JPL Publication 95-15

Proceedings of the Nineteenth NASA Propagation Experimenters Meeting (NAPEX XIX)

and the

Seventh Advanced Communications Technology Satellite (ACTS) Propagation Studies Workshop (APSW VII)

Held in Fort Collins, Colorado
June 14–16, 1995

Faramaz Davarian
Editor

August 1, 1995

NASA
National Aeronautics and
Space Administration

Jet Propulsion Laboratory
California Institute of Technology
Pasadena, California

JPL Publication 95-15

Proceedings of the Nineteenth NASA Propagation Experimenters Meeting (NAPEX XIX)

and the

Seventh Advanced Communications Technology Satellite (ACTS) Propagation Studies Workshop (APSW VII)

Held in Fort Collins, Colorado
June 14–16, 1995

Faramaz Davarian
Editor

August 1, 1995

NASA
National Aeronautics and
Space Administration

Jet Propulsion Laboratory
California Institute of Technology
Pasadena, California

This publication was prepared by the Jet Propulsion Laboratory, California Institute of Technology, under a contract with the National Aeronautics and Space Administration.

PREFACE

The NASA Propagation Experimenters (NAPEX) meeting is a forum convened each year to discuss studies supported by the NASA Propagation Program. The reports delivered at this meeting by program managers and investigators present our recent activities and future plans. Representatives from U.S. industry and organizations (domestic and international) who have an interest in radio wave propagation studies are invited to NAPEX meetings for discussions and information exchanges. This Proceedings records the content of NAPEX XIX and the ACTS Propagation Studies Workshop VII (APSW VII) that followed it.

The objective of the NASA Propagation Program is to enable new satellite communication applications. This objective is achieved by supporting propagation studies and experiments that meet the needs of the satellite communication community. In fact, such studies are planned with input from industry. The experiments are conducted mainly by universities.

NAPEX XIX took place at The University Club at Colorado State University, Fort Collins, Colorado, on June 14, 1995. I would like to express my sincere gratitude to our local host, Professor Bringi, his staff, and his student, John Beaver, for dealing with the local logistics of the meeting. Also, to their credit, we had a very interesting tour of the ACTS propagation terminal and the CHILL radar site.

Regretfully, Professor Robert Crane of the University of Oklahoma could not attend NAPEX XIX, as he was recovering from an earlier heart problem. In his absence, Dr. Louis Ippolito kindly agreed to cochair the ACTS Workshop Plenary Session with Dr. David Rogers. I would like to thank Drs. David Rogers and Louis Ippolito for chairing the plenary.

I would also like to thank Mardy Wilkins for helping me with the organization of the meeting and Janice Jones of the JPL Technical Information Section for coordinating the publication of this document.

The University of Alaska will host NAPEX XX in June 1996. The exact date of this meeting will be announced later. The eighth ACTS Propagation Studies Workshop will take place in Norman, Oklahoma in November 1995. Professor Robert Crane has kindly offered to be the local host for this meeting.

Faramaz Davarian

ABSTRACT

The NASA Propagation Experimenters Meeting (NAPEX), supported by the NASA Propagation Program, is convened annually to discuss studies made on radio wave propagation by investigators from domestic and international organizations. NAPEX XIX was held on June 14, 1995, in Fort Collins, Colorado. Participants included representatives from Canada, Japan, and the United States, including researchers from universities, government agencies, and private industry. The meeting focused on mobile personal satellite systems and the use of 20/30-GHz band for fixed and mobile satellite applications. In total, 18 technical papers were presented.

Following NAPEX XIX, the Advanced Communications Technology Satellite (ACTS) Propagation Studies Workshop VII (APSW VII) was held on June 15–16, 1995, to review ACTS propagation activities with emphasis on the experimenters' status reports and dissemination of propagation data to industry. The workshop included a tour of the ACTS propagation site in Colorado.

CONTENTS
NAPEX XIX MEETING

CONTENTS
APSW VII

NAPEX XIX AND MINIWORKSHOP ATTENDEES

Sergio Aguirre
Motorola, M/S OSC-V
2501 S. Price Road
Chandler, AZ 85248-2899
602-732-2765
602-732-2332 (FAX)
E-mail: sergio_aguirre-P25410.email.mot.com

Bruce Altmeyer
Allied Signal Avionics
6400 Wilkinson Drive
Prescott, AZ 86301
520-445-5711
520-445-7044 (FAX)

Robert Bauer
NASA Lewis Research Center
21000 Brookpark Rd., MS 54-6
Cleveland, OH 44135
216-433-3431
216-433-6371 (FAX)
E-mail: acbauer@lims01.lerc.nasa.gov

John Beaver
Colorado University
Dept. of EE
Ft. Collins, CO 80523
303-491-6758
303-491-2249 (FAX)
E-mail: jb686028@longs.lance.colostate.edu

Harvey L. Berger
TRW Space and Electronics Group
One Space Park
Redondo Beach, CA 90278
310-813-7692
E-mail: berger@gandalf.sp.trw.com

Scott Borgsmiller
Georgia Institute of Technology
Atlanta, GA 30332-0800
404-894-5280
404-853-9171 (FAX)
E-mail: gt3681c@prism.gatech.edu

V.N. Bringi
Colorado State University
Dept. of EE
Ft. Collins, CO 80523
303-491-5595
303-491-2249 (FAX)
E-mail: bringi@longs.lance.colostate.edu

Gulraiz Butt
University of Surrey
Centre for Satellite Eng. Research
Guildford, Surrey
GU2 5XH, U.K.
+44 1483 300800 ext. 2434
+44 1483 259504 (FAX)
E-mail: g.butt@ee.surrey.ac.uk

Junho Choi
U.S. Naval Research Laboratory
Code 8140.2
45455 Overlook Ave., S.W.
Washington, D.C. 20375-5354
202-767-9050/9792
202-767-1317 (FAX)

Faramaz Davarian
Jet Propulsion Laboratory
MS 67-204
4800 Oak Grove Drive
Pasadena, CA 91109
818-354-4820
818-393-0096 (FAX)
E-mail: davarian@qmail.jpl.nasa.gov

Asoka Dissanayake
Comsat Laboratories
22300 Comsat Drive
Clarksburg, MD 20871
301-428-4411
301-540-8208 (FAX)

Barry Fairbanks
NASA Lewis Research Center
21000 Brookpark Rd., MS 54-6
Cleveland, OH 44135
216-433-3541
216-433-6371 (FAX)
E-mail: acfair@lims01.lerc.nasa.gov

Yiping Fan
New Mexico State University
P.O. Box 30001
Las Cruces, NM 88003-0001
505-646-6417
505-646-1435 (FAX)

Julie Feil
Stanford Telecom
1761 Business Center Drive
Reston, VA 22090-5333
703-438-7846
703-438-7921 (FAX)
E-mail: jfeil@sed.stel.com

Robert J. Figucia
MIT/Lincoln Laboratory
244 Wood Street
Lexington, MA 02173-9108
617-981-4230
617-981-4583 (FAX)
figs@ll.mit.edu

Paul Flikkema
University of So. Florida
4202 E. Fowler Ave., ENB 118
Tampa, FL 33620
813-974-3940
813-974-5250 (FAX)
flikkema@sunburn.eng.usf.edu

Arhur Garrison
TRW Space and Electronics Group
One Space Park
Redondo Beach, CA 90278

Julius Goldhirsh
Applied Physics Lab.
Johns Hopkins University
Laurel, MD 20723-6099
301-953-5042
301-953-5458 (FAX)
E-mail: julius-goldhirsh@aplmail.
jhuapl.edu

Yoshiro Hase
Communications Research Laboratory
Space Communications Division
4-2-1 Nukui-Kitamachi
Koganei, Tokyo 184
Japan
+81 423 27 7506
+81 423 27 6825 (FAX)
E-mail: hase@crl.go.jp

Joshua Hayase
Information Systems International
2141 P Street NW, Suite 107
Washington, DC 20037
202-331-9353

Henry F. Helmken
Florida Atlantic University
P.O. Box 3091, MS SE/456
Boca Raton, FL 33431
407-367-3452
407-367-2336 (FAX)
E-mail: helmkenh@acc.fau.edu

Rudolph E. Henning
University of South Florida
College of Engineering
Tampa, FL 33620
813-974-4782
813-974-5250 (FAX)
E-mail: henning@eng.usf.edu

Hau H. Ho
TRW, MS R6-1587
One Space Park
Redondo Beach, CA 90278
310-812-1656
310-813-4719 (FAX)
E-mail: ho@qmail2.sp.trw.com

Stephen Horan
New Mexico State University
Dept. 3-0
P.O. Box 30001
Las Cruces. NM 88003-3001
505-646-5870
505-646-1435 (FAX)
E-mail: shoran@nmsu.edu

Louis J. Ippolito
Stanford Telecom.
1761 Business Center Drive
Reston, VA 21029
703-438-8061
703-438-8112 (FAX)
E-mail: lji@sed.stel.com

Lisa Judge
Hughes Spaceway
P.O. Box 92919
Los Angeles, CA 90009
310-364-4848
310-364-4841 (FAX)

Anil Kantak
Jet Propulsion Laboratory
4800 Oak Grove Drive, MS 67-204
Pasadena, CA 91109
818-354-1825
818-393-0096 (FAX)
E-mail: Anil.V.Kantak@ccmail.
jpl.nasa.gov

John A. Koukos
National Observatory of Athens
Space Research Institute
Lofos Nymphon, Thision
11810 Athens
Greece
+30-1-346-2710
+30-1-342-0022 (FAX)

Chuong Le
Jet Propulsion Laboratory
4800 Oak Grove Drive
MS 67-204
Pasadena, CA 91109
818-354-5996
818-393-0096 (FAX)
E-mail:
Chuong.A.Le@ccmail.jpl.nasa.gov

Charlie Mayer
University of Alaska, EE Dept.
P.O. Box 755900
Fairbanks, AK 99775-5900
907-474-6091
907-474-6087 (FAX)
E-mail: ffcem@aurora.alaska.edu

John C. Peterson
Hughes Spaceway
P.O. Box 92919
Los Angeles, CA 90009
310-364-4795/4869
310-364-4841/4775 (FAX)

Toby Prescott
Qualcomm Inc.
6455 Lusk Blvd.
San Diego, CA 92121-2779
619-658-3652
619-658-2112 (FAX)
E-mail: tprescott@qualcomm.com

David V. Rogers
Communications Research Centre
3701 Carling Avenue
Ottawa, Ontario
Canada K2H 8S2
613-998-5174
613-998-4077 (FAX)
E-mail: dave.rogers@crc.doc.ca

Tom Russell
Stanford Telecom
1761 Business Center Drive
Reston, VA 22090-5353
703-438-8082
703-438-7921 (FAX)

Fred Shimabukuro
The Aerospace Corportation
P.O. Box 92957
Los Angeles, CA 90009
310-336-6903
310-336-6225 (FAX)
E-mail: shimabukur@courier10.aero.org

Robert F. Slattery
Lockheed Martin Corporation
P.O. Box 8048
Philadelphia, PA 19101
610-531-5259
610-962-3599 (FAX)

Paul G. Steffes
Georgia Institute of Technology
School of Elec. & Computer Eng.
Atlanta, GA 30332-0250
404-894-3128
404-853-9171 (FAX)
E-mail: ps11@prism.gatech.edu

Scott Stephens
TRW Space and Electronics Group
One Space Park
Redondo Beach, CA 90278

Krisjani S. Suwitra
Jet Propulsion Laboratory
4800 Oak Grove Drive
MS 67-204
Pasadena, CA 91109
818-354-9250
818-393-0096 (FAX)
E-mail: suwitra@java.jpl.nasa.gov

Steve Townes
Jet Propulsion Laboratory
4800 Oak Grove Drive
MS 238-420
Pasadena, CA 91109
818-354-7525
818-354-6825 (FAX)
E-mail: townes@galway.jpl.nasa.gov

Randy Turcotte
Motorola, MS OSC-V
2501 S. Price Road
Chandler, AZ 85248-2899
602-732-3429
602-732-2332
E-mail: randy_turcotte-P16838@
email.mot.com

Arv Vaisnys
Jet Propulsion Laboratory
4800 Oak Grove Drive
MS 161-260
Pasadena, CA 91109
818-354-6219
818-393-4643
E-mail: avaisnys@qmail.jpl.nasa.gov

Wolf Vogel
EE Research Laboratory
University of Texas
10100 Burnet Road
Austin, TX 78758
512-471-8608
512-471-8609 (FAX)
E-mail: wolf_vogel@mail.utexas.edu

Xuhe Wang
University of Oklahoma
Room 1248
100 East Boyd St.
Norman, OK 73019-0628
405-325-6561
405-325-7689 (FAX)
E-mail:
xwang@metgem,gcn.uoknor.edu

David B. Westenhaver
WWW, I.
746 Lioness Ct. S.W.
Stone Mountain, GA 30087-2855
404-925-1091
404-931-3741 (FAX)
E-mail: 72622.3404@Compuserve.Com

Administrative Assistant

JPL:

Mardy Wilkins
818-354-1723
818-393-0096 (FAX)
E-mail: wilkins@qmail.jpl.nasa.gov

ACTS Electronic Address:

acts@java.jpl.nasa.gov

NAPEX XIX

NASA Propagation Experimenters Meeting
The University Club
Colorado State University, Fort Collins

June 14, 1995

OPENING REMARKS
Recent Accomplishments and Future Plans

Faramaz Davarian

Jet Propulsion Laboratory, California Institute of Technology

The NASA Propagation Experimenters (NAPEX) meeting is a forum for NASA investigators and other researchers to discuss topics in earth/space propagation. Research conducted during the last year and plans for the coming year will be reported here. We have also invited presentations by international speakers and members of the satellite communications industry.

The objective of the NASA Propagation Program is to enable the development of new Earth/space applications. This program supports studies and experiments that will assist industry to utilize space for telecommunication services. In fact, our plans are developed with input from industry.

I will now review the achievements of our program during the last year and report the plans for the coming year. Your feedback is sought to direct our efforts to best meet industry needs.

An important milestone was achieved last year. The Olympus propagation experimenters completed their work. Olympus with its three-frequency beacon package was used in a propagation campaign in the early 90s for Ku- and Ka-band measurements. The Olympus Propagation Experimenters (OPEX) completed their work last November by publishing the OPEX reports. Virginia Tech, supported by the NASA Propagation Program, was the U.S. participant in this experiment. Copies of the OPEX reports were provided to us courtesy of ESA and were distributed among NASA experimenters in January 1995.

The Advanced Communications Technology Satellite (ACTS) K_a-band campaign is currently a major element of our program. A two-day workshop is dedicated to this effort following today's meeting. During the last year, data were collected from several sites in North America. We also experienced a few growing pains. Hardware problems were corrected. A new preprocessing software was written, and later had to be revised. But we managed to collect data without interruption, and experimenters are now processing and analyzing the collected data. A new site also began operation at Georgia Tech to collect wideband data using ACTS.

The ACTS mobile propagation experiments concluded last year and the data have been analyzed. Measurements resulting from these experiments constitute the largest body of K_a-band propagation data to date. Later today we will hear the results of the ACTS mobile experiments from our investigator at the Applied Physics Laboratory.

Power control is an attractive means of propagation loss mitigation for K_a-band applications. To enhance our knowledge of this technique, an uplink power control experiment was successfully concluded by COMSAT Labs in Clarksburg, MD. We will hear a presentation on this topic by Dr. Dissanayake later today.

Another important element of the NASA Propagation Program is personal/mobile satellite communications. During the last year, our experimenters conducted a number of studies, and we have stayed abreast of industry advances in this area. As you may recall, last year the University of Texas introduced a concept known as "photogrammetric mobile satellite service prediction." This is a simple low-cost approach to characterizing user environment in a mobile/personal link. Images are taken through a fish-eye lens with 180° field of view. Recent efforts have been directed toward analyzing fisheye video sequences for predicting fading. A presentation on this topic is scheduled for this afternoon.

The University of Texas began a series of measurements using a six-channel GPS receiver for personal satellite communication applications. This effort provides an inexpensive approach for making shadowing, blockage, and multipath fading measurements. The effect of satellite path on signal availability can also be observed. A talk on this topic will be given this afternoon.

As is evident from the above two efforts, we are seeking inexpensive means to determine service availability and characterize the user environment for mobile/personal satellite communication applications. These efforts are in response to an industry need to assess quality of service over vast coverage areas.

During the last year, a series of in-building L- and S-band measurements were completed. During this experiment, several buildings were used for taking measurements. The results of this effort will be reported today. Similar measurements were also made using Tracking and Data Relay Satellite (TDRS) signals, the results of which will also be reported today. These efforts are in support of mobile satellite and direct broadcast satellite applications.

In collaboration with INTELSAT, the NASA Propagation Program is supporting an 11-GHz experiment at the University of Texas to collect long-duration statistics on low-elevation angle paths. This experiment is planned for eight years, and it will complete in June 1996. Results of this campaign have been previously published and the final report will be available in late 1996.

Most of you are familiar with the *Database for Propagation Models* for PC and Macintosh machines. An update to the software will be distributed in this meeting. This update includes new propagation models and contains an

enhanced user interface. This may be the last EXCEL release of the software. We are thinking of changing the software development platform from EXCEL to C++ for future releases.

Our work with the International Telecommunication Union (ITU) continued during the past year. I participated in Task Group 3/1 in September. The purpose of this task group was to address urgent issues on mobile/personal satellite propagation effects. It was recognized in this task group that there is an urgent need for data on non-geo satellite systems and links with hand-held receivers. Improvements to ITU-R Recommendation 681 were suggested. I provided the task group with an input document to clarify certain parts of the recommendation. I feel our program has obtained enough data in the last two years to make important contributions to Rec. 681. The NASA Propagation Program will provide the ITU with a document to improve this recommendation in the next year. Figure 1 shows the models included in Rec. 681, and Figure 2 shows the organizational chart of the ITU.

Figure 1. Recommendation 681

- Empirical roadside shadowing model
  - Valid for a frequency of 1.5 GHz; $\theta \geq 20°$; $1\% \leq P \leq 20\%$
- Attenuation frequency scaling model
  - Valid for a frequency range of 0.8–3.0 GHz; $30° \leq \theta \leq 60°$; $1\% \leq P \leq 30\%$
- Fade duration distribution statistics
  - Valid for a 5-dB fade threshold, and a frequency of 1.5 GHz
- Non-fade duration distribution statistics
  - Valid for a 5-dB fade threshold, and a frequency of 1.5 GHz
- Fading due to multipath model(fade depth)
  - Two models for mountainous and road-side tree environments, UHF and L-band
    - $1\% \leq P \leq 10\%$ for mountain, $1\% \leq P \leq 50\%$ for roadside tree
- Special consideration of hand held terminals (user blockage)

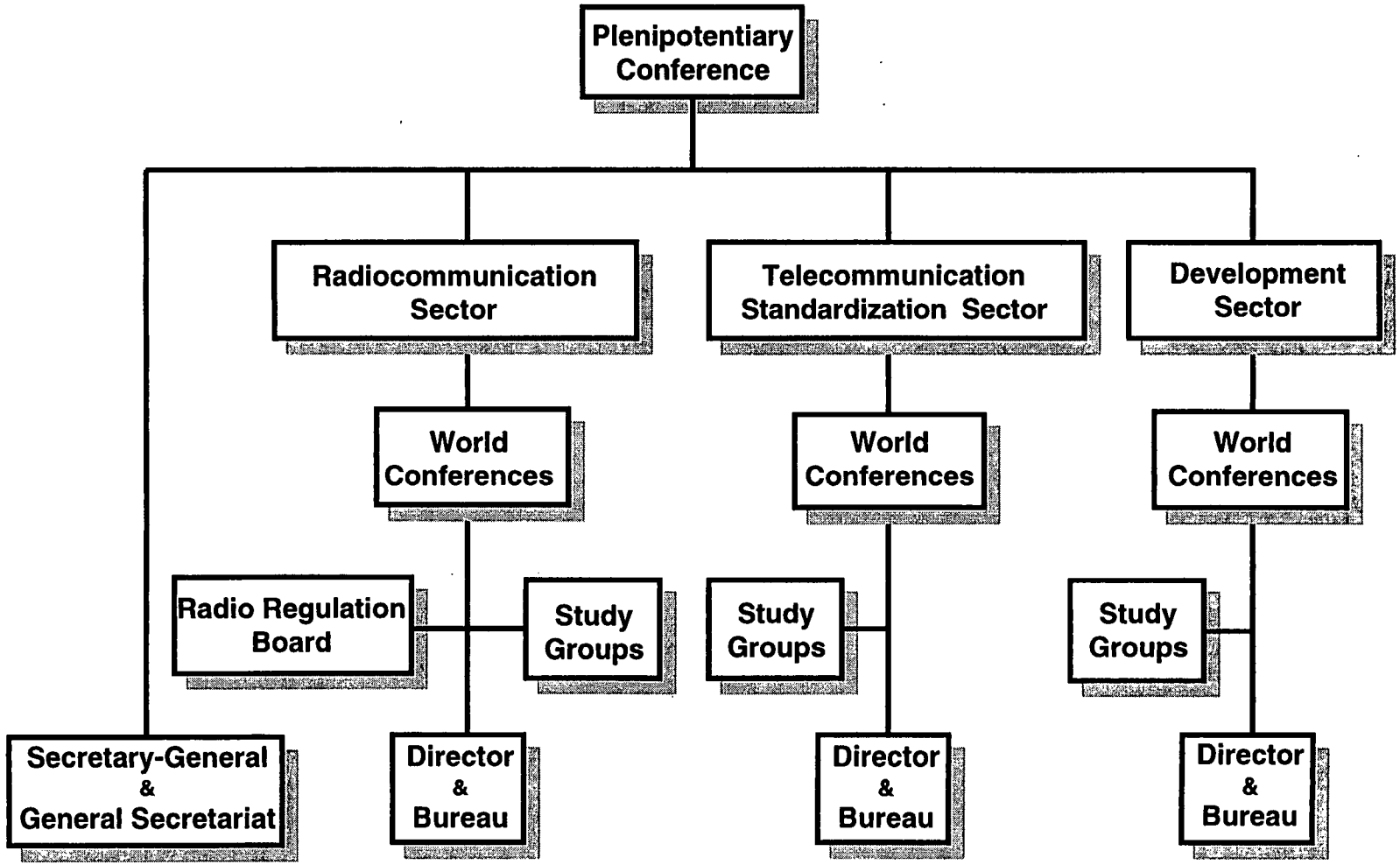

Figure 2. The Organizational Structure of the International Telecommunications Union

Earth-Space Links and Fade-Duration Statistics

F. Davarian
Jet Propulsion Laboratory, California Institute of Technology
818-354-4820

Abstract

In recent years, fade-duration statistics have been the subject of several experimental investigations. A good knowledge of the fade-duration distribution is important for the assessment of a satellite communication system's channel dynamics: What is a typical link outage duration? How often do link outages exceeding a given duration occur?

Unfortunately there is yet no model that can universally answer the above questions. The available field measurements mainly come from temperate climatic zones and only from a few sites. Furthermore, the available statistics are also limited in the choice of frequency and path elevation angle.

Yet, much can be learned from the available information. For example, we now know that the fade-duration distribution is approximately lognormal. Under certain conditions, we can even determine the median and other percentiles of the distribution. This paper reviews the available data obtained by several experimenters in different parts of the world. Areas of emphasis are mobile and fixed satellite links. Fades in mobile links are due to roadside-tree shadowing, whereas fades in fixed links are due to rain attenuation.

Introduction

Digital radio communication systems are influenced by the dynamics of fade events, that is, fade rate, fade duration, and inter-fade duration. In a digital receiver, signal decoding and synchronization (timing and phase) can be affected by the distribution of fade events. For long fades, a receiver could lose lock, and reacquisition may become necessary. Therefore, fades and their statistical distribution influence service availability, receiver loss of lock probability, and decoder performance. We will examine fade-duration statistics on Earth-space links.

On satellite links, fade events can result from atmospheric causes (rain) or, in the case of mobile satellite links, from tree shadowing and blockage. The analysis of measured data has shown that both types of fade give rise to fade-duration statistics that can be approximated with a lognormal distribution [1–3].

The lognormal probability density function is given by

$$p_z(z) = \frac{1}{sz\sqrt{2\pi}} \exp[-\frac{(\ln(z)-m)^2}{2s^2}] \qquad (1)$$

where z denotes the random variable, and s and m are the standard deviation and the mean of ln(z). The cumulative distribution of z can be obtained by integrating the above function from Z to infinity resulting in the probability that z is larger or equal to Z:

$$P(z \geq Z) = \frac{1}{2} erfc[\frac{\ln(Z)-m}{s\sqrt{2}}] \qquad (2)$$

where *erfc* denotes the complementary error function. For convenience, Eq. (2) can be multiplied by 100 to express the probability as a percentage.

Fade-Duration Statistics in Mobile Satellite Links

Fade-duration statistics caused by tree shadowing were obtained from measurements made in south-eastern Australia at a frequency of 1.5 GHz and a path elevation angle of 51° [1]. The data were shown to fit the lognormal distribution with good accuracy when m = -1.514 and s = 1.215, for a 5-dB fade threshold. The distribution encompassed road types that exhibit moderate and extreme shadowing —see reference 1 for a description of shadowing types. This distribution is shown in Figure 1. Note that fade duration is given in meters rather than seconds. Distance durations may be converted to time durations by dividing the former by the speed of the vehicle, which was nominally 25 m/s in the Australian experiment.

For this example, 50 percent of all the fade events consisted of fades shorter than 0.22 m. At a speed of 25 m/s, this translates to less than 0.01 s. Ninety-nine percent of all fade events consist of fades with durations shorter than 4 m, which is equivalent to a time duration of 0.16 s. Therefore, it appears that, for this example, fade durations are generally short enough to avoid receiver synchronization problems (at least for most of the time). Other experimental data have shown that for tree shadowing, fade durations increase with decreased elevation angle. For instance, the fade duration for a 30° elevation angle has been observed to be twice that of a 60° elevation angle at the same probability level [1]. If this observation is applied to the data presented in Figure 1, the fade-duration distribution for an elevation angle of about 25° can be estimated by adding the constant ln (2) to m. The result is shown by the dashed curve in Figure 1.

Rain Attenuation

Fades due to rain attenuation have been investigated in several experimental campaigns. Signals propagating through the atmosphere experience both attenuation and scintillation effects. Since signal fluctuations due to scintillation contain higher frequency components than the ones caused by rain attenuation, low-pass filtering of the observed signal can remove the scintillation effect. To focus our discussion to fade events due to rain attenuation, only data with scintillation-induced fluctuations removed are considered.

Reference [2] reports on a four-year experiment in Texas, where the elevation angle is 6° and the signal frequency is 11 GHz. Fade-duration statistics for fade thresholds from 5 to 20 dB are shown to be approximately lognormally distributed with the 50% probability level corresponding to a fade duration of about 300 s. Figure 2 shows the lognormal fit to the data. In this example, 50% of all fades are shorter than 300 s, and 90% of all fades are shorter than 2500 s. For a threshold of 20 dB, measured fade durations are shorter than the lognormal model predictions at high duration values. The asterisk at the 2000 s duration value in Figure 2 shows the measured data for a threshold of 20 dB. This means that, for a fade threshold of 20 dB, fades longer than 2000 s are rare.

There is evidence that the lognormal model also applies to a mix of data taken at different sites and different frequencies. Figure 3 taken from [3] shows an approximate lognormal fit to data obtained from three sites, one in the U.S. (Virginia) and two in Europe. The data include three frequencies of 12, 20, and 30 GHz, and fade thresholds in the range of 4 to 10 dB. The Virginia site[1] had the lowest path elevation angle of 14°. The 50 percentile value in this case is 200 s compared to 300 s in Figure 2. Another difference between these two cases is that the

[1] One full year of data was acquired in the 1990–92 period using the Olympus spacecraft.

percentage of very long fades, that is, fades longer than 1000 s, is less in this case than in Figure 2. This may be attributed to the data in Figure 2 corresponding to the very low elevation angle of 6°.

Another subject of interest is the absolute number of fades at a given threshold. The absolute number of fades depends on the frequency of the signal. The number of fade events increases with increasing frequency. For the Virginia site, Reference [4] shows the number of fades as a function of fade duration for frequencies of 12, 20, and 30 GHz and an elevation angle of 14°. For example, at a fade threshold level of 5 dB the number of fade events with fades equal to or exceeding 1 minute is 108 at 12 GHz, 605 at 20 GHz, and 935 at 30 GHz. These values for a fade threshold of 15 dB are 6 at 12 GHz, 75 at 20 GHz, and 200 at 30 GHz. Clearly, the number of fade events decreases when the threshold level increases. Since system engineers use the fade threshold information to determine the required fade margin in a system, it is useful to further explore the relationship between the fade duration statistics and the fade threshold (attenuation level). The next section will address this topic.

Fade Duration and Attenuation Level

The probability of service availability is a very important parameter of link design in a satellite communication system. The availability of the service is directly related to the link margin. Therefore, it is important to examine the fade-duration distribution as a function of signal attenuation. Presenting fade duration in this fashion will enable system designers to conveniently plan the optimum value of the fade margin for a system. Note that too little margin will result in an unacceptable grade of service, whereas too much link margin will give rise to high system costs.

Reference [5] considers this issue by relating the occurrence of fades of a certain duration to attenuation level. Although the model presented in [5] is a preliminary one, it is noteworthy in that it addresses an important system need. In this approach, fade durations have been binned into predetermined intervals. For example the model for fade durations between 30–60 s is given by

$$FT_{12} = 8900\exp(-1.315A + 0.118A^2 - 0.004A^3) \qquad (3)$$

where FT_{12} denotes the cumulative fade time in seconds for a frequency of 12 GHz and A is the attenuation level in dB ($3 \leq A \leq 16$). Figure 4 shows a plot of Eq. (3) for attenuation levels from 3 to 16 dB. For example, at a margin of 9 dB all fades lasting for 30–60 s add up to 500 s of link outage in one year of observation. The data used for this model were also obtained from the Virginia site mentioned earlier with a path elevation angle of 14° to the satellite.

Because the database used to develop Eq. (3) also included 20 and 30 GHz data, this equation was extended to a model that predicts fade time for three frequencies [5]. This model is given as

$$FT_f = 8900(-8.899 + 0.915f - 0.008f^2)\exp(-1.315A + 0.118A^2 - 0.004A^3) \qquad (4)$$

where FT_f is the cumulative fade time in seconds for the 30–60 s fade duration interval at a given frequency, f is the frequency in GHz, and A is the attenuation in dB. The dashed curve in Figure 4 shows the above model for 20 GHz. An extension of the above model to other fade duration intervals, e.g., 60–120 s, is also given in [5].

Although Eq. (4) offers a powerful tool for determining fade-duration distribution as a function of attenuation, there is a caveat associated with this tool: The model was developed based on measurements at a single elevation angle and in a single rain climate zone. Therefore, its extension to other elevation angles and climate zones is not clear. The model may also be contaminated by statistical noise because it is based on only one year of observations. Measurements at different sites and for longer time durations will very likely contribute to the improvement of the model's accuracy and robustness.

Summary

Fade-duration statistics on satellite links can be approximated by the lognormal distribution. This distribution can be uniquely described by the mean and the standard deviation of the natural logarithm of the samples. This model applies to fades due to rain attenuation (fixed satellite) as well as fades due to tree shadowing (mobile satellite).

For shadowing-induced fades, fade-duration statistics seem to be insensitive to the amount of shadowing, i.e., light to heavy shadowing. However, a moderate dependence on elevation angle has been observed in field measurements. This dependence gives rise to longer fade durations with decreased elevation angle.

For rain-attenuation-induced fades, it appears that for temperate site locations, elevation angles above 14°, and frequencies between 12–30 GHz, the fade-duration statistics are not strongly dependent on site location, elevation angle, or frequency.

A simple model to relate fade time for a given fade duration to attenuation level is also discussed. This approach is useful for examining the impact of fades on the receiver, allowing for an estimation of total receiver downtime. Note that total downtime is the sum of the fade duration and system reacquisition time.

The models presented in this paper are based on a limited amount of experimental data. Further study is required to substantiate their application to specific slant path configurations.

Acknowledgment

The work conducted for this paper was carried out by the Jet Propulsion Laboratory, California Institute of Technology, under a contract with the National Aeronautics and Space Administration.

References

1. J. Goldhirsh and W. Vogel, *Propagation Effects for Land Mobile Satellite Systems,* NASA Reference Publication 1274, Feb. 1992, pp. 41–45.
2. M. Rice, et. al., "K-Band Land-Mobile Satellite Channel Characterization using ACTS," *International Journal of Satellite Communications,* will be published in late 1995.
3. W. Vogel, et al, "Rain Fades on Low Elevation Angle Earth-Satellite Paths: Comparative Assessment of the Austin Texas, 11.2 GHz Experiment," *Proc. IEEE,* vol. 81, no. 6, Jun. 1993, pp. 885–896.
4. J. Baptista, et al, ed., *Reference Book on Attenuation Measurement and Prediction,* ESA WPP-083, Nov. 1994, pp. 101–107.
5. W. Stutzman, et al, "Results from the Virginia Tech Propagation Experiment Using the Olympus Satellite 12, 20, and 30 GHz Beacons," *IEEE Trans. Antennas and Propagation, vol 43, no 1, Jan. 1995, pp. 54–62*
6. H. Ajaz and A. Saffaai-Jazi, *Fade and Inter-Fade Durations in Ku- and Ka-Band Frequencies Measured From the Olympus Satellite Beacons,* Satcom Report 93-17, VPI&SU, Oct. 1993.

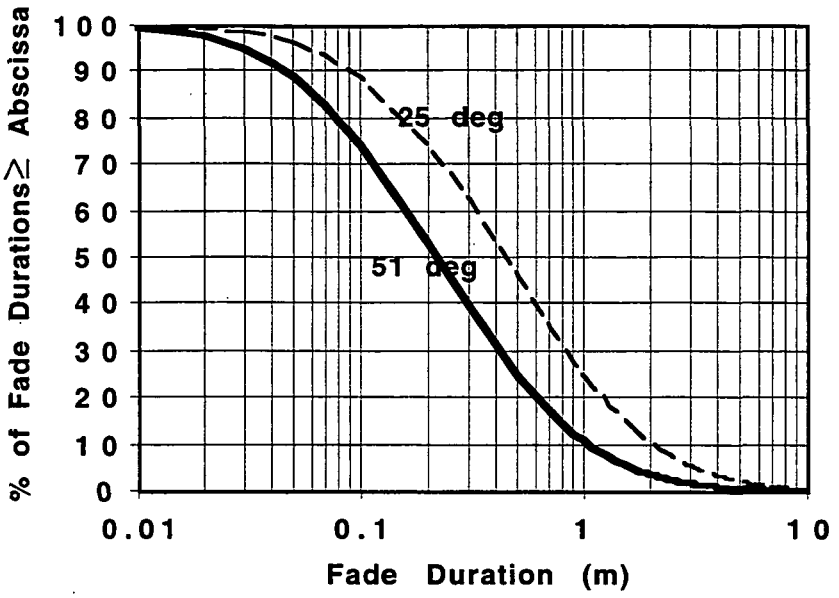

Figure 1. Fade Duration Distribution for Mobile Satellite Links (elevation angles 51° and 25°)

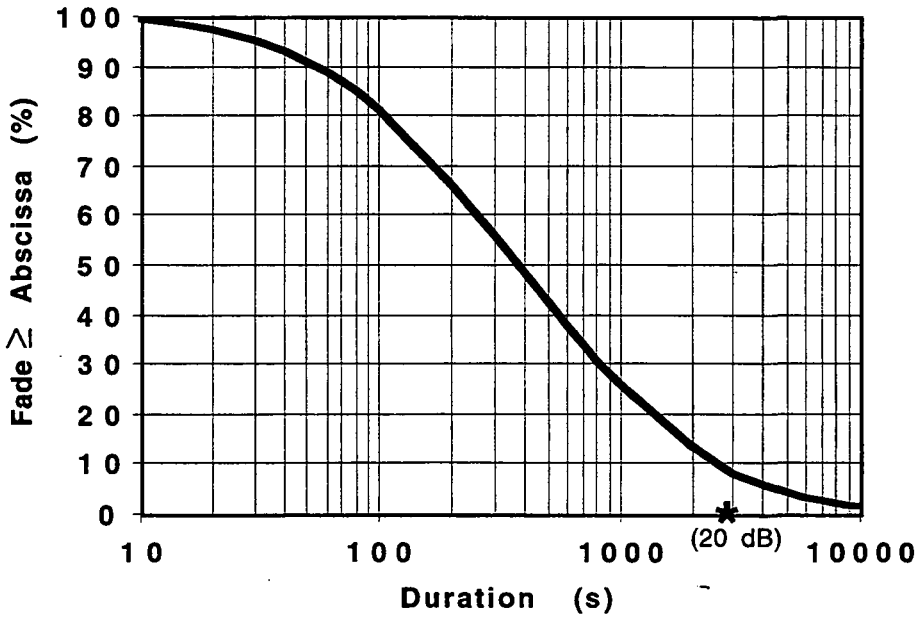

Figure 2. Texas 11-GHz Data

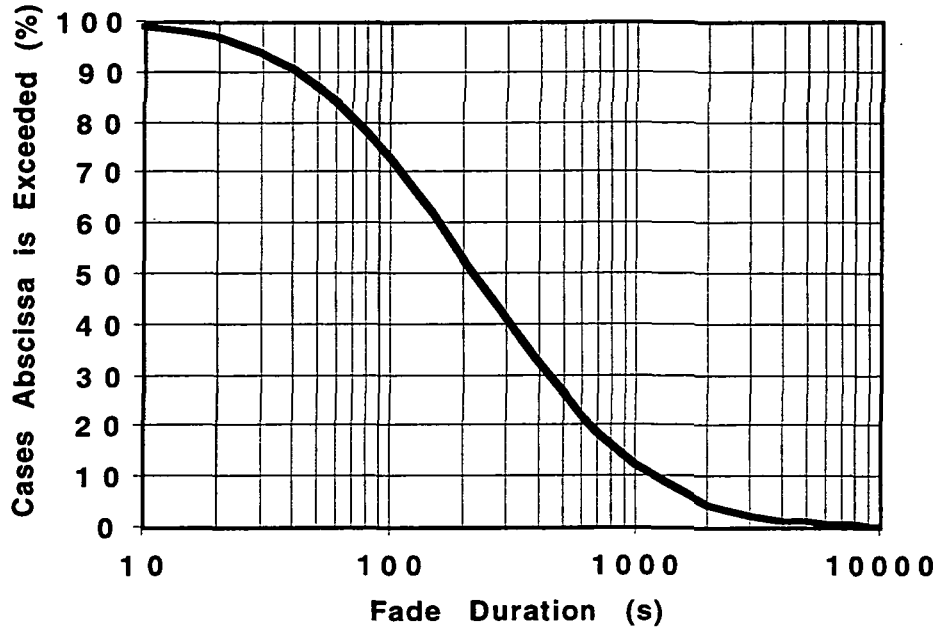

Figure 3. OPEX 12-, 20-, and 30-GHz Data

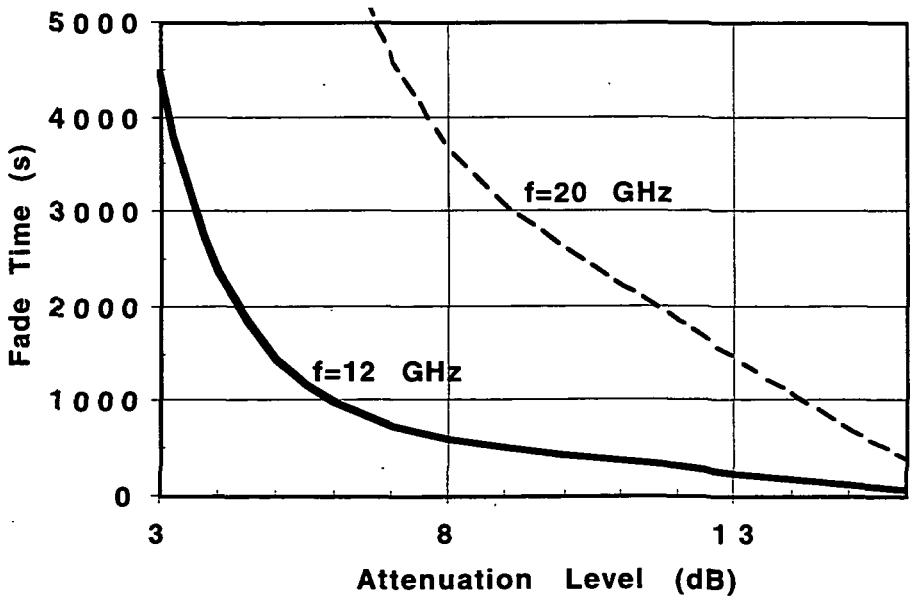

Figure 4. Annual Fade Time for 30–60 s Fade Durations

ON LOCAL RAIN FADE MODELING AND PREDICTION FOR MM-WAVE SATCOM SYSTEM ENGINEERING

NAPEX XIX, June 1995

Ft. Collins, CO

PAUL FLIKKEMA[†], HENRY HELMKEN[‡], and RUDY HENNING[†]

[†]University of South Florida [‡]Florida Atlantic University

Outline

Satcom systems engineering (brief history)

Potential Improvements

- Refined statistics
- Improved event prediction methods

Example: Event prediction via radiometric data

Open Issues (?)

Satcom Systems Engineering

First generation –

- Link budget analysis
- Rain attenuation statistics
  - Fade margin
  - Outage probability analysis

Second generation –

- Power control and coding
- Dynamic capacity allocation (trunking effect)
- Site diversity

Potential Improvements

Must maximize network operating efficiency

Resources must be used to combat rain fades – combinations of 2nd generation methods

Approaches:

- Refined statistics for optimum efficiency
  - Maximize efficiency by using multiple data classes (priorities)
  - Implies multi-tiered service/cost structure
  - Challenge: deep fades
- Improved prediction methods for adaptivity

Improved Prediction Methods

(e.g., nowcasting)

Adaptive approaches — desired properties:

- Successful in anomalous phenomena (can always have a bad day)
- Responsive to fine structure (short-term fade statistics)
- Site-nonspecific (robust)
- Can use information correlated in space and time, e.g.:
  - IR/visual satellite data
  - Radar data
  - Radiometric data

Attenuation Prediction via Radiometric Data

Approach: Analysis of correlation between fluctuations in sky temperature and attenuation caused by rain

Data reduction/processing software:

- C program for generation of "clean" data from PV1 files:
  - data/status unpacking
  - detection of missing data
  - flexible processing of status data
  - calibration processing
- MATLAB for statistical data processing
- MATLAB/Excel for plotting

Attenuation Prediction via Radiometric Data (cont'd)

Goal: Investigate usefulness of on-site radiometer sky temp measurements for prediction of link attenuation due to rain

Example: Time difference of level crossing — *a posteriori* event detection analysis (preliminary)

For rain event k, TDLC is

$\Delta^{(k)}(l_b, l_r) = t_b^{(k)}(l_b) - t_r^{(k)}(l_r)$

where

$t_b^{(k)}(l_b)$ = time beacon attenuation crosses l_b dB

$t_r^{(k)}(l_r)$ = time ARD crosses l_r dB

Preliminary Results

Data set: 13 days in 1994 (16 events)

Parameters:

- Rain event designated if both beacon atten. and ARD > 7 dB
- Beacon data filtered using 9-point median filter

TDLC computed for *known* events => includes times only for correctly detected rain events.

Sample mean:

$\bar{\Delta}(l_b, l_r) = \frac{1}{N} \sum_{k=1}^{N} \Delta^{(k)}(l_b, l_r)$

$\bar{\Delta}(5, 5) = 7.2$ sec

Summary

Complete solutions will require integration of techniques

Fading unavoidable => Mapping of outage statistics to service structure

Deep fading => Prediction using temporally/spatially correlated data

—> What is Needed?

Experimental Evaluation of Open-Loop Uplink Power Control Using ACTS

Asoka Dissanayake
COMSAT Laboratories
22300 COMSAT Drive
Clarksburg, MD 20871

1. Introduction

Satellite communication systems operating in the 20/30 GHz frequency band are subjected to degradations produced by the troposphere that are much more severe compared to those found at lower frequency bands. These impairments include signal absorption by rain, clouds, and gases, and amplitude scintillations arising from refractive index irregularities. For example, rain attenuation at 20 GHz is almost three times that at 11 GHz. Although some of these impairments can be overcome by oversizing the earth station equipment such as antenna and high power amplifier, the current trend of migrating to smaller, low-cost earth stations that can be easily deployed at user premises runs counter to using such brute force methods. As a consequence, most Ka-band systems are expected to employ some form of fade mitigation that can be implemented relatively easily and at modest cost. In this regard NASA's Advanced Communication Technology Satellite (ACTS) which operates in the 20/30 GHz band, provides an excellent opportunity to develop and test such techniques. The present investigation conducted under NASA sponsorship examines the potential of up-link power control as a fade mitigation technique.

Some of the methods applicable for countering rain fading include:

- site diversity
- satellite resource sharing
- up-link power control

Site-diversity takes advantage of finite size of rain cells to enable two earth stations seprated by several tens of kilometers and interconnected via a terrestrial line to provide a continuous link to the satellite. Extra cost of a second earth station and the terrestrial line between them usually make site-diversity a less attractive proposition. Satellite resource sharing involves reallocation of either power or bandwidth to those earth terminals affected by rain. Invariably this increaes the complexity and cost of the satellite. Up-link power control (ULPC) essentially counters fading on the up-link by increasing the power transmitted by the earth station. Other potential candidates for fade mitigation include orbital diversity and selective use of lower frequncy channels.

Up-link power control can be implemented in several forms, including:

- open-loop
- closed-loop
- feedback-loop

The open-loop scheme relies on estimating the up-link fade by independent means such as monitoring a satellite borne beacon signal or radiometry. In closed-loop implementations, the transmitting earth station uses its own transponded carrier to estimate the up-link fade. With feedback-loop, a central control station commands each earth staion in the network to adjust its power to compensate for fading on its own up-link. In terms of implementation complexity open-loop is the least complex since it can be deployed at an earth station without any systemwide considerations. Closed-loop control is not always realizable since the availability of the transponded carrier depends on the network configuration. Feedback-loop control is more complex requiring systemwide considerations and additional resources, both on the ground and on the spacecraft.

Power control accuracy is a major concern for systems prone to adajacent channel interferences. In addition, transmission of exeessive power can cuase harm to the spacesegment and to adjacent satellites. Closed-looop and feedback-loop power control systems can provide superior power control accuracy. In the case of open-loop systems, accuracies akin to the other two systems may be obtained using a beacon signal close to the transmit frequency to estimate the up-link fade. Mainly spurred by this requirement, a frequency allocation for an up-link beacon for Ka-band satellite systems was instituted by the World Adminstattive Radio Conference in 1992. However, reception of a weak beacon signal which lies close to a strong transmitting signal poses few problems. Although these can be surmounted easily, the additional investment required for a complex feed system and a receiver operating in a frequency band different from the down-link can be a burden on VSAT type applications where end-user cost is a major concern. Instead of using an up-link frequncy beacon, a beacon signal within the down-link frequency band can be used to estimate the fading on the up-link. This method is less accurate since fading on up- and down-link are not highly correlated. However, through careful considerations of propagtion factors involved in the fading process, acceptable accuracy levels may be achieved.

The present investigation deals with the implementation of open-loop up-link power control using a beacon signal in the down-link frequency band as the control parameter. A power control system was developed and tested using the ACTS satellite. ACTS carries beacon signals in both up- and down-link bands with which the relationship between the up- and down-link fading can be established. A power controlled carrier was transmitted to the ACTS satellite from a NASA operated ground sataion and the transponded signal was receieved at COMSAT Laborotories using a terminal that was routinely used to monitor the two ACTS beacon signals. The experiment ran for a period of approximately six months and the collected data were used to evaluate the performance of the power control system.

A breif review of propagation factors involved in estimating the up-link fade using a beacon signal in the down-link band are presented in Section 2. Section 3 describes the power controller design and the experiment configuration. Results of the experiment are discussed in Section 4.

2. Propagation Considerations

Propagation factors that have an impact on the design of Ka-band open-loop up-link power control systems that use a down-link signal to infer the up-link fade include:

- gaseous absorbtion
- cloud and rain attenuation
- tropospheric scintillations

The detected down-link fade is a combination of these factors. The power controller has to translate the down-link fade to the up-link using frequency sacling ratios applicable for each of the above factors. In general, the frequency scaling ratios for different propagation phenomena are not the same. Within the 20/30 GHz frequency band the gaseous absorption follows a complex frequency scaling law which is a function of the atmospheric water vapor content. For rain and clods the fade ratio can be approximated by $(f_1/f_2)^2$, where f_1 and f_2 are the frequencies at which fades are measured, and for topospheric scintillations the scaling ratio has the form $(f_1/f_2)^{7/12}$[1]. It is generally not feasible to seperate the absorptive components (gases, clouds, and rain) from each other; however, the non absoptive tropospheric scintillations can be separated from absorptive components using filtering techniques[2]. Since rain attenuation is the main factor a power control system has to contend with, the frequency sacling ratio for rain is of primary importance for the contoller design. The frequency scaling behaviour of rain attenuation is essentially a function of the rain type (stratiform, thunderstorm etc.); in addition, it can vary considerably during a single rain event. Figure 1 shows the frequency scaling ratio between 20 and 27 GHz fades observed during a summer rain event at a site in Clarksburg, MD; Fig. 1a shows the fade levels observed on the 20 and 27 GHz ACTS beacons, Fig. 1b shows the fade ratio as a function of the 20 GHz fade, and Fig. 1c shows the time series of the fade ratio. At low fade levels (<3 dB) the fade ratio is essentially determined by the gaseous absorption; Fig 1b also shows the combined effect of gaseous absorption and rain attenuation as predicted by theory. It is evident that considerable variation in the fade rato exist at high fade levels where rain fade is the dominant factor.

Figure 2a shows the distribution of the instentaneous frequency scaling ratio between 20 and 27 GHz fades coressponding to an observation period of 12 months; Fig. 2b shows the fade ratio on an equiprobable basis for the same observation period. Based on the instentaneous values, it is seen that for fades larger than about 3 dB the mean frequency scaling ratio is of the order of 1.8 dB. The equiprobable ratio has a similar magnitude. The distrbution of the instenteneous ratio around the mean is such that 90% of the values are contained within approximately ±10% of the mean value. This imples that the use of a constant frequency scaling ratio will limit the power control accuracy to approximately 10% of the fade level being compensated. The alternative of using a variable frequency scaling ratio which must adapt to the prevailing rain conditions is rather complex and may require additional information on the rain process. The experiment described in the next section was designed to evaluate power control error bounds resulting from the use of fixed frequency sclaing ratios.

3. Experiment Description

In order to evaluate the effectiveness of open-loop power control for Ka-band applications, a power control system was designed and fabricated. Figure 3 shows the main components of the control system. The control functions are carried out by a board level computer based on an Intel-80386 processor. The main input signal to the control system is the down-link beacon signal which is sampled at a rate of approximately 5 Hz. The computer processor first estimates the down-link fade and then translates it the up-link frequency. The power control is applied through a PIN diode attenuator placed in the signal path at an intermediate frequncy (IF) stage. Several safety features and alarm circuits are built into the system to prevent excessive power being transmitted towards the satellite. In case of an alarm a safety relay is activated and the power controller becomes transparent to the incoming signal.

The basic building blocks of the power control algorithm are shown in Figure 4. The incoming beacon signal samples are first used to obtain an estimate of carrier-to-noise ratio (C/N) over an averaging interval of 2 min. Next, the beacon level is separated into a clear sky reference level and a propagation contribution. The clear sky reference is the beacon level that would have been measured if negligible amounts of propagation impairments were present. The reference level is determined by drifts in the earth station receiver and thermal effects at the satellite. As a consequence, the clear-sky level esentially follows a diurnal pattern. The propagation contribution extracted after removing the clear-sky level is further divided into rain fade and signal scintillations. The frequency scaling laws applicable to rain and scintillation are applied to these components. The resulting values are added together to obtain the up-link fade level. The transmit power is then adjusted to compensate for the up-link fade.

The identification of the clear sky level is based on a filtering process in which relatively slow variations induced by the equipment are separated from somewhat faster varying propagation effects. This division is not always a clear-cut one. Slow propagation induced variations such as cloud attenuation and water vapor absorption cannot be factored out easily. Provided these effects are relatively small (< 1 dB), they can be lumped together with equipment effects without adversely affecting the control accuracy. On the other hand, complete isolation of propagation activity from equipment induced variations can be achieved by knowing the system noise temperature and determining the C/N to a high degree of accuracy. The extra effort required, however, is not commensurate with the resulting gain in link performance at such low levels of propagation activity. Variations in the C/N estimate over a two minute averaging period together with the slope of the beacon level are used for identifying the clear sky level. If the estimates are found to be within pre-set limits, the corresponing mean value of the beacon level is used to construct the clear-sky baseline; otherwise the base-line level is estimated from the previous clear-sky estimates using a predictive algorithm. The prediction makes use of samples collected during the previous two hours (60 samples). During rain fade events that last over several hours, the baseline predictive algorithm may not perform adequately. Under such circumstances, the baseline level from the previous day has a dominant influence on the current baseline estimate.

Once the baseline is established, any variation around this level is assumed to be induced by propagation phenomena. Two types of propagation factors are accounted for by the algorithm: fading caused by rain and heavy clouds and tropospheric scintillations. The two types can co-exist and they need to be separated before determining their contributions to the up-link. Scintillations are fast variations in signal level induced by tropospheric refractive irregularities. Variations are largely symmetrical about a mean level and fluctuations are restricted to frequencies above about 0.5 Hz. A running average of the estimated fade level, taken over a 20 second interval, appears to be sufficient to remove almost all scintillation effects. A delay of 10 seconds is introduced by the 20 seconds averaging filter. Therefore, to obtain the current rain fade level, a predictor similar to the one used for the baseline level is used. The predictor is based on maximum entropy[3] and can be applied to non-stationary processes such as rain.

After separating the rain and scintillation components, frequency scaling laws are applied to the two components. The up-link rain attenuation, A_{uR} can be approximated by:

$$A_{uR} = A_{dR} (f_u/f_d)^2 \ \text{(dB)} \qquad [1]$$

where A_{dR} is the down-link rain attenuation, and f_u and f_d are the up- and down-link frequencies, respectively. The factor involved in the scaling of 20 GHz fade to 27 GHz is 1.85. The measured fade ratio shown in Fig. 2 includes the effects of gaseous absorption and scintillations, and therefore, somewhat smaller compared to the ratio for rain alone.

For tropospheric scintillation, the scaling law employed is:

$$S_u = S_d (f_u/f_d)^{7/12} \ \text{(dB)} \qquad [2]$$

where S_u and S_d are the scintillation levels at the up- and down-link frequencies.

The up-link signal level, L_u, is given by:

$$L_u = A_{uR} + S_u \qquad [3]$$

In these calculations all quantities are in logarithmic scale (dBs).

In order to evaluate the performance of the power control system developed, a long-term test using the ACTS satellite was conducted. The test involved transmitting a power controlled carrier from the NASA ACTS ground station in Cleveland to the ACTS satellite and receiving the transponded carrier at an earth station in Clarksburg. Figure 5 shows the basic experiment configuration. The satellite was configured in the microwave switch matrix mode (MSM) and the E-08 spot beam of the satellite was used to beam the pilot signal towards Clarksburg. Starting from May, 1994, the experiment ran for a period of about 6 months. The power control evaluation was one of many experiments conducted using the satellite, and the actual satellite time used for the experiment was approximately 350 hours. During the test period several rain events

were encountered and these were deemed sufficient to evaluate the controller performance. In addition, off-line evaluation of the system was carried out using beacon data collected at Clarksburg.

At the transmit site in Cleveland, where the elevation angle to the ACTS satellite is 39°, the ACTS beacon signals are received via the 3.5 m NASA Ground Station (NGS) antenna using the beacon measurement system (BMS). The 20 GHz beacon signal is used by the power controller unit to estimate the down-link fade. The power controlled carrier at 70 MHz was derived from a signal synthesizer and fed to the power controller. The power controlled carrier coming out of the controller was fed to an up-converter that translates the 70 MHz input to an L-band frequency suitable for feeding the transmit chain of the Link Evaluation Terminal (LET); the transmit frequency was 29.5 GHz. The power amplifier of the LET saturates at an input of approximately 30 dBm. The nominal output of the power controller is maintained at a level close to 0 dBm, giving a total power control range in excess of 30 dB. The separation between the NGS antenna and the LET antenna is about 15 feet. Because of this, some decorrelation between fading on the up- and down-link was observed. However, the impact of the antenna separation on the general outcome of the experiment was thought insignificant.

At the receive site the antenna used was a 1.2 m offset reflector which can receive both the beacons, the pilot carrier at 20.3 GHz, and sky noise at 20 and 27 GHz. Beacon signals were received with a receiver detection bandwidth of 65 Hz; the pilot carrier detection bandwidth was 400 Hz. Clear-sky signal to noise ratio for the beacon channel was 33 dB; that for the pilot signal was 35 dB. The 20 GHz beacon level was used to remove any propagation induced variations occurring on the down-link leg of the pilot carrier thus enabling to estimate the received pilot levelat the satellite. In addition to the beacon signals and skynoise levels, several meteorological parameters are recorded in this data logger; these are rain intensity, humidity, and wind speed.

4. Results

Use of a narrow-band carrier signal allowed the power controller to be operated with a maximum fade compensation range of 25 dB. In operational systems the usable power control range would normally be much smaller. In view of this, results and analysis presented in this section pertain to a fade control range of 15 dB. During the entire experiment period the power controller was operated with the same configuration.

The collected data from the two sites were analyzed to evaluate the performance of the power controller unit. This required the extraction of fade depths from recorded signal levels. One of the difficulties encountered during this process was the lack of absolute levels to obtain precise fade levels. Session to session variations in received power levels could not be accurately defined. In addition, level variations caused by the slow drift of the spot beam pointed towards the Clarksburg site could not be removed completely. The overall uncertainity due to these error sources is of the order of 0.5 dB.

Clear-sky conditions were investigated to examine the degree to which the controller was able track out equipment effects as well as slowly varying propagation

effects. Fading conditions were investigated through analysis of individual rain events as well as statistical analysis of the control error. In addition, an off-line analysis of the power control algorithm was conducted using beacon signal data collected with the Clarksburg propagation measurement terminal.

Under clear-sky conditions the power controller is expected to remove slow variations in the beacon level caused by thermal effects and minor propagation contributions that includes gaseous absorption and light cloud situations. Figure 6 shows a 12 hour period during which only low-level propagation activity was present at the transmit site in Cleveland (maximum up-link fade around 2 dB). The two beacon levels and the up-link fade estimated by the power controller (EIRP with respect to nominal) are shown. It is seen that the power controller was adjusting the baseline in response to slow variations in the 20 GHz beacon level. This was due to the fact that the original software used in the controller did not use adequate sampling to estimate the C/N and proper thresholds in the detection of slow fades, especially under conditions of signal scintillations. An additional flaw in the software was that the baseline level was allowed to drift below the average beacon level, thus producing small amounts of undercompensataion. However, these shortcomings were found to be rather benign, and in most cases the errors were contained within about ±1 dB. The periodic pulses on the 20 GHz beacon channel are produced by ranging tones and the power controller reacts to them assuming the pulses are caused by propagation activity. The pulse amplitude is around 0.4 dB, and this was considered insignificant to be corrected by the control software. The negative going narrow pulses of approximately 4 dB appearing on the EIRP channel are the synchronization pulses inserted every hour to enable synchronization of data files generated at the two sites.

The power control error can be depicted in one of two forms: received pilot level at Clarksburg or the difference between the 27 GHz beacon fade and the predicted up-link fade at Cleveland. The pilot level at Clarksburg indicates how well the power controller managed to maintain the power at the satellite close to the nominal level; the down-link propagation effects on the pilot must be removed using the 20 GHz beacon. Since the transmit and receive antennas at Cleveland were not identical, the pilot level does not give a true measure of the power control error. The main objective of the pilot measurement was to evaluate the power controller behavior under operational conditions. On the other hand, the difference between the predicted and the measured fade at the transmit site can be considered a better indicator of the power control error. However, the frequency for which the up-link fade is predicted is 2.1 GHz away from the beacon frequency of 27.5 GHz, and the differential attenuation between the two frequencies can affect the control error estimate. The differential attenuation can be as much as 2 dB at fade levels closer to 15 dB.

Figure 7a shows a rain event recorded at Cleveland; fade levels at 20 and 27 GHz together with the up-link fade predicted by the power controller are shown. The up- and down-link fades were estimated by taking the clear-sky levels before and after the event, and therefore, do not include contributions from gaseous absorption. The event lasted about 30 minutes and the up-link fade exceeded the 25 dB level for more than two minutes. The transmit EIRP plot clearly shows that the power controller was tracking out the gaseous absorption component. Figure 7b depicts the power control

error in terms of the pilot level received at Clarksburg as well as the difference between the 27.5 GHz fade and the predicted up-link fade at Cleveland. The control error is blanked out for periods during which the controller was predicting fades in excess of 15 dB. The under compensated area starting around the 45 min. mark was the result of the controller reacting to a modulation pulse. The effect is compounded by the fact that the control error was derived after subtracting the 20 GHz beacon level.

The two error curves shown in Fig. 6-5b do not track each other very well due to somewhat differing propagation conditions in front of the transmit (LET) and receive (NGS) antennas at Cleveland. As an example, the period in between the two attenuation peaks show opposite behavior; fading on the LET antenna appears to be smaller than that on the NGS antenna. However, the overall appearance of the two error plots, both in terms the maximum value and the average value, are quite similar. This suggests that, from a statistical point of view, the separation between the antennas did not have any significant impact on the error estimate. Although the antenna separation of approximately 15' is sufficient to have complete decorrelation of scintillation, to a large extent, rain fading can be considered correlated.

A second rain event recorded at Cleveland is shown in Figure 8. The event consisting of three distinct peaks lasted approximately one hour. The first peak caused the 20 GHz beacon to lose lock, and as a consequence, the power controller was unable to recover from the fade correctly. It is also seen that the onset of the third peak at the two antennas occurred at different times.

Rapid rise and fall of deep fades makes it difficult to follow them accurately, and this is clearly evident in control error plots. During both events the power controller was able to maintain the control error within about ±2.5 dB, except during the recovery of the 20 GHz beacon from loss of lock.

Performance of a power control system may be evaluated at least on two criteria: overall improvement to link availability, and control error at the satellite. The overall improvement to the link availability requires continuous measurements spanning a minimum period of one year to account for seasonal differences in precipitation and scinitillation activity. This information may be obtainable through an analysis of the long-term beacon data collected with the Clarksburg propagation terminal. Evaluation based on the control error should also be carried out using long-term measurements or post processing of long-term propagation data. However, the control error can be considered less sensitive to seasonal variations, and therefore the error statistics obtained from to the limited set of measurements can still be considered representative.

Error statistics generated for the duration of the experiment are shown in Figure 9; the control error for several exceedance probabilities ranging from 1% to 99% are plotted against the up-link fade. Statistics shown pertains to all rain events observed at the Cleveland site and the control error was derived from the fade on the up-link beacon and the pilot carrier output of the power controller. To account for the frequency difference between the pilot carrier and the up-link beacon, a correction of 1 dB was applied to carrier levels in excess of 10 dB. It is seen that the control error increases with the up-link fade. This is partly due to the increase of differential

attenuation between the pilot and the up-link beacon, which was only partially compensated by the above mentioned correction. By applying full compensation for the frequency difference (i.e. correction of approximately 2 dB at 15 dB of up-link fade), the control error may be limited to ±2.5 dB instead of ±3.5 dB shown in the figure. With the increase of the up-link fade the spread of the error tend to increases as well. The lower bound of the control error is largely determined by the uncertainty in baseline estimation. Since the control algorithm used during the measurements was not optimized, the spread appears to be overly large. Errors in the signal enhancement region (negative fades) are dominated by those arising from modulation pulses. The power output from the controller was below the nominal level for the entire duration of the pulse thus producing a negative control error.

5. Conclusions

In this work a detailed study of issues pertaining to the design and operation of open-loop up-link power control for Ka-band applications was undertaken[5]. The ACTS satellite and the NASA ground station facilities in Cleveland, OH, were instrumental in the successful conduct of the investigation. Rain impairment amelioration techniques which can be implemented at modest cost are expected to play a pivotal role in commercial exploitation of the 20/30 GHz frequency band. The investigation proved that power control, even when implemented as an open-loop system, is quite effective in combating rain fading. Open-loop power control can be made more robust by using a beacon signal closer to the up-link frequency band; regulatory provision for such beacons in future Ka-band satellite systems has been mandated. However, the power controller was designed around a beacon signal in the down-link band as a way of keeping the system cost to a minimum.

Spurred by the same cost consideration, a design based on IF control was selected. The alternative of using RF control entails the use of expensive RF components as well as operational complexities. One of the advantages of RF control is that it allows for multi-carrier operation in large earth stations. However, the present design can be easily adapted for multi-carrier operation by incorporating additional IF stages driven by a single master controller. This will add only a small incremental cost to the power control system.

In the evaluation of the design, the same control algorithm was used from the beginning to the end of the experiment period. Data analysis at the end of the period reveled several shortcomings of the algorithm. However, these did not have a major impact on the power controller performance during the two dozen or so rain events observed at the transmit site. Although the experimental setup used for the investigation was less than ideal, the data collected allowed the assessment of the performance bounds of the controller.

The rain events encountered during the experiment period were mainly of summer thunderstorm type with durations averaging between 0.5 to 1 hour. On-line evaluation of the controller under lingering rain, which can last several hours, could not be accomplished. However, off-line analyses have indicated that the event duration did not affect the controller performance significantly.

The investigation was limited to a power control range of 18 dB (15 dB of fading and 3 dB of enhancement). This level of control was thought to represent an upper bound on the power control ability of most commercial systems. In general, the power control system was capable of regulating the EIRP within ±2.5 dB over the selected range. It was determined that the clear-sky power control uncertainty can be further reduced through careful selection of the control parameters. At the high end of the fade range the control error is due to the combined effects of the controllers inability to follow deep fades and the hysterisis in fade scaling ratio normally observed with deep fade events. Reduction of the error at this error may be attempted through refinements to the control algorithm. One such refinement could be an implementation based on estimating the short-term fade rates and adapting the fade prediction accordingly. Use of a frequency scaling ratio sensitive to the fade depth would also help reduce the control error.

The range of power compensation applied is essentially a function of the desired link availability and the associated earth station equipment cost. Up to the selected upper bound, performance of the controller is not very sensitive to the control range. As a result the decision as to what level of compensation should be applied can be made solely on the basis of the service type and other aspects of the satellite network.

6. References

1. ITU - Radiocommunication Sector Recommendation 618, 1992

2. Allnutt, J. E., 'Satellite-to-ground Radiowave Propagation'
   Peter Peregrinus, London, 1989

3. Macina N. A; Maximum Entropy Modeling for Identification and Detection of Certain Classes of Dynamic Events
   RCA Review, Vol. 42, March 1981, pp. 85-110

4. ACTS Up-Link Power Control Experiment: Final Report
   NASA Contract NAS 326402, COMSAT Laboratories, 1995

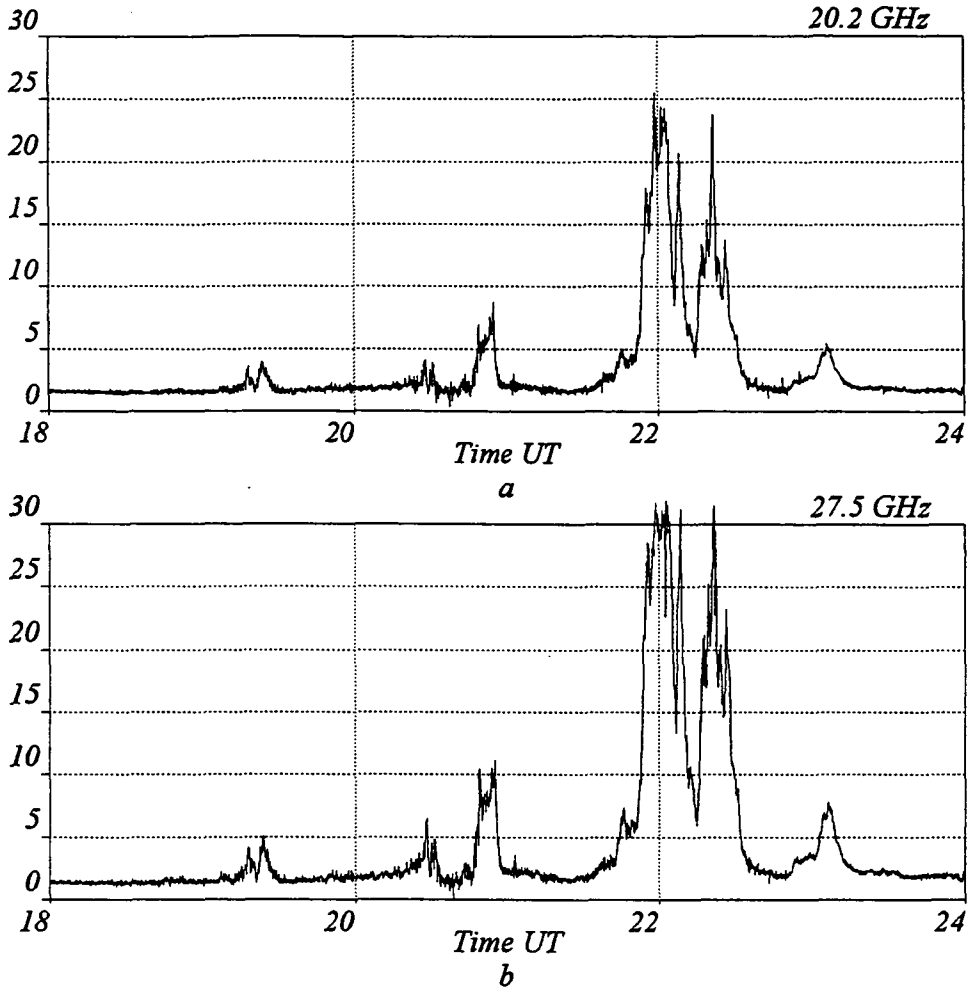

Figure 1a,b Attenuation at 20 and 27 GHz; Rain Event on 14 August, 1994

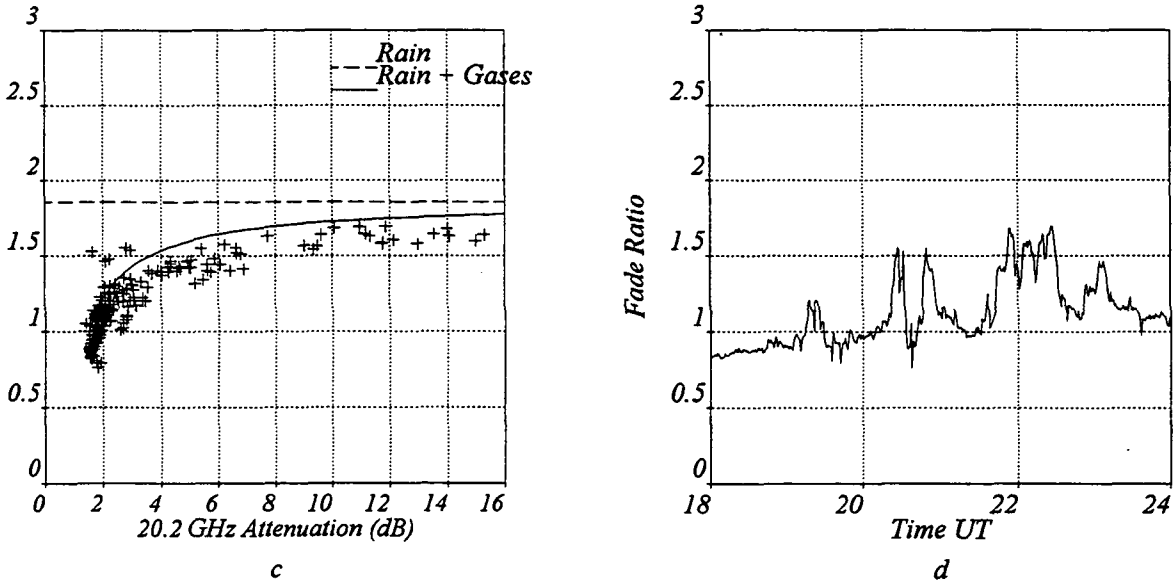

Figure 1c,d Ratio between 27 and 20 GHz Fades; Rain Event on 14 August, 1994

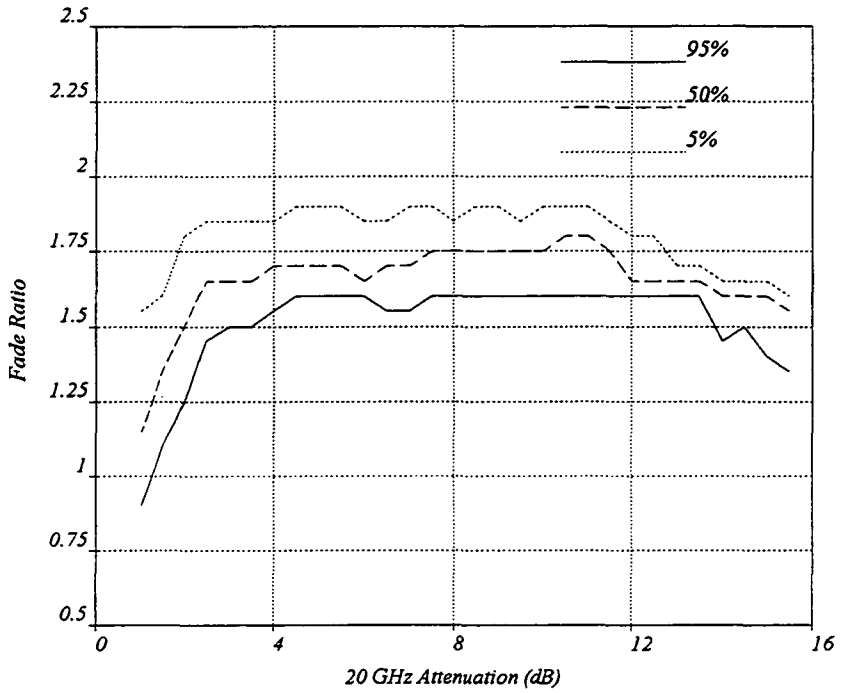

Figure 2a Distribution of Instantaneous Fade Ratio Between 27 and 20 GHz

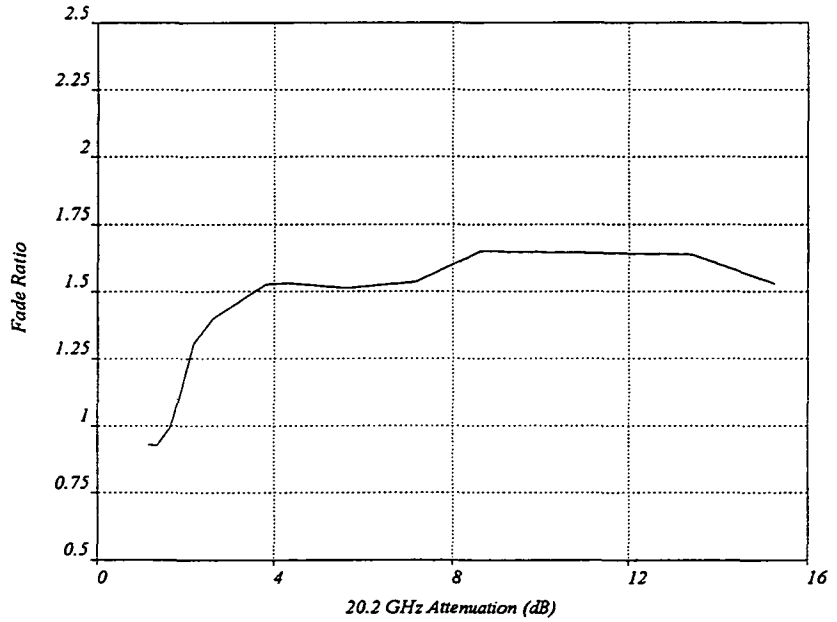

Figure 2b Equiprobable Fade Ratio Between 27 and 20 GHz

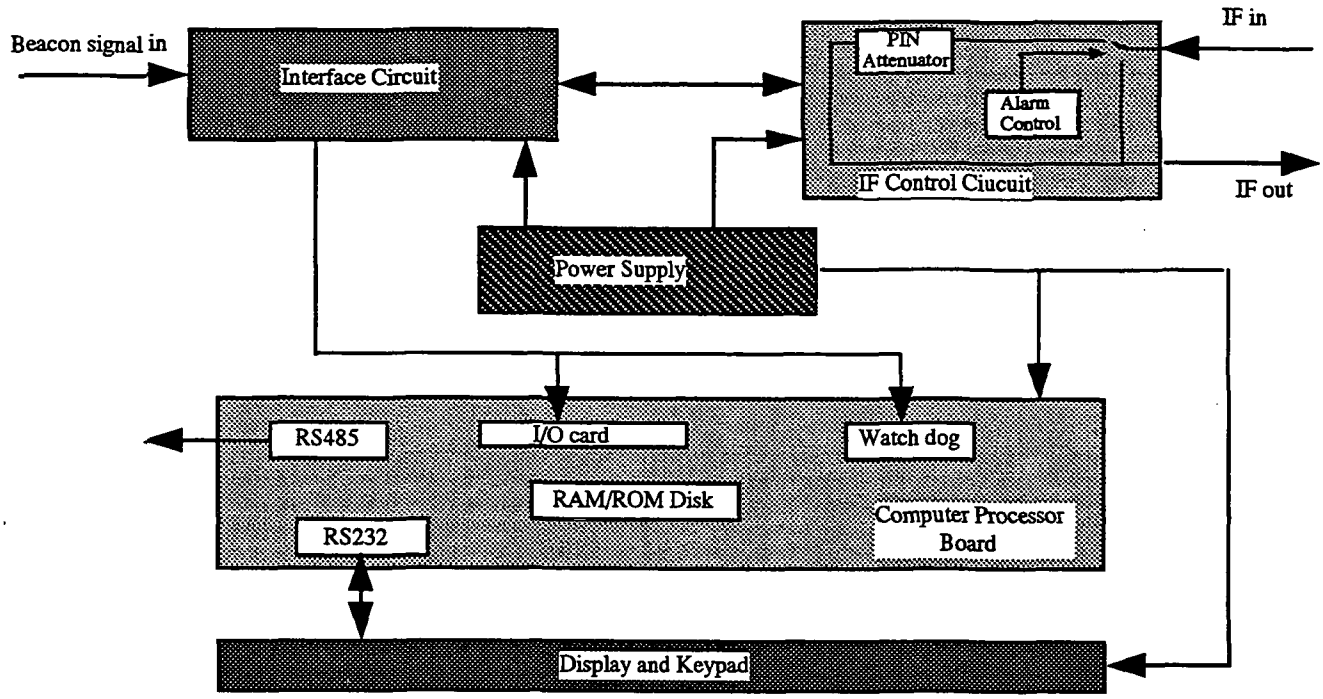

Figure 3 Functional Block Diagram of the Up-link Power Controller

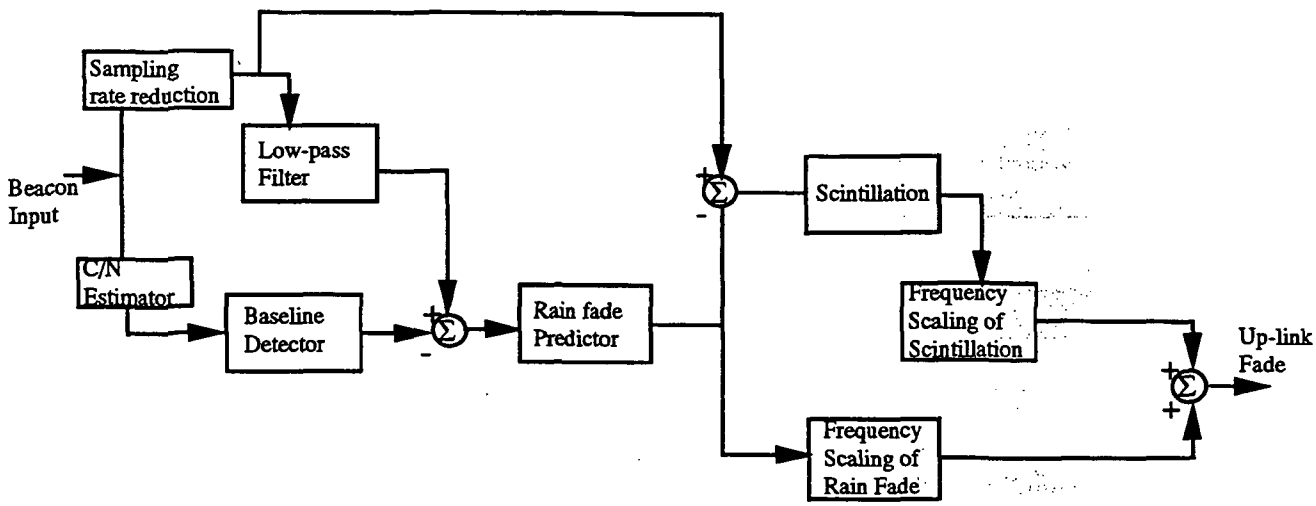

Figure 4 Up-link Fade Estimation Algorithm

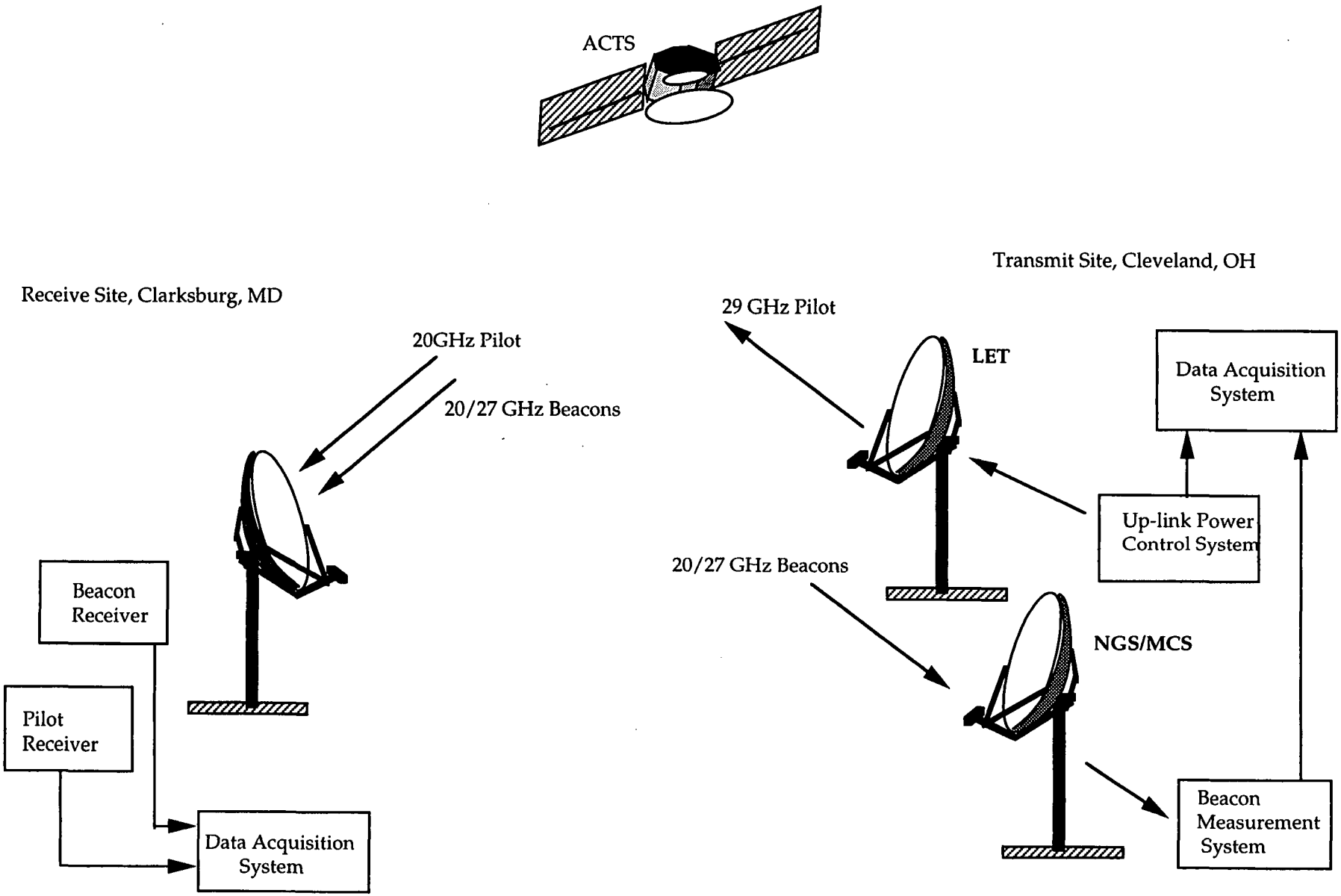

Figure 5 ACTS Up-link Power Control Experiment Configuration

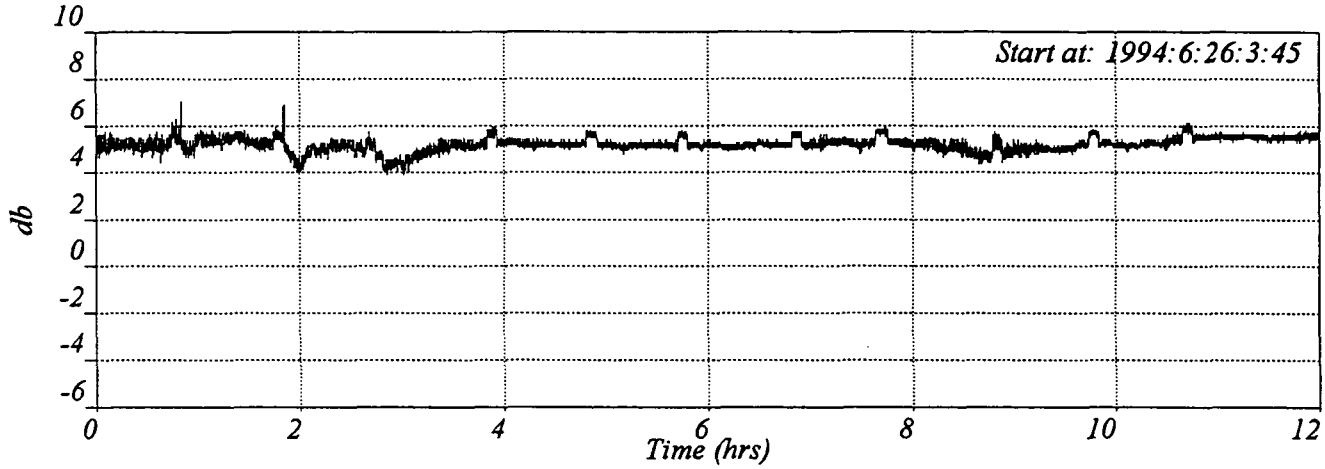

20.2 GHz Beacon Level

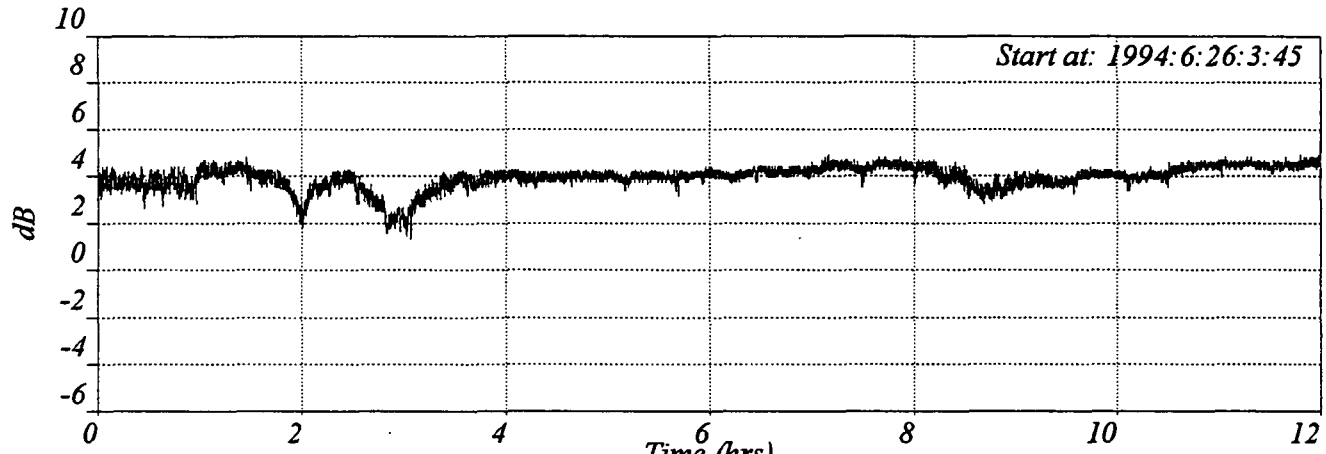

27.5 GHz Beacon Level

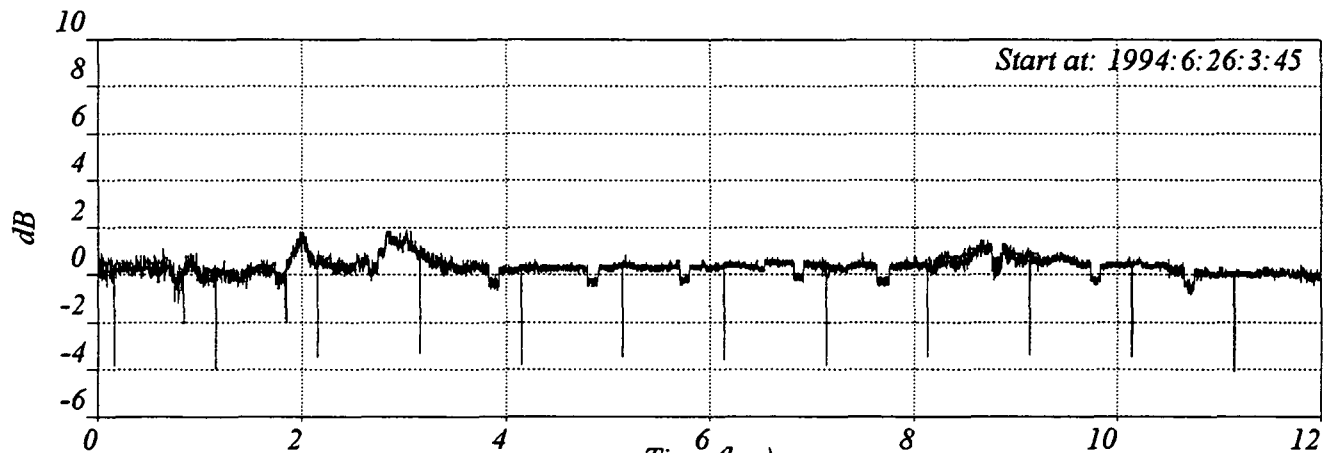

Transmit EIRP Relative to Nominal

Figure 6 Clear-sky Performance of Power Controller

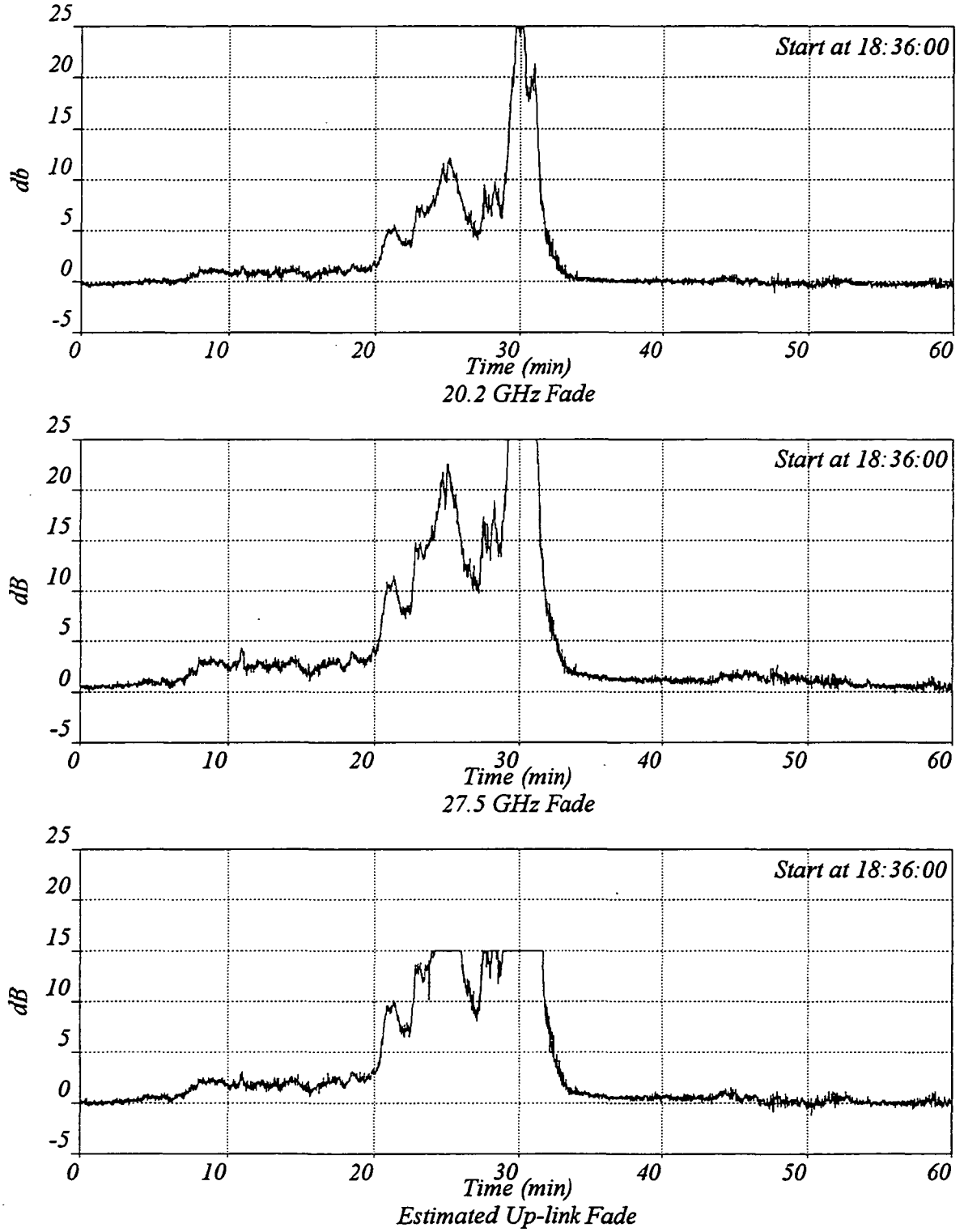

Figure 7a Rain Event 1 on 31 May, 1994

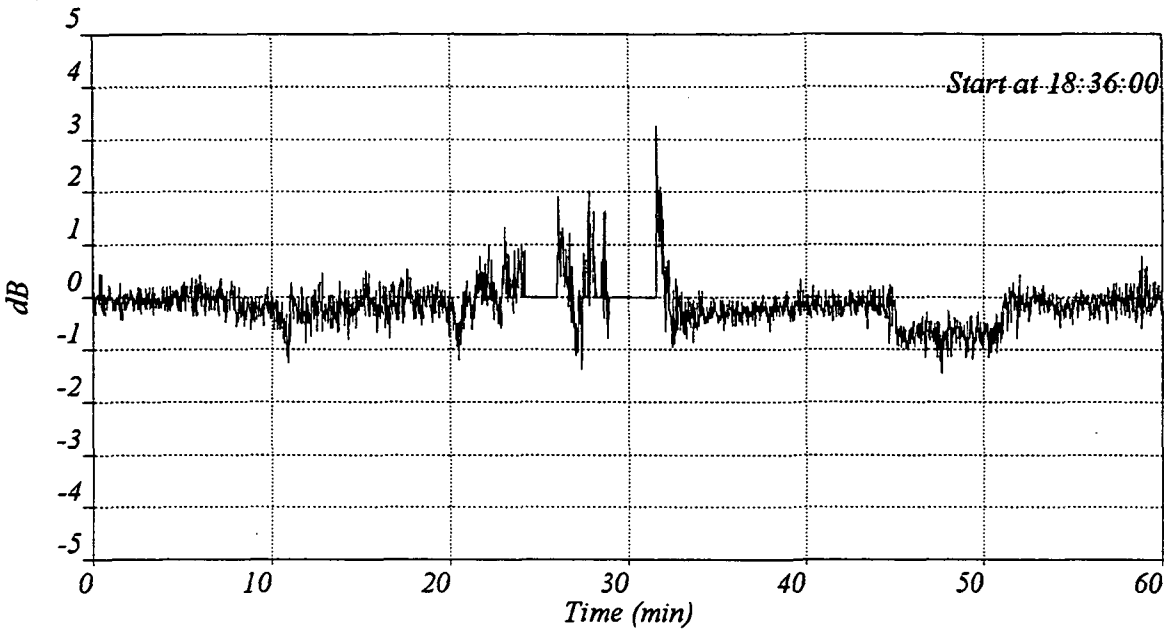

Control Error at Cleveland

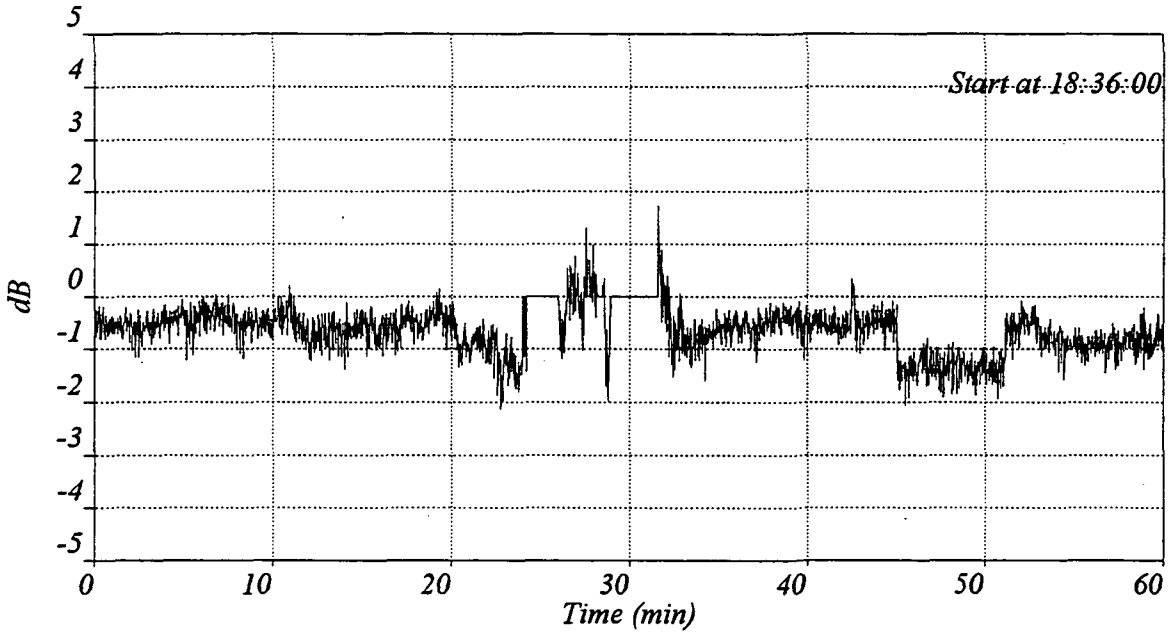

Pilot Level at Clarksburg

Figure 7b Control Error; Rain Event 1; May 31, 1994

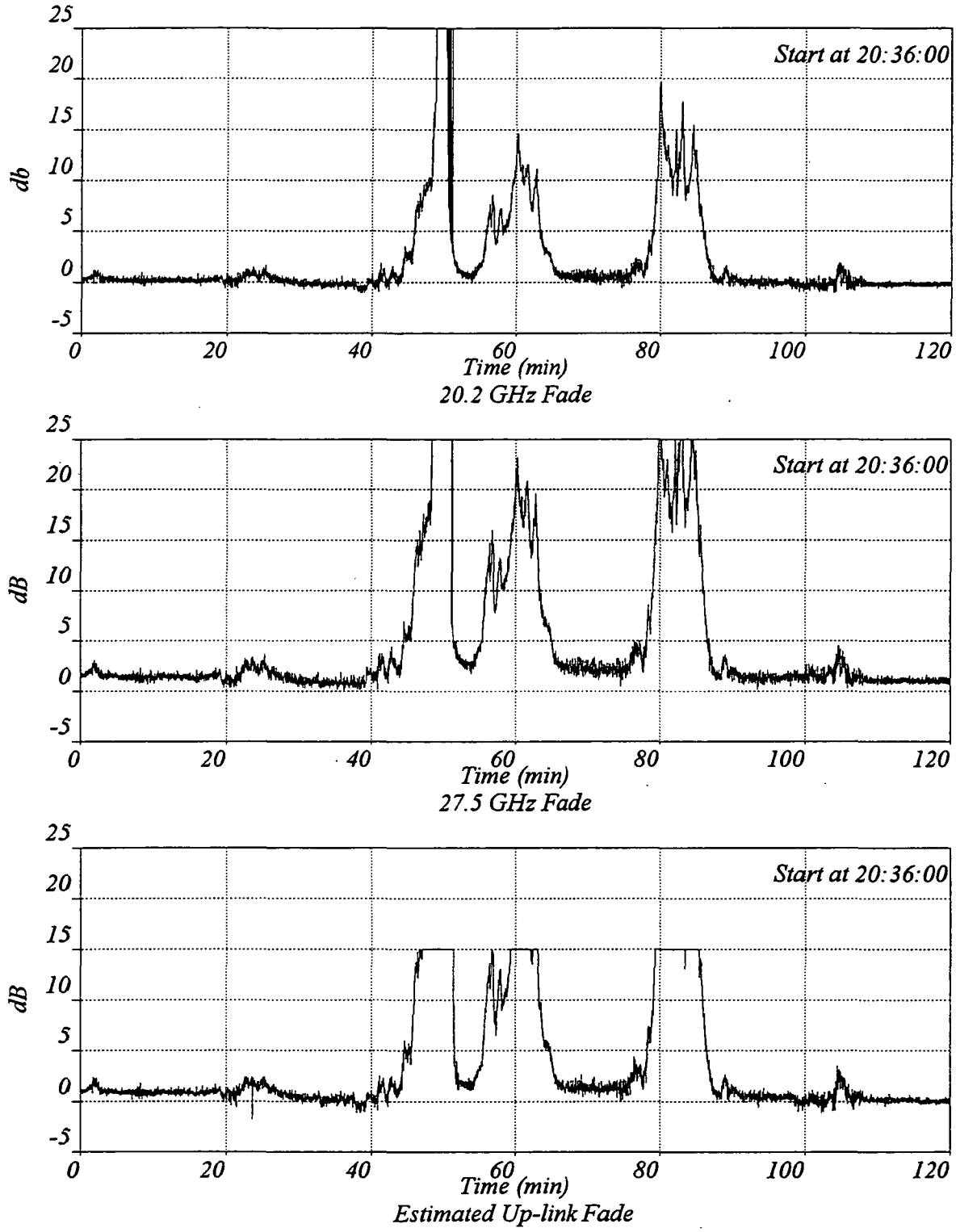

Figure 8a Rain Event 2 on 31 May, 1994

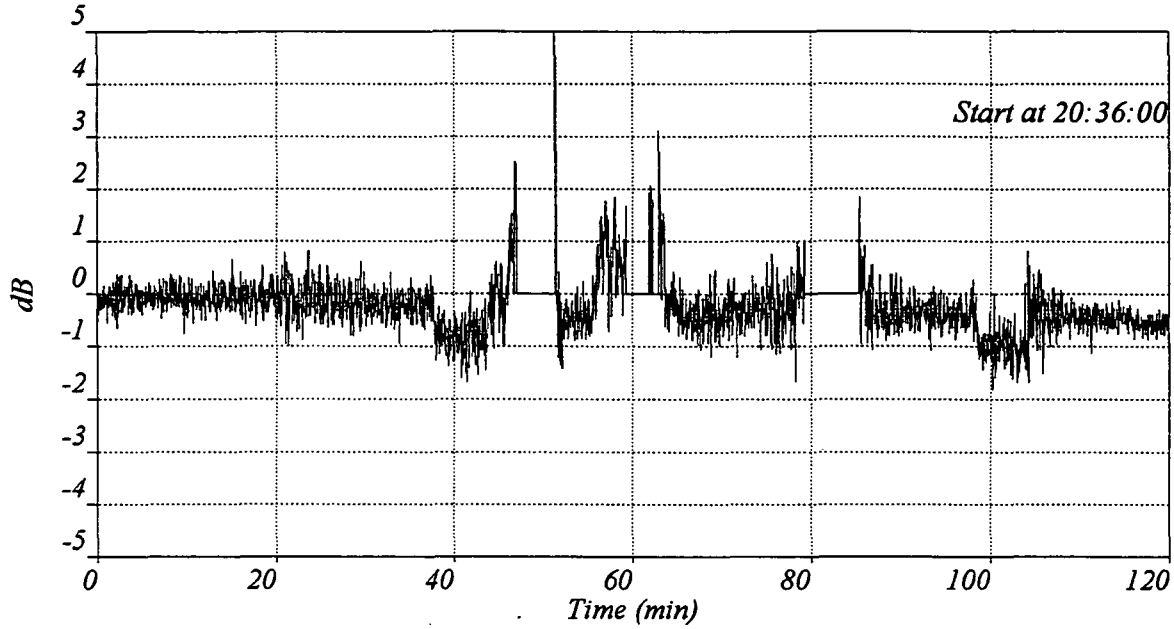

Control Error at Cleveland

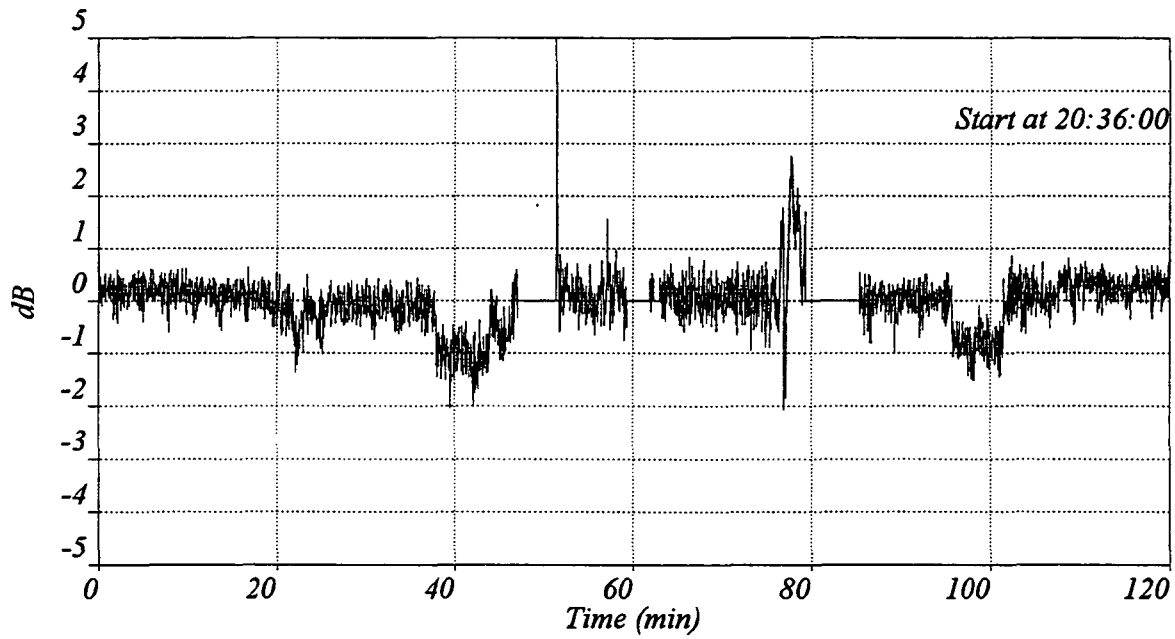

Pilot Level at Clarksburg

Figure 8b Control Error; Rain Event 2; May 31, 1994

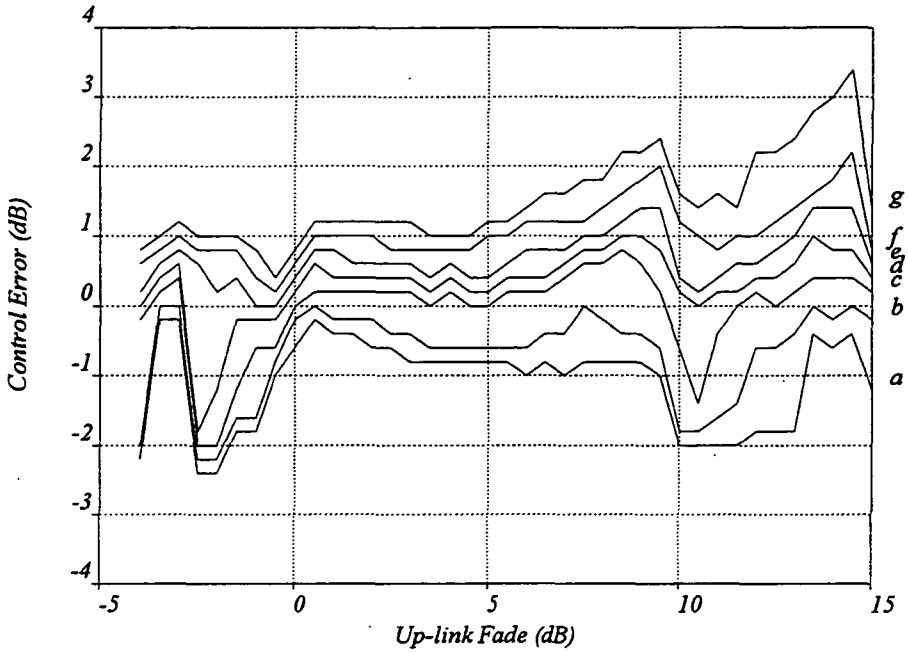

Figure 9 Distribution of Power Control Error;

a: 99%, b: 95%, c: 75%, d: 50%, e: 25%, f: 5%, g: 1%

N96-10447

Modeling Ka-band Low Elevation Angle Propagation Statistics

Thomas A. Russell, John Weinfield, Chris Pearson, and Louis J. Ippolito
Stanford Telecom
1761 Business Center Drive
Reston, VA 22090

Abstract

The statistical variability of the secondary atmospheric propagation effects on satellite communications cannot be ignored at frequencies of 20 GHz or higher, particularly if the propagation margin allocation is such that link availability falls below 99%. The secondary effects considered in this paper are gaseous absorption, cloud absorption, and tropospheric scintillation; rain attenuation is the primary effect. Techniques and example results are presented for estimation of the overall combined impact of the atmosphere on satellite communications reliability. Statistical methods are employed throughout and the most widely accepted models for the individual effects are used wherever possible. The degree of correlation between the effects is addressed and some bounds on the expected variability in the combined effects statistics are derived from the expected variability in correlation. Example estimates are presented of combined effects statistics in the Washington D.C. area at 20 GHz and 5° elevation angle. The statistics of water vapor are shown to be sufficient for estimation of the statistics of gaseous absorption at 20 GHz. A computer model based on monthly surface weather is described and tested. Significant improvement in prediction of absorption extremes is demonstrated with the use of path weather data instead of surface data.

I. Introduction

Traditionally, the allocation of power margin for propagation effects in a satellite communications link budget requires a statistical distribution of rain attenuation based on climatic region together with a fixed estimate of gaseous absorption derived from the mean temperature and humidity at the ground. The absorption level is subtracted from the link budget, and the statistics of link reliability are mapped directly from the statistics of rain attenuation. In the Ka band (30 GHz uplink / 20 GHz downlink) and above, however, fluctuations over the course of the year in gaseous absorption, cloud absorption, and tropospheric scintillation produce strong fades that often may occur simultaneously. Since rain attenuation is also higher at Ka band, the impact of these secondary effects (where rain attenuation remains the primary effect) depends on the level of total available propagation margin and the corresponding expected link availability.

The high levels of link availability (99.5% or higher) achievable at lower frequencies are very expensive to maintain at Ka band in light of the strong rain attenuation. Hence, lower availability levels (99% and less) are often accepted, corresponding to low rain rates (often 3 mm/hr and less), where the secondary effects become more pronounced relative to the rain attenuation. Such systems are referred to as low fade margin or low availability systems. For these systems, the statistical variability of the secondary effects should be combined with the statistics of rain attenuation in a way that incorporates the expected

correlations, in order to produce legitimate and useful estimates of the expected link availability. Similar assertions are made in [1-3]. In addition, significant work has been produced by the Helsinki University of Technology on many aspects of this topic [4-7].

Figure 1 presents an example of the relative fades produced by the three relatively slow-fading effects, fades which could at times produce a total attenuation equal to the sum of the individual fade levels. Scintillation is relatively quick-fading, and should be considered separately (see Section IV). The scenario used for all calculations in this paper is 20 GHz, 5° elevation angle, and the Washington D.C. area climate. The 5° elevation angle was selected as it produces especially strong contributions from all effects, and is probably the lower limit for useful communications (5° is being considered for extending coverage of fixed and mobile satellite systems). In Figure 1, the absorption by gas and clouds is calculated using a humid summertime scenario with moderate-heavy clouds. The surface water vapor density of 20 g/m^3 is used together with a Slobin height profile [8] that results in an integrated water vapor density of 4 cm, a value that is exceeded in Washington D.C about 10% of the time [5]. The cloud extends from 1 km above ground to 2 km above ground, with a uniform liquid water concentration of 1.0 g/m^3, giving a total liquid water content of 1.0 kg/m^2 . In statistics published by Salonen et al. [5], this level is exceeded approximately 5% of the time near Washington D.C.; it also corresponds to the total liquid water in Slobin's Case 8 cloud model [9], the lightest of the three 'Heavy Clouds'. The rain attenuation plotted is exceeded 2% of the year (98% availability) according to the Crane model [10] for climate region D2 (point rain rate = 1.5 mm/hr).

Figure 2 shows a comparison of the combined gaseous and cloud absorption for the scenario described above with radiometer measurements in Blacksburg, [11] and Wallops Island, [12] Virginia, both at 20.6 GHz, and with calculations at LaGuardia Airport, NY [9] at 18 GHz based on radiosonde measurements. This is an imprecise statistical comparison because, among other reasons, the Virginia measurements were for 1-2 month periods; nevertheless, the rough agreement observed is encouraging.

The modeling approach described here considers each effect individually, using accepted models where available. Each effect has a different mechanism of signal loss: rain produces Mie scattering of the wave, cloud water droplets produce absorption, water vapor and oxygen molecules undergo transitions that absorb energy, and turbulence refracts and diffracts the wave to produce scintillation. The different mechanisms require individual models to ensure that dependence on frequency, elevation angle, and weather parameters is correct for each effect.

The combination of these individual statistics requires the full joint distribution, for which sufficient information is not available. However, by describing the expected statistics of each effect by season or month instead of by year, we capture some of the nature of the correlation between effects. For example, weather-dependent models for gaseous absorption and tropospheric scintillation will both exhibit stronger effects in summer and weaker effects in winter.

The short-term correlations must also be considered. A cumulative distribution function (cdf) is developed for each effect, and the individual statistics are combined according to assumptions of either perfect statistical correlation ($\rho = 1.0$) or no statistical correlation (statistical independence, $\rho = 0.0$). Two random variables (RV's) which are perfectly correlated will experience extreme maxima simultaneously, and the same will be true of extreme minima. Accordingly, the cdf of the RV representing the combined process can be calculated simply by adding equiprobable values of the two constituent cdf's. For example, if the levels of gaseous absorption and cloud absorption not exceeded 90% of the summer are 6.8 dB and 1.2 dB, respectively, then under the assumption of perfect correlation, the level of combined absorption not exceeded 90% of the summer is 6.8 dB + 1.2 dB, or 8.0 dB.

The sum of two independent RV's is obtained by convolving the two probability density functions (pdf's) to obtain the pdf of the combined process, or by convolving one cdf with one pdf to obtain the cdf of the combined process.

We will describe two modeling approaches in this paper: summer statistics, for which example results of combined effects models will be presented; and month-by-month statistics. The latter approach can also be used to produce seasonal and annual statistics; we point out in the following sections some of the components of such an approach. The following sections consider each effect individually in terms of a monthly model, a summertime model, and preliminary approaches for combining with other effects. PMOD (Propagation MODel), the software propagation analysis tool developed by Stanford Telecom, will incorporate the models discussed in this paper

II. Gaseous Absorption

Water vapor and oxygen are the two gasses that contribute significant attenuation in the microwave region [13]. In the Ka band, oxygen absorption is typically an order of magnitude (in dB) smaller than water vapor absorption, and the fluctuations in water vapor absorption dominate the gaseous absorption statistics in this band. In addition, the variation in water vapor absorption depends principally on the total water vapor in the path. These last two points are demonstrated in Figure 3.

Figure 3 depicts the predictors of gaseous (both water vapor and oxygen) absorption. The sample points were calculated by integrating the Liebe model for specific absorption [13] over radiosonde profiles of temperature, pressure, and humidity taken during the summer of 1994 (June through mid-September) in the Washington D.C. area. Temperature (Figure 3a) is a poor predictor; surface humidity (Figure 3b) is fairly good but flawed, as will be discussed below; but integrated water vapor (Figure 3c) is an excellent predictor. The correlation between integrated water vapor and *water vapor* absorption alone has been shown by Salonen et al. [4] to be even better. (The non-zero y-intercept in Figure 3c represents the oxygen absorption.) Thus, we may reduce the height profiles of three parameters to the integrated value of a single parameter, water vapor, and incur very little error in the calculation of absorption. Moreover, note also the linearity of the relation between integrated water vapor and gaseous absorption. This allows the statistics of

integrated water vapor to be mapped directly to statistics of gaseous absorption, which greatly simplifies computer calculations of absorption statistics.

This characteristic has led to a preliminary computer model (included in PMOD) which implements long-term surface weather data. The program stores, for each month, the mean surface temperature and a tabulated cdf of the surface humidity. The user may specify the desired non-exceedance probability (analogous to availability) and the program takes the corresponding level of surface water vapor, the mean surface temperature, and the standard surface pressure, and integrates the Liebe specific absorption model over the resultant height profiles. This approach was tested by comparing with the accumulated statistics resulting from integrations of the Liebe model over the Slobin profiles at each hourly measured set of surface temperature/pressure/humidity over 10 years, and the cdf's were in very good agreement (see Figure 4).

The model, however, is not complete, because surface water vapor does not adequately characterize the water vapor over the radio path (for systems with high elevation angles, however, the error may be small). See Figure 5, which presents a cdf of gaseous absorption based on integrated water vapor, and a second cdf based on surface water vapor density and the Slobin average height profiles. This figure derives from the same data shown in Figure 1. The average profiles produce accurate estimates of the mean absorption, but miss many of the higher values of absorption, which are most important to link design. The data represented by the solid line will be used as the summertime absorption statistics in combined effects modeling in the following sections.

In future work, we will derive from radiosonde data the long-term statistics of integrated water vapor by month, which will provide for an improved mapping to monthly absorption statistics. An alternative source of this information is available in Salonen et al. [5], based on analysis of global ECMWF (European Center for Medium Range Weather Forecasts) data.

III. Cloud Absorption

Absorption by clouds is the most difficult to model statistically at the current time. The relevant cloud parameter is the total liquid water content, which is required in the form of a cdf, preferably by month or season. The importance of cloud absorption is enhanced because it occurs in conjunction with all other effects considered here. Rain occurs in the presence of clouds. Tropospheric scintillation is produced by turbulence, which is often associated with clouds (observations of the connection between scintillation and clouds were reported by Cox et al. [14], among others). Finally, gaseous absorption increases with humidity, which is also associated with increased water content in the cloud (higher absolute humidity makes more water vapor available for condensation into cloud liquid water).

Salonen et al. [15] have developed a model for cloud liquid water content that uses measured vertical weather profiles to estimate the existence, extent, and density of clouds. They have also published extensive statistics for Europe and the globe on cloud liquid

water [5]. These statistics are based on one full year of data and are not broken into season or month. In our estimates of summer statistics we have applied a scaled (in frequency and elevation angle) version of the full-year cloud absorption statistics reported for Finland (which under-estimates the summer absorption statistics). The results compare well with Slobin's models of typical cloud types [9]. Figure 6 illustrates the combination of gas and cloud absorption into a total absorption amount using two reasonable extremes: total correlation and total independence (negative correlation is not expected so it is not included). The two estimates of combined absorption differ by up to 2 dB at high percentages. Salonen et al. [7] have compared results based on these two extremes with the true combined statistics in Europe and found better results with the equiprobable assumption in most of northern Europe, and better results with the independent assumption in Mediterranean climates.

In order to create monthly and seasonal statistics, we plan to apply the Salonen cloud detection and liquid water estimation model to local radiosonde data.

IV. Scintillation

Tropospheric scintillation is produced by turbulence in humid air, accordingly, both humidity and turbulence are necessary for strong scintillation. The model developed by Karasawa et al. [16] uses two levels of statistics to describe these dependencies. The first is a short-term (valid over 10-60 min) Gaussian distribution of the fade level, $f_1(x)$, with zero mean and a variable standard deviation (scintillation intensity) described statistically by the second tier. The second tier is a Gamma distribution, $f_2(\sigma)$, applied to month-long periods. A function is given for mapping mean temperature and humidity for the month into the mean of the Gamma distribution of intensity, σ_m. The cdf of the fade level is computed by:

$$P(x < X) = \int_{-\infty}^{X} \int_{0}^{\infty} f_1(z|\sigma) f_2(\sigma) d\sigma dz . \qquad (1)$$

One approach to combining scintillation and absorption is to assume independence over the course of the month, with the average levels for each month related through the mutual dependence on temperature and humidity. In this case, a convolution of fade level statistics gives the combined statistics. However, there is reason to expect greater correlation and higher scintillation intensity during particularly humid afternoons, for example. In fact, the correlation exists over any time period, it merely decreases as the period shortens. This has been observed, and the correlation has been quantified by Vogel et al. [17] over a range of time periods, down to 43% correlation over one hour periods. Therefore, an upper bound to the combined statistics would be an equiprobable relationship between gaseous absorption and scintillation intensity. Note that the appropriate relationship is *not* between absorption and scintillation fade level. During scintillation, the signal level rapidly fluctuates about a much more slowly fluctuating mean, so all values of the short-term scintillation distribution, positive and negative, occur during periods of extreme scintillation

The cdf of the combined effect in this case is obtained by integrating over the Karasawa relation in Eq. (1) with the modification that the mean of f_l is not zero, but rather is equal to the level of absorption equiprobable with the standard deviation (intensity) of the short-term statistics. The equiprobable mapping is thus between the cdf of absorption and the cdf of scintillation intensity, the latter described by the Gamma distribution.

Figure 7 shows the expected summer statistics with rain effects excluded. The equiprobable (worst-case) combination of gas and clouds is presented without scintillation for comparison, and combined with scintillation according to the independent and correlated assumptions. The mean scintillation intensity over the summer is taken as 0.8 dB.

V. Rain

The Crane rain model [10] applied to the D2 climate region is combined with secondary effects in two ways in Figure 8. In the first, the mean gaseous absorption is added to the rain attenuation distribution. This is a typical propagation analysis, but is applied here using the summer mean gaseous absorption rather than the annual. The second method is an independent combination of the rain statistics with the worst-case non-rain statistics. The non-rain curve, also shown in the figure, assumes correlation between gaseous absorption, cloud absorption, and tropospheric scintillation intensity. The gaseous absorption and scintillation data, discussed above, are based on summer weather, while the cloud and rain statistics are annual predictions. For this particular scenario and set of assumptions, the curves representing a basic mean absorption and a full combined statistics approach converge somewhere slightly above 99% availability, where rain attenuation asserts its dominance over the other effects. This estimate of combined effects statistics is rather optimistic, however, because rain attenuation is assumed independent of other effects. By correlating rain with the other effects (cloud absorption, in particular, is correlated), predicted availability will degrade.

A monthly model for rain statistics in the Washington area is possible through the rain rate statistics reported by Goldhirsh and Gebo[18] over 8 years at 10 sites. This will be incorporated in future work.

VI. Conclusions

The seasonal dependence of all of the propagation effects discussed here: gas and cloud absorption, scintillation, and rain attenuation, is very strong for most climates, and generally all effects are enhanced in the summer (for the northern hemisphere). The correlation between effects is variable, but bounds may be produced on the combined effects through bounds on the likely correlation. This work only begins to address the possible correlations. The combined effects estimates presented here, by building up from gaseous absorption to gas and clouds, etc., emphasized the non-rain propagation effects, which have not been considered statistically in the past. However, since rain is often dominant, estimates should also be made starting from the rain statistics and correlating various effects with rain. Useful information for this effort would include weather statistics (humidity and cloud water content) conditioned on the existence and possibly the

intensity of rain. Future work includes developing monthly conditional statistics of integrated water vapor and cloud liquid water, investigating cloud modeling further, and comparing ACTS beacon and radiometer data with models utilizing ACTS weather data.

VII. References

[1] G. Brussaard and D. V. Rogers, "Propagation considerations in satellite communication systems," *Proc. IEEE*, vol. 78, pg. 1275-1281, July 1990.

[2] J. E. Allnut and D. V. Rogers, "Low-fade-margin systems: propagation considerations and implementation approaches," *Proc. Int. Conf. Antennas Propagat.*, IEE Conf. Publ. 301, 1989, pg. 6-9.

[3] J. P. V. Poiares Baptista and G. Brussaard, "Propagation predictions for low-elevation, low-availability satellite systems," *El. Lett.*, vol. 25, no. 20., pg. 1391-1393, Sept. 1989

[4] E. Salonen et al., Study of propagation phenomena for low availabilities, Final Report for ESA under ESTEC contract 8025/88/NL/PR, 316 pg., Nov. 1990.

[5] E. Salonen et al., Study of improved propagation predictions, 1994, Final Report for ESA under ESTEC contract 9455/91/NL/LC(SC), Dec. 1994.

[6] E. Salonen et al., "Modeling and calculation of atmospheric attenuation for low-fade-margin communications," *ESA Journal*, vol. 16, no. 3, pg. 299-317, 1992.

[7] E. Salonen, "Prediction models of atmospheric gases and clouds for slant path attenuation," *Olympus Utilisation Conference*, Sevilla, pg. 615-622, April 1993.

[8] S. D. Slobin, Microwave noise temperature and attenuation of clouds at frequencies below 50 GHz, JPL Publ. 81-46, July, 1981.

[9] S. D. Slobin, "Microwave noise temperature and attenuation of clouds: Statistics of these effects at various sites in the United States, Alaska, Hawaii," *Rad. Sci.*, vol. 17, no. 6, pg. 1443-1454, Nov.-Dec. 1982.

[10] R. K. Crane, "Prediction of attenuation by rain," *IEEE Trans. Comm.*, vol. COM-28, no. 9, Sept. 1980.

[11] J. B. Snider et al., "Comparison of Olympus beacon and radiometric attenuation measurements at Blacksburg, Virginia," *Proc. NASA Propagat. Exper. Mtg., (NAPEX XV)*, June 1991.

[12] J. B. Snider et al., "Observations of attenuation at 20.6, 31.65, and 90.0 GHz - Preliminary results from Wallops Island, VA," *Proc. NASA Propagat. Exper. Mtg., (NAPEX XIII)*, June 1989.

[13] H. J. Liebe, "An updated model for millimeter-wave propagation in moist air," *Rad. Sci.*, vol. 20, no. 5, pg. 1069-1089, Sept-Oct. 1985.

[14] D. C. Cox, H. W. Arnold, and H. H. Hoffman, "Observations of cloud-produced amplitude scintillation on 19- and 28- GHz earth-space paths," *Rad. Sci.* vol. 16, pg. 885-907, Sept.-Oct. 1981.

[15] E. Salonen and S. Uppala, "New prediction method of cloud attenuation," *El. Lett.*, vol. 27, no. 12, pg. 1106-1108, June 1991.

[16] Y. Karasawa, M. Yamada, and J. E. Allnut, "A new prediction method for tropospheric scintillation on earth-space paths," *IEEE Trans. Antennas Propagat.*, vol. 36, pg. 1608-1614, Nov. 1988.

[17] W. J. Vogel, G. W. Torrence, and J. E. Allnut, "Scintillation fading on a low elevation angle satellite path: Assessing the Austin experiment at 11.2 GHz," *Proc. Int. Conf. Antennas Propagat.*, March 1993.

[18] J. Goldhirsh and N. E. Gebo, "Slant path attenuation statistics at 20 GHz and 30 GHz from an eight year data base of rain rates obtained from the mid-Atlantic coast rain gauge network," *ACTS Propagat. Studies Workshop (APSW VI)*, pg. 271-281, Nov. 1994.

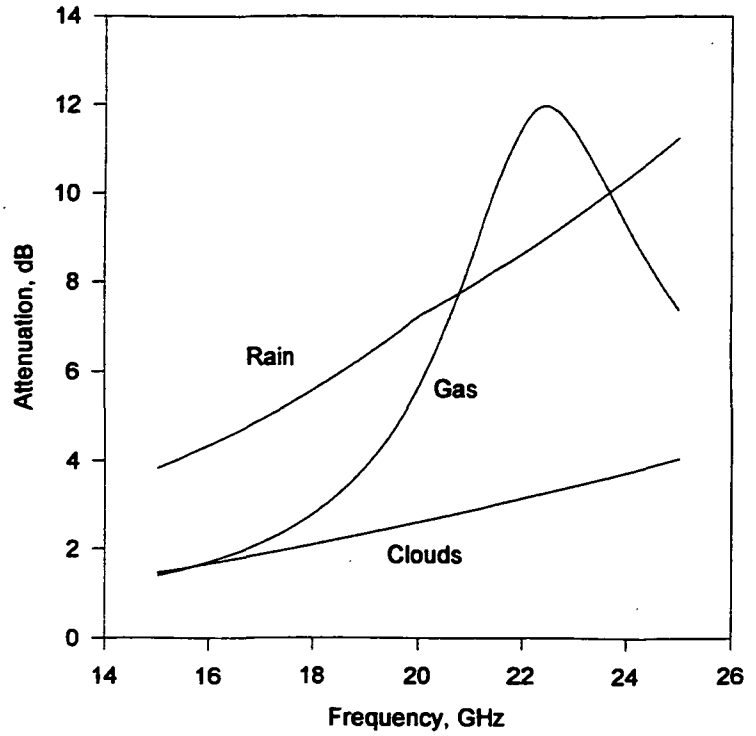

Figure 1. Individual propagation effects

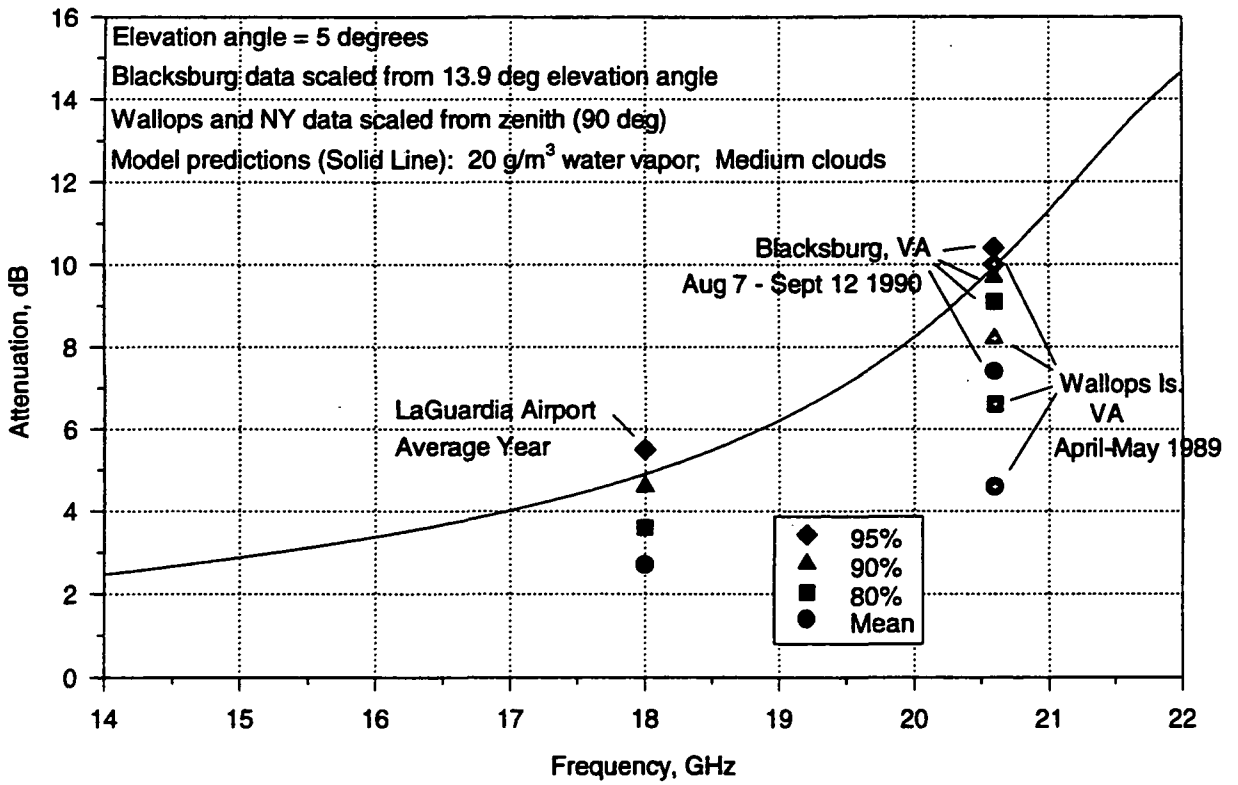

Figure 2. Predictions of absorption by gas and clouds with Liebe model, compared to radiometer measurements in Virginia and weather-based calculations in NY.

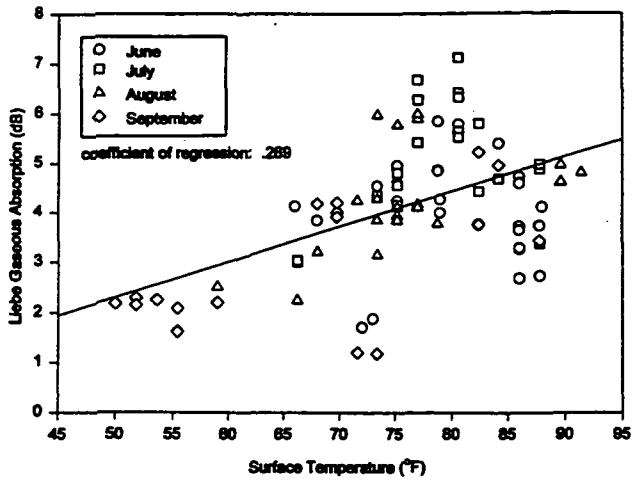

Figure 3a. Radiosonde-based Liebe gaseous absorption vs. surface temperature

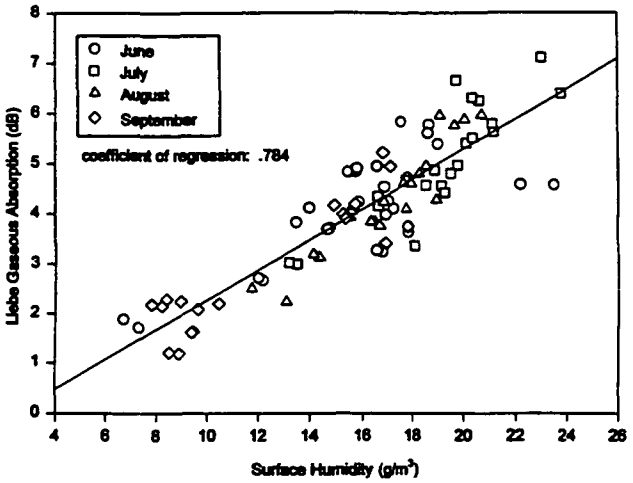

Figure 3b. Radiosonde-based Liebe gaseous absorption vs. surface humidity

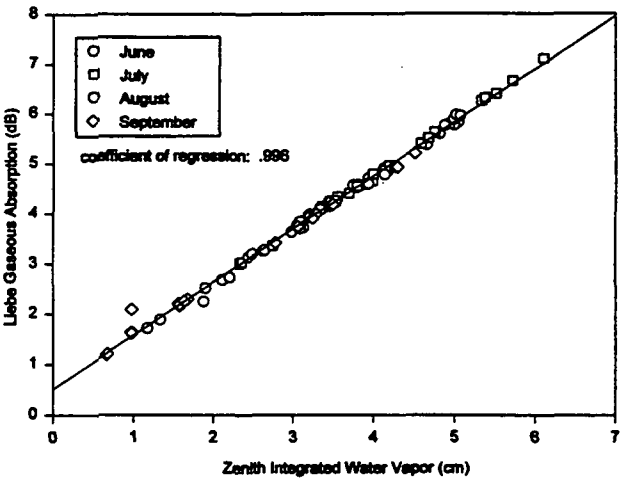

Figure 3c. Radiosonde-based Liebe gaseous absorption vs. integrated water vapor

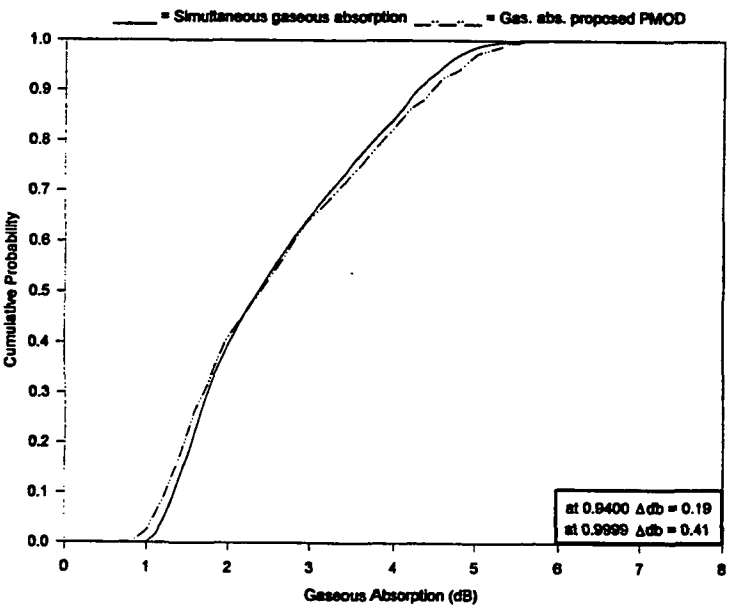

Figure 4. Annual gaseous absorption cdf's based on 1984-1994 surface observations: test of proposed model

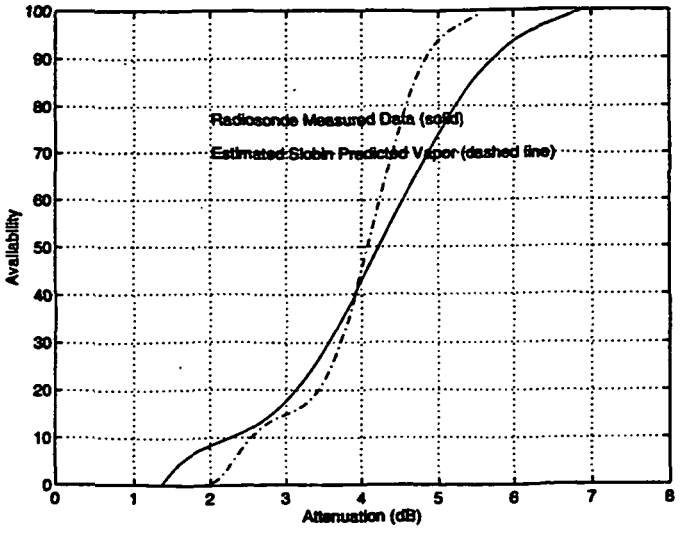

Figure 5. Error in surface-based gaseous absorption model

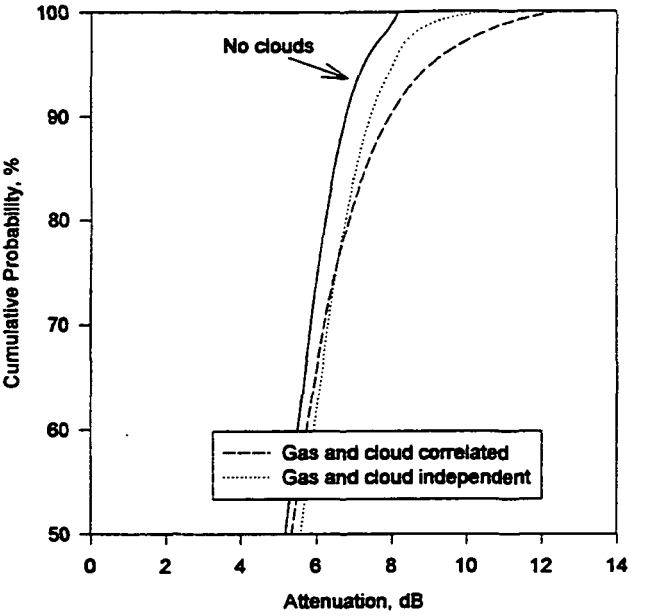

Figure 6. Absorption by gas and clouds; gaseous absorption based on summer radiosonde data, cloud absorption from Salonen and Uppala [15] (annual)

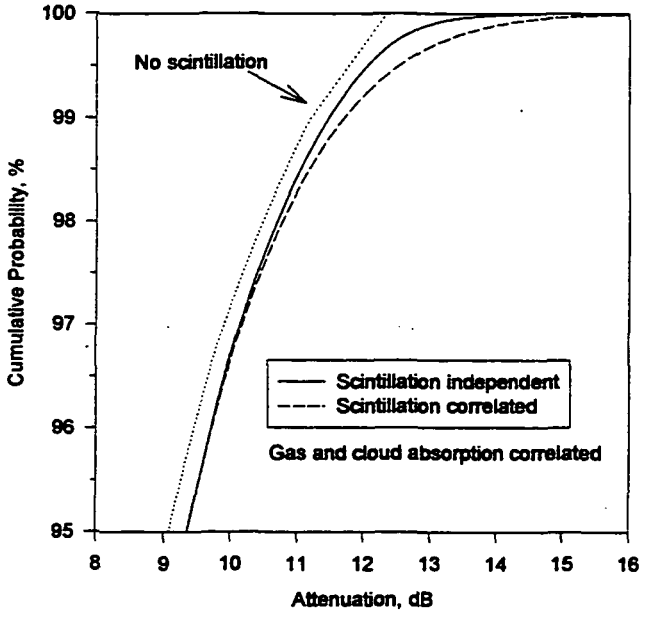

Figure 7. Attenuation by gas, clouds, and scintillation; summer statistics used for gaseous absorption and scintillation, annual for clouds

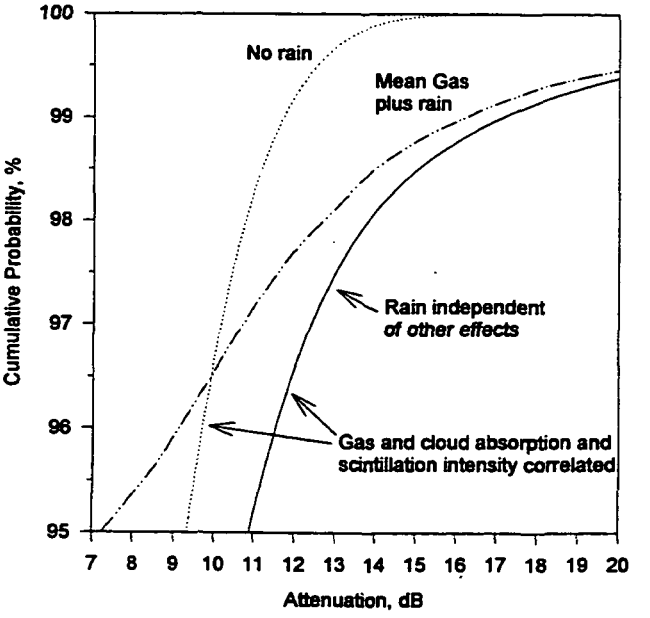

Figure 8. Attenuation by rain, gas, clouds, and scintillation; summer statistics used for gas and scintillation, annual for rain and clouds

N96-10448

SPACEWAY™

Providing Affordable

and

Versatile Communication

Solutions

Presented to the NASA Propagation

Experimenters Meeting

Fort Collins, Colorado

14 June 1995

For further information, please contact
E. J. Fitzpatrick, Vice President,
Hughes Communications, Inc.
Los Angeles, CA 90009
(310) 364-4840

ABSTRACT

By the end of this decade, Hughes' SPACEWAY™ network will provide the first interactive "bandwidth on demand" communication services for a variety of applications. High quality digital voice, interactive video, global access to multimedia databases, and transborder workgroup computing will make SPACEWAY™ an essential component of the computer-based workplace of the 21st century. With relatively few satellites to construct, insure, and launch -- plus extensive use of cost-effective, tightly focused spot beams on the world's most populated areas -- the high capacity SPACEWAY™ system can pass its significant cost savings onto its customers. The SPACEWAY™ network is different from other proposed global networks in that its geostationary orbit location makes it a truly market driven system: each satellite will make available extensive telecom services to hundreds of millions of people within the continuous view of that satellite, providing immediate capacity within a specific region of the world.

Introduction

This paper presents a summary description of SPACEWAY™, a global network of Ka band satellites being developed by Hughes Communications, Inc., to provide worldwide telecommunication services. The SPACEWAY™ network will utilize state-of-the-art technology to introduce a broad range of innovative and affordable satellite services on a global basis to consumer and commercial end-users. The outline of principal topics addressed in this paper is as follows:

1. System concept
2. Space segment characteristics
3. Ground segment characteristics
4. Link performance objectives and power budgets

1. System Concept

The SPACEWAY™ system[1] is a network of regional systems that will utilize satellites in the geostationary satellite orbit (GSO) to provide cost-effective, two-way voice, medium- and high-speed data, image, video and video telephony communications service to both business and individual users. Direct access to the satellites will be available on demand throughout the world via inexpensive ultra small aperture terminals (USATs). SPACEWAY™ is a high capacity, high quality, yet very versatile system. Figure 1 provides a summary of the performance available with each satellite. A two satellite regional configuration would therefore enable over 230,000 simultaneous telephone calls at 16 Kbps. The all digital 16 Kbps circuits utilized for telephony will ensure consistent high quality voice channels.

[1] Application filed by Hughes Communications Galaxy, Inc. with the Federal Communications Commission on 26 July 1994.

The high capacity of each SPACEWAY™ satellite is focused through the spot beams on the populated areas of the world thereby creating a significant cost advantage in the delivery of its telecom services. The flexibility of applications available through SPACEWAY™ is achieved through its broad range of data rates and is illustrated in Figure 1A.

The SPACEWAY™ network is different from other proposed global networks in that its geostationary orbit location makes it a truly market driven system: each satellite will make available extensive telecom services to hundreds of millions of people within the continuous view of that satellite, providing immediate capacity within a specific region of the world. SPACEWAY™ will be implemented in a phased, regional approach beginning in 1998, expanding into a network of four interconnected regional systems: (i) North America, (ii) Asia Pacific (iii) Central/South America, and (iv) Europe/Africa. The SPACEWAY™ network will provide in each of these regions the same low-cost, ubiquitous communications services at data rates up to multiple megabits per second, while also providing worldwide connectivity.

In developing countries, SPACEWAY™ will offer essential domestic and international telephone and facsimile services that will be seamlessly integrated into the public switched telephone network ("PSTN"). SPACEWAY™ will offer high bandwidth services for a variety of consumer and business applications, both for countries with existing telecom infrastructures and those with emerging needs for advanced services.

Figure 2 depicts the phased regional implementation of the SPACEWAY™ network. The first satellites in the SPACEWAY™ network will be operational in 1998. Each regional system will include two satellites. Our system plan accommodates the growth for up to four satellites per region. For these reasons, Hughes believes that the SPACEWAY™ network will become an essential element in the establishment of the Global Information Infrastructure (GII) by the turn of the century.

HUGHES
COMMUNICATIONS

14 June 1995

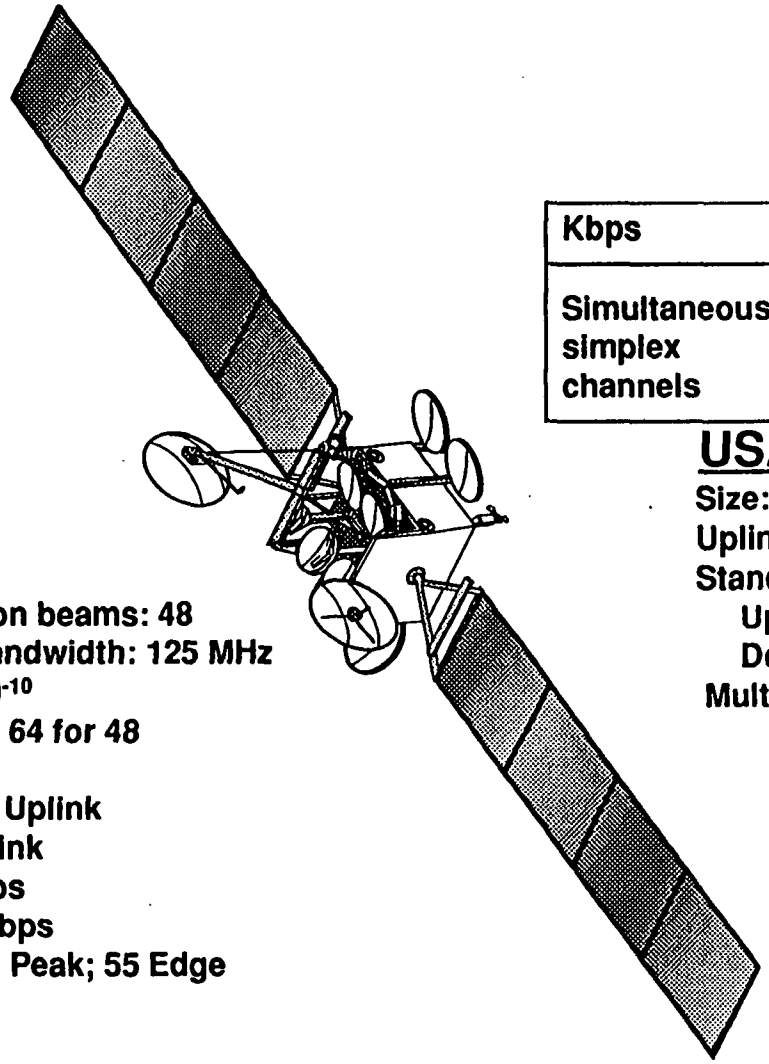

Satellite

Type: HS601
Lifetime: 15 yrs
Dry weight: 3,785 lbs
Eclipse capacity: 100%
Bandwidth: 500 MHz
Number of communication beams: 48
Communication beam bandwidth: 125 MHz
BER performance: 1 x 10^{-10}
Transmitter redundancy: 64 for 48
Modulation: QPSK
Data stream: FDM/TDMA Uplink
TDM Downlink
Data throughput: 4.6 Gbps
Downlink data rate: 92 Mbps
Downlink EIRP: 60 (dBw) Peak; 55 Edge

Capacity per satellite

Kbps	16	128	384	1,544	2,048
Simultaneous simplex channels	230,400	34,560	11,520	2,880	2,304

USAT

Size: 66 cm to 2 m
Uplink power: 0.1W to 2W
Standard Terminal:
Uplink data rates: 16 kbkps to 1.544 Mbps
Downlink data rates: 16 kbps to 92 Mbps
Multi Mbps with optional terminal

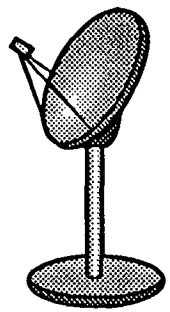

M941637-14

Fig. 1A. Performance summary.

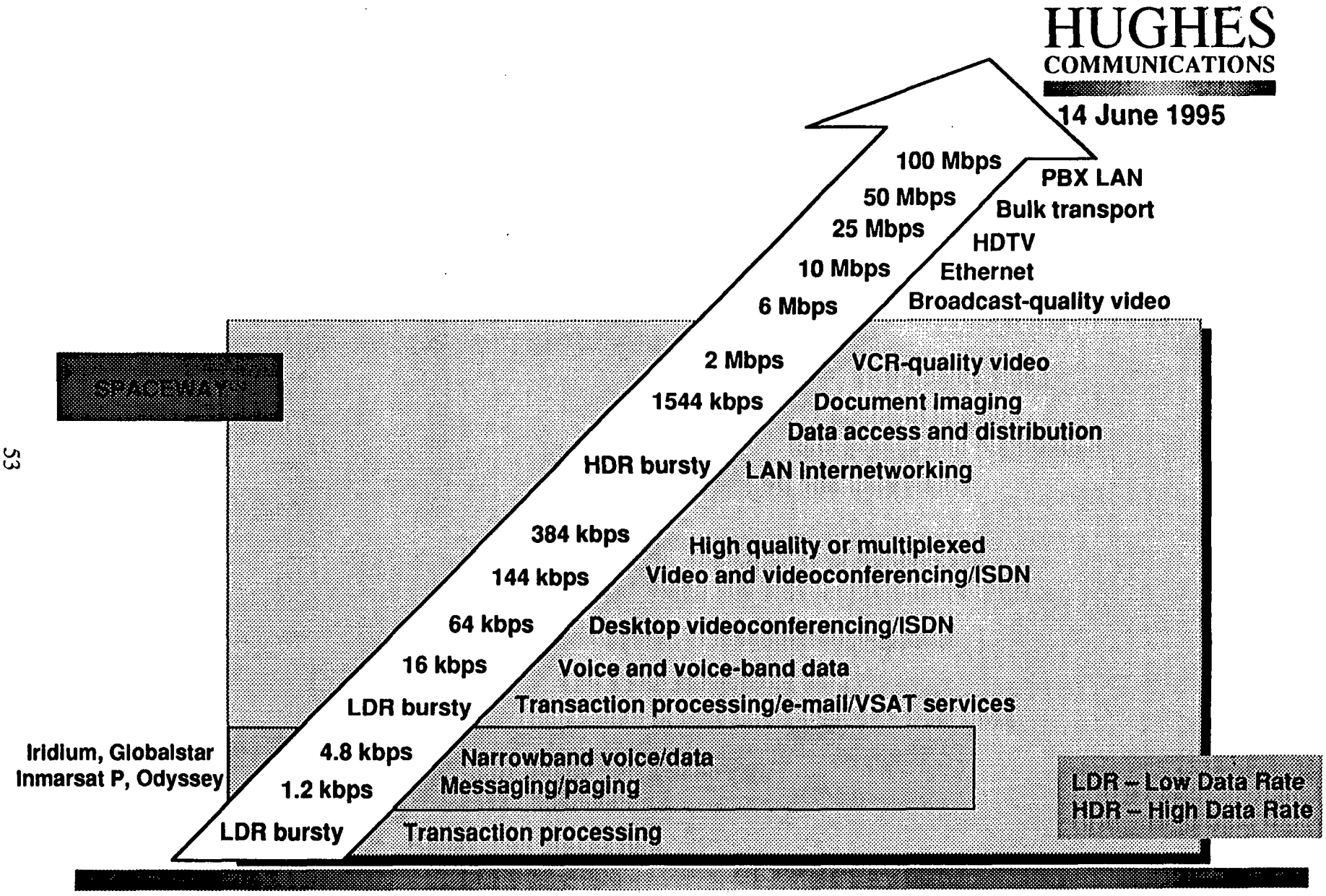

M950076-3A

Fig. 1B. Range of applications.

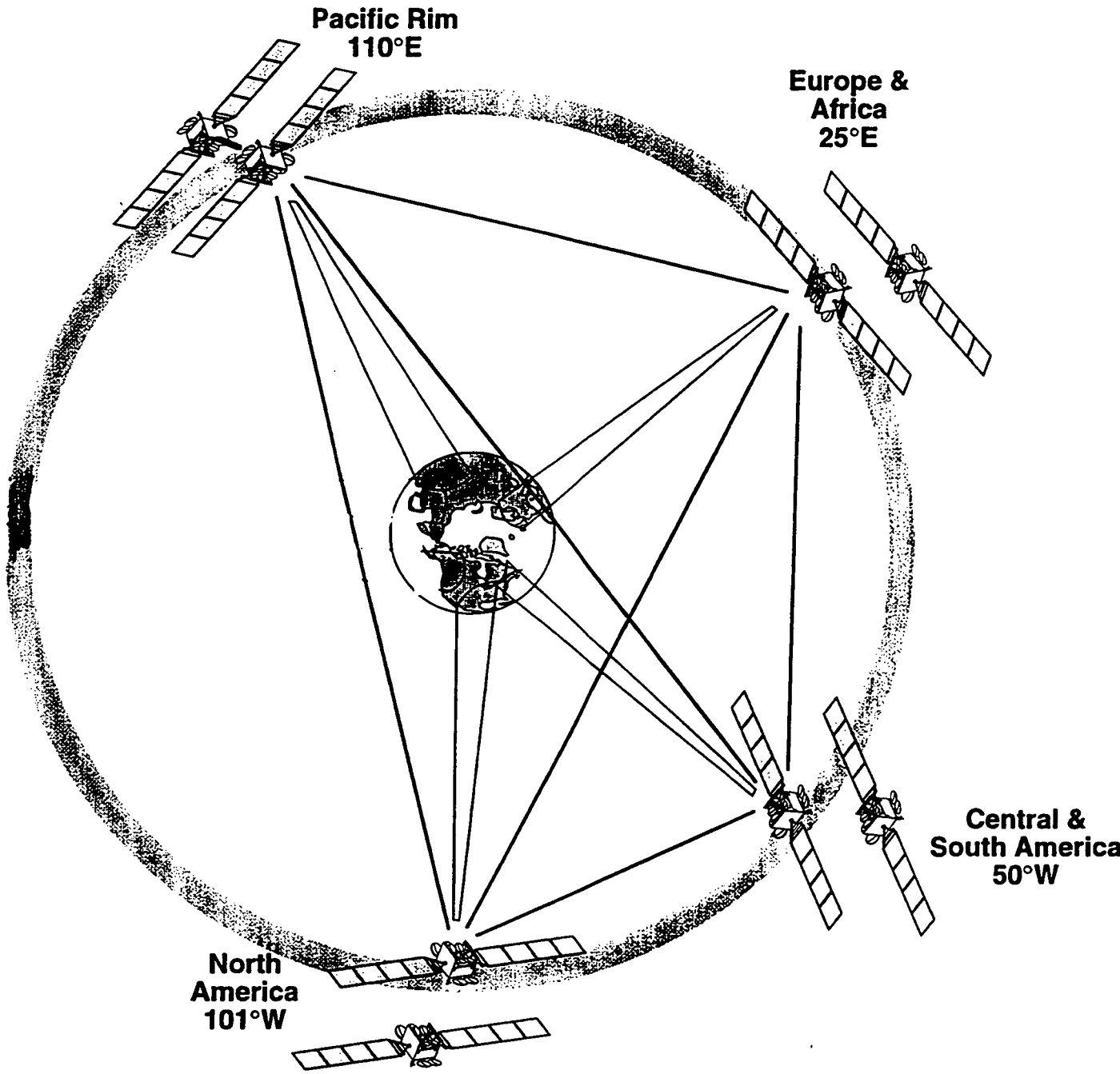

Fig. 2. Spaceway Global Network, Phase 1 (initial operating capability by 2000), showing orbital locations.

This innovative all-digital network will utilize state-of-the-art advances in satellite technology to provide full duplex interactive communications throughout the world. Its features include on-board signal processing, on-board switching, small, easily installed ground terminals, and digital transmissions at a variety of data rates.

A key component of the system architecture is the Ka-band spot beam network. This technology will allow the use of extremely small end user terminals (approximately 66 cm) and provide a high degree of spectrum efficiency. Each spot beam nominally will use 125 MHz of bandwidth. Narrow spot beams (about 1°) with a footprint approximately 650 km. in diameter will cover most of the populated world land mass. The satellite design will permit reuse of frequencies up to twelve times. Thus, the 500 MHz of spectrum utilized by each satellite will result in an effective 6 GHz of useful bandwidth per satellite.

The system allows symmetric and asymmetric data communications at transmission rates from 16 Kbps to 384 kbps, depending upon user requirements with the standard 66 cm terminal. Multi megabit per second applications can be accommodated with the SPACEWAY™ optional broadband terminal.

Each satellite will utilize a state-of-the-art on board switch/processor to provide individual end users with immediate access to the space segment, and to route transmissions within and between appropriate destination spot beams. This "on demand" satellite service will be competitively priced with many basic terrestrial telephone services especially in remote and underserved areas, where basic telephone services are neither economically feasible nor available. In addition, the use of off-the-shelf digital video compression equipment or optional codecs built into the earth terminals will allow end users to utilize a high quality, two-way interactive video telephony service. Availability of such teleconferencing facilities at low cost should help underserved countries improve the delivery of vital services such as health care and education.

SPACEWAY™ will offer a dramatic advancement in the functionality and affordability of business networks relative to today's VSAT capability. For businesses, the SPACEWAY™ USAT both advances the state-of-the-art in VSAT networking, and brings satellite technology to the economic threshold of a greater universe of customers. SPACEWAY™ USATs offer complete mesh connectivity without the need for expensive hubs: in essence a "hubless" network. Thus, through low cost USATs, smaller businesses -- for whom today's VSATs are unaffordable - can take advantage of satellite networking without requiring a large number of sites to amortize hub costs.

SPACEWAY™ will accommodate most conventional VSAT applications, including retail point-of-sale transaction processing, on-line reservations and inventory/pricing information updates. In addition, SPACEWAY™ will offer a variety of wideband services including video telephony and conferencing (allowing multiple meeting sites and interconnection with terrestrial videoconferencing equipment and services), telecommuting (home computer to office LAN connection), medical and technical tele-imaging, and CAD/CAM data and image transmission.

With its small size and low cost, the SPACEWAY™ USAT will make the benefits of satellite communications readily accessible to consumers. It is anticipated that consumers will use SPACEWAY™ for basic telephony and data communications, personal vidotelephony and high speed personal computer access to on-line services (such as Compuserve and Prodigy), as well as two-way interactive access to the wide array of multimedia information and entertainment services currently being developed for the "information superhighway" of tomorrow. The affordability of the SPACEWAY™ terminal will permit advanced telecommunications and media industries to reach an even wider audience.

The SPACEWAY™ network represents a giant stride forward for the transmission of data. The incorporation of on-board satellite switching/processing, multi-spot beam coverage, and advanced ground terminal semiconductor technology, will allow small, inexpensive end user terminals, immediate and on-demand access to space segment and very fast data transmission. For many applications, such as sending medical images (x-rays) to and from remote clinics, short transmission time is critical. The SPACEWAY™ network can dramatically reduce the retransmission time of important data by providing transmission at rates more than 150 times faster than conventional telephone lines. The following chart displays this relationship between time, information content and bandwidth.

IMAGE	INFORMATION CONTENT	ORDINARY PHONE LINE	SPACEWAY™ 384 Kbps	SPACEWAY™ 1.5 MBPS (T1)
Digitized Photo	1.0 megabit	1.7 min.	2.6 sec	0.7 sec
CAD/CAM	2.0 megabits	3.4 min.	5.2 sec	1.4 sec
CT Scan	5.2 megabits	9.0 min.	13.5 sec	3.4 sec
X-Ray	12.0 megabits	21.0 min.	31.3 sec	7.8 sec

In sum, the on-demand high-speed data transmission capability of the SPACEWAY™ network will facilitate an array of applications. In addition to those described above, many others could be made available through third-party service providers.

The SPACEWAY™ network will provide interconnected, bandwidth on demand services to virtually every populated area of the world. In this regard, the service area of the SPACEWAY™ network is similar to that of many of the low earth orbit ("LEO") satellite systems that have been proposed. The SPACEWAY™ network is different from these LEO systems in two significant respects: it is more spectrally efficient and it will not forestall the development of other geostationary satellite systems using the Ka band at other orbital locations. It is a geostationary satellite system that operates from a total of six orbital locations and complies with the United States Federal Communications Commission's 2° spacing policies. Thus, it is anticipated that it will be compatible with any other Ka band FSS system that may operate at any other geostationary orbital location that is at least 2° away. Assuming uniform 2° spacing around the world, making 180 orbital slots available, the 2.5 GHz that has been proposed for SPACEWAY™ could be reused to effectively provide 435 GHz of Ka band spectrum for other satellite services. No LEO system that has been proposed to date has offered this type of an opportunity for frequency reuse. In sum, unlike LEO satellite systems that have been proposed at Ka band, the SPACEWAY™ network supports the entry of multiple service providers at all or part of the 2.5 GHz that is available at Ka band.

2. Space Segment Characteristics

The deployment of the multibeam satellites at geostationary orbit will be accomplished on a phased regional implementation and is illustrated in Figure 2. The proposed assignment of frequencies and polarizations to satellite beams, the geographic coverage provided by these beams, and a description of the other satellite parameters are given below.

2.1 Frequency and Polarization Assignments

The SPACEWAY™ global network will utilize the 17.7 to 20.2 GHz portion of the Ka band for space-to-Earth (downlink) transmissions, and the 27.5 through 30.0 GHz portion of the Ka band for Earth-to-space (uplink) transmissions. This spectrum has been allocated on a worldwide basis for the Fixed-Satellite Service ("FSS").

The frequency plan for the SPACEWAY™ network is presented in Figures 3 and 4.

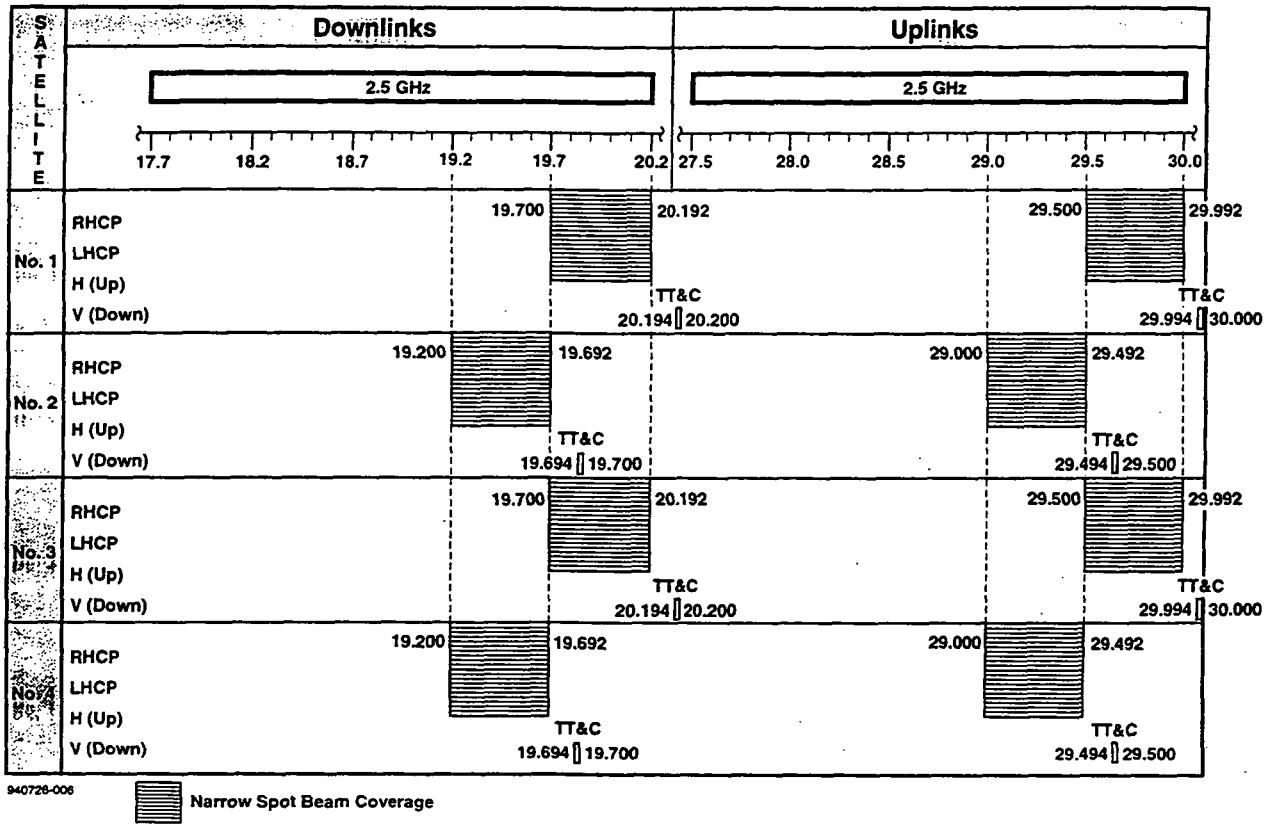

Fig. 3. Spaceway spectrum utilization in North America.

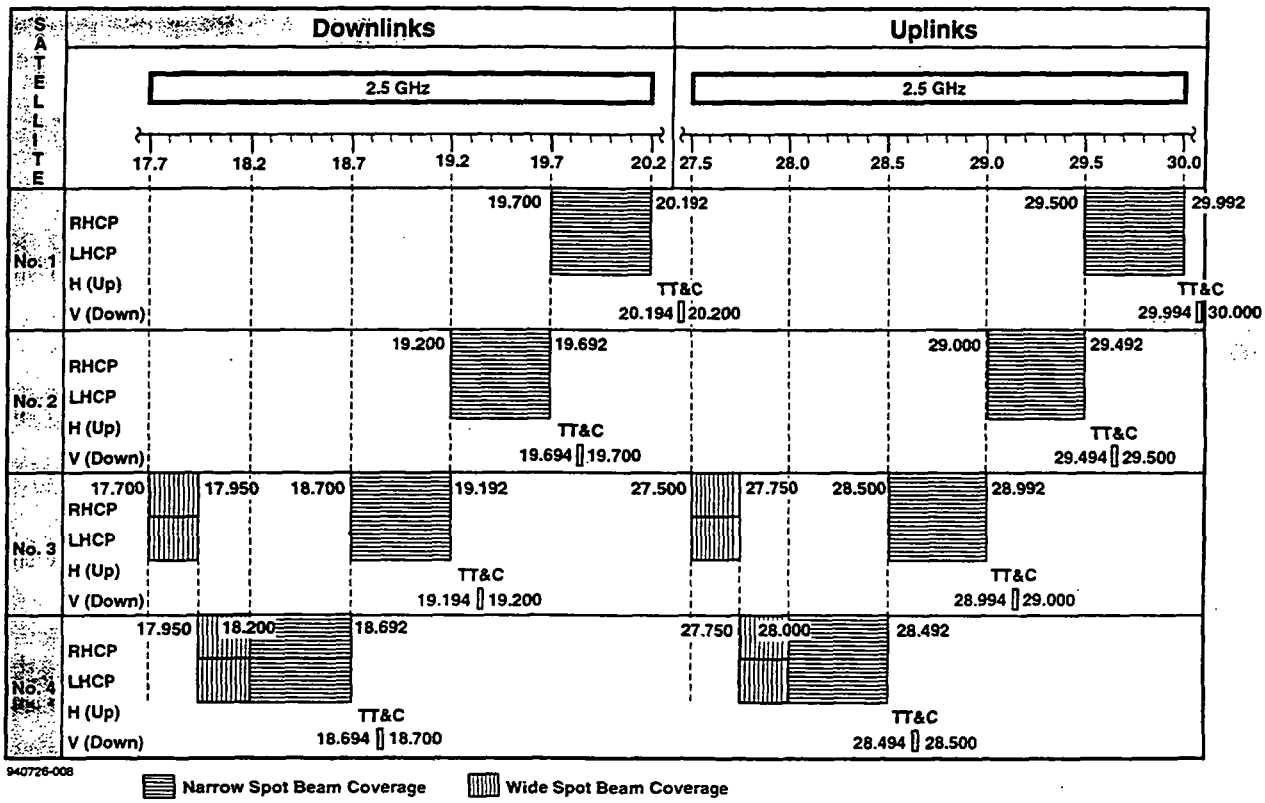

Fig. 4. Spaceway spectrum utilization in Central and South America, Europe, Africa, and Asia Pacific.

The plan for the four satellites serving the North America region is depicted in Figure 3. Satellites 1 and 2 will occupy the 101° W.L. position and will each employ 500 MHz of bandwidth. North American satellites 3 and 4 will be located 2° away at 99° W.L. and will employ precisely the same spectrum as North American satellites 1 and 2. North American coverage is provided by two satellites at each of 101° W.L. and 99° W.L. By placing two satellites at each of these locations, and using the same 1000 MHz of spectrum at each location, the system will have sufficient capacity to provide the full range of proposed satellite services.

Each of the four North American satellites will provide a total of forty-eight 125 MHz spot beams (24 beams used on opposite circular polarizations) for uplink and downlink transmission. In this way, each satellite effectively reuses the 500 MHz of spectrum assigned to it about 12 times.

Each of the other three regions is supported by a constellation of four satellites that will use the full 2.5 GHz of spectrum at a common orbit position as illustrated in Figure 4. This will allow any subscriber within any of these regions to use a single earth terminal to access capacity on any of the four satellites at that orbital position. In each region, satellites 1 and 2 are identical in frequency plan to their counterparts in North America and divide their 500 MHz into forty-eight 125 MHz spot beams in a manner similar to that shown in Table 1. However, satellites 3 and 4 in each region are assigned two different 500 MHz band segments so that they may be co-located with satellites 1 and 2.

2.2 Beam Coverage Areas

The proposed system will provide spot beam coverage of all inhabited land areas of the world. An eight satellite constellation provides service to 90% of the world's population. Figure 5 depicts the four regions of coverage by the SPACEWAY™ system. The two satellites per region provide high EIRP and G/T coverage to allow the use of small inexpensive earth terminals.

The system comprises two satellites per region:

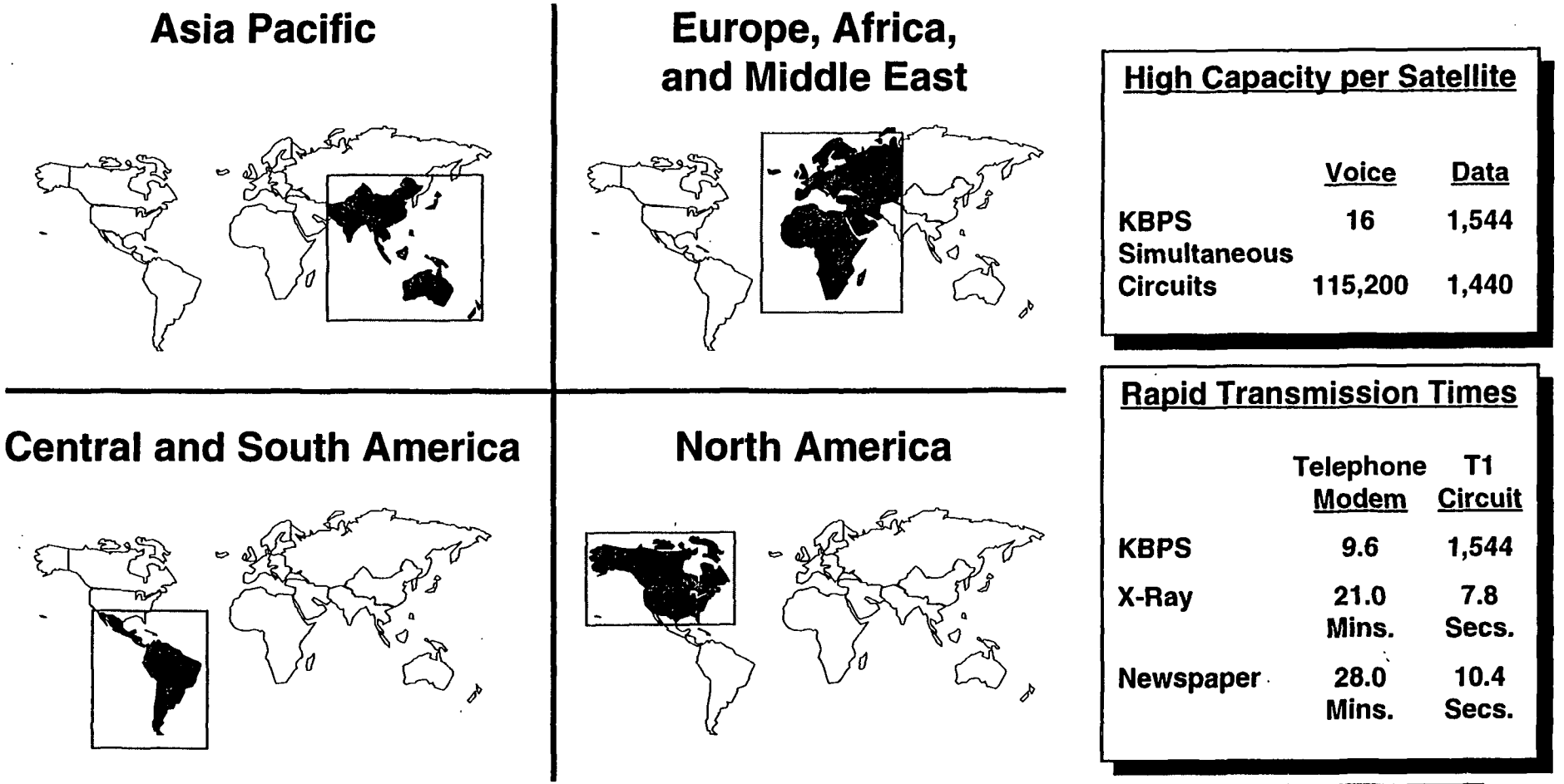

Fig. 5. An eight-satellite system provides service to 90% of the world's population.

2.3 Satellite Characteristics

The on-orbit configuration of the satellites is illustrated in Figure 6, and the major spacecraft characteristics are given in Table 1. The launch weight budget is presented in Table 2. The satellite receiver and transmitter parameters are given in Tables 3 and 4.

Table 1: Major Spacecraft Characteristics

General	
Spacecraft bus	HS-601
Stabilization	
Transfer orbit	Spin stabilization
On-station	3 axis. momentum bias
Mission life	15 years
Eclipse capability	100 percent
Station keeping	
North-South (orbital inclination)	±0.05°
East-West (longitudinal)	±0.05°
Antenna pointing	
Normal (Precision two-axis RF beacon tracking)	±0.1° N-S and E-W
Backup (Earth sensor)	±0.2° N-S and E-W
Beam rotation (antenna axis attitude)	±0.25°
Communications	
Number of communications beams (Satellites 1 and 2 over each region)[3]	48
Communications beam bandwidth	125 MHz
Transmitter redundancy	64 for 48
Communications channel receive flux density per Hz (narrow beams, edge of coverage)	-182.6 dBW/(m^2Hz)
Communications channel receive flux density per Hz (wide beams, edge of coverage)	-194.1 dBW/(m^2Hz)
Emission Limitations	
(Spurious level below unmodulated power)	
Frequency offset by 50% - 100% of BW	≤ -65 dBc
Frequency offset by 100% - 250% of BW	≤ -65 dBc
Frequency offset by > 250% of BW	≤ -65 dBc

[3] Satellites 3 and 4 in each region will have additional narrow spot beams and as many as five wide spot beams. However, only 48 beams in total, either narrow or wide, will be addressable at any time.

Table 2 Launch Weight Budget

Category	Weight, Lb.
Spacecraft dry	3785
10 year orbit sustenance propellant	883
Beginning of life (subtotal)	4668
Transfer orbit	3159
Total separated weight	7827

Table 3 Satellite Uplink G/T Budget

	Narrow Spot Beam	
	Peak	Edge of Cov.
Antenna gain (db)	46.50	41.50
System noise temperature (dB K)	27.60	27.60
G/T (dB/K)	18.90	13.90

Table 4 Satellite Downlink EIRP Budget

	Narrow Spot Beam	
	Peak	Edge of Cov.
Amplifier output power (db)	13.01	13.01
Repeater output losses (dB)	0.50	0.50
Antenna gain (dB)	46.50	41.50
EIRP (dBw)	59.01	54.01

3. Ground Segment Characteristics

3.1 SPACEWAY™ USATs

The SPACEWAY™ ground terminal will cover the range of communications required by the late 1990's; namely efficient and low cost telephony for areas of the world with emerging telecom infrastructure requirements as well as broad bandwidth multi-media requirements.

The SPACEWAY™ ground terminal is a multi-media ultra small aperture terminal (USAT) configured to enable direct exchange of packets with ATM type devices. Packets from video, voice and data inputs are assembled and transmitted in data bursts of up to 384 KBPS and received at TDM packet rates of up to 92 MBPS. The system with optional uplink terminals enables efficient transmission of both on-demand circuit-switched services such as ISDN, T1, and fractional T1, and packet-switched services such as frame relay and X.25.

The SPACEWAY™ system will incorporate two types of ground communications equipment: (i) end user USAT terminals and (ii) terrestrial network interfaces or gateways. The terminals will accommodate bi-directional transmissions from 16 Kbps up to 1.5 Mbps (T1) rates, using antennas ranging from 66 centimeters to 2 meters in diameter. However, virtually all mass market subscribers will utilize the 66 cm USATs which will be mass produced and easily installed.

Larger SPACEWAY™ ground terminals, or gateways, can support multiple carriers for much higher transmission throughout. Gateways are intended to provide interconnection between the global satellite system and the terrestrial public switched telephone network (PSTN), and will be strategically located to interface with inter-exchange and local exchange common carriers in the U.S. and telecommunications operators in various countries throughout the world.

Through on-board satellite switching and gateway earth stations that provide terrestrial interconnection, the system architecture will allow end users the greatest possible flexibility in making connections to each other. The system will allow both "private" network and "open" network communications. Private networks can be created where end-user terminals in a pre-defined "community" communicate with each other directly via a SPACEWAY™ satellite, with or without connection to the PSTN. Open networks allow system subscribers to connect with any other subscriber or with any other person or entity served by the PSTN through a SPACEWAY™ gateway.

The vast majority of the transmit/receive earth stations used to communicate with the global system will be owned by the end users of the service. It is anticipated that when fully deployed, the network will serve more than five million subscribers around the world, each of whom will own an earth terminal.

3.2 Availability and Rain Attenuation

In almost all areas,of the world SPACEWAY™ provides availabilities greater than 99 % with a standard ultra small aperture terminal (USAT) that includes a compact 66 cm antenna operating at a burst rate of 384 kbps. The SPACEWAY™ system offers a range of terminal options that achieve availability $\geq$ 99.5 % anywhere in the world. SPACEWAY™ incorporates uplink power control to maintain continuous service through moderate rain.

Ka-band is susceptible to rain fades that reduce availability statistics, but rain fades have a time character that is unlike an outage due to equipment failure or cable damage - which is the normal model for outages in terrestrial networks. NASA data on Ka-band propagation shows that rain fades are typically a few minutes due to the passage of a 'rain cell'. (Rain cells, which span about a kilometer, are bursts of heavy rain in a thunderstorm.) A few minutes of outage, after which service resumes unaffected, has very different consequences on an operating enterprise than the potential for hours of outage to carry out repairs normally associated with outages of terrestrial systems.

The SPACEWAY™ system availability has been evaluated over a wide range of geographical locations using the Crane[2] Rain model. In the United States the predicted link availability ranges from 99.1 % in Miami to 99.97% in Denver. The results from analyses for selected cities in the Asia Pacific region are summarized in Figure 6. The SPACEWAY™ availabilities shown in this figure. include both the standard USAT with a 66 cm antenna and availability improvements possible by using either a higher power uplink amplifier or slightly larger antenna. SPACEWAY™ will offer these optional USAT configurations so that users in the heavy rainfall areas of the world may have access to availability of at least 99.5%.

---

[2] Robert K. Crane, Predictions of Attenuation by Rain, IEEE Transactions on Communications, vol. COM-28, no 9, September 1980, pp. 1717-33.

SPACEWAY™ System Availability

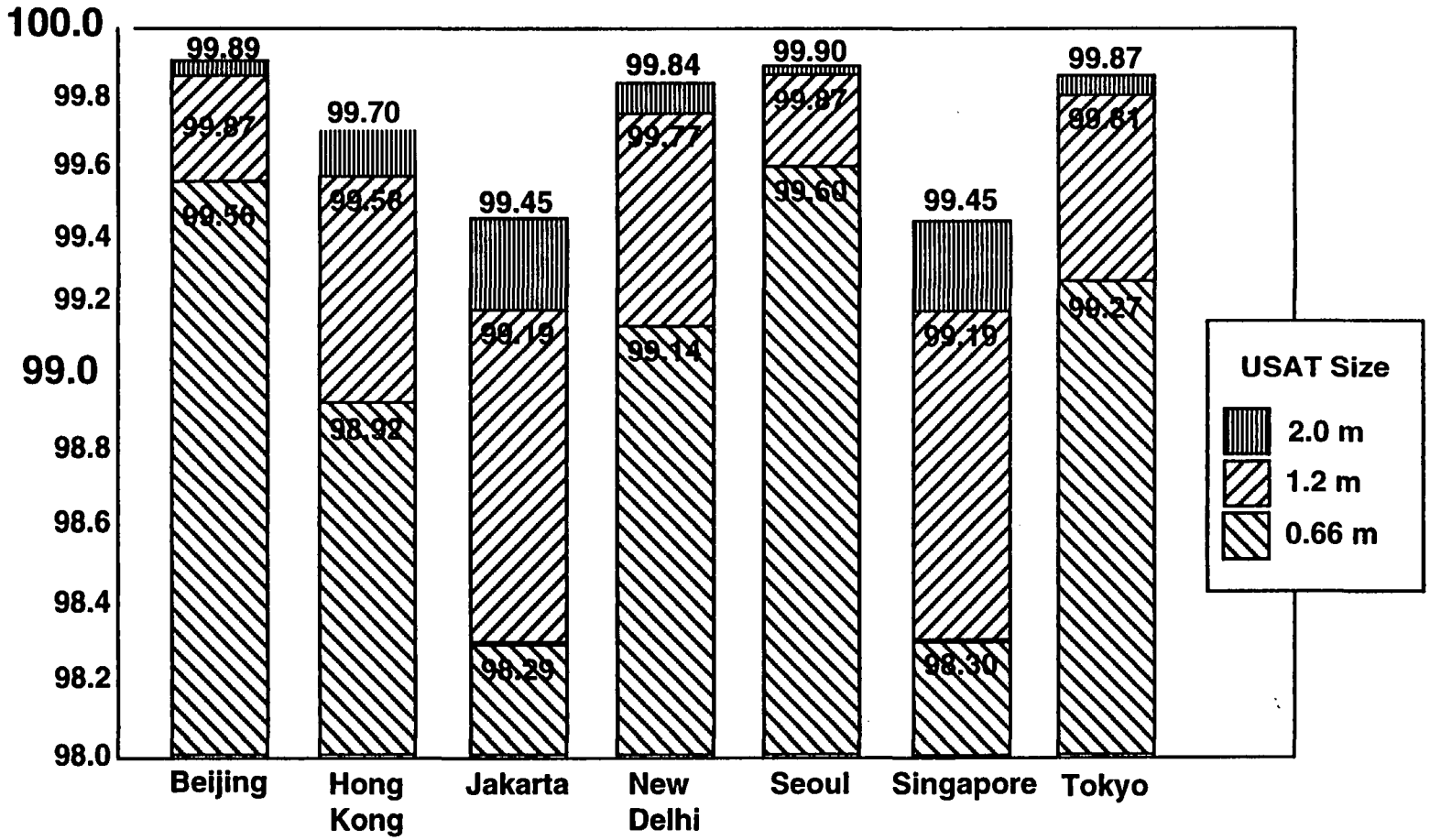

Fig. 6. Spaceway system availability in selected cities in the Asia Pacific region.

M941637-3

4. Link Performance Objectives and Power Budgets

4.1 Communication Links

Communication services will be provided at rates from 16 Kbps to 1,544 Mbps (T1). User terminals will have the capability to transmit and receive via 66 cm to 2 m aperture antennas with transmit powers that range from 0.1W to 2.0 W transmit power, depending on data rate and the amount of uplink power control used to compensate for rain attenuation. Up to 240 simultaneous 384 Kbps uplink signals may be supported in each beam for a data throughput of 92 Mbps per polarization per beam per satellite. With twelve-fold frequency reuse, the total data throughput is 4.4 Gbps per satellite.

The system performance objective is a bit error rate ("BER") of 10^{-10}. Because of on-board demodulation and remodulation of the signal, performance on the uplink and performance on the downlink are independent. Due to the error control coding used, the bit energy levels required of the two links are asymmetric. An E_b/N_0 of 8.0 dB on the uplink and 5.0 dB on the downlink are required to meet the targeted BER. Table 5 is a summary of the spot beam communication performance parameters for a data rate of 384 kbps.

Table 5. Summary of Spot Beam Communication Performance Parameters

Performance requirement	$1x10^{-10}$ BER
Transponder bandwidth	125 MHz
Modulation	QPSK
Uplink data rate	16 to 1,544 Kbps
Uplink channel bandwidth	500 to 2,000 KHz
Required uplink E_b/N_0	8.0 dB
Downlink data rate (per beam per polarization)	92 Mbps
Downlink channel bandwidth	125 MHz
Required downlink E_b/N_0	5.0 dB
Earth station diameter	66 cm to 2 m
Earth station amplifier power	1.0 - 2.0 W
Loss to antenna input	0.5 dB
Earth station receive system noise temperature	24.4 dBK

Tables 6 and 7 provide sample link analysis calculations for uplink peak and edge-of-coverage paths and downlink peak and edge-of-coverage paths, respectively, for the spot beams. Each table illustrates both clear sky and rain conditions. These calculations assume 384 kbps service.

Table 6. Uplink Power Budgets

Peak of Coverage

	Clear	Rain
Transmit power	- 9.73 dBW	- 3.01 dBW
Tramsmit losses	- 0.50 dB	- 0.50 dB
Ground transmit gain	44.45 dB	44.45 dB
Uplink path spreading	- 162.31 dB/M^2	- 162.31 dB/m^2
Uplink effective isotropic area	- 50.85 dB/m^2	- 50.85 dB/m^2
Atmosheric loss	- 0.96 dB	- 0.96 dB
Uplink rain loss	0.00 dB	- 8.77 dB
Satellite G/T (peak)	18.88 dB/K	18.88 dB/K
Bit rate	55.87 dB Hz	55.87 dB Hz
Boltzmann's constant	- 228.60 dBW/K/Hz	- 228.60 dBW/K/Hz
Thermal Eb/No	11.72 dB	9.67 dB
Cross-pol Eb/No	17.45 dB	17.45 dB
Adjacent beam co-pol Eb/I	17.95 dB	17.95 dB
Adjacent system (east) Eb/I	20.85 dB	20.85 dB
Adjacent system (west) Eb/I	20.85 dB	20.85 dB
Total Eb/I	9.29 dB	8.00 dB

Edge of Coverage

	Clear	Rain
Transmit power	- 4.73dBW	- 3.01 dBW
Tramsmit losses	- 0.50 dB	- 0.50 dB
Ground transmit gain (EOC)	44.45 dB	44.45 dB
Uplink path spreading	- 162.31 dB/M^2	- 162.31 dB/m^2
Uplink eff. isotropic area	- 50.85 dB/m^2	- 50.85 dB/m^2
Atmosheric loss	- 0.96 dB	- 0.96 dB
Uplink rain loss	0.00 dB	- 3.77dB
Satellite G/T	13.88 dB/K	13.88 dB/K
Bit rate	55.87 dB Hz	55.87 dB Hz
Boltzmann's constant	- 228.60 dBW/K/Hz	- 228.60 dBW/K/Hz
Thermal Eb/No	12.92 dB	5.66 dB
Cross-pol Eb/No	17.45 dB	17.45 dB
Adjacent beam co-pol Eb/I	17.95 dB	17.95 dB
Adjacent system (east) Eb/I	22.79 dB	22.79 dB
Adjacent system (west) Eb/I	22.79 dB	22.79dB
Total Eb/I	10.20 dB	5.00 dB

Table 7. Downlink Power Budgets
Peak of Coverage

	Clear	Rain
Transmit power	13.01 dBW	13.01 dBW
Tramsmit losses	- 0.50 dB	- 0.50 dB
Satellite transmit gain (peak)	46.50 dB	46.50 dB
Downlink path spreading	- 162.31 dB/M^2	- 162.31 dB/m^2
Uplink eff. isotropic area	- 47.34 dB/m^2	- 47.34 dB/m^2
Atmosheric loss	- 1.10 dB	- 1.10 dB
Downlink rain loss	0.00 dB	- 7.64 dB
Terminal G/T	18.56 dB/K	16.37 dB/K
Bit rate	79.64 dB Hz	79.64 dB Hz
Boltzmann's constant	- 228.60 dBW/K/Hz	- 228.60 dBW/K/Hz
Thermal Eb/No	15.78 dB	5.95 dB
Cross-pol Eb/No	17.45 dB	17.45 dB
Adjacent beam co-pol Eb/I	17.95 dB	17.95 dB
Adjacent system (east) Eb/I	18.50 dB	18.50 dB
Adjacent system (west) Eb/I	18.50 dB	18.50 dB
Total Eb/I	10.52 dB	5.00 dB

Downlink budget calculation SPOT beams
Table E-4 (A)

Edge of Coverage

	Clear	Rain
Transmit power	13.01 dBW	13.01 dBW
Tramsmit losses	- 0.50 dB	- 0.50 dB
Satellite transmit gain (EOC)	41.50 dB	46.50 dB
Downlink path spreading	- 162.31 dB/M^2	- 162.31 dB/m^2
Uplink eff. isotropic area	- 47.34 dB/m^2	- 47.34 dB/m^2
Atmosheric loss	- 1.10 dB	- 1.10 dB
Downlink rain loss	0.00 dB	- 2.64 dB
Terminal G/T	18.56 dB/K	16.37 dB/K
Bit rate	79.64 dB Hz	79.64 dB Hz
Boltzmann's constant	- 228.60 dBW/K/Hz	- 228.60 dBW/K/Hz
Thermal Eb/No	10.78 dB	5.95 dB
Cross-pol Eb/No	17.45 dB	17.45 dB
Adjacent beam co-pol Eb/I	17.95 dB	17.95 dB
Adjacent system (east) Eb/I	18.50 dB	18.50 dB
Adjacent system (west) Eb/I	18.50 dB	18.50 dB
Total Eb/I	8.36 dB	5.00 dB

For 384 Kbps service using narrow beams, the maximum earth station transmitter power is 1.0 W and is reduced to less than 0.1 W under clear sky conditions, as shown in Tables 6 and 7.

Propagation Experiment of COMETS Ka/Q-band Communication Link for Future Satellite Cellular System

Yoshihiro Hase
Communications Research Laboratory

Background

Mobile/Personal Satellite Communication Systems in L/S-bands are going into the operational phase. In the future, they will be operated in much higher frequency bands, for example in Ka-band, because the available bandwidth in L-band is limited. Systems with large on-board antennas in higher frequencies allow the same configuration as terrestrial cellular radio systems, since the on-board antennas will have many small spot beams. This may be true especially in a low earth orbit system such as Teledesic, which will use Ka-band.

The most important parameter of Satellite Cellular may be cell size, that is, a diameter of the spot beam. A system designer needs the local correlation data in a cell and the size of the correlative area. On the other hand, the most significant difficulty of Ka and higher band systems is the countermeasure to rain attenuation. Many-cell systems can manage the limited power of on-board transponders by controlling output power of each beam depending on the rain attenuation of each cell. If the cell size is equal to the correlative area, the system can probably achieve the maximum performance.

Propagation data of Ka and higher band obtained in the past shows a long term cumulative feature and link availability, but do not indicate the correlative area. The Japanese COMETS satellite, which will be launched in February 1997, has transponders in Ka and Q-band. The CRL is planning to measure the correlative area using 21GHz and 44GHz CW transmissions from the COMETS.

Propagation Research Plan

Earth stations with a receive-only function are set up in the meshed configuration with several km intervals, for example, 3x3 or 4x4. The functions of earth stations are to measure received level, precipitation, and cloudiness. Data from the stations are measured simultaneously, and recorded by data recorders or real-time transmitted to a center through a public telephone network. As the interval of meshed earth stations will be a parameter of this measurement, it will be changed in a certain period, for example, one year. Due to the different intervals, the measurement can be expanded in its dynamic range with a limited number of earth stations.

Accumulated data will be analyzed to estimate the correlative area. As the attenuation due to clouds is not negligible especially in mm-wave such as Q-band, the relation between a fade level and the cloudiness may be an interesting target for analysis.

In our tentative plan, the development of a bread-board model of the earth station will start this year, and at least 9 stations in Ka-band will be developed before the satellite is launched. The most significant difficulty in this research is the cost of receivers and antennas. As we would like to prepare many stations, we need cost effective antennas and receivers.

CRL's Propagation Research in Ka-band, mm-Wave and Optical Satellite Links

Y. Hase and Y. Arimoto
Communications Research Laboratory

1. Propagation Experiment of ETS-VI Optical Communication Link (Preliminary Result)
2. Propagation Experiment of COMETS Ka/Q-band Communication Link (Future Plan)

COMETS Satellite

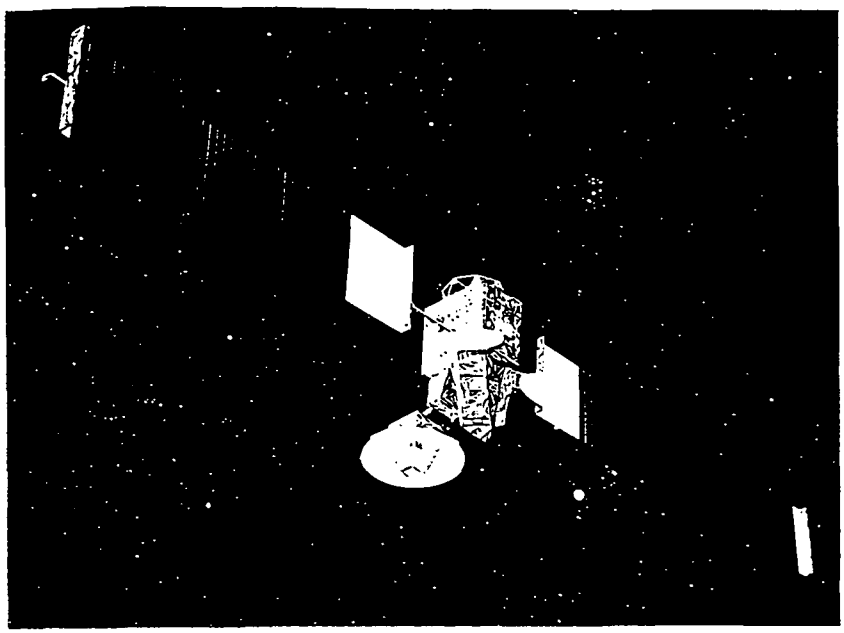

COMETS Project

Experimental Missions

Advanced Mobile Satellite Comm. (CRL)
Advanced Satellite Broadcasting (CRL/NASDA)
Inter-orbit Communication (NASDA)

Objectives of Advanced Mobile Sat-Com

To develop basic technology of future mobile/ personal satellite communication in Ka / mm-wave bands.

Features

Regenerative Transponder (SCPC/TDM)
Beam Interconnection

On-board Equipment

Mobile Mission

Freq.	: 21GHz / 44GHz
Tx Power	: 20W / 20W
ANT Gain	: 48dBi / 54dBi (2m)
EIRP	: 58dBW / 61dBW
Polarization	: LHCP

Broadcasting Mission

Frequency	: 20.7GHz
Tx Power	: 200W
ANT Gain	: 46dBi (2.3m)
EIRP	: 66dBW
Polarization	: RHCP

On-board Antenna Radiation Pattern in Ka-band

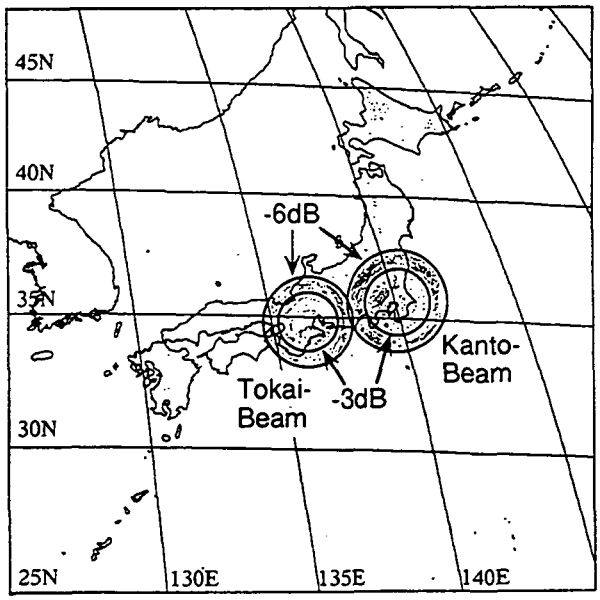

Radiation Pattern of Broadcasting ANT

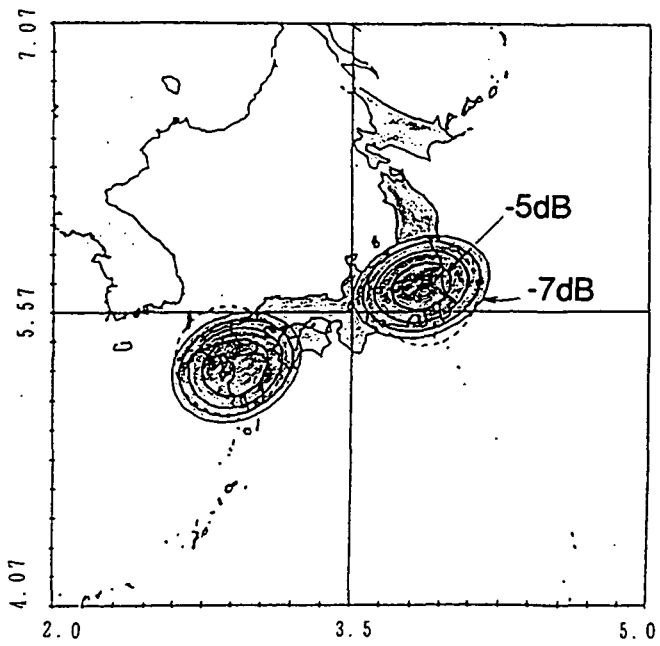

Future Mobile / Personal Satellite Communication

High Frequency
High EIRP
Low Earth Orbit

→

Satellite
Cellular

Cell size (spot beam size) will be the most important parameter from the viewpoint of rain attenuation.

Because the EIRP of each cell will be controled depending on the link condition of each cell.

Propagation Measurement Configuration

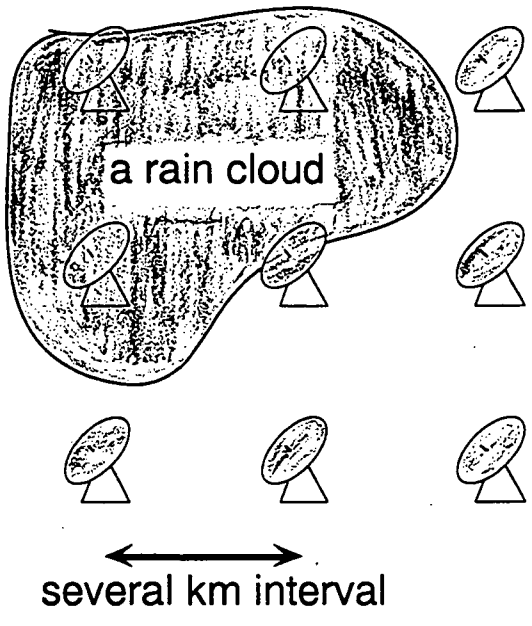

Simple Earth Station Hardware

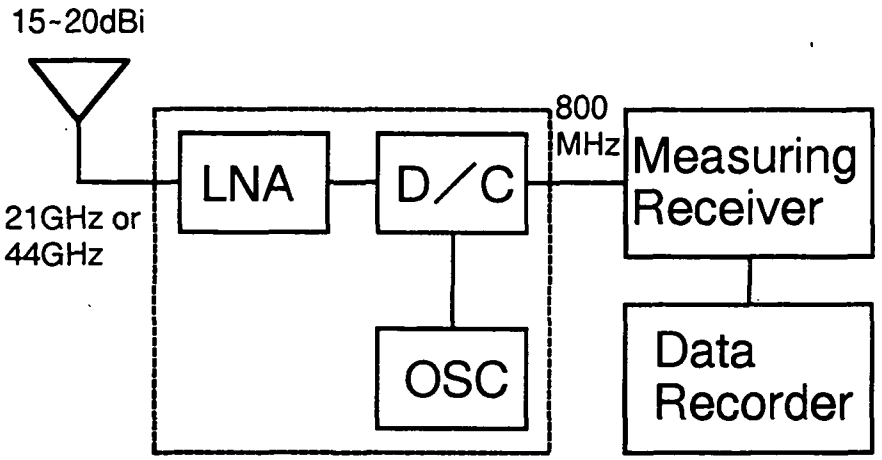

Summary

Propagation research for future satellite cellular communications

Using COMETS Ka/Q-band Transponders

Simultaneous measurement with array configuration of simple earth stations

Estimation of correlative area / cloud's effect

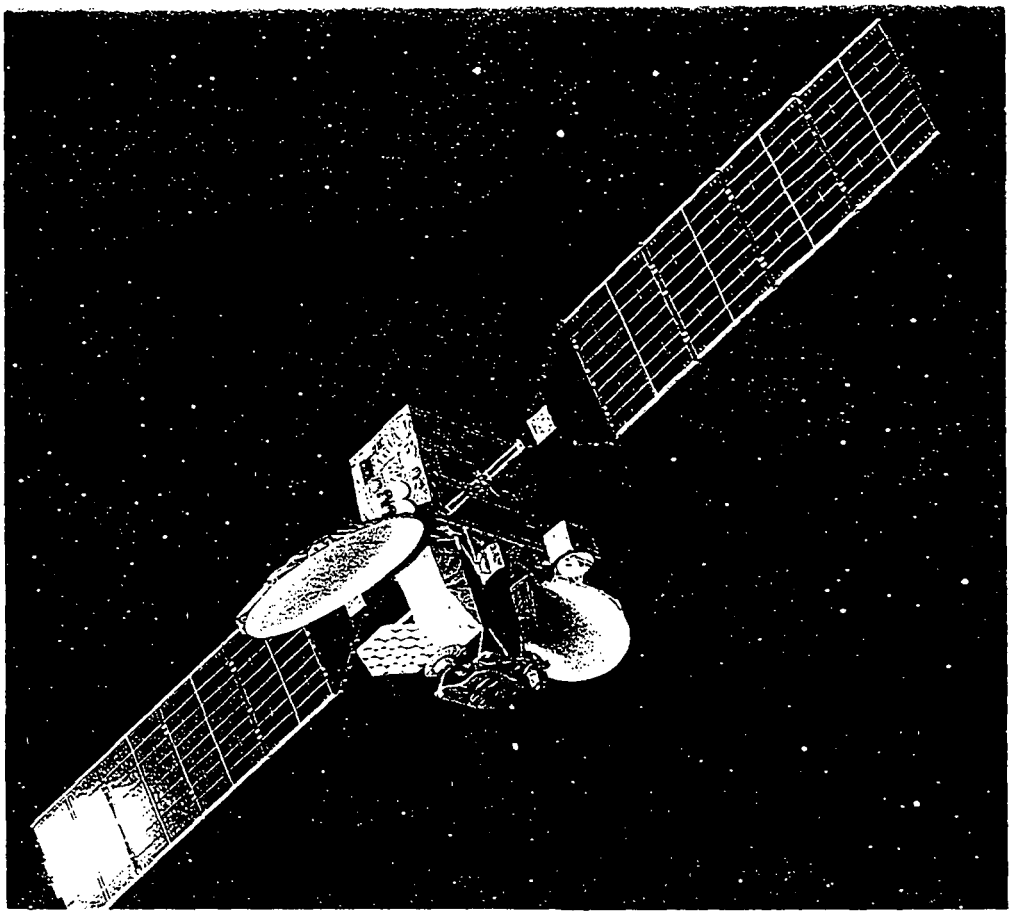

Current status of the ETS-VI satellite

- ETS-VI was launched on 28 August 1994 with a laser communication payload called LCE (Laser Communication Equipment).

- In November, ETS-VI was transferred into 3-day subrecurrent orbit suitable for communication experiment.

- It is necessary to make attitude bias-control by leaning the antenna pointing for communication with Japanese ground station.

- Because of the strong radiation effects in the Van Allen belt, electric power of the solar array is decreasing and this will limit the satellite lifetime.

Subrecurrent orbit of ETS-VI (three-day period)

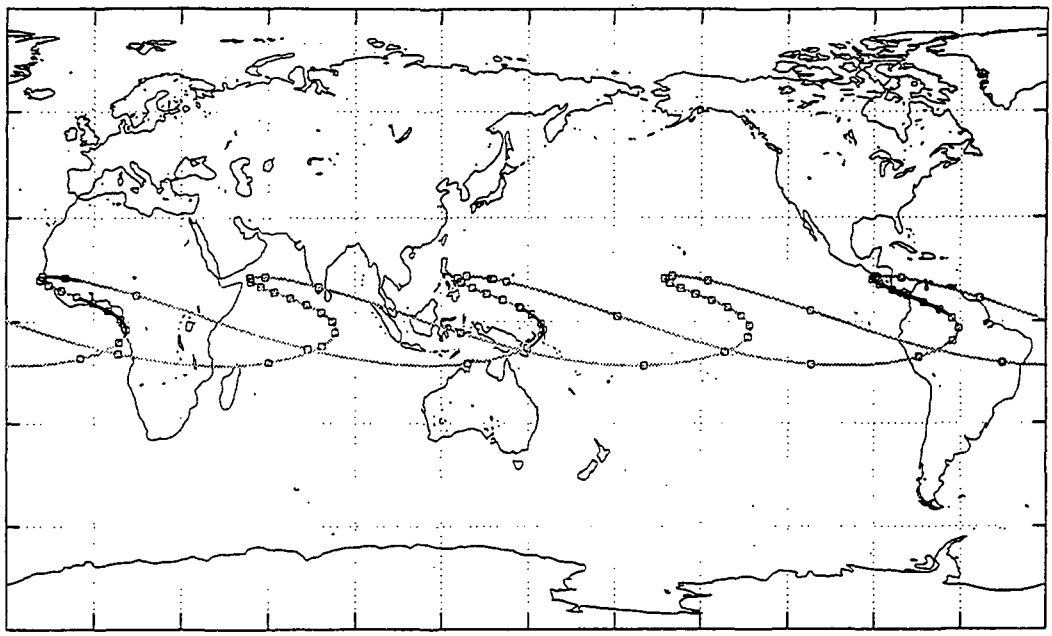

Three-day prediction of subsatellite point from Dec. 12, 1994, marker interval: 0.5 hour, thick line shows accessible region from ESA, Japan, and USA.

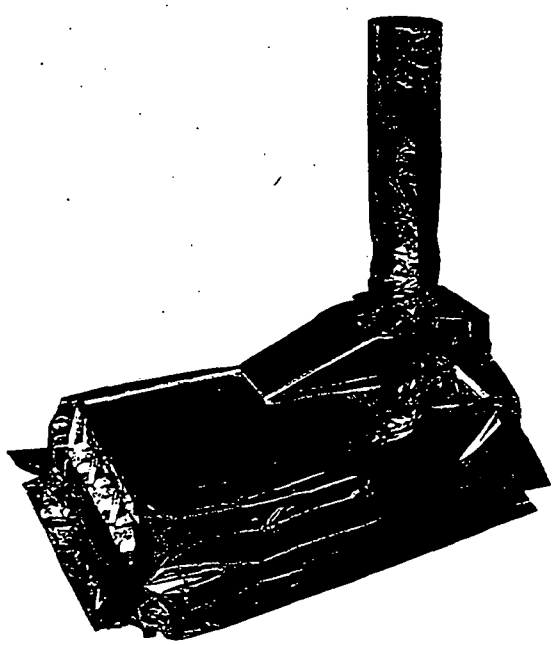

LCE光学部
LCE Optical Part

LCE光学部の内部
Layout of the LCE Optical Part

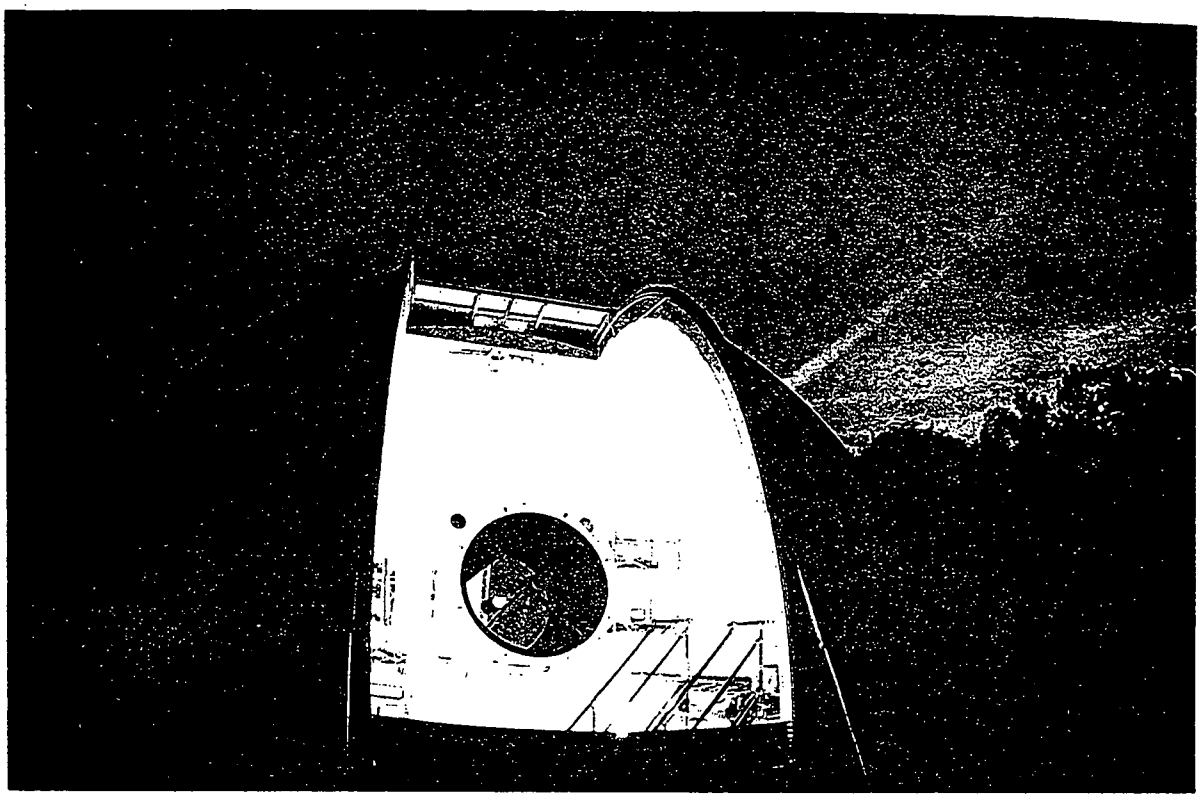

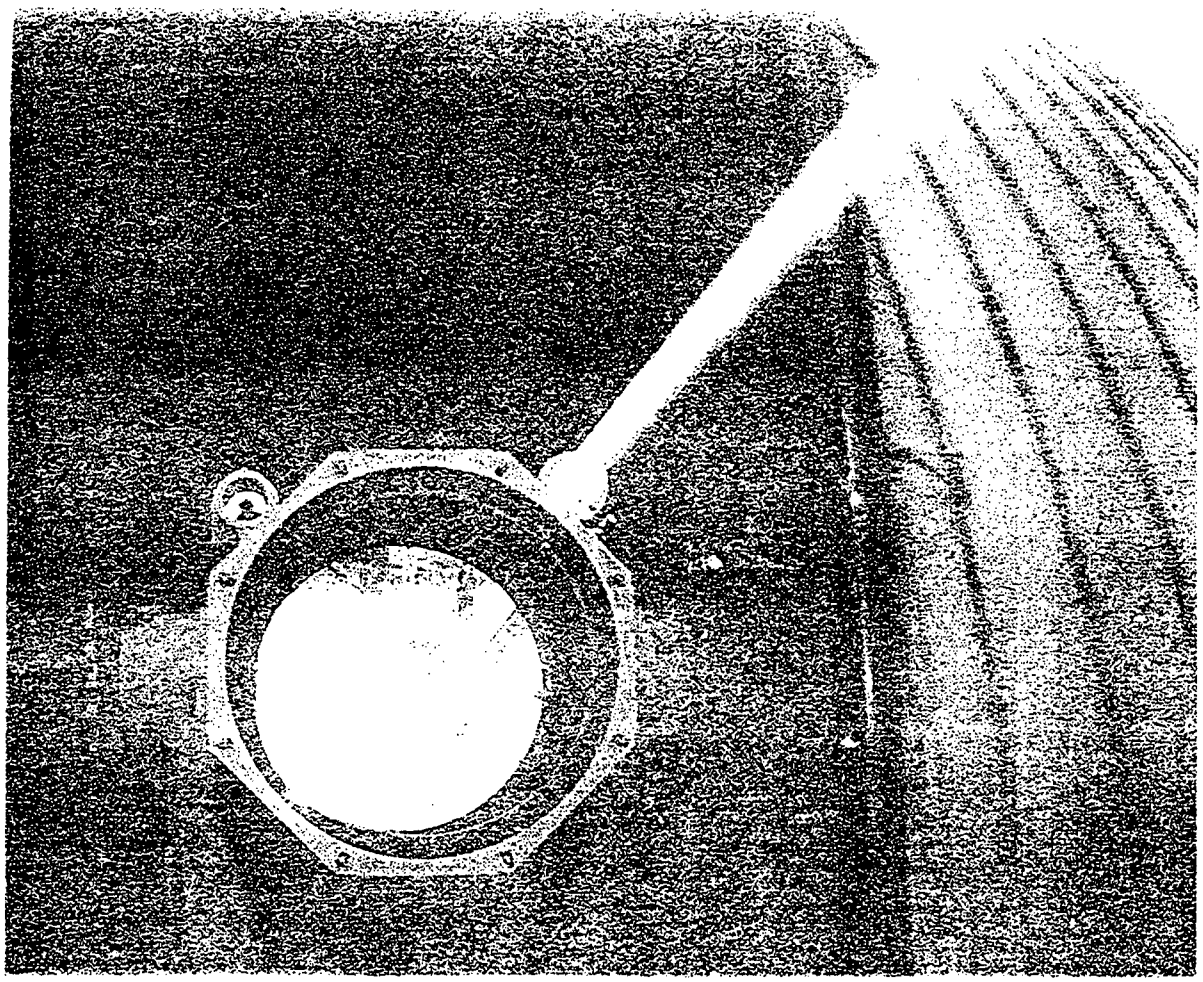

Receiving level of onboard CCD tracking sensor

February 23, 1995

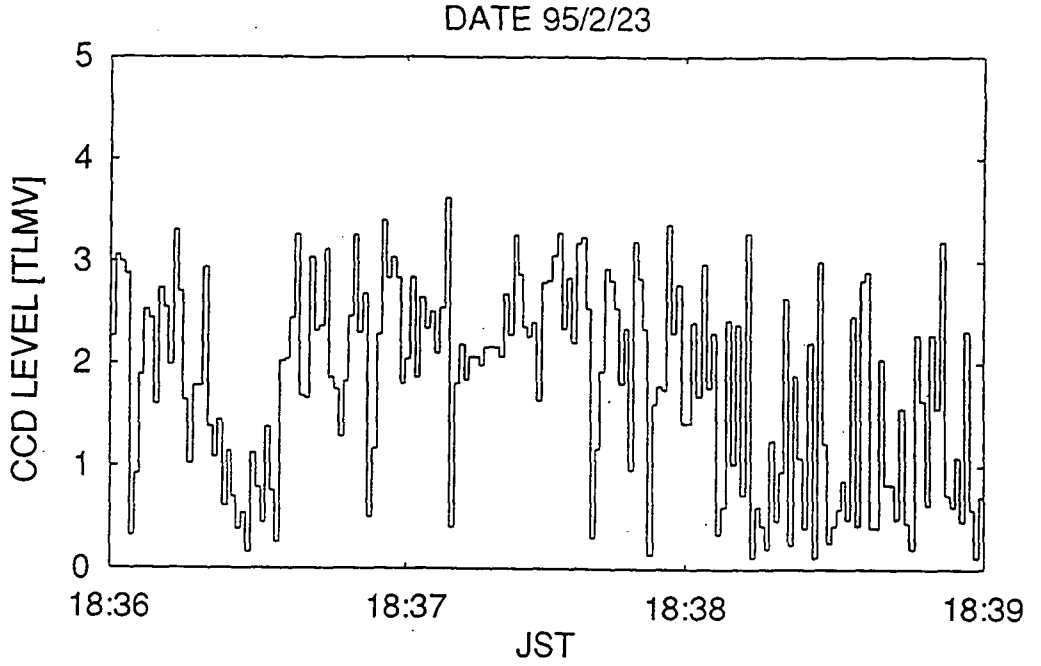

Receiving level of onboard fine tracking sensor (QD)

February 23, 1995

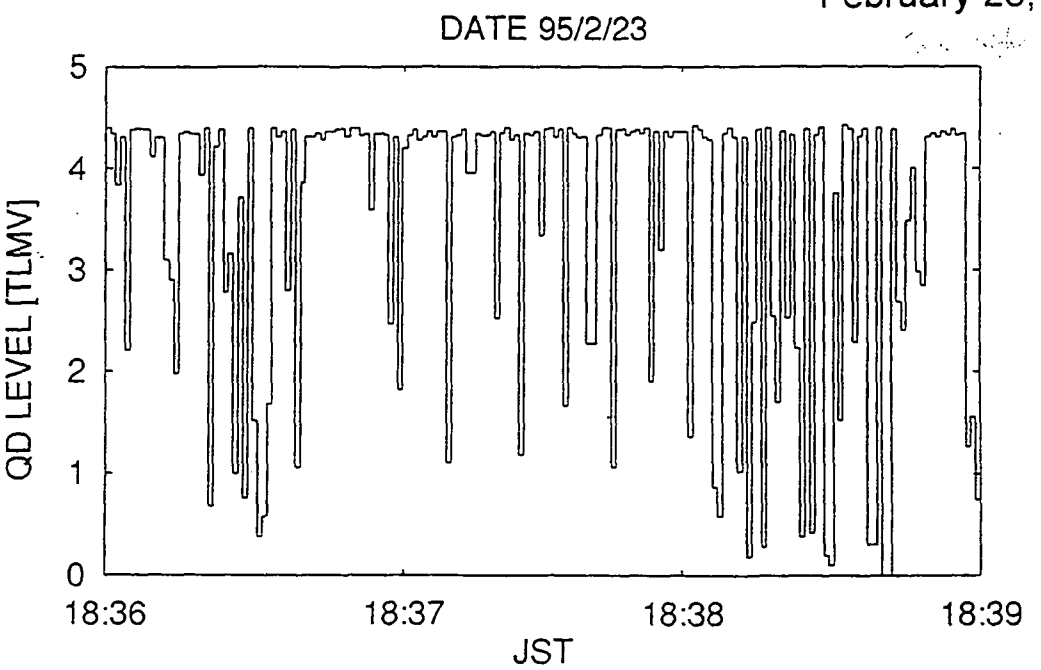

Cumulative probability of receiving laser power

January 15, 1995

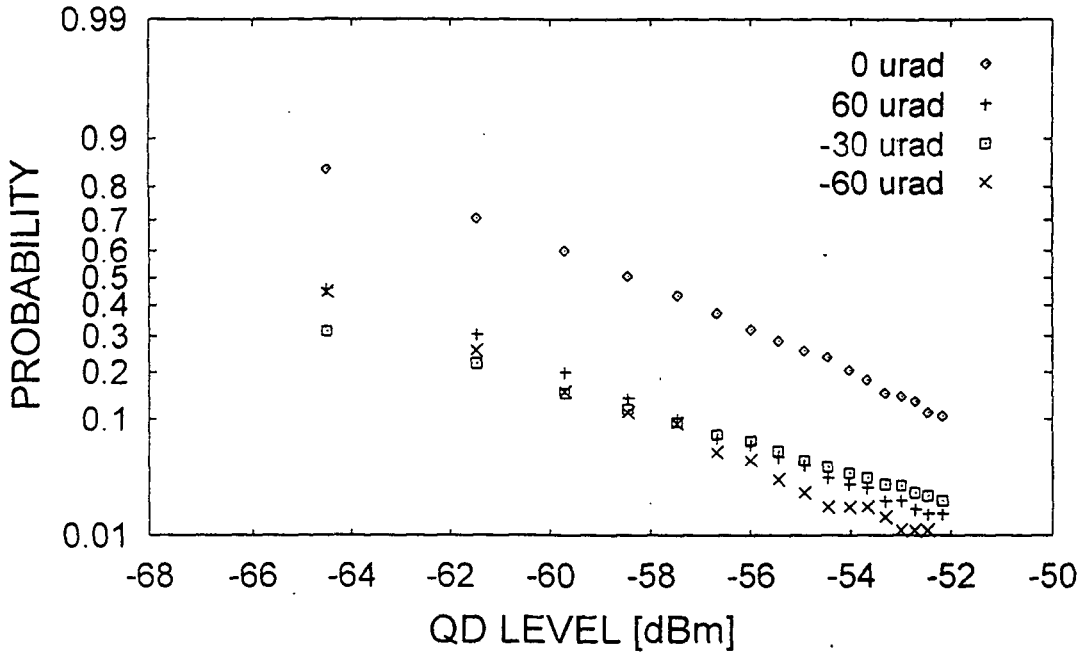

Cumulative probability of receiving laser power

March 1, 1995

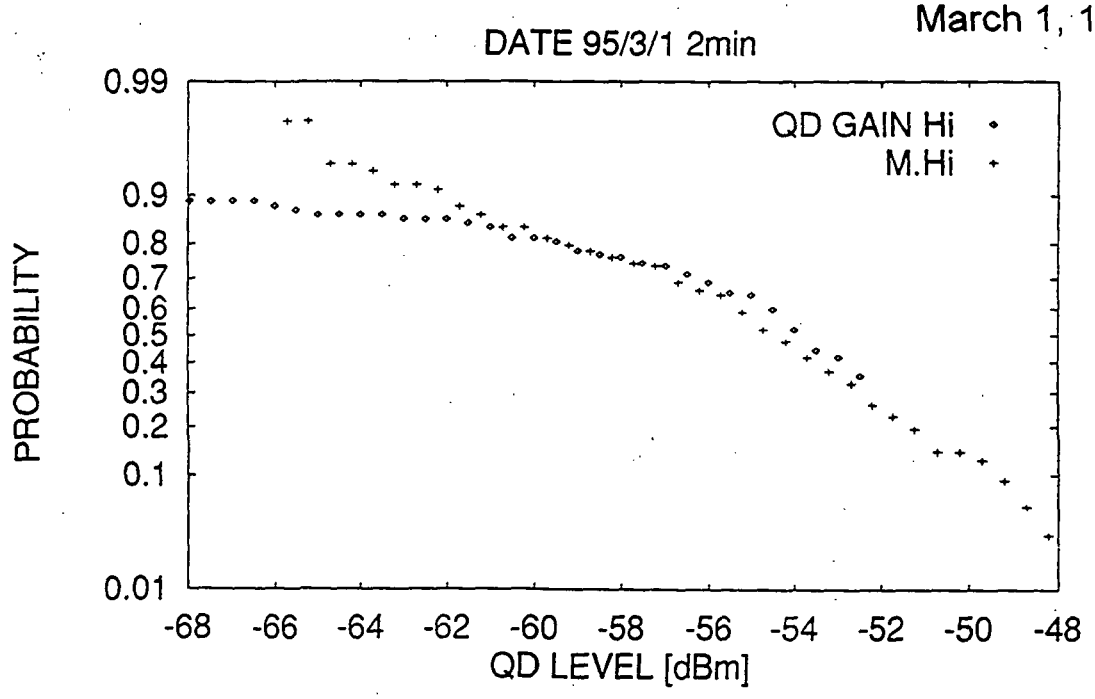

Application of Adaptive Optics for LaserCom

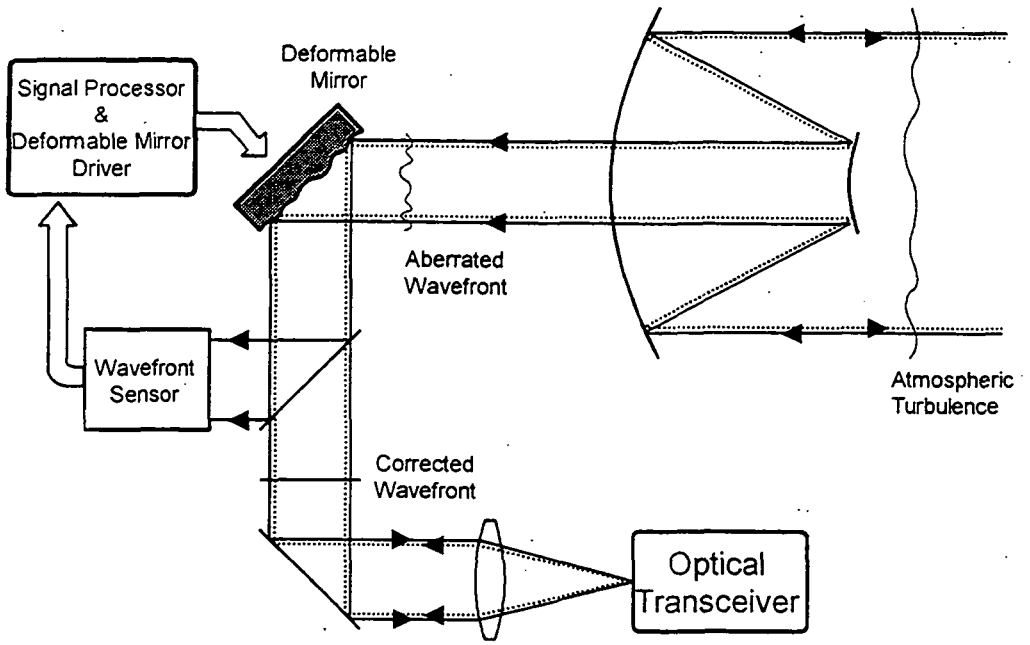

Conclusion

- All components and subsystem in the LCE are normal at present.
- LCE can be accessed from anywhere in the world if the satellite attitude can be maintained to point to the target ground station.
- There exist severe attenuation and scintillation in uplink laser light caused by atmospheric turbulences.

  and the variation of the scintillation gives good agreement with the log-normal distrobution.
- Adaptive optics will be able to decrease the severe attenuation (due to atmospheric turbulence) of up-link laser light in the ground-based laser communication experiment.

Earth-Space Propagation Research in Canada

D.V. Rogers and R.L. Olsen

Communications Research Centre

NAPEX XIX, Fort Collins, Colorado

14 June 1995

Communications Research Centre
Centre de recherches sur les communications

Propagation Impairments Affecting Satellite Communication Systems

Impairment	Physical Cause	Prime Importance
Signal attenuation, sky noise increases	Atmospheric gases, cloud, precipitation melting layer	Systems at f>10 GHz
Signal depolarization	Raindrops, ice crystals	Dual-polar systems at 6/4 and 14/11 GHz
Signal scintillations	Refractivity variations	Low-margin systems; low elevation angles; antenna tracking
Refraction, atmospheric multipath	Atmospheric gases	Systems operating at low elevation angles; antenna tracking
Reflection multipath, shadowing, blockage	Objects, vegetation on Earth's surface	Mobile-satellite services
Propagation delays & delay variations	Free-space, variations in troposphere	TDMA & position-location systems; adaptive control
Intersystem interference	Ducting, precipitation scatter, diffraction	6/4-GHz systems

ACTS Measurements in Canada

I. UBC, Vancouver / ACTS Propagation Terminal:
- Path elevation 29.4°, azimuth 150.4° CWN
- ITU-R Rain Climate D (maritime)

II. Teleglobe, Montréal:
- Site diversity (separation 93.6 km)
- Path elevation 31.5°, azimuth 214° CWN

III. CRC, Ottawa:
- Path elevation 32.2°, azimuth 212.4° CWN
- Radiometers at 12/20/29.5 GHz
- Possible communication experiments with RADC

Clear-Sky Link Budgets/Ottawa

	20.2 GHz	27.5 GHz
Beacon EIRP (dBW), nominal	16.6	15.1
Free-space Loss (dB)	- 210.2	- 212.9
Clear-sky Loss (dB), nominal	- 0.8	- 0.7
Polarization Loss (dB)	- 0.2	- 0.1
Earth Terminal Pointing Loss (dB)	- 0.2	- 0.4
Modulation Loss (dB), nominal	- 3.2	0.0
Earth Terminal G/T (dB/K), nominal	20.0	20.0
Received Power (dBW)	- 177.8	- 179.0
1/k (dB-Hz K/W)	228.6	228.6
C/N_0 (dB-Hz)	50.8	49.6
C/N in 65 Hz (dB)	32.7	31.5

Melting-Layer Attenuation Event

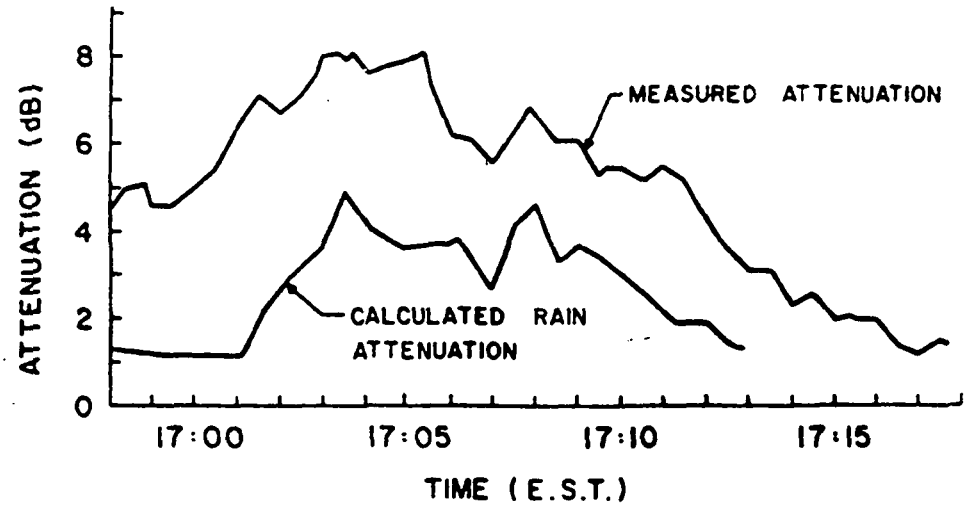

Measured at Ottawa using COMSTAR 28-GHz Beacon and 16.5-GHz Polarimetric Radar

Transmission Loss with and without Melting Layer

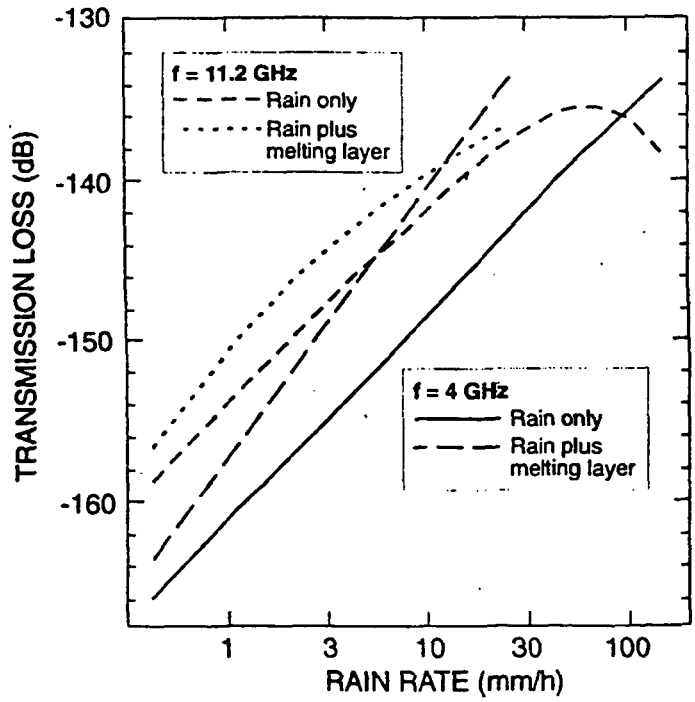

ITU-R Rain Zones

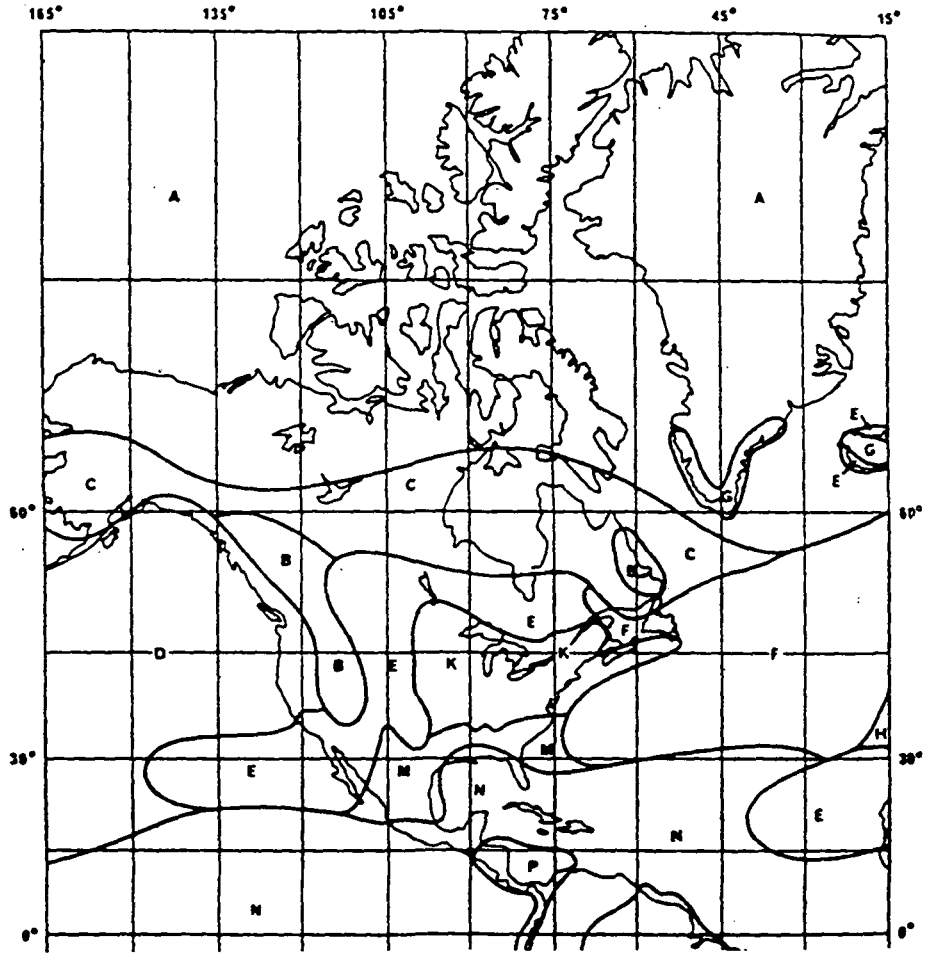

Climate Regions Based on 60-Minute Rainfall Observations

[Segal & Allnutt, 1991]

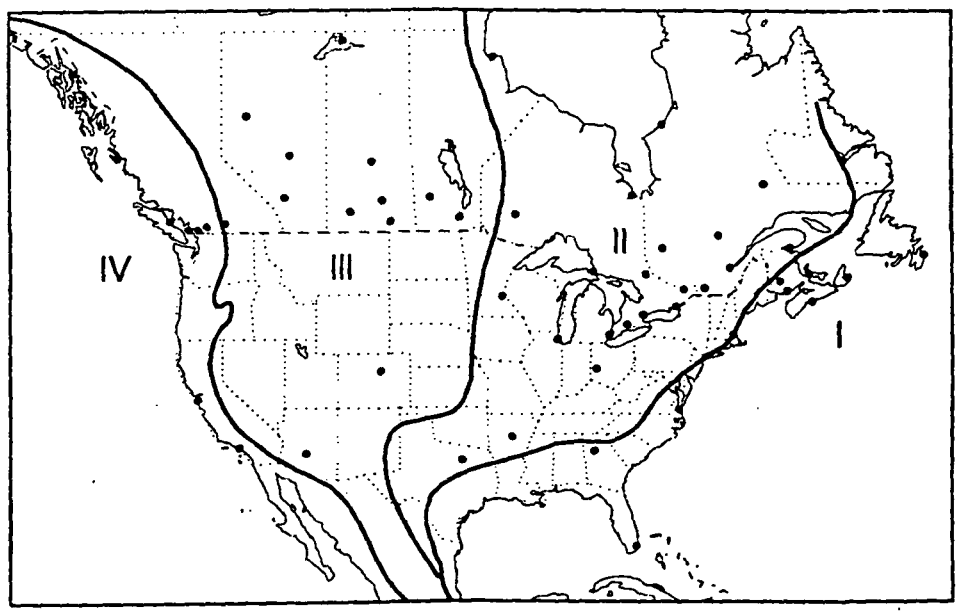

38-GHz Low-Angle Fade/Scintillation Data Measured at Alert, N.W.T.

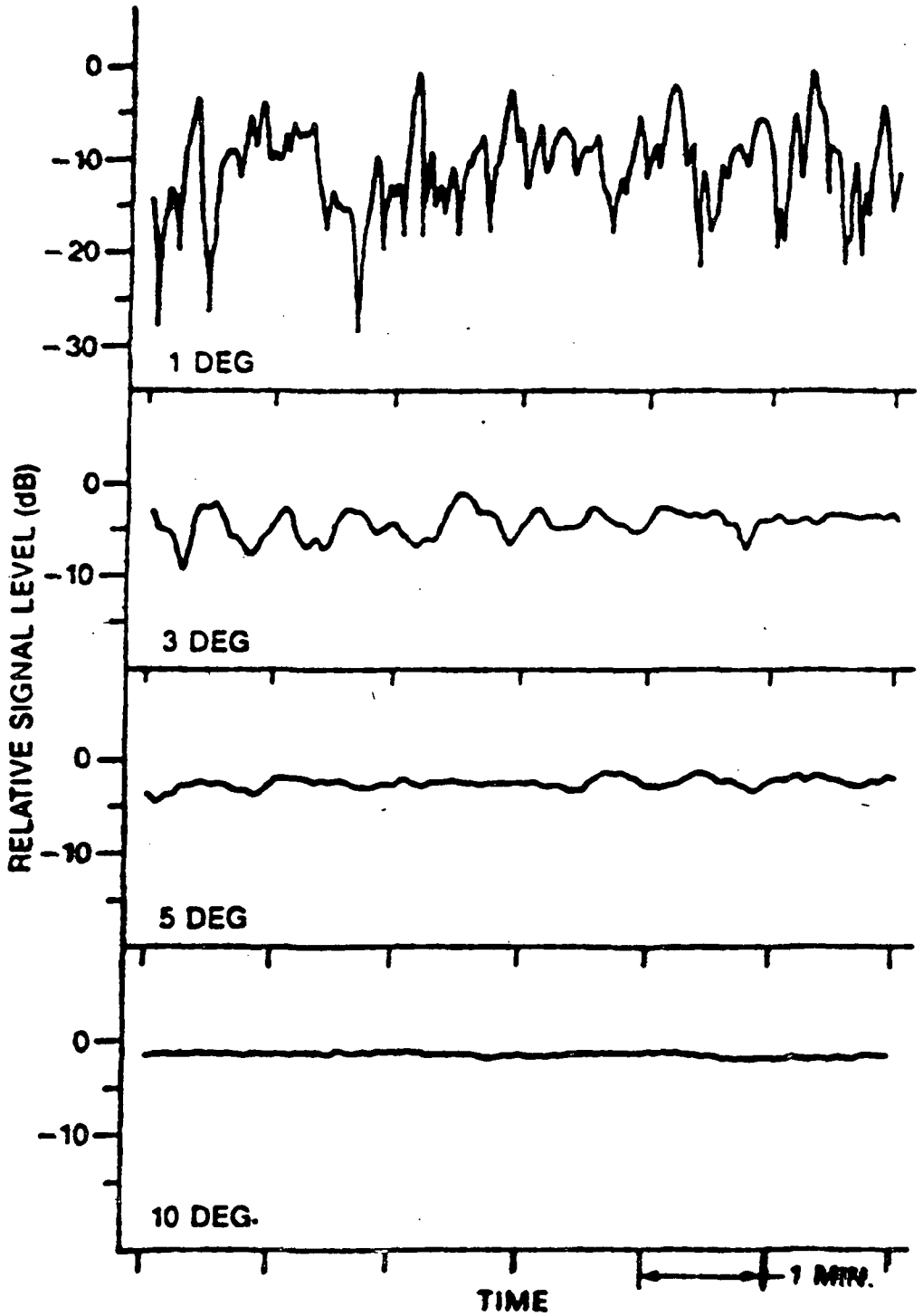

WORLDWIDE PROCEDURES FOR PREDICTING SCINTILLATION/MULTIPATH FADING DISTRIBUTION AT VERY LOW ANGLES (<5°)

- Fade depth A (>25 dB) exceeded for p % of the time in the average worst month:

$$A = G_W + 92 + 9 \log f - 55 \log(1+\varepsilon_o) - 10 \log p \quad \text{(dB)}$$

where $G_W = G_o + C_{Lat} + 15 \log p_L$

$$G_o = \begin{cases} -16 & \text{antenna height} \leq 700 \text{ m} \\ -22 & \text{antenna height} > 700 \text{ m} \\ -10 & \text{paths over water or adjacent coastal areas} \end{cases}$$

C_{Lat} = high latitude factor

p_L: Aug

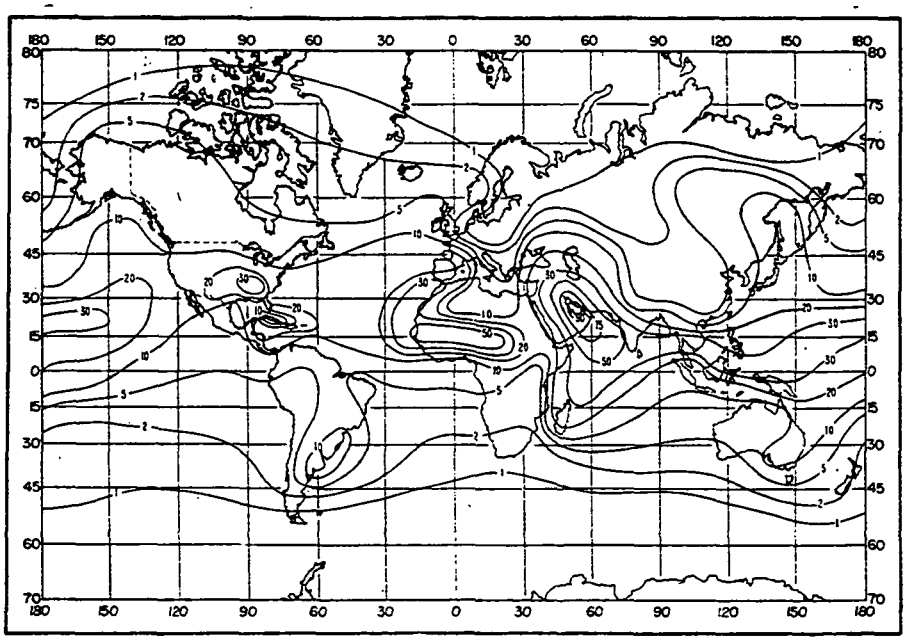

- Associated methods for shallow fading range (0-25 dB) and predictions in the average year

Communications Research Centre
Centre de recherches sur les communications

Low-Angle Fade Model Compared to Data

Comparison of model with average worst-month clear-air fading (3.2° elev. angle) Spitzbergen, Norway

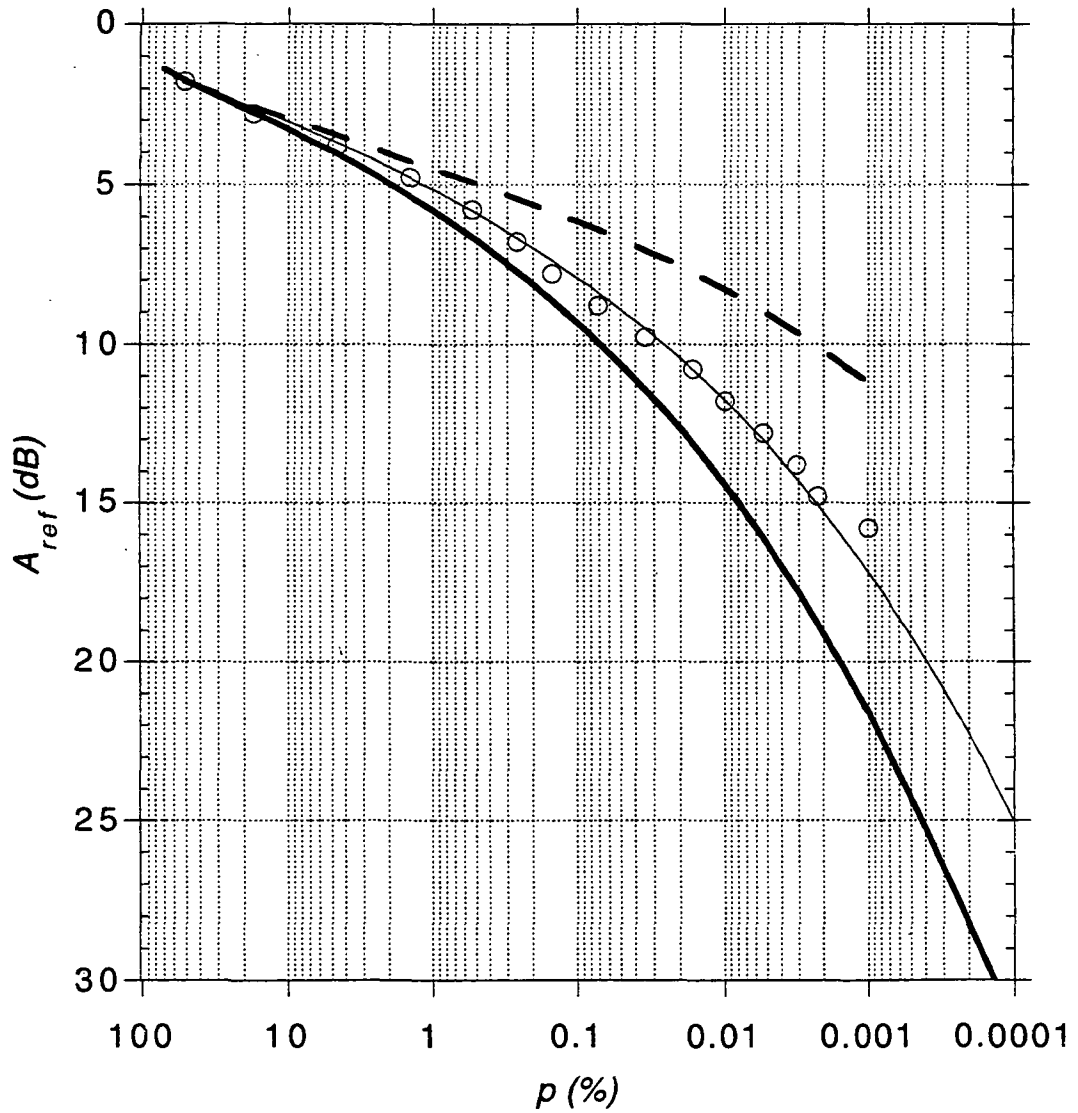

Circles: measured; Line: fit to measured data; Bold line: predicted; Dash line: predicted with extended ITU-R scintillation model

Extended Empirical Roadside Shadowing Model from ACTS Mobile Measurements

Julius Goldhirsh
The Johns Hopkins University, Applied Physics Laboratory
Johns Hopkins Road, Laurel MD 20723-6099

Wolfhard Vogel
The University of Texas at Austin, Electrical Engineering Research Laboratory
10100 Burnet Road, Austin, TX, 78758-4497

Abstract

Employing multiple data bases derived from land-mobile satellite measurements using the Advanced Communications Technology Satellite (ACTS) at 20 GHz, MARECS B-2 at 1.5 GHz, and helicopter measurements at 870 MHz and 1.5 GHz, the Empirical Road Side Shadowing Model (ERS) has been extended. The new model (Extended Empirical Roadside Shadowing Model, EERS) may now be employed at frequencies from UHF to 20 GHz, at elevation angles from 7° to 60° and at percentages from 1% to 80% (0 dB fade). The EERS distributions are validated against measured ones and fade deviations associated with the model are assessed. A model is also presented for estimating the effects of foliage (or non-foliage) on 20 GHz distributions, given distributions from deciduous trees devoid of leaves (or in full foliage).

1.0 Background

The Empirical Roadside Shadowing (ERS) is a formulation which describes the probability of exceeding Earth-satellite signal attenuation at frequencies between UHF (870 MHz) and S-Band (2.7 GHz) due to roadside trees for mobile scenarios [1,2]. This model was derived from systematic helicopter-mobile and satellite-mobile measurements over approximately 600 km of driving in central Maryland employing transmitters on helicopter and satellite platforms [2–4]. It corresponds to the median of a set of distributions (at fixed elevation angles) which describe roadside tree attenuation for highway and rural road scenarios with optical tree shadowing (at 45°) ranging between 55% to 75%; implying tree populations of at least this amount over the stretches driven. It corresponds to a worst case vehicle-satellite pointing aspect; namely, that in which the Earth-satellite path is orthogonal to the line of roadside trees. It also represents an overall average of various driving scenarios encompassing right and left lane driving, and opposite directions of travel along tree-lined highways and rural roads. In the acquisition of the data base, the dominant cause of attenuation was tree canopy shadowing where multipath fading played only a minimal role. The validity limitations of the model are enumerated as follows: (1) The probability range is from 1% to 20%. (2) The frequency interval is from 0.87 - 2.7 GHz. (3) The elevation

angle range is from 20°–60°. (4) The population of trees along the road is at least 55% of the distance driven. (5) The aspect of the Earth-satellite path is such that it cuts the line of roadside trees approximately orthogonal. An extended EERS model (EERS) is presented here which expands the first three of the above validity ranges as follows: (1) The probability interval ranges from 1% to 80%. (2) The frequency interval is from 0.87–20 GHz. (3) The path elevation angle ranges from 7° to 60°.

In deriving the EERS model, use was made of the original previously developed body of data at UHF and L-Band in central Maryland as well as more recently developed data bases. The more recent data bases correspond to mobile L-Band measurements of transmissions from MARECS B-2 in western United States [5], static K-Band measurements in Austin, Texas [6], and mobile K-Band measurements employing transmissions from the Advanced Communications Technology Satellite (ACTS) [7–9]. These latter measurements were performed during the first six months of 1994 during which a series of four 20 GHz mobile-ACTS campaigns were executed. The campaigns were performed in central Maryland (March, elevation = 39°), Austin, Texas (February and May, elevation = 55°), and Fairbanks, Alaska and environs (June, elevation = 8°) [7–9]. The mobile measurements in Austin, Texas during February and May enabled a determination of fading probability distributions for non-foliage and foliage conditions, respectively.

2.0 Review of Empirical Roadside Shadowing Model

The ERS model alluded to above, which also is a recommendation of the International Telecommunication Union, Radio Communication Study Groups (ITU-R) [10], is mathematically formulated as follows:

$$A(P,\theta) = -M(\theta)\ \ln P + N(\theta) \tag{1}$$

where

$$M(\theta) = a + b\,\theta + c\,\theta^2 \tag{2}$$

$$N(\theta) = d\,\theta + e \tag{3}$$

and where

$$\begin{aligned} a &= 3.44 \\ b &= 0.0975 \\ c &= -0.002 \\ d &= -0.443 \\ e &= 34.76 \end{aligned} \tag{4}$$

In (1), A(P,θ) is the L-Band (f = 1.5 GHz) fade (dB) exceeded at the percentage of driving distance P for an Earth-satellite elevation angle θ (deg). The fade is defined relative to non-shadowed and negligible multipath conditions. The equation had been previously validated in the elevation angle range between 20° to 60° over the percentage interval 1% to 20%.

Equation (1) had also been extended to include the frequency range between 870 MHz

(UHF) to 2.7 GHz (S-Band) employing the scaling relation

$$A(f_2) = A(f_L)\sqrt{\left(\frac{f_2}{f_L}\right)} \tag{5}$$

where $A(f_2)$ is the attenuation (dB) at a different frequency f_2 (GHz) valid between 0.87 to 2.7 GHz, $A(f_L)$ is the L-Band attenuation given by (1), and f_L is the L-Band frequency (1.5 GHz).

3.0 Extended Empirical Roadside Shadowing Model (EERS)

3.1 Extending ERS to Larger Percentages

In examining the original set of distributions at L-Band and UHF with the ERS model, it was found that the model may be conveniently extended to higher percentages employing a natural logarithmic fit which is continuous at the previously limiting 20% level and reaches 0 dB at P = 80%. That is, over the range of P from 20% to 80%, the model has been extended as follows:

$$A(P,\theta) = \frac{A(20°,\theta)}{\ln 4}\ln\left(\frac{80}{P}\right) \tag{6}$$

The rationale for selecting a logarithmic fit in the 20% to 80% range was based on the observation that most of the distributions similarly followed this variation. Furthermore, the distributions reached 0 dB fade in the 70% to 90% interval. Hence 80% was selected as the mid-level. Since the distributions coalesce in this interval, the exact value of probability (between 70% and 90%) at 0 dB fade plays an insignificant role. In employing the above fit, it was observed that the modeled distribution continued to maintain its median characteristic vis-a-vis the other measured distributions.

In Figures 1 through 4 are shown previously derived sets of distributions in central Maryland at 21° (MARECS B-2), and at 30°, 45°, and 60° (helicopter measurements) [2, 3]. These are compared with the extended ERS distribution (alternately referred to here as EERS model) at L-Band (thick solid curve) over the percentage range from 80% to 1%. We note that over the percentage range between 20% to 80%, the fade differences between the ERS model and the other distributions monotonically reduce, and the ERS distributions generally maintains its median characteristic. It should be emphasized that for the realm of percentages greater than 20% (fades < 3 dB), multipath effects play an important role.

3.2 Extending the ERS Model to 20 GHz

In Figure 5 are shown probability distributions derived from static measurements of attenuation due to the canopy of a Pecan tree in Austin, Texas at L-Band (1.6 GHz) and K-Band (20 GHz) [6]. In the determination of these distributions, measurements were made from a transmitter on a tower placed on one side of the tree canopy and a receiver was placed on the opposite side. The vertical scale in Figure 5 represents the percentage of locations for which the attenuation exceeds the abscissa value. In deriving these curves, the receiver was placed at different locations such that the transmitter-receiver path cut different parts

of the tree canopy, where at all receiver measurement aspects the tree optically shadowed the transmitter. An equal-probability frequency scaling function estimating the fade at the 10% probability at these two frequencies was developed given by

$$A(f_2) = A(f_1)\ \exp\left\{b \cdot \left[\frac{1}{f_1^{0.5}} - \frac{1}{f_2^{0.5}}\right]\right\} \tag{7}$$

where

$$b = 1.5 \tag{8}$$

and where $A(f_1)$ and $A(f_2)$ are the attenuations in dB at frequencies f_1 and f_2 (expressed in GHz). The above formulation shows a fade predictability for the static case (1.6 GHz to 19.6 GHz, and conversely) to within 0.2 dB at the 10% probability (see circled and triangular points in Figure 5).

We extend the ERS model to frequencies as high as K-Band (20 GHz) and as low as L-Band (1.6 GHz) employing (7) where

$$A(f_L) = A(f_2) \tag{9}$$

and where $A(f_L)$ is given by the left hand side of (1).

In Figure 6 is shown the K-Band distribution (elevation angle = 55° for a 10 km run along an evergreen tree-lined road in Bastrop, Texas. The Earth-satellite path generally cut the line of roadside trees on average at an angle of 57°. The population of trees were in excess of 55%, where there were considerable segments of road where the trees formed a tunnel of foliage overhead. Also shown plotted is the EERS model (dashed curve). We note that the EERS model underestimates the fade by at most 5 dB for probabilities between 1% and 20%. This deviation is within the variabilities expected in comparing the EERS model with measured distributions as exemplified in Figures 1–4 for the ERS model. The underestimation of the EERS model in Figure 6 at the smaller probabilities is caused by the prevalence of foliage tunnels giving a greater likelihood of fading at the higher elevation angles. Further validation examples related to extending the ERS model to 20 GHz is given in Section 3.4.

3.3 Extending the ERS Model to Low Elevation Angles

Extending ERS to elevation angles smaller than 20° is a complex task for the following reasons: (1) The ERS model tacitly assumes that the canopies of single tree shadows the Earth-satellite path. At lower angles, there is a greater likelihood that the path may cut the canopies of multiple trees or multiple tree trunks. (2) At smaller angles there is a greater likelihood that the terrain itself may block the Earth-satellite path creating high attenuation. (3) Ground multipath may be a factor. Based upon empirical experience for cases where the above caveats do not arise, it has been found that with good approximation, the ERS model at 20° elevation gives similar results to that at 7° or 8°. The rationale for this is that at 20° elevation the Earth-satellite path is already passing through the lower part of the tree canopies. Reducing the path elevation angle is likely to result in attenuation caused by tree

trunks which may tend to mitigate the path attenuation. On the other hand, attenuation effects may increase because of fading from those tree canopies which are further offset from the road (as was the case in Alaska). The combination of these two effects may result in the median fade statistics to be relatively invariant to angles below 20°, although larger deviations about the median are expected because of the breakdown of the aforementioned underlying assumptions.

In Figure 7 is shown an L-Band (1.5 GHz) cumulative fade distribution corresponding to a tree-lined road along an approximate 16 km stretch of road in Washington State (elevation angle = 7°), where the satellite path was orthogonal to the line of trees [5]. Also plotted (dashed curve) is the EERS model employing the assumption that the 20° fade is the same as that at 7°. The EERS distribution agrees with the measured distribution to within 2 dB for percentages smaller than 10% and larger than 50%, and is within 5 dB for the other percentage levels. The above deviations are comparable to those obtained when comparing the ERS model with L-Band distributions from multiple runs in central Maryland (Figures 1–4).

In Figure 8 are shown a set of K-Band distributions (elevation = 8°) derived from ACTS measurements in Alaska corresponding to different roads in which the Earth-satellite path was orthogonal to the line of roadside trees. Also shown is the EERS model. We note that the EERS model maintains its median characteristic, although the variability about the median is large. The low angle distributions are shown to vary considerably because of the reasons enumerated above, with the high probability fades caused by terrain blockage and multiple trees along the Earth-satellite path.

3.4 Validating the EERS Model in Central Maryland at K-Band

The difficulty in validating the EERS model in central Maryland employing the ACTS mobile measurements is that this data base was obtained during March when the deciduous trees were without foliage. A quasi-validation may however be made by converting a non-foliage run to a foliage case using a foliage conversion model described in the following paragraphs.

3.4.1 Modeling the Effects of Foliage at 20 GHz

In Figure 9 is shown a cumulative fade distribution (dashed curve) for an approximate 1 km segment of road driven in Austin, Texas during February when the trees (primarily Pecan trees) were devoid of leaves. Also shown is a distribution (solid curve) derived from a mobile run during May when the trees were in full foliage. The direction of travel for these run was approximately orthogonal to the satellite pointing direction, which represents a worst case fading situation. Furthermore, the optical blockage to the satellite during the full foliage period was estimated to be in excess of 55%.

Performing a least square fit associated with equal probability levels of the attenuations

for the two curves in Figure 9, the following relation was determined:

$$A(\text{Foliage}) = a + b \cdot A(\text{NoFoliage})^c \tag{10}$$

where

$$\begin{aligned} a &= 0.351 \\ b &= 6.8253 \\ c &= .5776 \end{aligned} \tag{11}$$

and where

$$1 \leq A(\text{NoFoliage}) \leq 15 \text{ dB} \tag{12}$$

and

$$8 \leq A(\text{Foliage}) \leq 32 \text{ dB} \tag{13}$$

Plots of the above mathematical fit at the equal probability levels show agreement to within 0.1 dB when compared to the measured distributions in Figure 9. Figure 10 represents an independent validation of the above foliage formulation. The solid curves represent the foliage and non-foliage static distributions at 19.6 GHz for the Pecan measurements alluded to previously relative to Figure 5. The dashed curves represent the predicted levels using the formulation given by (10). That is, the dashed curve on the right is the predicted level of A(Foliage) where equal probabilities of A(No Foliage) as given by the left solid curve was injected into (10). The left dashed curve represents the predicted levels of the A(No Foliage), where the measured levels of A(Foliage) as given by the right solid curve values were injected into (10). The formulation (10) generally produces agreement to within 1 dB or smaller over most of the probability range.

3.4.2 Comparison of EERS Model with K-Band Measurements in Central Maryland

In Figure 11 is shown a plot of a K-Band mobile measurements employing transmission from ACTS in March 1994 for Route 108 (traveling south-west). The solid curve to the left (with circled points) represents the actual measured distribution for the case in which the deciduous trees were without leaves. For this case, the satellite was on the left and the Earth-satellite path frequently cut the line of roadside trees at near orthogonal angles. Shown also is the right solid line distribution derived by applying the foliage formulation (10). This adjusted distribution thus represents a predictor of the full foliage case. Also shown is the EERS distribution at K-Band (dashed curve). We observe that the EERS distribution deviates from the adjusted measured distribution to within 5 dB and less.

The dot-dashed curve in Figure 11 was derived from previous L-Band helicopter measurements in June 1987 [3] employing the following procedures: (1) Distributions were examined which corresponded to the same scenario as for the K-Band measurements; namely, the vehicle was traveling in the southwest direction and the helicopter was on the left. (2) A resultant 39° distribution was derived by interpolating the 45° and the 30° distributions at L-Band. (3) The L-Band distribution was extended to K-Band employing (7). We note that relatively close agreement exists between the adjusted distribution (based on helicopter measurements), the adjusted ACTS distribution, and the EERS model.

4.0 Summary and Conclusions

A revised empirical roadside shadowing model has been derived which extends the previous ERS model such that it is now applicable to frequencies as high as 20 GHz and as low as 870 MHz. This model, now referred to as the extended empirical roadside shadowing model (EERS), may be applied to percentages from 1% to 80% and to elevation angles ranging from 7° to 60°. The model is representative of a median distribution of measured data which deviates from measured distributions generally to within ±5 dB at elevation angles above 20° (Figures 1–4, 6,7,11). At low elevation angles (Figure 8), terrain blockage and multiple tree attenuation may be prevalent and hence the deviation relative to the EERS model may be substantially larger.

To validate the EERS model in central Maryland, an empirical formulation was developed relating equal probability fades associated with distributions corresponding to foliage and non-foliage cases (equation (10)). This formulation was independently validated when applied to distributions for foliage and non-foliage scenarios associated with a Pecan tree employing static measurements at 20 GHz (Figure 10).

The EERS may be applied as follows: [1] We start with equation (1) which is the appropriate distribution model at L-Band in combination with (6), which extends the model from 20% to 80% over the elevation angle range between 20° and 60°. [2] To estimate distributions between the elevation angles of 7° and 20°, assume the value of A(P,θ) at 20°. [3] To extend the distribution to higher frequencies, apply the formulation (7), where $A(f_1) = A(f_L) = A(P,\theta)$, and where A(P,$\theta$) is given by (1). [4] To extend the L-Band distribution to lower frequencies (e.g., 870 MHz), greater accuracy may be achieved using (2) and the formulation (5).

5.0 Acknowledgements

This work was supported by NASA Lewis Research Center, Cleveland, Ohio and the NASA Propagation Program under Contract N00039-94-C-0001 for the Applied Physics Laboratory, The Johns Hopkins University, and contracts NAS3-26403 and JPL956520 for the Electrical Engineering Research Laboratory, The University of Texas at Austin.

6.0 References

[1] Goldhirsh, J. and W. J. Vogel, "Propagation Effects for Land Mobile Satellite Systems: Overview of Experimental and Modeling Results," *NASA Reference Publication 1274*, (Office of Management, Scientific and Technical Information Program), February, 1992.

[2] Vogel, W. J. and J. Goldhirsh, "Mobile Satellite System Propagation Measurements at L-Band Using MARECS-B2," *IEEE Trans. Antennas Propagat.*, Vol. AP-38, No. 2, February, 1990, pp. 259-264.

[3] Goldhirsh, J. and W. J. Vogel, "Mobile Satellite System Fade Statistics for Shadowing and Multipath from Roadside Trees at UHF and L-band," *IEEE Trans. Antennas Propagat.*, Vol. AP-37, No. 4, April, 1989, pp. 489-498.

[4] Vogel, W. J., J. Goldhirsh, and Y. Hase, "Land-Mobile-Satellite Fade Measurements in Australia," *AIAA Journal of Spacecraft and Rockets*, Vol. 29, No. 1, Jan-Feb, 1992, pp. 123–128.

[5] Vogel, W. J. and J. Goldhirsh, "Multipath Fading at L Band for Low Elevation Angle, Land Mobile Satellite Scenarios," *IEEE Journal on Selected Areas in Communications*, Vol. 13, No. 2, February, 1995, pp. 197–204.

[6] Vogel, W. J. and J. Goldhirsh, "Earth-Satellite Tree Attenuation at 20 GHz: Foliage Effects," *Electronics Letters*, Vol. 29, No. 18, 2nd September, 1993, pp. 1640–1641.

[7] Goldhirsh, J., W. J. Vogel, and G. W. Torrence "Mobile Propagation Measurements in the U.S. at 20 GHz Using ACTS," *International Conference on Antennas and Propagation (ICAP 95)*, Vol. 2, Conference Publication No. 407, Eindhoven, The Netherlands, 1995, pp. 381-386.

[8] Goldhirsh, J., W. J. Vogel, and G. W. Torrence, "ACTS Mobile Propagation Campaign," *Proceeding of the Eighteenth NASA Propagation Experimenters Meeting (NAPEX XVIII) and the Advanced Communications Technology Satellite (ACTS) Propagation Studies Miniworkshop*, Vancouver, British Columbia, June 16-17, (JPL Publication 94-19), 1994, pp. 135–150.

[9] Vogel, W. J., G. W. Torrence, and J. Goldhirsh, "ACTS 20 GHz Mobile Propagation Campaign in Alaska," *Presentations of the Sixth ACTS Propagation Studies Workshop (APSW VI)*, Sheraton Sand Key Resort, Clearwater Beach Florida, November 28-30, (JPL Publication JPL D-12350) 1994, April, 1989, pp. 283–294.

[10] International Telecommunication Union, Radio Communications Study Groups, "Propagation Data Required for the Design of Earth-Space Land Mobile Telecommunication Systems," *ITU-R Document 5/BL/42-E*, 15 March 1994.

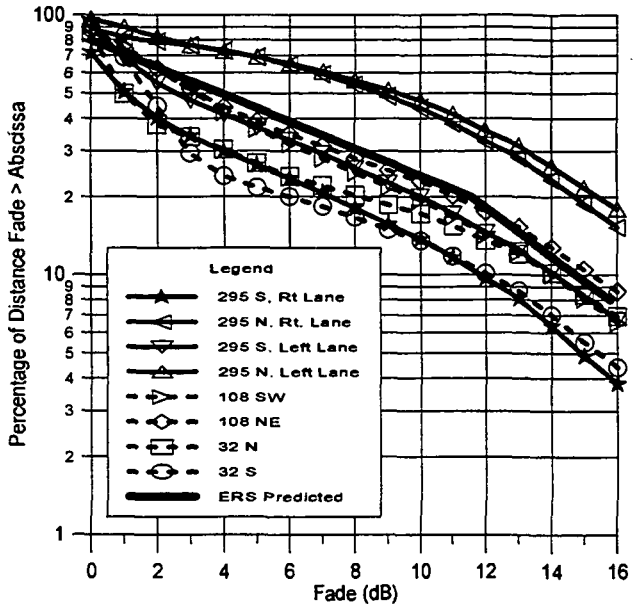

Figure 1: MARECS B2-mobile fade distributions at L-Band in central Maryland (elevation = 21.2°) and comparison with EERS model (thick solid curve).

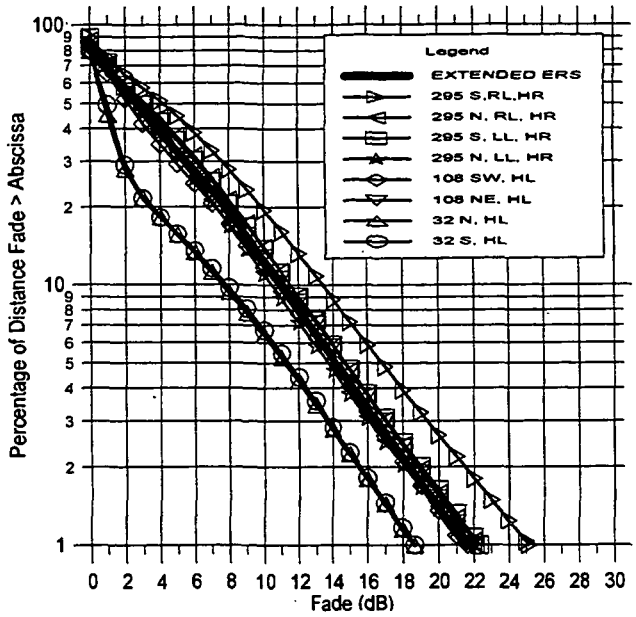

Figure 2: Helicopter-mobile fade distributions at L-Band in central Maryland (elevation = 30°) and comparison with EERS model (thick solid curve).

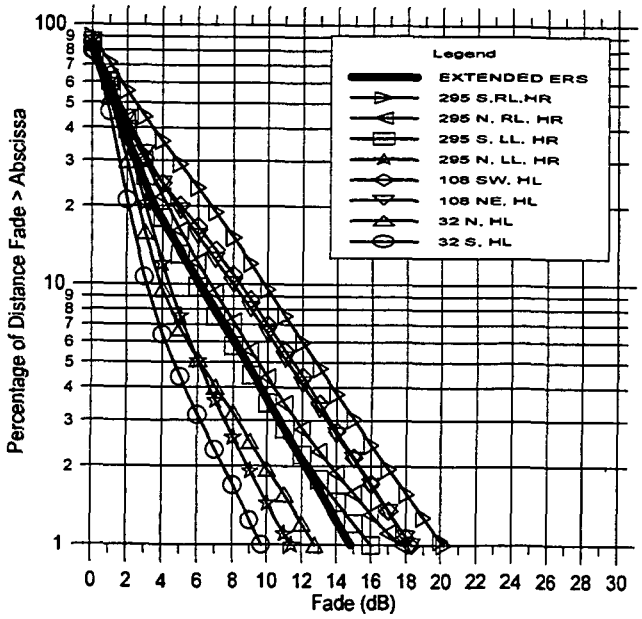

Figure 3: Helicopter-mobile fade distributions at L-Band in central Maryland (elevation = 45°) and comparison with EERS model (thick solid curve).

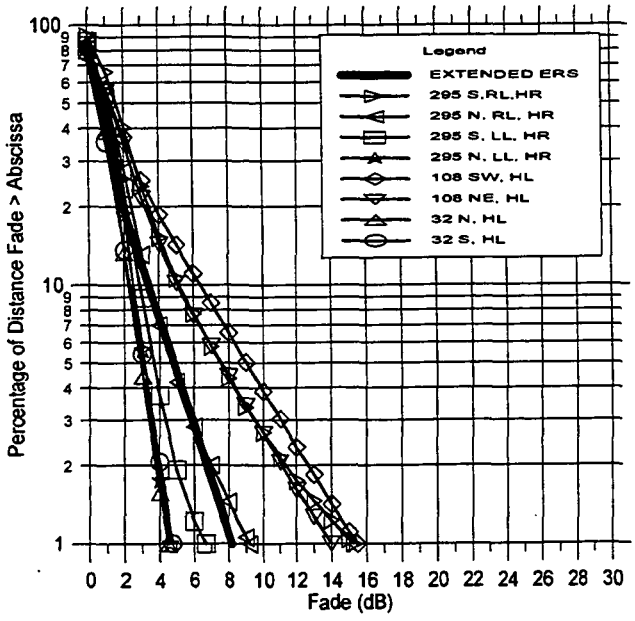

Figure 4: Helicopter-mobile fade distributions at L-Band in central Maryland (elevation = 60°) and comparison with EERS model (thick solid curve).

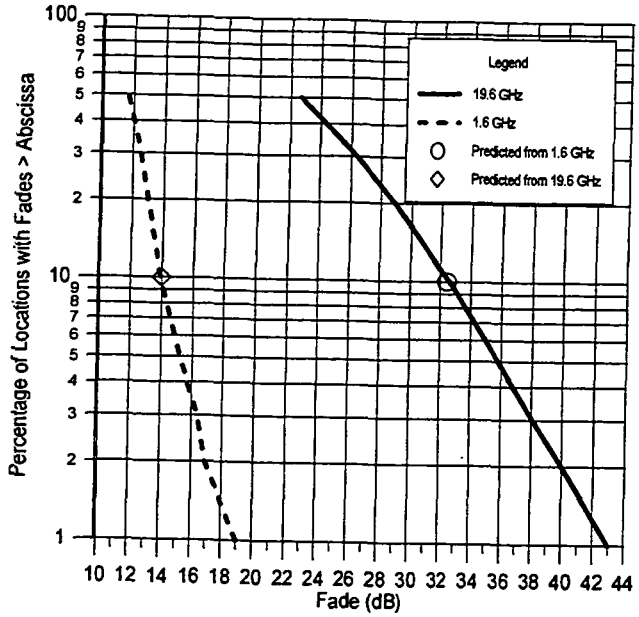

Figure 5: Fade distributions derived from static measurements of canopy attenuation of a Pecan tree at 19.6 and 1.6 GHz in Austin, Texas [6]. Circled and triangular points show prediction at the 10% probability using the formulation (7).

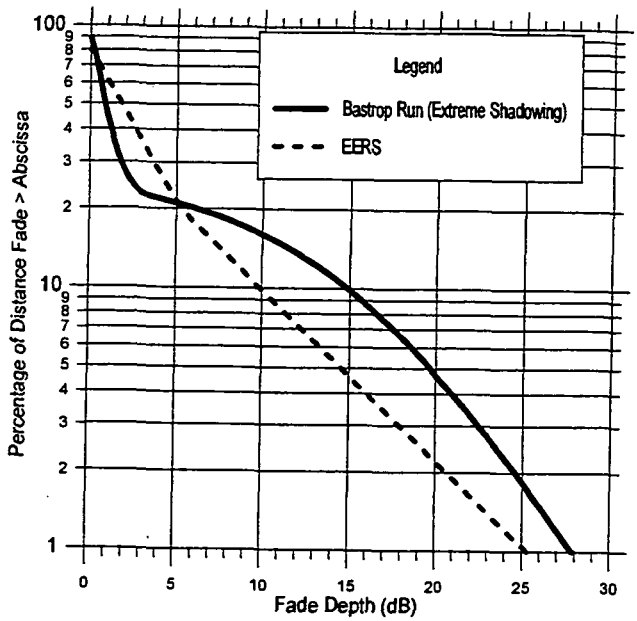

Figure 6: ACTS-mobile fade distribution at an elevation angle of 55° (solid curve) at 20 GHz for a 10 km tree-lined stretch of road in Bastrop, Maryland. Dashed curve is EERS predicted distribution.

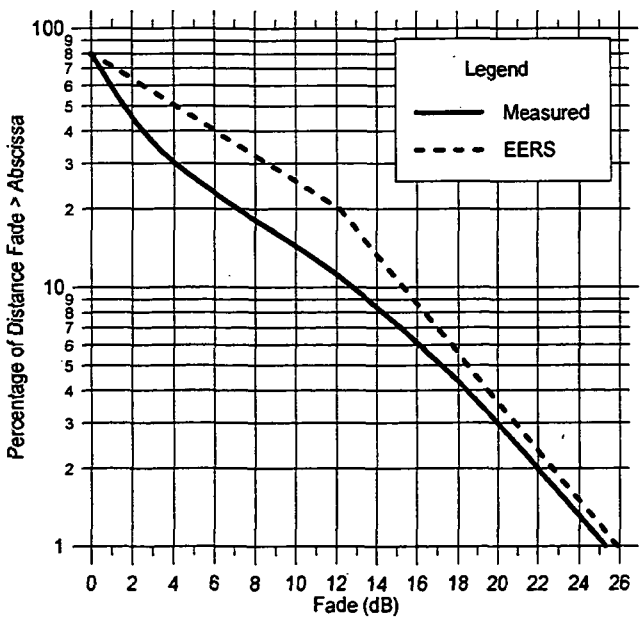

Figure 7: MARECS B2-mobile fade distribution at 1.5 GHz at elevation angle of 7° in Washington State over a 16 km tree-lined stretch (solid curve) [5]. Dashed curve is EERS predicted distribution.

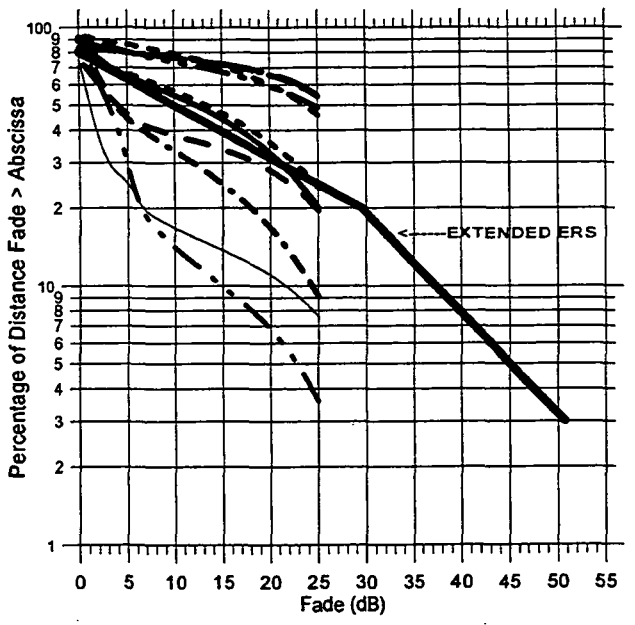

Figure 8: ACTS-mobile fade distributions in and around Fairbanks, Alaska (elevation angle = 8°) [7,9]. Thick sold curve is EERS predicted distribution.

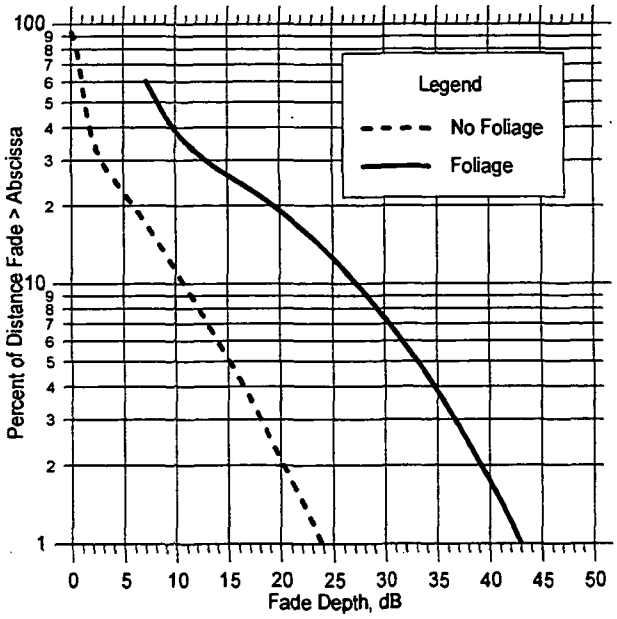

Figure 9: ACTS-mobile fade distributions at 20 GHz (elevation angle = 55°) in Austin, Texas with foliage (solid curve) and without foliage (dashed curve) for a 1 km stretch of a tree lined street.

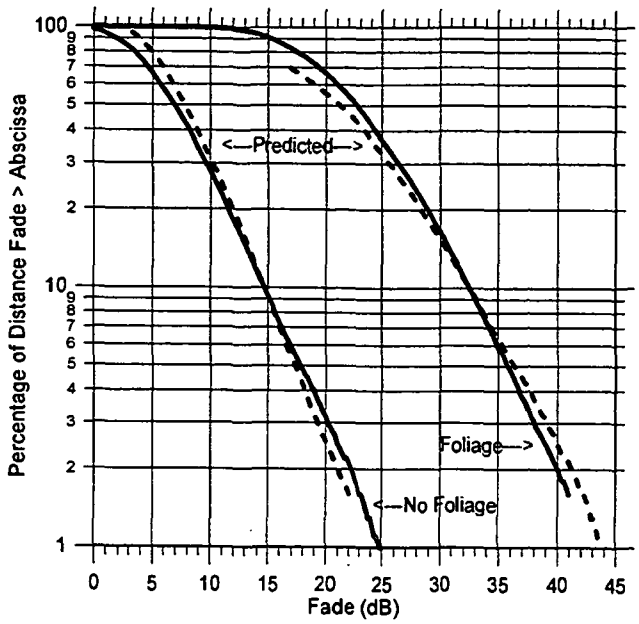

Figure 10: Fade distributions at 19.6 GHz derived from static measurements of a Pecan tree in Austin, Texas for foliage (right solid curve) and non-foliage (left solid curve) scenarios. Dashed curves are predicted distributions using the formulation (10).

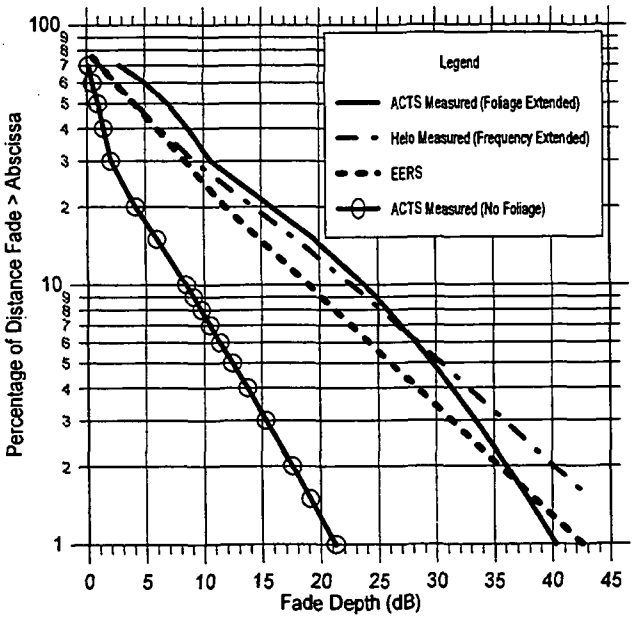

Figure 11: [1] The left solid curve with circled points represents the 20 GHz ACTS-mobile fade distributions for Route 108 (traveling S-W) during period in which trees were without leaves. [2] The right solid curve is the corresponding distribution when adjusted for foliage using (10). [3] The dot-dashed curve is the 20 GHz distribution obtained by frequency extending the helicopter L-Band distribution using (7). [4] The dashed curve is the predicted EERS distribution.

Effect of Attenuation Models on Communication System Design

F. I. Shimabukuro
The Aerospace Corporation

Introduction

The atmosphere has a significant impact on the design of a global communication system operating at 20 GHz. The system under consideration has a total atmospheric link attenuation budget that is less than 6 dB. For this relatively small link margin, rain, cloud, and molecular attenuation have to be taken into account. For an assessment of system performance on a global basis, attenuation models are utilized. There is concern whether current models can adequately describe the atmospheric effects such that a system planner can properly allocate his resources for superior overall system performance. The atmospheric attenuation as predicted by models will be examined.

Rain effects

To assess the impact of rain on overall system performance rain attenuation models are utilized. Figure 1 shows the predicted exceedance attenuation for two rain models, the CCIR and the Global at mid latitudes. For comparison similar rain regions, the K region for the CCIR model, and the D2 region for the Global are used. For the assumptions shown for the ground terminal, 40 degrees latitude, sea level, 30 degrees elevation, using circular polarization, there is reasonable agreement between the models. There is about a 1 dB difference at the 2 per cent level. The correspondence is not surprising, because these models have been tailored to fit the same available attenuation measurements, for which there is an ample data base for this climate region.

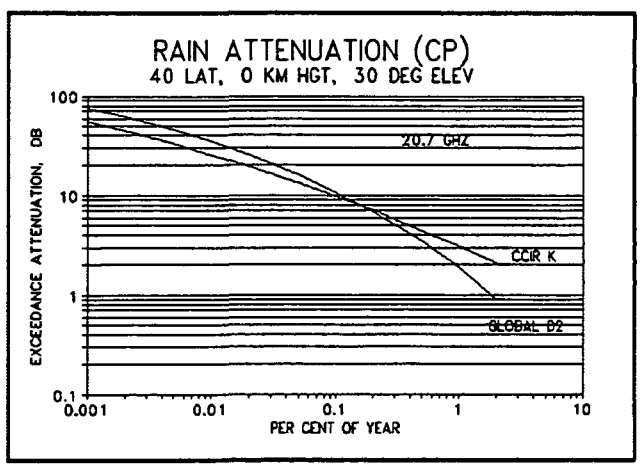

Fig. 1. Rain attenuation for CCIR K and Global D2 regions.

At 20 GHz, system performance would be most degraded by rain in tropical regions. In Fig. 2, exceedance attenuations are shown for the CCIR P and Global H climate regions. In this case we see a large discrepancy in the predictions. For example, for the assumed conditions here, there is a 30 dB difference at the 0.1 % level, and a 13 dB difference at the 0.5 % level. And these differences widen further at lower elevation angles. There are indications that even the CCIR model may overestimate the rain attenuation in tropical zones. The designer might feel a bit uneasy in planning for system operation in the tropical rain regions. Clearly, more rain data is needed in these areas. The NAPEX and ACTS programs will resolve some of these issues, but it would be more comforting if at least one of the ACTS terminals were in the tropics. In addition to the annual rain statistics the system planner is also interested in performance in the "worst" month. Suppose the rain margin is 4 dB. For region H, at an elevation angle of 30 degrees, the Global model predicts a link availability of 97.2 per cent. In the worst month, using the "average" CCIR Q value, the link availability decreases to 93 per cent. It is not clear how the Q statistics vary for different global regions, and these data would greatly benefit system planning.

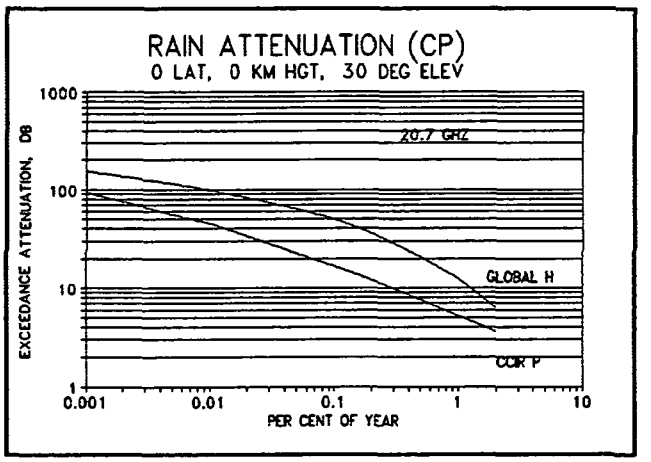

Fig. 2. Rain Attenuation for CCIR P and Global H regions.

Clear Air and Cloud Effects

Cloud effects cannot be adequately modeled at the present time, but suffice it to say, clouds will reduce the link availability. In Table 1 the molecular attenuation for a tropical and a mid-latitude (July) atmospheric model at elevation angles of 10 and 20 degrees. For the same models it is assumed that the relative humidity is 80 % when it is raining. We see that for a link margin of 5 dB, when it is raining, about to rain, or extremely hot and humid, the molecular attenuation can be sufficiently large to make the link unavailable. This is may be a more important factor at mid-latitudes than in the tropics for a global system, since the elevation angles will be smaller. A system planner would like to incorporate a global non-precipitating attenuation model, which would give

global statistics of molecular and cloud attenuation, in his planning. The ACTS program will give some input to this need but unfortunately the information is not available today.

Table 1.
20 GHz Clear Air Attenuation

Atm. Model	Temp. (Surf) Kelvin	RH (Surf) Per cent	Attenuation (dB) 10 deg. elev.	Attenuation (dB) 20 deg. elev.
Tropical	300	75	4.3	2.2
Mid-Lat (July)	294	75	3.3	1.7

Table 2.
20 GHz Clear Air Attenuation (Raining)

Atm. Model	Temp. (Surf) Kelvin	RH (Surf) Per cent	Attenuation (dB) 10 deg. elev.	Attenuation (dB) 20 deg. elev.
Tropical	300	80	6.3	3.2
Mid-Lat (July)	294	80	5.5	2.8

To summarize, more attenuation data is needed for the proper design a global communication system, with small link margins, operating at 20 GHz. In particular, rain data in tropic regions and a global non-precipitating attenuation model are needed.

N96-10452

Propagation Issues in the Globalstar System

Toby Prescott - Qualcomm, Inc.

Introduction

The purpose of the Globalstar system is to provide reliable, timely space based telecommunications services for fixed, handheld and mobile user telephones throughout the world. The system supports communication services for voice and data as well as low rate data services such as paging. The Globalstar system can also support user position determination. The purpose of this paper is to provide a brief introduction to the Globalstar system followed by a discussion of the propagation issues in the Globalstar system design.

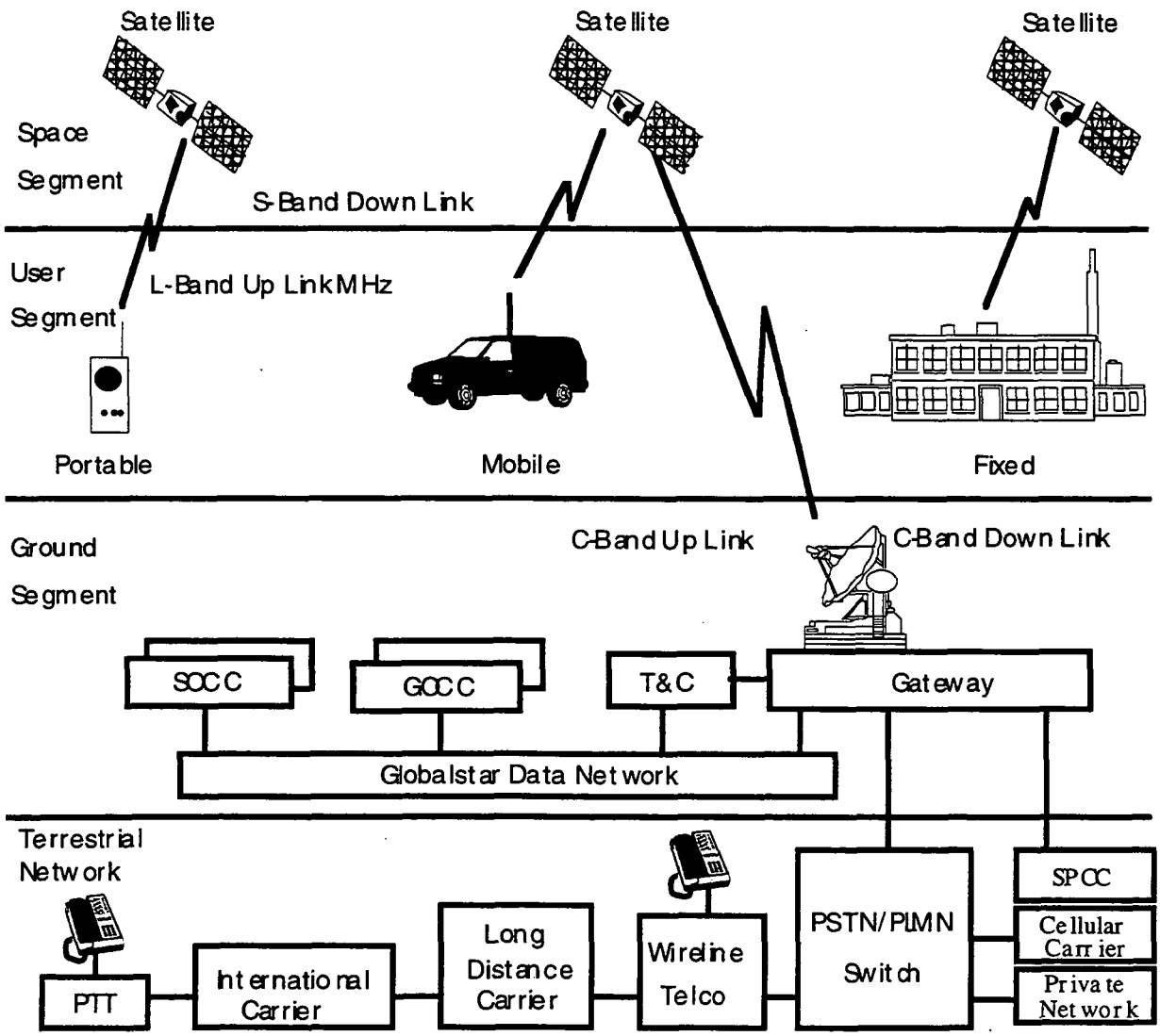

Figure 1 Globalstar System Integrates with Terrestrial Network

Globalstar System Overview

The Globalstar system consists of a space segment, a user segment, a ground segment, and a terrestrial network as shown in figure 1.

The Globalstar system provides communications from any point on the earth's surface to any other point on the earth's surface, exclusive of the polar regions. The Globalstar space segment consists of 48 satellites in 1410 km Low Earth Orbits. The low earth orbits permit low power handheld telephones to be used similar to the cellular telephones. These satellites are distributed in 8 orbital planes with 6 equally spaced satellites per orbital plane. User telephones are illuminated by the satellite antenna as it passes over the earth as shown by the antenna footprints in figure 2.

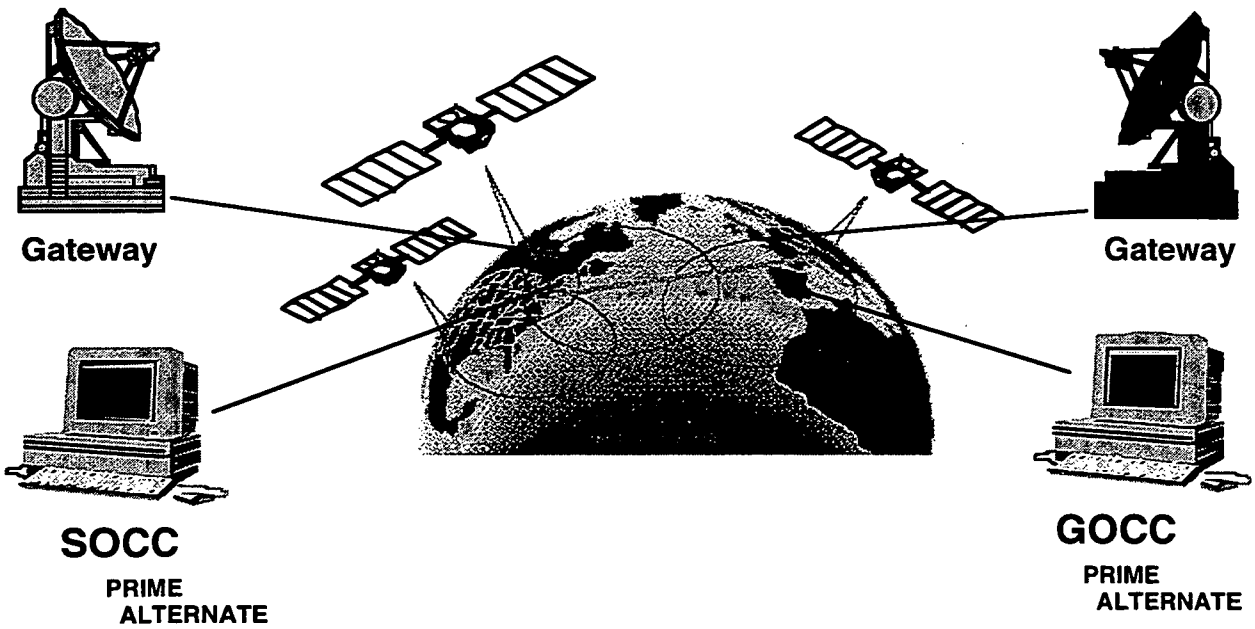

Figure 2 Ground Segment Accommodates Home Country Gateways

User telephones can be served by a satellite for up to 15 minutes per orbit. The inclined orbital planes provide full earth coverage with multiple satellites in view, providing space diversity, for a large percentage of time. Since the satellites are moving, the user is continuously being illuminated by different satellite beams and different satellites. Diversity combining within the receivers and Gateways supports a process of transferring traffic that is completely transparent to the user. The diversity combining process also

provides better call reliability. Normally a user is covered by more than one satellite. If the user moves into an area that shadows or blocks access to one satellite, the space diversity link through a satellite that is not blocked maintains uninterrupted user communications.

Gateways are illuminated by an earth coverage beam. The Gateway connects the user telephone to the terrestrial network through an earth terminal that acts as the gateway between the Globalstar system and the terrestrial network.

User Telephone Equipment

The user telephones come in several varieties - hand held units, mobile units and fixed station units. The candidate user telephones are listed in table 1.

Table 1 Pre-Production User Telephones

Fixed Terminal	*Mobile and Hand Held*
Globalstar Only	Globalstar Only
	Dual Mode Globalstar & GSM
	Tri Mode Globalstar & Terrestrial CDMA & AMPS

Hand Held. The radiating element of the antenna is positioned above the head of the user. The antenna is positioned vertically to effectively utilize the symmetrical radiation pattern of the hand held antenna.

Mobile. The mobile units consist of a hand held unit inserted in an adapter in the vehicle. The mobile units typically have a higher gain antenna, a lower noise receiver, and a higher RF power output that is provided by the adapter kit.

Fixed. Fixed station terminals are Globalstar only. The fixed user terminals have multiple antennas pointed at different portions of the sky. Each antenna element has higher gain than mobile or hand held units and one antenna is used at a time. This permits lower satellite power in the forward direction and lower interference in the reverse direction.

Gateway

The Gateways are geographically distributed by the service providers to serve their customer base. Gateways are designed for unmanned operation. The Gateway consists of up to four identical parabolic dish antennas, drive mechanisms for positioning the antenna, the Code Division Multiple Access (CDMA) equipment, PSTN interface equipment that interfaces with the terrestrial telephone network and computer equipment to operate the Gateway and collect status and performance data.

The Gateway connects the Globalstar space segment to terrestrial switching equipment. The Gateway receives telephone calls from the terrestrial switching equipment and generates Code Division Multiple Access (CDMA) carriers to transmit through the satellite. The satellite then re-transmits the signal to the user telephones. These user telephones may be either hand held, fixed or mobile and located anywhere within the satellite antenna footprint.

In the return direction, the Gateway receives transmissions from any user telephone and connects the call to terrestrial switching equipment that can then connect to any subscriber using the standard telephone system. Connections can also be made to terrestrial cellular subscribers or to other Globalstar user telephones.

Globalstar Satellite

The Globalstar satellite is a simple low cost satellite designed to minimize both satellite costs and launch costs. A pictorial of the satellite and some of the major characteristics are shown in figure 3.

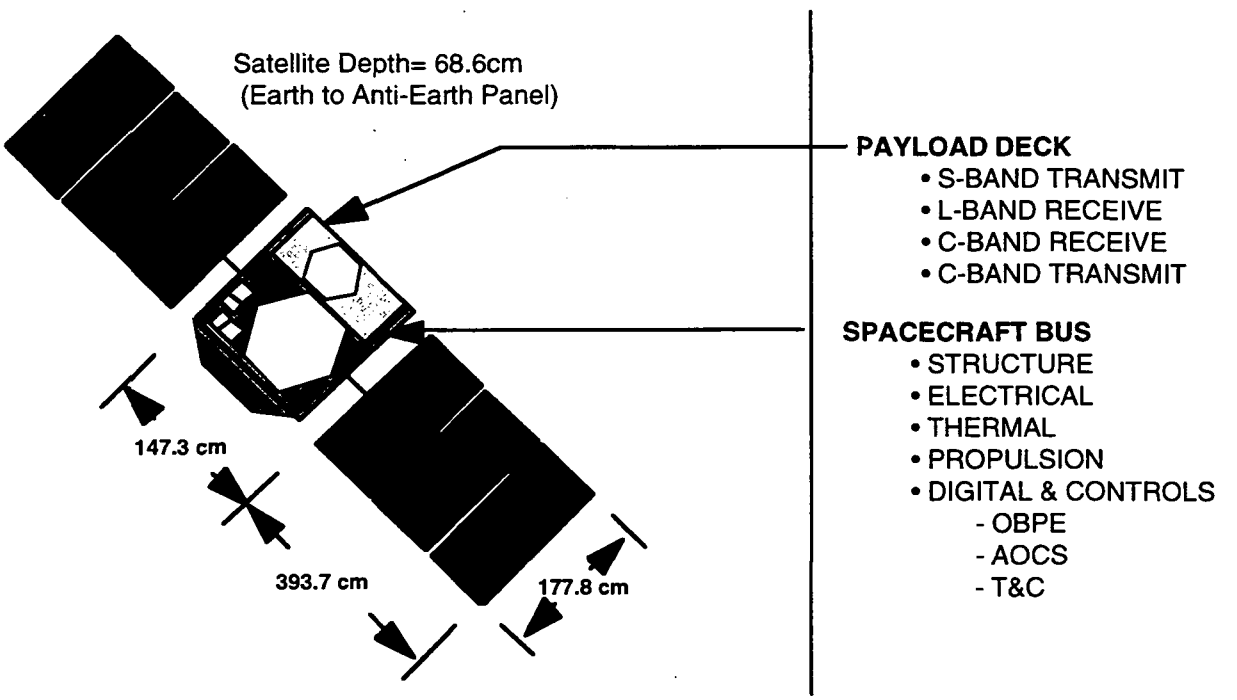

Figure 3 Globalstar Satellite Pictorial - Simple Satellite

A user telephone transmits to the satellite by L-Band. The signal enters the satellite through the L-Band low noise amplifier. It is amplified and then converted into a C-Band signal. This is radiated to the Gateway. The Gateway receives the signal and downconverts to an intermediate frequency. The communications traffic is presented to the CDMA equipment for demodulation.

In the transmit direction, the Gateway combines the up link CDMA signals with the signal from the command transmitter and radiates it at C-Band up to the satellite. The satellite then downconverts the signal and radiates an S-Band down link signal to the user telephones.

Ground Operations Control Center/Satellite Operations Control Center

Ground Operations Control Center is responsible for planning and management of the communications resources of the Globalstar satellite constellation. This is coordinated with the Satellite Operations Control Center that manages the satellites, controls the orbits and provides Telemetry and Command services for the satellite constellation.

Channel Propagation Considerations

The channel propagation modeling is of paramount importance in developing a communication system for both performance prediction and system design. For the terrestrial cellular telephone system, the propagation channel has been well studied. However, in the Globalstar environment further work is required to develop a comprehensive model. For the terrestrial system, typically the user equipment does not receive a direct line of sight signal component. Instead, the signal is composed of the reflections from many diffuse scatterers. In terrestrial CDMA, we employ a Rake receiver design to combine energies from different paths to offset some of the signal fading. For the Globalstar system, the typical scenario will enable the user telephone to maintain a direct line of sight component with the satellites in view. For the Globalstar system located in rural locations, most of the obstructions of the direct line of sight component will be due to vegetative shadowing that does not completely block the direct line of sight component, but rather simply attenuates it. Therefore, the Globalstar channel is significantly better than the terrestrial channel from a signal fading perspective.

Significant improvement in channel propagation comes from the use of continuous multiple satellite diversity employed in the design of the Globalstar system. The use of satellite diversity will help mitigate signal fading and greatly reduce the power requirements to originate and maintain calls relative to operations with a single satellite. Given two satellites in view at the same time, the probability of signal blockage or shadowing to both satellites is

significantly less than the probability of blockage to a single satellite.

Another difference with terrestrial system is vastly different forward and reverse link frequencies. The correlation between signal fades on the forward and reverse link frequencies will be used in developing strategies for power control. One of the major problems associated with the land mobile satellite channel is the long delays associated with the transit times to and from the Gateways through the satellite. This satellite link delay is tens of milliseconds long compared to less than a couple of milliseconds in the terrestrial case.

Signal Components

The signal received at a user phone is composed of three components: direct line-of-sight, specular reflection and diffuse reflection. The diffuse component is composed of a sum of a large number of individual terrain scatterers from outside the first Fresnel zone of the vehicle. This diffuse component is characterized by phase incoherent multipath with a uniform phase distribution and a Rayleigh amplitude distribution (hence known as Rayleigh fading). The signal fading associated with the diffuse component combining with the direct component produces the fast-fading characteristics of the propagation channel.

The direct signal component is subject to shadowing by obstacles in the local environment such as trees and buildings. This form of fading has fade rates that are significantly less than the Rayleigh component and is primarily due to the motion of the mobile unit with respect to the geometry of the object causing the shadowing. In the presence of vegetative shadowing, a direct line-of-sight signal is subject to attenuation by the surrounding vegetation. The direct line-of-sight signal has an amplitude characteristic that can best be described as being log-normally distributed [2]. This direct line-of-sight signal combined with the Rayleigh distributed multipath signal from the diffuse scatterers provides a composite Rician distribution with a line of sight signal amplitude variability defined by the log normal distribution.

In the case of travel through a city, the most significant characterization is the percentage of time the direct signal path is blocked due to the geometry of the local buildings with respect to the signal line-of-sight. It has been found that the description of the distribution function during times of direct line-of-sight signal blockage is best described by a Rayleigh distribution whose mean received power is described by a log-normal distributed variable. In instances where there is no signal blockage, the distribution is best described by a Rician distribution.

Channel Modeling

Given the limited satellite resources, estimation of system performance is critically dependent upon the signal propagation losses. The purpose of the channel modeling activity is to

accurately characterize the signal propagation from (or to) the satellite when communicating with a GS telephone user. Signal propagation characteristics are strongly dependent on the environment surrounding the user telephone such as the height and density of vegetation, the location of man made structures, nearby hills, etc. Therefore, the signal characterization must account for the type of terrain one expects to encounter and the location of objects in the environment that impede the direct line of sight between the satellite and user telephone.

At different locations and terrain types, we are concerned with determining the following signal characterizations for each of the states identified above:

1. The signal fade power probability distribution functions,
2. Characterization of the modeling parameters of the magnitude function for the direct line of sight component and the diffuse component
3. Temporal characterization of the diffuse signal component
4. Average fade and non-fade durations
5. Probability distributions of fade (and non fade) durations below (above) a series of signal thresholds
6. Time delay spread
7. Cross correlation of signal magnitude functions between L-band and S-band signals

This signal characterization at each location is dependent upon the geometry between the satellite and the user telephone (primarily satellite elevation angle and the line of sight vector between the satellite and the user telephone), motion of the user telephone, and the user telephone antenna characteristics.

Characterization of the environments to be encountered is also a big factor to be considered. This characterization involves determining the percentage of time one would anticipate encountering the various terrain types in a given locale.

System Design Considerations

The sections below provide an overview of some of the design issues in the Globalstar system with channel propagation considerations.

Power Control

To achieve the high capacity, quality and other benefits inherent in the CDMA waveform design, the Globalstar system will employ power control on both the forward link (Gateway to user telephone) and reverse link (user telephone to Gateway) communications. On the reverse link, the objective of the power control process is to produce the same nominal received signal power from each transmitting user telephone. On the forward link, the objective of the power control process is to provide a minimum power at each user telephone adequate to

achieve the desired quality of service for each user telephone.

The principal problem facing the designer of the Globalstar power control is the large round trip propagation delay that reduces the tracking capability of closed loop power control. Fortunately, the satellite channel is inherently Rician due to the strong line-of-sight component, as opposed to the Rayleigh channel prevalent in terrestrial cellular systems. This has the implication of reducing the tracking requirement for power control, which now has to contend only with the effects of shadowing and/or blocking by trees and buildings. These effects have different dynamics than diffuse multipath fading effects. The Globalstar system design also provides for multiple satellite diversity for most users. This has the effect of reducing the fluctuations in signal level. Due to the large round trip delay, the bandwidth of the fading processes that can be compensated for with power control is limited and must be compensated using a combination of interleaving, coding and open loop power control.

To compensate for the sluggishness in the closed loop power control, investigations of open loop power control strategies are being considered. In the open loop power control, the user telephone (or Gateway) measures the received forward (or reverse) link signal and adjusts the power of his transmit reverse (or forward) link signal. The open loop power control can be operated at higher operational bandwidths and can therefore react more quickly to its environment. Essential to the development of closed loop power control strategies is a better understanding of the cross correlation between L-band and S-band signaling.

System Capacity

Computation of the capacity of the Globalstar system is a complex problem. However, one of the overriding factors in the computation of the channel capacity is the inclusion of channel propagation characteristics. Satellite resources are finite and must be carefully controlled. The channel propagation characteristics coupled with the power control process dictates the amount of diversity gain to be achieved by employing multiple satellites, the peak power required by a satellite and the total power consumed by the satellite. Of paramount interest is the determination of propagation state probabilities as a function of satellite to user telephone geometry in a variety of different locations.

Low Level Design

The low level design of the Globalstar system is dependent upon the characteristics of the received signal after the application of the power control process. The residual channel characteristics are used for the design of plethora of different issues. In our application, the channel characteristics are primarily superior to those encountered in the cellular system.

Summary

In this paper, an overview of the Globalstar system was provided with emphasis on design issues associated with the channel propagation characteristics of the land mobile satellite channel. Based upon a comparison of the terrestrial cellular propagation channel, the land mobile satellite channel provides many advantages. However, further work is required to completely define the propagation channel for the Globalstar development effort.

INFORMATION SYSTEMS

INTERNATIONAL

TECHNICAL PAPER

AN APPROACH TO EFFECTIVE UHF (S/L BAND) DATA COMMUNICATIONS FOR SATELLITE PERSONAL COMMUNICATION SERVICE (PCS)

J.Y. Hayase

15 JUN 95

An Approach to Effective UHF (S/L Band) Data Communications for Satellite Personal Communication Service (PCS)

Land Mobile Service (LMS) satellite systems (SSs) providing Personal Communication Service (PCS), now under development after FCC authorization, could offer packet data communication service with an ecomomy exceeding that of conventional circuit-switched data carrying connections in voice channels. The subject access method allows users with personal digital assistants (PDAs), notepad/notebook personal computers (PCs) and PCs in general, to access such LMS SSs. Users can directly access the non-geosynchronous space vehicle (SV) constellation of an LMS SS to perform non-interactive processing functions. Examples are the execution of agent-based applications that exploit the client-agent-server paradigm, such as [1] "ORACLE in Motion"™, and the transfer of [2] computer-processed dictation of speech in text form on an anywhere-anytime basis.

Users that can access the non-geosynchronous SV constellation are mobile and/or fixed. The users are located in any of a large number of earth-based cells organized and serviced, through narrow beam antennas, by the SV constellation of the LMS provider. Frequency reuse may be performed on a 1 for 7 basis for time divided (TD) access or 1 for 1 for code divided (CD) access. The forward path, i.e., Gateway (GW) hub-to- SV-to-cell/user, at S-band is organized into frequency division (FD) channels and, within each such channel, either time division (TD) or code division (CD) is employed. The return path, i.e., user/cell-to-SV-to-GW hub, at L-band is also organized into FD channels with either TD or CD for users to access any one SV of a constellation.

The UHF transmission media and the problems associated with signaling through such fading media have been reported by many investigators. Lutz [3] et al report their findings and conclude that, " Moreover, the models show that reliable and efficient data transmission via the land mobile satellite channel should be achievable, if the transmission scheme is suitably adapted to the channel behavior." It is clear that an understanding of the UHF channel is necessary and adaptation to the vagaries of the channel is essential in achieving reliable communication.

A brief investigation of the recent literature dealing with fading

media modulation/demodulation techniques revealed the approach traditionally employed in addressing this problem. As summarized in Fig 1, modulation/demodulation techniques are traditionally selected on the basis of the relation between the symbol rate and Doppler or the signaling bandwidth to the coherence bandwidth. Since modulation/demodulation techniques used for signaling in a fading media cannot address all the problems, such as fading with all its vagaries, these are addressed through support techniques for fading media modulation/demodulation. These include the traditional arsenal used for HF and troposcatter at UHF, such as diversity, equalization, and error correction with interleaving and transmission strategies, such as the use of pilot tones. Pulse shaping and symbol constellation designs are part of this arsenal as well. Satellite transponder technology through development of linearized characteristics may offer an opportunity to reduce intermodulation in frequency division schemes for multiple access. These macro-level enhancement techniques are moving towards adapting to the media through techniques such as[4] decision feedback channel estimation and[5] adaptive equalization methods. The symbol constellation design is another effort in the adaptive direction.

Under the sponsorship of NASA Small Business Innovation Research (SBIR) Contract NAS7-1335, Information Systems International (ISI) has been exploring methods to achieve reliable, economical data communication by packet tranmission through LMS SSs offering PCS capability. Signaling functions that adapt to the vagaries of the UHF mobile satellite channel essential in the design of such a PCS via LMS SSs have been studied. Efficient design of packet data communication service over a LMS SS requires addressing a group of users in a cell. Severe latency grievously multiplies, if sequential methods are used to coordinate PCS data communication with each user in a cell. If PCS activities in a cell are coordinated through addressing a group, what percentage of the users will receive the information without error? System solutions are available to handle those that did not receive the information, but basic UHF transmission knowledge is required to understand the extent. Exceptions have to be made for those that did not receive coordinating information due to media vagaries. For that matter, on a point-to-point basis how reliable is the transfer of information for signaling functions? Is there a way to avoid the use of ACKs and NAKs, as in the case of high level data link control (HDLC) adapted to such Mobile Satellite Service (MSS) channels with non-geo SVs, either MEO (medium earth orbit) or LEO (low earth orbit)?

Fig 2 shows the latencies attendant with transmission times for MEO and LEO SVs servicing Boston-and Miami-based users. The MEO example has an on-board control function for the satellite PCS and

latency for this case would include on-board processing time and propagation delay times; in the figure, only the propagation times are considered. In the case of the LEOs, the satellite PCS control function is assumed to be performed at a gateway (G), which happens to be located in Washington, DC. A Miami-based user thus incurs the delay from Miami to the gateway, i.e., $\rho_{ML} + \rho_{GL}$, and the delay from the gateway to Boston, i.e., $\rho_{GL} + \rho_{BL}$. The figure shows the time axis starting at the time of ascending node crossing, at longitude -90 deg, of the first satellite of the LEO constellation. Data for this figure was generated by means of an ISI-developed APL2 program called TRAKCS.

In more aggressive moves, ISI has been investigating the feasibility of employing TRAKCS to operate in conjunction with a geographic information system (GIS), such as SPANS (AIX, OS/2, DOS)[6]*, to determine the user's environment for effective use of packet data service via LMS SSs providing PCS. In such systems, user activities in a cell are controlled from the hub (i.e., GW) location for the hub-and-spoke satellite system architecture which all currently authorized systems adopt. This arrangement is suited for operating a combined TRAKCS and GIS to establish a profile of the user's environment and the possible signaling environment for conducting system signaling functions. Through GIS and a user-position location system, such as the radio determination satellite service (RDSS), the user's environment--whether open highway, urban, or suburban--can be determined. Through TRAKCS and GIS, the elevation angle of a non-geosynchronous SV from the user can be determined to adapt the communication process.

Fig 3 shows the elevation angles observed at Miami, Washington, and Boston for the same LEO constellation and time span of Fig 2. Gaps in coverage are supported by SVs in adjacent orbital planes of the LEO constellation, which is not shown in Fig 3 (adjacent plane SV coverage is illustrated by the dashed curve of Fig 2). Users in a cell will have similar elevation angle profiles and users that view the non-geosynchronous SV at higher elevation angles, e.g., 35 deg, are expected, in general, to have the benefit of better satellite channels. A possible method of adapting the satellite PCS data communication system is to employ the HDLC ACKs and NAKs only when the user elevation angle is below, say, 35 deg. The packet data communication control function has the option to employ or not to employ the ACK/NAK mode, depending on its assessment of the user environment and the user-to-SV elevation angle profile.

---

* SPANS is a registered trademark of INTERNA TYDAC Technologies, Inc

The other more aggressive approach being pursued is investigation of the physical medium (the so-called "Layer Zero"), identified in the ISO layered architecture for OSI, to correct for fading and related vagaries of the UHF MSS channel. The physical medium in this case is essentially an attempt to make that channel approximate, as closely as possible, a terrestrial 4-wire full duplex (FDX) circuit (as used for Toll Quality transmission by telecommunication carriers or adminisrations) for which the ISO layered architecture was originally formulated. Since this is a process that requires a significant amount of information concerning fade characteristics of the media (including fade duration, occurrence of selective fading, fade depths, fade rates, and other relevent vagaries), a measurement program through a non-geosynchronous satellite with realistic user environments (including user mobility) is required.

The lack of a non-geosynchronous satellite with an S-band forward link and an L-band return link leaves no alternative for consideration but the use of INMARSAT, which operates at L-band only. Through a measurement program, it is hoped that channel fading information can be collected to design a physical layer (the first in the ISO layered architecture), in order to utilize existing network protocols, i.e., the data link layer, which have been extensively developed and refined.

Conclusion

Reliable signaling information transfer is fundamental in supporting the needs of data communication PCS via LMS SSs. The needs of the system designer can be satisfied only through the collection of media information that can be brought to bear on the pertinent design issues. We at ISI hope to continue our dialogue with fading media experts to address the unique data communications needs of PCS via LMS SSs.

Acknowledgement

The author extends his deepest graditude to his former IBM colleages that support this effort. Through Phil Bonomo, who brings 30 years experience in space systems engineering and APL analysis, the project developed invaluable insights into the dynamics of the non-geosynchronous satellite environment for PCS. The project is indebted to Ralph Metz, who brings 30 years of DOD and commercial satellite systems knowledge and the wisdom acquired supporting IBM's effort to establish a position in satellite digital communications service provision.

References

(1) ORACLE White Paper, "ORACLE in Motion™, Technical Product Summary, Sept 1994.

(2) IBM Software Vendor Operations, "Voice Type Dictation for OS/2 and Windows".

(3) Lutz,E., Cygan, D., Dippold, M., Dolainsky, F., Papke, W., "The Land Mobile Satellite Communication Channel-Recording, Statistics, and Channel Model", IEEE Transactions on Vehicular Technology, Vol 40, No 2, May 1991.

(4) Li, M., Bateman, A., and McGeehan, J. P., "Decision Feedback Channel Estimation-A Precursor for Adaptive Data Management", 41st IEEE Vehicular Technology Conference, 1991, p 730.

(5) Huang, W., and Rappaport, T. S., "A Comparative Study of Two Adaptive Equalizers for Mobile Radio", IEEE Vehicular Technology Conference, 1991, p 765.

(6) IBM Programming Announcement, 291-258, June 4, 1991.

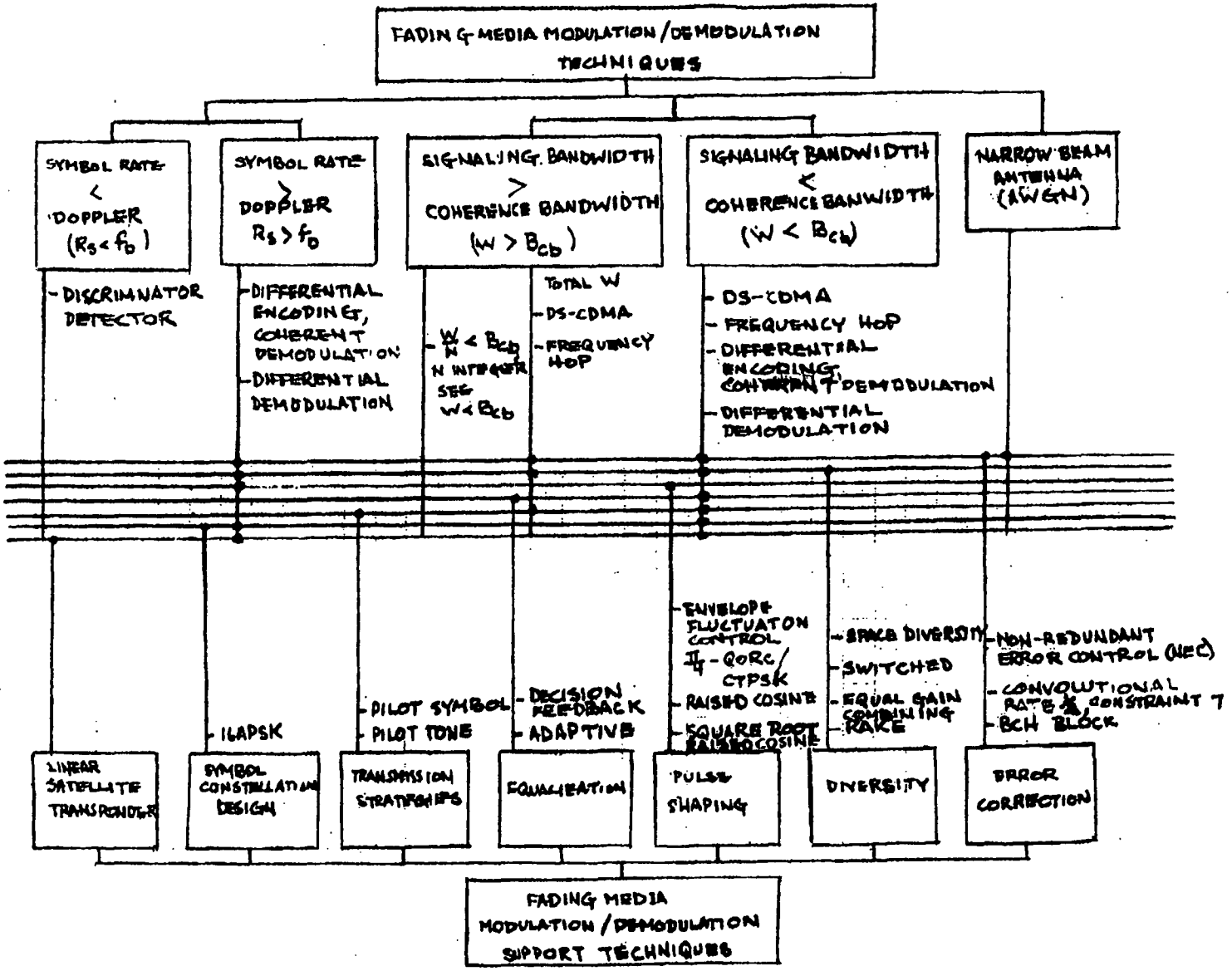

Fig. 1. Modulation / demodulation approaches for access system.

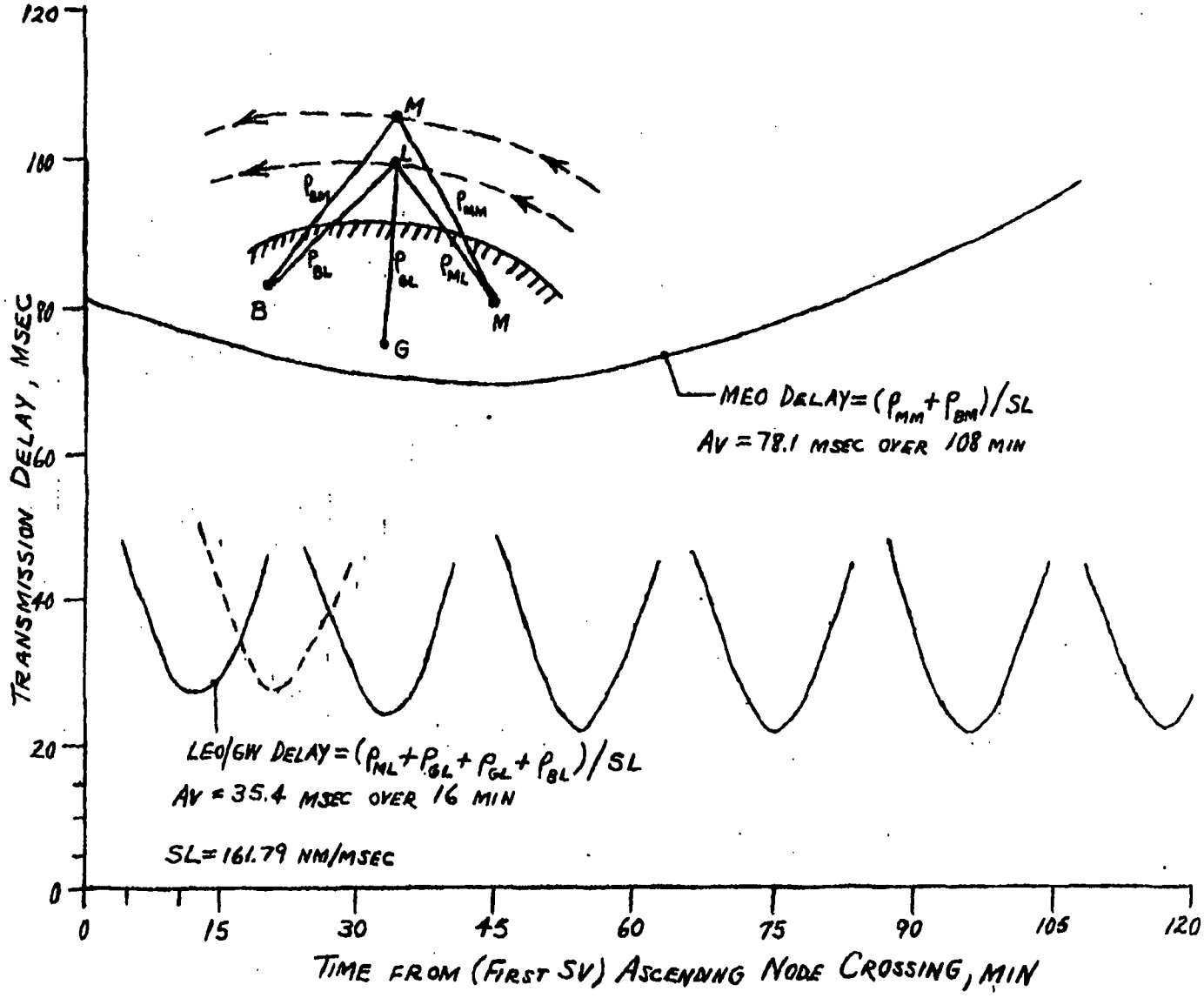

Fig. 2. Miami to Boston transmission time delays through MEO and LEO/GW.

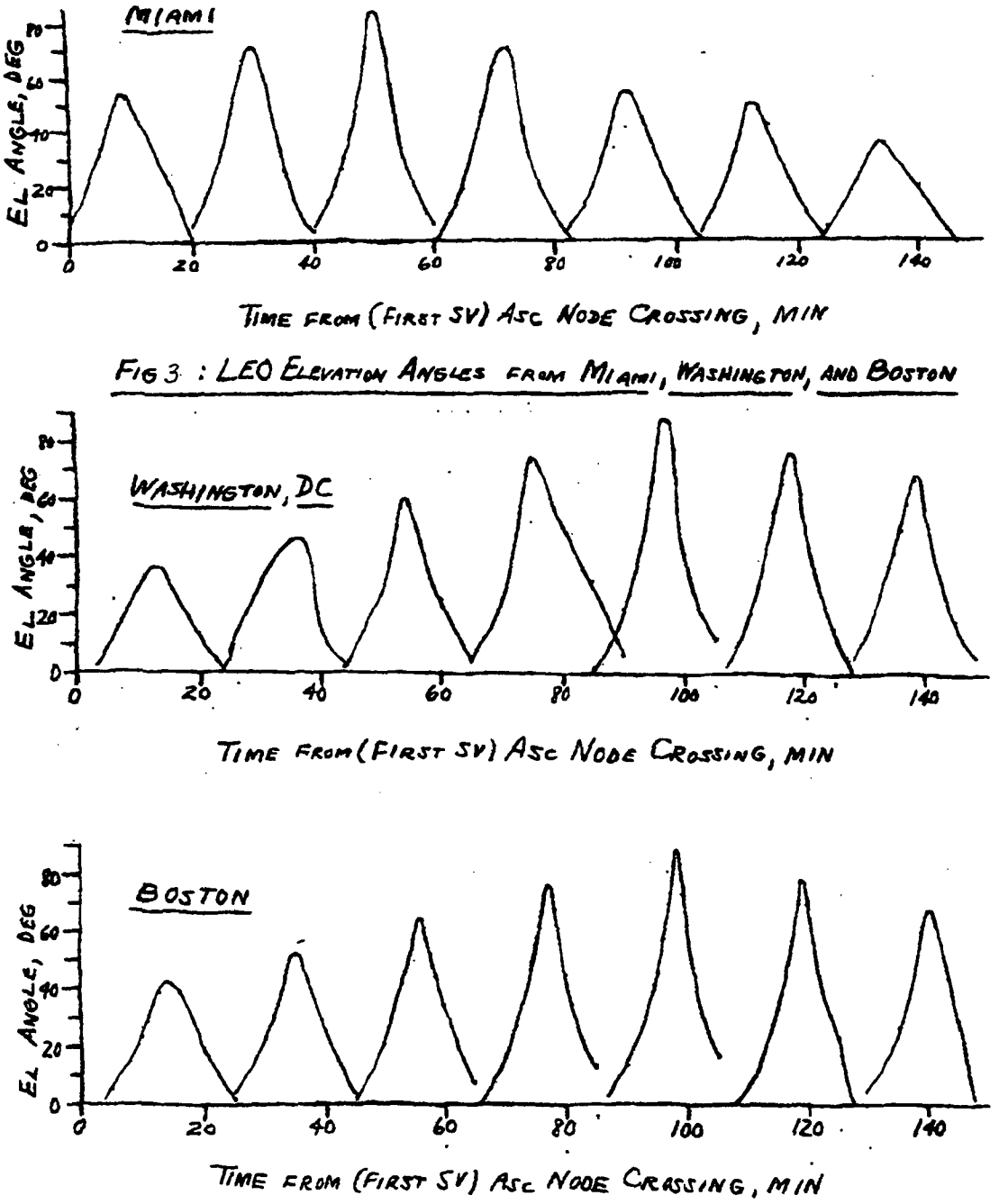

FIG 3 : LEO ELEVATION ANGLES FROM MIAMI, WASHINGTON, AND BOSTON

Fig. 3. LEO elevation angles from Miami, Washington, and Boston.

OPTICALLY DERIVED ELEVATION ANGLE DEPENDENCE OF FADING FOR SATELLITE PCS

R. Akturan and W. J. Vogel
Electrical Engineering Research Laboratory
The University of Texas at Austin
Austin, Texas 78758-4497
e-mail: Wolf_Vogel@mail.utexas.edu

Abstract - Images of urban Japan taken vertically through a 180° fisheye lens were analyzed to derive, as a function of elevation the fraction of sky that is clear, shadowed by trees, or blocked by buildings. At 32° elevation, results match those derived from satellite measurements fit to a 3-state fade model. Using the same model, for the first time the elevation angle dependence of mobile satellite fading is predicted.

INTRODUCTION

Fading for mobile satellite communications can be modeled by assuming that distinct signal level statistics pertain to three major propagation states, i.e., when the line-of-sight is clear (C), shadowed by trees (S), or blocked by buildings (B). In [1], Karasawa et al. derived percentages of (C, S, B) by fitting L-Band satellite fade data obtained in urban Japan at 32° elevation to a cumulative probability distribution consisting of a weighted linear combination of Rice (C), Loo (S) [2], and Rayleigh (B) fading, as in

$$f_v(v) = C * f_{Rice}(v) + S * f_{Loo}(v) + B * f_{Rayleigh}(v), \tag{1}$$

where $f(v)$ denotes the density function for the signal envelope [3] and the individual fade distributions are the Ricean density function,

$$f_{Rice}(v) = \frac{v}{\sigma^2}\exp\left[\frac{-(v^2+a^2)}{2\sigma^2}\right] I_0\left(a\frac{v}{\sigma^2}\right), \tag{2}$$

Loo's density function,

$$f_{Loo}(v) = \frac{8.686\,v}{P_S\, s\sqrt{2\pi}} \int_0^\infty \frac{1}{z}\exp\left[-\frac{(20\log(z)-m)^2}{2s^2} - \frac{(v^2+z^2)}{2P_S}\right] I_0\left(\frac{vz}{P_S}\right) dz, \tag{3}$$

and the Rayleigh density

$$f_{Rayleigh}(v) = \frac{v}{\sigma^2}\exp\left[\frac{-v^2}{2\sigma^2}\right]. \tag{4}$$

The parameters assumed for the three fade distributions, with a, the direct signal's voltage set to $\sqrt{2}$ for a direct power of P_d=1, are given in Table 1.

Table 1 Parameters for fade densities

state	distribution	parameter	Karasawa	optical fit
C	**Rice** scattered power P_S relative to direct power P_a	$\sigma = 10^{P_S(dB)/20}$	-8 dB	-7.5 dB
S	**Loo**			
	diffuse power P_S relative to direct power	$P_S = 10^{P_S(dB)/10}$	-13 dB	-13 dB
	mean power of lognormal process	$m\ (dB)$	-10 dB	-10 dB
	standard deviation of lognormal process	$s = 10^{s(dB)/10}$	3 dB	3 dB
B	**Rayleigh** diffuse power relative to direct power	$\sigma = 10^{P_S(dB)/20}$	-20 dB	-17 dB

We employed an optical method [4], applied to 236 fisheye lens images taken in urban Japan during the fall of 1993, to evaluate where the Earth-satellite path is clear, shadowed, or blocked as a function of the elevation angle. The photogrammetrically derived fade state probabilities are compared to [1] at 32° and then used to predict, for the first time, fade probabilities for elevation angles from 5° to 85°.

PHOTOGRAMMETRIC RESULTS

The fisheye images were taken at random urban locations in Tokyo, Kyoto, Nara, Hiroshima, and Kamakura, Japan. As the fisheye lens gives a full hemispheric view, the 35mm camera was always pointed vertically. The lens was held 1¾m above ground near the street-side edge of any sidewalk and its direction was aligned with a compass. The fraction of potential satellite paths with clear, shadowed, or blocked line-of-sight was calculated in 5° elevation angle increments from 0° to 89° and is plotted in Fig. 1. For example, in the low-elevation interval from 10° to 14°, 17% of the sky is clear, 8% is shadowed, and 75% is blocked, compared against the higher elevation interval of 60° to 64°, where (C, S, B) equals (80%, 3%, 17%). The environment states from 0° to 89° in 5° increments for urban Japan are also listed in Table 2.

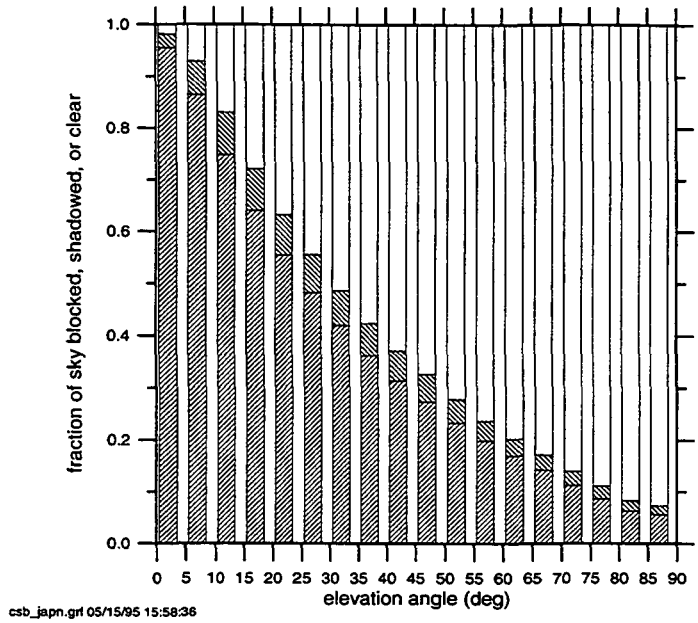

Fig. 1 The fraction of urban Japanese sky that is clear (white), shadowed by trees (diagonal hatch, down), or blocked by buildings (diagonal hatch, up) as a function of elevation angle.

Table 2 Environment states in urban Japan

Elevation	Clear	Shadowed	Blocked
0-4	2%	3%	95%
5-9	7%	6%	86%
10-14	17%	8%	75%
15-19	28%	8%	64%
20-24	37%	8%	56%
25-29	44%	7%	48%
30-34	51%	7%	42%
35-39	58%	6%	36%
40-44	63%	6%	31%
45-49	67%	5%	27%
50-54	72%	5%	23%
55-59	76%	4%	20%
60-64	80%	3%	17%
65-69	83%	3%	14%
70-74	86%	3%	11%
75-79	89%	2%	9%
80-84	92%	2%	6%
85-89	93%	2%	6%

COMPARISON TO SATELLITE MEASUREMENT

In Fig. 2, three cumulative fade distributions are drawn for comparison. The circles represent the satellite beacon measurement at 32° elevation and the dashed line the fit to the data in [1], with (C, S, B) estimated at (55%, 10%, 35%). The solid line is the result of applying the photogrammetrically derived states (C, S, B) of (51%, 7%, 42%) at 32° with the distribution parameters adjusted (see Table 1) to minimize the squared deviation from the measurement on the logarithmic scale. As a small fraction of fading was due to tree shadowing, only the parameters for the C and B states were allowed to vary. Although no attempt was made to link the propagation measurement locations to the image locations other than through their generic "urban Japan" description, the agreement between distributions is quite close and validates the optical method. The divergence between the fade measurement and the fitted and optically predicted distributions at fades greater than 25 dB is most likely due to the limited fade margin of the satellite system. The oscillating prediction error might call for further refinement of the 3-state model.

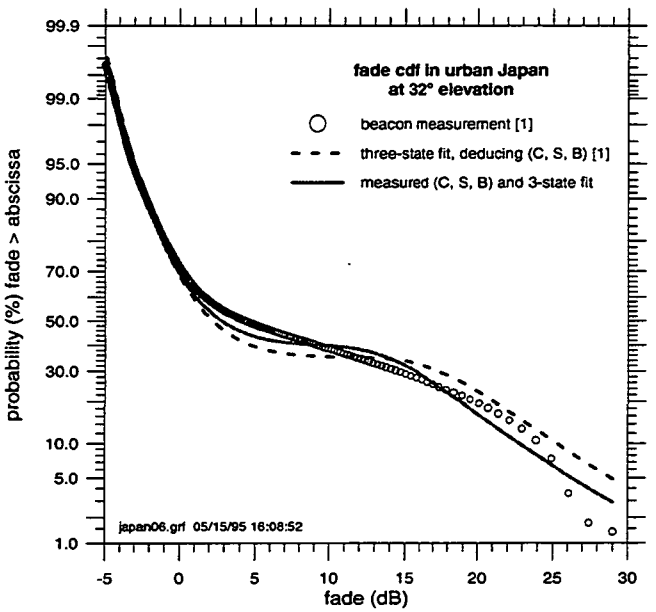

Fig. 2 Cumulative fade distributions resulting from satellite measurement and fit [1] vs. the photogrammetric environment sensing method.

ELEVATION ANGLE DEPENDENCE OF FADING

By inserting the environmental state probabilities of Table 2 with the optically derived distribution parameters of Table 1 into (1), we obtain a family of cumulative fade distributions, as shown in Figure 3. It shows, for instance, that in the urban area a system with a 25 dB fade margin can give 90% coverage at an elevation angle of 17°, respectively. This procedure assumes that the three-state model can be extended over the entire elevation angle range with the parameters give in Table 2. At elevations below

about 20°, specular ground reflections can become significant [5] and might influence the overall distribution. That effect, however, is mainly significant in open, rural environments. Similarly, high elevation angle distributions might be affected by reflections from vertical building surfaces prevailing in urban areas. Such effects can be included in the model once data are available for verification.

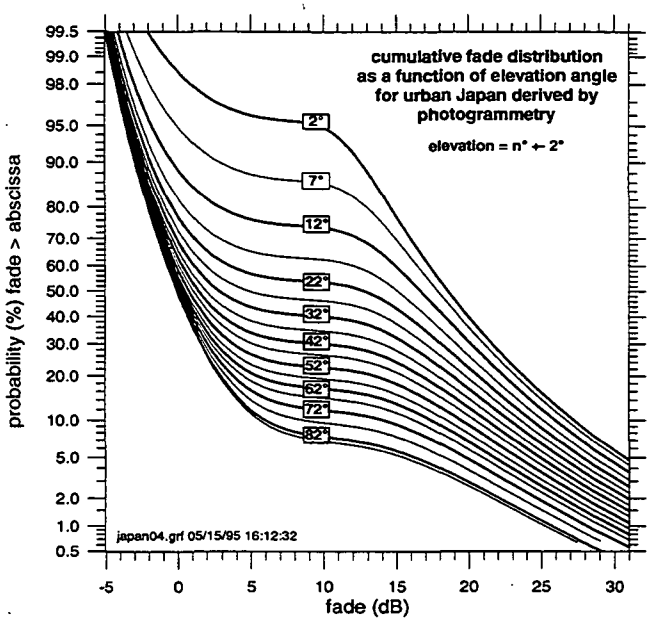

Fig. 3 Cumulative fade distributions for urban Japan as a function of elevation angle derived using photogrammetry combined with 3-state modeling.

DISCUSSION

The dominance of building blockage fading in urban areas is expressed in the terracing of the cumulative distribution. As a consequence, increasing the coverage significantly beyond what is available with a 5 dB fade margin requires a quantum-increase to beyond 15 dB. Once in the Rayleigh domain, the minimum elevation with 90% coverage decreases by about 5° per dB of additional fade margin.

Acknowledgments

This effort was jointly supported by Loral Aerospace Corporation, Motorola Inc., and the NASA Propagation Program under Contract JPL-956520.

References

1 KARASAWA, Y., MINAMISONO, K., and MATSUDO, T., "A propagation channel model for personal mobile-satellite services," Proceedings of the 1994 Progress in

Electromagnetics Research Symposium, ESA, Noordwijk, The Netherlands, July 11-15, 1994

2 LOO, C., "A statistical model for a land mobile satellite link," *IEEE Trans. on Vehic. Tech.*, 1985, **VT-34**, 3, pp. 122-127

3 GOLDHIRSH, J. AND VOGEL, W. J., "Propagation Effects for Land Mobile Satellite Systems: Overview of Experimental and Modeling Results," *NASA Reference Publication 1274*, February 1992

4 AKTURAN, R. AND VOGEL, W. J., "Photogrammetric mobile service prediction," *Electron. Lett.*, 1995, **31**, 3, pp. 165-166

5 VOGEL, W. J. and GOLDHIRSH, J., "Multipath fading at L band for low elevation angle, land mobile satellite scenarios," *IEEE J. Sel. Areas Comm.*, 1995, **13**, 2, pp. 197-204

INTO BUILDING FADING AT L- AND S-BAND FOR SATELLITE PCS

Wolfhard J. Vogel, Geoffrey W. Torrence, and Hsin Piao Lin

Electrical Engineering Research Laboratory
The University of Texas at Austin
Austin, Texas 78758, USA

Abstract - Selected results from L- and S-Band slant-path fade measurements into six different buildings employing a tower-mounted transmitter and dual-frequency receiver are presented. The objective of the measurements was to provide information for personal communications satellite design on the correlation of fading inside buildings between frequencies near 1620 and 2500 MHz. Fades were measured along horizontal directions with 5 cm spacing. Fade differences between L- and S-Band exhibited a normal distribution with means usually near 0 dB and standard deviations from 7.2 to 8.2 dB. After spatial averaging over a few wavelenghts, the correlation between L- and S-Band was significantly improved. Simultaneous swept measurements over 160 MHz spans showed that the standard deviation of the power levels as function of frequency increased linearly with average fade depth from a minimum of about 1.3 dB and increased by .2 dB per 1 dB of fade. Fade slopes were also a function of fade level, with LMSS-Band averages in the range of 1 to 2 dB/MHz for 10 dB fades and increasing to about 3 to 4 dB/MHz at a 30 dB fade.

I. INTRODUCTION

While voice service into buildings may demand more link margin than can be provided economically from a satellite, other services, such as call-alert or paging with lower data rates and, therefore, higher fade margin, might be feasible. To characterize the penetration of satellite signals into buildings on slant paths, it is necessary to measure and understand the typical power level structure in the time, space, and frequency domains.

Propagation measurements for slant-path into-building fading have previously been reported for the frequency range from 700 to 1800 MHz [1]. Those measurements were targeted towards the application of broadcasting from geostationary satellites, however, and used a relatively directive receiving antenna. It is expected that the azimuthally omni-directional antennas used in this experiment interact more fully with the multipath environment inside buildings and produce somewhat different fade results. This experiment used one wideband transmit antenna and two separate receiving antennas, which were mounted 5 cm apart in the direction of the receiver motion. Because of this, L-Band and S-Band data were obtained at the same receiver location consecutively, with a time interval of about 2 seconds. Data were generated in either fixed- or swept-cw modes, thus permitting a deterministic comparative assessment of the temporal, spatial, and frequency structure of the received power levels at L- and S-Band. We present the

results from our "simultaneous" L- and S-Band into-building measurements in terms of the observed temporal, spatial, and frequency characteristics and draw some conclusions.

II. Experimental Details

The measurement system consists of a dual-frequency sweeping transceiver located in a van, a 20 m crank-up transmitter tower mounted to the van, and a remote receiving antenna, filter, and preamplifier mounted on a linear positioner. The system has been described previously [3]. To maintain the same signal structure for the consecutive L- and S-Band observations performed at the same location, the tower was tethered and measurements were obtained only on days with (at most) very light winds.

The receiving antennas are quadrifilar helixes mounted with 5 cm spacing in direction of motion of the linear positioner; either a pair of left- or right-hand polarized antenna can be used. The receiving antennas are narrow-band, azimuthally omni-directional, and have peak gain at about 30° elevation.

The receiver positioner holds the receiving antenna on a computer-controlled linear motion arm. The motion can be along any direction and over a range of 80 cm. The axis of motion is horizontal, 1.4 m above ground. To take data over a wider range of receiver positions, the entire positioner has to be moved in 80 cm increments.

Measurements were made into six different buildings during the Fall of 1994. The names of these buildings, pertinent construction details, and the path elevation angle are given in Table 1. The transceiver-van was parked on one side of the building under test with the transmitter tower fully extended to 20 m. The antenna positioner was placed inside the building on the first floor and moved along a horizontal direction. The building was in the far-field of the transmitting antenna in all cases.

Table 1: Building Names, Construction Details, and Elevation Angle.

Building name	Approx. year of constr.	Construction type	No. of stories	Roof type	Average elevation (°)	Distance measured (m)
Commons	1987	concrete tilt wall	1	tar	16	16
EERL Office	1944	block brick	1	tar	30	8.8
Farmhouse	1880	wood frame	2	wood shingle	57	19.2
House	1958	wood frame	1	composition	40	12
Motel	1980	brick	2	composition	26	8
Store	1967	steel frame	1	tar	37	16

All L- and S-Band levels, $P_{L\text{-}Band}$ and $P_{S\text{-}Band}$, have been implicitly adjusted relative to the co-polarized clear-path level and all results are presented relative to the co-polarized clear-path level.

III. RESULTS

A. Time Variability

Time series were obtained to support the assumption that variations observed during the 2 s separated consecutive frequency sweeps are due to changes with frequency as opposed to time. As an example, data are shown in Fig. 1 as the tower was being retracted. One can observe that motion of the transmitter has a dramatic impact on the received signal level and that guying of the tower for the measurements was necessary.

Comparing the standard deviations of the timeseries data with those of the spatial and frequency variations to be presented in the following sections (typically 0.5 dB vs. 8 dB), one can say that the system's data acquisition rate of L-Band and S-Band signal levels at the same location taken within 2 seconds of each other and the frequency sweep rate of 2000 MHz/s was sufficiently fast to ensure that space or frequency variability as opposed to time variability was measured during frequency sweeps.

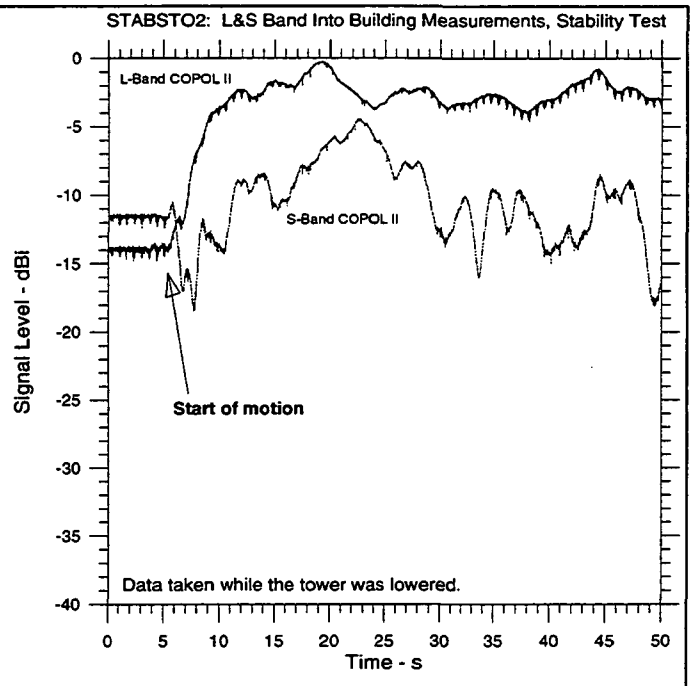

Fig. 1: Time variations without and with transmitter motion.

B. Space Variability

Figure 2 illustrates the typical spatial variation of power levels received at 1618 and 2492 MHz with co-polarized antennas as a function of position inside a building. Some general observations can be made while inspecting the plots. As expected, there is a macroscopic correlation between power levels at the two frequencies, i.e., both L- and S-Band are attenuated by the intervening structures, with 10 to 20 dB being typical values. The fades at the two frequencies often overlap in the graphs. On a finer distance scale, however, there are many deviations from equality which will be quantified below.

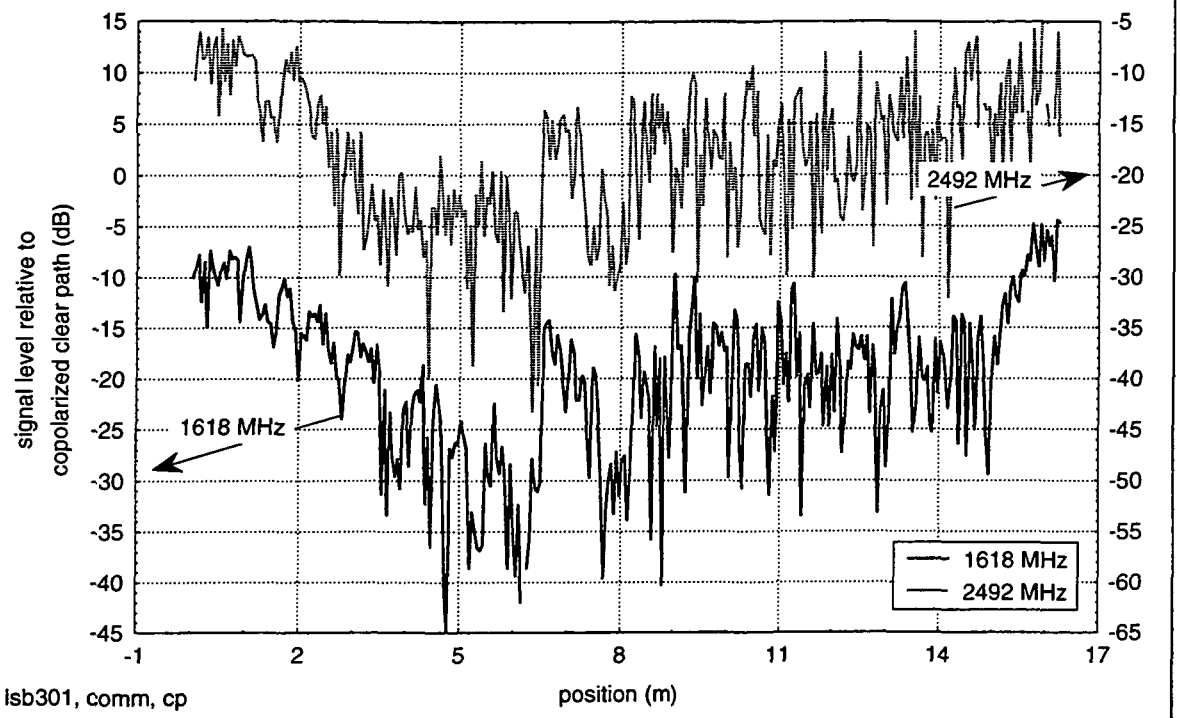

Fig. 2: The L-Band (left scale) and S-Band (right scale) signal levels vs. position in the Commons building.

The mean and standard deviation for each building and frequency band are summarized in Table 2 and some of the results are plotted in Figure 3. Also given in Table 2 are the differences between the received power levels at 1618 and 2492 MHz. One would expect that the building attenuation at S-Band on average exceeds that at L-Band, as for instance in the Store location, where the mean S-Band fades were 4.8 dB higher than the mean L-Band fades. At four other locations, however, the absolute difference was only 1 dB or less, which is about the accuracy of the measurement and at another location, the Commons, the average L-Band fades were about 2 dB greater than those at S-Band. Considering that fading into buildings depends on both the absorption by building materials and the reflection and scattering properties of the building skeleton, it is not entirely surprising to observe counter-intuitive results. A window, for instance, represents a larger opening at S-Band than at L-Band, but its attenuation may primarily depend on its frequency-independent metallic reflective coating. Similarly, steel mesh embedded in concrete may be less transmissive at the longer wavelength. In [1], median fades increased significantly over the frequency range from 700 to 1800 MHz. It is not clear, however, whether or not the fades tend to level off above about 1500 MHz. Preliminary results from wideband swept measurements into buildings from 500 to above 3000 MHz indicate at best a weak frequency dependence of the fading.

Table 2: Summary of Spatial Variation Results for Scans Inside Buildings

	L-Band		S-Band			Difference Power	
Building	**Mean (dB)**	**Std (dB)**	**Mean (dB)**	**Std (dB)**	**corre-lation**	**S-Band - L-Band Mean (dB)**	**Std (dB)**
Commons	-19.9	8.1	-18.0	7.2	0.56	1.9	7.2
EERL	-15.0	6.9	-15.6	6.9	0.34	-0.6	7.9
Farmhouse	-7.4	6.1	-7.9	7.1	0.28	-0.5	7.9
House	-10.6	5.7	-9.6	5.1	0.13	1.0	7.2
Motel	-19.8	6.3	-20.1	5.6	0.05	-0.3	8.2
Store	-14.7	6.2	-19.5	7.3	0.34	-4.8	7.8

Spatial moving averages were found for the scans in the six buildings, with an averaging interval of 60 cm or 12 positions, i.e., 3.2λ and 5λ at L- and S-Band, respectively. The correlation of the slowly-varying, low-pass filtered signal levels is larger than that of the unfiltered levels, ranging from a high 0.89 for the Commons to a low of 0.21 for the Motel. As an example, unfiltered L-Band and S-Band levels in the Commons are correlated by 0.54, increasing to 0.89 after low-pass filtering. The high-frequency variations, however, have consistently low correlations, in this case about zero (-0.02).

C. Frequency Variability

Similar to spatial variability, rapid changes with frequency occur only when the average power level vs. frequency is comparable to the diffusely scattered power. Inside buildings the multipath power is assumed to be about 10 dB or more below the clear path power level. A close-up view of the typical frequency selectivity of into-building fading has been plotted for EERL's laboratory building in Fig. 3. Four cases were selected from all positions, namely frequency scans with mean received power vs. frequency of 20, 15, 10, and 5 dB below the clear-path level. The graph illustrates that at high signal levels only limited frequency selectivity is exhibited over a narrow bandwidth but that the variability increases with decreasing mean in a scan, exhibiting deep and relatively sharp nulls for the -15 and -20 dB mean scans. The 16.5 MHz LMSS up- and

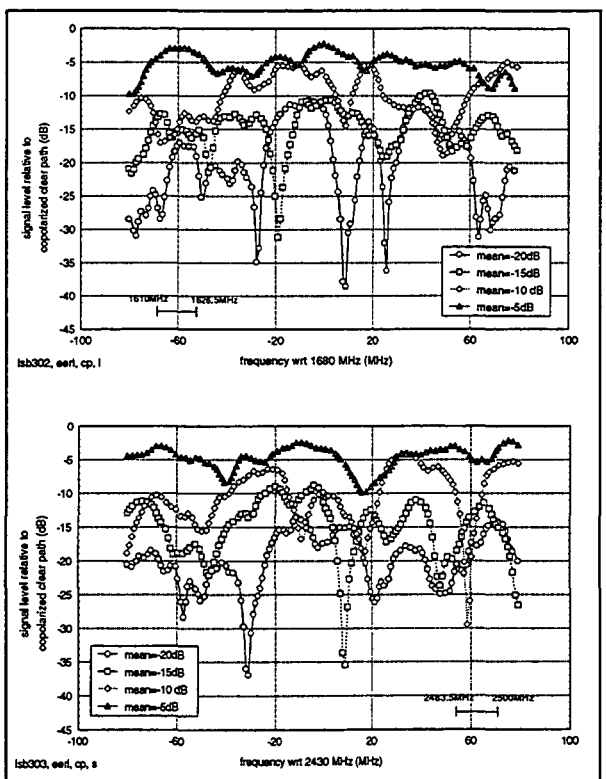

Fig 3: Fading vs. frequency at 4 positions.

down-link bands are marked in these graphs by horizontal bars. Another indicator for frequency variability is the fade slope vs. frequency, defined by

$$fadeslope = \frac{dS}{dF} \text{ (dB/MHz)} \qquad (1)$$

where dS is the change in received co-polarized power over the measurement frequency resolution dF, i.e., 1.0 MHz. Figure 4 presents an overview of the fade slopes observed at L- and S-Band in the six buildings.

The fade slope has been determined for all co-polarized signals within the MSS bands and regression coefficients for the standard deviation of the fade slope as a function of the mean signal level have been derived using

$$\sigma_{fs} = a + b\mu_{sl} + c\mu_{sl}^2, \qquad (8)$$

where σ_{fs} is the standard deviation of the fade slope and μ_{sl} is the mean signal level over the frequency span. Scatter plots of average fade slope as a function of average co-polarized signal level are shown in Figures 39 to 44, and the polynomial fit coefficients of (8) are summarized in Table 3.

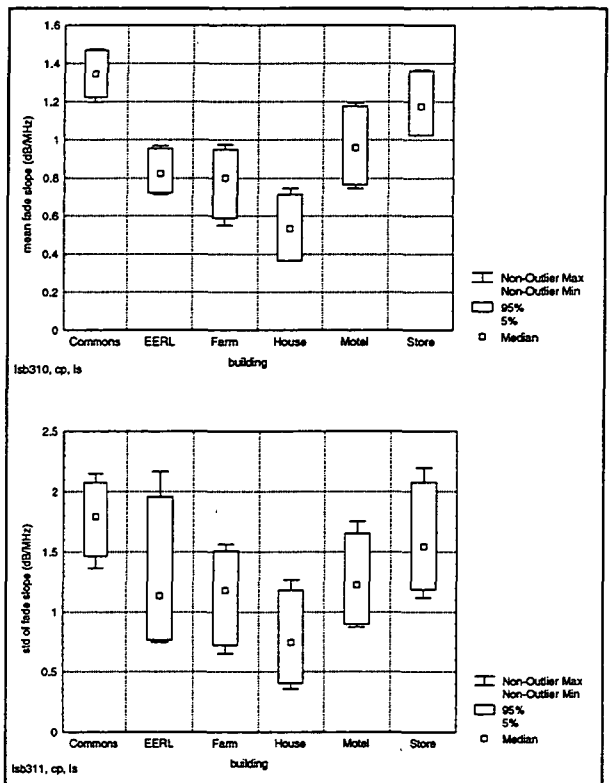

Fig. 4: Mean and std of the fade slope.

Table 3: Fit Parameters for the Fade Slope in the LEO Bands

LOCATION	L-Band a	L-Band b	L-Band c	S-Band a	S-Band b	S-Band c
Commons	-0.589	-0.11	0.000	-0.52	-0.123	-0.001
EERL	0.323	0.038	0.004	0.296	0.027	0.003
Farm	0.298	-0.047	0.003	0.196	-0.014	0.003
House	0.169	-0.015	0.002	0.237	0.026	0.004
Motel	0.531	0.063	0.004	0.342	0.047	0.004
Store	0.379	0.008	0.004	0.549	0.057	0.004

IV. CONCLUSIONS

We have observed the time, space, and frequency domain structures of L- and S-Band simulated satellite signals propagated into six buildings on a slant path. Our findings are:

1. Power level variations at L-Band are not correlated with those measured in the same location at S-Band. By forming spatial averages of power levels over a few wavelengths, the correlations increase.
2. Time variations are small if there is little wind and the receiver and transmitter are stationary. This means that for satellite communications systems with fade margins less than about 15 dB, time variations of mobile terminal power at the satellite will be spatial variations converted to time variations primarily by user motion and secondarily by satellite motion.
3. Power level variability in the space and frequency domains increases with increasing attenuation, because as the direct signal is reduced, multipath scattering has a greater effect.
4. Simultaneous swept measurements over 160 MHz spans showed that the standard deviation of the power level variation with frequency increased linearly with average fade depth from a minimum of about 1.3 dB and increased by 0.2 dB per 1 dB of fade.
5. Fade slopes were also a function of fade level, with LMSS-Band averages in the range of 1 to 2 dB/MHz for 10 dB fades and increasing to about 3 to 4 dB/MHz at a 30 dB fade.

ACKNOWLEDGMENT

This effort was supported jointly by Loral Aerospace Corporation and JPL under Contract JPL 956520, via the JPL Technology Affiliates Program, coordinated by the JPL Commercialization Office.

REFERENCES

[1] Vogel, W. J. and G. W. Torrence, "Propagation Measurements for Satellite Radio Reception Inside Buildings," *IEEE Transactions on Antennas and Propagation*, Vol. 41, No. 7, pp. 954-961, July 1993

[2] Shapiro, S.S., Wilks, M.B. & Chen, H.J., "A comparative study of various tests of normality," *Journal of the American Statistical Association*, vol. 63, pp. 1343-1372, 1968

[3] Vogel, W. J., G. W. Torrence, and H. P. Lin, "Simultaneous Measurements of L- and S-Band Tree Shadowing for Earth-Space Communications," accepted for publication, *IEEE Transactions on Antennas and Propagation*

MEASUREMENT OF SATELLITE PCS FADING USING GPS

Wolfhard J. Vogel and Geoffrey W. Torrence

Electrical Engineering Research Laboratory
The University of Texas at Austin
Austin, Texas 78758, USA

Abstract - A six-channel commercial GPS receiver with a custom-made 40° tilted, rotating antenna has been assembled to make fade measurements for personal satellite communications. The system can measure up to two times per minute fades of up to 15 dB in the direction of each tracked satellite from 10° to 90° elevation. Photographic fisheye lens images were used to categorize the fade data obtained in several test locations according to fade states of clear, shadowed, or blocked. Multipath effects in the form of annular rings can be observed when most of the sky is clear. Tree fading by a *Pecan* exceeding 3.5 dB and 12 dB at 50% and 10% probability, respectively, compared with median fades of 7.5 dB measured earlier and the discrepancy is attributed to the change in ratio when measuring over an area as opposed to along a line. Data acquired inside buildings revealed "rf-leaky" ceilings. Satellite diversity gain in a shadowed environment exceeded 6 dB at the 10% probability.

I. Introduction

To characterize Earth-satellite fading for personal satellite communications (PSC) at L- and S-Band, many campaigns have been carried out with either stratospheric balloons, helicopters, or airplanes employed as *non-orbiting* transmitter platforms [1]. Other measurements have used *satellites of opportunity*, such as INMARSAT's Atlantic or Pacific Ocean Satellite with L-Band pilot tones [2] and NASA's S-Band tracking and data relay satellites (TDRS) [3], or a *dedicated* satellite, i.e., Japan's experimental test satellite (ETS-V) at L-Band [4]. Not much, if any, fade data have been reported which were derived from global positioning satellite (GPS) observations, probably because of their inherent low sampling rate and fade margin. Nevertheless, some information useful for PSC design can be gleaned from such measurements, and at relatively low cost. The most obvious advantage of GPS measurements is the fact that the satellite constellation sweeps out a large part of the sky. This allows the collection at any one location of data at a large variety of elevation and azimuth angles and such data can be used to predict satellite diversity gain of low Earth orbit (LEO) communications systems, when they are combined with specific constellation parameters.

Table 1: Comparison of Transmitter Platforms

	Non-Orbiting Platform (NOP)	Satellites (GEO)	GPS
Frequency	As desired	~1.45 and ~2.05 GHz	1.575 GHz
SNR	>40 dB easily	40 to 20 dB	~21 dB
Sampling interval	1 ms	10 to 1 ms	0.5 to 1 s
Number of simultaneous sources	up to 2	up to 2	up to 6
Elevation angles covered	variable (~5° to 90°)	fixed, depending on location	variable (~5° to 90°)
Information derived	Amplitude, Phase	Amplitude, Phase	Amplitude only
Measurement time	ms	ms	24 h
Cost	High	Medium	Low
Data suitability	primary and secondary statistics, channel simulation	primary and secondary statistics, channel simulation	primary statistics categorized by fade state and elevation angle

A comparison among the different platforms for acquiring fade data is given in Table 1. Although the GPS fade data lack phase information, are obtained at a rate of only 2 or 1 sps and have at best a mere 21 dB signal-to-noise ratio, they come with angular coverage over much of the sky within a 12 hour measurement period, thus making them applicable for LEO or other non-geostationary orbit constellations. In this vein, we describe initial results derived from GPS observations, using a consumer-grade GPS receiver and a fisheye-lens imaging system [5]. These elements were combined to derive cumulative fade distributions categorized by fade state (i.e., clear, shadowed, or blocked).

II. Experimental Setup and Measurement Details

The GPS receiver employed for the measurements is a Trimble Model SVeeSix 6-channel OEM unit supplied with external active patch antenna and RS-232 interface. A computer program monitors the health of the receiver and stores the information decoded by the GPS receiver up to twice per second, such as time, location, satellite positions and signal strengths. The signal level for each monitored satellite is normalized to the maximum expected signal level for this receiver/antenna combination, which is -105.7 dBm. The lowest measurable signal level is 127.6 dBm, corresponding to a dynamic range of 21.9 dB. Backing off by the customary 7 dB results in a measurement fade margin of about 15 dB.

When used in its intended operation as a location determination device, the GPS receiver's antenna is mounted to a horizontal surface, has maximum gain in the zenith direction and decreasing gain with decreasing elevation angle. As fading is expected to increase with decreasing elevation angle, the antenna was canted at an elevation angle of 50° and rotated in azimuth at a rate of 2 rpm. This resulted in a reduction of the data rate from 1 sps to 2 samples per minute. For each satellite the computer program saves the peak signal level up to 2 times per minute. As the measurements are performed by keeping the receiver in the same location for at least 12 hours and as the environment seen by the receiver does not change (statistically speaking), the data rate reduction is irrelevant. The system with the rotating tilted antenna was used to make measurements at several locations, including inside two office buildings, close to a long three-story building, inside a vehicle, and several others at sites impacted by tree shadowing or object blockage.

To relate the observed signal levels to each fade state (*Clear*, *Shadowed*, or *Blocked*) in specific azimuth and elevation angle directions, fisheye lens images were also taken from the approximate position of the receiving antenna at each measurement site. The images were divided manually into fade state regions and used to categorize the signal level observations.

Using only a six-channel GPS receiver has biased the data to make fewer measurements available for the blocked state, however, especially at locations where only a part of the sky is blocked. The GPS receiver will try to acquire and use the six strongest signals that give a strong solution, hence the weakest, i.e., the blocked signals, do not get measured. There are two strategies for dealing with this problem. One is to make the measurements with a 10-channel receiver. As the maximum number of satellites visible is usually 10 or less for elevation angles above 5°, even the weakest satellites would be measured (within the dynamic range of the system).

III. Results

Details for three of the GPS experiments have been summarized in Table 2. For each measurement set, two types of figures have been included: (1) an overlay of the fisheye image with the signal strength encoded azimuth-elevation traces of the GPS satellites and (2) a plot of cumulative distribution functions categorized by fade state (clear, shadowed, or blocked) with the addition of a cdf for the indeterminate transition regions between any two fade states and the overall cdf. The transition region is defined as the area contained within about ±4° from the line separating the fade state regions.

The fisheye overlay images are in color and the GPS satellite traces are color-coded in 2 to 3 dB steps of signal strength. Common features in the images are elevation angle contours at 30° and 60° and north is at the top and west on the right. Due to the orbit inclination of the GPS constellation and Austin's latitude of 30.4°N, no satellites appear in the northern-most part of the sky.

Measurement Set 1 in Figure 1 was acquired under a canopy of trees. More than 96% of the measurement points are categorized as shadowed. The fade cdf has a median of 1.5 dB and a 1% value of 10 dB. Clear sky is seen in the second set, taken north of a water tower and depicted in Figure 2. It demonstrates the blockage by the water tower and also shows "cold-spots" in the clear sky region due to multipath reflections. The cdf, for the blocked and clear states has a 1% value of 13.5 dB and 4 dB, respectively. A third measurement was performed on the top-floor of a 6-story office building, where the receiving antenna was placed on the sill of a south window. There was no tree-shadowing and the glass was plain plate glass. The fisheye pictures and resulting cumulative distribution functions are shown in Figure 3. At this site some energy was received through the reinforced concrete ceiling. Diffraction effects along the window edges cause the GPS signal strength to vary over the directions defined by the window aperture, but the strongest signals are close to the clear-path level. Due to these multipath effects, the clear state fades at the 10% probability have attenuations exceeding between 6.5 and 7.5 dB.

Table 2: Details for Selected Measurement Sites

Set	Location	Characteristic
1	Under *Pecans* and *Oaks*	Shadowing
2	North of a water tower	Clear & Blockage
3	South window, top floor, no trees	Building Penetration

Figure 1: Tree-shadowed location under Pecans and Oaks.

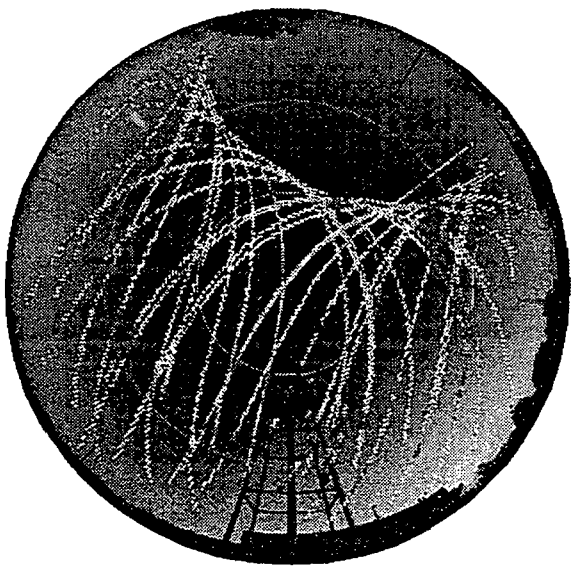

Figure 2: Clear LOS with some blockage by a water tower.

Figure 3: View from a southern window on the sixth and top floor of an office building.

IV. Diversity Analysis

The GPS data collected in the shadowed environment at Site 1 (Figure 1) have been analyzed for satellite diversity gain. There are 7 hours of data at 1 sample per minute in the set. At any one time, typically 5 or 6 satellites were visible. Output from an orbit program, *SATPRO* [8], predicted GPS satellite trajectories. The orbit data were used to randomly select two theoretically visible satellites (elevation angle > 5°) once every minute. The signal strengths for the chosen satellites (see Figure 1) were binned into three separate histograms: one for each satellite and a joint histogram for the stronger signal of the two. The cumulative distribution functions derived from the three histograms are plotted in Figure 4. The benefits of satellite diversity in a shadowed environment can be appreciated by comparing the two single-satellite CDFs (solid line, filled circles and dashed line, diamonds) to the joint distribution (solid line, empty circles), defined by the stronger of two different satellite signals. Because the entire sky was shadowed and a new satellite pair was randomly chosen every minute, the distributions are constellation independent. At the 10% probability, over 6 dB diversity gain is achieved.

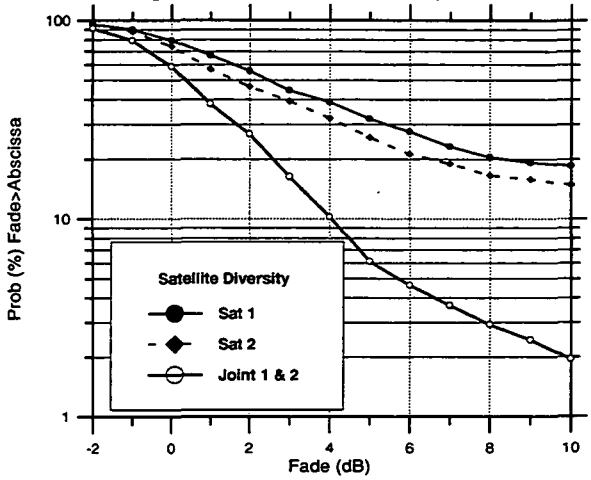

Figure 4: Satellite diversity gain in shadowed environment.

V. Conclusions

A six-channel GPS receiver was configured to make fade measurements for personal satellite communications propagation research. This included tilting the antenna 40° from vertical and rotating it in azimuth to mitigate the loss of measurement sensitivity due to the antenna pattern. Although the data rate was reduced to one measurement in 15 seconds per satellite, this did not impact the results, as the GPS fade measurements are limited to a stationary receiver anyway. The advantage of the GPS measurements is that over the course of a day transmitters are moving over much of the sky and allow the collection of fade data with varying azimuth and elevation angles. The system can measure fades up to 15 dB. By combining the fade results with fisheye lens images taken at the same spot, the fades could be categorized according to the fade state in a particular direction.

We found the median tree attenuation to be less than that measured previously by scanning a receiver laterally across the shadow zone of the tree. This may be due to the fact that the GPS measurement is an area (or solid angle) measurement and includes a larger fraction of less attenuating tree periphery than the linearly scanning measurement. In the open, with clear sky conditions, the GPS measurements revealed annular rings and isolated spots of fading due to (specular) multipath reflections. In rooms with plain glass the signal was strongest within the window aperture, but diffraction affected the signal over the entire region of visible sky. Satellite diversity gain in a shadowed environment was found to be greater than 6 dB at the 10% probability level. The measurement system could be improved in two ways. For one, using a ten-channel receiver would provide more blocked fade state data, especially at locations that are only partially blocked. With the six-channel receiver, often all six channels are locked to satellites which are in the clear or shadowed part of the sky, leaving no channel to search for weaker blocked signals.

ACKNOWLEDGMENT

This effort was supported jointly by Loral Aerospace Corporation and the NASA propagation program under Contract JPL 956520, via the JPL Technology Affiliates Program, coordinated by the JPL Commercialization Office.

REFERENCES

[1] Goldhirsh, J. and W. J. Vogel, "Propagation effects for land mobile satellite systems: overview of experimental and modeling results," *NASA Reference Publication 1274*, February 1992

[2] Vogel, W. J. and J. Goldhirsh, "Multipath fading at L-Band for low elevation angle, land mobile satellite scenarios," *IEEE Journal on Selected Areas in Communications*, Vol. 13, No. 2, pp. 197-204, Feb. 1995

[3] Vogel, W. J. and G. W. Torrence, "Satellite fade statistics and diversity gain for personal and broadcast satellite communications systems derived from TDRS observations," *Proc. of NAPEX XVIII*, Vancouver, Canada, June 17, 1994, JPL Publication 94-19, JPL, 4800 Oak Grove Drive, Pasadena, CA

[4] Hase, Y., W. J. Vogel and J. Goldhirsh, "Fade-durations derived from land-mobile-satellite measurements in Australia," *IEEE Transactions on Communications*, Vol. 39, No. 5, pp. 664-668, May 1991

[5] Akturan, R. and W. J. Vogel, "Photogrammetric mobile satellite service prediction," *Electronics Letters*, Vol. 31, No. 3, pp. 165-166, Feb. 2, 1995

[6] Vogel, W. J. and G. W. Torrence, "Simultaneous measurements of L- and S-Band tree shadowing for space-Earth communications," submitted to *IEEE Transactions on Antennas and Propagation*

[7] Vogel, W. J. and G. W. Torrence, "Propagation measurements for satellite radio reception inside buildings," *IEEE Transactions on Antennas and Propagation*, Vol. 41, No. 7, pp. 954-961, July 1993

[8] SatellitePro™ DOS High Accuracy Satellite Predictions, Zephyr Services, 1900 Murray Ave., Pittsburg, PA 15217

Channel Fading for Mobile Satellite Communications using Spread Spectrum signaling and TDRSS[1]

Jeffrey D. Jenkins, Yiping Fan, and William P. Osborne

Department of Electrical and Computer Engineering
New Mexico State University, Las Cruces, NM 88003

Abstract

This paper will present some preliminary results from a propagation experiment which employed NASA's TDRSS and an 8 MHz chip rate spread spectrum signal. Channel fade statistics were measured and analyzed in 21 representative geographical locations covering urban/suburban, open plain, and forested areas. Cumulative Distribution Functions (CDF's) of 12 individual locations are presented and classified based on location. Representative CDF's from each of these three types of terrain are summarized. These results are discussed, and the fade depths exceeded 10% of the time in three types of environments are tabulated. The spread spectrum fade statistics for tree-lined roads are compared with the Empirical Roadside Shadowing Model.

1. Introduction

Many previous measurements of the mobile satellite channel have used narrow band signaling techniques [1], [2], and have been primarily obtained at UHF, L-Band, and K-Band frequencies. In contrast, this paper will describe an experiment which measured the characteristics of the mobile satellite propagation channel at 2090 MHz using spread-spectrum signaling techniques.

The results from mobile satellite experiments summarized in [3] have confirmed that fades due to shadowing and multipath are significant. To mitigate the fading on such channels, system architects have looked towards spread spectrum signaling. One of the principal advantages of spread spectrum systems is their performance gain against jamming or interfering signals. This is true even when the interference is a multipath component of itself, provided that the time delay of the multipath is longer than one chip time (the chip time being a design parameter of the system). Under such conditions, spread systems should not experience the same degree of fading as unspread systems. It is unknown how much of these gains may be realized in practice since it depends on the distribution of multipath delay spreads.

[1]The authors wish to acknowledge the funding of this research under NASA Grant NAG-5-2142, and for the arrangements which NASA made to permit the use of TDRSS in making these propagation measurements.

Recent work by Ghassemzadeh et al [4] as well as Ikegami et al [5] has been aimed at using spread spectrum measurement apparatus to measure delay spreads in urban and indoor environments. However, no work appearing in the literature has attempted to measure such channel properties in a large number of environments, and no direct comparison of fade statistics for narrow band and spread signaling has been made in typical operating conditions.

The experiment described in this paper utilized NASA's Tracking and Data Relay Satellite System (TDRSS) as a signal source, and measured the channel characteristics with a mobile receiver. This data collection experiment covered 21 representative geographical locations in the Western and Southeastern regions of the United States. For the sake of brevity, Cumulative Distribution Functions (CDF's) for the fading in only 12 of these regions are presented: four each for cities, tree-lined roads, and open areas. Representative CDF's for these three classes of areas are summarized, and the CDF from the tree-lined road areas are compared with a narrow band measurement model. For each of these types of areas, the best case, worst case, and median fade levels observed are tabulated. The sections that follow will describe the experiment in sufficient detail to understand how the propagation data were gathered. Following this description, the basic statistics of the mobile channels will be presented.

2. Experimental Overview

To accomplish the task of measuring channel fade statistics for a spread spectrum communications link, a spread signal was transmitted from geostationary orbit to an instrumented mobile receiver. For this research, the spread signal was uplinked at Ku-Band through the White Sands Ground Terminal (WSGT), to TDRS F3, from which the signal was relayed back to the mobile receiver at S-Band. Figure 1 illustrates the basic concept of the measurement.

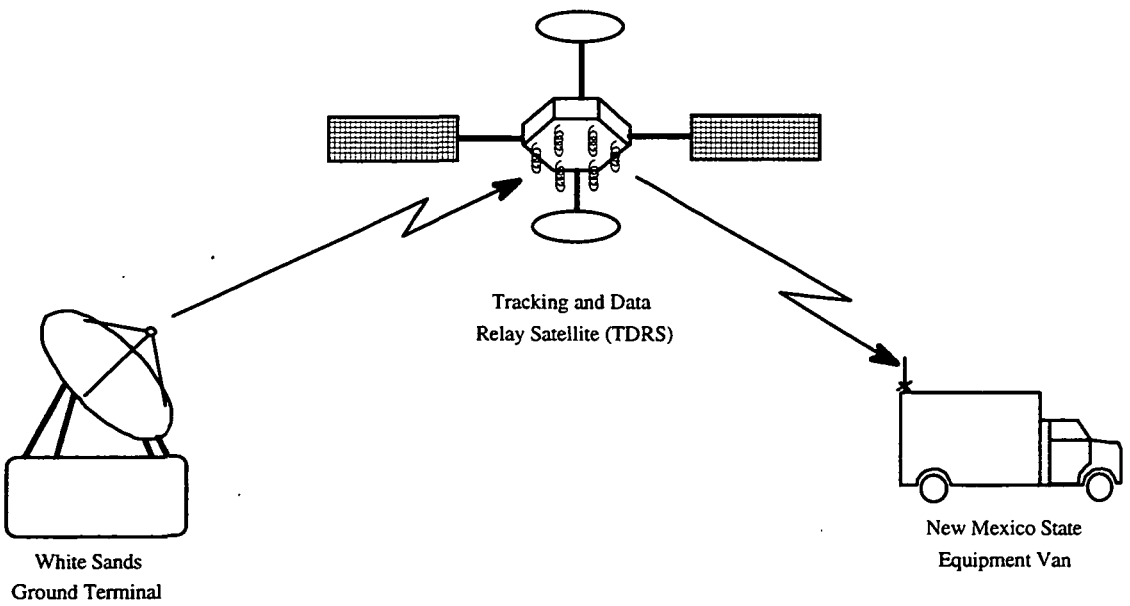

Figure 1. S-Band Test Concept

The performance of the channel was characterized by measuring the energy in the received wave form as the instrumentation was moved through the test areas. The receiver was calibrated against line-of-sight signal levels, providing statistics of the excess path loss due to shadowing and multipath effects. To achieve the goal of developing accurate empirical channel models for a *variety* of environments, it was important to pick appropriate locations in which to collect the data. These locations should be representative both in elevation angle to the satellite, and in topographical features. Using TDRS F3 located at 61° W, the elevation angle contours to the satellite were as shown in Figure 2 below. It can be seen that the elevation angles vary from about 55° in southern Florida, to about 8° in the Olympic Peninsula of Washington.

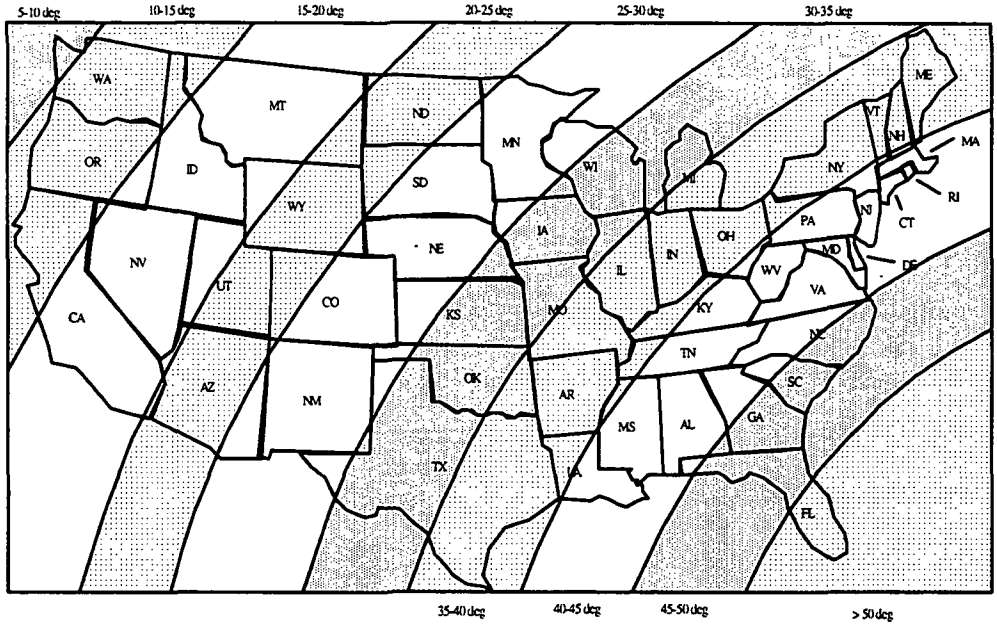

Figure 2. Look Angles to TDRS F3 at 61°W.

The NMSU measurement system was designed around an analog SAW matched filter[2]. The filter was matched to a 1024-bit acquisition sequenced derived from a much longer Gold code. The transmitter located at WSGT continuously transmitted this 1024-bit sequence as it was clocked out at an 8 MHz rate. The resulting BPSK signal, after filtering, occupied nearly 16 MHz of bandwidth. After propagation through the channel, this signal was received, amplified, and down converted for processing through the matched filter. At the output of the envelope detector, a wave form may be observed such as that depicted in Figure 3. There is a large response from the matched filter once per 1024-bit cycle. This response occurs when the pattern of the incoming signal envelope is aligned with the geometry of the SAW device in the filter. The amplitude of the peak response is directly related to the total energy in the 1024-bit symbol.

[2]For complete details of the design, fabrication, and verification of the spread spectrum measurement system, see [6].

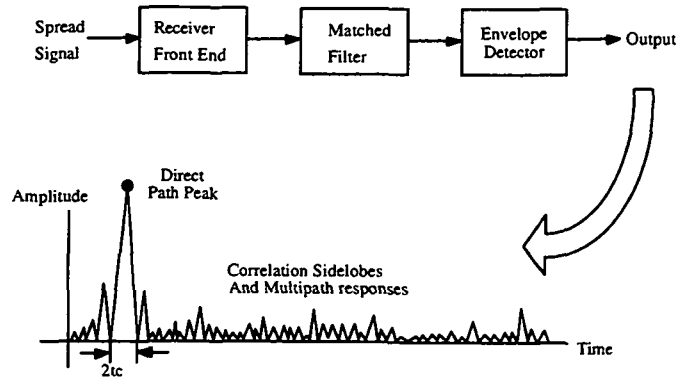

Figure 3. Response at receiver output

The principle of operation of the receiver structure is as follows. If there is no multipath present on the channel, there will be only one response at the output per 1024-bit sequence. If, however, multipath is present, it will appear as a time delayed and attenuated response at the output. Sampling the output of the matched filter provides a measurement of the delay profile for the channel for each sequence repetition, and the amplitude of the largest response in this profile provides statistics on the channel fading that would be observed by a single channel receiver.

The propagation data presented in this paper were collected by sampling the output of the matched filter at a 50 MHz rate. Sampling was not uniform since it was only desired to observe multipath returns from a few miles away. Figure 4 shows the timing of the samples. A receiver circuit synchronized the data collection with the incoming signal, and samples were collected in 20 μs bursts around each peak response. Each burst of data collection provides a measurement of the delay profile of the channel, extending from -2 to +18 μs relative to the direct-path response. With the hardware employed, it was possible to collect 30 delay profiles before pausing the collection to transfer samples to storage. The transfer took approximately 3 seconds, so that 3 second gaps exist in the data collection every 30 profiles.

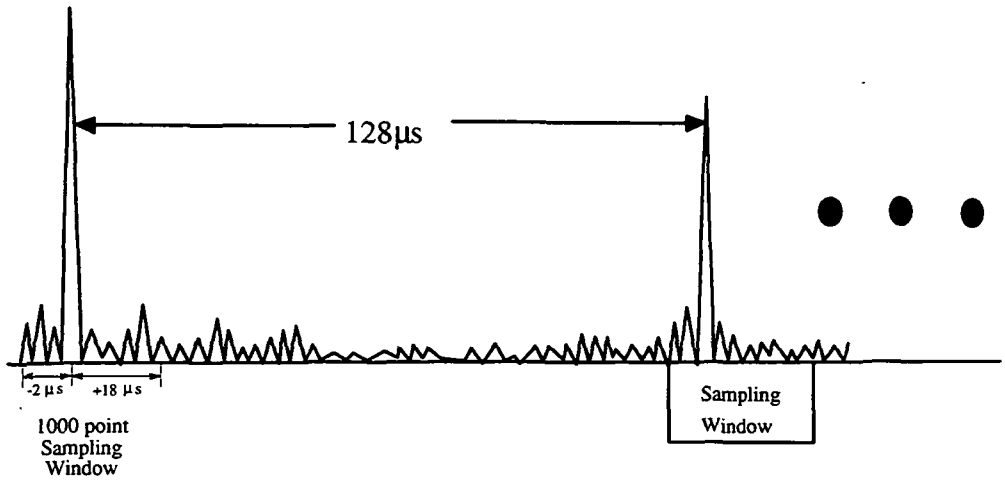

Figure 4. Timing of waveform sampling at the receiver output.

3. Data Collection

Data collection proceeded in two phases. First, the function of the system was verified with a satellite loop-back test. Details pertaining to the system validation testing are given in [6]. Following the equipment check-out, propagation data were collected during two journeys through the United States. The routes were selected to provide measurement opportunities in a variety of environments. Route 1, shown in Figure 5a, passed through the Western US, following a route North from Las Cruces, NM, to Denver, to the Olympic Peninsula of Washington, South to San Francisco, and Eastward back to Las Cruces. Route 2, shown in Figure 5b, encompassed much of the Gulf Coast region of the US, passing from Las Cruces across Texas to Houston along I-10, northward through Mississippi and Arkansas, and finally across the plains of Oklahoma and the Texas Panhandle back to Las Cruces.

Several propagation issues were involved in selecting the test areas. In order to address questions about the performance of spread spectrum systems in multipath environments, it was necessary to collect data in such areas. Geometrical considerations lead to that the conclusion that the delay spread profile in a "city canyon" environment would be quite different from that found in mountainous or real canyon areas. In response to these considerations, sites were selected in several major cities as well as in mountain and canyon areas. Another question addressed by this experiment was to examine how different the fade statistics for spread systems are compared with models developed from CW measurements under shadowing (non-multipath) conditions. This led to the selection of test areas in both heavy and light tree-shadowed environments. Finally, several sites were selected in open areas, where fading was expected to be light. The resulting fade distributions were expected to be identical (in a statistical sense) with similar distributions measured by CW experiments.

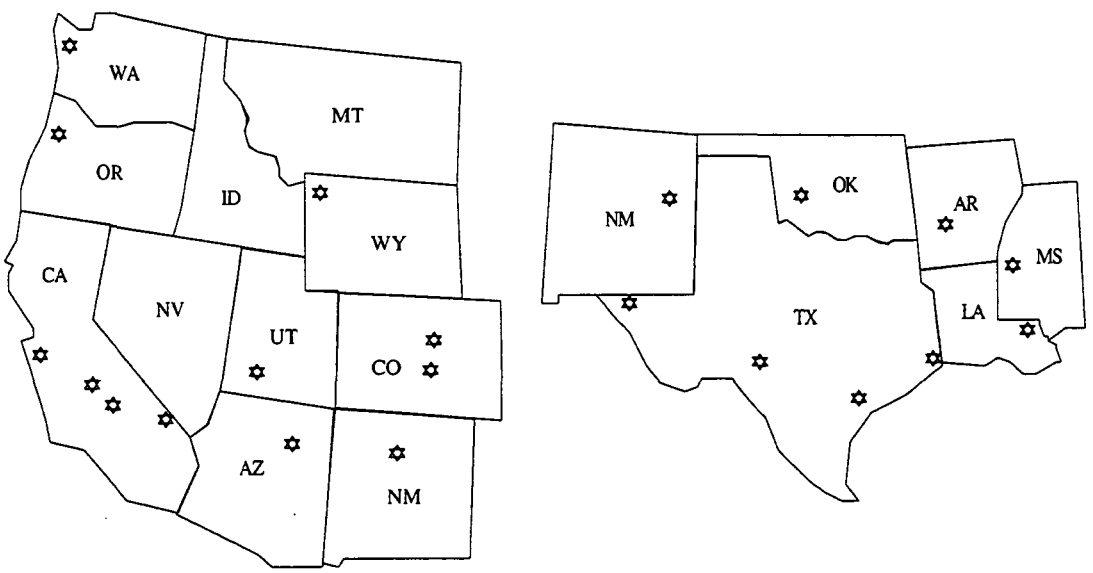

Figure 5. Details of the routes along which data was collected. (a) Western route, and (b) Southeastern route.

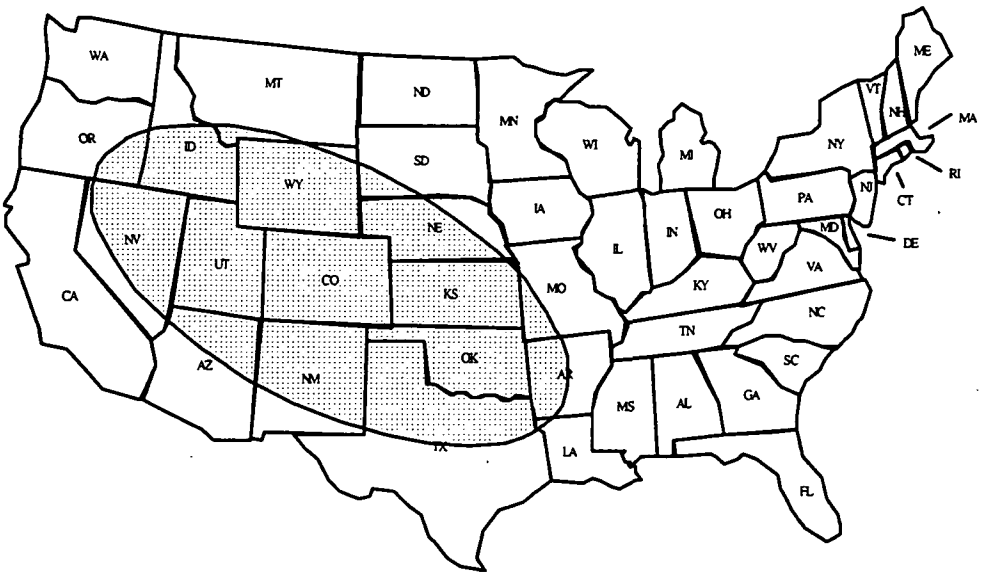

Figure 6. A Typical TDRSS S-Band 3 dB footprint. Shown here with the beam centered on Denver, CO.

In the two figures above, locations with a ✡ represent regions where propagation data was collected. The twelve locations along Route 1 included: Albuquerque; Pikes Peak; Denver; Yellowstone Park; the Olympic Peninsula of Washington; Portland, OR; San Francisco; Yosemite Park; Sequoia Park; the Mojave Desert; Zion Park; and US-180 across Arizona. Tests along Route 2 included: I-10 East of El Paso, TX; I-10 West of San Antonio, TX; I-10 through Houston; Galveston, TX; New Orleans, LA; Vicksburg, MS; Central Arkansas; Central Oklahoma; and Eastern New Mexico. Figure 6 shows how the half power beam width of the TDRSS S-Band antenna compares with the size of the test areas. Under worse case conditions, where the receiver was moved at 65 mph during the three hours of data collection, the expected amplitude change due to movement through the footprint would be less than 0.5 dB. In addition, the Doppler observed on the signal due to the motion of the vehicle was on the order of 200 Hz, which also had no measurable effect on the received signal strength.

4. Fade Distributions

Following the test plan summarized in the previous section, propagation data was collected in each of the locations specified. Approximately 100,000 individual delay profiles were measured at each location. To improve the effective signal-to-noise ratio, wave form averaging was employed. The 100,000 unaveraged delay profiles were processed into about 3000 averaged profiles. The CDF's shown below represent the distribution of fades observed on the amplitude of the strongest return observable within each averaged delay profile. The fade depths are all referenced to unobstructed line-of-sight levels. Given the relatively small number of samples available for statistical analysis, probabilities less than 0.01 are not shown on the graphs.

In Figure 7, several representative fade distribution curves are shown from urban areas. Figure 8 presents fade distributions for areas where unobstructed line-of-sight propagation was predominant. In Figure 9, the distributions from routes along shadowed roads are presented. Finally, Figure 10 shows an overlay of the fade distributions from Figures 7 through 9.

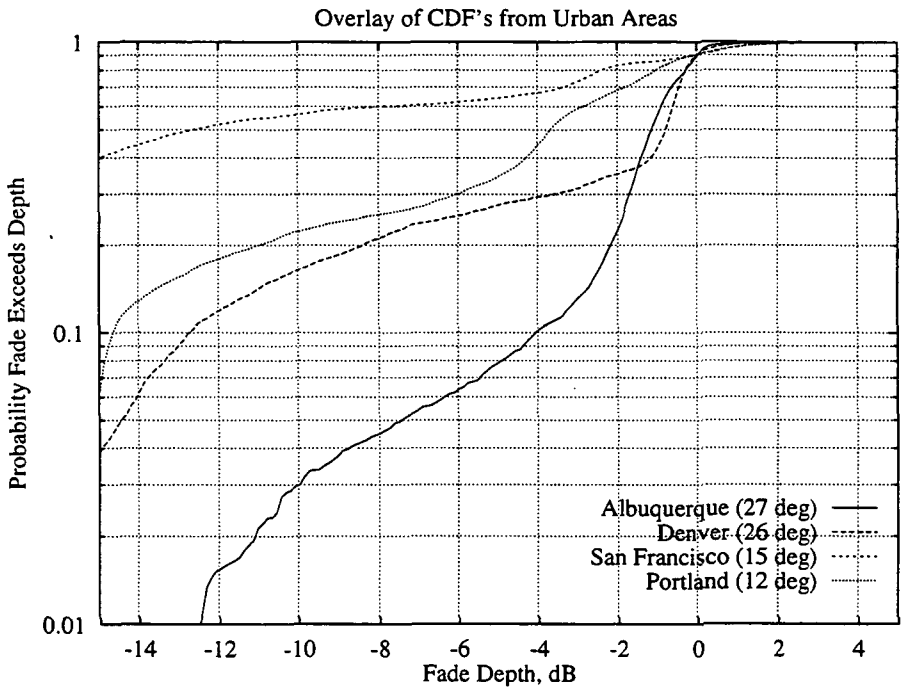

Figure 7. CDF's for Urban Areas

5. Discussion and Conclusions

In the previous section, the fade distributions observed by the S-Band receiver were presented. These curves exhibit two principle slopes. First, in the relatively open areas, the CDF's fall off very rapidly, with very low probability of deep fades. Those fades which do occur are primarily due to ground multipath and atmospheric effects. To see this, one may examine the geometry shown in Figure 11. The height of the mobile antenna is given as h, with the path elevation angle to the satellite given by θ. The differential path length is given as

$$\Delta = (R'+D) - R = R\left(\sqrt{1-4\frac{h^2}{R^2}\cos^2\theta} - 1\right) - \frac{2h\cos^2\theta}{\sin\theta} + \frac{2h}{\sin\theta} \cong 2h\sin\theta \qquad (1)$$

where the approximation holds as h/R goes to zero. This differential path length is less than $2h$ for all elevation angles, or 24 feet in the case of the NMSU experiment. This corresponds to an excess path delay of about 24 ns, which is much less than the chip time

of 125 ns. Thus, the multipath is not eliminated by the spread receiver, and can contribute to fades.

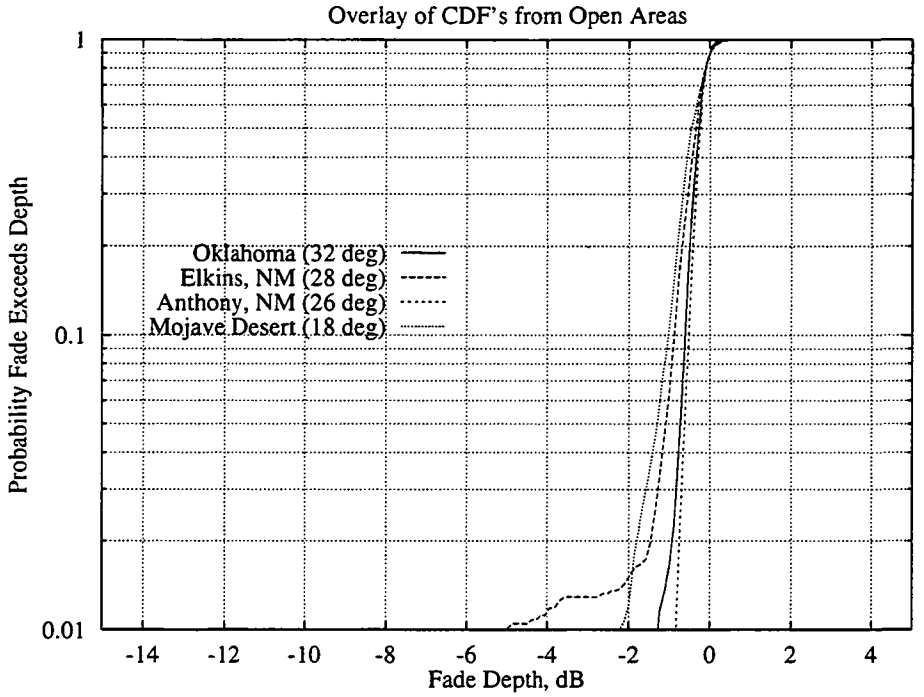

Figure 8. CDF's from Open Areas

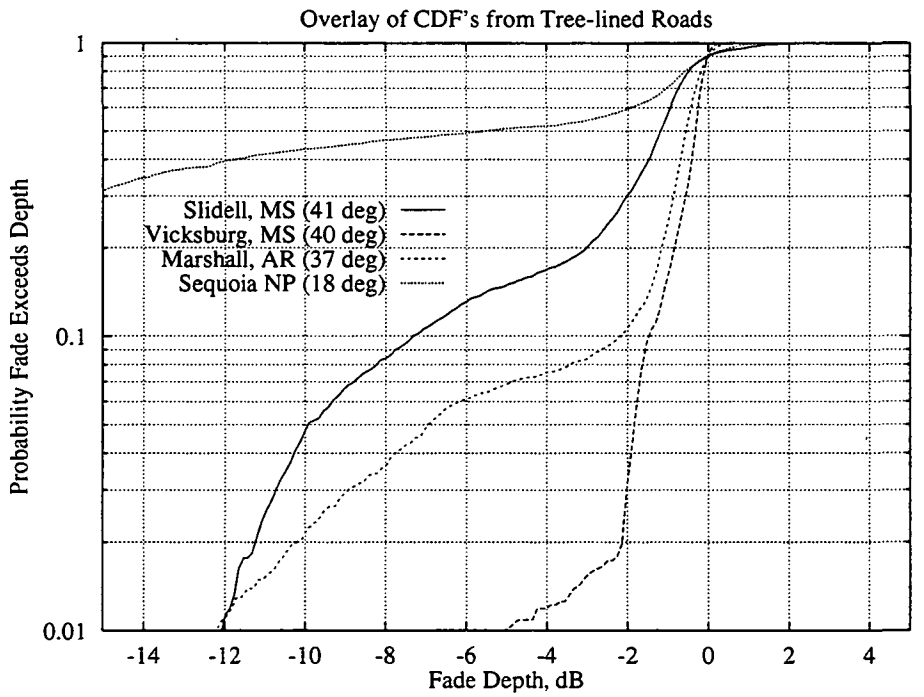

Figure 9. CDF's from Tree-lines Roads

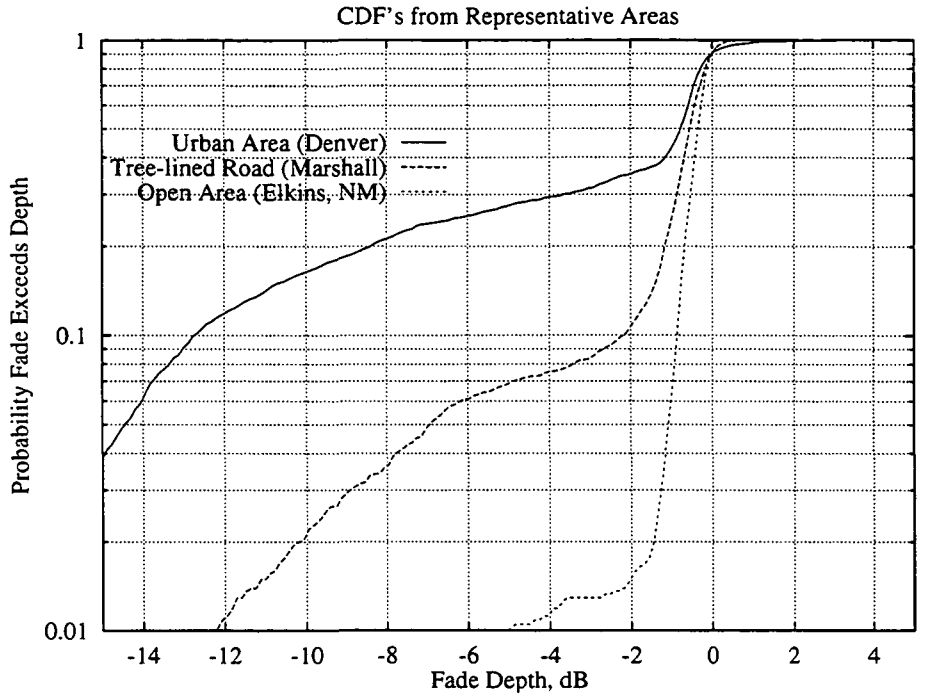

Figure 10. Overlay of the curves from three representative areas.

In the heavily shadowed areas, the CDF's fall off very slowly, with high probability of deep fades. The open areas and shadowed areas comprise the two characteristic slopes for the CDF's. Test areas with a mixture of open and shadowed regions exhibit both slopes, with a knee separating the regions where each effect (shadowing and "flat fading") is dominant.

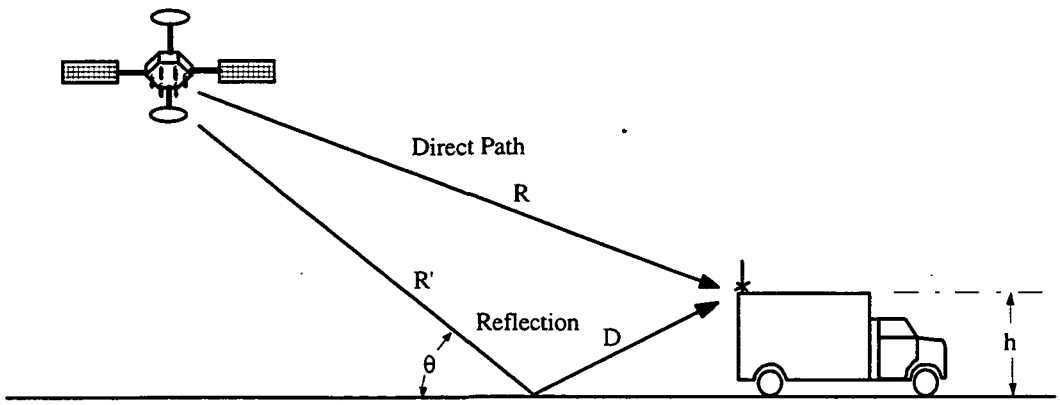

Figure 11. Multipath geometry on flat terrain.

Several statements may be made about the degree to which the fade statistics vary from one type of region to another. Refer to Figure 7, which shows the CDF's in several cities. At the 0.1 probability level, there is a 13 dB separation between the best and worst case fade depths exceeded (the worst case is actually off of the scale of the figure). The curves generally follow a pattern from low elevation angle to high, with the more severe

fades occurring in the cities with lower elevation angles. However, it is seen that the fades in Portland (12 degrees elevation) are not as severe as the fades in San Francisco (15 degrees elevation). This demonstrates that not only elevation angle, but also many other features of the city itself determine the severity of the fading that will be observed.

Figure 8 does not hold many surprises. In the open areas, the fade distributions were strictly a function of elevation angle to the satellite. The best case fade distribution was measured in Oklahoma (where the highest elevation angle to TDRS F3 was observed), while the worst case fade distribution was measured in the Mojave Desert (where elevation angles were the lowest).

Figure 9 shows a similar trend in the tree-shadowed environments to that of Figure 7. Generally, the lower the elevation angle to the satellite, the more severe the fades become. The data collected between Slidell, LA, and Bolton, MS appears to have experienced deeper fades than elevation angle alone would account for. Again, the specific type of tree, size of the crown, and spacing between trees are all factors which impact the degree of fading observed.

The performance differences between heavy shadowing (urban), light shadowing (roadside trees), and open areas is clearly evident in Figure 10. The knees in the curves which separate the regions where flat fading and shadowing dominate are also evident. Flat fading is observed in all environments; however, the more sever the shadowing is, the sooner the shadowing effect dominates the fade distribution. In the open area, the knee occurs below the 0.01 probability level and is not observed in the distribution. With light to moderate shadowing, such as along tree-lined roads, the knee occurs at about the 0.1 probability level. Finally, in the urban environment, the knee has moved all the way up to the 0.3 level, and dominates nearly the entire fade distribution curve. The best-case, worst-case, and median fade levels observed during the data collections are summarized in Table 1.

Geographic Area	Best-Case	Median	Worst-Case
Urban Areas	-4 dB	-10 dB	-17 dB
Tree-line Roads	-1.5 dB	-8 dB	-16 dB
Open Areas	-0.5 dB	-0.8 dB	-1.0 dB

Table 1. Summary of fade depths at the 0.1 probability level in three types of environments.

It is interesting to examine how the fade statistics derived from the spread measurements compare with models derived from CW measurements. Using the Empirical Roadside Shadowing Model described in [7], the fade statistics for a mobile system operating in a roadside tree environment at 37° elevation angle were computed. In Figure 12, this curve has been overlaid with the fade statistics from the spread measurements in Central Arkansas. The spread measurement clearly shows the presence

of two types of fading - flat fading (multipath from the ground) and shadowing. The knee in the curve marks the transition between the two. The slope of the shadowing portion of the CDF is identical with that of the ERS model, but is shifted to the right. This shift to the right is accounted for because roadside tree shadowing was not present for the entire duration of the data collection.

The knee occurs at a fade depth of between 2 and 3 dB. If the portion of the CDF of interest (between 1% and 20% probability) is extrapolated, and shifted so that the resulting line passes through the origin, then the dashed line in Figure 12 results. The agreement between the ERS model and spread measurement is good. The minor difference in slope is most likely due to differences in the density of the tree canopy. This result indicates that spread systems exhibit the same degree of fading in tree-shadowed environments as do unspread modulation systems.

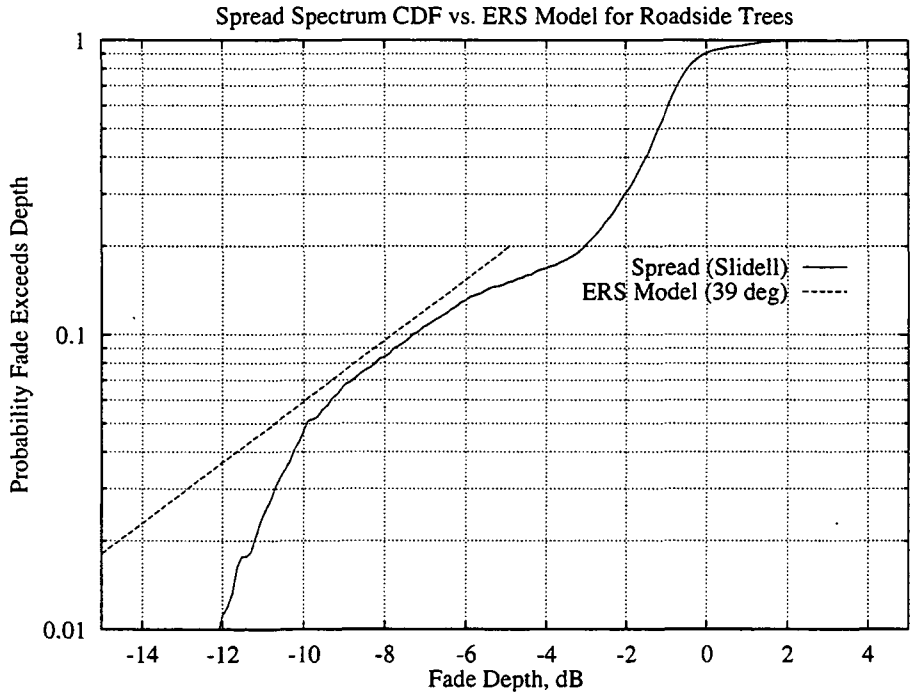

Figure 12. A comparison between the Empirical Roadside Shadowing model and the observed fade distribution at a 37° elevation angle.

Some insight is gained by comparing measurements against models. However, to actually determine the improvement offered by spread signaling in typical operating conditions, it is necessary to collect simultaneous fade statistics with both spread signaling and a CW beacon. Such information will allow the system engineer to determine if there are sufficient gains available from employing spread signaling to justify building such a system for a given operational area. An experiment to simultaneously measure the performance of spread and narrow band systems in the same environments is currently being pursued to address these questions.

References

[1] Vogel, W. and J. Goldhirsh, "Fade measurements at L-Band and UHF in mountainous terrain for land mobile satellite systems," *IEEE Trans. Antennas Propagat.*, vol. AP-36, no. 1, pp. 104-113, Jan. 1988

[2] Goldhirsh, J. and W. Vogel, "Mobile satellite system fade statistics for shadowing and multipath from roadside trees at UHF and L-Band," *IEEE Trans. Antennas Propagat.*, vol. AP-37, no. 4, pp. 489-498, April 1989

[3] Goldhirsh, J. and W. Vogel, "Propagation effects for land mobile satellite systems; overview of experimental and modeling results," NASA Reference Publication 1274, February 1992

[4] Ghassemzadeh, S. et al, "On the statistics of multipath fading using a direct sequence CDMA signal at 2 GHz, in microcellular and indoor environments," *International Journal of Wireless Information Networks*, vol. 1, no. 2, 1994

[5] Ikegami, T. et al, "Field tests of a spread spectrum land mobile satellite communication system," *IEICE Trans. Commun,* vol. E76B, no. 8, August 1993

[6] Jenkins, J., Y. Fan, and W. Osborne, "Wideband propagation measurement system using spread spectrum signaling and TDRS," to appear in the *Proc. NAPEX XIX*, June 1995

[7] Goldhirsh, J. and W. Vogel, "Mobile satellite system propagation measurements at L-Band using MARECS B-2," *IEEE Trans. Antennas Propagat.*, vol. AP-38, no. 2, pp. 259-264, February 1990

Acknowledgment

The authors wish to acknowledge the support of NASA under grant NAG-5-2141 for funding this research and making the TDRSS resources available for the measurements. We also wish to express our gratitude to the many people who worked on fabrication and test of the experimental hardware and the NMSU Engineering Department's mobile experiment van.

An Experiment on Fade Statistics

for Spread and Unspread Modulation Systems in the Mobile Multipath Environment

Jeff Jenkins
Yiping Fan

Why Spread?

- **One reason for looking at spread spectrum in mobile systems is to combat multipath:**

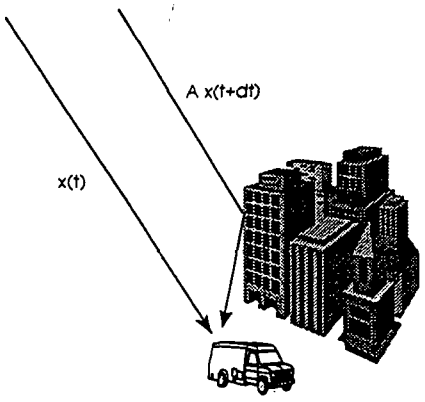

$$r(t)=x(t)+Ax(t+\tau)$$

If we can make the amplitude of the multipath component *at the decision device* small, its effect will be small.

How can Spread Modulation Help?

- We take advantage of the correlation properties of the spreading functions. The most important of these is the following:

$$R_{xx}(\tau)=\int PN(t)\times PN(t+\tau)=0, \text{ for } \tau > \text{chip time}$$

- If the time delay is *not* less than one chip period, the amplitude of the multipath component *after the matched filter* is still reduced linearly with the time delay

Waveform from Matched Filter

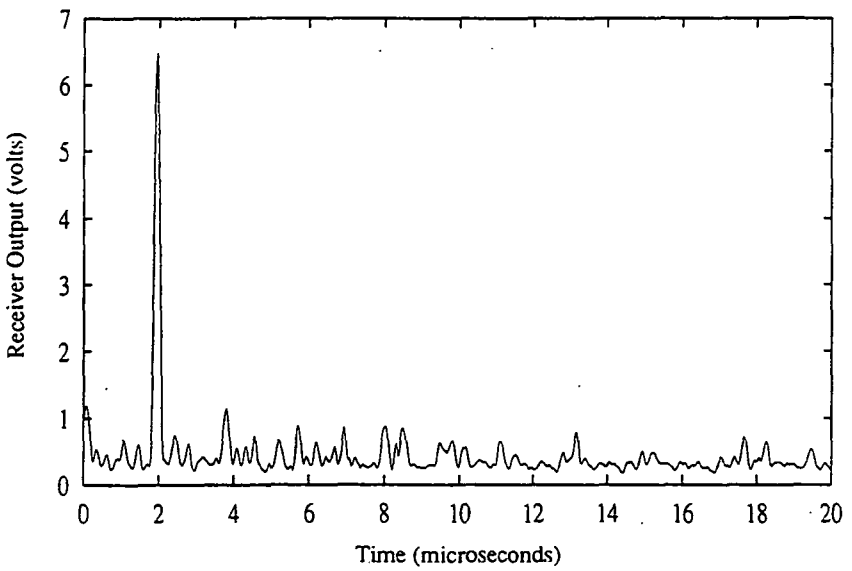

Review of Previous Results

- Fade Statistics were collected in 21 areas of the US during Summer of 1993
- These data provide useful information on what types of fades are likely to be encountered by spread systems in these environments
- Little to nothing has been learned about how spread systems perform compared to unspread modulation systems

Data Collection - Western Route (Summer, 1993)

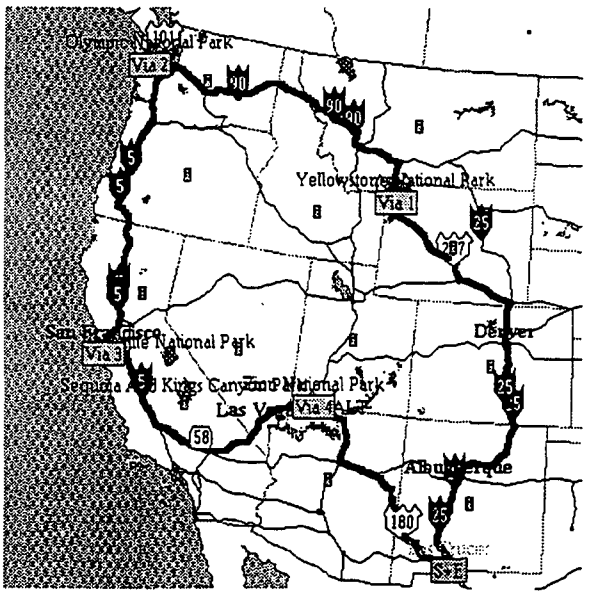

Data Collection - Southeast (Summer, 1993)

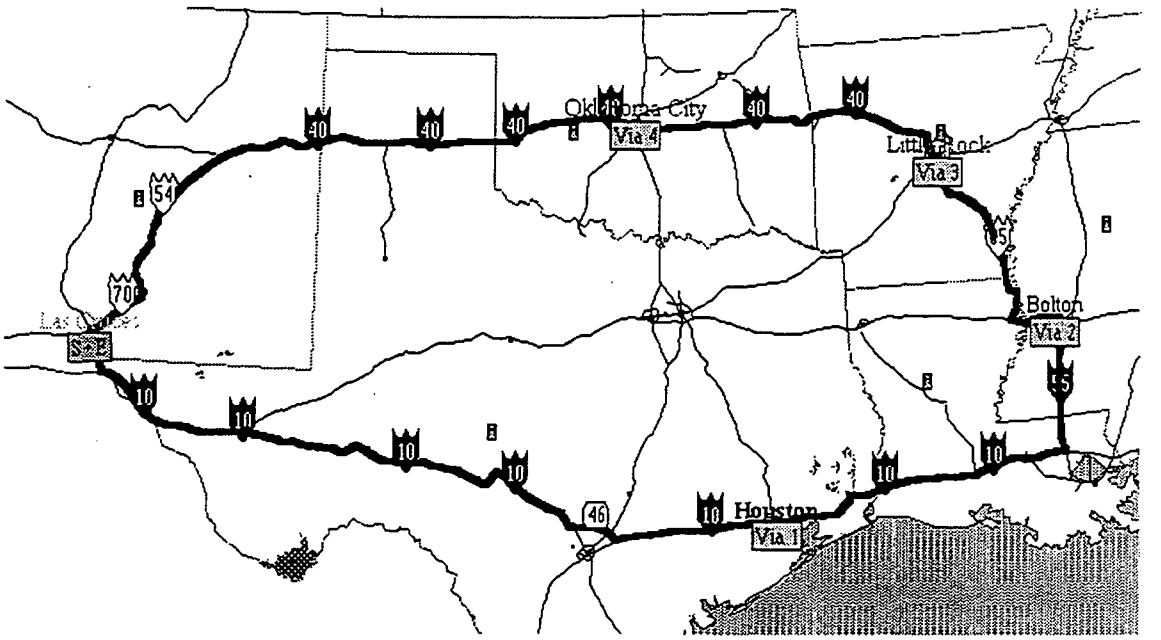

Open Area Fade Statistics

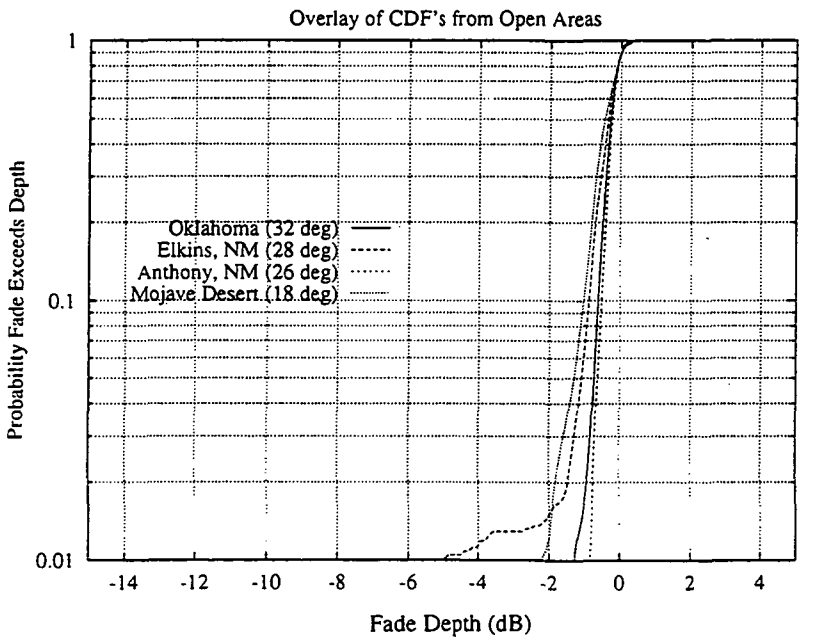

Tree-Line Roads Fade Statistics

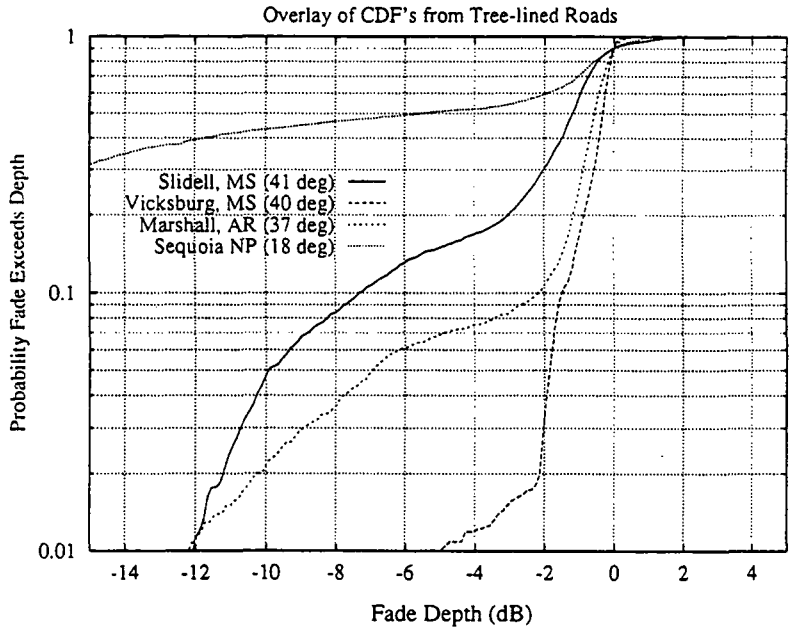

. Urban Areas Fade Statistics

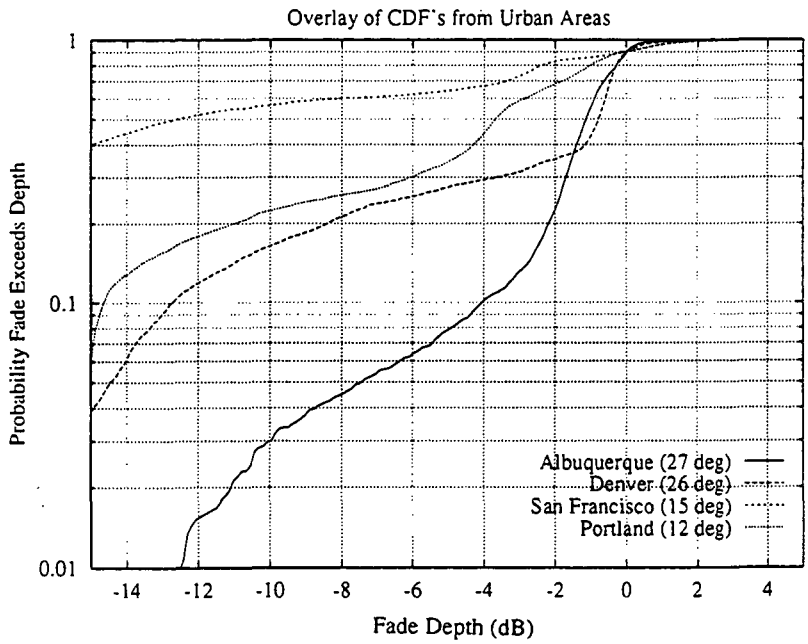

The Big Question

- **In practice, can spread modulation systems effectively reduce the severity of multipath fades?**

- **To answer this question, a side-by-side comparison between spread and unspread systems must be made.**

- **Parameters of the spread system should be typical of practical systems. Ideally, the chip rate should be variable.**

Dual Beacon Data Collection (Summer, 1995)

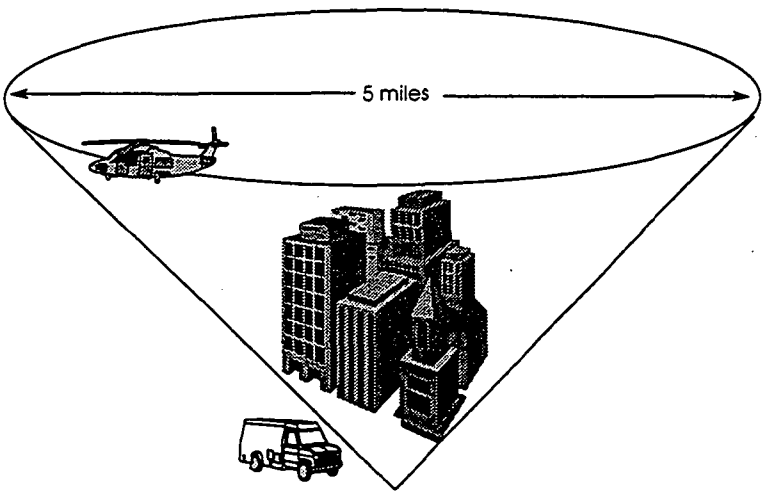

Airborne Platform will be a Cessna 172

Elevation angles from 15 to 45 degrees achievable

Las Cruces, El Paso, Denver, Albuqueque, Tucson, Phoenix, San Antonio, Austin, Dallas/Ft. Worth

Transmitter

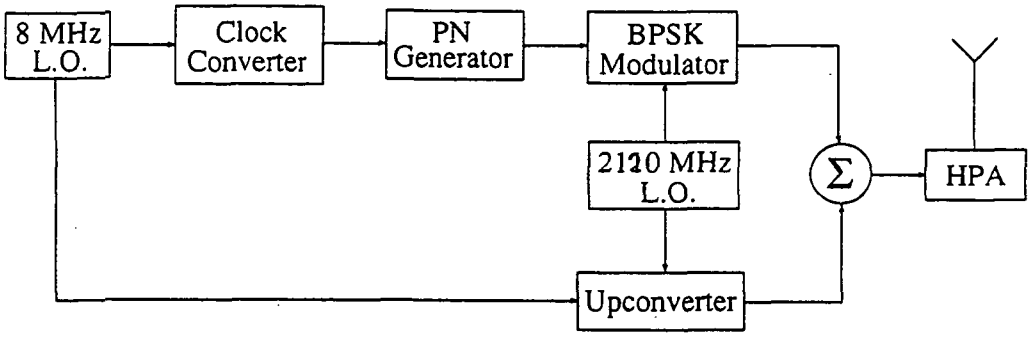

Receiver and Data Collection Equipment

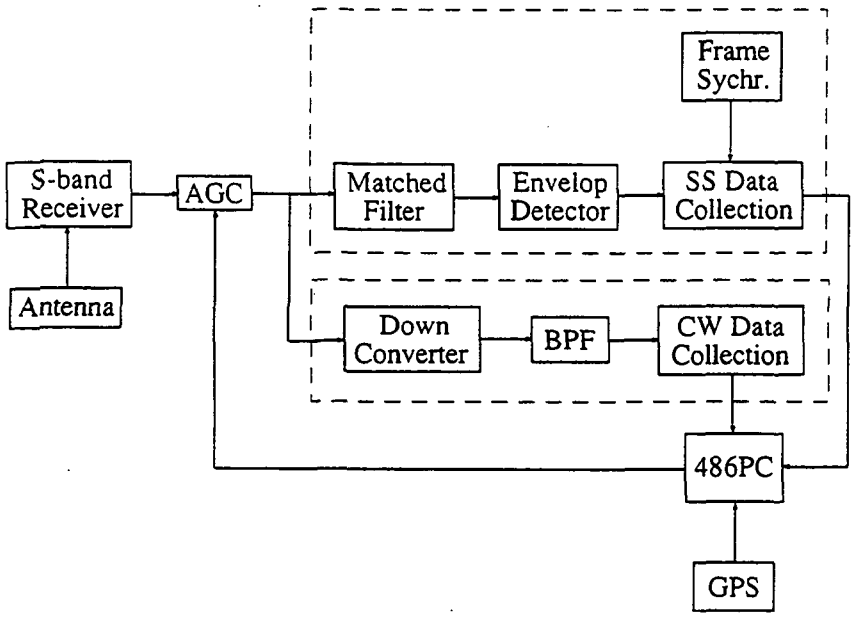

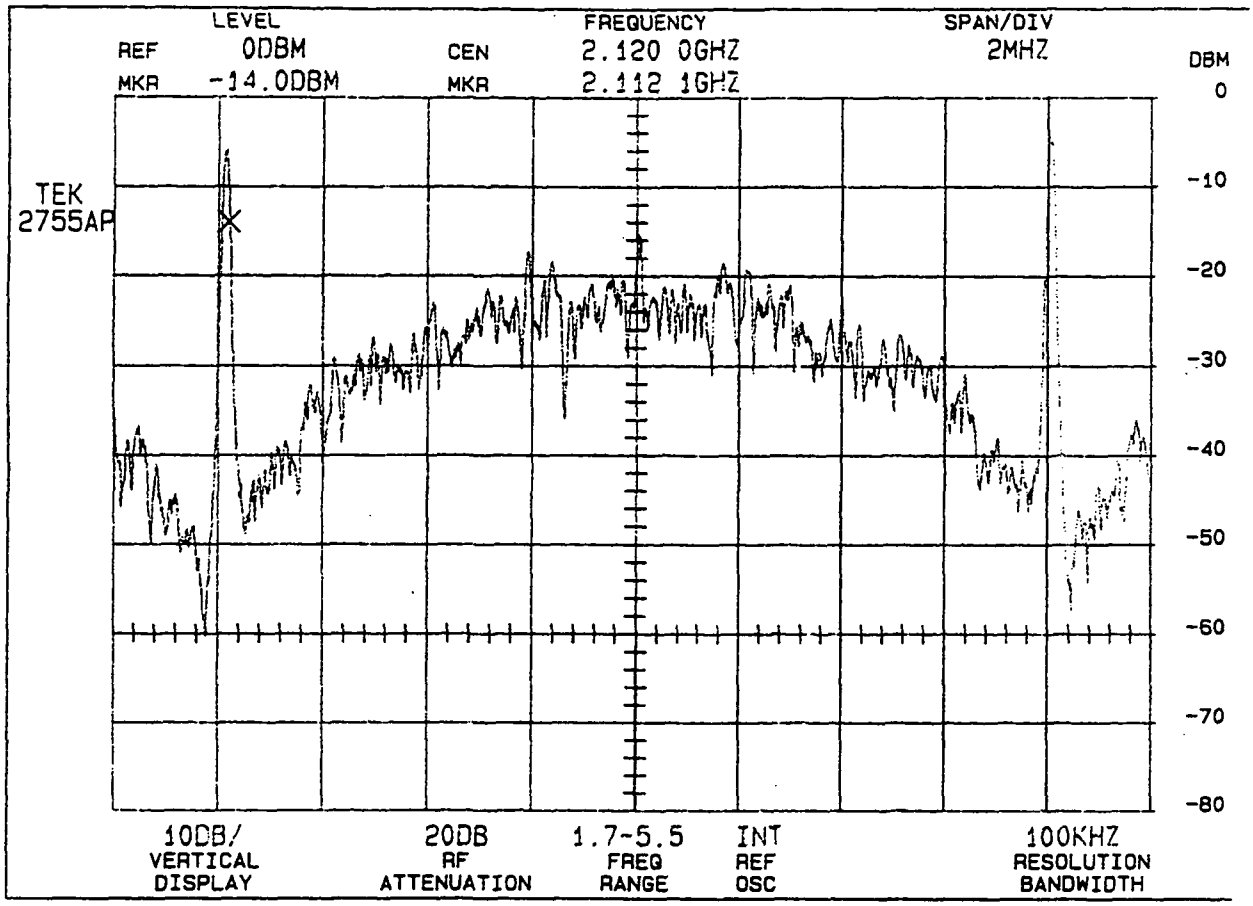

Data Collection Locations & Schedule

- LAS CRUCES & EL PASO (Week of June 19)
- ALBUQUERQUE & DENVER (Week of June 26)
- DALLAS/FT WORTH (Week of July 10)
- AUSTIN& SAN ANTONIO (Week of July 10)
- TUCSON & PHOENIX (Week of July 24)

Wideband Propagation Measurement System Using Spread Spectrum Signaling and TDRS[1]

Jeffrey D. Jenkins, Yiping Fan and William P. Osborne

Department of Electrical and Computer Engineering
New Mexico State University, Las Cruces, NM 88003

Abstract

In this paper, a wideband propagation measurement system, which consisted of a ground-based transmitter, a mobile receiver, and a data acquisition system, was constructed. This system has been employed in a study of the characteristics of different propagation environments, such as urban, suburban and rural areas, by using a pseudonoise spreading sequence transmitted over NASA's Tracking and Data Relay Satellite System. The hardware and software tests showed that it met overall system requirements and it was very robust during a 3-month-long outdoor data collection experiment.

1. Introduction

It is fundemental to have a good understanding of the channel characteristics in the planning and designing of mobile satellite systems. Otherwise, one will either suffer very poor system performance or come up with an unrealistic fading margin. Although many results have been presented in characterizing channels [1], more experimental and analytical works on propagation are needed, since the channels are statistical and frequency dependent in nature. As a part of the effort, a study of wideband propagation characteristics by using spread spectrum signaling over NASA's Tracking and Data Relay Satellite-F3 (TDRS-F3) was conducted. This study filled a gap in the propagation data base (model) of wideband signals at S-band and provided an experimental view of multipath phenomenon in real environments.

The study was divided into two phases. In the first phase, a wideband propagation measurement hardware and software system was developed. The field data collection and post data analysis were carried out in the second phase. Only the first phase work is discussed here[2]. Since there is no standard product available for wideband propagation measurement, it is hoped the knowledge and experience gained in the development of this hardware system will be useful to others.

---

1 The authors wish to acknowledge the funding of this research under NASA grant NAG-5-2143, and for the arrangements which NASA made to permit the use of TDRS-F3 in making the propagation measurement.

2 Refer to [2], if interested in the second phase work.

The hardware system consisted of a transmitter, located at White Sands Ground Terminal (WSGT), a receiver in a van and a data acquisition system. Figure 1 shows how the system is used in a data collection experiment. A 1024-bit-long psuedonoise (PN) spreading signal was transmitted by WSGT at Ku-band and received by the NMSU mobile receiver at S-band, where *td* is the path delay of the line-of-sight signal and *tr1+tr2* is the path delay of one of the multipath signals. At the receiving end, a surface acoustic wave (SAW) matched filter tuned to this sequence will produce autocorrelation pulses whose amplitudes and time locations can be used to indicate symbol energy, fading depth, and multipath delay spread.

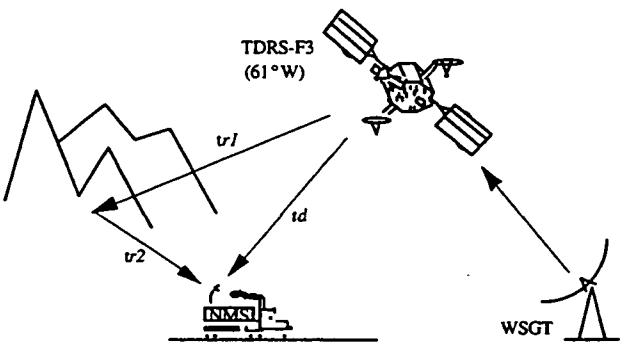

Figure 1. Wideband propagation measurement experiment

System parameters were selected based upon the availability of resources and system components as well as the existing system belonging to Mobile Datacom Corporation, which is representitive of new mobile satellite spread systems which are currently under development.

A link analysis is given in Table 1 which indicates that the available E_s/N_0 is 26.1 dB. With the minimum E_s/N_0 required for signal detection of 5 dB, the resulting dynamic range of the measurement is 21.1 dB.

Table 1. Link budget

EIRP @ TDRS-F3	+ 47 dBW
Receiver Antenna Gain	+ 5.0 dBic
Free Space Path Loss @ 2090 MHz	- 191.8 dB
Carrier Power @ Ground	- 139.3 dBW
Antenna Temperature	300 K
LNA Temperature	124 K
System Temperature	235 K
kTsys	- 204.9 dB
C/kT	+ 65.6 dB
Symbol Rate	+ 39 dB
Es/No	+ 26.1 dB
Minimum Es/No for Detection	+ 5 dB
Dynamic Range	+ 21.1 dB

Before the hardware system was used in data collection, it was tested and verified in the lab using two input sources: (1) an IF source with varying E_s/N_0; (2) a RF source from TDRS-F3 with varying transmitting power. The test showed that the system met the data collection requirements and functioned over a dynamic range of 20 dB.

The measurement system has been applied to wideband data collection in 21 different geographical locations of the western and southeastern parts of the country in the summer of 1993. During this 3-month-long data collection campaign, this system was very robust and functioned very satisfactorily.

2. Wideband Propagation Measurement System

2.1 Transmitter

The transmitter hardware, located at White Sands Ground Terminal (WSGT), consisted of a PN-generator with an 8 MHz clock and a BPSK modulator. The general block diagram is shown in Figure 2.

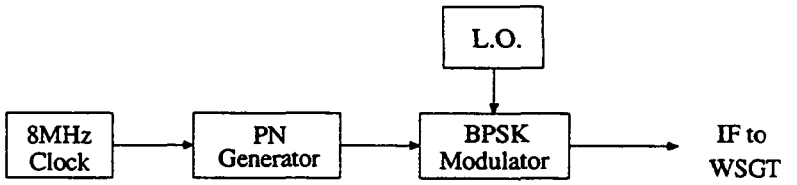

Figure 2. Block diagram of transmission equipment

The PN generator produced a 1024 chip sequence to match that of the SAW matched filter at the receiving end. This sequence consisted of four 256 bit code sequences in a non-inverted/inverted/non-inverted/non-inverted pattern. This means that the first sequence of 256 chips is the non-inverted code; the second one is the same code sequence, but inverted; the third and fourth 256 chip blocks are identical to the first sequence.

This 1024 chip sequence, driven by the 8MHz clock, was input to the BPSK modulator working at an intermediate frequency (IF) of 370.000 MHz to provide a spread spectrum signal operating at 8 MChips/sec with null-to-null bandwidth of 16 MHz. This spread spectrum signal was transmitted to TDRS-F3 by the WSGT at K-band unlink and received by the mobile receiver at S-band (2090 MHz) via the TDRS-F3 satellite downlink. WSGT transmitted the 1024 chip sequence continuously for the duration of the test.

2.2 Receiver

The receiver hardware set in the van consisted of an antenna, an S-band receiver, a SAW matched filter, and an envelope detector. The general block diagram of the receiver subsystem is depicted in Figure 3. The S-band receiver unit mixed the received signal with

the proper frequencies to bring the signal down to an intermediate frequency matching that of the SAW matched filter. The envelope detector converted the output of the matched filter into a baseband signal which was fed to the data acquisition system (DAS) for digitizing, sampling and data storage.

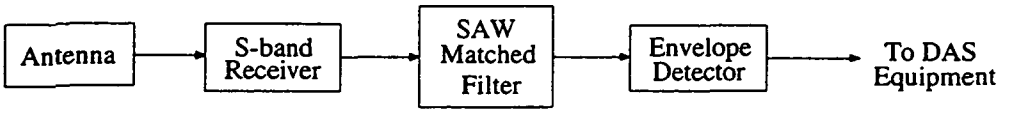

Figure 3. Block diagram of receiver equipment

Antenna

The antenna subsystem, mounted on the roof of the van, was composed of a Quad Helix antenna and a low noise amplifier (LNA). The Quad Helix antenna was selected to obtain omnidirectional coverage. It had a left hand circular polarization and a peak gain of 5 dBic. To minimize the SNR degradation due to cable loss between the antenna and the S-band receiver, a low noise amplifier with 20 dB gain was mounted immediately following the antenna. The electric field patterns of the antenna are depicted in Figure 4, (a) for an incident angle of 30° and rotation angle of 0° – 360° and (b) an incident angle of 0° – 360° and a rotation angle of 90°. These two antenna patterns were sufficient to cover all likely driving conditions in the data collection campaign.

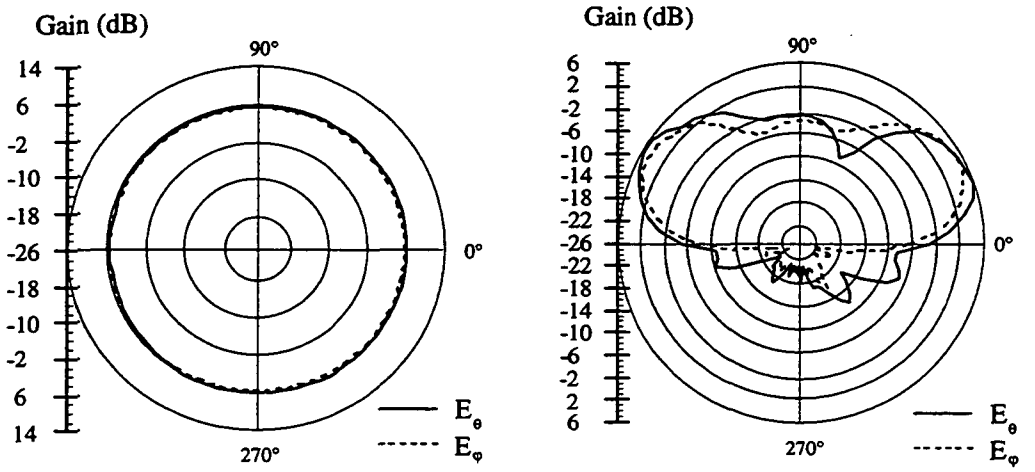

(a) incident 30° and rotation 0° – 360° (b) incident 0° – 360° and rotation 90°

Figure 4. Antenna patterns

S-Band Receiver

The S-band receiver contained the down-conversion hardware as shown in Figure 5. The S-band signal from TDRS-F3 was received through the Quad Helix antenna and entered a band pass filter (BPF) centered at 2090 MHz to reject out-band noise. The

output of the BPF was mixed with a 1930 MHz source from L.O. 1 (HP8657B signal generator), and a second BPF was used to pass the desired frequencies centered at 160 MHz. The signal was mixed a second time, with 87.997 MHz supplied by L.O. 2 (HP-8656B signal generator). A 135 MHz low pass filter (LPF) was used to reject the mixer product of 247.997 MHz. The signal was then band-pass filtered at 75 MHz to isolate the required frequencies (centered at 72.003 MHz, i.e., the IF frequency of the SAW matched filter) of the mixer. This resulting signal was fed into the SAW matched filter. Several amplifiers and pads were used to provide isolation and the desired signal gain.

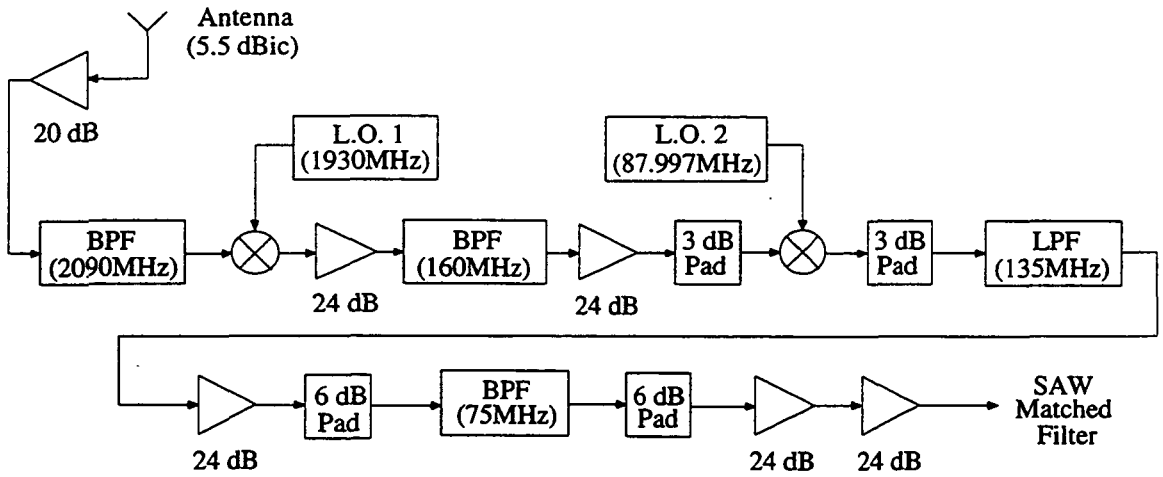

Figure 5. S-band receiver

SAW Matched Filter[3]

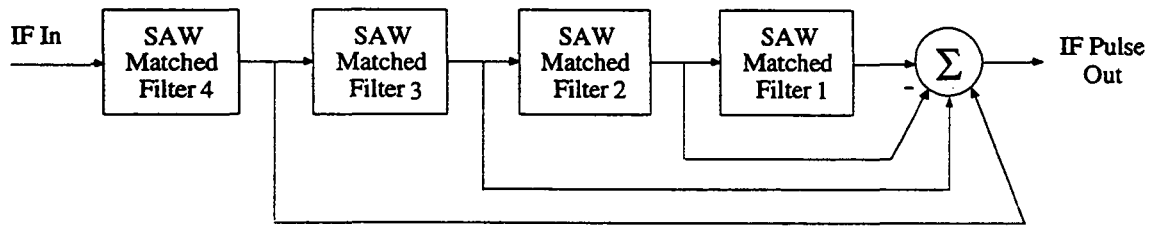

Figure 6. Matched filter configuration

The SAW matched filter converted the modulated PN sequence to an IF autocorrelation pulse. This special matched filter was comprised of four SAW sub-filters, as depicted in Figure 6 above. Each sub-filter matched the same 256-chip sequence of non-inverted code. Functionally, the third sub-filter matched to the 256-chip sequence of inverted code, because of its negative contribution to summer. This structure theoretically ensured that (1) when each sub-filter aligned with this 256-chip sequence and the received sequence pattern was non-inverted/inverted/non-inverted/non-inverted, the output of the matched filter would produced an IF autocorrelation pulse of width 250 ns, and (2) when

[3] The SAW matched filter was supplied by Mobile Datacom Corporation.

either the pattern or the 256-chip sequence was misaligned, no output or noise with very small magnitude, would be generated. Figure 7 shows a typical output of the SAW matched filter in response to the 1024 PN sequence after the demodulation by the envelope detector. Since the DAS sampled only 1000 points per waveform at 50 MSa/s, Figure 7 gives a fraction (20 μs out of 128 μs) of the response around the auotcorrelation pulse.

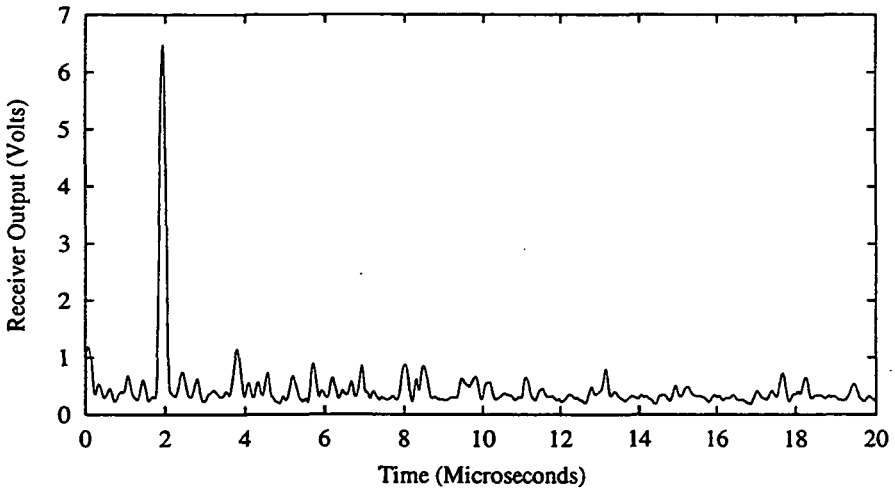

Figure 7. Typical reponse of the matched filter after demodulation

Envelope Detector

The IF output of the SAW matched filter was demodulated with the HP model 420B envelope detector. Because this particular envelope detector provided a negative pulse, it was inverted and then amplified to provide a baseband autocorrelation pulse.

2.3 Data Acquisition System

The DAS was responsible for the digitization, sampling and storage of the output of the SAW matched filter. Some basic functions of the DAS were:

1) Digitize, sample and store waveforms;
2) Acquire GPS data every minute;
3) Determine the synchronization state or lock condition;
4) Record multipath signals with maximal differential distance of 3 miles.

The autocorrelation pulse to be digitized was 250 ns wide (two-times the bit duration at 8 Mchips/sec). The pulse was sampled at 50 MSa/s. This gave 12 samples along the autocorrelation pulse to allow pulse reconstruction and peak estimation.

Objects within a few miles are of concern because they may cause significant multipath interference in received signals. Multipath signals from objects farther than a few miles away are attenuated to atmospheric noise levels and are therefore not necessary to

observe. It was necessary to digitize enough points so that a total multipath differential distance (distance traveled by the multipath signal minus that traveled by the direct signal) of several miles was included in the waveform record. At a sample rate of 50 MSa/s, a waveform with 806 samples was able to see a multipath distance less than or equal to 3 miles. For simplicity, the number of samples per waveform was selected to be 1000 which resulted in a total of 20 μs of data per waveform. Accounting for 2 μs of data, collected prior to the peak (Figure 8), a total of about 18 μs was left for the autocorrelation pulse and multipath. Hence, the multipath effect which could be seen from the waveform had a maximal distance of 3.35 miles.

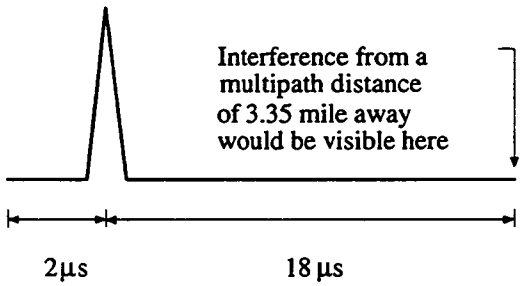

Figure 8. Theoretical Received Waveform

The DAS consisted of a frame synchronizer, a GPS antenna, a GPS receiver card, an HP digitizing oscilloscope, a 486-33 MHz computer and a tape backup system. A video camcorder was also present to record actual paths traversed by the van. This allowed us in part to review weather conditions and objects causing interference in data analysis. A general block diagram of the DAS equipment is shown in Figure 9.

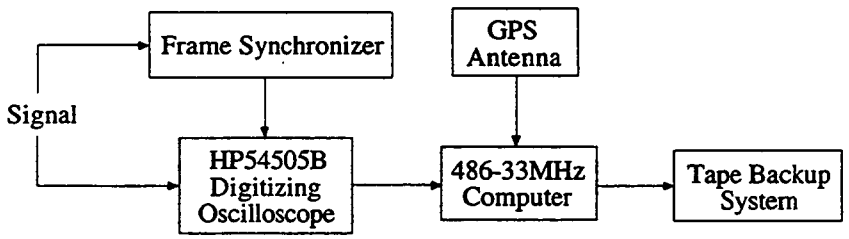

Figure 9. Block diagram of the DAS

Frame Synchronizer

The baseband autocorrelation pulse from the envelope detector was supplied to the frame synchronizer. The frame synchronizer board used a digital phase locked loop design to acquire and track a pulse of known period. The circuit then provided an external trigger pulse to the oscilloscope signifying both the lock condition of the board and the imminent occurrence of the tracked pulse within a known window of time so that data could be sampled. Figure 10 is a block diagram of the frame synchronizer.

In a locked condition, the incoming pulse occurred within a "look" window. If the pulse was away from the center of the window, a feedback mechanism was involved such

that the VCO input voltage was altered which forced the center of the window tracking the incoming pulse. Board timing was derived from two counter circuits. The first circuit operated at 16 MHz and consisted of a 24 bit counter used to set the desired pulse period. The second counter circuit operated at 2 MHz and adjusted the length of the window.

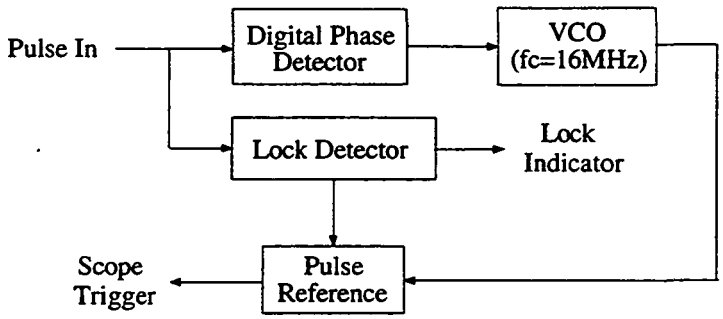

Figure 10. Frame synchronizer block diagram

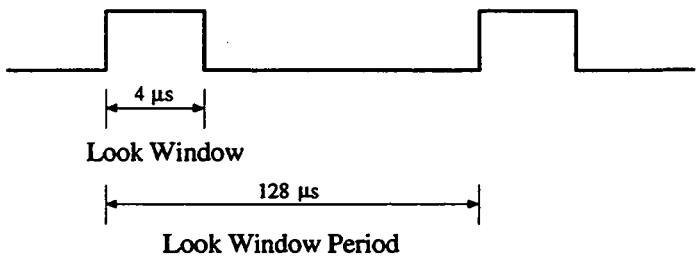

Figure 11. Frame timings

The look window period (Figure 11) was selected to be 128 µs which was the elapsed time between autocorrelation pulses generated by the matched filter. The window duration was selected to be 4 µs, 16 times the pulse width of 250 ns.

The lock detector circuit was also built to indicate the lock condition. The lock condition remained in effect as long as pulses occurred in the window. This sustained lock allowed the system to momentarily lose the incoming pulse and still maintain the same location in time to find it when it came back (should it be lost due to a short duration fade). The maximum time to remain in lock without a pulse was approximately 20 ms. When the circuit was out of lock, any pulse occurring within the window reset the period counter and lock was instantaneously achieved.

GPS Antenna

The GPS antenna allowed the NOVATEL Model 711 GPS receiver card, located inside the computer, to receive data from the GPS satellites. The GPS receiver card gave GPS time, latitude, longitude, altitude and standard deviations of those measurements.

HP Digitizing Oscilloscope

The HP54505B digitizing oscilloscope sampled the auto-correlation pulse from the envelope detector in the receiving equipment. The trigger pulse created by the frame synchronizer was fed directly into the scope trigger input. The 486-33MHz computer controlled the digitization process via IEEE-488 interface. The HP54505B digitizing oscilloscope was selected due to its 125 MHz bandwidth, 500 MSa/sec maximum sample rate and versatility.

486-33 MHz PC

The 486-33MHz computer with 32 Mbytes of RAM, controlled the digitization, collection, and storage of waveform data. It also controlled the collection and storage of GPS data. Writing to the hard drives while in transit could damage them. To overcome this problem, 28 Mbytes of RAM was configured into virtual RAM drives. With the Quarterdeck memory manager software, the largest configurable size of a RAM drive was 4096 KBytes, so 7 virtual drives (each with 4 Mbytes) were created. It took 3 seconds to digitize, transfer and store 30 waveforms and took about 20 minutes to fill all 7 RAM drives with data. After 7 RAM drives were full of waveform data, the DAS prompted the user to stop the van so that a safe transfer from volatile RAM to the hard drive could be executed.

Because GPS data was collected every minute, a means to correlate the GPS information to waveform record was required. A CPU time and GPS number was introduced in the data format (Figure 12) to achieve this correlation. At the beginning of a collection, the GPS number was zero and GPS data was collected, followed by a number of groups of 30 waveforms. Each time a new group of 30 waveforms was collected, and the elapsed time was less than 60 seconds, the GPS number was incremented. When 60 seconds had elapsed, a new GPS fix was collected and the GPS number was reset to zero. Therefore, GPS data was directly correlated to the time a group of 30 waveforms was collected by noting when the GPS number was zero. Since each sample took 16 bits, one waveform record with 1000 samples occupied 2000 bytes.

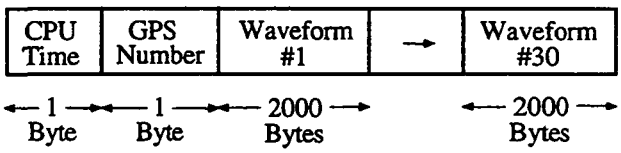

Figure 12. Data format for 30 waveforms

Tape Backup System

The tape backup system was the Colorado Jumbo 250 MByte Tape drive and software. This was used to back-up the hard drive data at the end of each days

measurement. It was necessary to clear the hard drives of all waveform data before a new data run could be executed.

3. System Test

Once the transmitter, receiver and data acquisition system were constructed, in-lab tests were conducted to confirm proper operation and to examine system performance. Two kinds of tests were done: (1) IF loop-back; (2) satellite reception of signals from TDRS-F3.

In-lab IF loop-back

In this test, the 1024-chip PN sequence, with BPSK modulation at an IF of 72.003 MHz, was supplied to the SAW matched filter. This test confirmed proper PN sequence generation, matched filter operation, demodulation, frame synchronization and DAS operation. Through varying E_s/N_0 of the input signal, these subsystems were checked over the entire operating range. Figure 13 shows the output voltage at the envelope detector with a varying E_s/N_0 from 25 dB to 5 dB in one decibal steps. The time indices from 1 to 30 correspond to an input E_s/N_0 of 5 dB. The next group of 30 indices has a E_s/N_0 of 6 dB, and so on. Therefore, the last group of indices from 600 to 630 represents an input E_s/N_0 of 25 dB. It was seen that although there was a nonlinear relation between the input and the output (primarily due to the envelope detector), this relation was consistent as expected. The test also showed that this system functioned over a dynamic range of 20 dB which was almost identical to the theoretical range of 21.1 dB given in Table 1, accounting for there were some uncertainties in the link budget calculation.

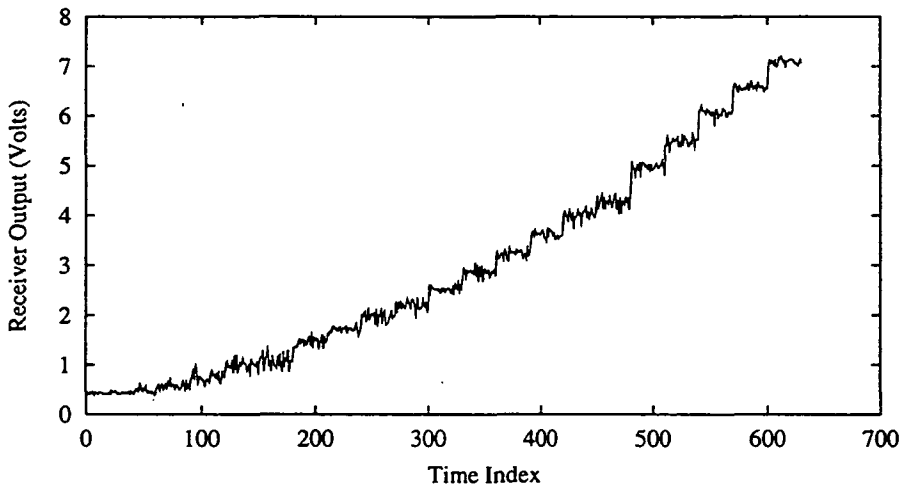

Figure 13. Voltage at receiver output during system calibration

In-lab satellite reception

The in-lab reception of the PN sequence from TDRS-F3 tested all subsystems in the entire link from the transmitter to DAS. During the test, TDRS-F3 alternately transmitted the PN signal and carrier so that E_s/N_0 level could be analyzed. The entire range of E_s/N_0 was checked by varying the transmitted power of TDRS-F3. Figure 14 shows the actual E_s/N_0 vs the observed E_s/N_0 in dB. The actual E_s/N_0 was varied approximately 2 dB each step. The test data was indicated by the points and the curve fitting was represented by the solid line. This fitting curve of the 3rd order polynomials was used to compensate the nonlinearity of the measurement system in propagation data processing so that the actual signal strength level could be restored. Again, the input-output relationship was consistent and the test was a success.

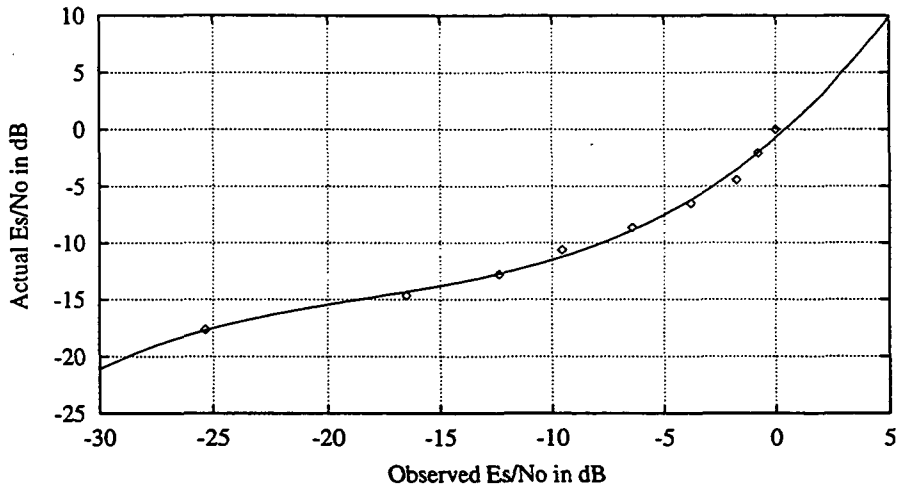

Figure 14. Measurement system calibration curve input vs output

4. Conclusions

A spread spectrum measurement system, which consisted of a ground-based transmitter, a mobile receiver and a data acquisition system, was fabricated. Two kinds of tests demonstrated that the system met the requirements for the data collection. This system allowed us to conduct experimental studies of channel fading by using spread spectrum signaling over NASA's Tracking and Data Relay Satellite. It has been used in a data collection campaign in many different geographical areas, including cites, canyons, prairies, wooded tree roads, etc. During the 3-month-long operation, the system was very robust and functioned very satisfactorily. Since the system used the spread spectrum technique, it was also capable of measuring multipath phenomena.

References

[1] Goldhirsh, J. and W. J. Vogel, " Propagation Effects for Land Mobile Satellite Systems: Overview of Experimental and Modeling Results ", NASA Reference Publication 1274, February 1992.

[2] Jenkins, J. D., Y. Fan and W. P. Osborne, "Channel Fading for Mobile Satellite Communications Using Spread Spectrum Signaling and TDRSS", Proc. NAPEX XIX, June, 1995.

[3] Goddard Space Center, " Performance Specification for Service via the Tracking and Data Relay Satellite System ", Revision C, July 1989.

[4] Osborne, W. P. and W. Drozdick, Jr., " Data Acquisition System for S-band Propagation Study ", Technical Report, NMSU-ECE-93-019, December 1993.

Acknowledgment

The authors wish to thank Steve Kelly for his efforts in system fabrication and installation, Al Carrier, Abe Valdez, Ted Wolcott and Bill Drozdick for their work in system fabrication and test, and Bill Linde for his software development of DAS. The authors would also like to thank Dr. Les Snively of Mobile Datacom Corporation for supplying the 1024-bit SAW matched filter used in the receiver. This study was supported by NASA under Grant #NAG 5-2142.

Satellite and Terrestrial Narrow-Band Propagation Measurements At 2.05 GHz

A. Vaisnys Jet Propulsion Laboratory, California Institute of Technology
W. Vogel EERL/University of Texas at Austin

1. Introduction

A series of satellite and terrestrial propagation measurements were conducted on 15 and 16 December, 1994 in the vicinity of the Jet Propulsion Laboratory (JPL), Pasadena, California, in support of the VOA/JPL DBS-Radio Program. The reason for including terrestrial measurements was the possible use of terrestrial boosters to improve reception in some satellite digital audio broadcasting system service areas.

The signal sources used were the NASA TDRS satellite located at 171 degrees West and a terrestrial transmitter located on a high point on JPL property. Both signals were unmodulated carriers near 2.05 GHz, spaced a few kHz apart so that both could be received simultaneously by a single receiver. An unmodulated signal was used in order to maximize the dynamic range of the signal strength measurement. A range of greater than 35 dB was achieved with the satellite signal, and over 50 dB was achieved with the terrestrial signal measurements.

Three test courses were used to conduct the measurements:

- A 33 km round trip drive from JPL through Pasadena was used to remeasure the propagation of the satellite signal over the path previously used in DBS-Radio experiments in mid 1994. A shortened portion of this test course, approximately 20 km, was used to measure the satellite and terrestrial signals simultaneously.

- A 9 km round trip drive through JPL property, going behind buildings and other obstacles, was used to measure the satellite and terrestrial signals simultaneously.

- A path through one of the buildings at JPL, hand carrying the receiver, was also used to measure the satellite and terrestrial signals simultaneously.

Below is a photograph of the view from the terrestrial transmit site down to JPL and toward Pasadena. The horizon is Colorado Boulevard, which marks the far point of the Pasadena runs. Building 161, which was the site of the indoor measurement, is indicated.

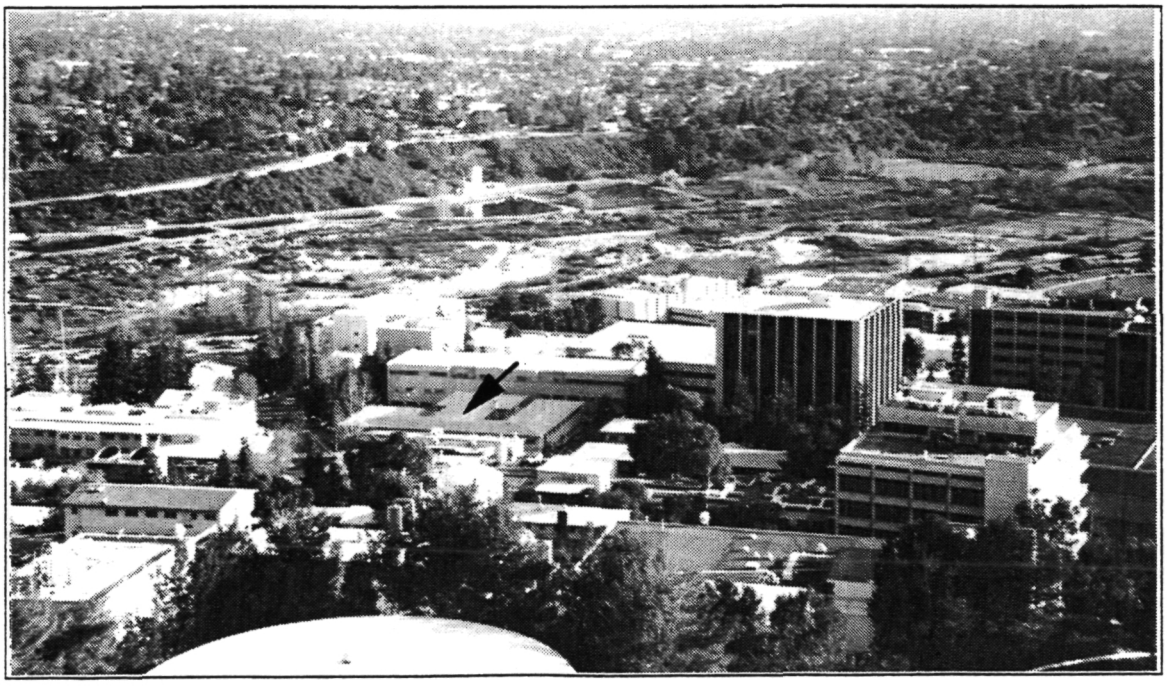

2. Test Configuration

The receiving system configuration for the automobile mounted equipment is shown in Figure 1. The receiving antenna was a bifilar helix with a gain of 8 dBi at 25 degrees' elevation.This was followed by a low noise amplifier and a receiver which converted the signal to the audio frequency range between 2.5 kHz and 7.5 kHz. This signal was recorded on a digital audio tape (DAT) recorder at a sampling rate of 48 kHz. Post processing was then used to filter and detect the signal amplitude and phase. The resultant data was provided at a sample rate of 1000 samples per second.

The configuration used indoors was the same except that the antenna was omnidirectional, with approximately 0 dBi gain.

All of the outdoor tests also included recording with two vehicle mounted video cameras, one facing forward and the other a fisheye lens facing up. A global positioning system (GPS) receiver was used to record vehicle position, speed and heading.

The direction to the satellite was 248 compass degrees (South of West) and the elevation angle was 22 degrees. The direction to the terrestrial transmitter was generally to the North or Northwest.

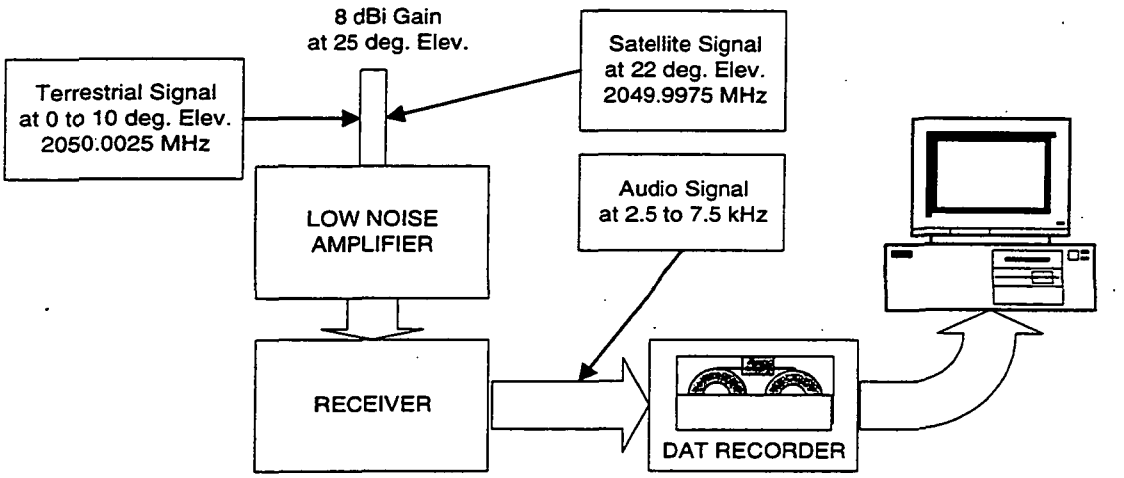

Figure 1. Receiving System Configuration

3. Test Results

The complete set of test data is documented in University of Texas Report EERL-95-B1, 10 February, 1995. This paper presents a selection of the test results and some conclusions on the differences in propagation of satellite and terrestrial signals.

3.1. Pasadena Run 1 - Satellite Signal.

The Pasadena long path was used in a previous test, in mid 1994, to test the performance of the VOA/JPL DBS Receiver with TDRS. Signal drop-outs were experienced due to blockage by buildings and trees. The signal strength measurement showed sharp signal drops during blockage, but being a wide band measurement, it could not achieve a dynamic range of more than about 10 dB. The main purpose of the December 1994 test run 1 was to retest this path with a much wider dynamic range signal measurement.

Figure 2 shows a map of the test route, with a short description of the terrain given in Table 1. Figure 3 shows a GPS derived plot of the vehicle position during the test run.

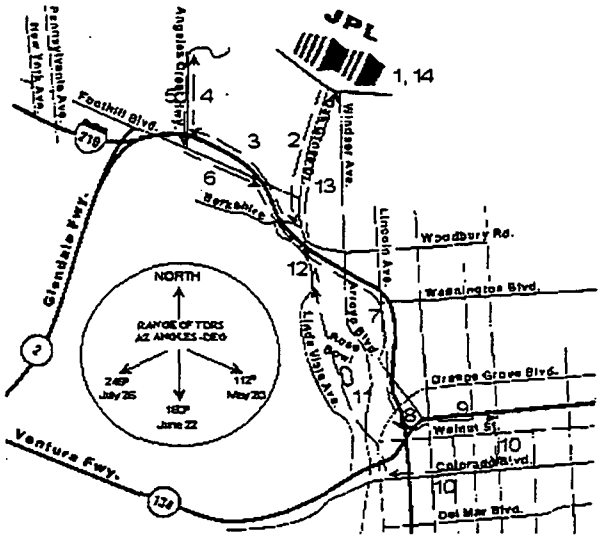

Figure 2. Test Route

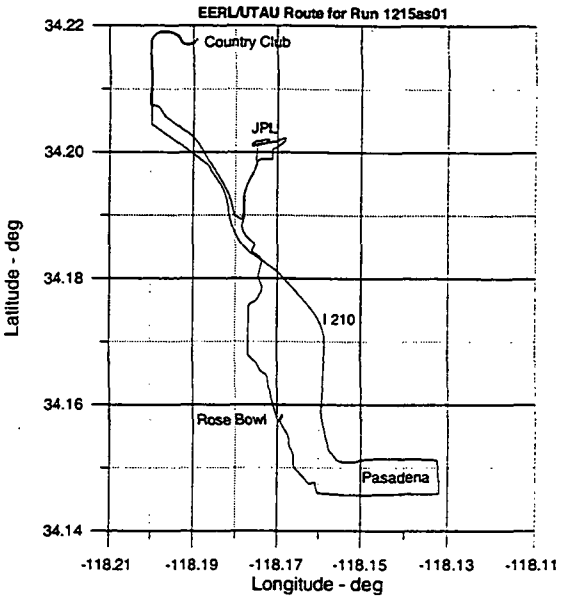

Figure 3. GPS Derived Vehicle Position

Table 1. Test Route Description

Buildings and trees on JPL property	1
Medium width, 4 lane , street with trees at varying distance from roadway	2
Above street level freeway with occasional overpasses	3
Wide, 4 lane, street with trees at varying distance from roadway (North)	4
Wide, 4 lane, street with trees at varying distance from roadway (South)	5
Commercial with low buildings	6
Above street level freeway with occasional overpasses	7
Two long tunnels	8
Below street level freeway with occasional overpasses	9
Commercial, mostly 3 story, but some tall buildings	10
Mixed open and some trees close to road	11
Residential heavily shaded by trees	12
Medium width, 4 lane , street with trees at varying distance from roadway	13
Buildings and trees on JPL property	14

Figure 4 is a plot of the received signal power, at 100 samples per second, relative to a line-of-sight value referenced to 0 dB. The measurement indicates that there is very little multipath under line-of-sight conditions. Most impairments are due to signal blockage by buildings and trees. Figure 5 shows the histogram and cumulative probability of the received signal power samples, which indicate that signal attenuation under the test conditions exceeded 15 dB about 10 percent of the time and 30 dB about 2 percent of the time.

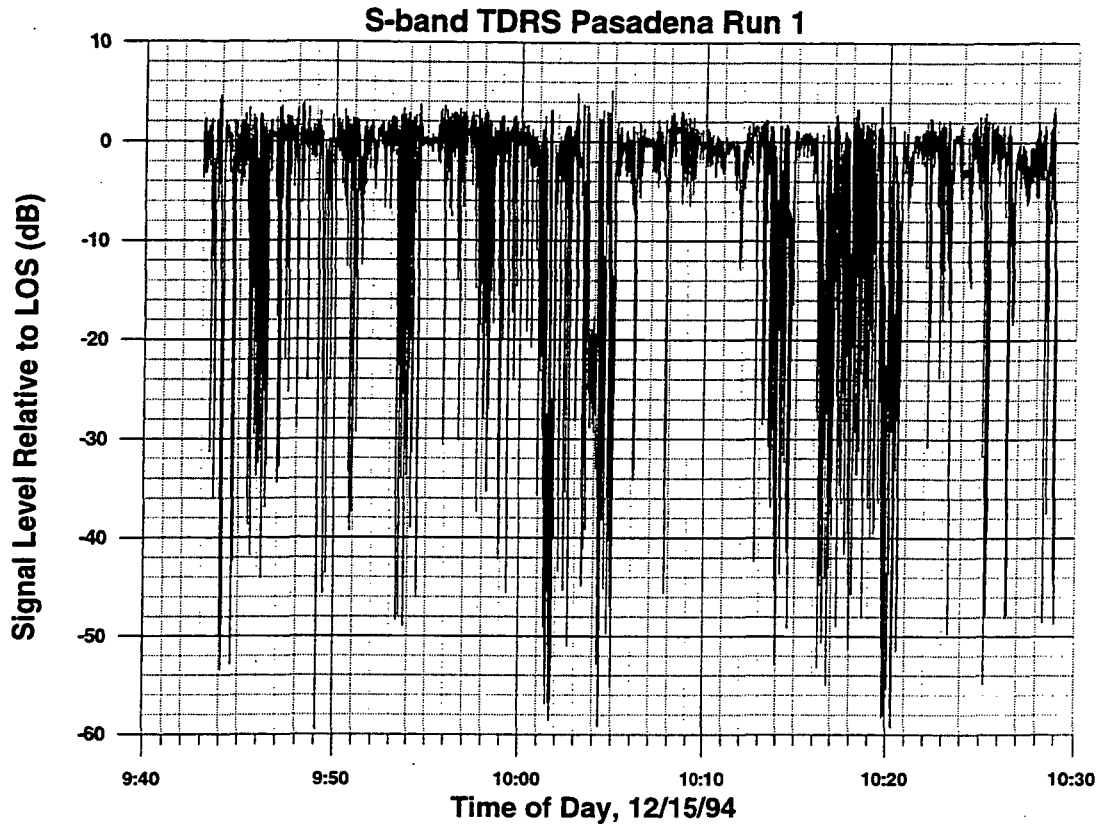

Figure 4. Received Satellite Signal Power for Run 1 (100 samples/sec.)

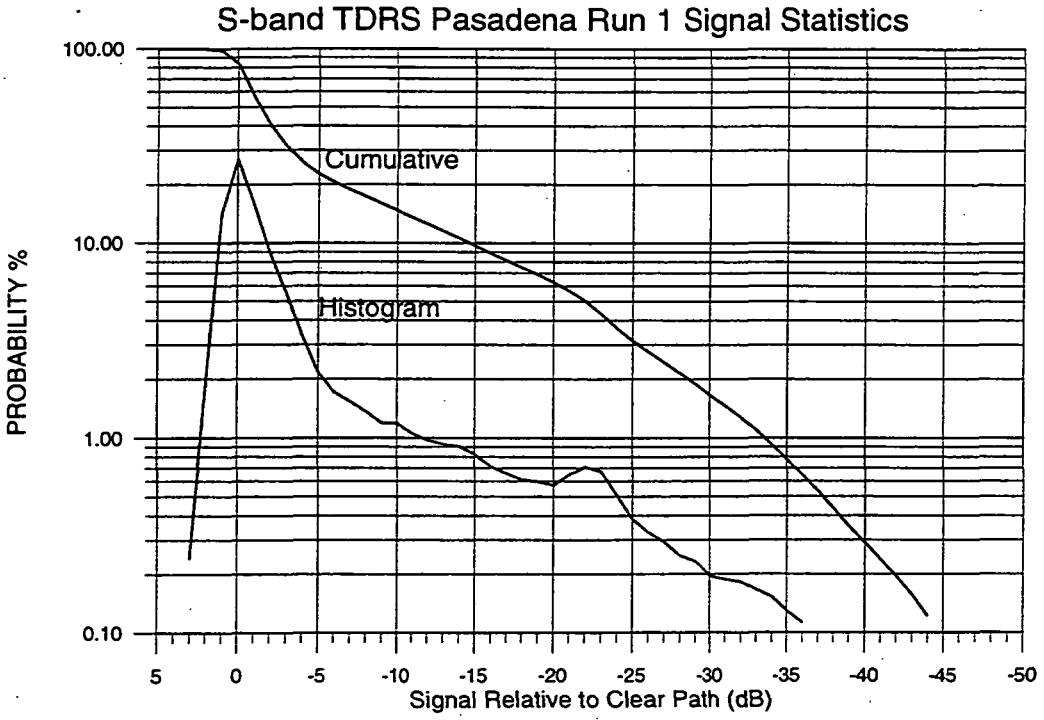

Figure 5. Signal Statistics for Run 1

3.2. Pasadena Runs 6 and 7 - Satellite and Terrestrial Signals.

These runs were conducted over the same test course as run 1, with the exception of sections 3 through 6 to the West of JPL. These sections could not be covered by the terrestrial transmitter.

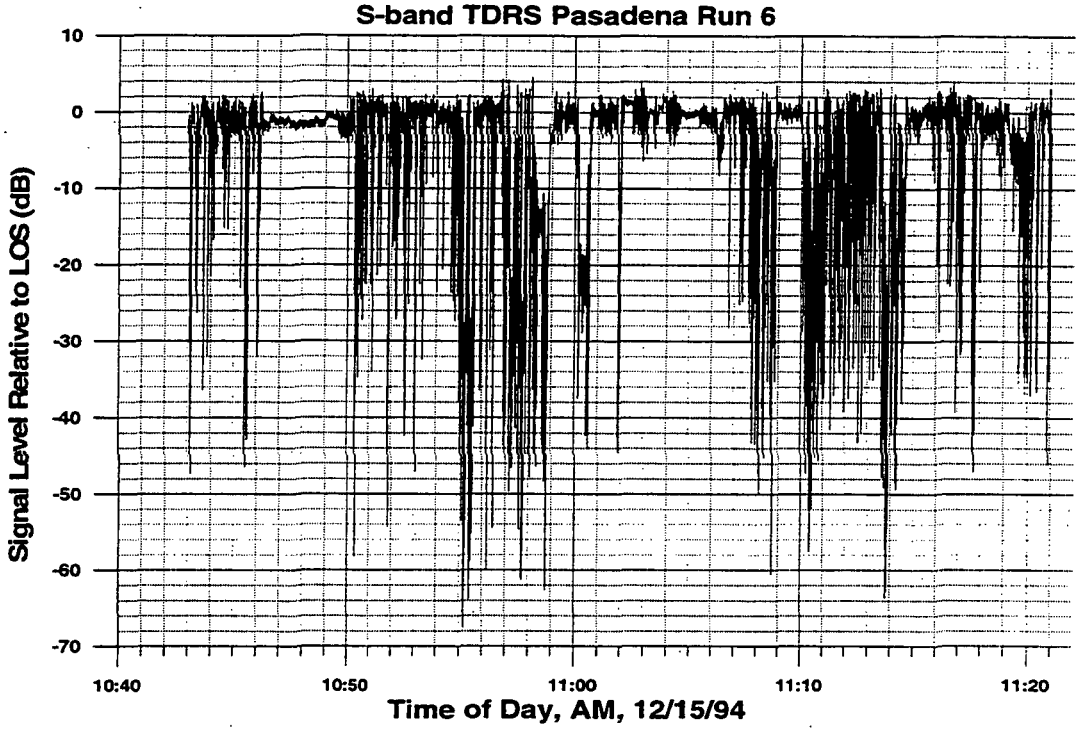

Figure 6. Received Satellite Signal Power for Run 6

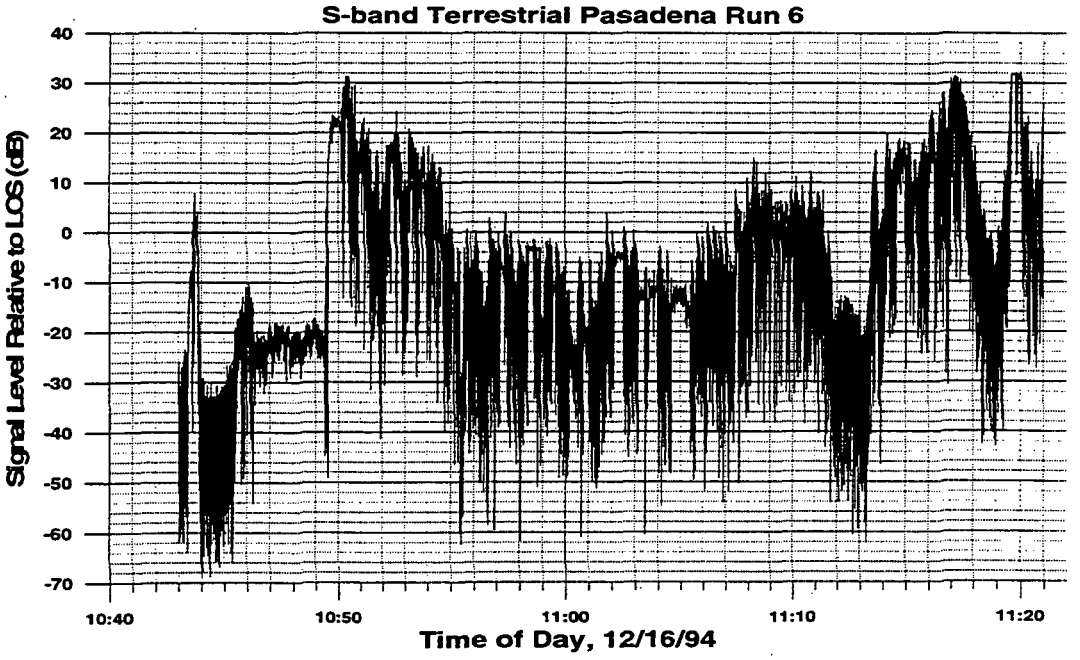

Figure 7. Received Terrestrial Signal Power for Run 6

Because of transmission at a lower elevation angle, the terrestrial signal suffers much more multipath than the satellite signal. In addition there is a greater chance of terrain blockage. Run 6 started on the hill near the terrestrial transmit site. In the initial part, from 10:43 to 10:49, the signal was blocked by the ridge upon which the transmitter was located. There are also indications of signal blockage by terrain at 11:12 and at 11:19.

Run 6 included several 360 degree loops in a parking lot. Figure 8 shows a plot of the satellite and terrestrial signal during the parking lot calibration circles. This plot also indicates that there is much more multipath for the terrestrial signal path.

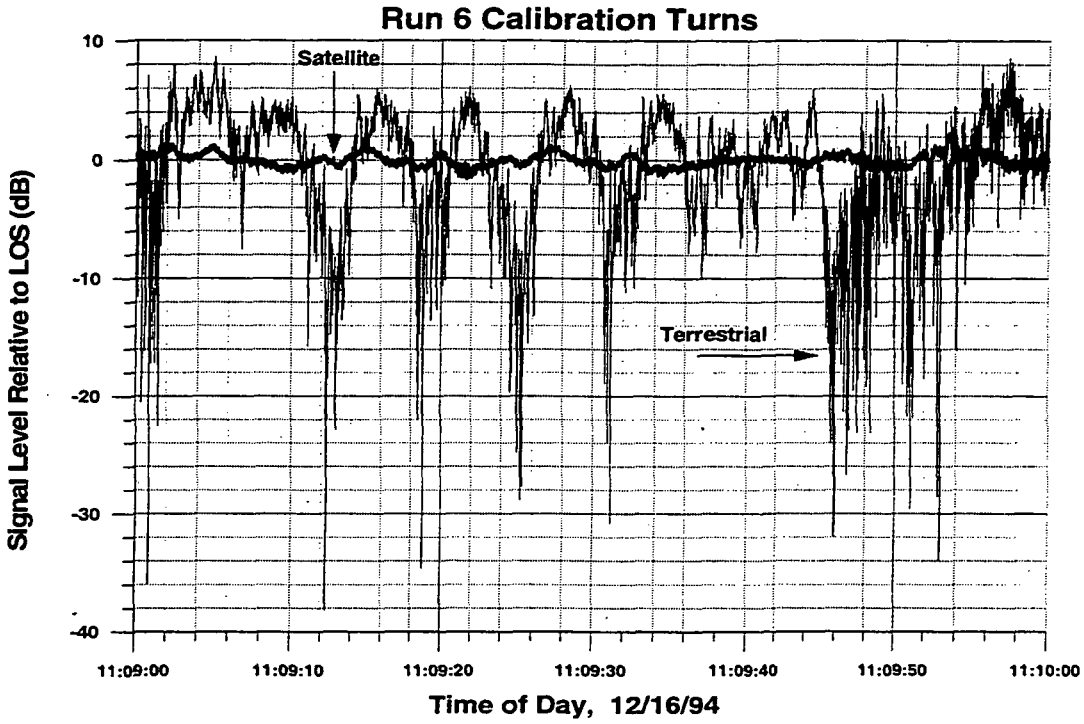

Figure 8. Satellite and Terrestrial Signal Measurement During Calibration Turns on Run 6.

Run 7 was conducted over the same test course as run 6, except that it was started past the initial area of terrestrial signal blockage. Run 7 also included a segment with the terrestrial signal turned off, which provided a calibration of the noise floor of the receiver for the terrestrial signal measurement.

Figures 9 and 10 show the received satellite and terrestrial sampled signals for run 7.

Figure 11 shows the received terrestrial signal averaged with a one second running average. This shows that much of the signal fluctuation structure seen in Figure 10 is of a short term nature, a good indication that signal fluctuations are caused by multipath. Multipath effects can be overcome to some extent by antenna diversity.

The average attenuation of the terrestrial signal over the test course was not excessive. Since it is possible to have larger terrestrial signal transmitter power, the use of wide area terrestrial boosters for augmenting satellite signal reception at S-band appears promising.

Figure 12 show the signal statistics for the satellite and terrestrial signal measurements of run 7.

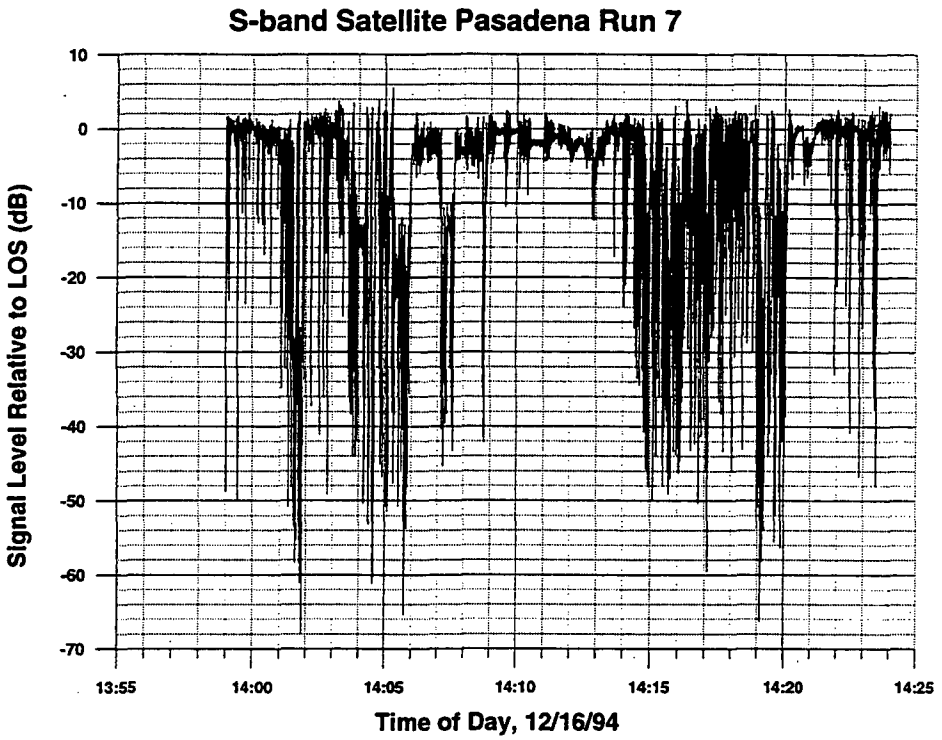

Figure 9. Satellite Signal Measurement

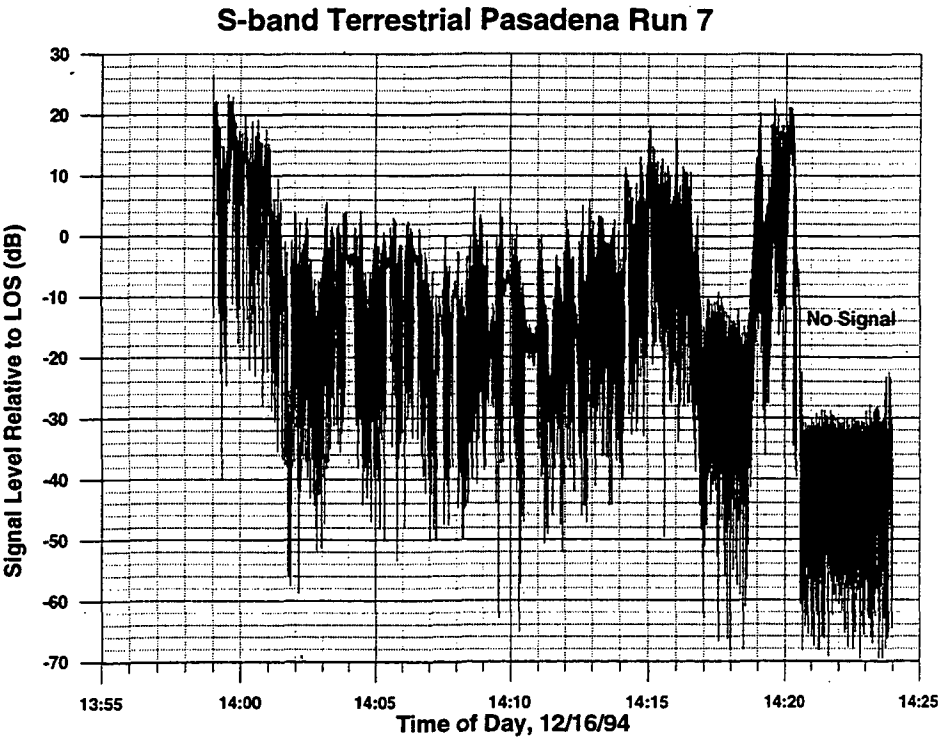

Figure 10. Received Terrestrial Signal Power

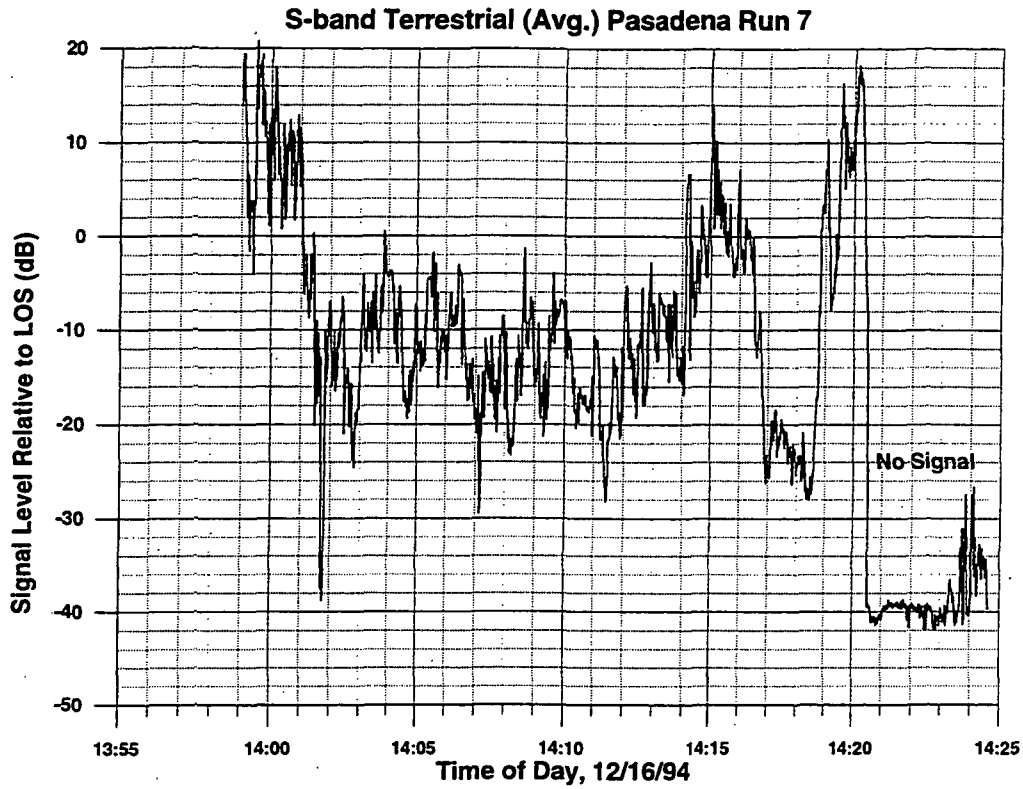

Figure 11. Received Terrestrial Signal Power for Run 7 - One Second Averages

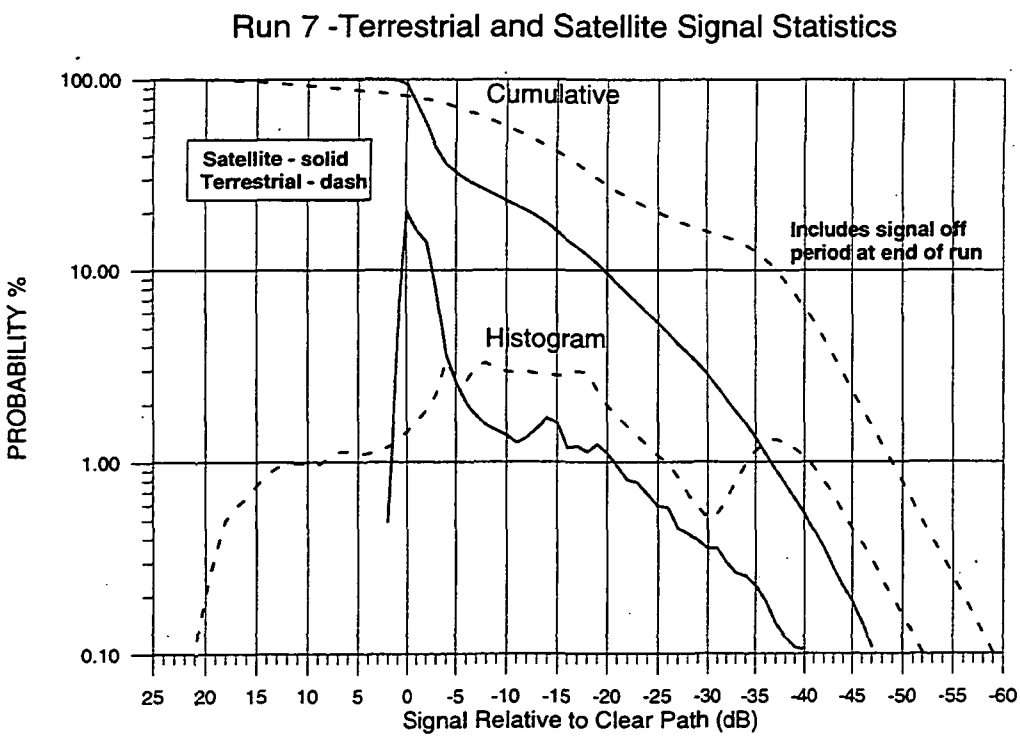

Figure 12. Histograms and Cumulative Probabilities of Received Signal Power for Run 7

3.3. JPL Run 5 - Satellite and Terrestrial Signals on JPL Test Run.

Run 5 was also a simultaneous measurement of the satellite and terrestrial signal, except that it was conducted over a shorter course within JPL. Figure 13 shows a map of JPL, while Figure 14 shows the GPS derived vehicle position during the test loop. Some drift in the latitude determination is apparent from this plot.

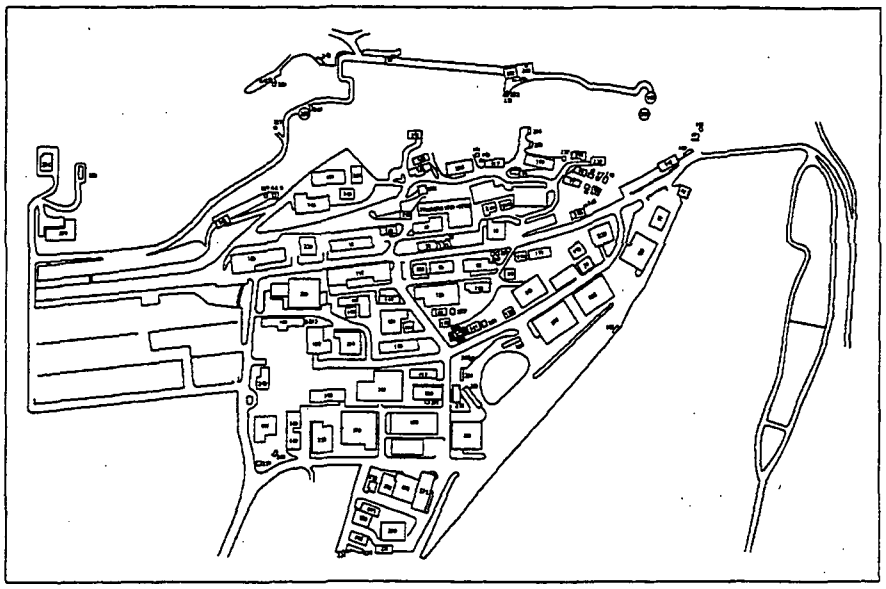

Figure 13. Map of the Jet Propulsion Laboratory

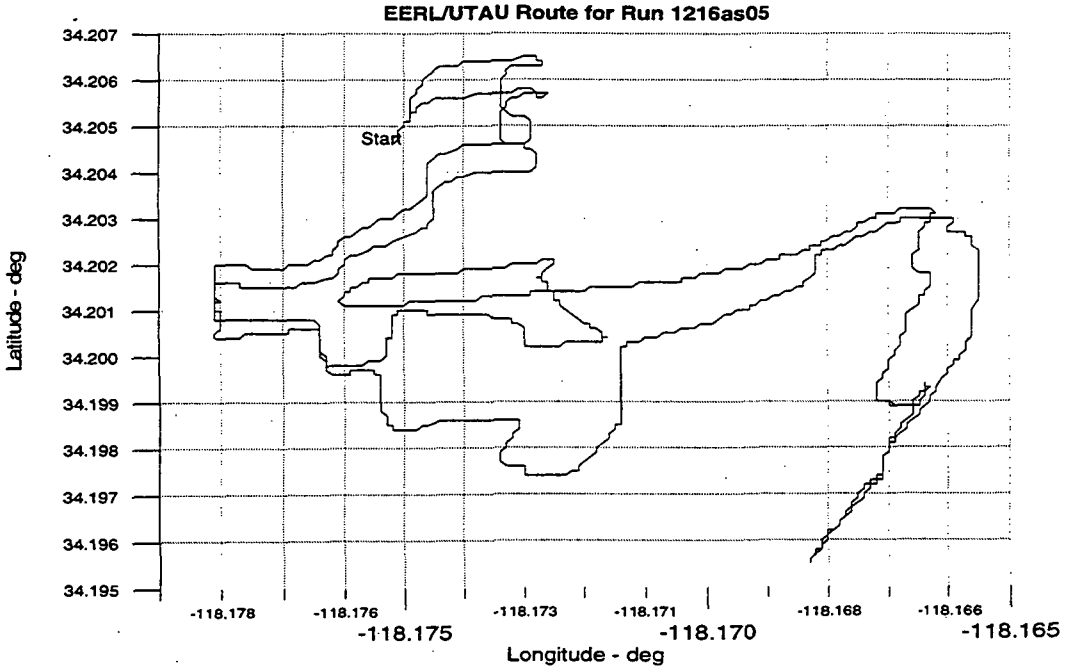

Figure 14. GPS Derived Position During Run 5

Figures 15 through 17 show the signal measurements and signal statistics for Run 5.

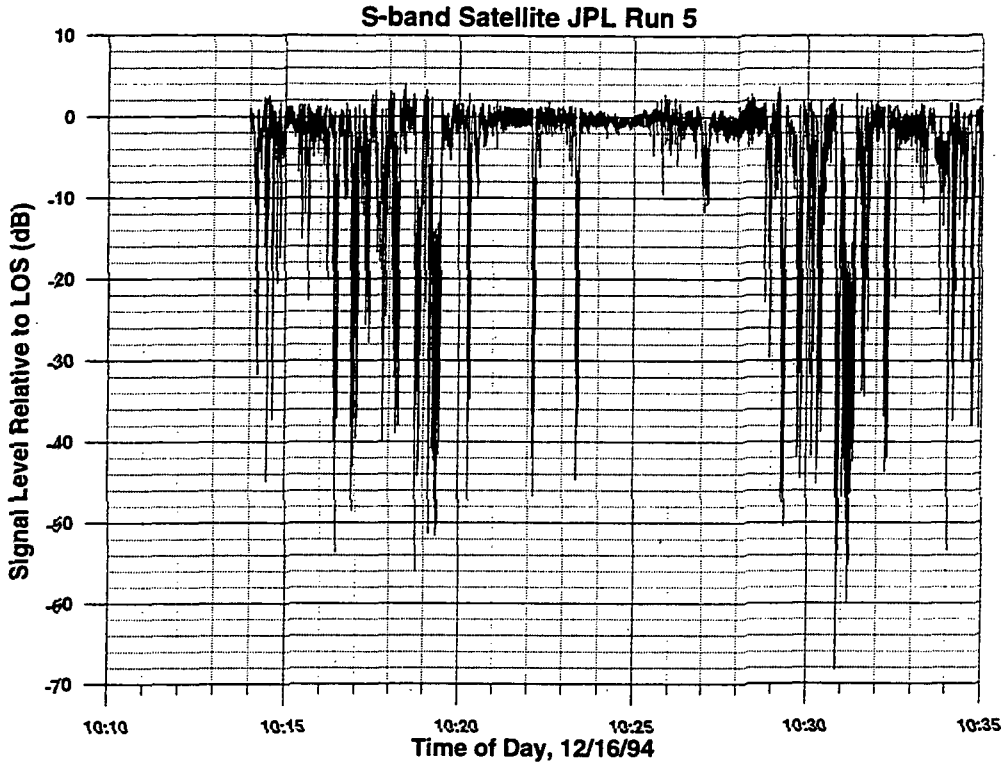

Figure 15. Received Satellite Signal Power

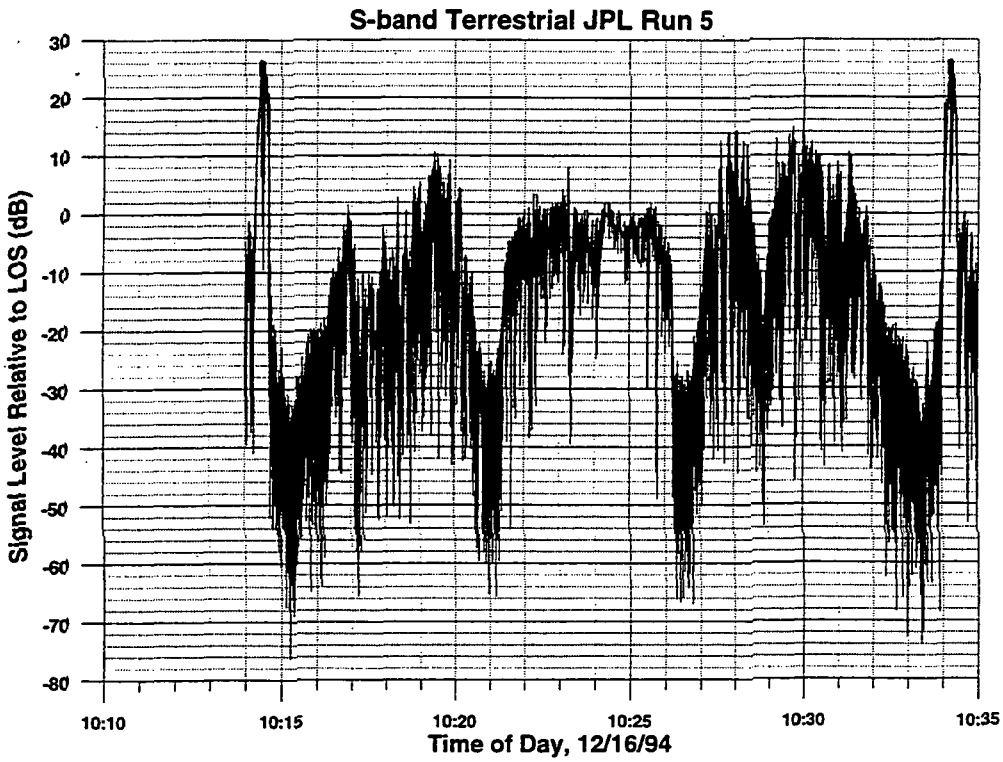

Figure 16. Received Terrestrial Signal Power

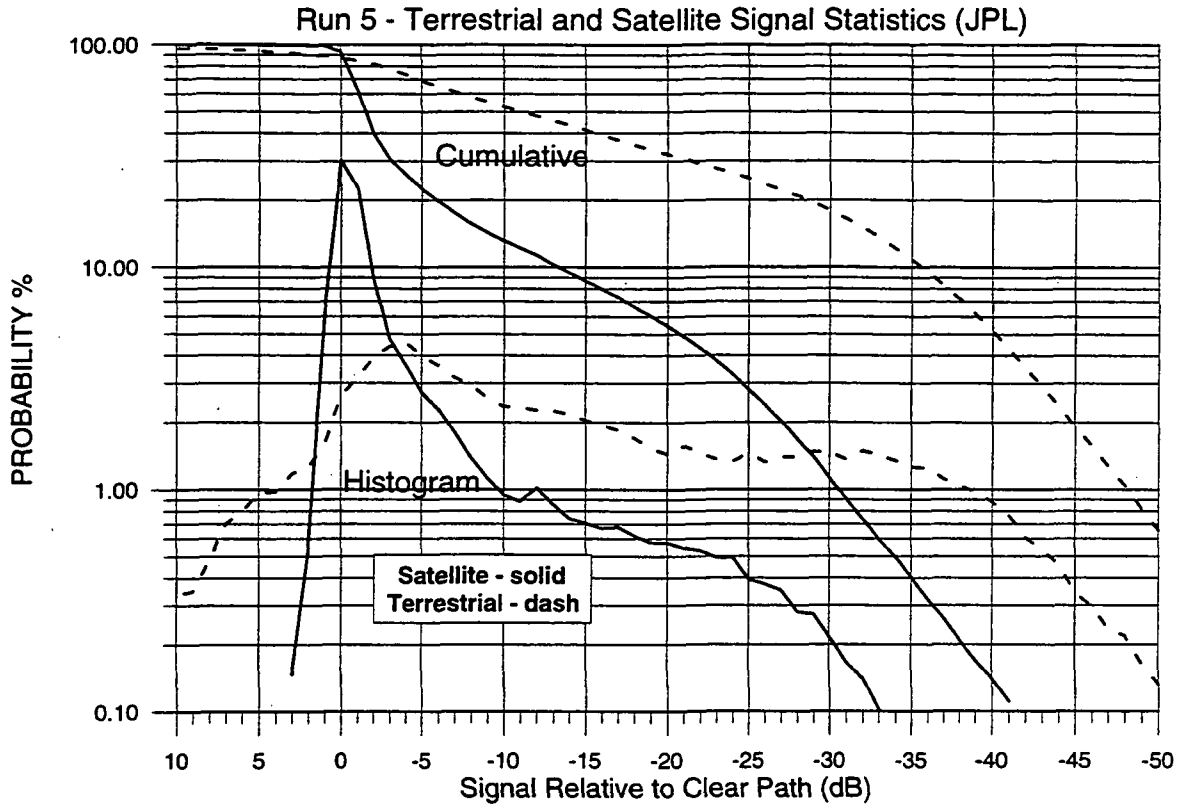

Figure 17. Histograms and Cumulative Probability of the Received Signal Power Samples for Run 5

3.4. JPL Indoor (Building. 161) - Satellite and Terrestrial Signals.

Run 8 of the measurements was conducted indoors, walking through JPL building 161. Shown below is a close-up photo of Building 161, looking from the general direction of the terrestrial transmit site.

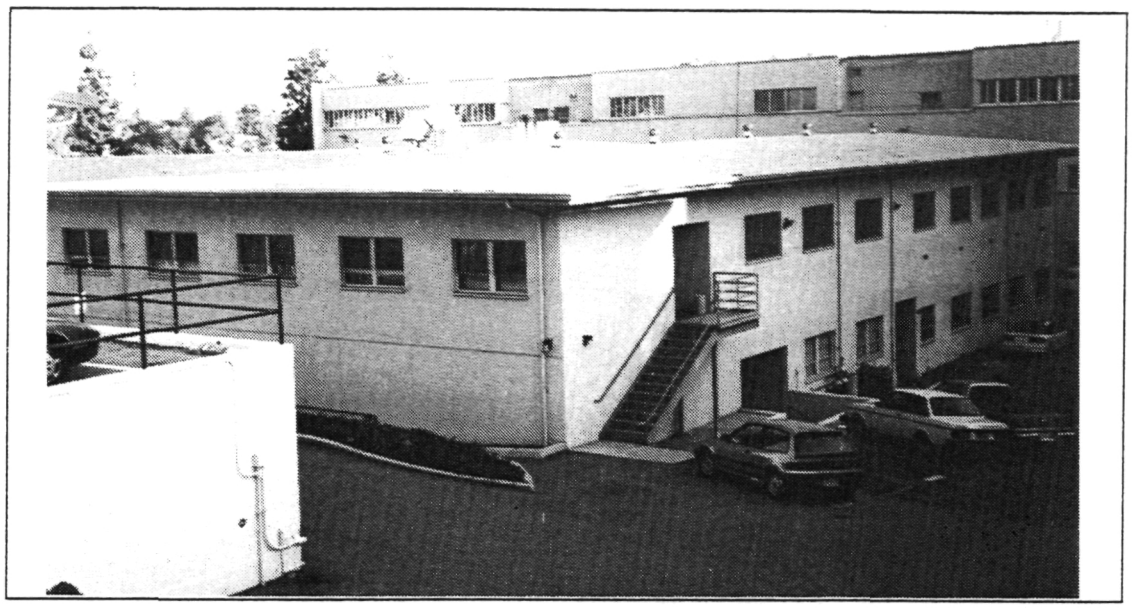

The receiver was carried into the second floor East entrance to the building, carried through the North corridor, out through the West door (at 14:35:30), back in and down the West corridor, then back all the way to the East entrance and outside (at 14:39:40).

Figure 18 shows the signal statistics. Figures 19 through 20 show the signal power measurements. including one second averages.

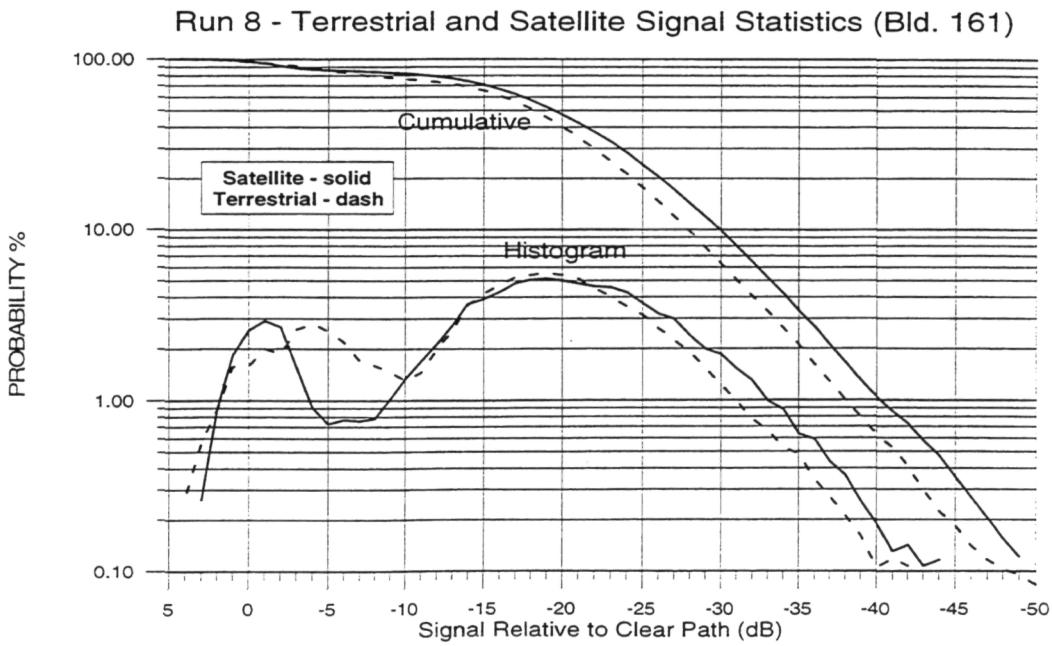

Figure 18. Signal Statistics for Run 8

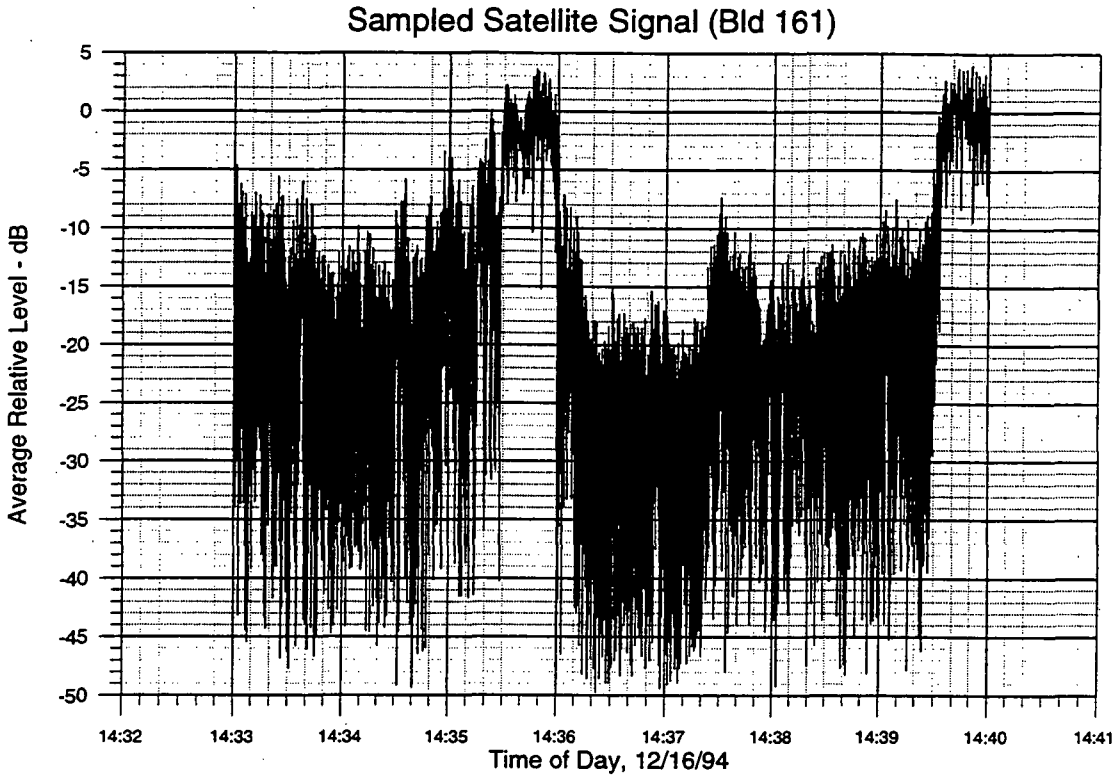

Figure 19a. Received Satellite Signal

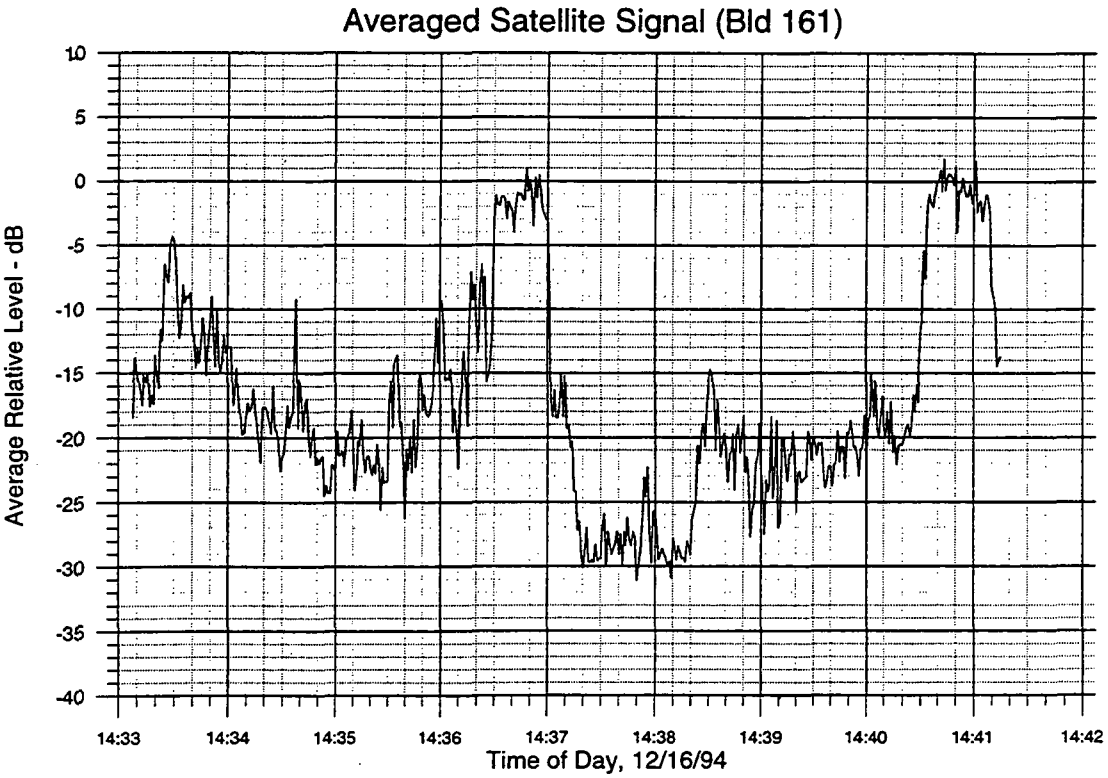

Figure 19b. Received Satellite Signal- One Second Averages

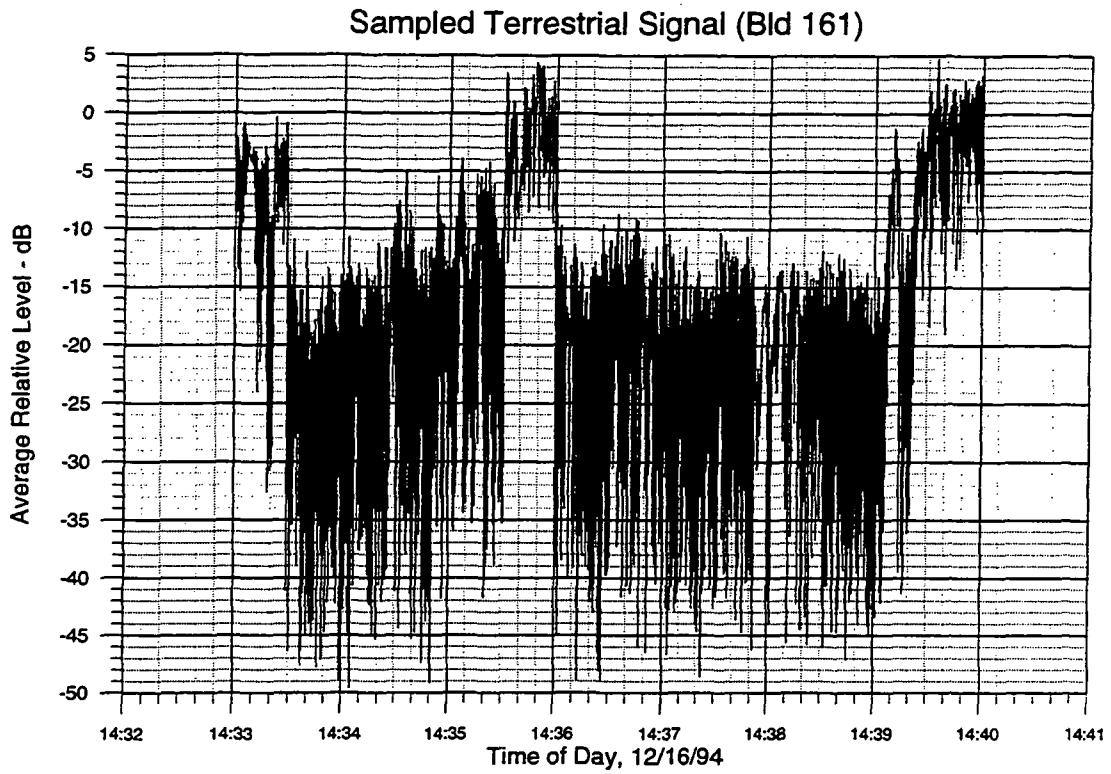

Figure 20a. Received Terrestrial Signal

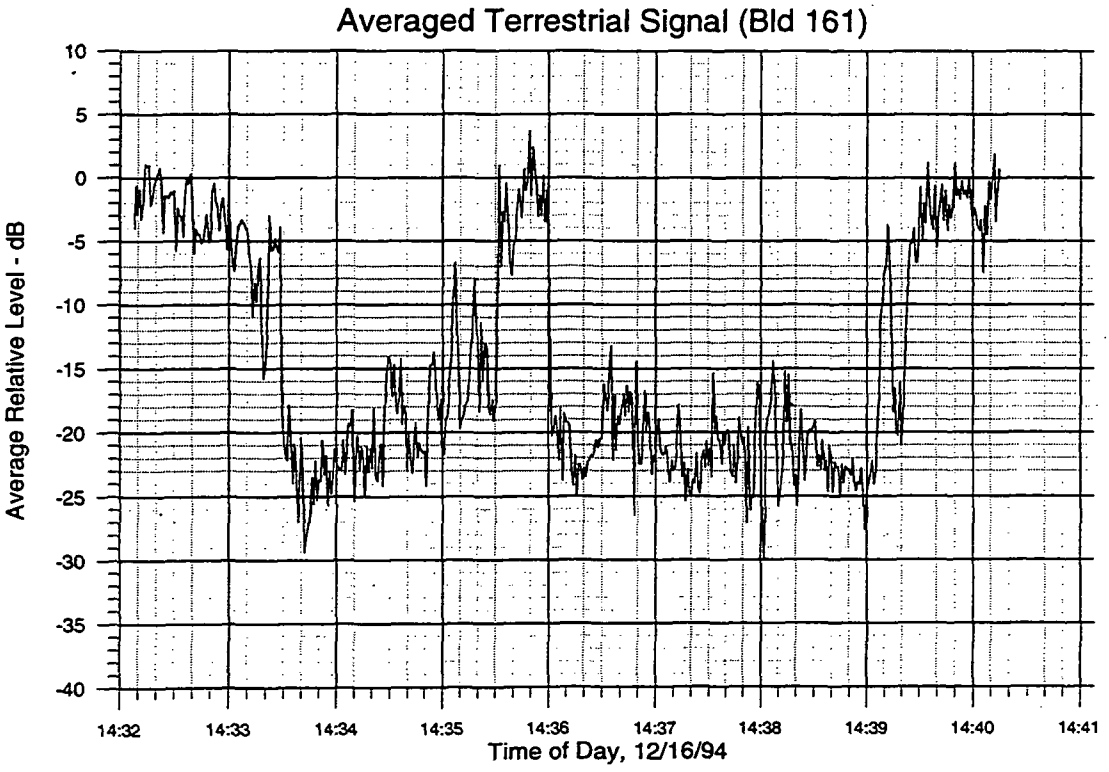

Figure 20b. Received Terrestrial Signal - One Second Averages

4.0 Summary and Conclusions.

A propagation data base at 2 GHz has been obtained through an extensive set of measurements using both a satellite and terrestrial, narrow band, signal source. The measurements were made in a variety of environments, including indoors. A video record of the outdoor measurements is available to identify the cause of the propagation impairments.

Propagation of a satellite signal, even at an elevation of 22 degrees, is characterized by minimal multipath, but very large (> 30 dB) signal drop outs due to blockage by buildings and trees. These effects cannot be compensated for by reasonable amounts of link margin. Signal or time diversity is the only viable option for improving performance.

Terrestrial transmission provides a signal which fluctuates rapidly with receiver position. Under these conditions, receiving antenna diversity, with a reasonably small antenna separation, may be effective in improving reception.

Indoors, the effect on both a satellite and terrestrial signal is similar. There is a complex standing wave structure with signal peaks and troughs on the order of fractions of wavelengths apart. This wave structure has been shown to be wide band (on the order of several MHz), as well as stable in time [1]. Because of this, it is theoretically possible to find strong signal points by moving the receive antenna around. In practice, however, this may be difficult. Receive antenna diversity may be the only practical strategy if the antenna cannot be moved outdoors or to a window facing the satellite.

5.0 References

[1] W.J. Vogel and G. W. Torrence, "Propagation Measurements for Satellite Radio Reception Inside Buildings, " *IEEE Transactions on Antennas and Propagation*, Vol. 41, No. 7, pp. 954-961, July 1993.

N96-10460

A Database For Propagation Models

Anil V. Kantak, Krisjani Suwitra and Chuong Le
Jet Propulsion Laboratory
California Institute of Technology
Pasadena, California 91109.

1.0 Introduction

To design a telecommunications system, the systems engineer usually needs at least a few parameter values governing the radio wave propagation through the channel associated with the system. To obtain the definition of the channel, the systems engineer generally has a few choices. A search of the relevant publications such as the CCIR's, NASA propagation handbook, etc., may be conducted to find the desired channel values. This method may need excessive amounts of time and effort on the systems engineer's part and there is a possibility that the search may not even yield the needed results. Another possible method to define the channel is to find other similar systems and use the needed values from them for the design of the present system. This method has the obvious disadvantage that very rarely two telecommunications systems are exactly alike, and hence, the values to be transported to the system design at hand may not produce correct results.

The best method of obtaining the pertinent parameter values is to generate them using the propagation models describing the channel in question. This method is by far the best because the parameter values are produced for a particular set of system requirements. The obvious disadvantage of this method is that the systems engineer must resort to programming the propagation phenomena models of interest to obtain the parameter values to be used in the system design. The systems engineer must either be a skillful computer programmer or must hire a programmer. This, of course, increases the cost of the effort; an increase in cost due to the inevitable programming effort may seem particularly inappropriate if the data generated by the experiment is to be used to substantiate the already well-established models, or a slight variation thereof.

The National Aeronautics and Space Administration's (NASA's) Propagation Program supports academic research that models various propagation phenomena in the space research frequency bands. NASA supports such research via schools and institutions prominent in the field. The products of these efforts are particularly useful for telecommunications systems engineers and researchers in the field of propagation

phenomena. To help the researcher and the systems engineers, it was recommended by the conference participants of NASA Propagation Experimenters (NAPEX) XV (London, Ontario, Canada, June 28 and 29, 1991) that a software should be produced that contains propagation models and the necessary prediction methods of most propagation phenomena. Moreover, the software should be flexible enough for the user to make slight changes to the models without expending a substantial effort in programming.

2.0 Properties of the Propagation Database

The Propagation Model Database described here creates a user friendly environment that makes using the database easy for experienced users and novices alike. The database allows sufficient freedom for users to custom fit the propagation phenomena model of interest to their requirements. The database is designed to pass data through the desired models easily and generate relevant results quickly. The database already contains many propagation phenomena models accepted by the propagation community and every year new models are added to it. Only minimal computer operations knowledge is necessary to run the database.

The major sources of models included in the database are the NASA Propagation Effects Handbook or the CCIR publications, sometimes they are taken from other publications such as the IEEE Journal etc. Every model included in the software contains a reference to the document from which the model was obtained, and if desired, a brief description of the model itself can be brought up on the screen or even printed. Also, when applicable, the related model names to the active model are also indicated. The parameters of every model in the database are shown explicitly, and the units of the parameters are defined completely so that the user does not have to invest time investigating them. Wherever possible, to make the use of the model obvious to the user, default values of the parameters are given. The default values are generally values that are used most frequently with the model; the users are free to change them to more appropriate ones for their own case. One possible use of the default values is to compare the already known results using the default values with the newly obtained values in an experiment.

Sometimes a propagation phenomenon model may have many formulas, numbers generated by one formula are used by the next, and so on until the final result is generated. In such cases, to include them as single step models in the database would make their use and understanding quite difficult, if not impossible. To avoid this inconvenience, such models are broken down into several logical steps as appropriate, and parameters as well as outputs of each step are described in detail one step at a time. The software makes use

of the extensive charting capabilities offered by the Microsoft Excel software to produce charts for the model under use and the users can use these charting capabilities to change any attribute of the produced chart. Where feasible, the actual charting process is made transparent to the user and involves the user only when a choice must be made between the possible inputs or outputs.

The database also allows the user to make changes, within some guidelines, to the model being run. The main restriction is that the user may make changes in mathematical functions and operations used in the model using only already existing input parameters of the model; no new definitions of parameters will be permitted. In general, this restriction is a reasonable restriction and the user can test slight variations of the existing model generated by utilizing different mathematical functions and operations than the original model.

Every model in the database has the same operating procedure and instructions, thus the user needs to learn the procedure for only one model in order to use the entire database effectively. All the necessary precautions to ensure the correct use of the database are incorporated in the program. When incorrect inputs are made or when an action conflicts with the general directives of the model at hand, the user is alerted with a warning, and where possible, suggestions are made to correct the input.

User friendly procedures are used to call the available mathematical functions of Excel software, such as curve fitting, statistical analysis, etc. This allows the user to apply these functions to the data whenever needed.

3.0 Software Selection to Host the Propagation Database

In the early stages of the software development, a study was conducted to evaluate the advantages and disadvantages of currently available compiler-based programs versus spreadsheet programs for hosting the propagation database software. The results of this study indicated that between the spreadsheet/database software and the compiler based software available then, because of its very nature of dealing with data in columns without extra effort, the spreadsheet software will easily create a product such as the Propagation Models Database.

Of the many commercially available spreadsheet programs at that time, Microsoft Excel was selected to host the Propagation Models Database. Excel provides an extensive list of the database and mathematical functions necessary to implement the propagation models. Excel also has excellent charting capabilities that include many versions of two-and three-

dimensional charts, which can be easily used or automated using the macro language. Excel also offers the dialog box utility, which can be effectively used for input and output functions of the Propagation Models Database. Another notable advantage of Excel is that it can call any executable programs written in C, which is a compiler-based program. This arrangement is ideal because it combines the advantages of a spreadsheet environment with the speed of the compiler-based software for number-crunching purposes.

4.0 Software and Hardware Requirements

To run the Propagation Models Database, Microsoft Windows 3.1, and Microsoft Excel 4.0, or later versions are required. A personal computer equipped with an 80386 cpu, accompanied by its 80387 math coprocessor chip, with at least 4 Mbytes of RAM, is required to run the software. The clock speed should be at least 20 MHz. An 80486 or Pentium based system with higher clock speed is preferable. Any other computer (e.g., an 80286-based PC) with sufficient RAM will run the software, however, it will be very slow.

For the Macintosh version of the database, a Macintosh II ci or better computer accompanied with its coprocessor chip and having at least 4 Mbytes of RAM is needed to run the software. The clock speed should be at least 20 MHz.

It is recommended that a color monitor be used so that the charting can be done more effectively. Also, needed is a hard disk with at least several megabytes of storage space available for the software.

5.0 The Propagation Database

The Propagation Database is divided into six categories: the Ionospheric models, the Tropospheric models, the Land Mobile Systems models, the Effects of Small Particles models, the Rain models, and the Radio Noise models. These six categories are further divided into subcategories to include all the models to be housed in the software.

Ionospheric Models:

Tropospheric Models:

Index of Refraction Profile Model, Gaseous Attenuation Model, Refraction and Fading Model, and Scintillation Model

Mobile Satellite System Models:

The mobile satellite models are subdivided into 'Land Mobile System Models' and 'Maritime Mobile System Models'.

Land Mobile Satellite System Models:

Attenuation Frequency Scaling Model, Cumulative Distribution of Fade Duration Model, Cumulative Distribution of Non Fade Duration Model, Diffusely Scattering Model, Diversity Improvement (Tree Shadowing) Model, Empirical Regression Models, Empirical Roadside Shadowing Model, Faraday Rotation Model, Fresnel Zones, Frequency Reuse Using Orthogonal Polarization Model, Raleigh Model, and Reflection Coefficient Model.

Maritime Mobile Satellite System Models:

Fading Due to Sea Reflection Model, and Interference Due to Reflection Model.

Effect of Small Particles Models:

Cloud Model

Rain Models:

CCIR Model, COMSAT Model, Global Model, Depolarization Model, and Site Diversity Model.

Radio Noise Models:

Noise Model

The access to any model is carried out using Excel's dialog box user interface. Each dialog box is divided into six distinct areas to help the user to provide the inputs easily.

The six areas of the dialog box are described below. The first area is used to provide general information about the model selected by the user. This step describes any particular conditions required by the model, the parameter ranges as well as the number of steps the model has, and so on. The second area is used to display formulas describing the model selected. The formula can be modified by the users to a certain extent using legal expressions in Excel. Once the formula is created, the software will use this formula for the current run only. Loading the software again will bring back the original formula. The third area is the parameter definition area, where all the parameters of the model are defined appropriately. The fourth area is called the input area. This area is used to acquire input parameter(s) for the model. The fifth area is used to display intermediate or final result(s) of the particular model. The sixth area has a few buttons to help the user and to produce the output(s) of the model (or step). For some models, this area also has buttons to allow creation of a table of output values of the model as a function of the range of the selected input parameter. The following figures show the run of the CCIR rain attenuation model included in the database software.

6.0 Future of the Propagation Models Database

From the inception of the idea of Propagation Database till present, Microsoft Excel has been the underlying software. The reason for adopting Excel was that it truly offered unique capabilities of charting and scientific functionality. However, Excel has some drawbacks such as the slow execution of the program, the large memory requirement, and the need to own the Excel software by the users. Another disadvantage Excel entails is that whenever a newer version of Excel is released, such as Excel 5.0, it may not be fully compatible with the older versions such as Excel 4.0. This makes it difficult, if not impossible, for programmers to develop a long-term program. Having taken all these disadvantages into consideration, it was decided that future versions of the database shall be written in the 'C' language because this language offers some attractive qualities such as faster execution, efficient use of computer memory, and complete independence from the compiler software once the program is compiled.

7.0 Conclusion

A database of various propagation phenomena models that can be used by telecommunications systems engineers to obtain parameter values for systems design is presented. This is an easy-to-use tool and is currently available for either a PC using Excel

software under Windows environment or a Macintosh using Excel software for Macintosh. All the steps necessary to use the software are easy and many times self explanatory, however, following is a sample run of the CCIR rain attenuation model.

A Sample Run of the CCIR Rain Attenuation Model

The following pages show a sample run of the CCIR model, which contains 6 steps:

Step 1: Calculates h_R, the effective rain height in kilometers.

The model used for the effective rain height, h_R, is as follows:

$$h_R = 3.0 + 0.028 * Phi \qquad 0 \le Phi < 36^0$$
$$h_R = 4.0 - 0.075 * (Phi - 36) \qquad Phi \ge 36^0$$

where

Phi is the station's latitude in degrees.

- Enter *Phi* (the station's latitude) in degrees, e.g., 30 degrees.
- Click the Output button to see h_R (the effective rain height).
- Click the Step 2 button to go to the next step.

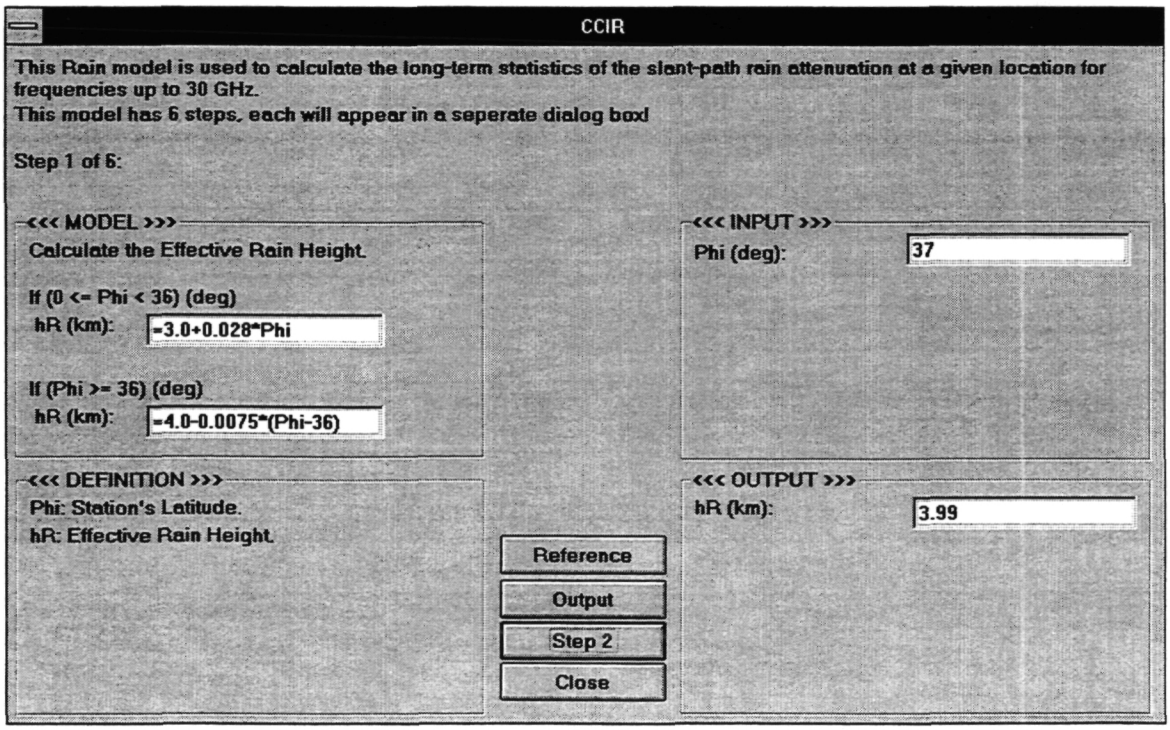

Step 2: Calculates L_S, the slant-path length below rain height in km.
The model used for the slant-path length, L_S, is as follows:

$$L_s = \frac{(h_R - h_s)}{\sin(Theta)} \qquad Theta \geq 5^0$$

$$L_s = \frac{2(h_R - h_s)}{\left(\sin^2(Theta) + \frac{2(h_R - h_s)}{R_e}\right)^{1/2} + \sin(Theta)} \qquad Theta < 5^0$$

where

h_R is the effective rain height in kilometers.
h_S is the height mean sea level of the earth station in kilometers.
Theta is the elevation angle in degrees.
R_e is the modified earth radius (defaulted to 8500 km).

- h_R was computed in Step 1.
- Enter h_S (the height mean sea level of the earth station) e.g., 0.632 km.
- Enter *Theta* (the elevation angle) e.g., 14 degrees.
- Change R_e (the earth radius) if necessary.
- Click the Output button to see L_S (the slant-path length).
- Click Step 3 to go to the next step.

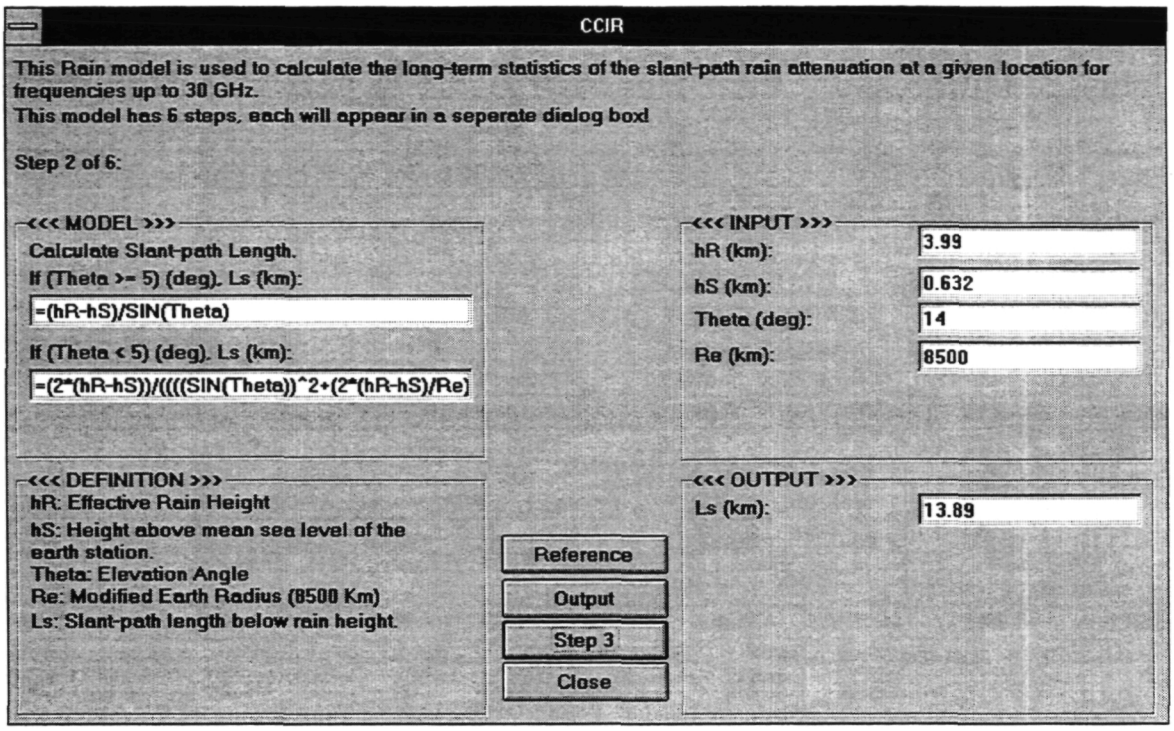

Step 3: Calculates L_g, the horizontal projection of the slant-path length in kilometers. The model used for the horizontal projection of the slant-path length, L_g, is

$$L_g = L_s \cos(Theta)$$

where

L_S is the slant-path length below rain height in kilometers.
Theta is the elevation angle in degrees.

- No input is required for this step.
- Click the Output button to see L_g (the horizontal projection of the slant-path length).
- Click the Step 4 button to go to the next step.

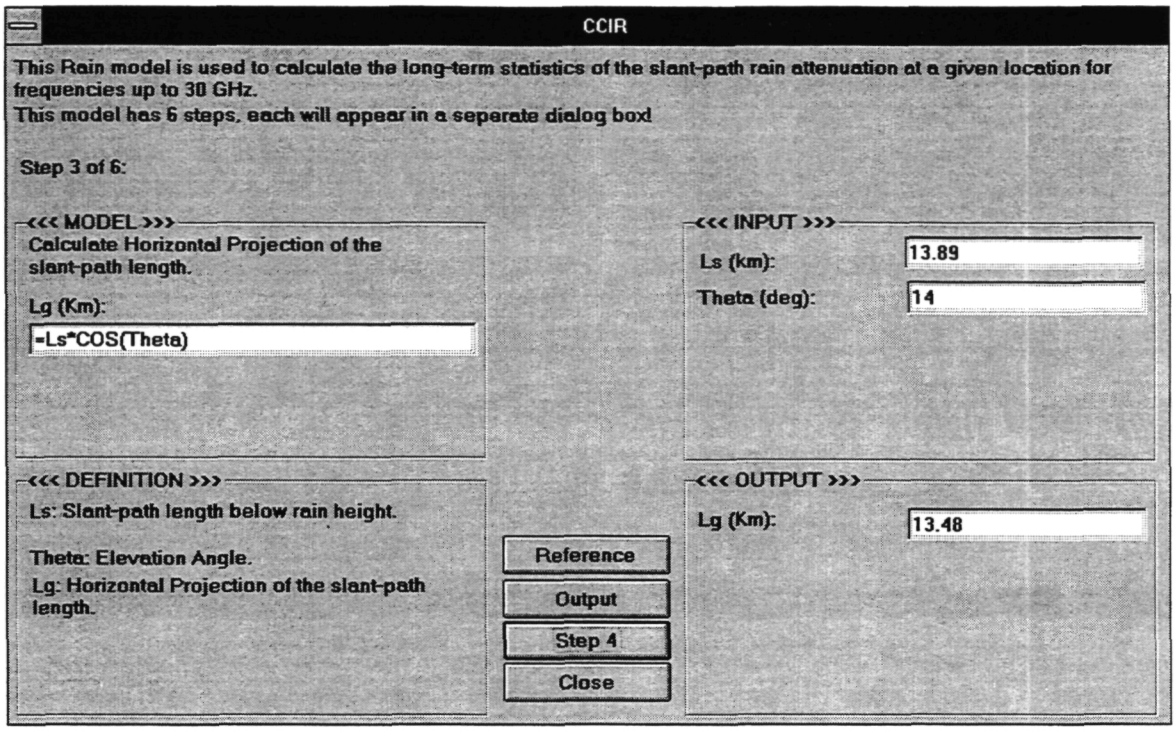

Step 4: Obtains $R_{0.01}$ (dB), the rain intensity exceeded for 0.01% of an average year and calculates $r_{0.01}$, the reduction factor.

The model used for the reduction factor, $r_{0.01}$, is

$$r_{0.01} = \frac{1}{1 + L_G / L_o}, \quad L_o = 35\exp\left(-0.015 R_{0.01}\right)$$

where,

$R_{0.01}$ is the rain intensity exceeded for 0.01% of an average year in mm/hr.

$r_{0.01}$ is the reduction factor.

- Select the Rain Climatic Zone, such as K for this example.
- Click the Output button to see $r_{0.01}$ (the reduction factor).
- Click the Step 5 button to go to the next step.

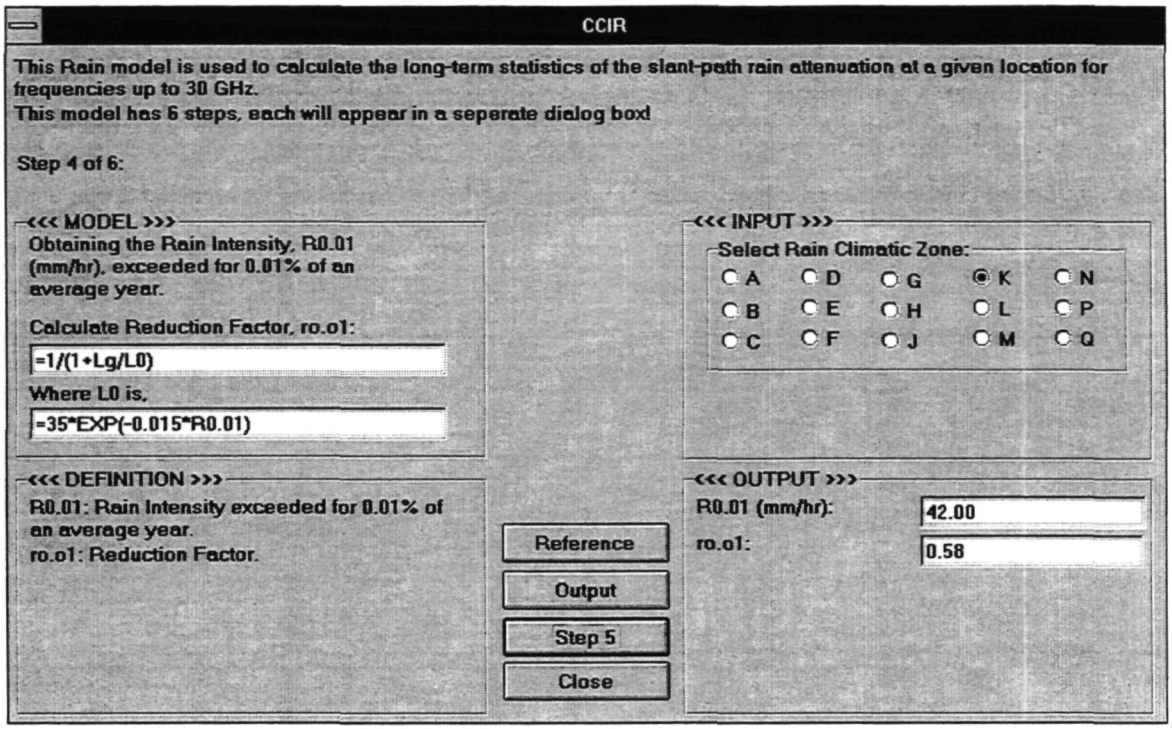

Step 5: Calculates *GammaR*, the specific attenuation using the frequency-dependent coefficient in dB/km. The formula used to calculate *GammaR* is as follows:

$$GammaR = kR_{0.01}^{\alpha},$$

$$k = [k_H + k_V + (k_H - k_V)\cos^2(Theta)\cos(2Tau)]/2$$

$$\alpha = [k_H\alpha_H + k_V\alpha_V + (k_V\alpha_H - k_V\alpha_V)\cos^2(Theta)\cos(2Tau)]/2k$$

where

Theta is the elevation angle in degrees.

Tau is the polarization tilt angle in degrees.

k and α are coefficients taken from Reports of the CCIR, 1990. Table 1. Regression Coefficients for Estimating Specific Attenuation.

- Enter *Frequency*, e.g., 12.5 GHz.
- Select *Tau*, e.g., 45 degrees for circular polarization.
- Click the Output button to see *GammaR*.
- Click the Step 6 button to go to the next step.

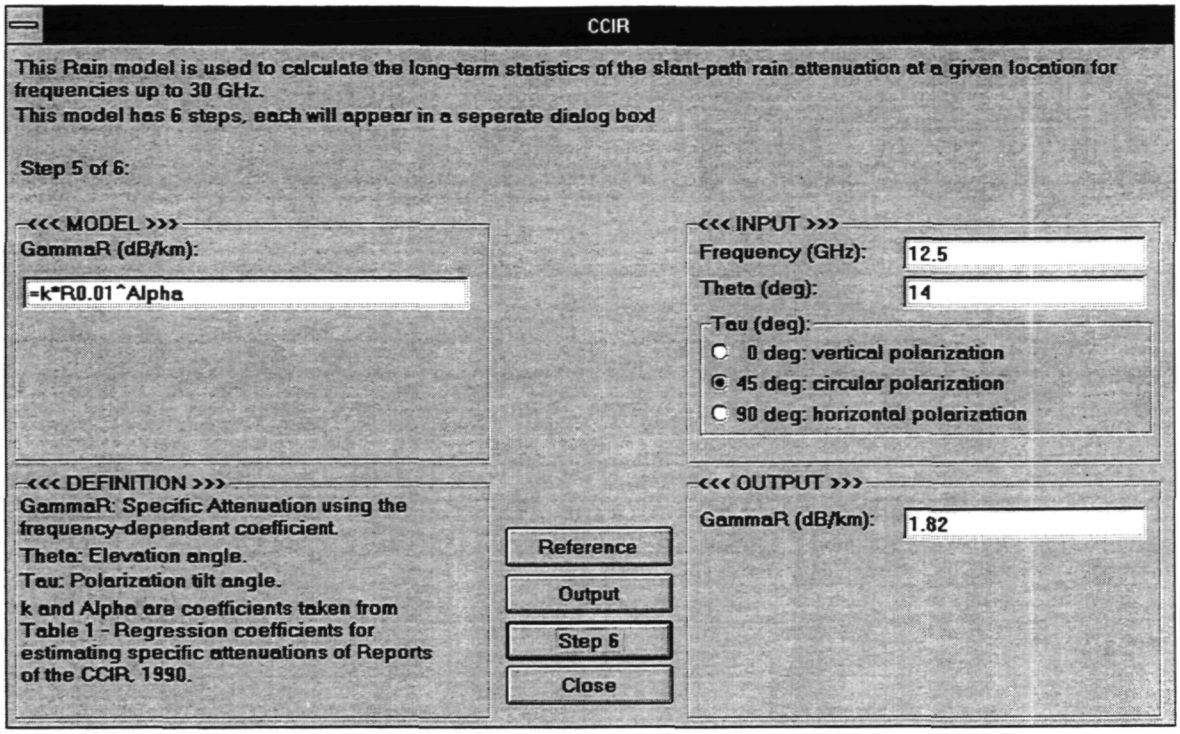

Step 6: Calculates $A_{0.01}$, the attenuation exceeded for 0.01% of an average year in decibels.

The formula used for the attenuation exceeded for an average year, $A_{0.01}$ is:

$$A_{0.01} = GammaR * L_s * r_{0.01}$$

where

GammaR is the specific attenuation using the frequency dependent coefficient in dB/km.
L_S is the slant-path length below rain height in kilometers.
$r_{0.01}$ is the reduction factor.

Click the Output button to see $A_{0.01}$ (the attenuation exceeded for 0.01% of an average year).

Click the "Other p (%)" button to find attenuation exceeded for other percentages of an average year (0.001 to 1.0 %).

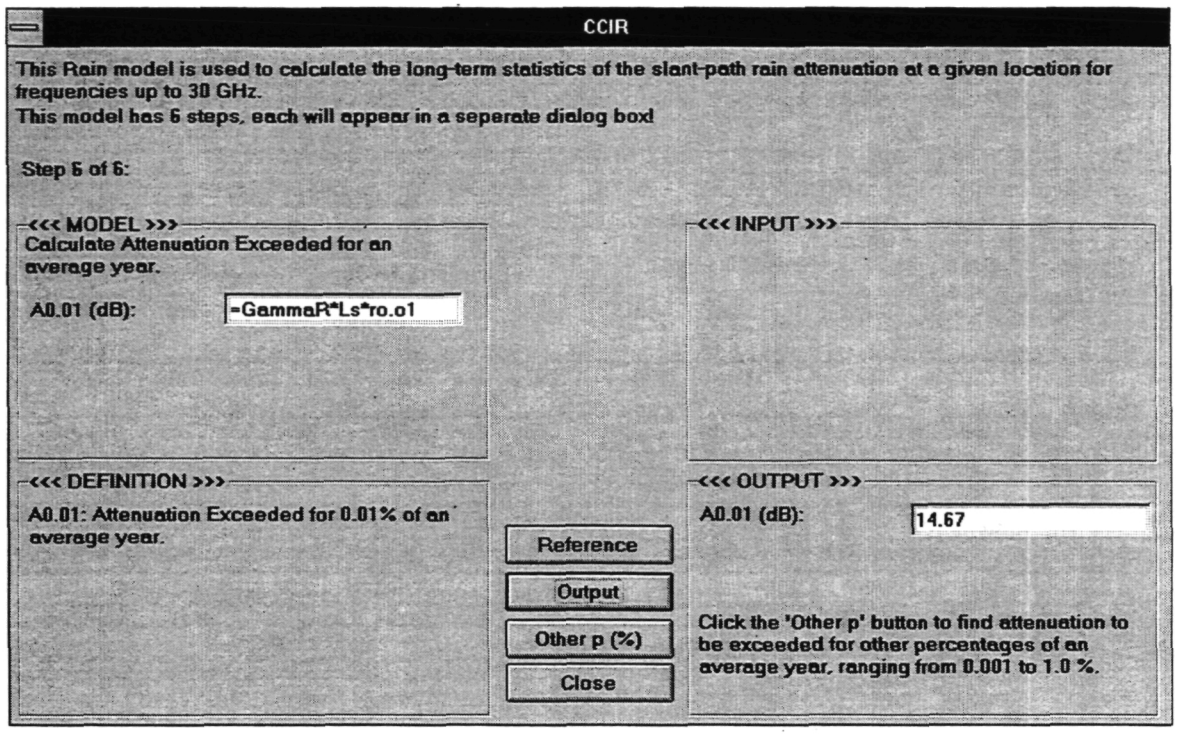

This step also calculates attenuation exceeded for an average year for other percentages (0.001 - 1.0 %).

The formula used for *p* percent of the attenuation exceeded for an average year is as follows:

$$A_p = A_{0.01} * 0.12 * p^{-(0.546+0.043\log(p))}$$

where

p is the percentage of the attenuation exceeded.

Ap is the attenuation exceeded for *p* percent.

$A_{0.01}$ is the attenuation exceeded for 0.01 percent.

- Enter the *p* (percentage) of an average year.
- Click the Output button to see *Ap*, attenuation of *p* percentage and ratio of $Ap/A_{0.01}$

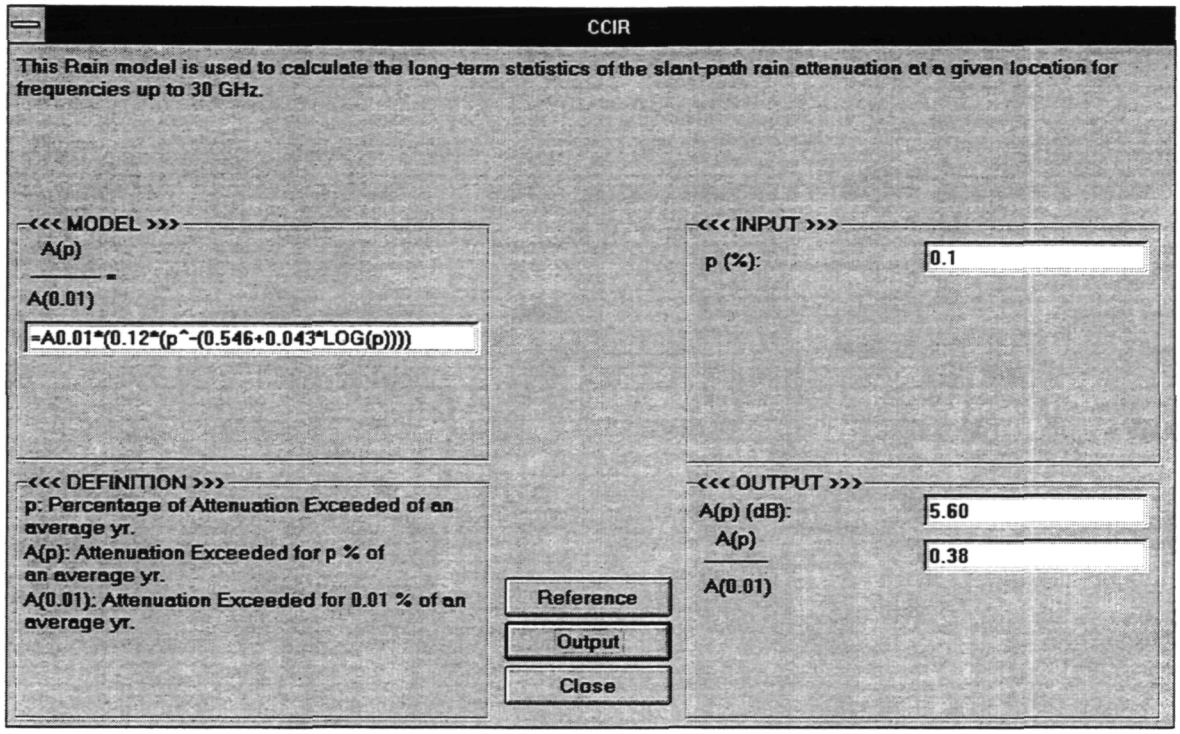

When the close button is clicked the following dialog box appears

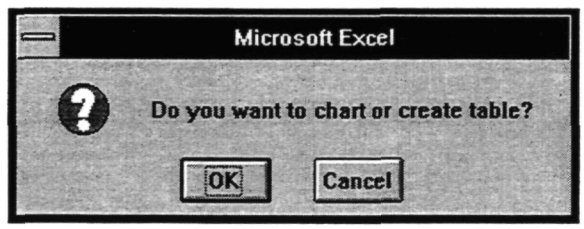

- Click OK to see the response.

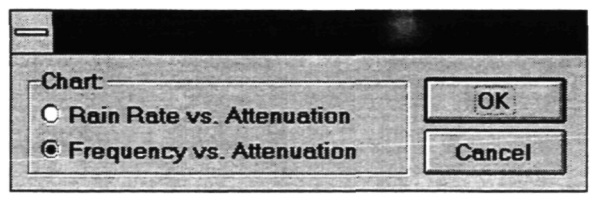

- Select one of the options, e.g., the Frequency vs. Attenuation.
- Click OK.

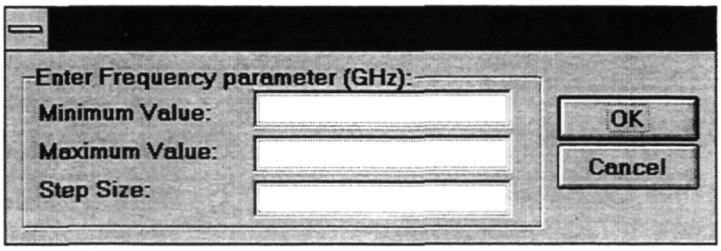

- Enter the minimum, maximum and step values
- Click OK

A new worksheet will then be invoked to store all of the parameters used, the table, as well as the selected chart.

The 'Print' option is available after this step.

This ends the sample run of the CCIR model.

APSW VII

A WORKSHOP ON ADVANCED COMMUNICATIONS TECHNOLOGY SATELLITE (ACTS) PROPAGATION STUDIES

ACTS Workshop Opening Remarks

Faramaz Davarian
Jet Propulsion Laboratory, California Institute of Technology

ACTS propagation data are collected at different sites in North America through NASA's financial support. NASA has two-year contracts with the experimenters. These contracts will expire in late summer 1995. The extension of the ACTS propagation contracts has kept Bob Bauer and myself preoccupied for the last six months. Tasked with an action item in our last workshop (Florida, December 1994), I compiled a letter to NASA Headquarters, see attachment. This letter presents strong arguments for continuing data collection beyond the original two-year period. Bob and I provided data and justification on many occasions to the ACTS program office and Headquarters in the last six months. We have made good progress on this important topic. Bob will discuss the situation this morning.

The data-analysis phase of our campaign has begun. Hardware issues are mostly behind us. Thanks to the engineering support received from David Westenhaver, the terminals are behaving themselves. Mr. Westenhaver will give an update on the health of the ACTS propagation terminals and the associated software.

To the best of my knowledge, all the sites are processing and analyzing data. I was able to receive analyzed data from all the sites for the paper that I wrote for the *International Journal of Satellite Communications*. The only exception was Georgia Tech because this site joined our group only recently. Examples of data received from the sites are given in the following table:

DATA TYPE	SITE
Uplink Power Control	COMSAT
Beacon & Radar Data	Colorado
Scintillation Results	Alaska
Worst Month	Oklahoma
Frequency-Scaling Data	British Colombia
Prediction Model Rain Attenuation	New Mexico
Fade-Duration Data	Florida

The wide scope of the ACTS propagation experiments is evident from the above table. Clearly the next step is to compare our findings with models and use our results to improve those models and develop new ones as required. For these activities, good data calibration is a must, and comparisons should be made correctly. For example, if the 27-GHz channel loses lock, we must account for this anomaly in the statistics when comparing them to the 20-GHz statistics.

Emphasis should be given to industry needs. Several companies are going to use Ka band for their proposed systems: Hughes for SpaceWay, Teledesic, Motorola for Iridium, and TRW for Odyssey. The next set of NASA's TDRS satellites will be equipped with a Ka-band experimental payload, and Milstar uses 20- and 40-GHz

frequencies. Therefore, we seek feedback from industry to ensure that their requirements are addressed in our efforts: data, models, format, etc.

As we get more involved in data analysis, many questions surface. For example, should scintillation be separated from attenuation when calculating fade duration? Or should gaseous attenuation be distinguished from rain attenuation, or . . . Some of these questions can be answered in the plenary session by simply agreeing upon how to do a task. Some can be resolved by receiving feedback from industry. Yet others can be answered by observing what earlier researchers have done. Good sources of information include OPEX reports, Virginia Tech Olympus reports, and the reports of the long-duration experiment at the University of Texas.

To facilitate industry participation, I was asked to prepare a short write-up on our campaign's objectives, structure, and logistics at our meeting in Florida. In response to this action item, I prepared an article that appeared in *The ACTS Propagation Newsletter* last February. To publicize ACTS goals and achievements, our community published many papers and organized conference sessions. All of you have played a role in publicizing ACTS. Please continue doing so. I would particularly like to acknowledge Rudy Henning's efforts in this area. Rudy is always working on a new outreach idea to better inform the user community of our campaign.

To facilitate the dissemination of ACTS data and make our reports easy to read and comprehend, our community is urged to present data in a common format. For example, in the last workshop, it was recommended that cumulative statistics be plotted on the ordinate with attenuation on the abscissa, see Figure 1. Please follow the format of Figure 1 when plotting cumulative statistics. Also note that Figure 1 is the format adopted by the *NASA Propagation Handbook* (NASA Ref. Pub. 1082).

The *ACTS Propagation Newsletter* continues to be published by Kris Suwitra. To publish in this newsletter, please contact her. Kris also maintains the ACTS Propagation Home Page on the World Wide Web (http://www-seg.jpl.nasa.gov/~suwitra/acts.html).

NASA has announced a results conference for ACTS in September (September 11–13). There will be several minisessions on propagation. I would like to invite you to join this conference. By attending, one can become informed of ACTS results beyond our own area.

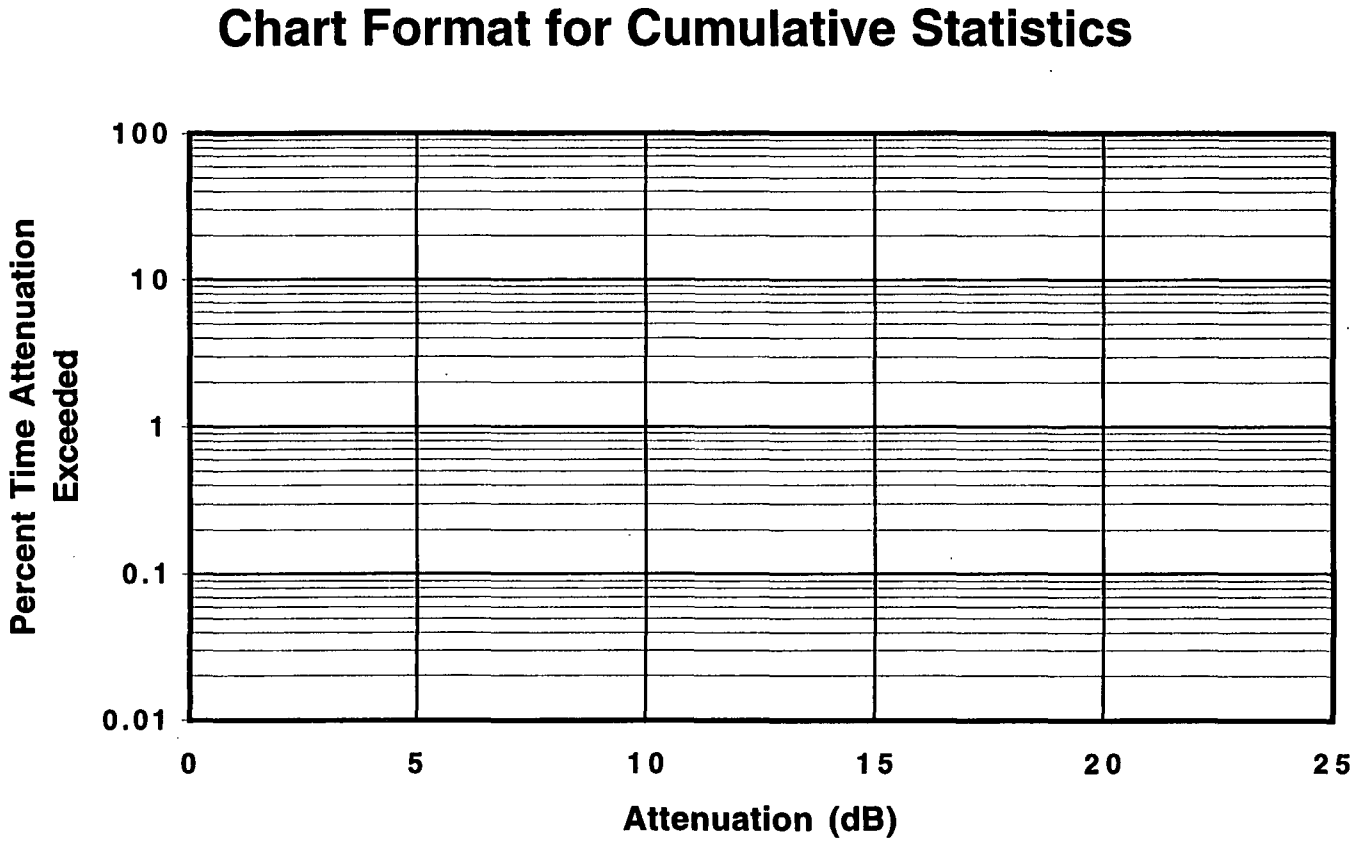

Fig. 1. Common format adopted for ACTS cumulative statistics, with statistics plotted on the ordinate and attenuation on the abscissa.

Jet Propulsion Laboratory
California Institute of Technology

4800 Oak Grove Drive
Pasadena, California 91109-8099

(818) 354-4321

JPL

December 15, 1994

Mike Smith
NASA Code XS

Dear Mike:

I would like to take this opportunity to report to you on the status of the ACTS propagation campaign. JPL has awarded a contract to David Westenhaver of WWWI for engineering support of the experiment terminals. I am glad to report that ACTS experimenters are now receiving uninterrupted engineering support, and they are most appreciative. Major hardware and software problems have already been addressed, and other issues are currently being worked out in a collaborative effort.

JPL hosted the sixth ACTS Propagation Studies Workshop (APSW VI) at the Florida site of the ACTS propagation measurements, November 29–30, 1994. Attendees consisted of the experimenters and users of propagation data. User participation included such organizations as Hughes, TRW, Stanford Telecom, Teledesic, COMSAT, GTE, Lincoln Lab, E-Systems, and the U.S. Army. These and other users are playing a vital role by helping to define user requirements for ACTS propagation data.

The experimenters reported that they have completed one year of measurements and are beginning the second year of data collection[1]. Due to the deficiencies of the software that had been delivered by the terminal manufacturer, the processed data have not been calibrated properly. Since we had become aware of this problem earlier, with help from Professor Robert Crane of the University of Oklahoma, David Westenhaver had rewritten the preprocessing software and had distributed it a week or two before the workshop. The day after the workshop, on December 1, Professor Crane conducted a hands-on class to familiarize the experimenters with the new preprocessing software. Soon all the experimenters will reprocess their data using the new software to obtain appropriate signal calibration and improved statistical accuracy.

During the workshop, Dr. Wolfhard Vogel of the University of Texas reported that the ACTS Data Center has received nearly one year of raw and preprocessed data from the experimenters. It was noted that due to occasional, but generally infrequent, hardware crashes, segments of data are missing in the first year. However, it is anticipated that hardware-related data loss will be kept to negligible levels during the second year. The ACTS Data Center is a depository for all ACTS raw and preprocessed propagation data. U.S. industry and other users of propagation measurements can conveniently obtain data stored on CD-ROM disks from the ACTS Data Center at the University of Texas.

Plans for 1995 are as follows:

- Process the 1994 raw data using the new software and, as measurements are made, process 1995 data.
- Analyze the 1994 data, and begin the analysis of 1995 data.
- Develop models to predict Ka-band propagation effects on satellite links. These models will reduce the risk of implementing new satellite communication services at Ka-band.
- Begin the dissemination of ACTS propagation results to industry.

It should be noted that, whereas prior measurement campaigns' accuracy was generally poorer than 1 dB, our measurement precision is about 0.5 dB with an RMS measurement error of 0.1 to 0.2 dB. For low-cost, i.e., low margin, satellite systems, this is a very attractive feature of our experiment because for the first time we will be able to separate attenuation by the physical phenomena causing the loss. This can be used to model attenuation at low levels needed for the design of VSAT systems.

[1] The ACTS campaign began its data collection phase December 1, 1993.

A very important subject that was discussed during the workshop was the duration of the ACTS propagation measurements. Both experimenters and users feel strongly that a two-year period is not adequate for establishing sufficient statistics for modeling propagation effects, particularly in light of some missing data during the first year. Here are some of the reasons for their concern:

- If the experiment period is not extended, the goals of the campaign will be compromised. This will have an adverse affect on proposed Ka-band communication systems because the propagation risk factor cannot be appropriately treated in estimates of system reliability. Without an extended campaign period, statistical errors will far exceed measurement errors.
- Because of non-average year climatic conditions, some of the sites showed results which substantially deviated from the norm. This anomaly can only be remedied by multi-year measurements.
- The International Telecommunications Union has requested member administrations for multi-year Ka-band propagation data to assist in the development of system risk models.
- Past theoretical studies and empirical observations have shown weather cycles in the order of about seven years. For this reason, a three- to four-year observation period seems to be the minimum recommendable duration.
- The June 1993 Proceedings of the IEEE published a study on the risks associated with Earth–satellite attenuation prediction. This study concluded that to specify a link budget with a precision of better than 1.5 dB, when the fade margin is 10 dB, more than three prior years of observations are necessary.
- The users present at the workshop felt that, since the ACTS propagation experiments are going to be the last major Ka-band campaign, NASA should see to it that adequate data are collected to enable the development of low-risk applications in this band. This sentiment was especially voiced by industry representatives at the workshop.

It should also be noted that the hardware and logistical expenses associated with initiating the measurement campaign are nonrecurring, and the cost of obtaining additional data with the existing installations is rather modest by comparison.

The workshop concluded with a plenary session, where recommendations were issued and action items were assigned. Bob Bauer and myself were given the task of communicating the needs of our users, i.e., industry, to our NASA sponsor: ***The user community is requesting that the ACTS propagation experiments be extended for at least one more year, with additional time given to experimenters to complete data analysis, i.e., years 1996–1997.***

I might also mention that the experimenters' contracts will end between September and November of 1995, preventing some of the sites from even collecting a complete two-year set of data and not allowing time to analyze all of the collected data. Due to the logistical necessities of the universities, there is a pressing need to inform the contractors of the continuation of the ACTS propagation program by early spring, 1995. This requirement is because of the advanced notice needed to employ or continue the employment of university students.

The proceedings of the APSW VI will be distributed in early January, and you will be receiving a copy.

Best regards,

Dr. Faramaz Davarian
NASA Propagation Program

cc: R. Bauer, R. DePaula, R. Knight, W. Rafferty, R. Schertler

Session I: Overview

ADVANCED COMMUNICATIONS TECHNOLOGY SATELLITE (ACTS) PROGRAM

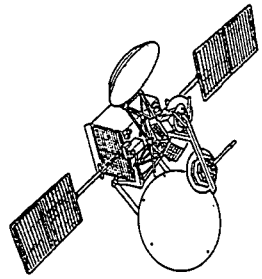

Robert Bauer

Spacecraft & Program Updates

APSW VII
Ft. Collins, CO
June 15-16, 1995

ACTS NASA

SPACECRAFT STATUS

- Hydrazine depletion being re-estimated (~May '98)
- Fourth eclipse season of the mission was completed 4/13/95. Operations were normal
- Autotrack control (as opposed to Earth sensor) continues to be primary attitude reference

SPACECRAFT STATUS

- Transmit reflector biax drive to be routinely used for daily compensation of diurnal MBA distortions beginning 6/12/95
  - Received signal variations reduced by 1.5-3.0 dB
  - Signal varies only +/- 0.5 dB over 14 hour diurnal period
  - SBA movements and biax drive corrections not mutually compatible as expected

ACTS NASA

EXPERIMENT OPERATIONS

ACTS EXPERIMENTS PROGRAM

- EXPERIMENTS APPROVED 80

- PIs, CO-PIs & AFFILIATED ORGANIZATIONS

INDUSTRY	39
UNIVERSITY	28
GOVERNMENT	26
CCDS	2
	95

	EXPERIMENTS				
TYPES	INDUSTRY	UNIVERSITY	CCDS	GOV'T	TOTAL
APPLICATION	20	11	1	18	50
TECHNOLOGY VERIFICATION	4	0	1	12	17
PROPAGATION	5	8	0	0	13
TOTAL	29	19	2	30	80

ACTS NASA

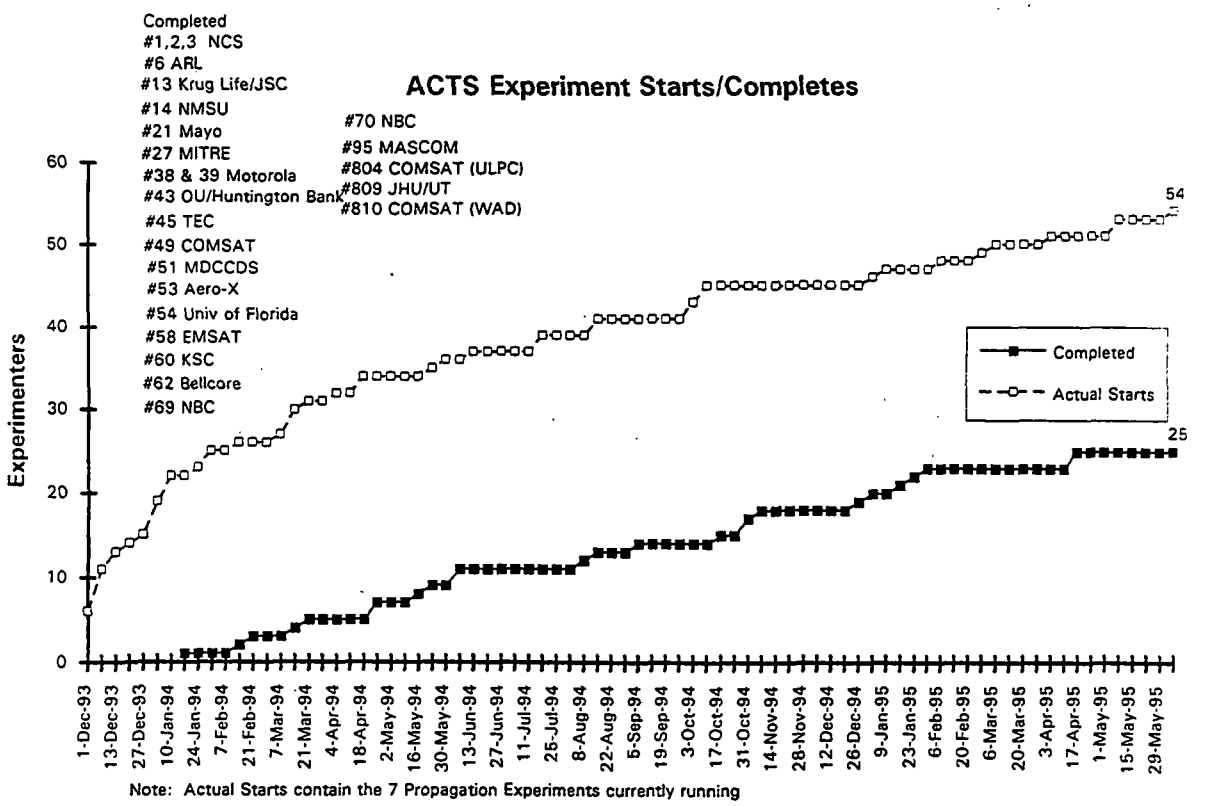

Note: Actual Starts contain the 7 Propagation Experiments currently running

ACTS NASA 6/7/95

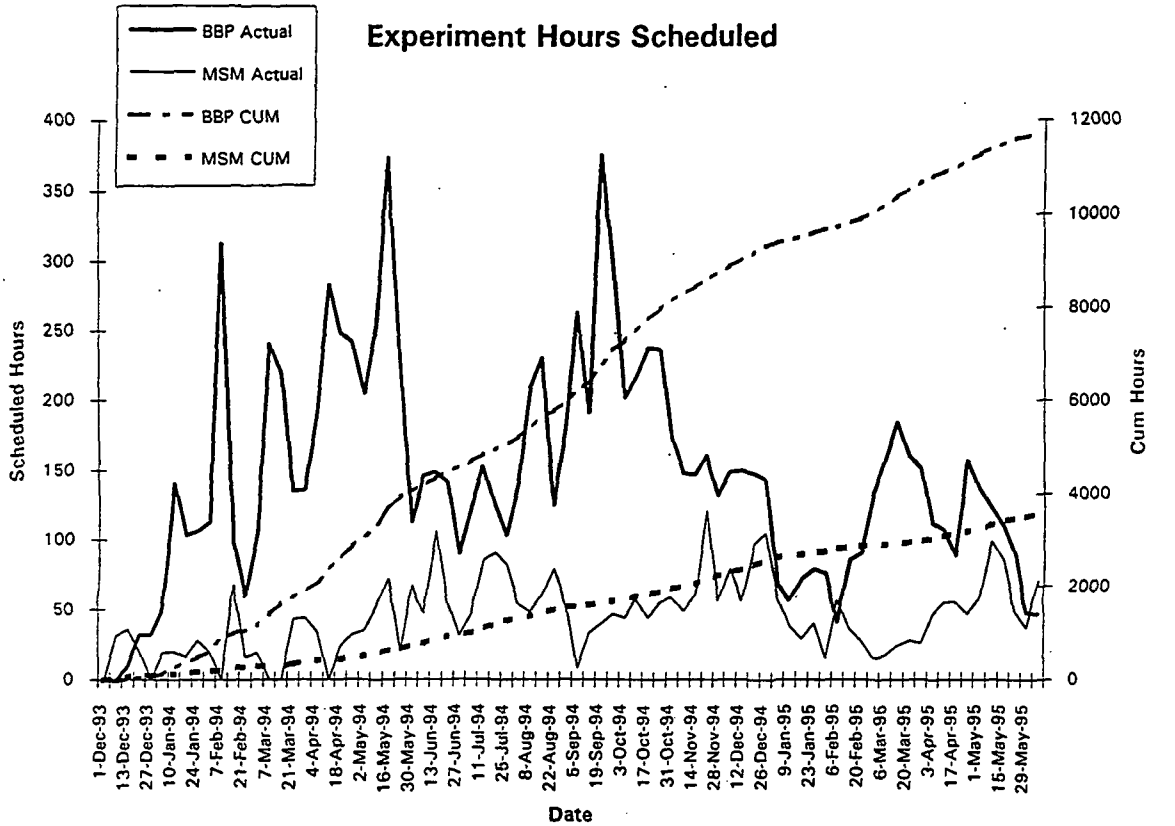

ACTS

NASA 6/6/95

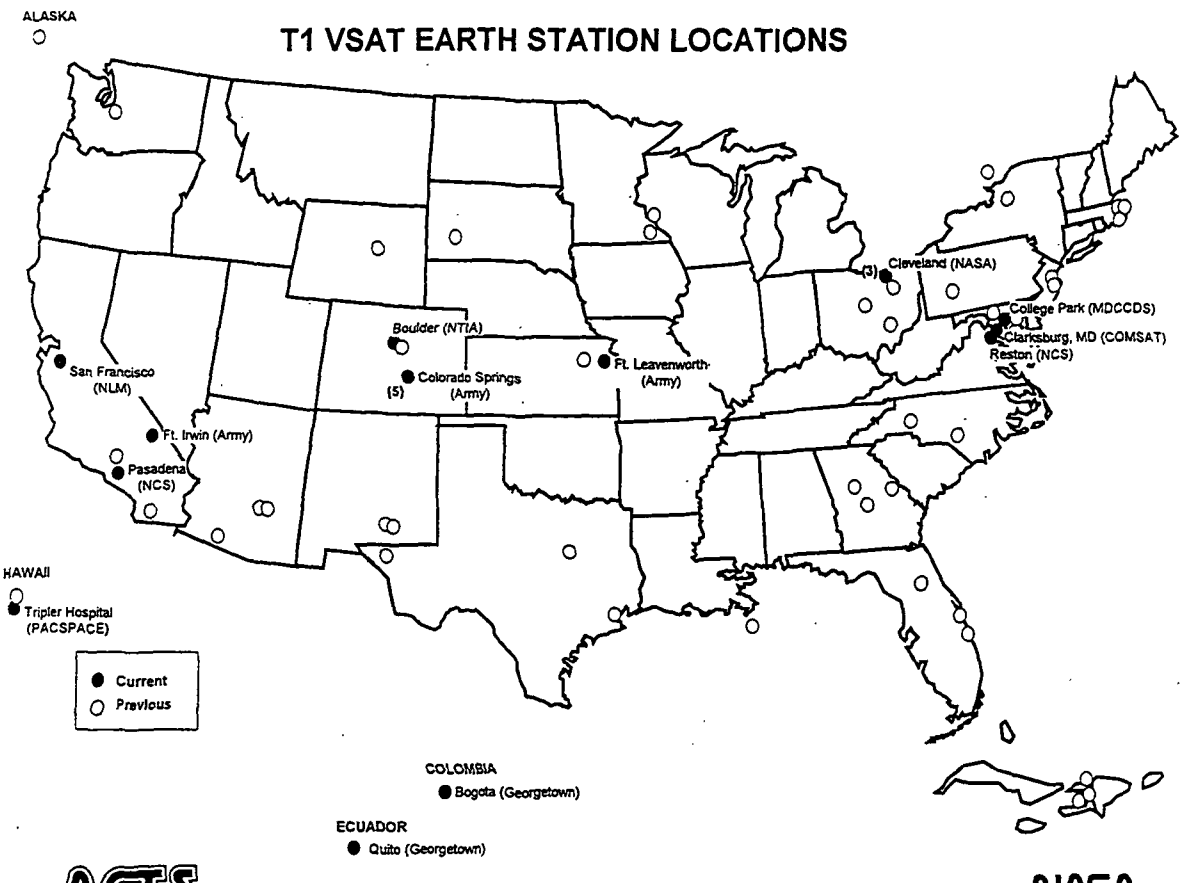

ACTS

NASA

AMOCO

ARIES PROJECT
Demonstration Profile

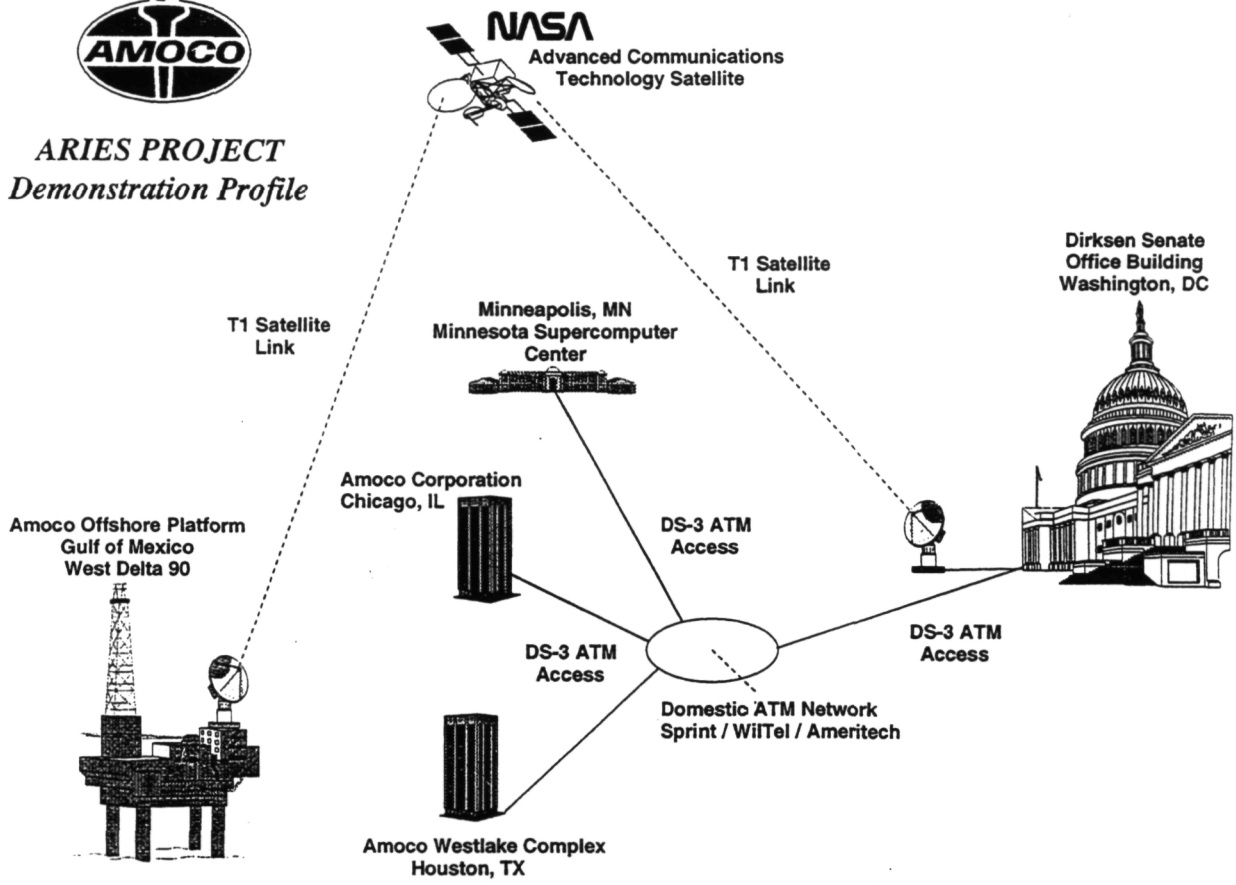

AMOCO OFFSHORE PLATFORM - West Delta 90 area of Gulf of Mexico, December, 1994

HDR STATUS

#1 At Boeing	Operational
#2 At BBN going to HI	TWTA sent to OSC
#3 At OSC Check-out	TWTA replaced with 2's.
#4 At NCAR	Operational
#5 At Lewis	Down, TWTA failed in early May

- Spacecraft limits # of hops to 40 per frame. No real impact to program due to small number of users.
- Operational limit of 2 HDR stations per each beam (e.g., 2 in West or East beam)

ACTS NASA

HDR EARTH STATION LOCATIONS
PLANS FOR EXPERIMENTS

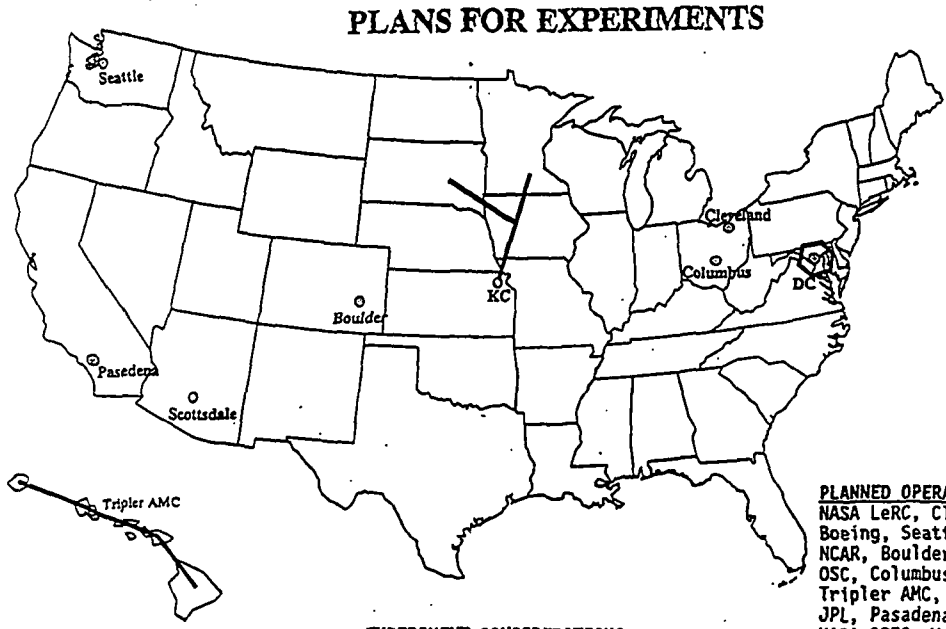

PLANNED OPERATIONAL EARTH STATIONS

NASA LeRC, Cleveland	March 95 - June 95
Boeing, Seattle	March 95 - June 95
NCAR, Boulder	April 95 - Sept 95
OSC, Columbus	April 95 - Sept 95
Tripler AMC, Hawaii	June 95 - 2Q FY97
JPL, Pasadena	July 95 - 2Q FY97
NASA GSFC, Wash. DC	July 95 - 2Q FY97
Sprint, Kansas City	Oct 95 - 2Q FY97
Mayo, Scottsdale	Oct 95 - April96
OSC, Columbus	May 96 - 2Q FY97

EXPERIMENT CONSIDERATIONS
5 HDR Earth Stations
Multiple Experiments
9 Geographic Sites
3 Terrestrial Fiber Networks
- ATDnet encircling DC
- MAGIC from KC to Minneapolis
- State of Hawaii

ACTS NASA

Experiment Starts and Completes by Week (actuals)

As of: 6/7/9

Line #	Date	Expt. #	Organization	Description	Mode	Static
1	1-Dec-93	803	Univ of Alaska - Fairbanks, AK	Propagation		
2		801	Univ. of British Columbia - Vancouver, BC	Propagation		
3		802	Colorado State Univ. - Ft. Collins, CO	Propagation		
4		807	Univ. of Oklahoma - Norman, OK	Propagation		
5		808	Univ of South Florida - Tampa, FL	Propagation		
6		806	Stanford Telecom Inc. - Las Cruces, NM	Propagation		
7		812	Teleglobe Canada	Propagation		
8	6-Dec-93	8	JPL	Mobile	MSM	AMT/LE
9		905	LeRC	Tech Verif Exp. (TVE) - Rain	BBP	NGS
10		907	LeRC	Tech Verif Exp. (TVE) - ATRK	BBP	NGS
11		908	INTEX	Tech Verif Exp. (TVE)	MSM	LET
12	13-Dec-93	38	Motorola	TVE	BBP	2, 13
13		39	Motorola	TVE	BBP	13
14	20-Dec-93	49	COMSAT	Business Network	BBP	1, 7
15	27-Dec-93	45	TEC	DoD	BBP	19, 20
16	03-Jan-94	1	NCS	PSN	BBP	1, 4, 5
17		13	JSC/Krug	Telemedicine	BBP	9, 12
18		43	OU/Huntington Bank	Business	BBP	10, 11
19		58	EMSAT	Mobile	MSM	AMT/LE
20	10-Jan-94	2	NCS	PSN	BBP	4, 5
21		7	Army	DoD Strat/Tact	BBP	16, 17, 1
22		27	Mitre	ISDN	BBP	5, 7
Completed	17-Jan-94	39	Motorola	TVE	BBP	13
23	24-Jan-94	901	MBA Performance	TVE	BBP	As Require

Experiment Starts and Completes by Week (actuals)

As of: 6/7/9

Line #	Date	Expt. #	Organization	Description	Mode	Statio
24	31-Jan-94	4	NCS	PSN	MSM	AMT/LE
25		701	NASA Demo	Demo	BBP	1, 9
26	14-Feb-94	809	JHU/UT	Mobile Propagation	MSM	LET
Completed		2	NCS	PSN	BBP	4, 5
Completed	21-Feb-94	13	JSC/Krug	Telemedicine	BBP	9,12
27	14-Mar-94	5	NTIA	ISDN	BBP	9
28		6	ARL	ISDN	BBP	2, 7, 8
29		17	COMSAT	ISDN	BBP	5, 7
Completed		38	Motorola	TVE	BBP	2, 13
30	15-Mar-94	805	COMSAT Labs - Clarksburg, MD	Propagation		
31	21-Mar-94	21	MAYO	Telemedicine	BBP	12,13
Completed		58	EMSAT	Mobile/Telemedicine	MSM	AMT/LE
32	04-Apr-94	53	AERO-X	Aero	MSM	LET
33	18-Apr-94	54	University of Florida	ISDN	BBP	3
34	18-Apr-94	3	NCS	PSN	BBP	1, 4, 5
Completed	25-Apr-94	1	NCS	PSN	BBP	1, 4, 5
Completed	25-Apr-94	3	NCS	PSN	BBP	1, 4, 5
Completed	16-May-94	54	University of Florida	ISDN	BBP	3
35	23-May-94	804	COMSAT Uplink Power Control	Propagation	MSM	LET
Completed		43	OU/Huntington Bank	Business	BBP	10, 11
36	30-May-94	903	LET MSM Performance	Propagation	MSM	LET
Completed	6-Jun-94	27	Mitre	ISDN	BBP	5, 7

Experiment Starts and Completes by Week (actuals)

As of: 6/7/9

Line #	Date	Expt. #	Organization	Description	Mode	Static
Completed	6-Jun-94	809	JHU/UT	Mobile Propagation	MSM	LET
37	13-Jun-94	14	NMSU	Tele Science	BBP	10, 11
38	18-Jul-94	51	MDCCDS	Data Network	BBP	8, 9
39	18-Jul-94	56	COMSAT	Data Network	MSM	LET
Completed	08-Aug-94	53	AERO-X	Aero	MSM	LET
40	15-Aug-94	911	USAT Checkout	TVE	MSM	USAT
41	15-Aug-94	62	Bellcore	Mobile	MSM	AMT
Completed	15-Aug-93	45	TEC	DoD	BBP	19, 20
Completed	05-Sep-94	21	MAYO	Telemedicine	BBP	12,13
42	3-Oct-94	60	KSC/Lockheed	Distance Education	BBP	12,13
43	3-Oct-94	810	COMSAT - Wide Area Diversity	Data Network	BBP	5,7
44	10-Oct-94	69	NBC	Mobile	MSM	AMT
45	10-Oct-94	95	MASCOM	Mobile	MSM	LET
Completed (Cancelled)	17-Oct-94	60	KSC/Lockheed	Distance Education	BBP	12,13
Completed	31-Oct-94	14	NMSU	Tele Science	BBP	10, 11
Completed	31-Oct-94	95	MASCOM	Mobile	MSM	LET
Completed	7-Nov-94	804	COMSAT Uplink Power Control	Propagation	MSM	LET
Completed	26-Dec-94	810	COMSAT - Wide Area Diversity	Data Network	BBP	5,7
Completed	29-Dec-94	49	COMSAT	Business Network	BBP	1, 7

Experiment Starts and Completes by Week (actuals)

As of: 6/7/95

Line #	Date	Expt. #	Organization	Description	Mode	Statio
46	02-Jan-95	906	LeRC	Tech Verif Exp. (TVE) - DYNM	BBP	NGS
47	09-Jan-95	70	NBC	Data Network	BBP	2, 4, 21
Completed	15-Jan-95	62	Bellcore	Mobile	MSM	AMT
Completed	20-Jan-95	70	NBC	Data Network	BBP	2, 4, 21
Completed	27-Jan-95	69	NBC	Mobile	MSM	AMT
48	08-Feb-95	111	ARPA (UGV)	Mobile	MSM	AMT
49	02-Mar-95	50	PACSPACE	Data Network	BBP	1, 5, 11
50	06-Mar-95	811	Georgia Tech	Propagation	MSM	Other
51	03-Apr-95	99	LeRC/Boeing Inlet Simulation	HDR	MSM	HDR01, 0
Completed	14-Apr-95	51	MDCCDS	Data Network	BBP	8, 9
Completed	14-Apr-95	6	ARL	ISDN	BBP	2, 7, 8
52	08-May-95	41	Southern Cal Edisón	Data Network	MSM	USAT
53	11-May-95	98	NASA Ames (Kuiper)	Aero	MSM	Kuiper Je
54	30-May-95	67	National Library of Medicine	Telemedicine	BBP	1, 8, 10

PROPAGATION PROGRAM STATUS

ACTS NASA

INDUSTRY LETTER

- Sent in Jan. '95 from NASA LeRC Center Director requesting industry's value in extending Prop. program:

Comsat World Systems	Orbital Sciences
Motorola	Martin Marietta
GE American	GM Hughes Elect.
Teledesic	Hughes Spaceway
Space Systems/Loral	Hughes S & C
TRW	AT&T Skynet

ACTS NASA

INDUSTRY LETTER

- Responses received from:
  - Teledesic
  - Space Systems/Loral
  - Martin Marietta Astro Space
  - Comsat World Systems
- Responses added vital industry/commercial support to continue program

NASA

BUDGET STATUS

- Date for announcing ACTS budget is TBD
- Funds have been requested by Lewis to extend through FY 96
- Actual funding level will be set by HQ. May be less than fully funded if by NASA alone. **Any industry support?!**
- One year at a time is being considered

NASA

PROGRAM'S FUTURE

- Three paths program may take
  - 1) Extend program - **decision made soon** before contracts end
  - 2) Extend program - **decision delayed** until contracts end, or nearly so
  - 3) End program - **decision delayed** until contracts end, or nearly so

ACTS NASA

1) EXTEND PROGRAM - DECISION MADE SOON

- Extend contracts
- Continue data collection
- Prepare results/final report as usual

ACTS NASA

2) EXTEND PROGRAM - DECISION DELAYED

- No cost extension
- Prepare final report per current contracts
- Continue data collection/analysis once contract funding restored
- Amend report at end of extension

ACTS NASA

3) END PROGRAM - DECISION DELAYED

- No cost extension
- Prepare final report per current contracts
- Amend report at end of extension as needed

ACTS NASA

NO COST EXTENSIONS

- Will need, most likely, until funding is decided
- Keeps contracts active
  - Prevents re-bid, possible loss of contract
  - Keeps long term data collection at sites currently selected
- No work required during extension period

NASA

PROGRAM COMPLETION

- Assuming 1 year continuation:
  - Collect data through June '96 (or whatever date is sufficient and reasonable to amend report; should be same for all)
  - Program would end Sept. 30, 1996 unless second extension granted
  - Final reports due 30 days later

NASA

ACTS RESULTS CONFERENCE

- September 11 - 13, 1995, in Cleveland
- Focus is on results of all experiments performed so far
- Audience is sat. comm. providers, developers, manufacturers, users, and researchers from govt., univ., and industry
- By invitation only - see me if interested
- Alert to authors - papers due July 01, 1995!

NASA

Acts Propagation Terminals

Engineering Support and Systems Upgrades

David Westenhaver
Westenhaver Wizard Works, Inc.
June 15, 1995

Westenhaver Wizard Works, Inc.

Software Status / Deficiencies and Known Problems

DRX software status:
- Current version 15 of 9/26/94.
  - Remove Post FFT AFC Filter.

DACS software status:
- Current version 8 of 9/26/94.
- Testing version 9:
  - Correct Tipping Bucket Tip Time.
  - Automatic re-start of DRX.

TSR software status:
- Current version 8 of 9/26/94.
  - Testing Using GPS Time via RS-232.
  - Data missing from RV0; Defragment Disk.

ActsView software status:
- Current version 3 of 9/26/94.
  - Add display tipping bucket gauge.

Actspp PreProcessing software status:
- Current version 5.1 of 4/20/95.

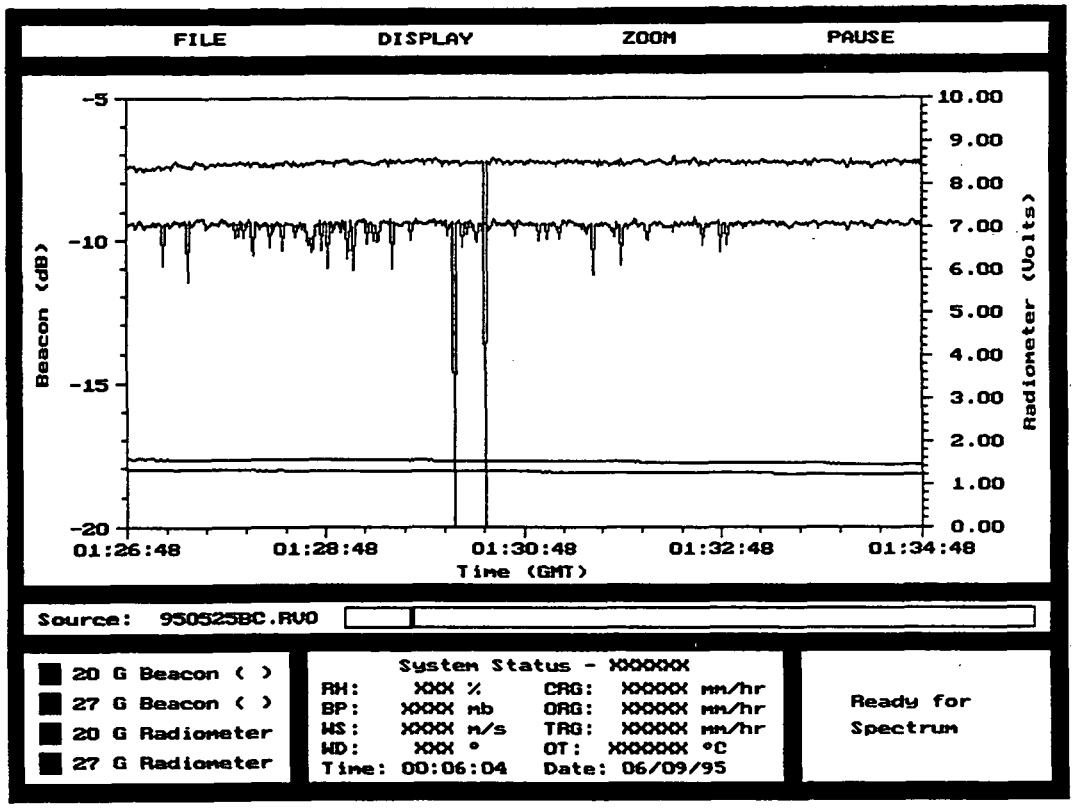

950524BC.FFT P3

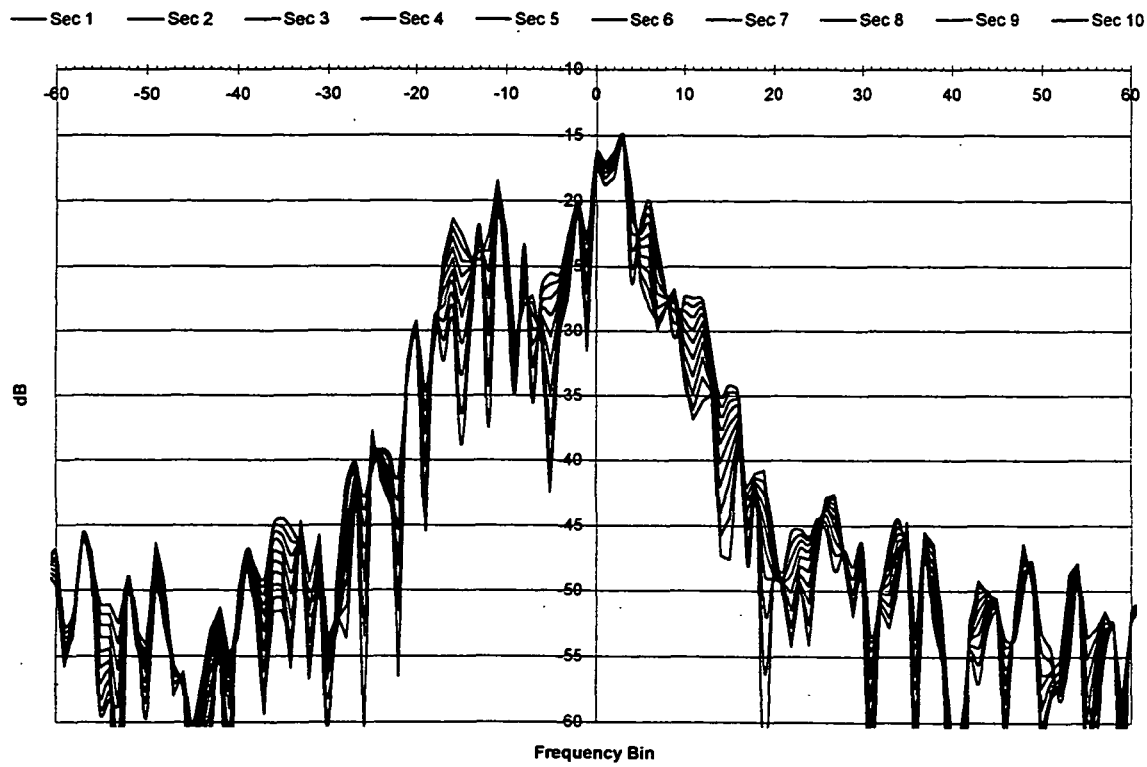

Figure 2

950524BC.FFT P2

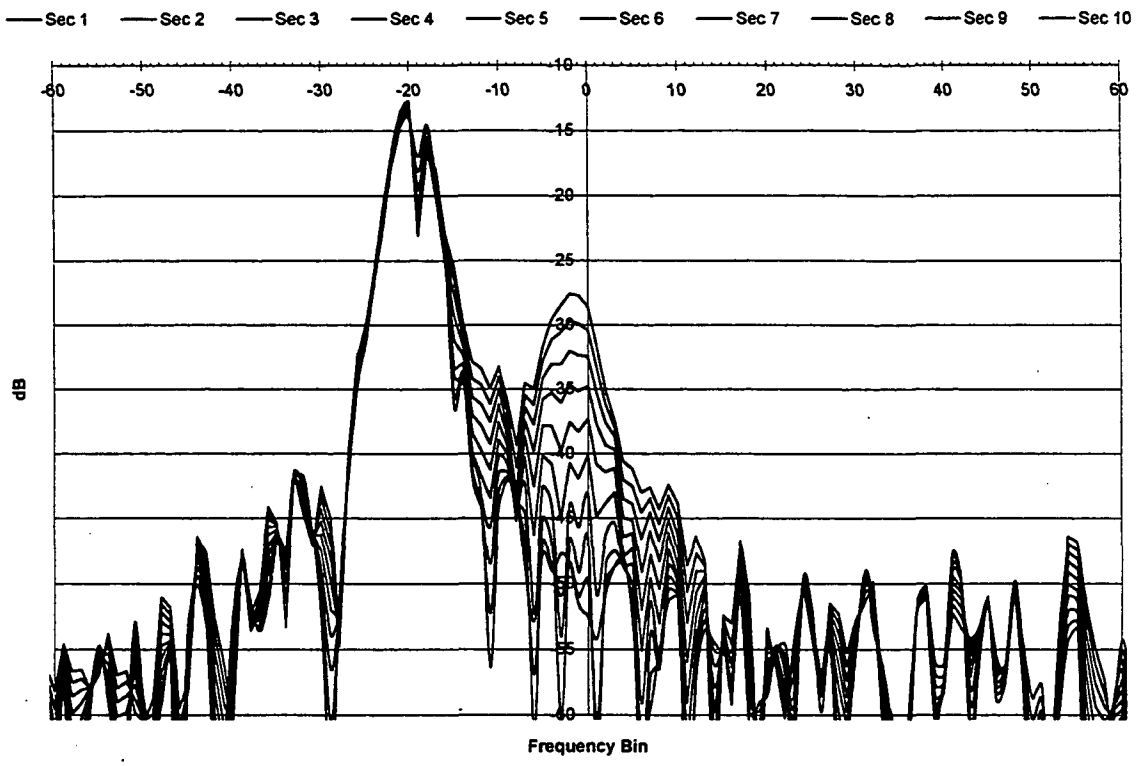

Figure 3

950525BC.FFT P1

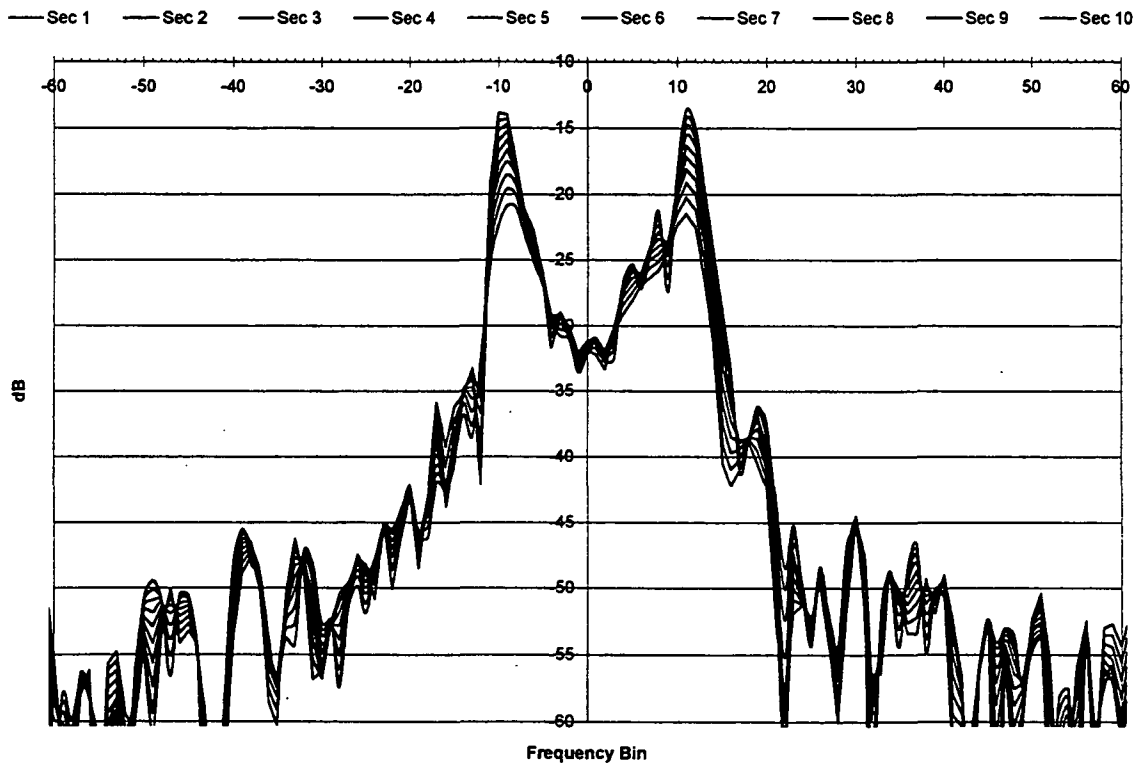

Figure 4

System Hardware Status / Deficiencies and Known Problems

Upper Fan Shroud Installed:

Lowers delta temperatures inside enclosure.

RF Temperature Controller:

The primary design features of this design are:

The FET's are run at less than 50% their ratings.

The balanced output filtering removes all high frequencies from the output. The output ripple is a very low level 7.5 KHz sine wave.

The control loop contains an error integrator making the control loop a type II loop.

Micro-Controller uses smart controls and protection.

WWV clock:

Problems: Start up & signal loss; Date jumps.

Solution: GPS

Antenna placement (signal level & cable length)

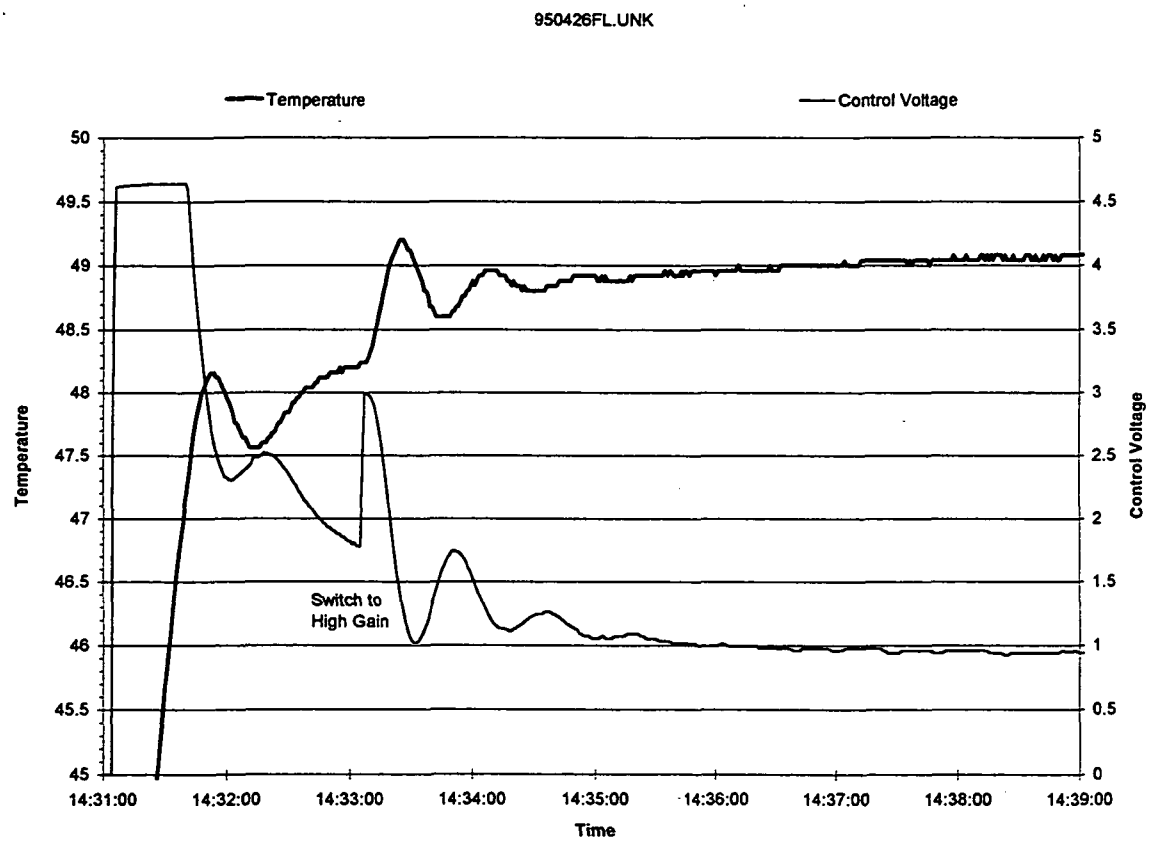

Figure 5

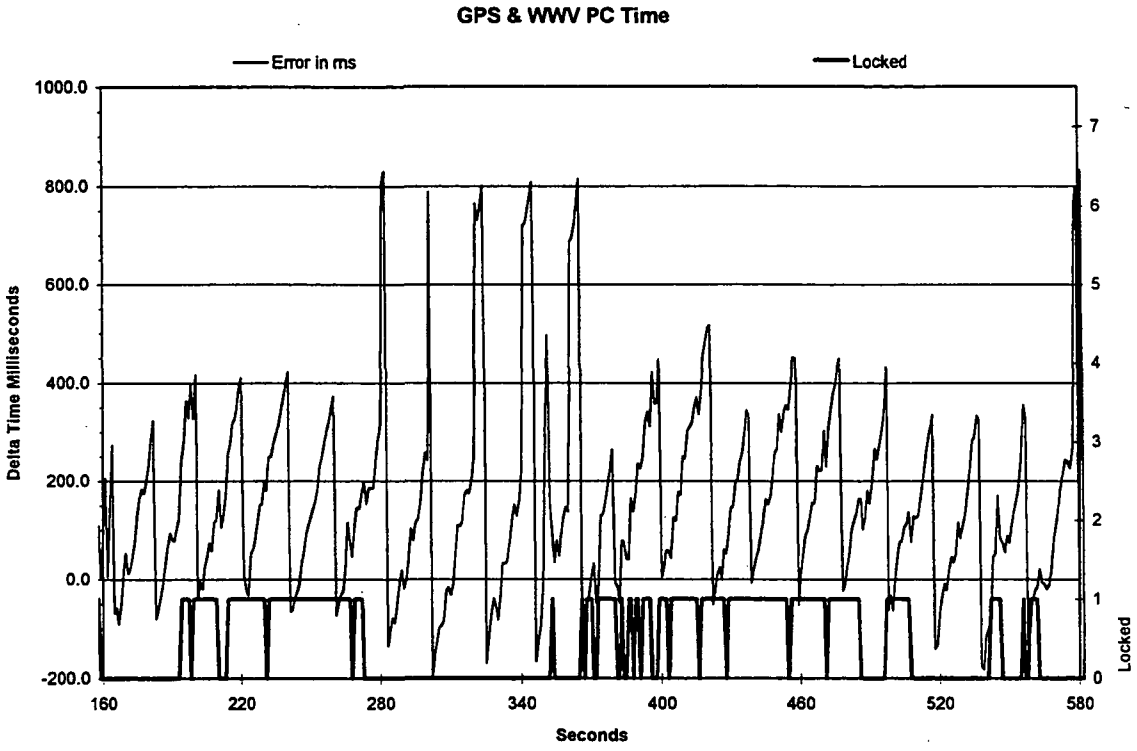

Figure 6

Westenhaver Wizard Works, Inc.

Decoding System Effects using PreProcessing

Polarization test:

Figure 7 Beacon Levels Vs Polarization Angles:

System Stability

Figure 8 DRX Calibration noise diode & ref. load Vs Time.

Figure 9 Radiometer Calibration; slope and offset Vs Time.

Figure 10 DRX Calibration noise diode & ref. load Vs Time, With A Hardware Change.

Figure 11 Radiometer Calibration; slope and offset Vs Time, With A Hardware Change.

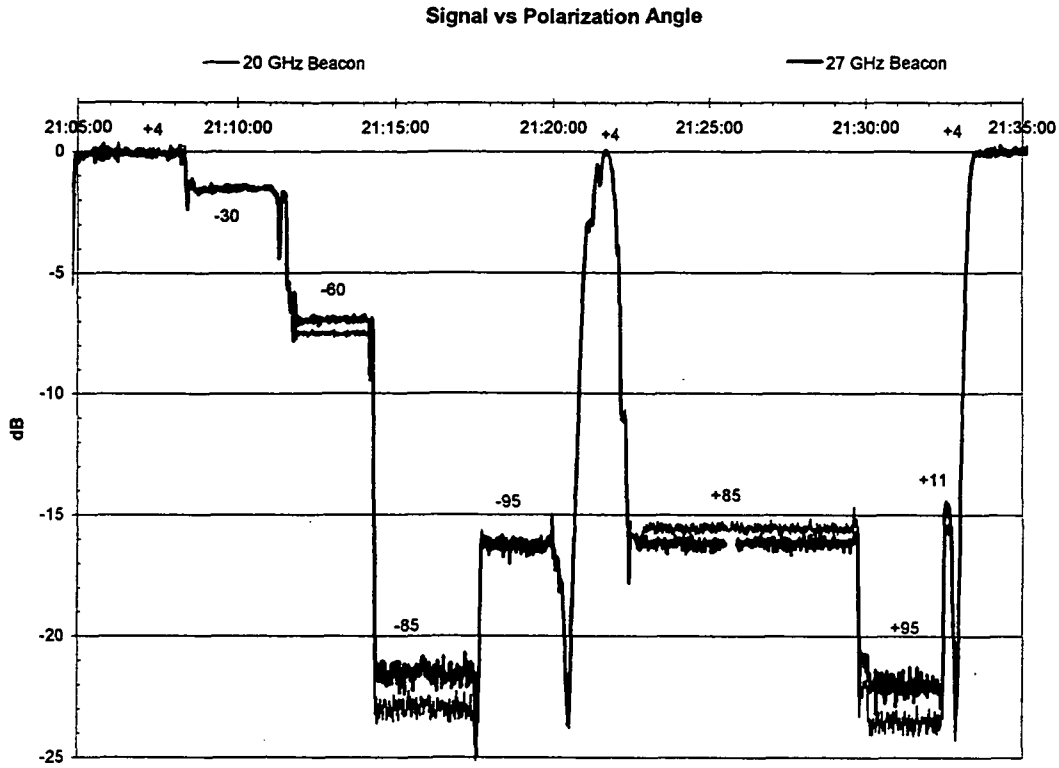

Figure 7

950226FL.SUM

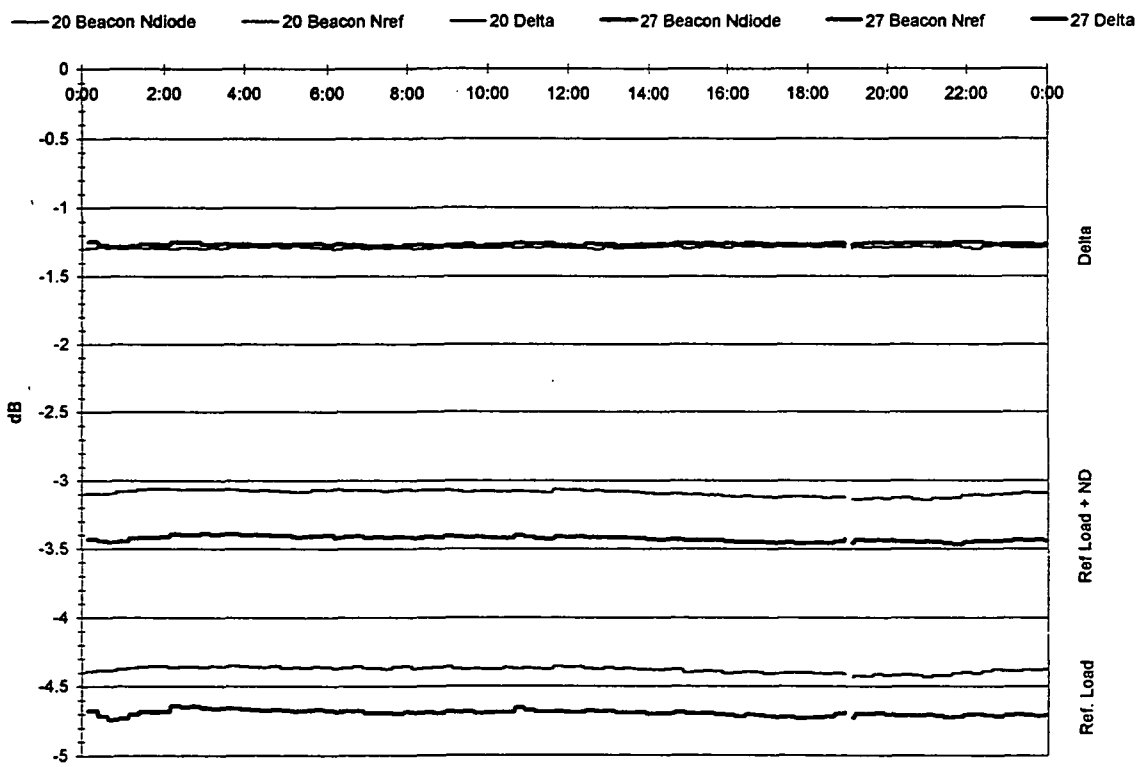

Figure 8

950226FL.SUM

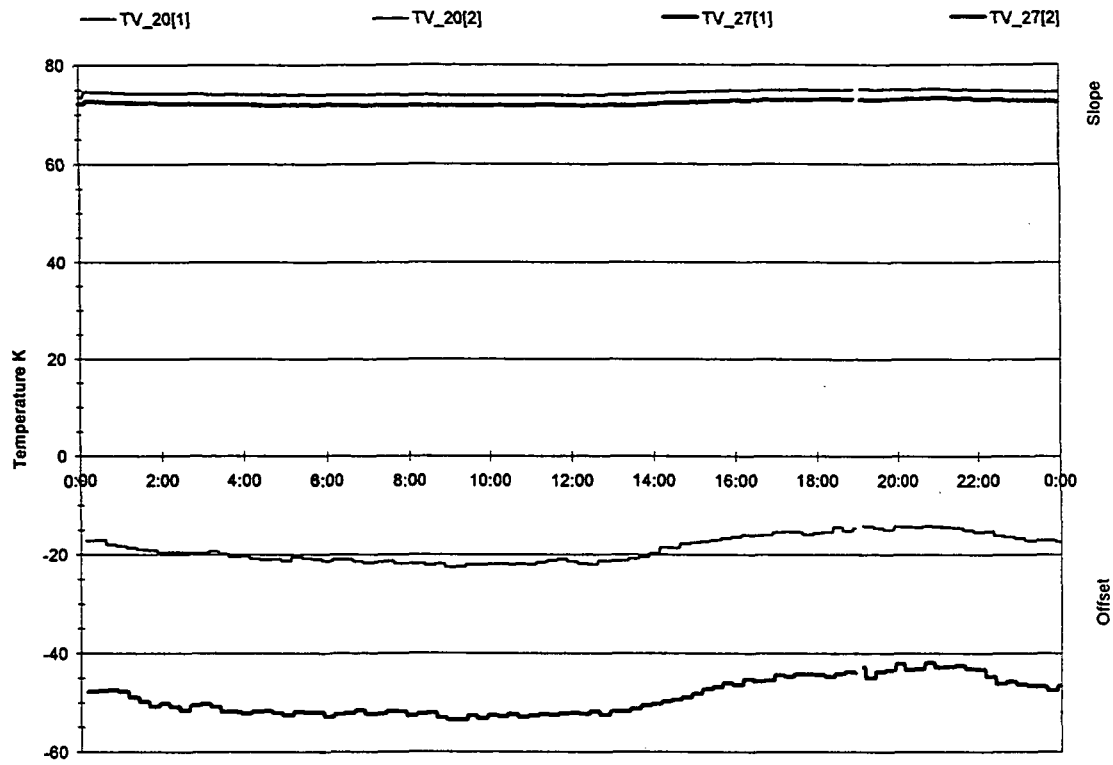

Figure 9

941201BC.SUM

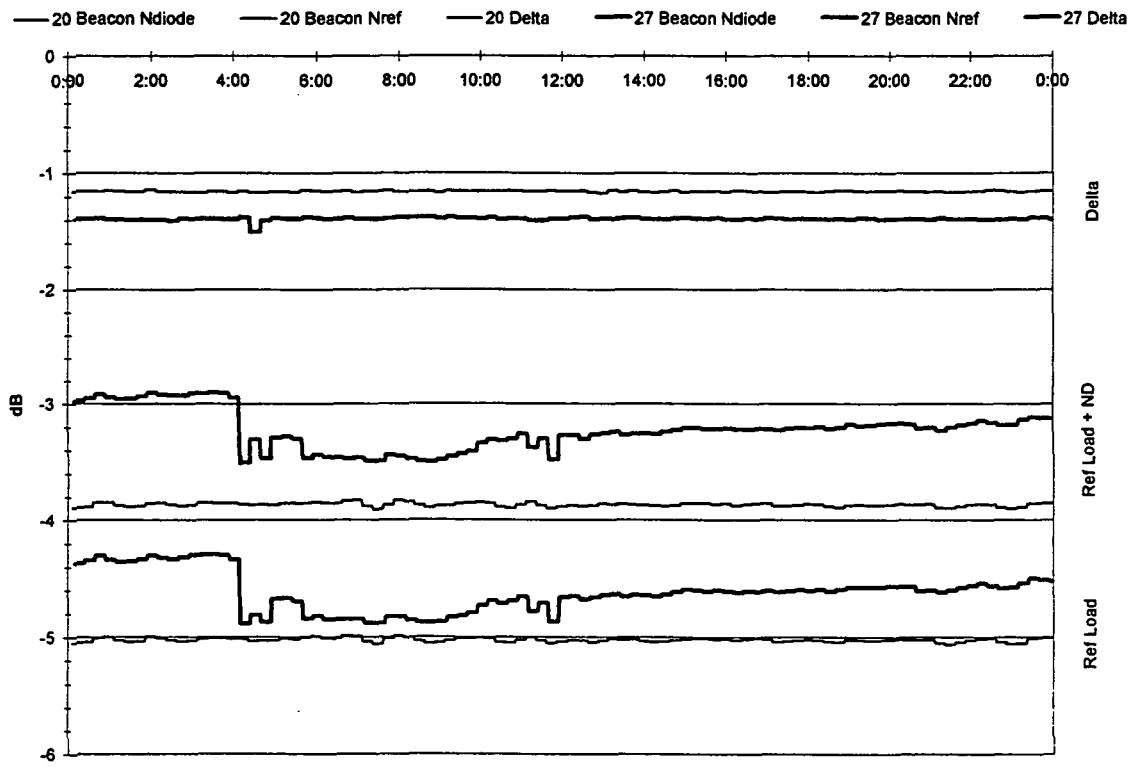

Figure 10

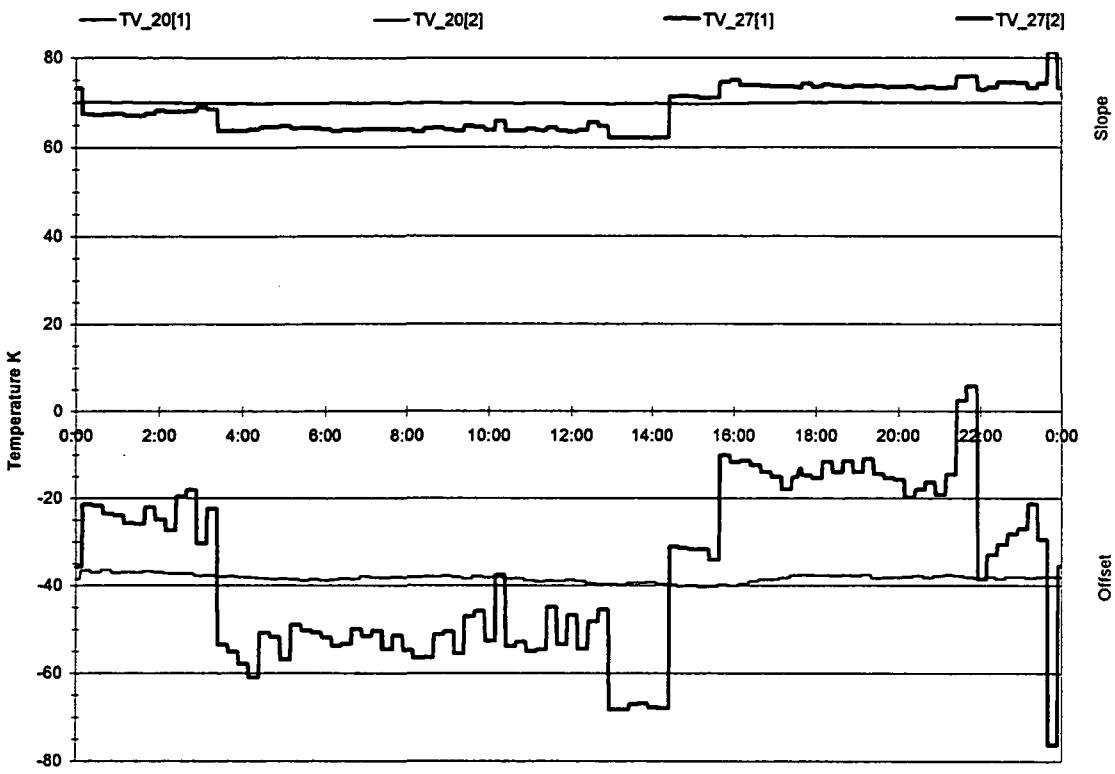

Figure 11

Westenhaver Wizard Works, Inc.

Conclusions

Systems are collecting almost all of available data 99.9%.

Systems are Dependable.

Systems are Accurate. 0.1 - 0.2 dB, 10- 12 ° K

A Few Potential problems:

LOs or PLOs or LNA's have frequency instability causing dropouts.

IFs and Radiometers have gain instability causing random shifts.

Hardware failures.

PC problems.

EERL / Univ. of Texas

DATA CENTER STATUS REPORT

BY
ALI SYED
&
WOLFHARD J VOGEL

EERL/UTAU
10100 BURNET RD
AUSTIN, TX 78758-4497
PRESENTED AT APSW VII
FORT COLLINS, CO
JUN 15, 1995

1

EERL / Univ. of Texas

Current DC Activities

- ☑ Archive Raw Data from Stations
- ☑ Distribute Raw Data on CD-ROM to Stations
- ☑ Archive Event & Fault Logs from Stations
- ☑ E-mail Weekly Data Received Status
- ☑ Audit Pre-processed Data & E-mail Reports
- ☑ Perform Basic Statistical Analysis

EERL / Univ. of Texas

Raw Data Received

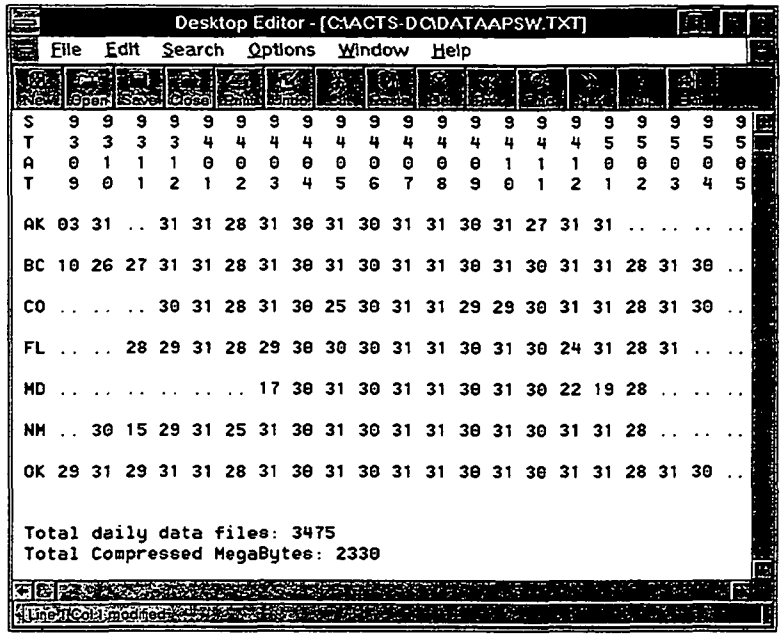

3

EERL / Univ. of Texas

Pre-processed Data Received

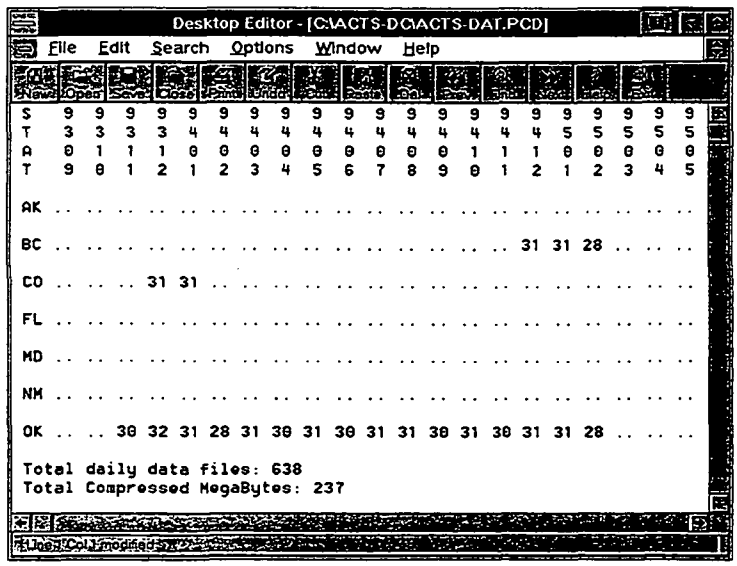

4

EERL / Univ. of Texas

TOTAL RAW DATA ON 4 CDs

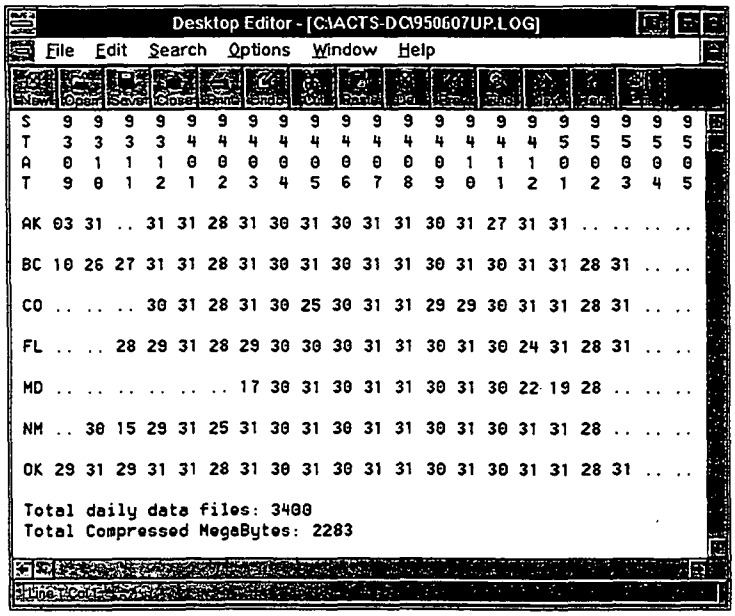

5

EERL / Univ. of Texas

CD-ROM DIRECTORY STRUCTURE

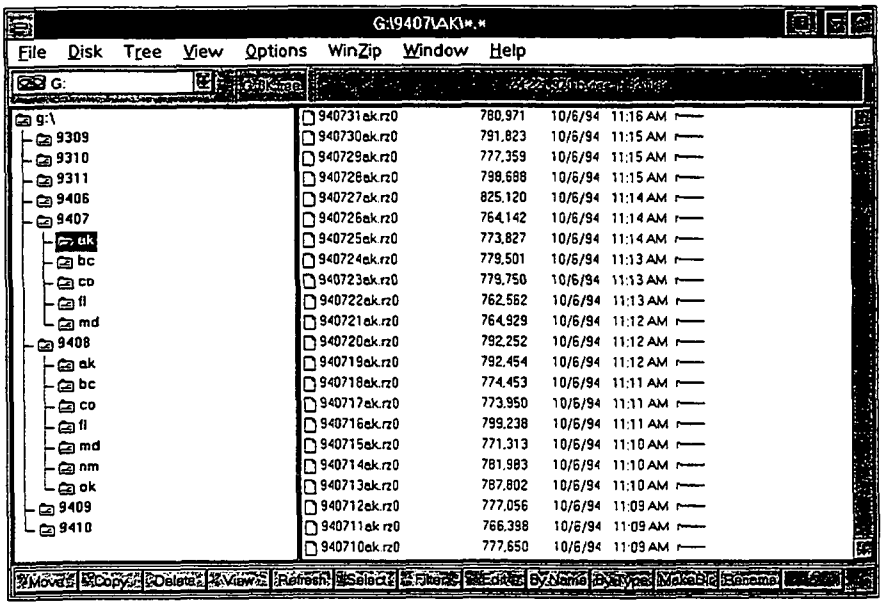

6

EERL / Univ. of Texas

ACTS DATA COMPRESSION RATIOS

RAW DATA ON CDs

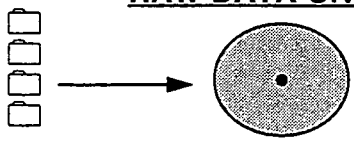

2283 MBytes in 3400 Files

C.R = 1.96

P-P DATA ON HARD DISK

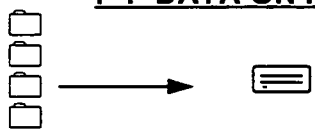

237 MBytes in 638 Files

C.R = 3.55

7

EERL / Univ. of Texas

DATA CENTER AUDIT PROGRAM

TO AUDIT	STATES
BEACON	GOOD / BAD / QUESTIONABLE / MISS
	CAL. MODE / TOTAL POWER MODE
RADIOMETER	GOOD / BAD / QUESTIONABLE / MISS
	CAL. MODE
RAIN RATE	GOOD / BAD
REL. HUMIDITY	GOOD / BAD
AIR TEMP.	GOOD / BAD

STATES LEGEND:

GOOD	GOOD DATA
BAD	BAD DATA
MISS	MISSING DATA
QUEST	OUT OF RANGE DATA, FORCED CALIB. ETC
CAL.	NOISE DIODE CALIBRATION MODE DATA
TOTAL PWR.	BEACONS IN TOTAL POWER MODE DATA

EERL / Univ. of Texas

ACTS DATA AUDIT

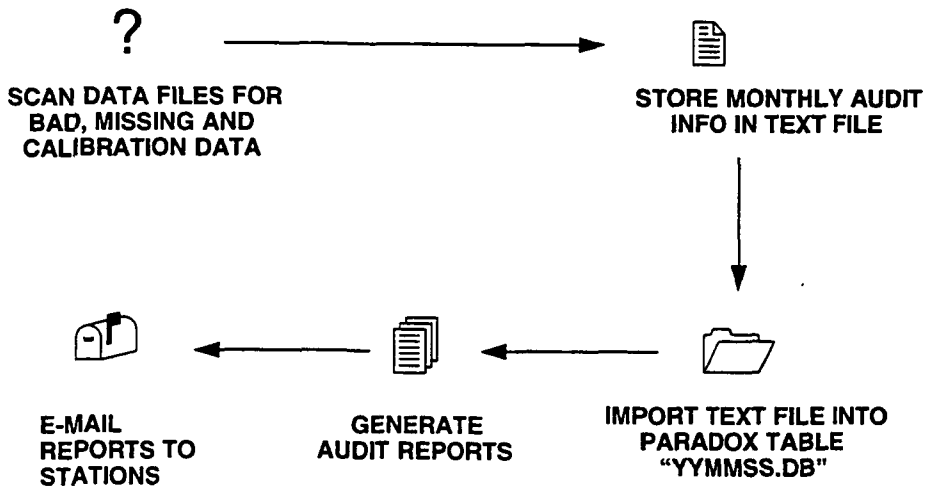

9

EERL / Univ. of Texas

AUDIT REPORT E-MAILED TO STATIONS

Desktop Editor - [C:\DATA\PDOX\9412BCAT.TXT]

File Edit Search Options Window Help

```
ACTS DATA CENTER AUDIT REPORT
~~~~~~~~~~~~~~~~~~~~~~~~~~~~

STATE              DEFINITION
~~~~~              ~~~~~~~~~~

GOOD               Good data
BAD                Bad data
QUES               Questionable data, e.g forced calibrations
                   Attenuation > 40dB < -10 dB etc
TPWR               Beacon in total power mode
CAL                Noise-diode calibration

                   ~~~~~~
                   9412BC
                   ~~~~~~

Parameter          State    #Events  Seconds
~~~~~~~~~          ~~~~~    ~~~~~~~  ~~~~~~~

Beacon20           CAL      2974     68402
Beacon20           QUES     3        949
Beacon20           TPWR     13       179
Beacon27           CAL      2980     68540
Beacon27           QUES     49       1295
Beacon27           TPWR     30       276
FILE               GOOD     31       2678163
FILE               MISS     3        237
RECEIVER           GOOD     31       2678400
Radiom20           CAL      2973     68379
Radiom20           QUES     4        1076
Radiom27           CAL      2969     68287
Radiom27           QUES     60       1851
RainRate           BAD      65       1637
RelHumid           BAD      18       190758
```


10

EERL / Univ. of Texas

MISSING PV1 DATA SUMMARY

9412BC	GOOD	31	2678163		9311OK	GOOD	29	2111033
9412BC	MISS	3	237		9311OK	MISS	163	567561
9501BC	GOOD	31	2677912		9312OK	GOOD	31	2561668
9501BC	MISS	65	488		9312OK	MISS	125	116732
9502BC	GOOD	28	2419032		9401OK	GOOD	31	2677891
9502BC	MISS	56	168		9401OK	MISS	66	509
					9402OK	GOOD	28	2417902
	GOOD	7775107			9402OK	MISS	14	1130
	MISS	893	0.011485		9403OK	GOOD	31	2677809
					9403OK	MISS	67	591
9312CO	GOOD	30	2395504		9404OK	GOOD	30	2585687
9312CO	MISS	247	282899		9404OK	MISS	87	6313
9401CO	GOOD	31	2678127		9405OK	GOOD	31	2677283
9401CO	MISS	63	273		9405OK	MISS	71	1117
					9406OK	GOOD	29	2505345
	GOOD	5073631			9406OK	MISS	59	86655
	MISS	283172	5.581249		9407OK	GOOD	30	2676719
					9407OK	MISS	62	88081
					9408OK	GOOD	31	2678400
					9409OK	GOOD	30	2587946
					9409OK	MISS	8	4054
					9410OK	GOOD	31	2664110
					9410OK	MISS	83	14905
					9411OK	GOOD	30	2569867
					9411OK	MISS	70	22133
					9412OK	GOOD	31	2676193
					9412OK	MISS	66	2207
					9501OK	GOOD	31	2672359
					9501OK	MISS	12	6041
					9502OK	GOOD	28	2410732
					9502OK	MISS	18	8468
						GOOD	41150944	
						MISS	926497	2.25146

11

EERL / Univ. of Texas

DATA CENTER ANALYSIS PROGRAM

TO ANALYZE	STATISTICS
BEACONs	CDFs & CORRELATIONs
RADIOMETERs	CDFs & CORRELATIONs
RAIN RATE	CDFs

"C" PROGRAM

STORE MONTHLY ANALYSIS INFO IN TEXT FILES

IMPORT TEXT FILE INTO EXCEL SPREADSHEET "YYMMSS.XLS"

EXCEL MACROS

GENERATE STATISTICS

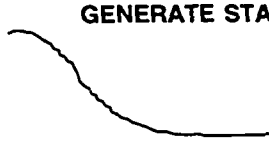

12

EERL / Univ. of Texas

ANALYSIS RESULTS - CDFs

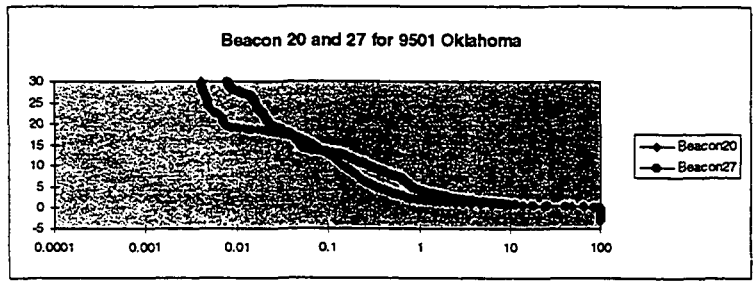

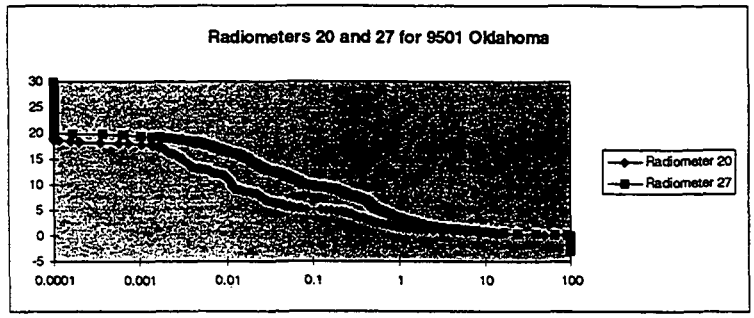

13

EERL / Univ. of Texas

ACTS-DC SYSTEM STATUS

COMPUTER SYSTEM OK

TRAKKER 240MB OK
COLORADO BACKUP LITE VER 2.01

CD-R SYSTEM OK
PSCRIBE UPGRADED TO *WinSCRIBE*
NEW SOFTWARE FEATURES:
- CD-ROM / CD-AUDIO TO CD-R TRANSFER
- INCREMENTAL MULTI-SESSION, WRITE-PROTECTION

ACTS-DC PROGRAMS FOR COMPRESSION & DECOMPRESSION OK
AUDIT & ANALYSIS WERE MODIFIED FOR PV1 FILES

14

EERL / Univ. of Texas

CONCLUSIONS

- RAW & PRE-PROCESSED DATA ARCHIVAL IS WORKING
- WEEKLY STATUS REPORTS FOR RECEIVED DATA WILL CONTINUE TO BE E-MAILED
- MONTHLY AUDIT REPORTS FOR RECEIVED DATA WILL CONTINUE TO BE E-MAILED

15

Session II:
Topics in Ka-Band Propagation

USING ACTS PROPAGATION DATA IN SUPPORT OF MILITARY EHF SATELLITE COMMUNICATION

ROBERT J. FIGUCIA
MIT LINCOLN LABORATORY

NASA ACTS PROPAGATION STUDIES WORKSHOP (APSW VII)
15 JUNE 1995

OUTLINE

- INTRODUCTION
- NEED FOR PROPAGATION DATA
- DESIRED ACTS DATA PROCESSING

RJF - 2

INTRODUCTION

- U.S. MILITARY RELIES ON SATELLITES FOR LONG-HAUL COMMUNICATIONS
- "MILITARY EHF" SATCOM IS CRITICAL FOR PRESENT AND FUTURE CAPACITY
  - — LOW AND MEDIUM DATA RATE (≤ 1.544 MBPS) COMMUNICATIONS
  - — ASSURED ACCESS (HIGH AVAILABILITY)
  - — ROBUST (ANTI-JAM)
- RAIN LOSS DRIVES AVAILABILITY IN THE EHF BAND
- ACCURATE CHARACTERIZATION OF RAIN AND ATMOSPHERIC LOSSES NEEDED FOR EFFICIENT DESIGN

RJF - 3

FREQUENCIES USED FOR SATCOM

STANDARD 521 FREQUENCIES (GHz)*	USES
UHF-BAND (0.3 - 1)	→MILITARY UHF (225 - 400 MHZ) - FLTSAT, AFSATCOM
L-BAND (1 - 2)	IRIDIUM, INMARSAT
S-BAND (2 - 4)	TT&C
C-BAND (4 - 8)	INTELSAT, INMARSAT, MARISAT
X-BAND (8 - 12)	→MILITARY SHF (8/7 GHZ) - DSCS
Ku-BAND (12 - 18)	TDRS, INTELSAT, HUGHES DBS
K-BAND (18 - 27)	→MILITARY EHF DOWNLINK (20 GHZ) - MILSTAR, FEP, UFO-E; ACTS (20 GHZ BEACON)
Ka-BAND (27 - 40)	→MILITARY UPLINK (30 GHZ); ACTS (27.5 GHZ BEACON)
MILLIMETER WAVES (30 - 300)	→MILITARY EHF UPLINK (44 GHZ) - MILSTAR, FEP, UFO-E

- LINK DEGRADATION DUE TO WEATHER BECOMES SIGNIFICANT ABOVE 10 GHZ
- MILITARY EHF SATCOM (44/20 GHZ) AND ACTS BEACONS (27/20 GHZ) WILL EXPERIENCE SIMILAR DEGRADATION

* MORGAN AND GORDON (1989).

RJF - 4

NEED FOR EHF PROPAGATION DATA

- TO DETERMINE IF USERS CAN TOLERATE SMALLER WEATHER MARGINS ALLOWING FOR LIGHTER, LOWER-COST TERMINALS
- TO CHARACTERIZE/MODEL OUTAGE STATISTICS
- TO EXTEND AVAILABILITY PREDICTIONS BELOW 98%

RJF - 9

BENEFITS OF USING ACTS PROPAGATION DATA

- ADVANTAGES
  - — EXTENSIVE, CALIBRATED ATTENUATION MEASUREMENTS
  - — BEACON FREQUENCIES CLOSE TO MILITARY EHF BAND
  - — ELIMINATES NEED FOR COSTLY MILITARY PROPAGATION EXPERIMENT
  - — UNSURPASSED EXPERTISE IN THE FIELD
- CONCERN
  - — SPECIAL PROCESSING NEEDED TO APPLY DATA TO EHF MILSATCOM

RJF - 10

REQUESTS FOR PROCESSING ACTS DATA

- USE UNIFORM DATA FORMAT FOR ALL SITES
- SCALE DATA TO GIVE CORRESPONDING EHF LOSS
  - — FROM 20.185 AND 27.5 GHZ
  - — TO 20.7 AND 44.5 GHZ
- SCALE DATA TO GIVE INFORMATION AT SAME ELEVATION ANGLES
  - — RANGE OF INTEREST FROM UNDER 10° TO 90° (ESPECIALLY 20°)
- REPORT RESULTS FOR DIFFERENT WEATHER MARGINS
  - — 20.7 GHZ MARGINS FROM 1 TO 6 dB
  - — 44.5 GHZ MARGINS FROM 6 TO 14 dB
- COMBINE SITE DATA FOR CONTINENTAL/GLOBAL PREDICTIONS

RJF - 11

STATISTICAL INFORMATION DESIRED

- FADE CHARACTERISTICS
  - — DEPTH OF FADE (PDF)
  - — OUTAGE DURATION (PDF) VS. MARGIN
  - — OUTAGE FREQUENCY (MTBO) VS. MARGIN
- ATTENUATION VS. PERCENT AVAILABILITY
  - — WITH COMPARISON TO EXISTING MODELS
- SKY TEMPERATURE (PDF) AT 20.7 GHZ
  - — AS A FUNCTION OF PATH ATTENUATION

RJF - 12

OPEN QUESTIONS

- CAN A MODEL FOR OUTAGES BE FORMULATED ?

- HOW SHOULD YOU MODEL THE COMBINED EFFECTS OF RAIN, ATMOSPHERIC ATTENUATION AND SKY TEMPERATURE?
  - — I.E., WHAT HAPPENS TO WATER VAPOR CONCENTRATION IN RAIN?

- HOW TO BEST ACCOUNT FOR INFLUENCE OF OTHER VARIABLES?
  - — INSTANTANEOUS METEOROLOGICAL CONDITIONS
    EX., RAIN RATE, RAIN HEIGHT, DROP SIZE/CONCENTRATION, HUMIDITY, TEMP
  - — VARIATION BY MONTH, YEAR, AND CLIMATE
  - — POLARIZATION

RJF - 13

SUMMARY

- ACTS PROPAGATION EXPERIMENT HAS POTENTIAL TO IMPROVE THE UNDERSTANDING OF WEATHER EFFECTS ON EHF MILSATCOM

- SPECIAL DATA PROCESSING AND FORMATTING WILL ENHANCE THE VALUE TO USERS AND PLANNERS

RJF - 14

APL-COMSAT-Mitre 20 GHz Diversity Experiment Using ACTS

Julius Goldhirsh, Bert Musiani,
Applied Physics Laboratory, JHU
Asoka Dissanayake, K. T. Lin,
COMSAT Laboratories

Background

- Three Site Diversity Link Initiated September 1, 1994
- APL Contract Commenced 4/10/95
- 20 GHz Receivers at APL, COMSAT, Mitre Locations
  - Central Maryland and Virginia
  - Transferred to Stanford Telecom 4/8/95 (0.5 km Distance)
- COMSAT Provided All Receivers and Oversees Health
  - Provides APL with COMSAT and Mitre (or Stanford Telecom) Data
  - APL Performs Diversity Analysis

Long Term Objectives

- Establish Single Terminal and Joint Probability Distributions
  - Three Site Scenario
  - Monthly
  - Annual
- Establish Diversity Gains
  - Three Site Scenario
  - Monthly
  - Annual
- Compare Results with Previous Models

Objectives Today's Talk

- Provide Background Regarding Experiment
- Single Terminal and Joint Probability Distributions
  - Sept., Oct., Nov. 1994
  - APL-COMSAT Scenario
- Diversity Gains
  - Sept., Oct., Nov. 1994
  - APL-COMSAT Scenario

GEOMETRY FOR APL-COMSAT-MITRE DIVERSITY LINK

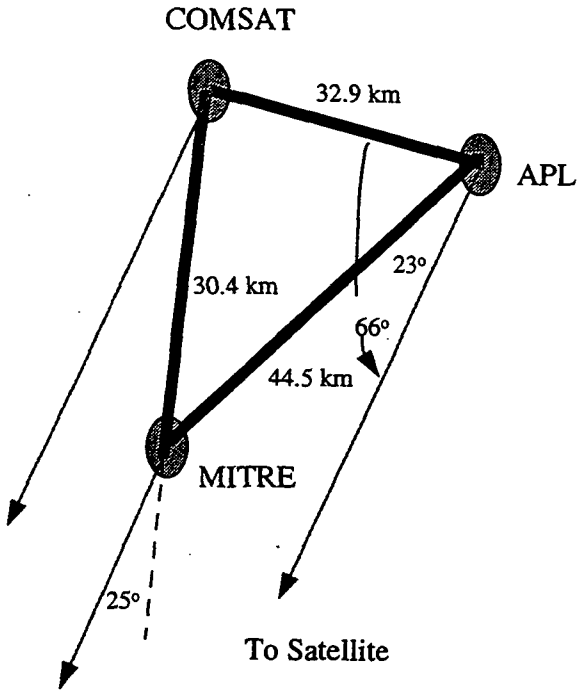

Geometrical and Nominal Electrical Parameters of APL-COMSAT-MITRE Link

PARAMETERS	ALL	APL	COMSAT	MITRE
GEOMETRIC				
Latitude of Sites (deg)		39°10'7.5"	39°13'12"	38°57'
Longitudes of Sites (deg)		77°53'55.5"	77°16'30"	77°19'48"
Azimuth Pointing (deg)		214.0	213.5	213.6
Elevation (deg)		38.7	38.8	39.1
Dist. from APL (km)			32.9	44.5
Dist. from COMSAT (km)		32.9		30.4
ELECTRICAL				
Frequency	20.185			
Polarization	V			
Beacon EIRP (dBW)	19			
Rec. Antenna Diameter (m)	1.2			
Rec. Antenna Gain (dB)	45.9			
Rec. Beamwidth (deg)	.85			
Rec. Bandwidth (Hz)		400	65	20
Carrier to Noise (dB)		28	34	36
Rec. Dynamic Range (dB)		22	28	30

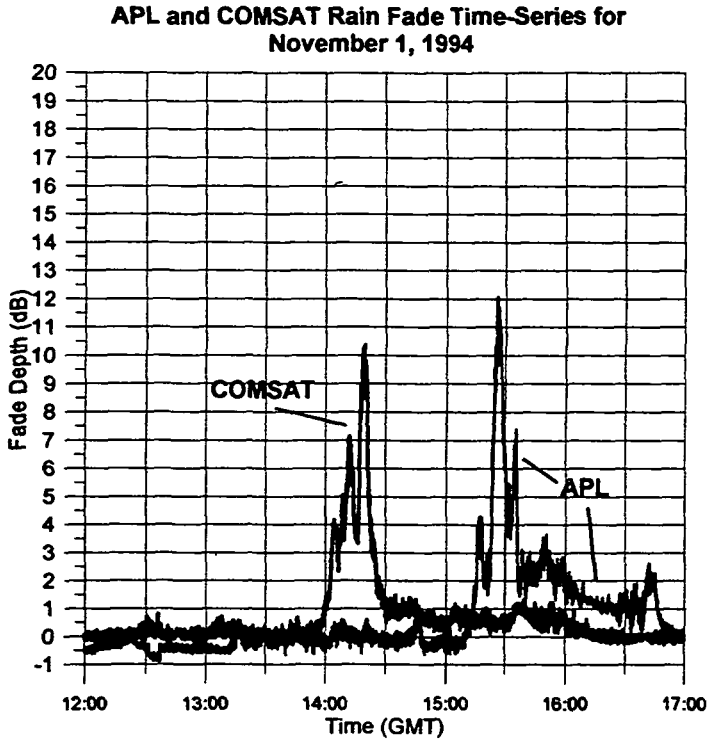
APL and COMSAT Rain Fade Time-Series for November 1, 1994
Fade Depth (dB)
20
19
18
17
16
15
14
13
12
11
10
9
8
7
6
5
4
3
2
1
0
-1
COMSAT
APL
12:00
13:00
14:00
15:00
16:00
17:00
Time (GMT)

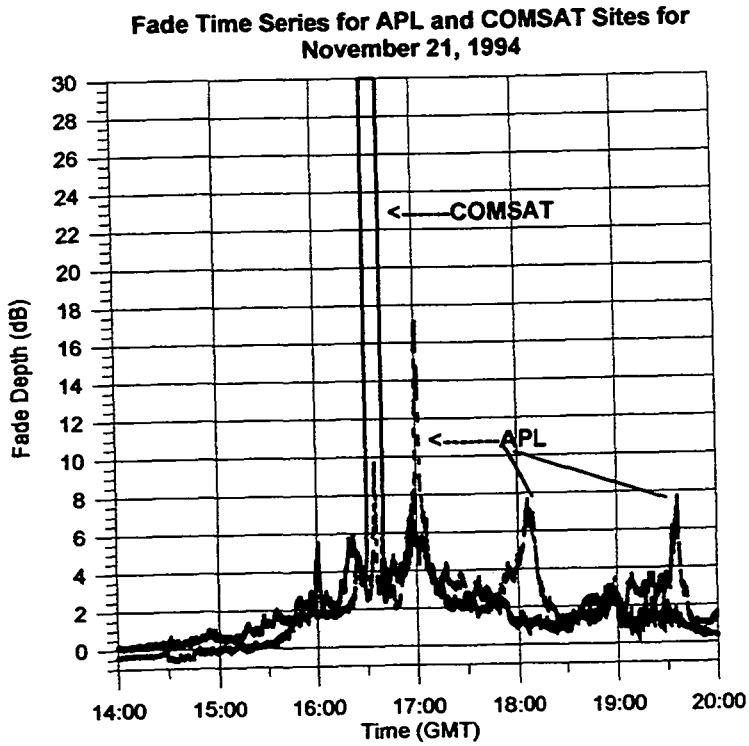
Fade Time Series for APL and COMSAT Sites for November 21, 1994
Fade Depth (dB)
30
28
26
24
22
20
18
16
14
12
10
8
6
4
2
0
<——COMSAT
<——APL
14:00
15:00
16:00
17:00
18:00
19:00
20:00
Time (GMT)

ACTS 20 GHz Single Terminal and Joint Fade Distributions for APL and COMSAT Sites - September, 1994

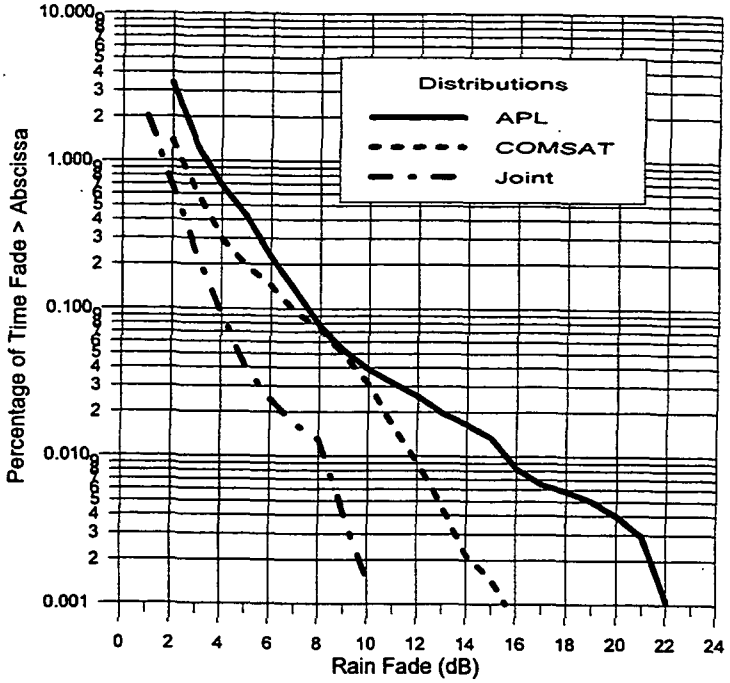

ACTS 20 GHz Single Terminal and Joint Fade Distributions for APL and COMSAT Sites - October, 1994

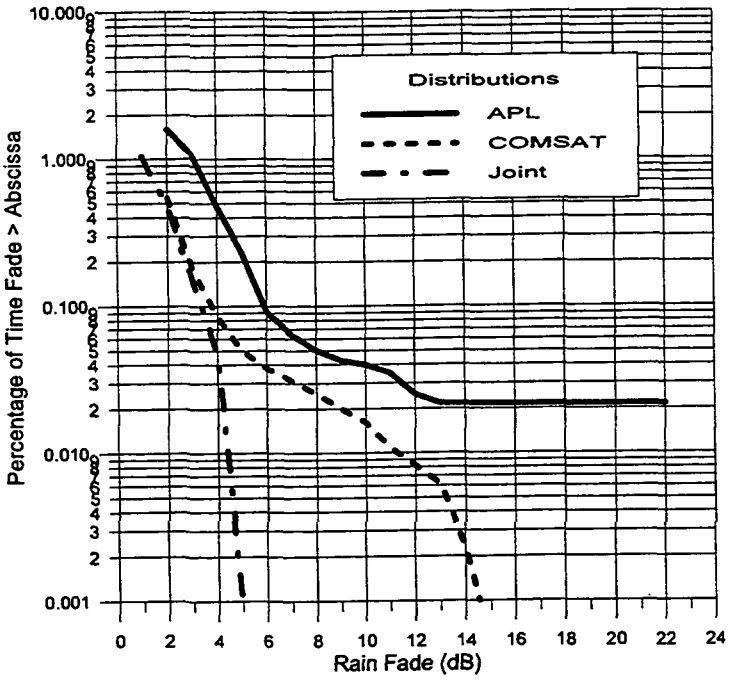

Single Terminal and Joint Cumulative Distributions for APL and COMSAT Sites for November 1994

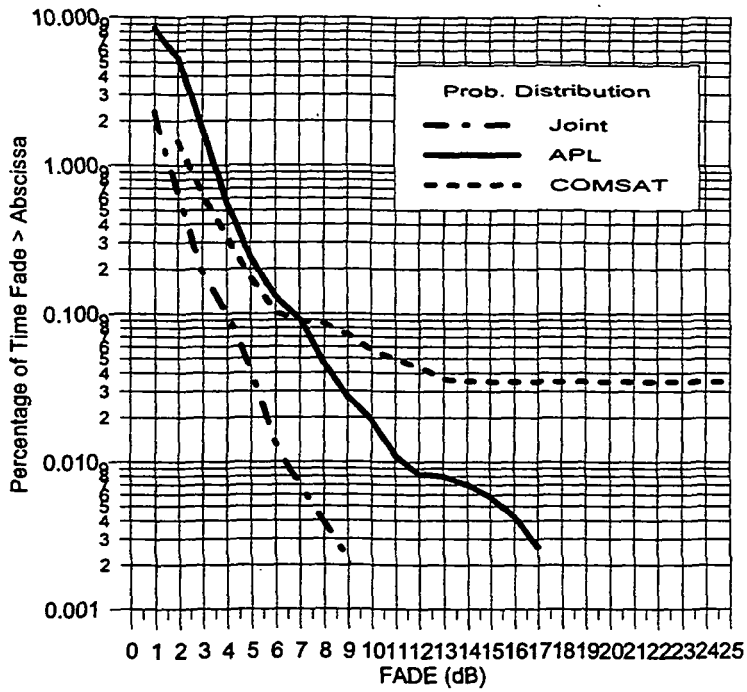

ACTS 20 GHz Single Terminal and Joint Fade Distributions for APL and COMSAT (Sept, Oct, Nov. 1994)

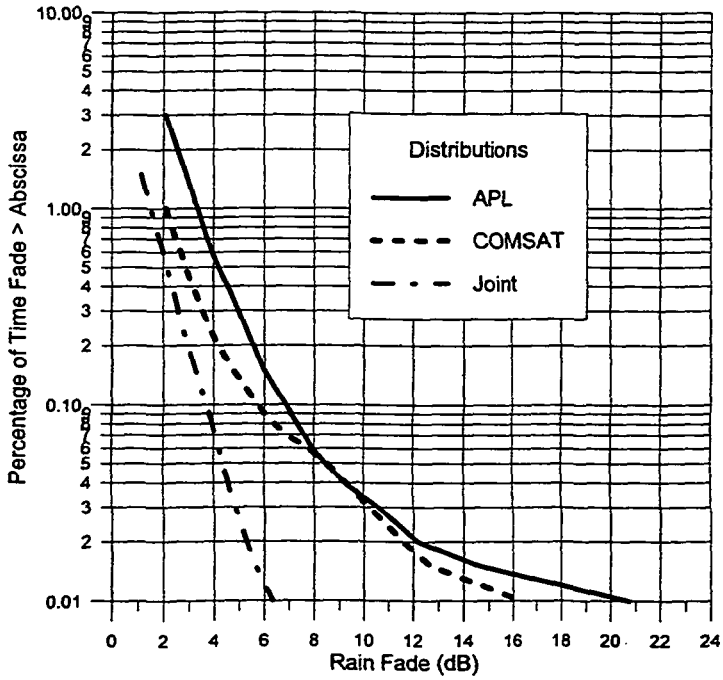

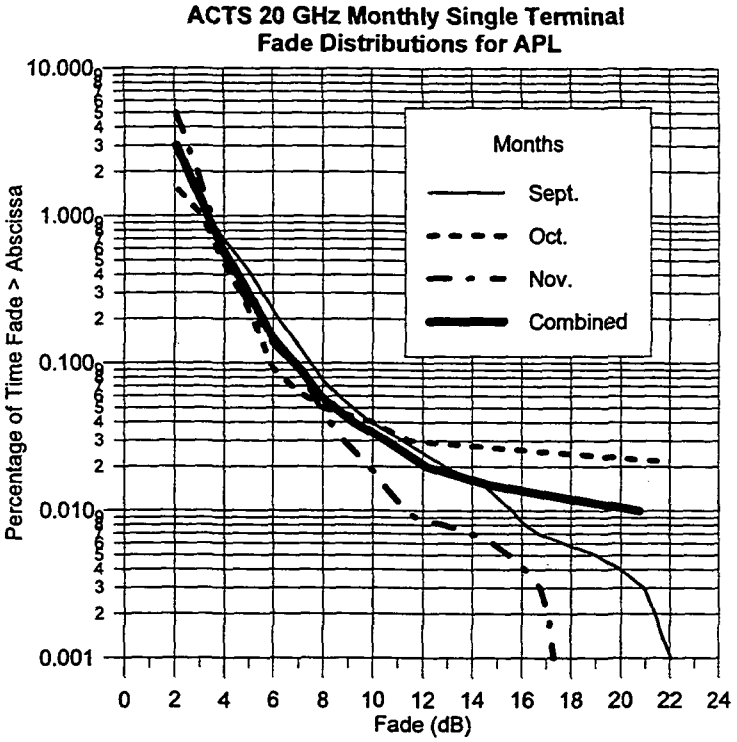
ACTS 20 GHz Monthly Single Terminal
Fade Distributions for APL
Percentage of Time Fade > Abscissa
10.000
1.000
0.100
0.010
0.001
0 2 4 6 8 10 12 14 16 18 20 22 24
Fade (dB)
Months
Sept.
Oct.
Nov.
Combined

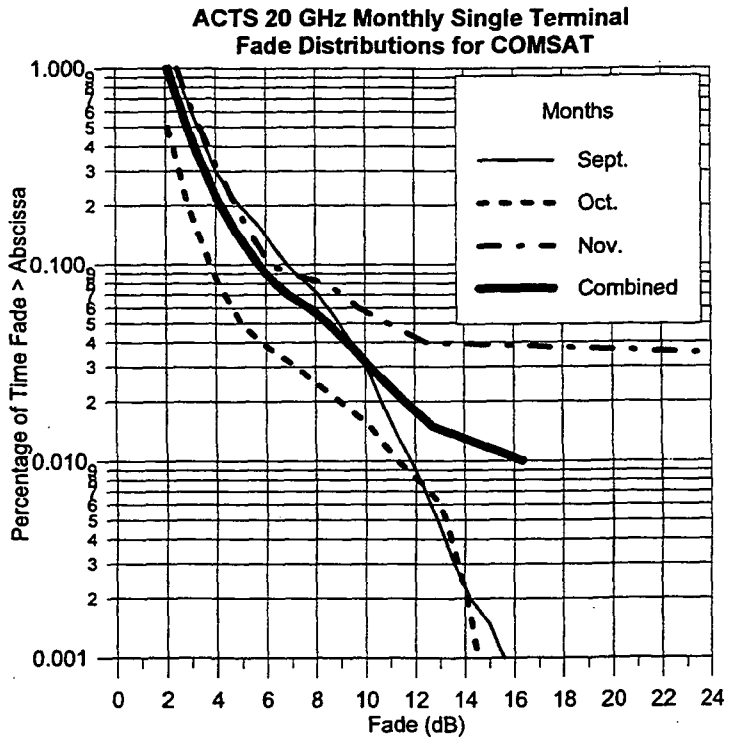
ACTS 20 GHz Monthly Single Terminal
Fade Distributions for COMSAT
Percentage of Time Fade > Abscissa
1.000
0.100
0.010
0.001
0 2 4 6 8 10 12 14 16 18 20 22 24
Fade (dB)
Months
Sept.
Oct.
Nov.
Combined

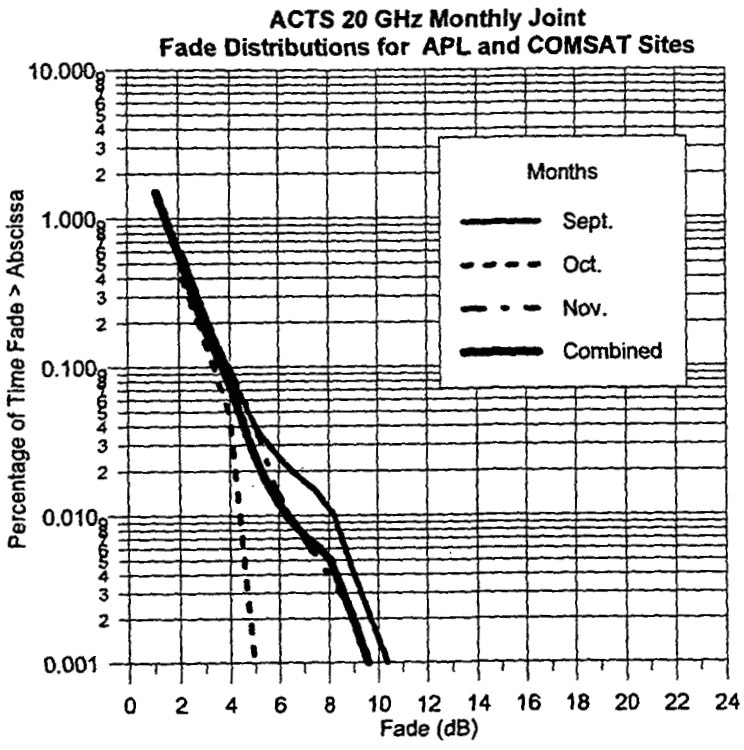
ACTS 20 GHz Monthly Joint
Fade Distributions for APL and COMSAT Sites
Percentage of Time Fade > Abscissa
10.000
1.000
0.100
0.010
0.001
0 2 4 6 8 10 12 14 16 18 20 22 24
Fade (dB)
Months
Sept.
Oct.
Nov.
Combined

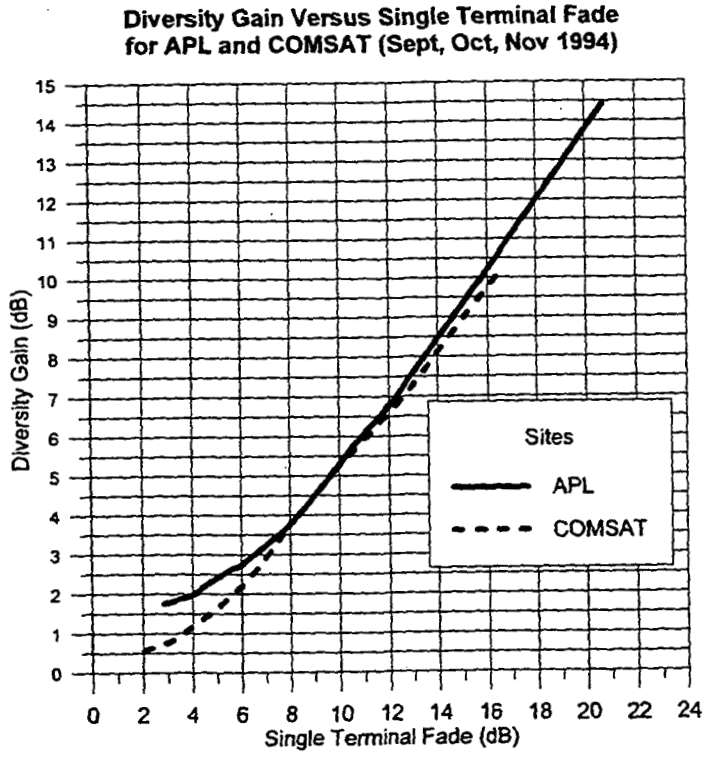
Diversity Gain Versus Single Terminal Fade
for APL and COMSAT (Sept, Oct, Nov 1994)
Diversity Gain (dB)
0 1 2 3 4 5 6 7 8 9 10 11 12 13 14 15
0 2 4 6 8 10 12 14 16 18 20 22 24
Single Terminal Fade (dB)
Sites
APL
COMSAT

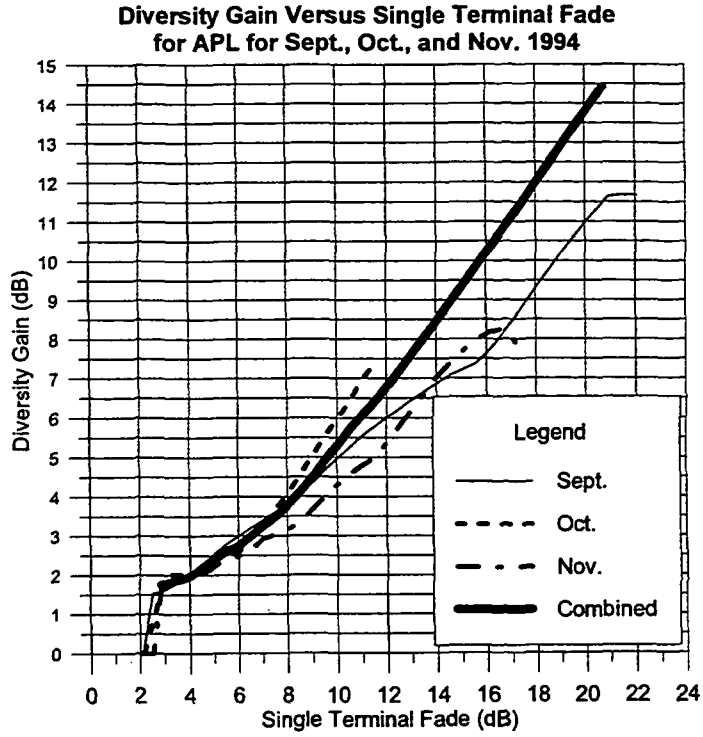
Diversity Gain Versus Single Terminal Fade
for APL for Sept., Oct., and Nov. 1994
Diversity Gain (dB)
Single Terminal Fade (dB)
Legend
Sept.
Oct.
Nov.
Combined

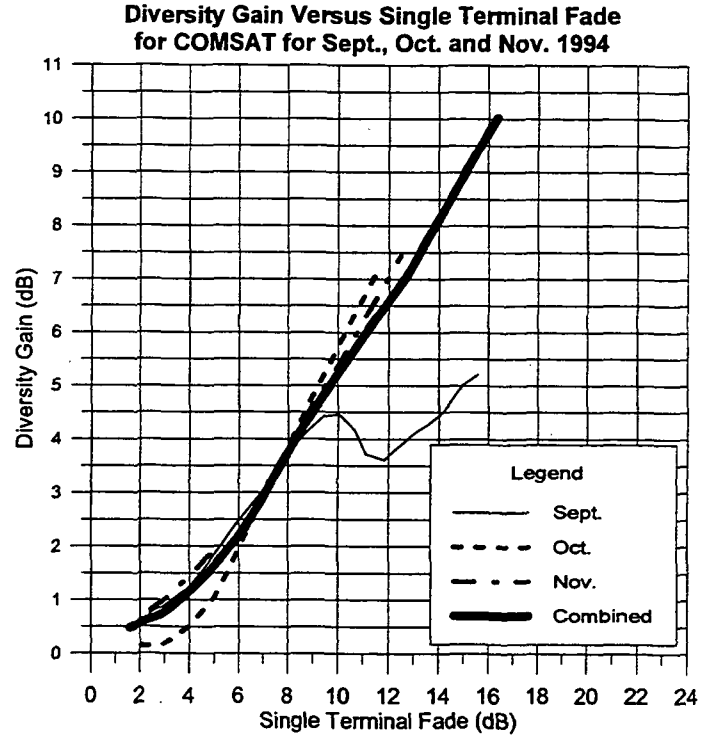
Diversity Gain Versus Single Terminal Fade
for COMSAT for Sept., Oct. and Nov. 1994
Diversity Gain (dB)
Single Terminal Fade (dB)
Legend
Sept.
Oct.
Nov.
Combined

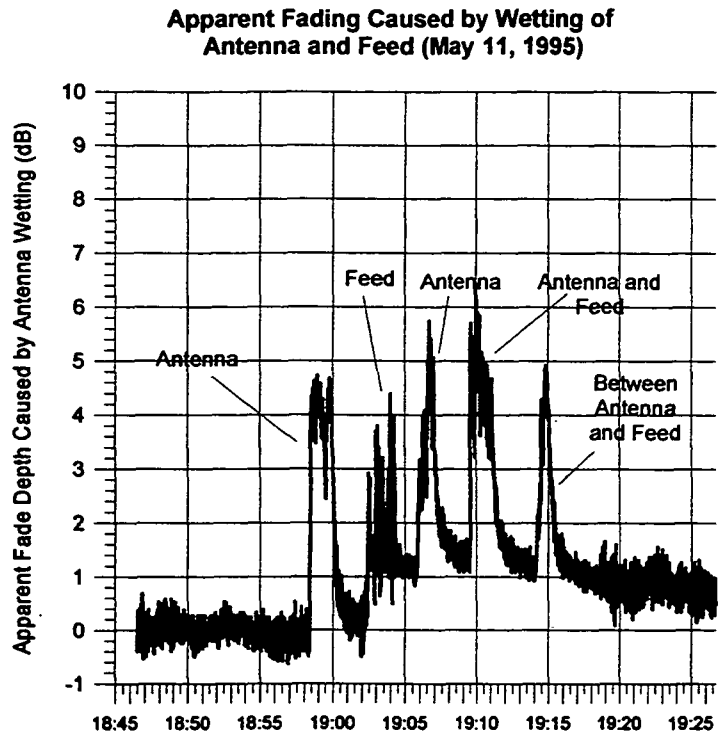

Salient Conclusions

- Assuming a 0.01% Probability for APL - COMSAT Diversity Operation
  - 6 dB Rain Fade Margin Required
    - 21 dB APL Margin
    - 16 dB COMSAT Margin
  - Month to Month Variability is 4 dB
    - 4 dB Margin Required in October
    - 8 dB Margin Required in September
- Diversity Gains of COMSAT and APL - Average Case
  - Within 2 dB from 1% to 0.01%
- Monthly Variability of Diversity Gain for 10 dB Single Terminal Fade
  - DG = 5 dB +/- 1 dB for APL
  - DG = 5 dB +/- 0.5 dB for COMSAT

EERL / Univ. of Texas

12-GHz Rain Fade Measurements Using DBS Signals

Wolfhard J. Vogel
Ali Syed
G. W. Torrence

Electrical Engineering Research Laboratory
The University of Texas at Austin

Presented at APSW VII
Fort Collins, Colorado
June 15, 1995

1

EERL / Univ. of Texas

Introduction

- 12 GHz DBS is transmitting from 101° W
- ACTS is at 100°
- For ACTS sites (except Alaska) a 3rd frequency
- Inexpensive and easy implementation
- Significant enhancement of ACTS measurements

2

EERL / Univ. of Texas

Required Hardware

- RCA Model DRD203RW Advanced DBS receiver system
  - Antenna, LNA, Receiver = $900
  - 75Ω cable from antenna to receiver = $30
  - RS232 cable from receiver to PC = $10
- PC - an older model (286 or 386) is good enough

3

EERL / Univ. of Texas

Subscription to DirecTV

- Personal subscription
  - $29.95 per month
  - >30 channels
- Commercial subscription
  - $59.95 per month
  - >30 channels

4

EERL / Univ. of Texas

Channels and Strength

Channel	Xponder	Signal	Content
224	15	91	Disney
206	***2***	***90***	***ESPN***
245	2	90	Bloomberg
201	7	90	Preview
220	8	90	TCM
225	8	90	Discovery
254	11	90	Travel
247	19	90	AmerTalk
272	19	90	EncoreLV
210	27	90	
229	27	90	USA
276	27	90	EncoreTS
100	4	89	Preview
200	4	89	Preview
202	4	89	

5

EERL / Univ. of Texas

Required Software - Inquiry

Path: geraldo.cc.utexas.edu!usenet
From: Wolf_Vogel@mail.utexas.edu (Wolfhard J Vogel)
Newsgroups: rec.video.satellite.dbs
Subject: ***Hacker Challenge***
Date: 11 May 1995 02:47:39 GMT
Organization: The University of Texas at Austin
Lines: 9
Message-ID: <3ortsb$4r1@geraldo.cc.utexas.edu>
NNTP-Posting-Host: slip-13-7.ots.utexas.edu
X-Newsreader: WinVN 0.90.4

The RCA DBS unit has an RS232 port, so it is probably possible to read the state of the receiver (e.g., the mail messages or signal level) or to control the unit without the remote.
The manual, of course, does not even mention the purpose of the connector.

Will a hacker rise to the challenge and figure out the protocol?

If you have the time and the skills - please let me know the result and I will be forever grateful. Thanks.

6

EERL / Univ. of Texas

Required Software - Response I

Date: Fri, 12 May 1995 01:01:31 -0400
To: Wolf_Vogel@mail.utexas.edu (Wolfhard J. Vogel)
From: an174356@anon.penet.fi
Organization: Anonymous forwarding service
Reply-To: an174356@anon.penet.fi
Date: Mon, 15 May 1995 10:56:48 UTC
Subject: DBS Hacking

Maybe this partial explanation of the DBS codes will be useful. I am working on completing this sometime in the future. Wait times were determined by trial and error. Good luck.

7

EERL / Univ. of Texas

Response II

SIGNAL STRENGTH:

TO DBS-Box:

Command-prefix Byte: 0xFA ; send first
Wait 15msec
Command-byte to request signal strength: 0x10
Wait 15msec

FROM DBS-Box:

Acknowledged-Command Byte: 0xF0
*** Error *** Command-Prefix Not Sent: 0xFB
Signal-Strength Byte: 0xSS
Command-Completed-OK Byte: 0xF4

X= DBS-Box Signal Strength Number
Y= CNR (dB)

y=(a+clnx+e(lnx)^2+g(lnx)^3)/(1+blnx+d(lnx)^2+f(lnx)^3)

a= 0.254791 e= -0.116899
b= -0.749124 f= -0.016554
c= 0.157723 g= 0.019983
d= 0.192953

8

EERL / Univ. of Texas

Response III

Change CHANNEL:

TO DBS-Box:
- Command-prefix Byte: 0xFA ; send first
- Wait 15msec
- Command-byte to change channel: 0x46
- Wait 600msec

FROM DBS-Box:
- Acknowledged-Command Byte: 0xF0
- *** Error *** Command-Prefix Not Sent: 0xFB

TO DBS-Box:
- Channel=0xHHLL
- Channel-Byte HI: 0xHH
- Wait 600msec
- Channel-Byte LO: 0xLL
- Wait 600msec

FROM DBS-Box:
- Acknowledged-Parameter Byte: 0xF2
- Command-Completed-OK Byte: 0xF4

9

EERL / Univ. of Texas

Response IV

TRANSPONDER ID:

TO DBS-Box:
- Command-prefix Byte: 0xFA ;send first
- Wait 15msec
- Command-byte to get status: 0x03
- Wait 1sec

FROM DBS-Box:
- Acknowledged-Command Byte: 0xF0
- *** Error *** Command-Prefix Not Sent: 0xFB

36 Bytes returned by DBS-Box:

|B01|,|B02|,..|B13|,..|B36|

|_____ Command-complete-OK byte: 0xF4

|_____ Transponder Number

10

EERL / Univ. of Texas

Receiver Dynamics

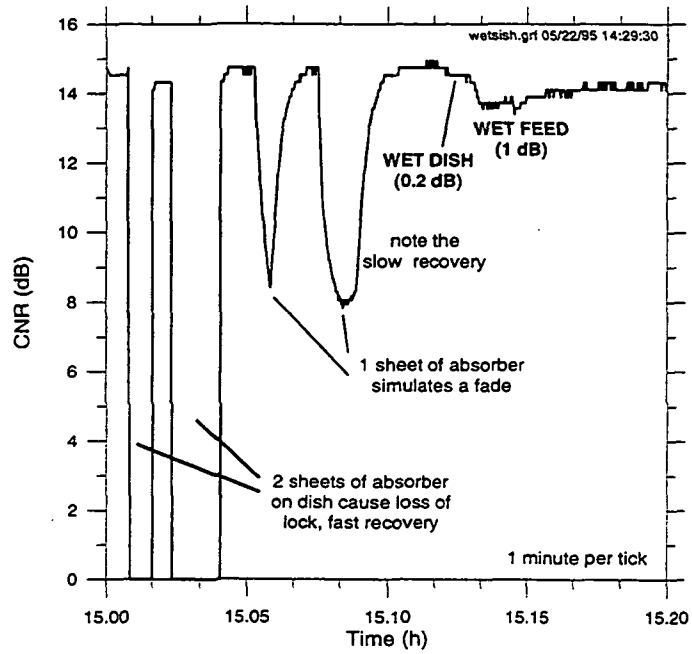

11

EERL / Univ. of Texas

Rain Fade Event

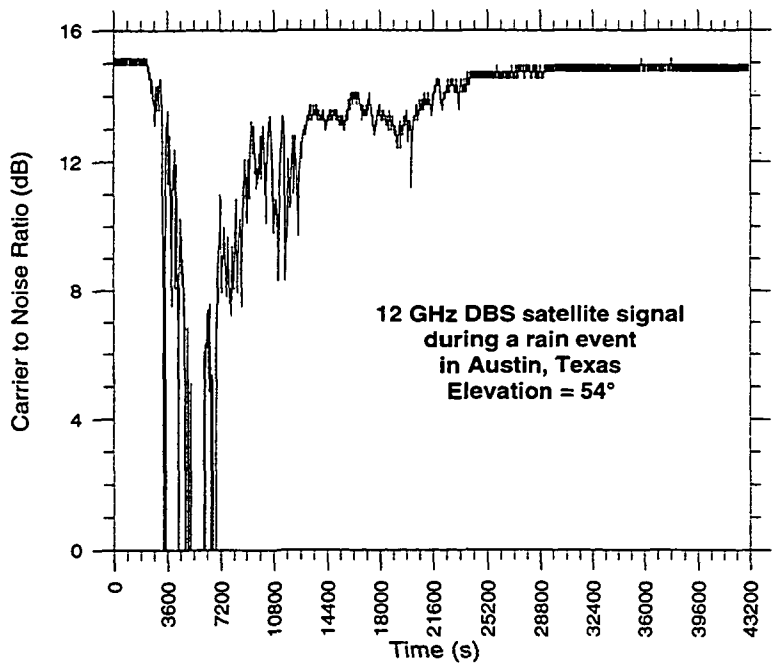

12

EERL / Univ. of Texas

Conclusion

- CNR has a long time constant
- 1 measurement / 10 s is adequate
- fade measurement margin 10-12 dB
- Valuable addition to 20/30 measurements

13

Georgia Tech ACTS Propagation Experiment

Status Report

Prepared by: D. H. Howard and P. G. Steffes (Principal Investigators) and M. S. Alouini, S. A. Borgsmiller, D. J. Collins, and M. A. Hoover

Presented by: P. G. Steffes and S. A. Borgsmiller

Presented to: NAPEX XIX and Seventh ACTS Propagation Studies Workshop - (APSW VII) Fort Collins, CO

Date: 15 June 1995

GT ACTS Experiment Phases

- Phase I : Terminal and link RF Measurements:
  - CW/swept CW, noise, PSK, SBM modulations used for typical end-to-end link characterization measurements:
    - Clear air/inclement weather
    - Phase iitter as key measurement
- Phase II : CDMA Measurements
  - Use lab equipment to generate CDMA test signal with background CDMA traffic:
  - Build code CDMA receiver for BER measurements
    - Use spectrum analyzer and digital waveform capture for signal snapshots, cross-correlation measurements
    - Scintillation effects on CDMA as key point of interest

Schedule/Milestones

Develop and Test RF Terminal	Completed, May 95
Phase I Measurements	May 95 - Jul 95
Develop and Test CDMA Modem	Completed, May 95
Integrate CDMA/RF Terminal and Weather Station	Jun 95 - Jul 95
Phase II Measurements	Aug 95 - Oct 95
Additional Measurements	Nov 95
Final Report and Data Archiving	Nov/Dec 95

Transmitter/Receiver Configuration

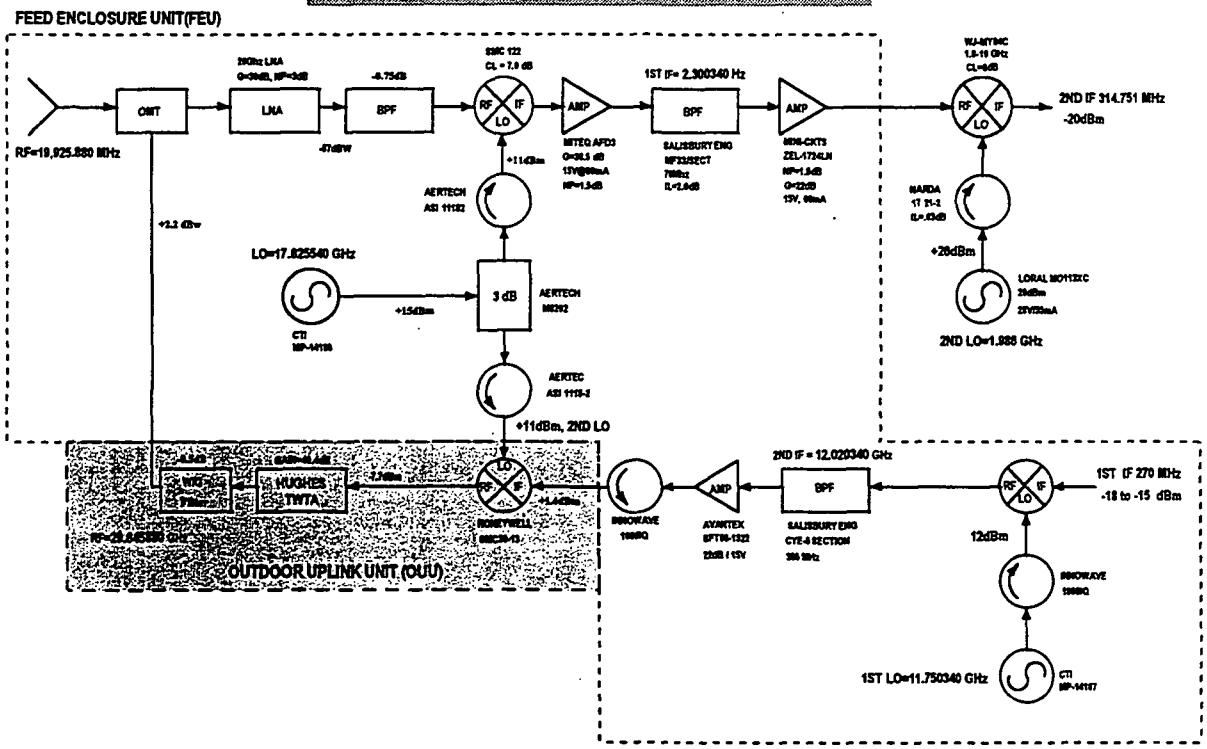

Georgia Tech RESEARCH INSTITUTE Information Technology and Telecommunications Laboratory Georgia Tech School of Electrical and Computer Engineering

Georgia Tech NASA ACTS RF Measurements Block Diagram

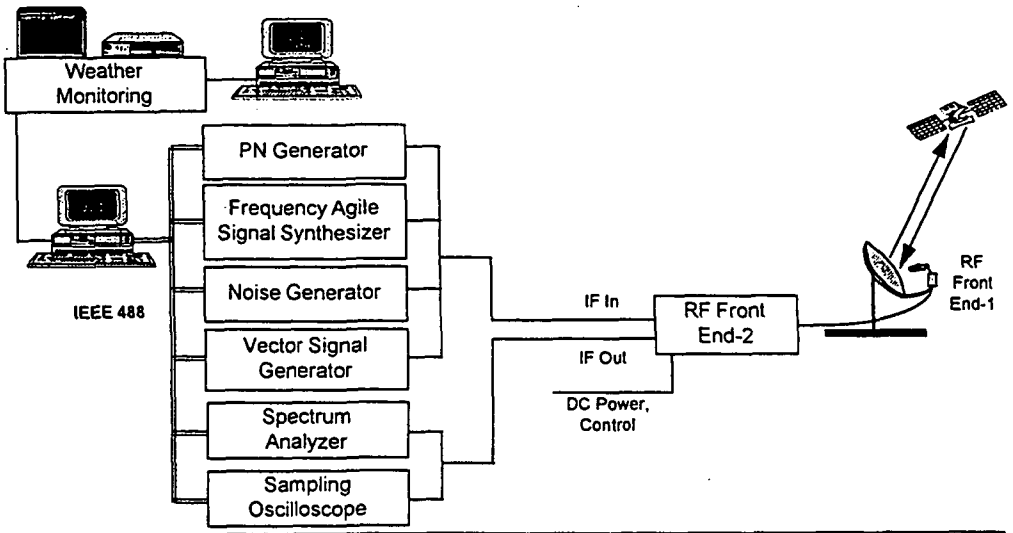

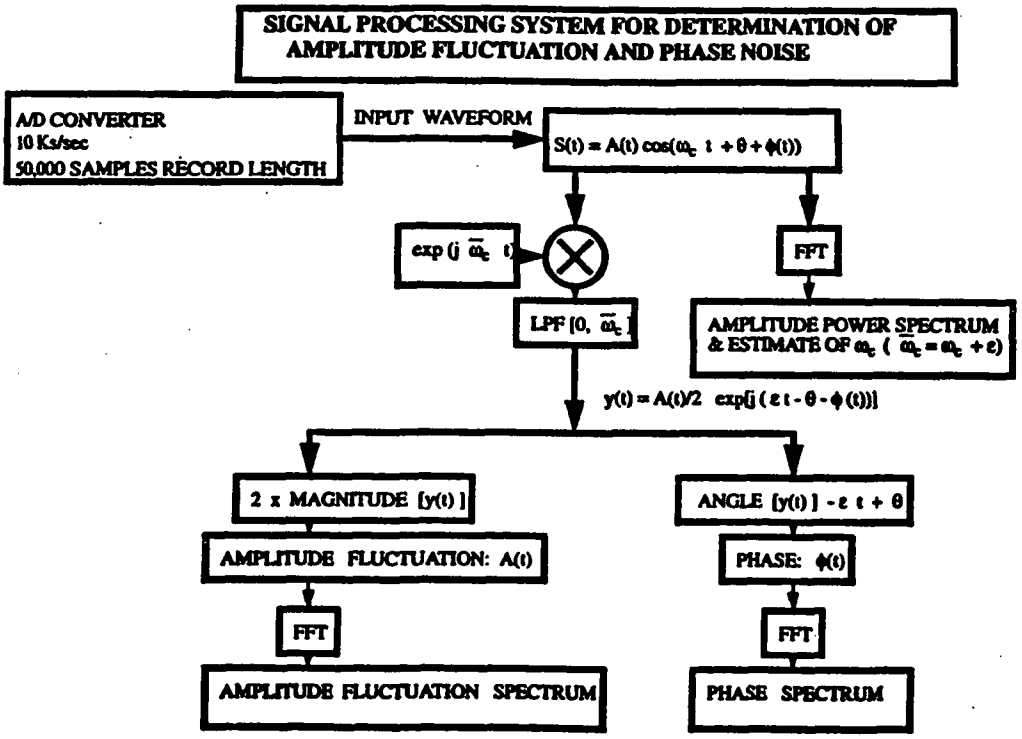

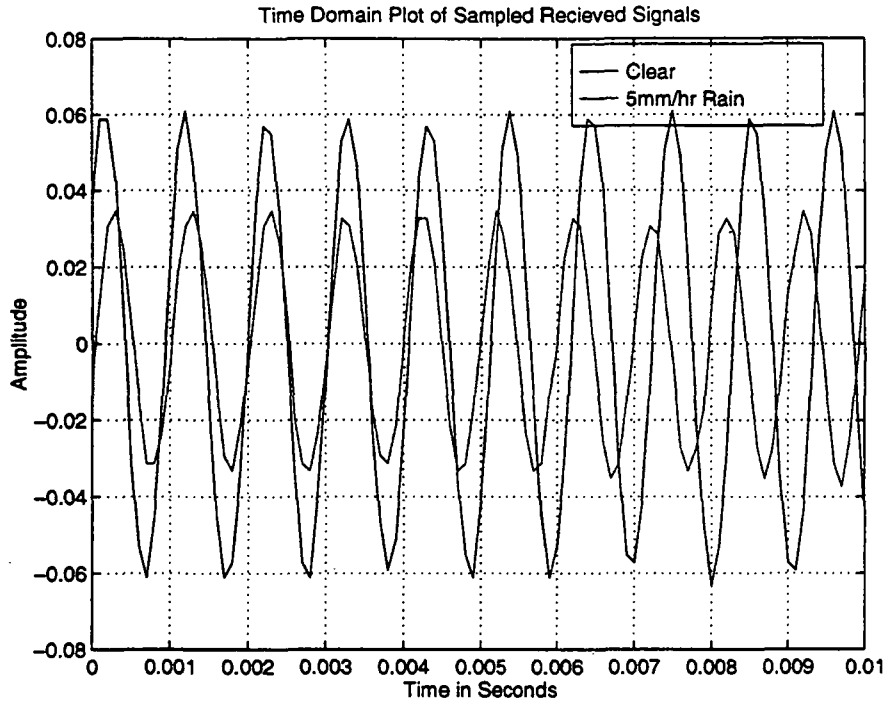

7

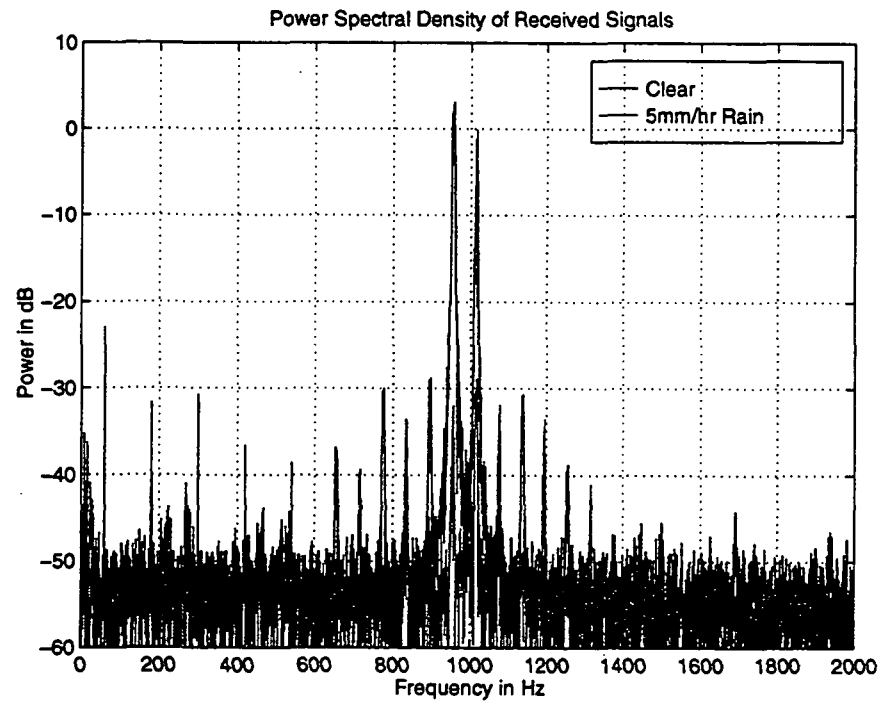

8

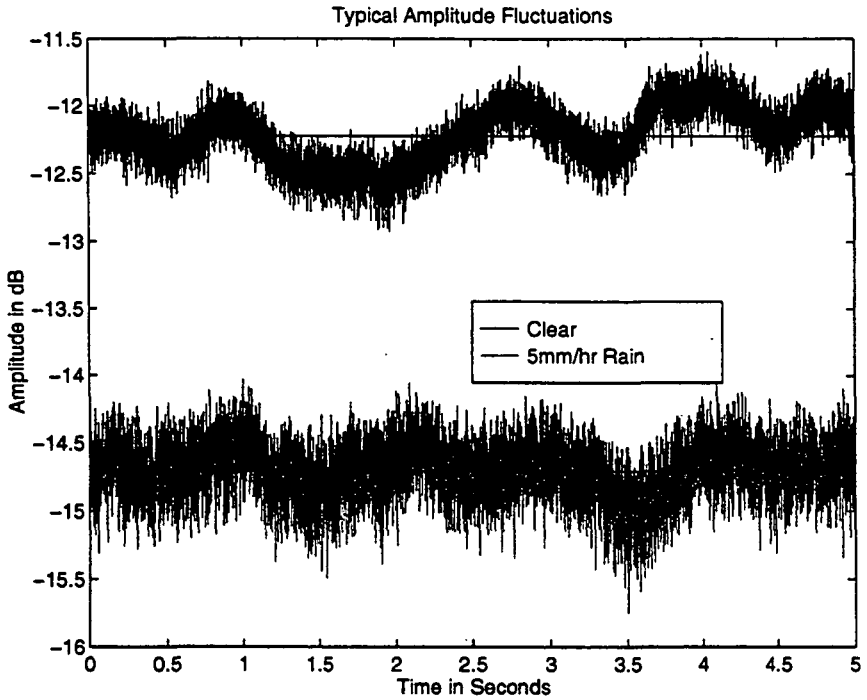
Typical Amplitude Fluctuations
Amplitude in dB
Time in Seconds
Clear
5mm/hr Rain
-11.5
-12
-12.5
-13
-13.5
-14
-14.5
-15
-15.5
-16
0
0.5
1
1.5
2
2.5
3
3.5
4
4.5
5

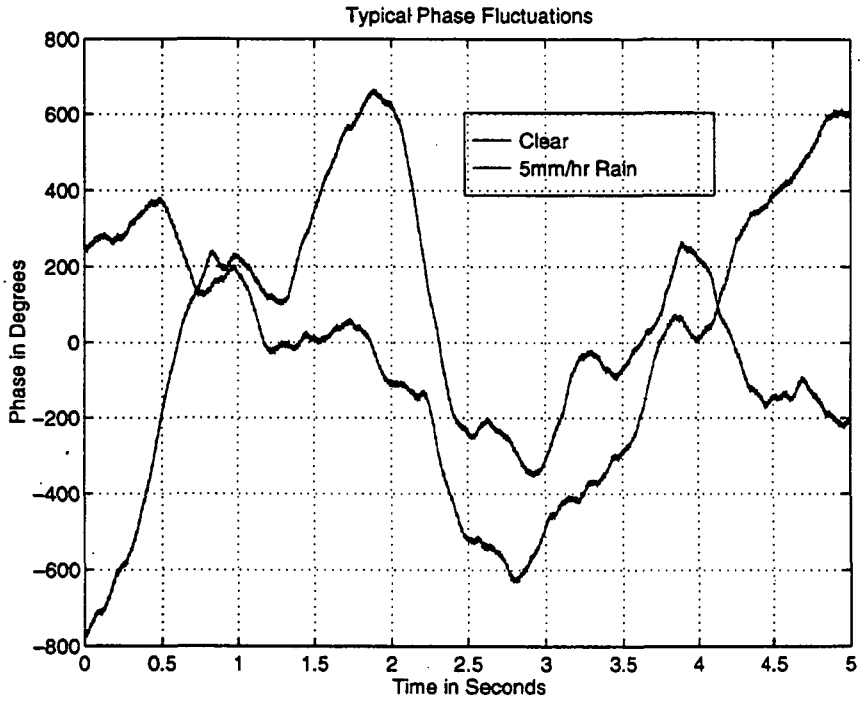
Typical Phase Fluctuations
Phase in Degrees
Time in Seconds
Clear
5mm/hr Rain
800
600
400
200
0
-200
-400
-600
-800
0
0.5
1
1.5
2
2.5
3
3.5
4
4.5
5

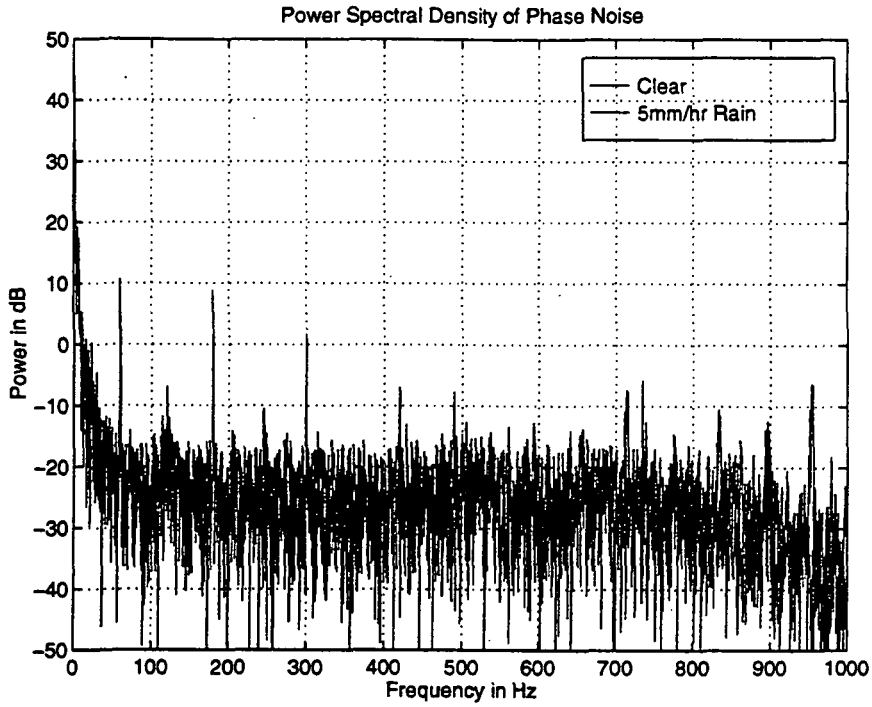

RF Measurements Conducted During Phase I

- BER vs. Eb/No for selected digital modulations (underway)
- Amplitude response vs. frequency (complete)
- Group delay vs. frequency
- Pulse parameters (rise time, fall time, distortion, etc.)
- CNR degradation (complete)
- Intermodulation and spurious signal response (complete)
- Eye/vector/constellation diagrams for selected digital modulations (underway)
- Others TBD

Automated Weather Station

- Based around Davis Instruments Weather Monitor II weather station
  - Automatically records a wide variety of weather data:
    - Temperature
    - Wind Speed
    - Wind Direction
    - Humidity
    - Barometric Pressure
    - Rainfall Rate
    - Rainfall Accumulation
    - Dew Point
- Interfaces to IBM-compatible PC for data storage and analysis
- Also recording video of Doppler radar from local television

CDMA Receiver

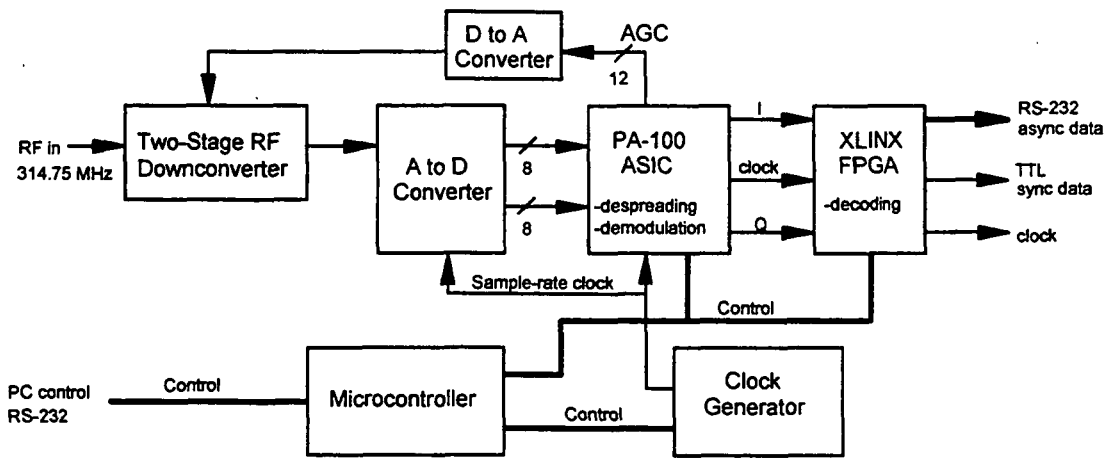

CDMA Modulator

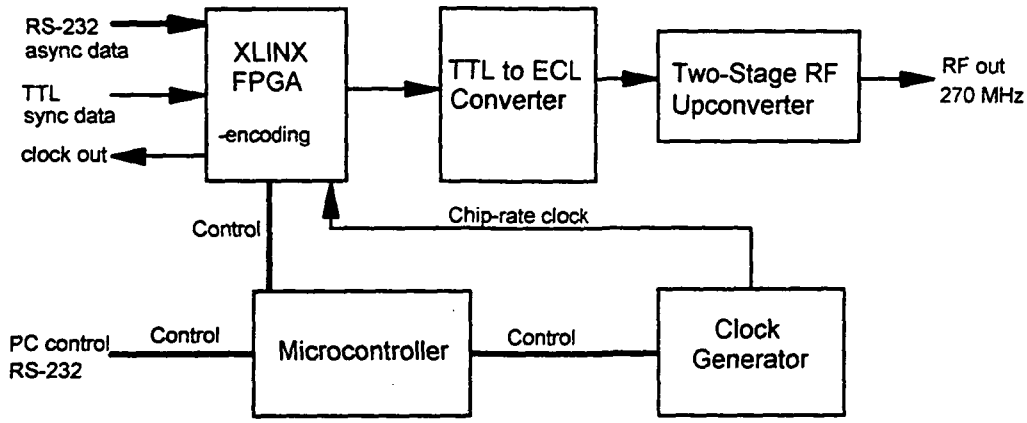

Modem Spectrum
Output Spread at 8 Mcps

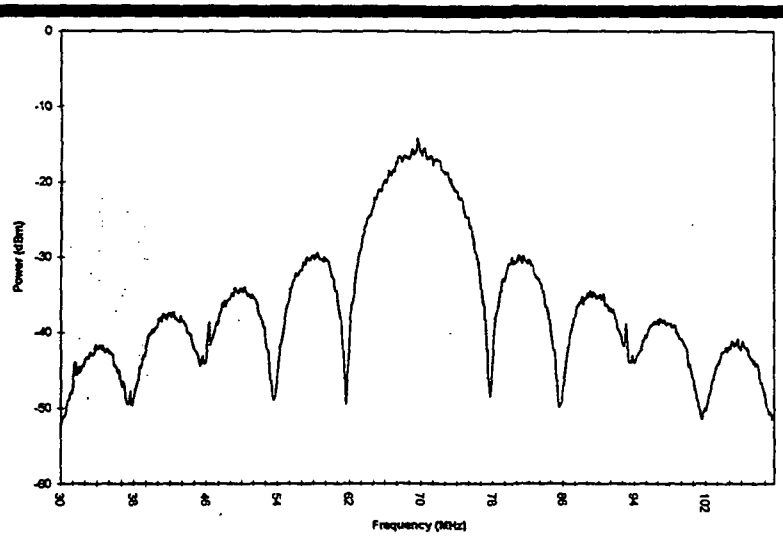

Modem Spectrum
Output Spread at 32 Mcps

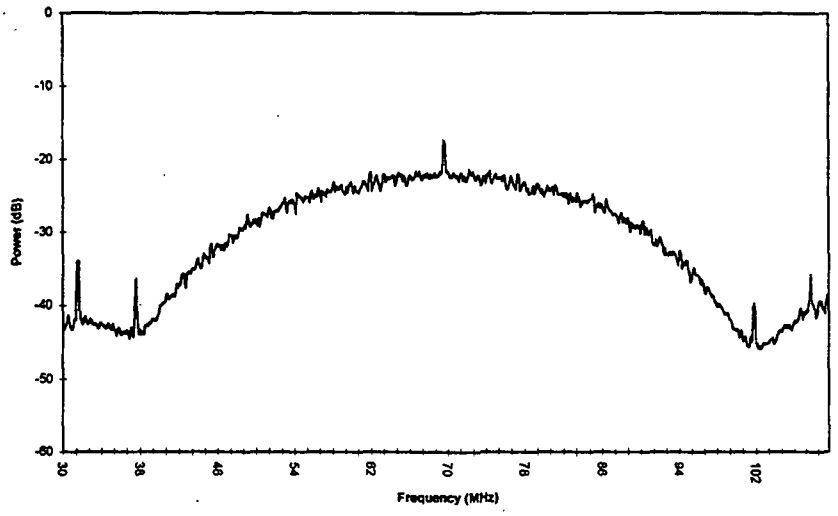

Georgia Tech RESEARCH INSTITUTE | Information Technology and Telecommunications Laboratory | Georgia Tech School of Electrical and Computer Engineering

17

Session III:
Experimenter Status Reports

ON THE ANALYSIS OF FADE DURATION AND SUMMER SCINTILLATIONS

NAPEX XIX and APSW VII
FT. COLLINS, CO
JUNE 14 - 16, 1995

CHARLIE MAYER
BRAD JAEGER
UNIVERSITY OF ALASKA FAIRBANKS

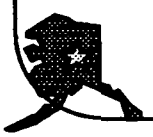

OUTLINE

I. APT OPERATIONAL STATUS

II. PREPROCESSING STATUS

III. SCINTILLATIONS

IV. FADES
- A. ULTIMATE FADE DEPTH
- B. FADE DURATIONS

V. ATTENUATION RATIO

VI. CONCLUSIONS

PROBLEMS ENCOUNTERED

- WWV CARD ERRONEOUS TIME
  - CONCATENATE FRAGMENTED FILES
  - EDIT CORRECT TIME INTO .RV0 FILES
  - NEED TO RESUBMIT NOVEMBER RAW DATA TAPE TO DATA COLLECTION CENTER AT UT

Alaska ACTS Propagation

PROBLEMS ENCOUNTERED, 2

- 20 GHz BEACON DROP-OUTS
  - BEACON DISAPPEARS
  - RADIOMETER STILL PRESENT
  - CTRL-ALT-DEL DOES NOTHING
  - RELOADING DACS DOES NOTHING
  - CYCLING POWER OFF/ON RESTORES BEACON
  - SENT FILES TO DAVE
  - REFERENCE OSCILLATOR CABLE OPEN CIRCUITED
  - STRAIGHTENED ANACONDA CONDUIT TO REDUCE TENSION ON COAXIAL CENTER CONDUCTOR
  - PROBLEM REDUCED BUT STILL PRESENT
  - WE PLAN TO EXAMINE THE SMA CONNECTOR AND EITHER REPAIR OR REPLACE

Alaska ACTS Propagation

PROBLEMS ENCOUNTERED, 3

- 27 GHZ MINI-DROP-OUTS
  - CHARACTERIZED BY RAPID VARIATIONS IN BEACON LEVEL
  - MAGNITUDE IS A FEW DB
  - RADIOMETER IS UNCHANGED
  - LIKE THE SIGNAL IS DRIFTING RAPIDLY IN AND OUT OF THE DETECTION PASSBAND
  - OPENED DETECTION BANDWIDTH FROM 20 HZ TO 40 HZ
  - MINI-DROP-OUTS DISAPPEARED
  - BUT THIS GIVES 3 DB LESS DYNAMIC RANGE

PREPROCESSING STATUS

	Jun-94	Jul-94
20 GHz Spillover Temperature	74	74
27 GHz Spillover Temperature	58	58
20 GHz Antenna Efficiency	0.63	0.60
27 GHz Antenna Efficiency	0.63	0.66
20 GHz Std. Bias Error	0.26	0.11
27 GHz Std. Bias Error	0.19	0.13

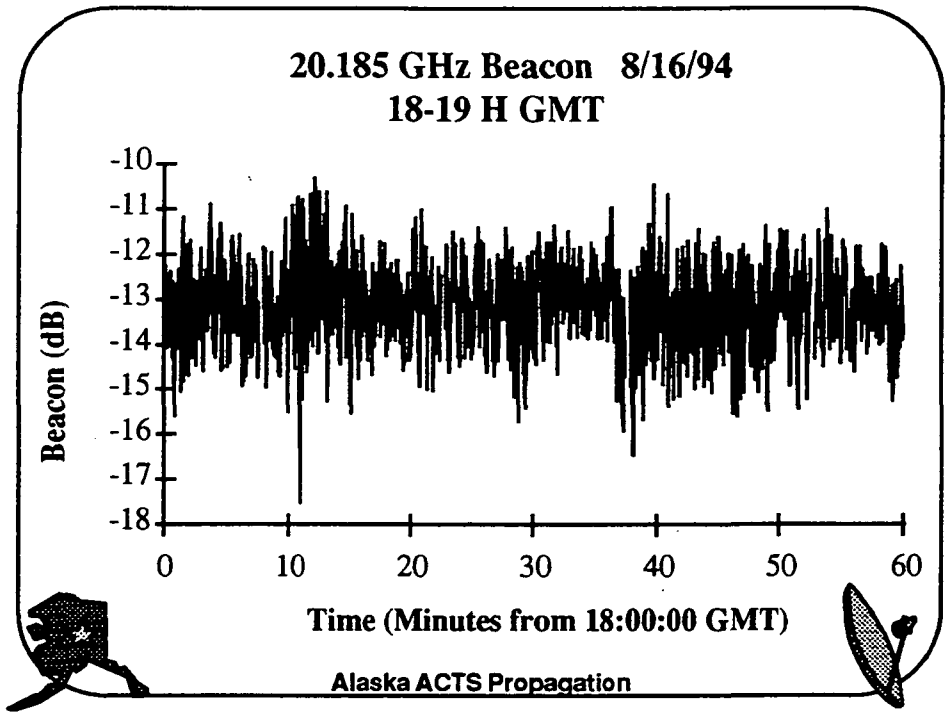
20.185 GHz Beacon 8/16/94
18-19 H GMT
Beacon (dB)
-10
-11
-12
-13
-14
-15
-16
-17
-18
0
10
20
30
40
50
60
Time (Minutes from 18:00:00 GMT)
Alaska ACTS Propagation

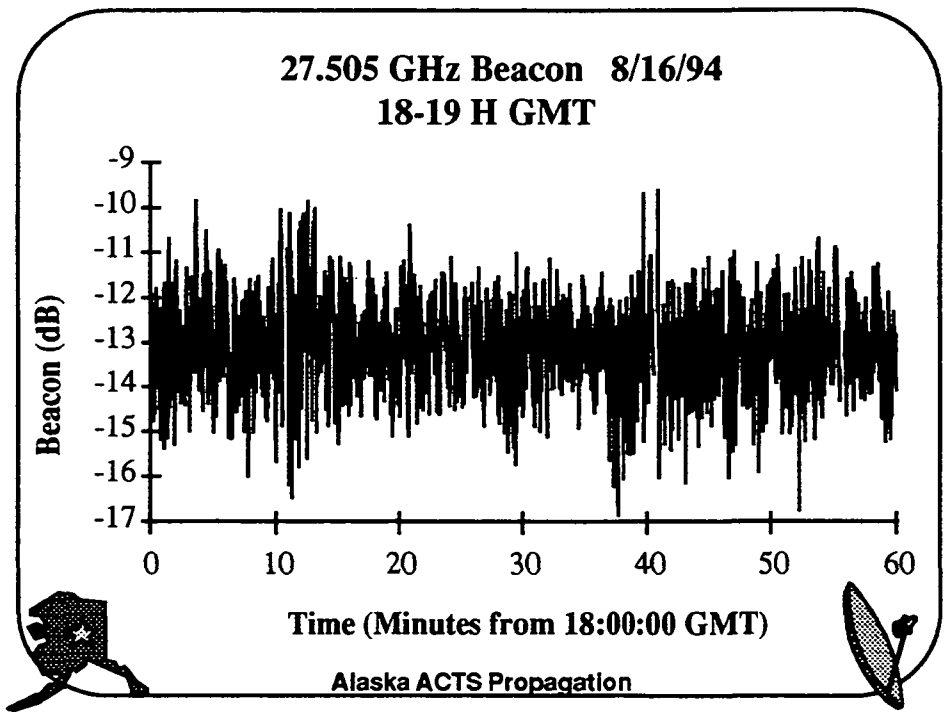
27.505 GHz Beacon 8/16/94
18-19 H GMT
Beacon (dB)
-9
-10
-11
-12
-13
-14
-15
-16
-17
0
10
20
30
40
50
60
Time (Minutes from 18:00:00 GMT)
Alaska ACTS Propagation

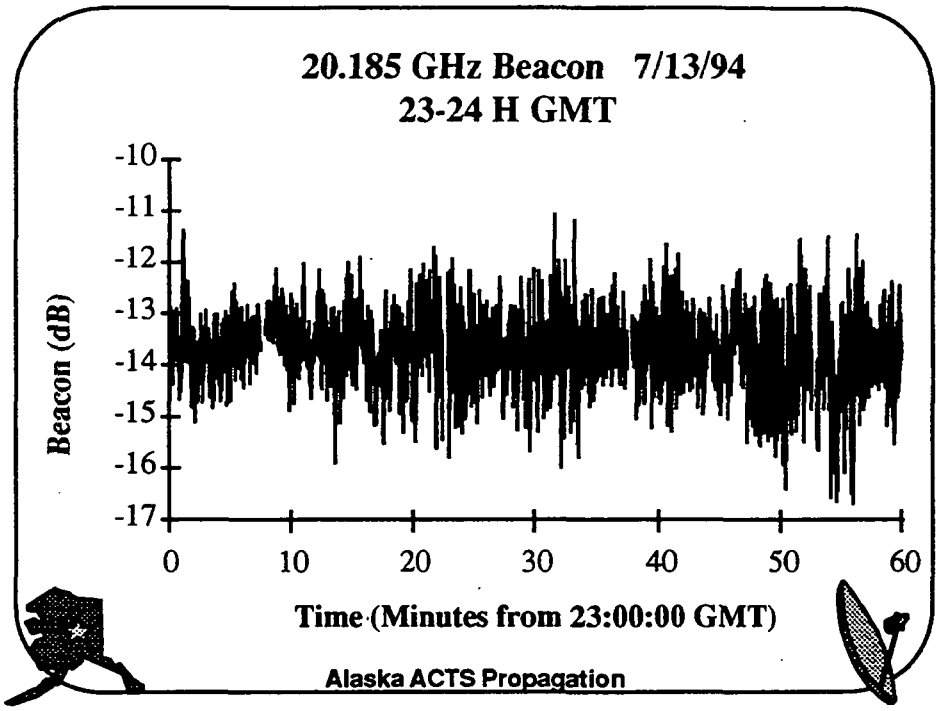
20.185 GHz Beacon 7/13/94
23-24 H GMT
Beacon (dB)
-10
-11
-12
-13
-14
-15
-16
-17
0
10
20
30
40
50
60
Time (Minutes from 23:00:00 GMT)
Alaska ACTS Propagation

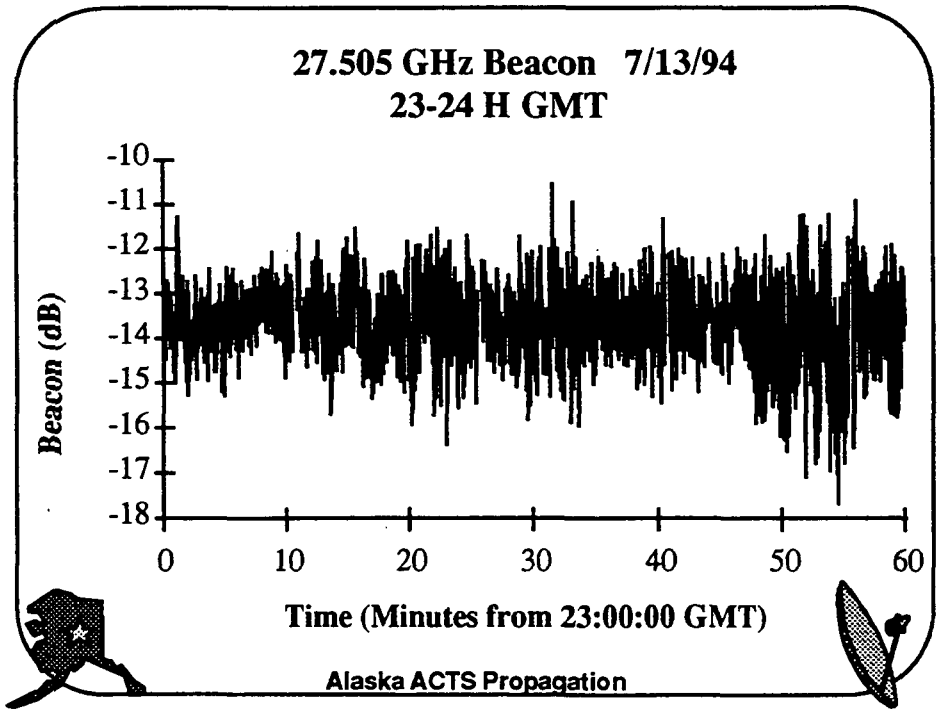
27.505 GHz Beacon 7/13/94
23-24 H GMT
Beacon (dB)
-10
-11
-12
-13
-14
-15
-16
-17
-18
0
10
20
30
40
50
60
Time (Minutes from 23:00:00 GMT)
Alaska ACTS Propagation

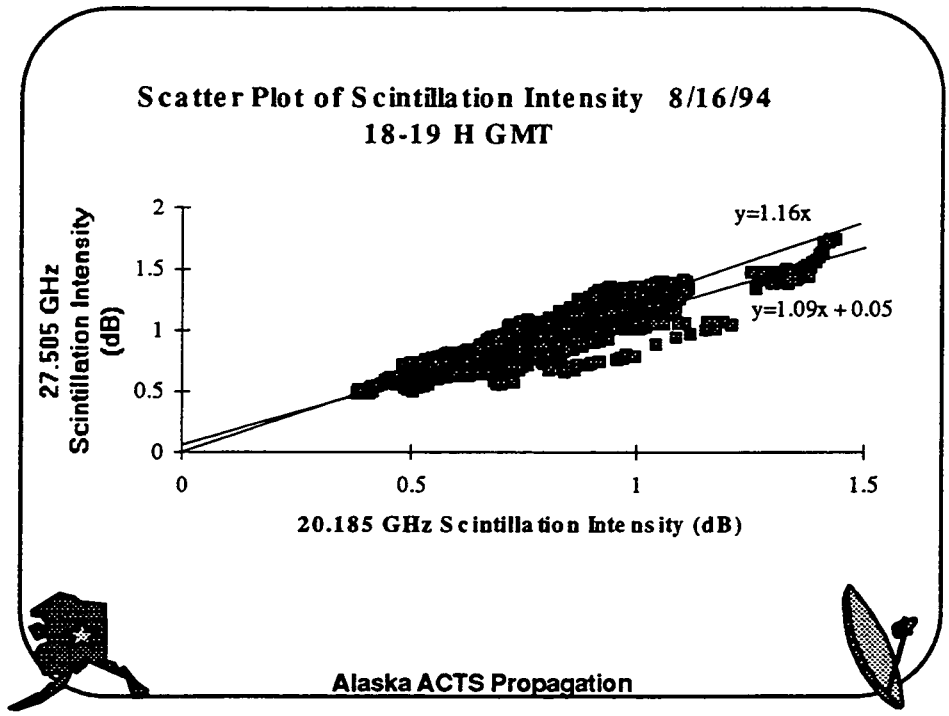
Scatter Plot of Scintillation Intensity 8/16/94
18-19 H GMT
27.505 GHz Scintillation Intensity (dB)
2
1.5
1
0.5
0
0
0.5
1
1.5
y=1.16x
y=1.09x + 0.05
20.185 GHz Scintillation Intensity (dB)
Alaska ACTS Propagation

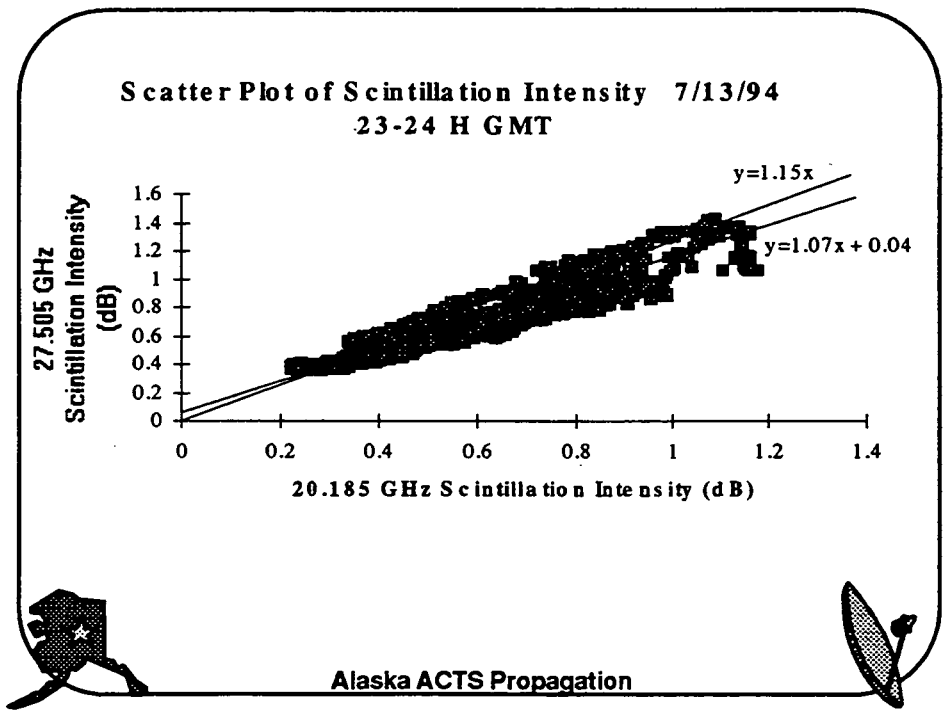
Scatter Plot of Scintillation Intensity 7/13/94
23-24 H GMT
27.505 GHz Scintillation Intensity (dB)
1.6
1.4
1.2
1
0.8
0.6
0.4
0.2
0
0
0.2
0.4
0.6
0.8
1
1.2
1.4
y=1.15x
y=1.07x + 0.04
20.185 GHz Scintillation Intensity (dB)
Alaska ACTS Propagation

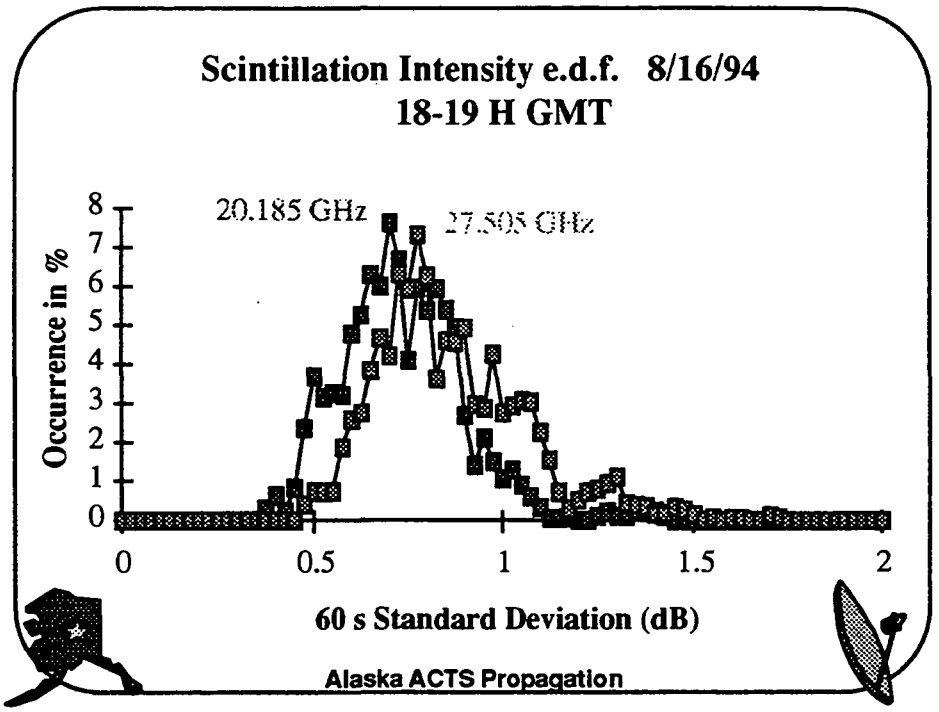
Scintillation Intensity e.d.f. 8/16/94
18-19 H GMT
20.185 GHz
27.505 GHz
Occurrence in %
8
7
6
5
4
3
2
1
0
0
0.5
1
1.5
2
60 s Standard Deviation (dB)
Alaska ACTS Propagation

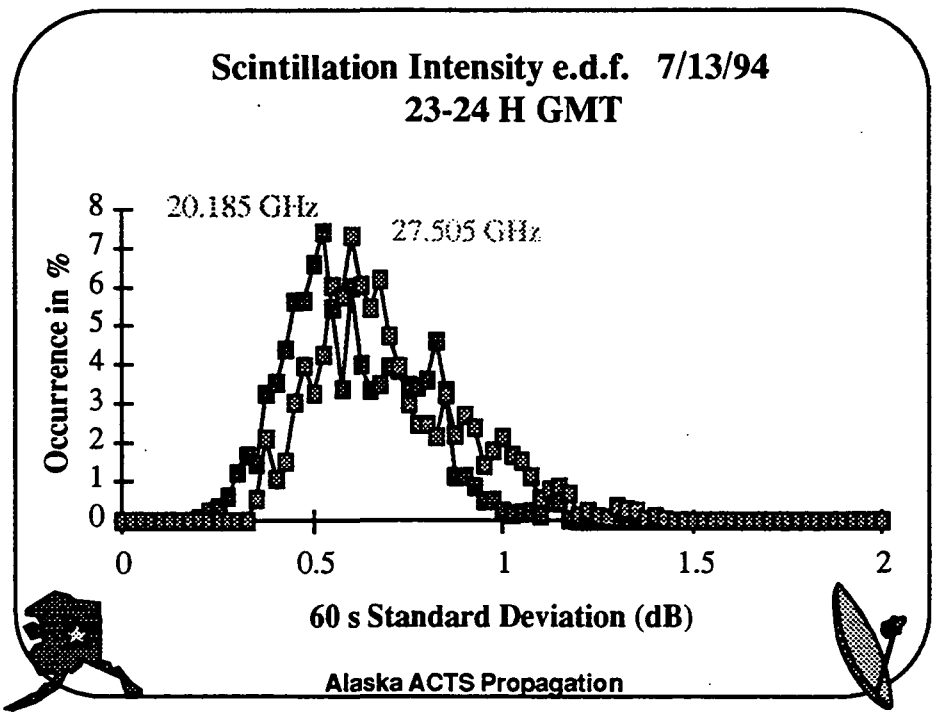
Scintillation Intensity e.d.f. 7/13/94
23-24 H GMT
20.185 GHz
27.505 GHz
Occurrence in %
8
7
6
5
4
3
2
1
0
0
0.5
1
1.5
2
60 s Standard Deviation (dB)
Alaska ACTS Propagation

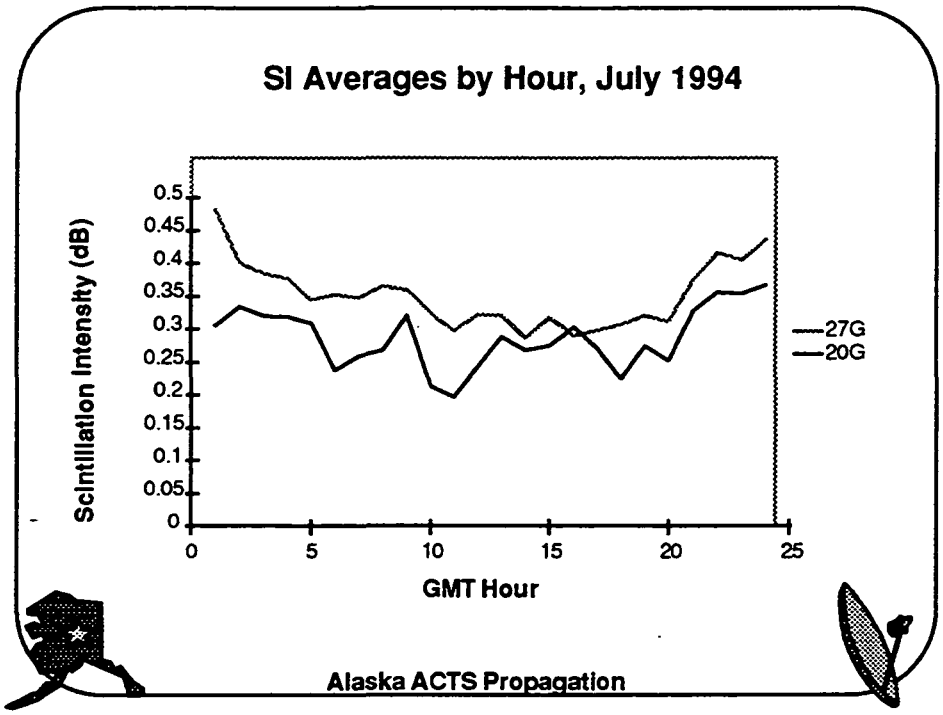
SI Averages by Hour, July 1994
Scintillation Intensity (dB)
0.5
0.45
0.4
0.35
0.3
0.25
0.2
0.15
0.1
0.05
0
0
5
10
15
20
25
GMT Hour
27G
20G
Alaska ACTS Propagation

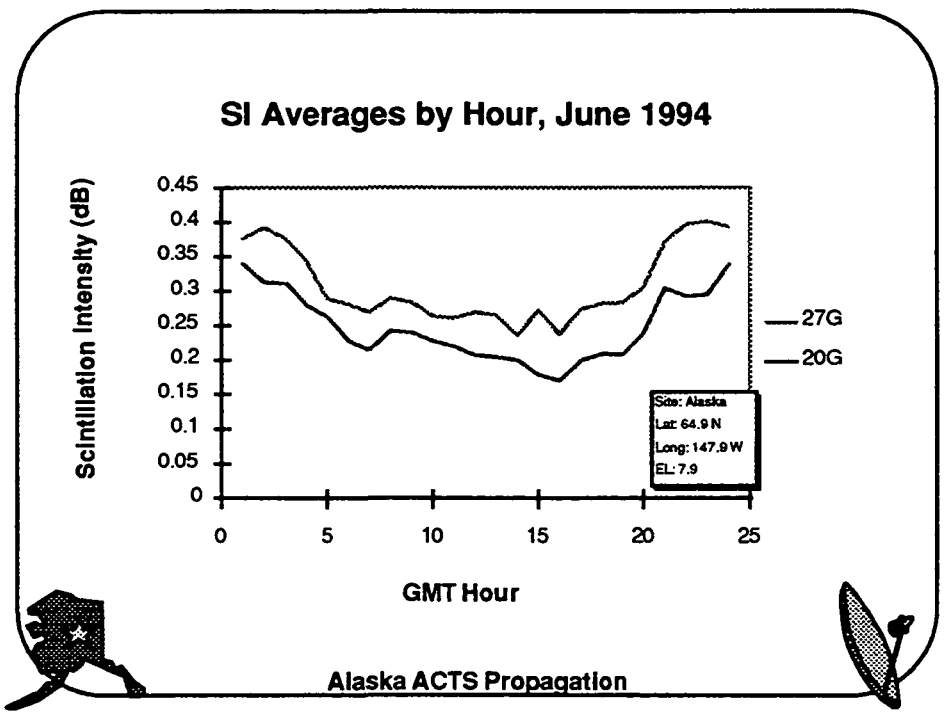
SI Averages by Hour, June 1994
Scintillation Intensity (dB)
0.45
0.4
0.35
0.3
0.25
0.2
0.15
0.1
0.05
0
0
5
10
15
20
25
GMT Hour
27G
20G
Site: Alaska
Lat: 64.9 N
Long: 147.9 W
EL: 7.9
Alaska ACTS Propagation

THRESHOLDING:
30s BEACON AVERAGE vs. TIME

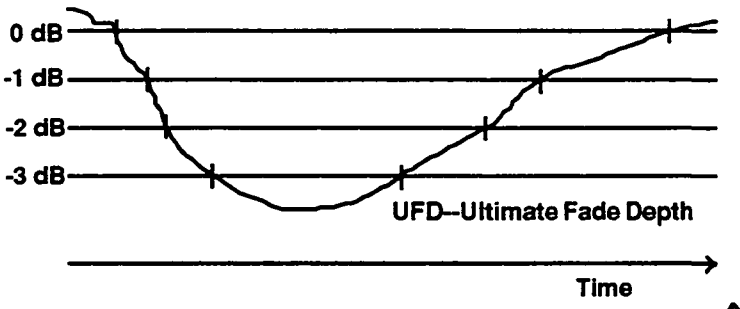

Alaska ACTS Propagation

UFD* at 20.185 GHz, June 1994

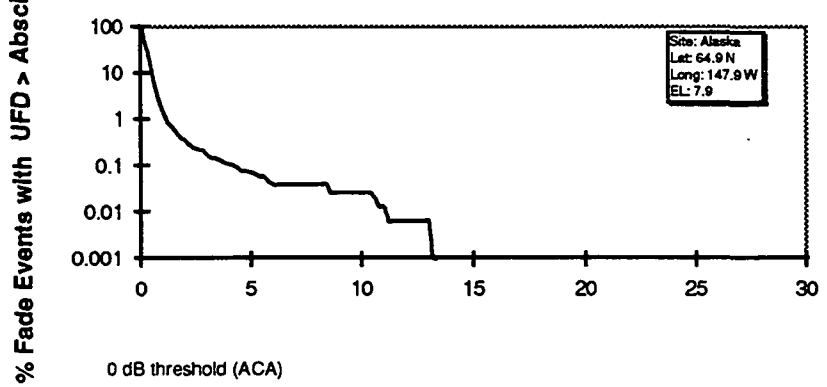

Alaska ACTS Propagation

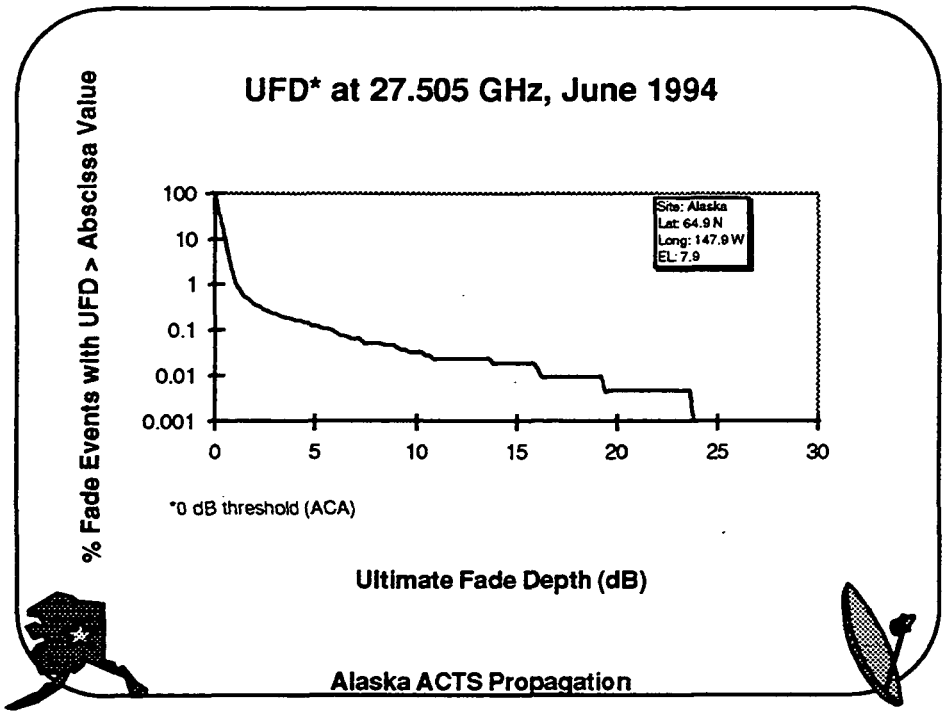
UFD* at 27.505 GHz, June 1994
% Fade Events with UFD > Abscissa Value
100
10
1
0.1
0.01
0.001
0
5
10
15
20
25
30
Site: Alaska
Lat: 64.9 N
Long: 147.9 W
EL: 7.9
*0 dB threshold (ACA)
Ultimate Fade Depth (dB)
Alaska ACTS Propagation

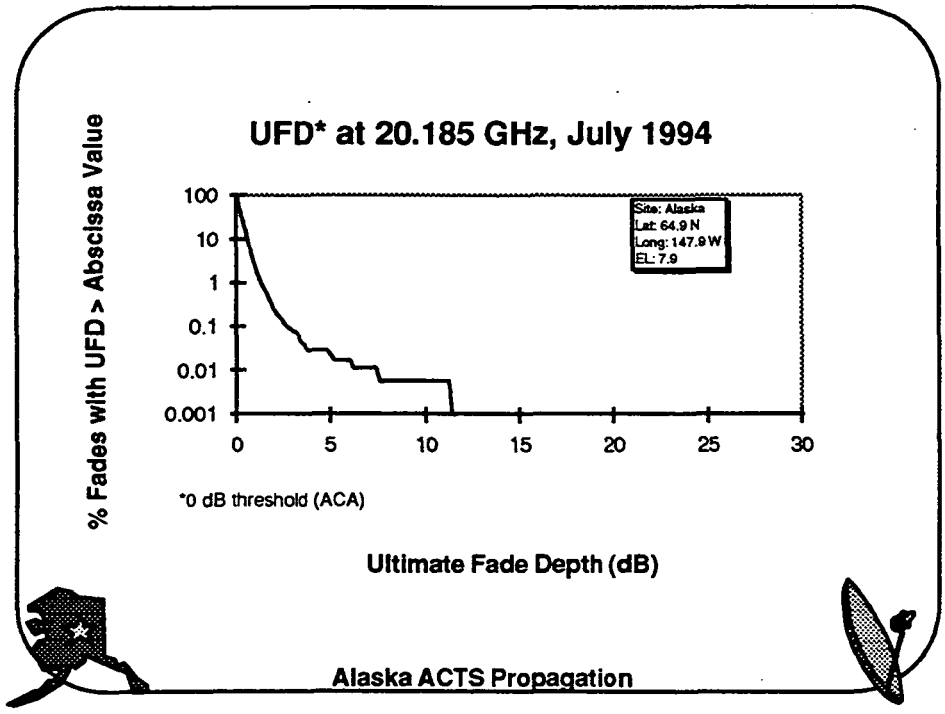
UFD* at 20.185 GHz, July 1994
% Fades with UFD > Abscissa Value
100
10
1
0.1
0.01
0.001
0
5
10
15
20
25
30
Site: Alaska
Lat: 64.9 N
Long: 147.9 W
EL: 7.9
*0 dB threshold (ACA)
Ultimate Fade Depth (dB)
Alaska ACTS Propagation

UFD* at 27.505 GHz, July 1994

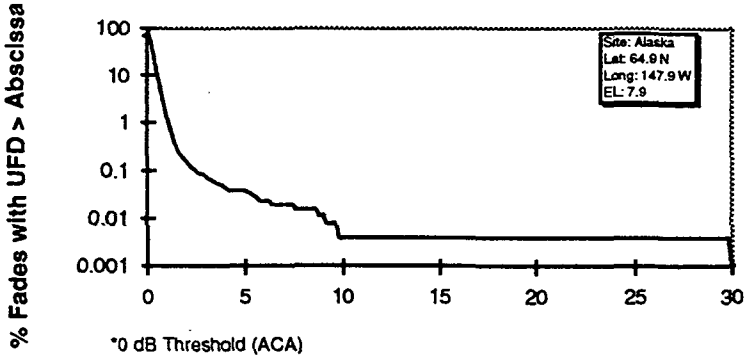

Alaska ACTS Propagation

20.185 GHz Fade Distributions, July 1994

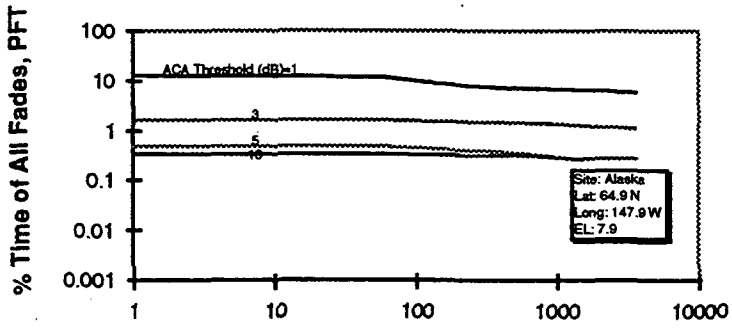

Alaska ACTS Propagation

27.505 GHz Fade Distributions, July 1994

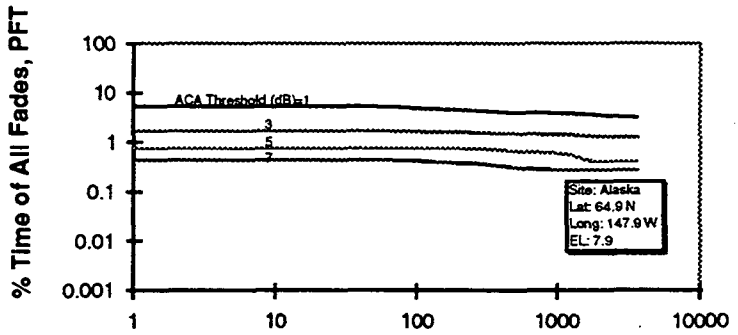

Alaska ACTS Propagation

20.185 GHz Non-fade Distributions, July 1994

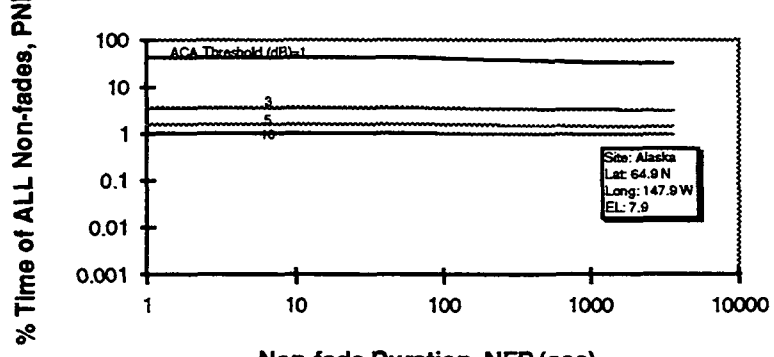

Alaska ACTS Propagation

27.505 GHz Non-fade Distributions, July 1994

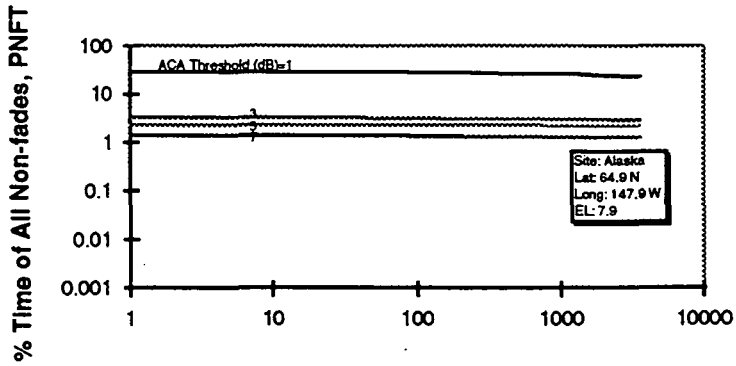

Alaska ACTS Propagation

Fade Durations* at 20.185 GHz, July 1994

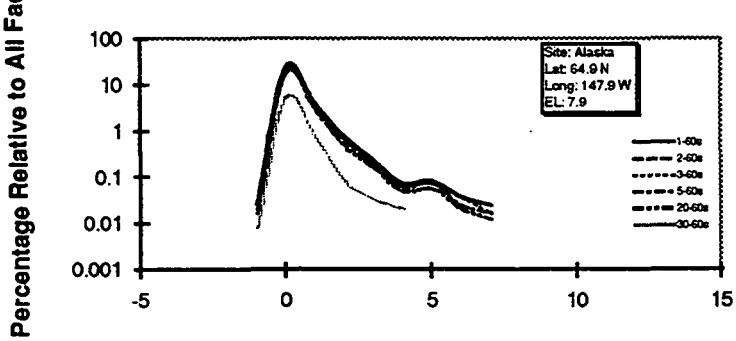

*with respect to 30s average of ACA

Alaska ACTS Propagation

Fade Durations* at 27.505 GHz, July 1994

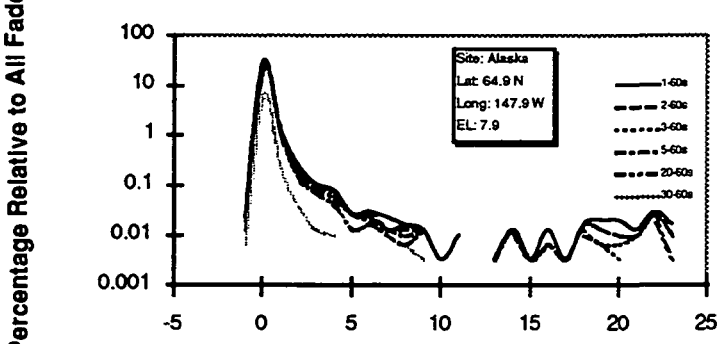

*with respect to 30s average of ACA

Fade Level (dB)

Alaska ACTS Propagation

20.185 GHz Fade Distributions, June 1994

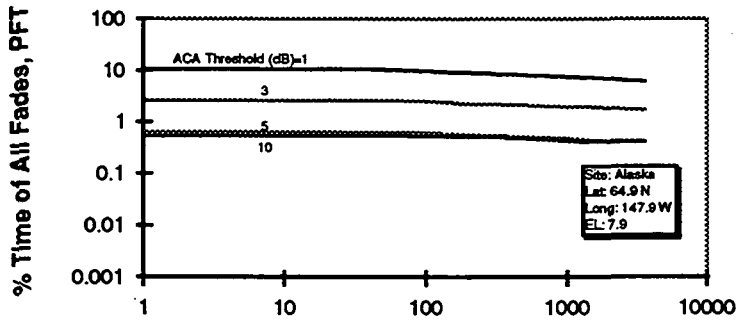

Fade Duration, FD (sec)

Alaska ACTS Propagation

27.505 GHz Fade Distributions, June 1994

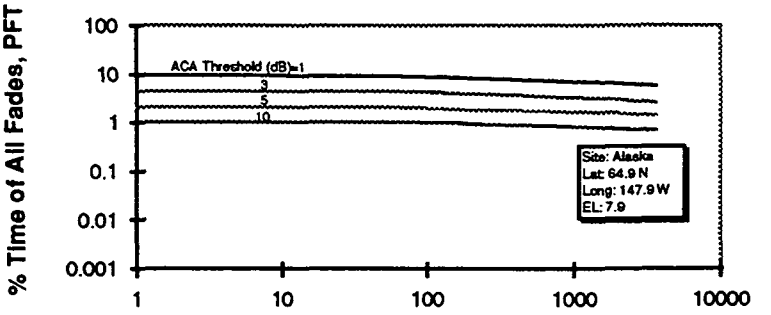

Alaska ACTS Propagation

20.185 GHz Non-fade Distributions, June 1994

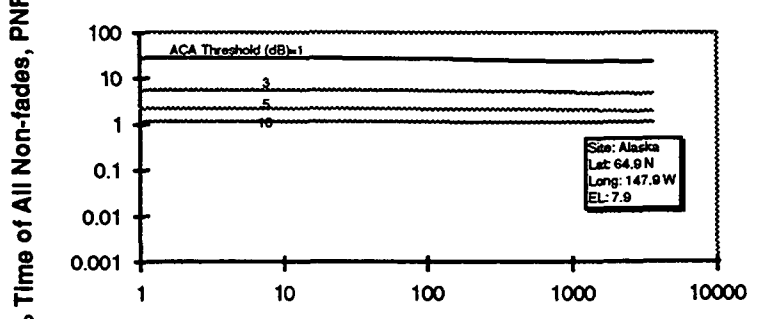

Alaska ACTS Propagation

27.505 GHz Non-fade Distributions, June 1994

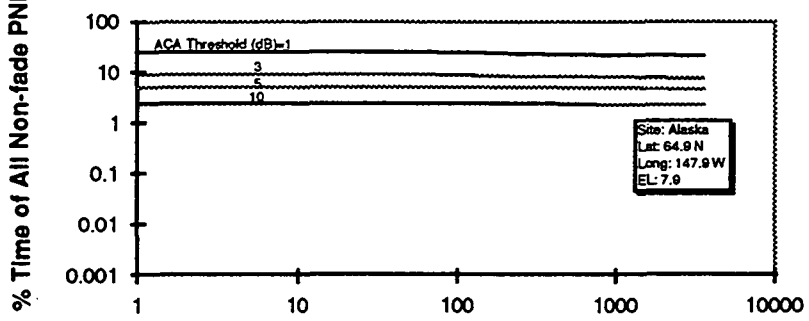

Alaska ACTS Propagation

Fade Durations* at 20.185 GHz, June 1994

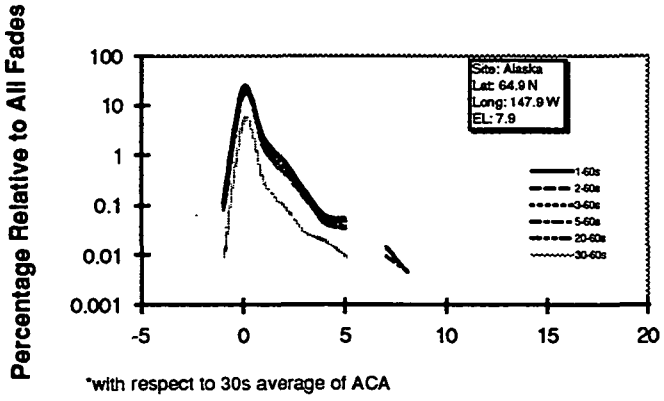

Alaska ACTS Propagation

Fade Durations* at 27.505 GHz, June 1994

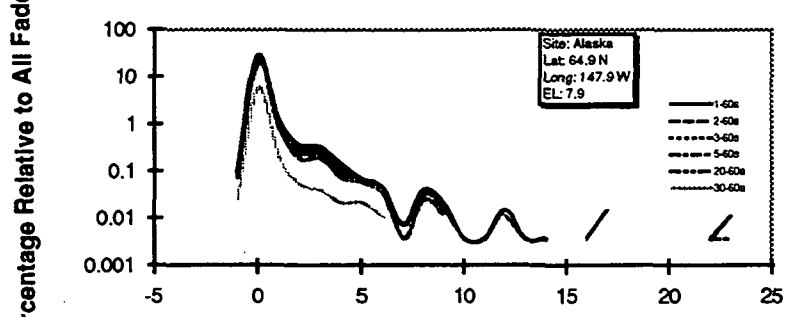

*with respect to 30s average of ACA

Fade Level (dB)

Alaska ACTS Propagation

27/20 Attenuation Ratio
Level of Occurances, June 1994

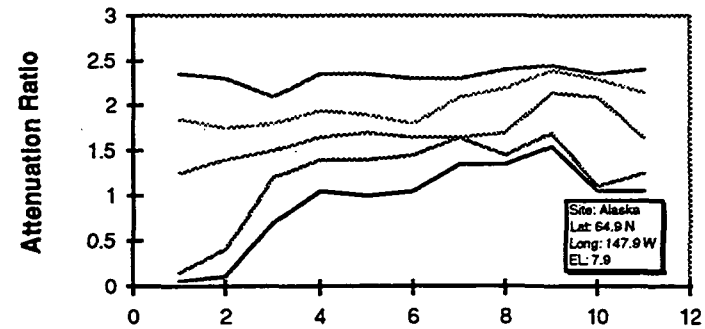

20.185 GHz Attenuation (dB)

1% 10% 50% 90% 99%

Alaska ACTS Propagation

U.B.C. ACTS PROPAGATION EXPERIMENT

M. Kharadly
B. Dow

Presented by D. Rogers

Electrical Engineering Department
University of British Columbia

June, 1995

OUTLINE

- STATUS
- SUPPLEMENTAL EQUIPMENT
- SOME PROBLEMS
- NEW PREPROCESSING SOFTWARE
- SAMPLE STATISTICS

STATUS

THE LATEST SOFTWARE UPDATE WAS INSTALLED ON APRIL 24, 1995

THE RAW DATA, AND FAULT AND EVENT LOGS UP TO AND INCLUDING APRIL 1995 HAVE BEEN SENT TO ACTS DATA CENTER

THE DATA FOR NOVEMBER 1994 - FEBRUARY 1995 WAS PREPROCESSED WITH THE NEW SOFTWARE AND SENT TO THE ACTS DATA CENTER

CAPACITIVE RAIN GAUGE CALIBRATION WAS SUSPENDED AS OF JANUARY 23, 1995

HOT AND COLD CALIBRATION WAS SUSPENDED AS OF MARCH 22, 1995

ANTENNA ALIGNMENT CHECKED BY MR. WESTENHAVER AND SIGNAL LEVELS IMPROVED AS OF MAY 23, 1995

SUPPLEMENTAL EQUIPMENT

A THERMOSTATICALLY CONTROLLED RADIANT HEAT SOURCE WAS INSTALLED BEHIND THE DISH ON DECEMBER 30, 1994

It is set to turn on when the temperature drops below 3° C so as to melt any ice or snow before it can accumulate on the dish.

AN AUTOMATIC ILLUMINATION SYSTEM WAS INSTALLED ON JANUARY 30, 1995

It is set to turn on at dusk and off at dawn so as to illuminate the area around the dish. This makes it easier to see this area via the monitoring camera at all times of day.

THE TIPPING BUCKET RAIN GAUGE ON THE ROOF OF THE ELECTRICAL ENGINEERING DEPARTMENT

We are exploring the possibility of disconnecting the gauge from a separate collection computer and connecting it directly to the DACS computer.

AN ACCURATE HUMIDITY "TRANSMITTER" HAS BEEN ACQUIRED (OMEGA ENGINEERING, INC. MODEL HX92; ACCURACY ±2% RH)

It will be used to replace the present humidity sensor, which has been indicating relative humidities higher than 100%.

A NEW RF TEMPERATURE CONTROLLER, FAN, AND SHROUD WERE INSTALLED ON MAY 24, 1995

SOME PROBLEMS

INTERMITTENT NEGATIVE-GOING 1 - 5 DB SPIKES ARE BEING OBSERVED ON THE 27 GHZ BEACON

These appeared during February 18, 1995; existed for several days before disappearing, then returned a few days later. To our knowledge at the time (email requesting information was sent to all sites February 28, 1995), no other site had reported seeing this phenomenon (we now know that the Alaska site is experiencing similar problems). The attenuation remained constant during the periods spikes were observed, however. (see Fig. 1). It is now suspected that the negative-going spikes are due to the master LO, the LO frequency multiplier or the LNA.

HUMIDITY IN THE ANTENNA FEED HORN WAS NOTICED (AGAIN!) ON MARCH 22, 1995

This was indicated by higher than normal radiometer voltage readings and lower than normal beacon signal value readings (on clear days).

The suspected cause is that there was no escape route for any moisture that did make its way into the feed horn.

The feed horn was removed on March 28, 1995, and the feed horn and waveguide were dried. A small hole was drilled in the barrel of the feed horn. Beacon and radiometer levels are now back to "normal."

NEW PREPROCESSING SOFTWARE

We had some difficulties trying to use the software until we received the user's manual on February 20, 1995.

Other problems regarding the new calibration method and relative humidity scaling were solved after consulting with Dr. Crane and Mr. Westenhaver. However, we found that the program that we were using to generate the CDFs could not read the new preprocessed files. New software was supplied by Ali Syed.

Subsequent months will be preprocessed as soon as the ranging tone files are received from the ACTS Data Center. Previous months are currently being preprocessed. There was, however, a problem involving the new preprocessing software; files created by older versions of the data collection software caused it to terminate with various error messages. Mr. Westenhaver provided an updated version of the new preprocessing software that, so far, seems to have solved the problem.

JUMPS IN RADIOMETER VOLTAGE LEVELS WERE OBSERVED SINCE NOVEMBER 29, 1995

The jumps were first noticed in the 27 GHz radiometer voltage levels. Mr. Westenhaver recommended checking and tightening the connectors on the cable at the front end and at the receiver. This seems to have solved the problem at 27 GHz, but we are still seeing occasional small jumps at 20 GHz.

SNOW ACCUMULATION SEEN ON ANTENNA DISH

Occasional heavy snowfalls during February 1995 deposited a relatively large amount of snow on the dish that was not "immediately" melted with the present radiant-heat arrangement. The heater will be repositioned so as to be more effective.

A POWER OUTAGE OCCURRED ON APRIL 13

An extended power outage drained the UPS battery, resulting in loss of data between 7:13 and 7:34 and between 9:53 and 11:56.

SAMPLE STATISTICS

These are shown in Figs. 2 - 4. The data in Fig. 4 excludes the month of July, 1994, when hot and cold calibrations were improperly performed as one of the calibrate buttons was held down by a covering insulating box.

NEW SIGNAL LEVELS

The present signal levels, after antenna adjustment by Mr. Westenhaver, are shown in Fig. 5.

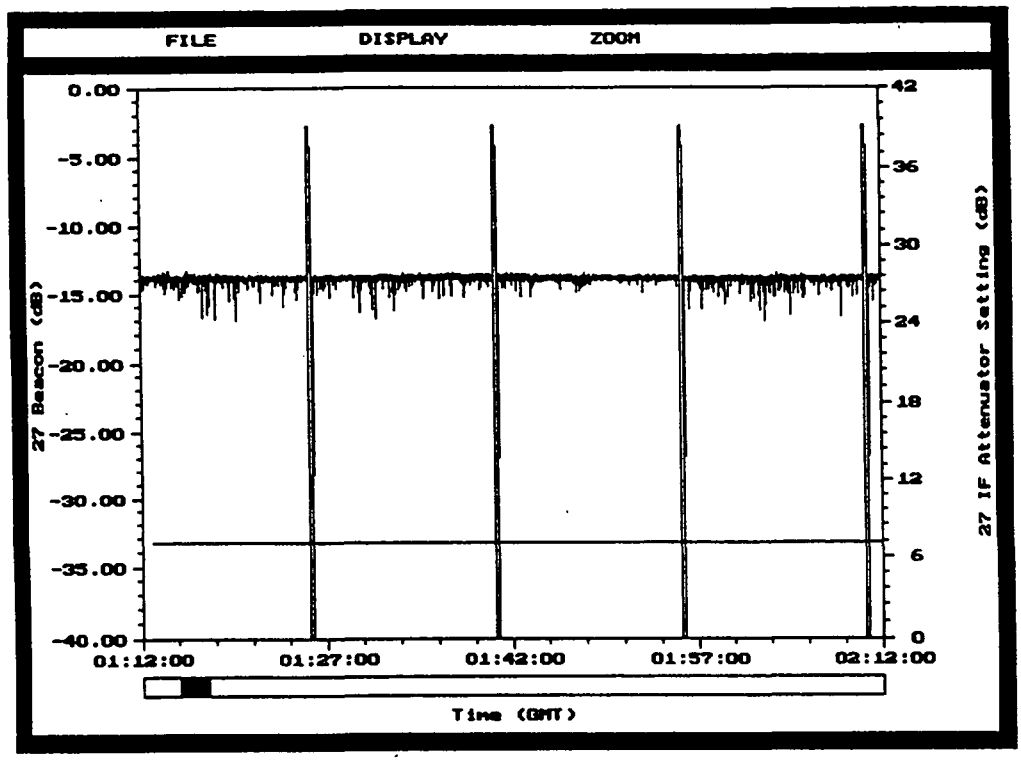

Figure 1: Negative-going spikes as observed on the 27 GHz beacon signal on May 1, 1995.

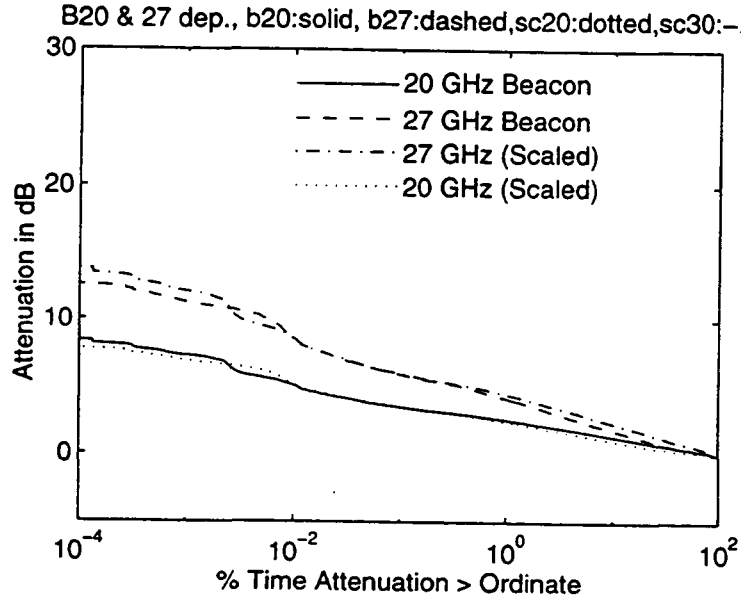

Figure 2: CDFs comparing the 20 and 27 Ghz beacon attenuation with the attenuation scaling model described in CCIR rev. rec. 618-1 for the month of January, 1995.

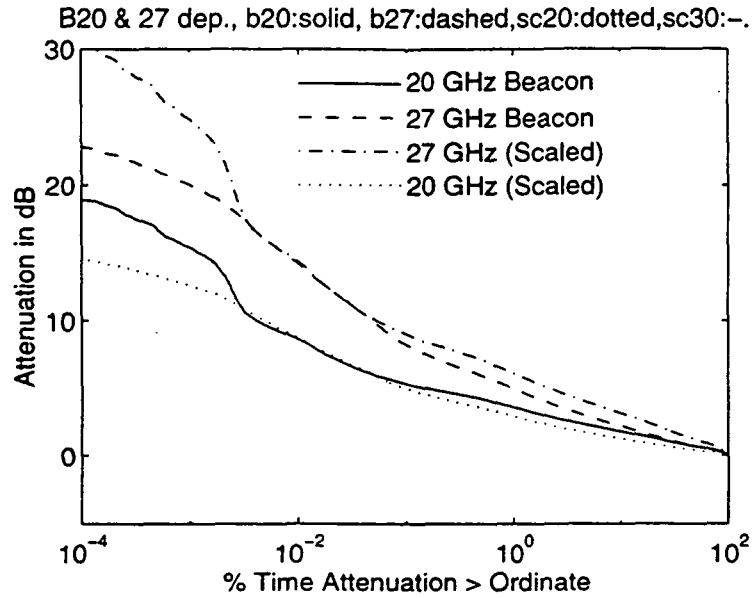

Figure 3: CDFs comparing the 20 and 27 Ghz beacon attenuation with the attenuation scaling model described in CCIR rev. rec. 618-1 for August 1994 - January 1995 inclusive.

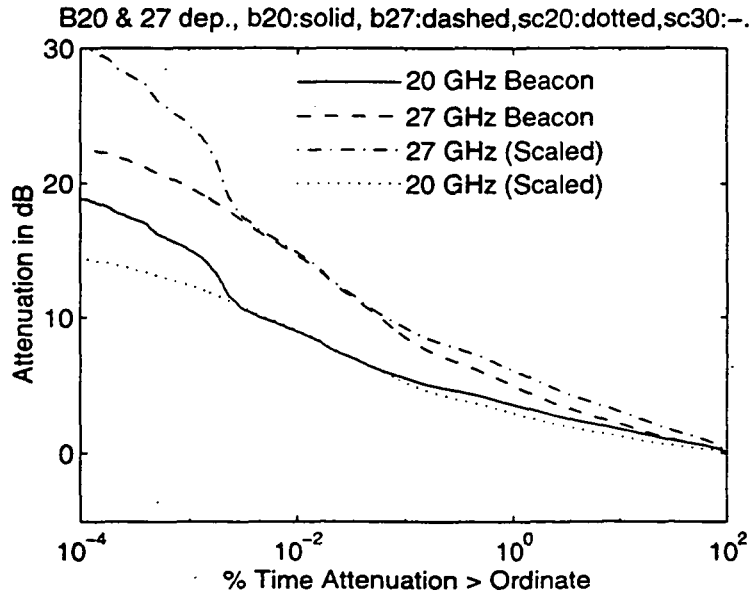

Figure 4: CDFs comparing the 20 and 27 Ghz beacon attenuation with the attenuation scaling model described in CCIR rev. rec. 618-1 for June 1994 - January 1995 inclusive, excluding July 1994.

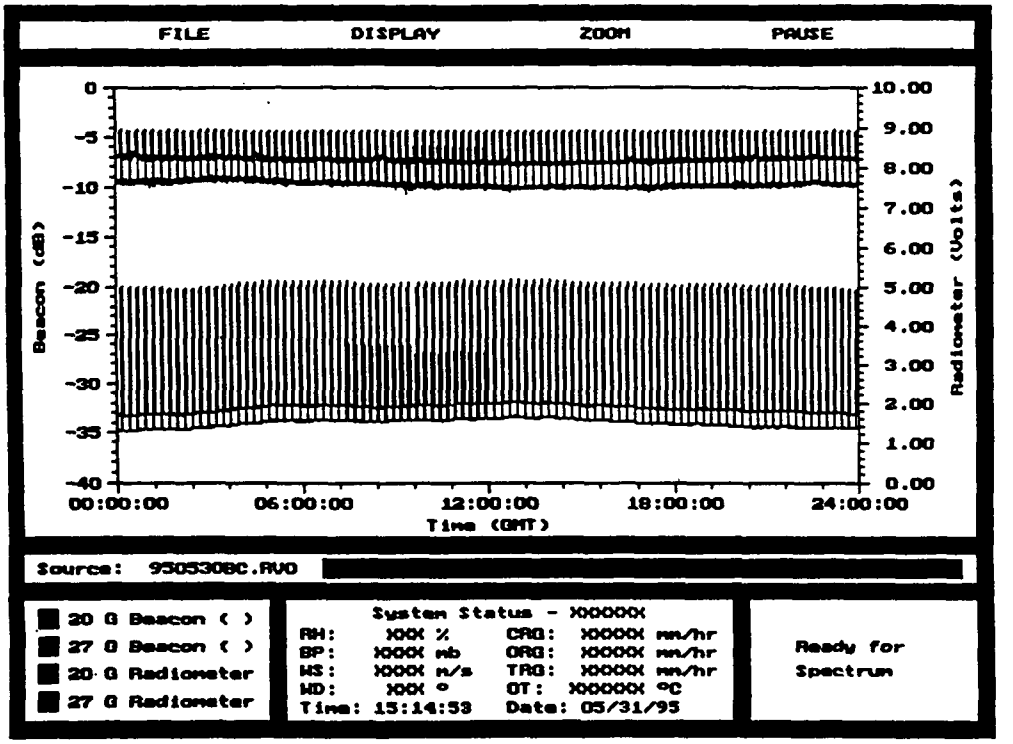

Figure 5: Signal levels for May 30, 1995 (after adjustment by Mr. Westenhaver).

KA-BAND PROPAGATION STUDIES USING THE ACTS PROPAGATION TERMINAL AND THE CSU-CHILL MULTIPARAMETER, DOPPLER RADAR

J. Beaver*, J. Turk† and V.N. Bringi*

Colorado State University
Fort Collins, Colorado

1 INTRODUCTION

An increase in the demand for satellite communications has led to an overcrowding of the current spectrums being used – mainly at C and Ku bands. To alleviate this overcrowding, new technology is being developed to open up the Ka-band for communications use. One of the first experimental communications satellites using this technology is NASA's Advanced Communications Technology Satellite (ACTS).

In September 1993, ACTS was deployed into a geostationary orbit near 100° W longitude. The ACTS system employs two Ka-band beacons for propagation experiments, one at 20.185 GHz and another at 27.505 GHz. Attenuation due to rain and tropospheric scintillations will adversely affect new technologies proposed for this spectrum. Therefore, before being used commercially, propagation effects at Ka-band must be studied.

Colorado State University is one of eight sites across the United States and Canada conducting propagations studies; each site is equipped with the ACTS propagation terminal (APT) [1]. With each site located in a different climatic zone, the main objective of the propagation experiment is to obtain monthly and yearly attenuation statistics. Each site also has secondary objectives that are site dependent.

At CSU, the CSU-CHILL radar facility is being used to obtain polarimetric radar data along the ACTS propagation path. During the expected two to four year period of the project, it is hoped to study several significant weather events. The S-band radar data will be used to obtain Ka-band attenuation estimates and to initialize propagation models that have been developed, to help classify propagation events measured by the APT [2].

Preliminary attenuation estimates for two attenuation events will be shown here – a bright band case that occurred on May 13, 1994 and a convective case that occurred on June 20, 1994. Section 2 will detail the computations used to obtain Ka-band attenuation estimates from S-band radar data. In Section 3, results from the two events will be shown.

2 COMPUTATIONS

As a preliminary step in obtaining attenuation estimates for Ka-band using S-band radar data, a Mie solution for spherical water particles is used. Attenuation estimates for 20 and 27 GHz versus reflectivity at 3 GHz are obtained by varying the parameters of the gamma drop size distribution

$$N(D) = N_0 D^m e^{-\gamma D} \tag{1}$$

where

$$\gamma = \frac{3.67 + m}{D_0} \tag{2}$$

and $N(D)$, given in $mm^{-1}m^{-3}$, is the number of drops per unit volume per unit size interval, D is the equivalent drop size diameter in mm, N_0 is given in $mm^{-1}m^{-3}$, D_0 is the median drop size in mm and m is the shape factor. Scatter plots were obtained for 20 and 27 GHz by varying the DSD parameters (N_0, D_0, m). The attenuation curves were then computed by applying an 8^{th} order polynomial fit to the data. The result for 27 GHz is shown in Figure 1.

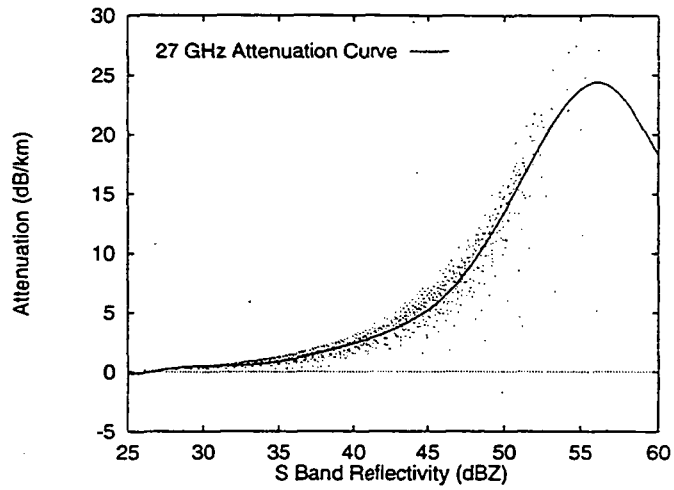

Figure 1: Attenuation for 27 GHz versus reflectivity at 3 GHz, obtained using a Mie solution for spherical particles.

Attenuation estimates at Ka-band were also obtained using specific differential phase, KDP, at S-band and are shown in Figure 2. Here a T-matrix solution was used to obtain the scattering amplitudes for oblate raindrops ranging in size from 1–8 mm. S-band KDP and specific attenuation at Ka-band were then computed from the Mueller matrix, averaged over

*Colorado State University, Dept. Of Electrical Engineering, Fort Collins, CO 80523

†Naval Research Lab, 7 Grace Hopper Ave, Monterey, CA 93943

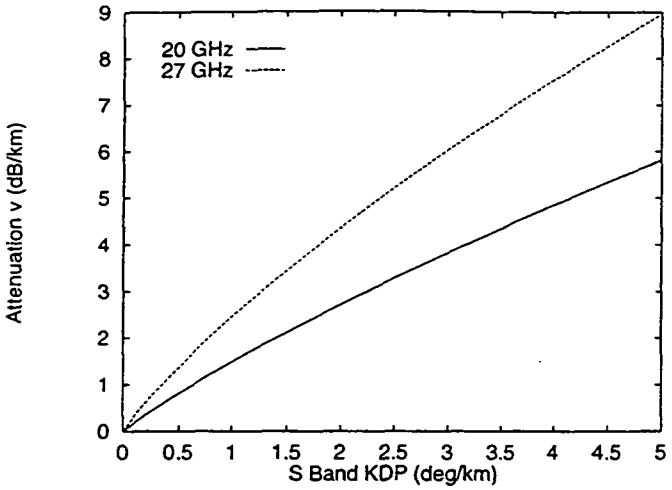

Figure 2: Attenuation for 20 and 27 GHz versus specific differential phase at 3 GHz, obtained via T-matrix and Mueller matrix solutions.

an exponential DSD (m = 0). The attenuation curves were derived by varying the DSD parameter D_0, while N_0 was fixed at 8000 $mm^{-1}m^{-3}$.

3 RESULTS

The May 13 bright band case is examined first. Attenuation measurements taken by the CSU-APT are shown in Figure 3. A range profile of radar observables, along the propagation path, is shown in Figure 4. The horizontal reflectivity, Z_H, profile shows a well defined bright band at a height of approximately 1.93 km, with values of 40 to 45 dBZ. The increase in reflectivity is due to the aggregation of ice particles and an increase in the dielectric constant as the particles begin to melt. The differential reflectivity, Z_{DR}, profile indicates values of 0.9 to 1.2 dB in the bright band. The enhanced region of Z_{DR} can be attributed to the fact that the aggregates have reached their largest size and are becoming more oblate as they melt. The increasing dielectric constant also contributes to the increase of differential reflectivity. The cross correlation coefficient, ρ_{HV}, profile is also shown. This is at the base of the melting layer, the point just before the aggregates collapse into raindrops. Values of ρ_{HV}, in the bright band are typically .93 to .94, which indicates of a wide distribution of shapes in this region. Finally the differential phase shift upon backscatter, δ, is shown. The presence of δ gives an indication of large Mie particles in the melting layer. It is located between the peak values of Z_H and Z_{DR} [3].

There are three periods of time when the CSU-CHILL radar took scans along the ACTS propagation path during this event. Reflectivity, (Z_H), measurements at 3 GHz are available at 150 m increments along the path. The corresponding 20 and 27 GHz attenuation estimates are determined from the data shown in Figure 1 and multiplied by the appropriate distance. The results using the reflectivity-attenuation curves for 20 GHz are given given in Table 1, while those for 27 GHz are given in Table 2. For this particular event S-band KDP values were to small too obtain

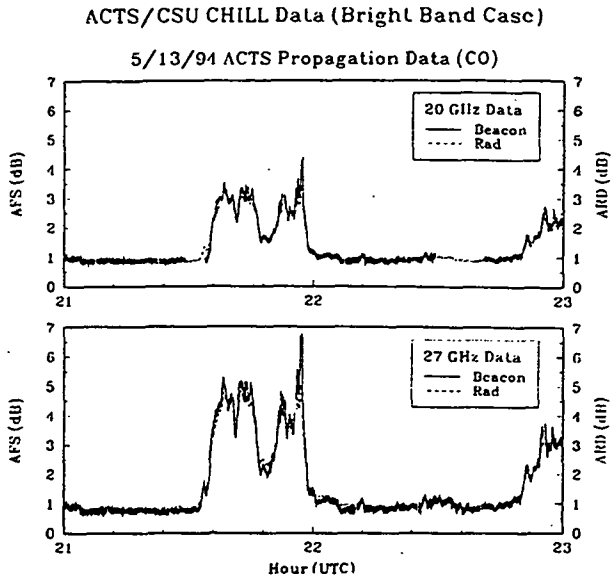

Figure 3: CSU-APT attenuation curves for May 13, 1994 bright band case.

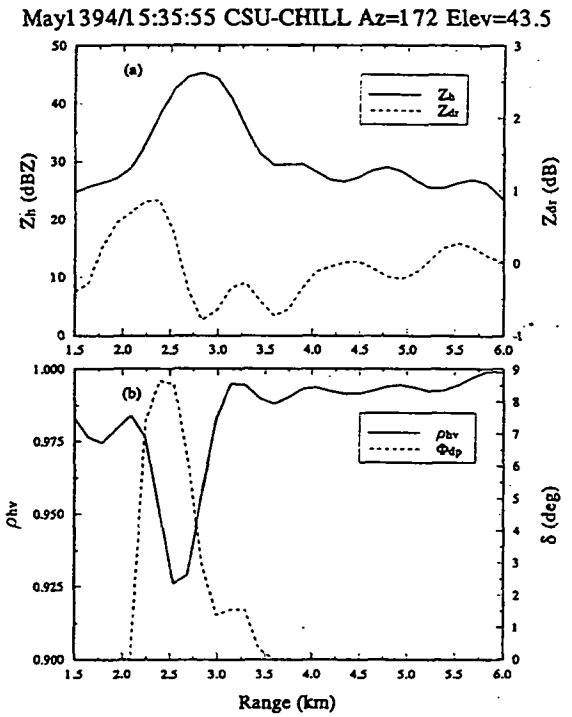

Figure 4: Range profile of Z_h, Z_{DR}, ρ_{HV} and δ for the May 13, 1994 convective case.

Time (GMT)	ACTS Attn (dB)	CHILL Attn (dB)
21:35:55	2.26	2.43
21:53:00	3.06	2.01
21:55:18	2.38	2.23

Table 1: 20 GHz attenuation estimates obtained by the CSU-APT and from CSU-CHILL S-band radar data.

Time (GMT)	ACTS Attn (dB)	CHILL Attn (dB)
21:35:55	3.51	3.86
21:53:00	4.49	3.08
21:55:18	3.55	3.48

Table 2: 27 GHz attenuation comparisons obtained by the CSU-APT and from CSU-CHILL S-band radar data.

attenuation estimates.

A rain event that occurred on June 20, caused a signal loss at 27 GHz for approximately 15 minutes. The 20 GHz signal bounced in and out of lock several times, but for only very short durations. Figure 5 shows attenuation data for both the 20 and 27 GHz channels. A range profile of Z_h, Z_{DR}, ρ_{HV} and KDP along the propagation path is shown in Figure 6. Starting at 2 km, along the propagation path, reflectivity values are on the order of 45 dBZ. At 6.5 km Z_H reaches a maximum of 54 dBZ. Low values of Z_{DR}, combined with high reflectivity values, a dip in the cross correlation coefficient, and measurable values of specific differential phase, KDP, at 6 km indicates a region with a mixture of melting hail and raindrops along the ACTS propagation path. There were 43 radar scans taken throughout the duration of the event. Attenuation estimates from reflectivity data and KDP data are derived from these scans. The results are shown Figure 7.

As seen in Figure 7, the CSU-CHILL reflectivity derived attenuation estimates follow the attenuation measurements obtained from the APT very closely. The maximum difference is about 5 db, while for the most part the CSU-CHILL derived estimates are within 1-2 dB of those measured by the CSU-APT. The attenuation estimates derived from KDP data alone grossly under estimated the attenuation caused by this event. This may be explained by examining Figure 8, a scatter plot of the APT measured 20 GHz attenuation versus the one way differential phase measured by the CSU-CHILL radar.

One way differential phase, Φ_{DP}, and its derivative KDP are only sensitive to the oblateness of a particle, therefore the difference seen between the maximum and minimum values of the fitted curve in Figure is caused by the presence of various sizes of oblate rain drops throughout the medium. If the medium were comprised of only raindrops the y-intercept of the fitted curve would be at zero; however, if the fitted curve is extended back to $\Phi_{DP} = 0$, the y-intercept is at 23.97 dB. This indicates that a large amount of attenuation was due to spherical, water coated ice particles. As indicated previously, there was indeed a region of mixed phase along the propagation path, however from Figure 8 and the fact that KDP data alone grossly underestimates the attenuation is

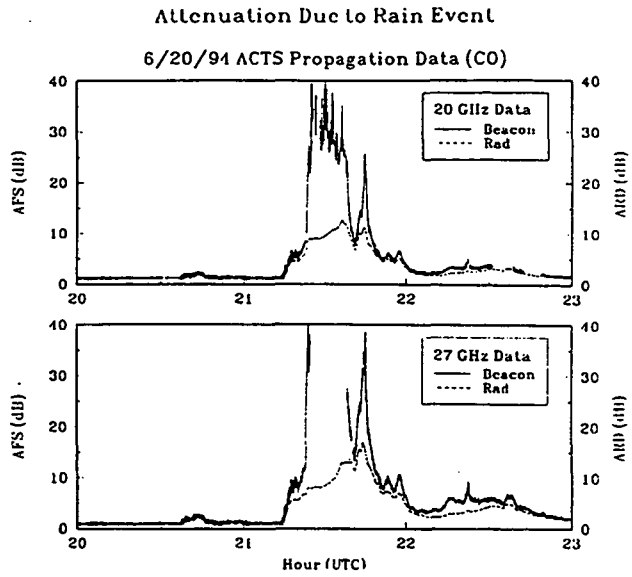

Figure 5: June 20, 1994 rain event, measured by the CSU-APT.

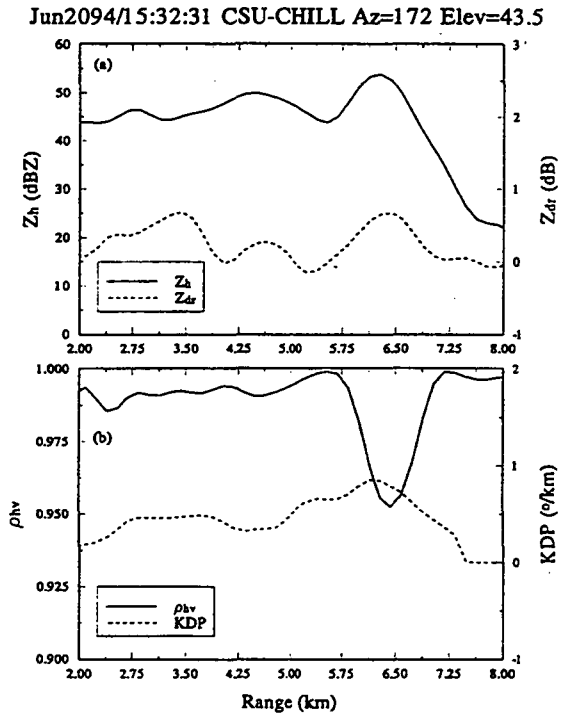

Figure 6: Range profile of Z_h, Z_{DR}, ρ_{HV} and KDP for the June 20, 1994 convective case.

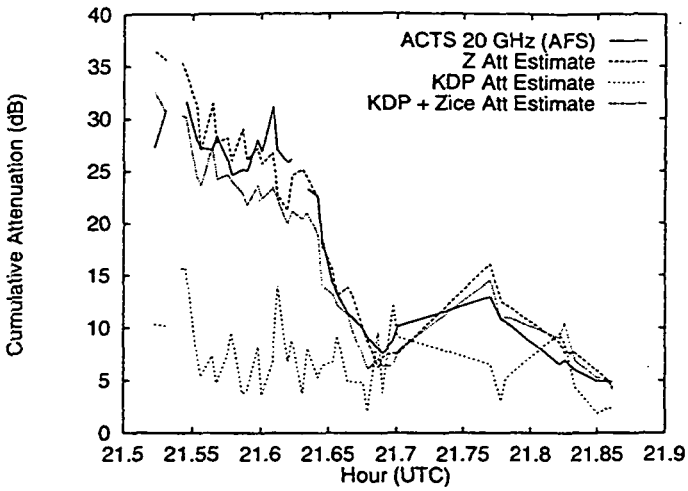

Figure 7: Comparison of measured CSU-APt attenuation and 20 GHz attenuation estimates derived from CSU-CHILL data.

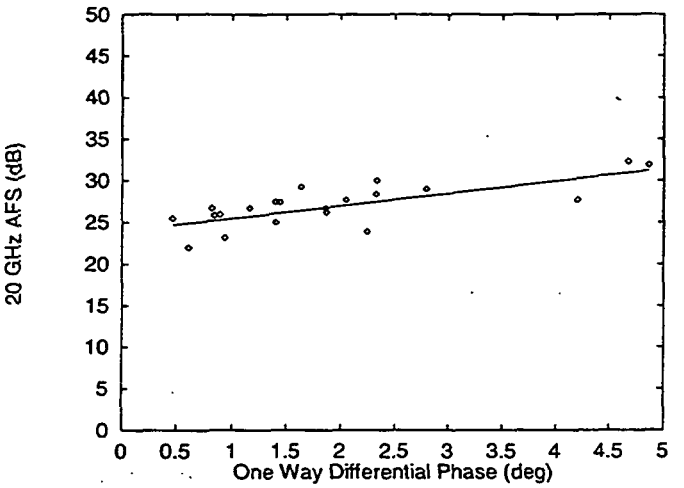

Figure 8: 20 GHz attenuation versus one way differential phase, for the June 20, 1994 convective case.

an indication that water coated ice particles could have been present throughout the propagation path during this event. Considering this to be the case, the next step is to determine the reflectivity due only to the water coated ice particles along the propagation path from the total reflectivity measured by the CSU-CHILL radar. This is done by using Z_{DR} to determine the ice fraction content in the range resolution volume at each 150 m increment along the propagation path. Once the ice fraction content is determined, the reflectivity due to the water coated ice particles is computed and used to determine the attenuation at 20 and 27 GHz due to these particles alone, while the attenuation due to the oblate raindrops is computed using KDP data.

The combined results are shown in Figure 7, while the attenuation estimates are still slightly underestimated for the most part, the CSU-CHILL derived attenuation estimates us-

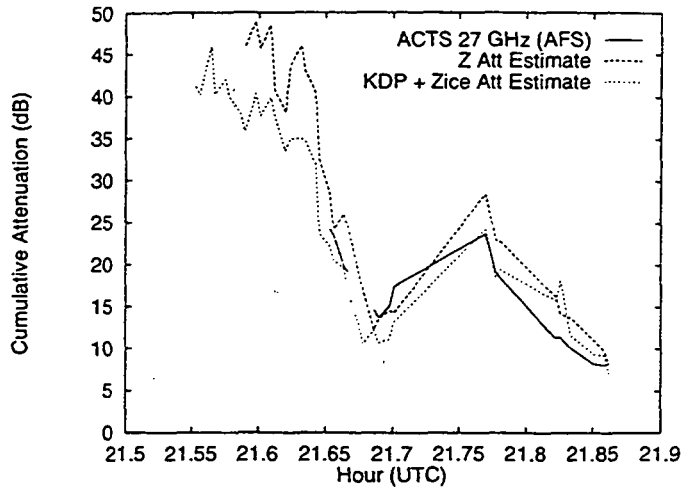

Figure 9: Comparison of measured CSU-APT attenuation and 27 GHz attenuation estimates derived from CSU-CHILL data.

ing KDP and Z_{ICE} are within 1 to 2 dB of the the attenuation values obtained by the CSU-APT. The 27 GHz results are shown in Figure 9.

While these are just preliminary results, they are very encouraging. The June 20 convective case is a good example of how the different parameters available from the CSU-CHILL radar can be used to determine the nature of precipitation particles along the propagation path. Currently, other events for which radar data is available are being analyzed, in addition to refining the methods used to obtain the attenuation estimates from S-band radar data.

References

[1] W. L. Stutzman, et al., "ACTS Propagation Terminal Hardware Description Report," Virginia Tech Report No. EESATCOM 93-9, June 1993.

[2] V.N. Bringi, V. Chandrasekar and Y. Golestani, "Polarimetric Radar Measurements in Convective Storms," *Direct and Inverse Methods in Radar Polarimetry, Part 2*, 1992.

[3] D. Zrnic, N. Balakrishnan, C. Ziegler, V.N. Bringi, K. Aydin and T. Matejka, "Polarimetric Signatures in the Stratiform Region of a Mesoscale Convective System," *Journal of Applied Meteorology*, vol. 32, April 1993.

Acknowledgement

The authors would like to acknowledge support from NASA contract NAS3-26410. We would also like to thank Pat Kennedy, Dave Brunkow and Ken Pattison of the CSU-CHILL radar facility, for their help in collecting radar data. Finally we would like to thank David Westenhaver for his continued support in keeping the terminal operational.

COMSAT LABORATORIES

ACTS Propagation Measurements

Asoka Dissanayake, Kuan-Ting Lin

COMSAT LABORATORIES

Diversity Geometry

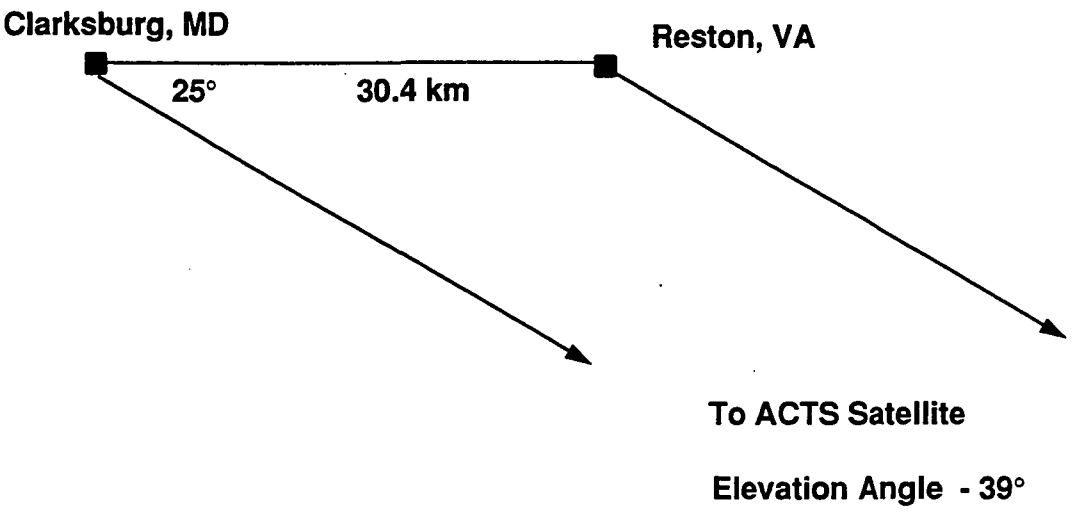

COMSAT LABORATORIES

ACTS Propagation Terminal

- Terminal moved to a new site (Stanford Telecom) approximately 0.5 km from the original site (MITRE).

- Data collection at the new site started on 4/8/95. Approximately three days of down time due to relocation.

- Reasons for relocation: easier access to the terminal and active support of STEL staff in maintaining the terminal.

- Due to the short distance involved data from the two sites can be pooled together without affecting any of the statistical results.

- After the relocation several problems were rectified: installing new DACS software, new rain gauge interface board, new RF temperature control unit, replacement of faulty temperature sensors etc.

- A tipping bucket rain gauge was added to the system.

COMSAT LABORATORIES

ACTS Propagation Terminal

- Un resolved issues: humidity gauge still giving faulty readings, Young rain gauge does not register rain correctly.

- Data Analysis:
  - data from March, 1994 to February, 1995 (12 months) have been analyzed.
  - temperature and humidity data from Washington-Dullas airport were used for the analysis.
  - manual editing carried out to remove anomalous readings due to eclipse operation , 20 GHz radiometer interference, faulty reference load temperature sensor in the 27 GHz radiometer channel.

COMSAT LABORATORIES

COMSAT Propagation Terminal

- Data collection continued with several minor problems:
  - local oscillator in the 20 GHz channel failed causing data loss over 24 hour period in February, 1995.
  - refurbishment work on the terminal was carried out in March, 1995; 2.5 days down time mostly during clear sky conditions.
  - 27 GHz channel suffered gain reduction in the RF stage; repair work caused 2 days of down time in April, 1995.

- Data analysis for the period November, 1993 to April, 1995 have been completed.

COMSAT LABORATORIES

Results

- Almost identical cumulative statistics of attenuation from the two sites; results given for the measurement period from March, 1994 to February, 1995.

- Results include several snow events.

- Rain zone rain rates are much smaller compared with the measured rain rates.

- Attenuation predictions made with the ITU-R model using measured rain rate appear to provide reasonable agreement with measurements;

- Smaller diversity gains predicted by the ITU-R model.

Rain Rate Distribution : Clarksburg, MD: March,1994 - February,1995

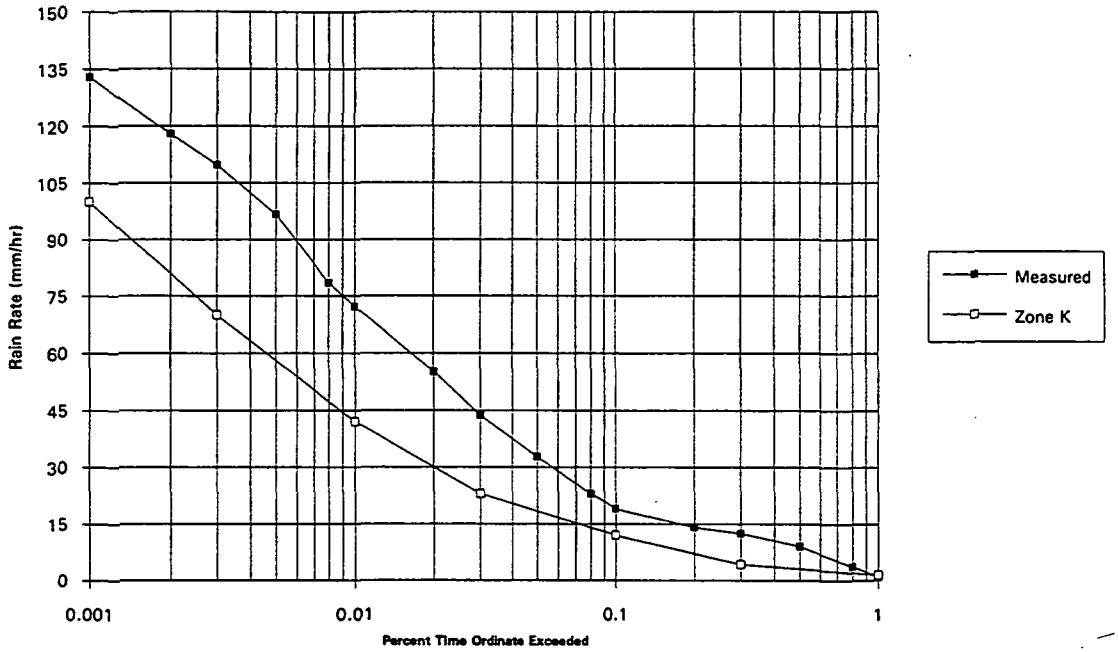

Cumulative Distribution of 20 and 27 GHz Attenuation: Clarksburg, MD: March,1994 - February,1995; ITU-R Prediction Using 0.01% Rain Rate of 72 mm/hr

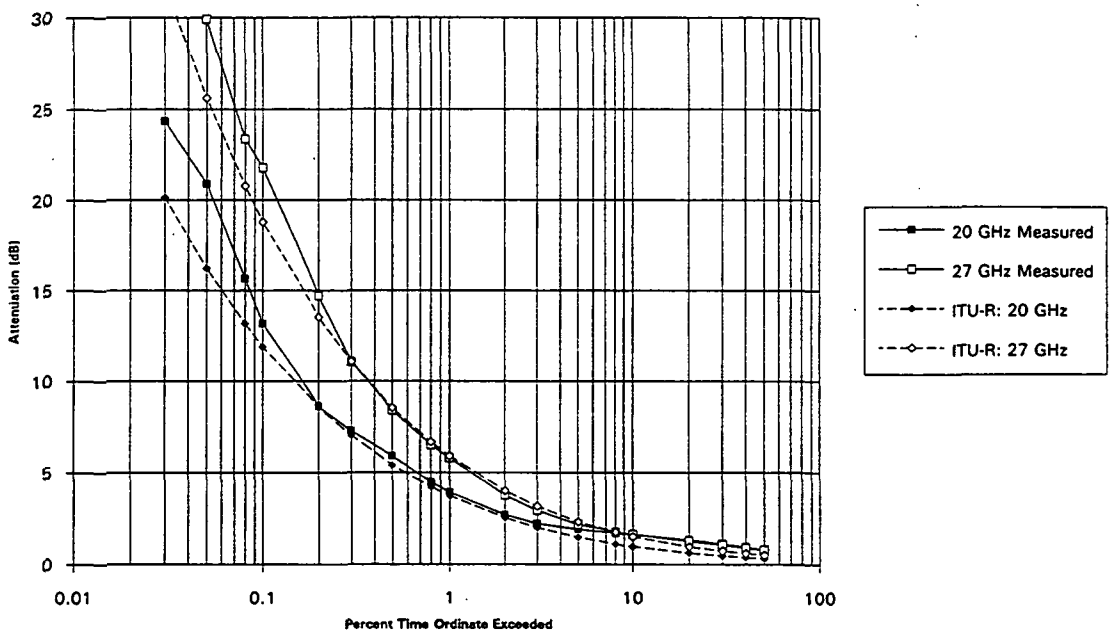

Cumumative Distribution of 20 and 27 GHz Attenuation; Clarksburg, MD; March,1994 - February,1995; ITU-R Prediction Using 0.01% Rain Rate of 42 mm/hr

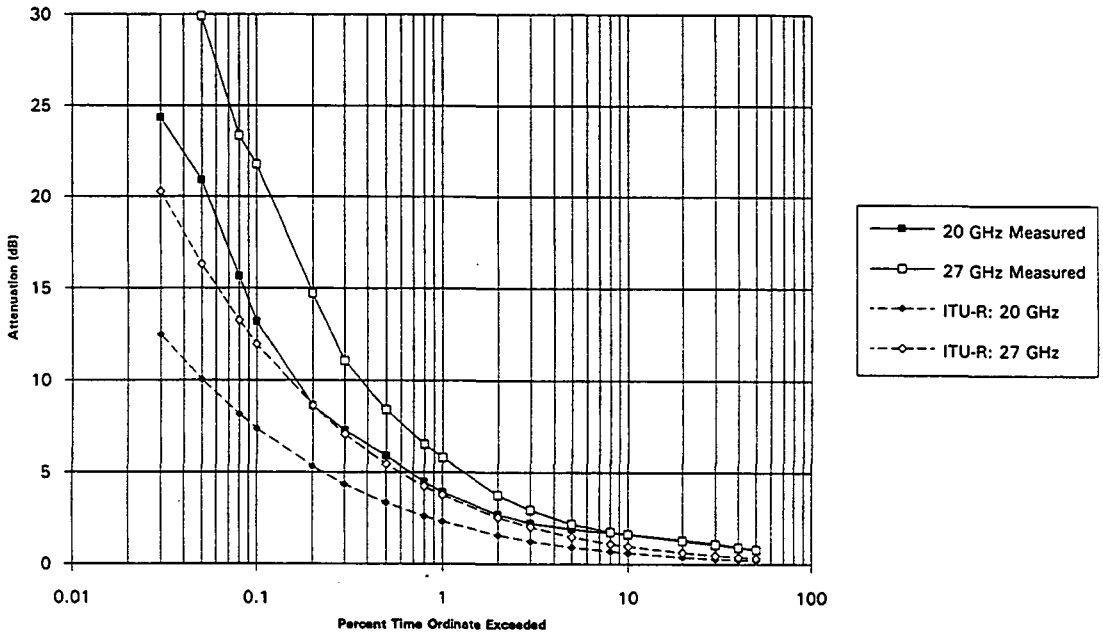

Cumumative Distribution of 20 and 27 GHz Attenuation; Reston, VA; March,1994 - February,1995; ITU-R Prediction Using 0.01% Rain Rate of 42 mm/hr

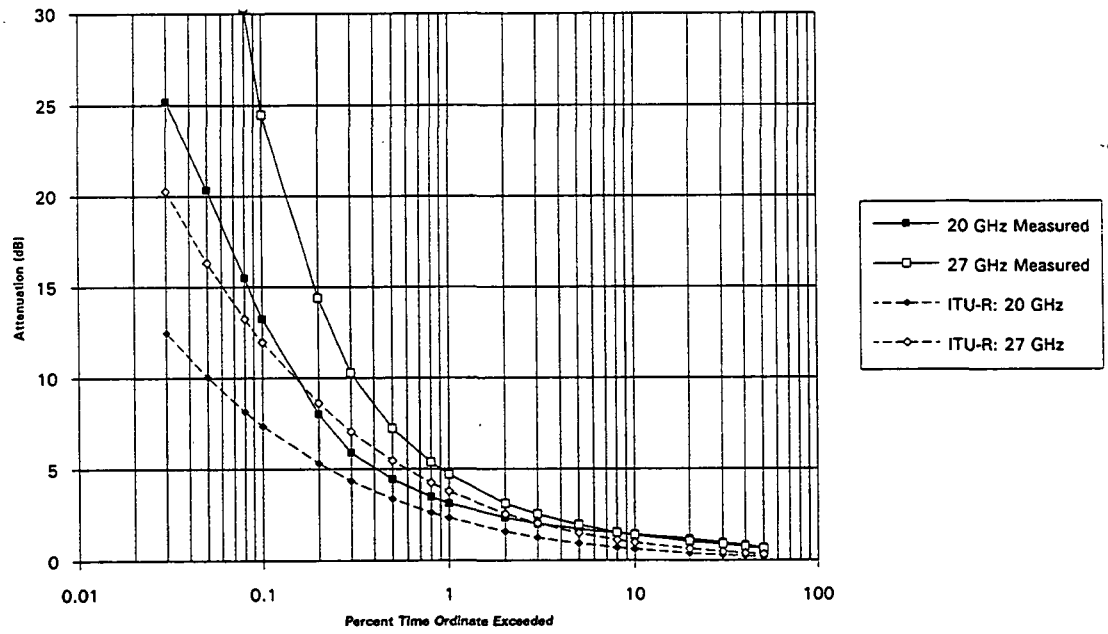

Cumumative Distribution of 20 GHz Attenuation; Reston, VA and Clarksburg, MD; March,1994 - February,1995

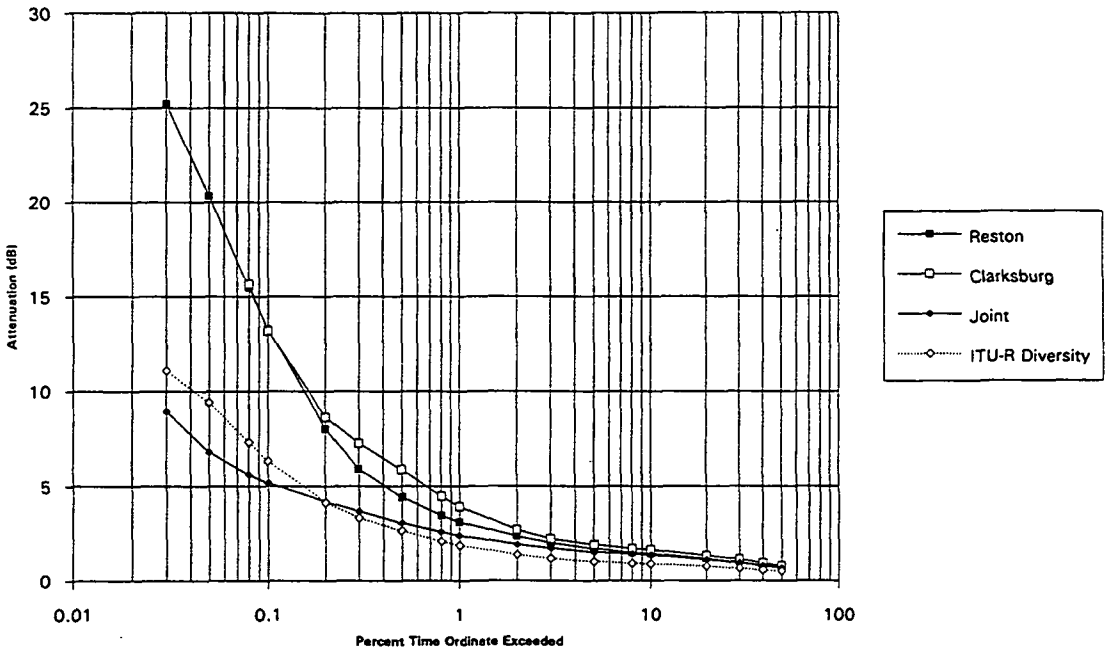

Cumumative Distribution of 27 GHz Attenuation; Reston, VA and Clarksburg, MD; March,1994 - February,1995

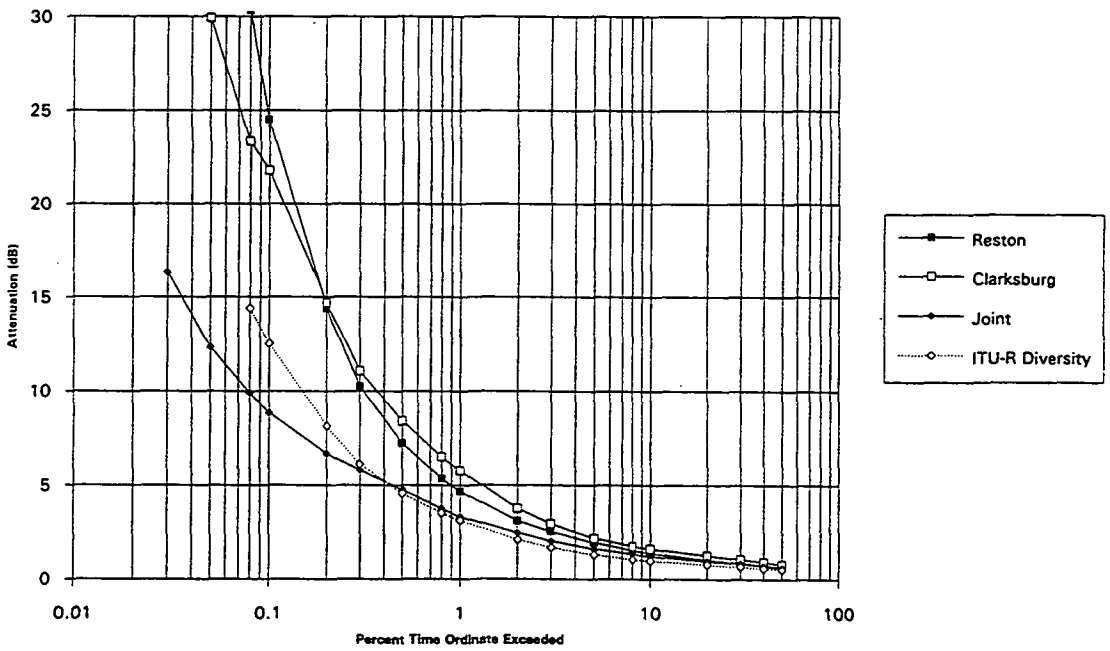

Worst Month Distribution of 20 and 27 GHz Attenuation; Reston, VA; March,1994 - February,1995

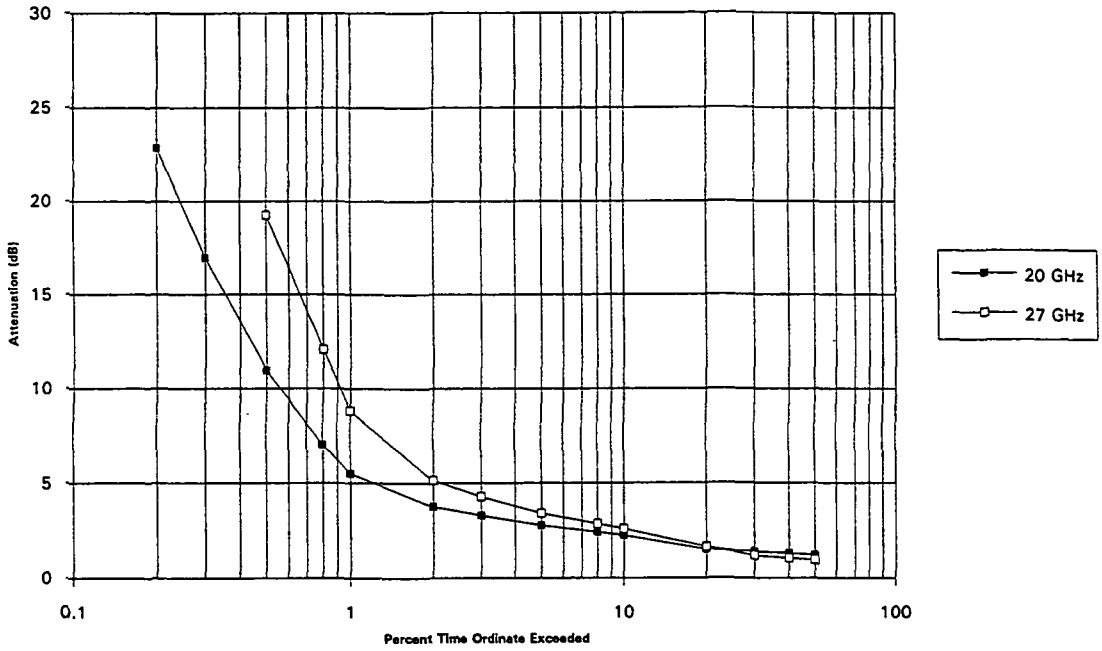

Worst Month Distribution of 20 and 27 GHz Attenuation; Clarksburg, MD; March,1994 - February,1995

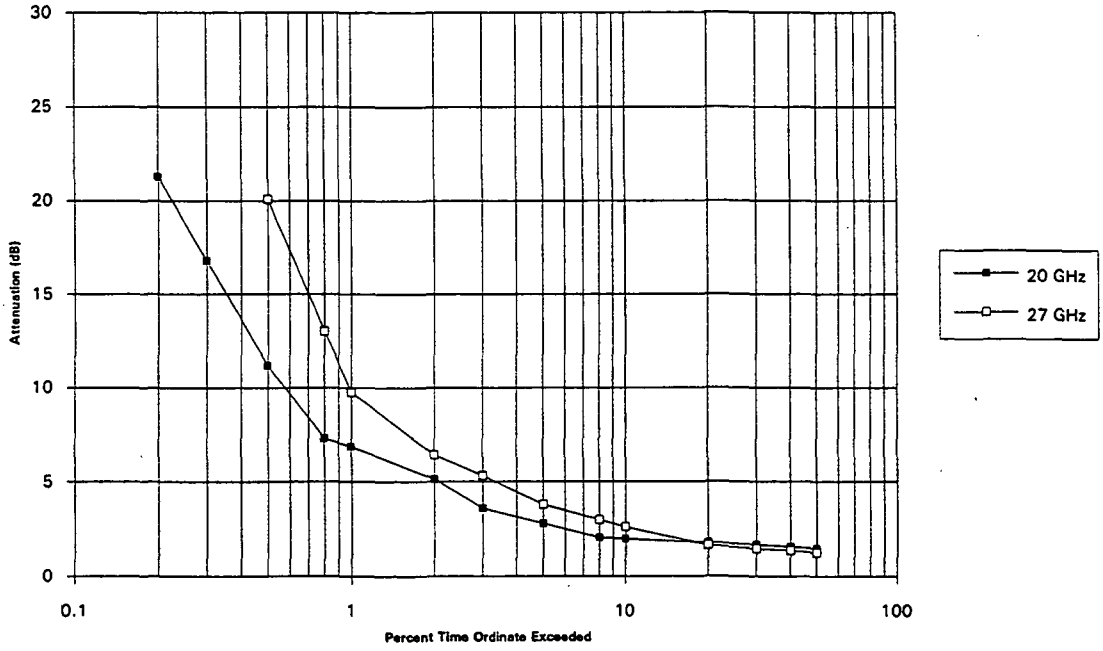

SPACE COMMUNICATIONS TECHNOLOGY CENTER

(SCTC)

SATELLITE Ka-BAND PROPAGATION MEASUREMENTS IN FLORIDA

HENRY HELMKEN
FLORIDA ATLANTIC UNIVERSITY (FAU)

&

RUDY HENNING
UNIVERSITY OF SOUTH FLORIDA (USF)

June 15, 1995

FLORIDA PROGRAM GOALS

* Generate CDF's for Sub-tropical Region
* Sub-tropical Fading Statistics
* Diversity Gain
* Radiometer Development
* Sub-tropical Rain Models

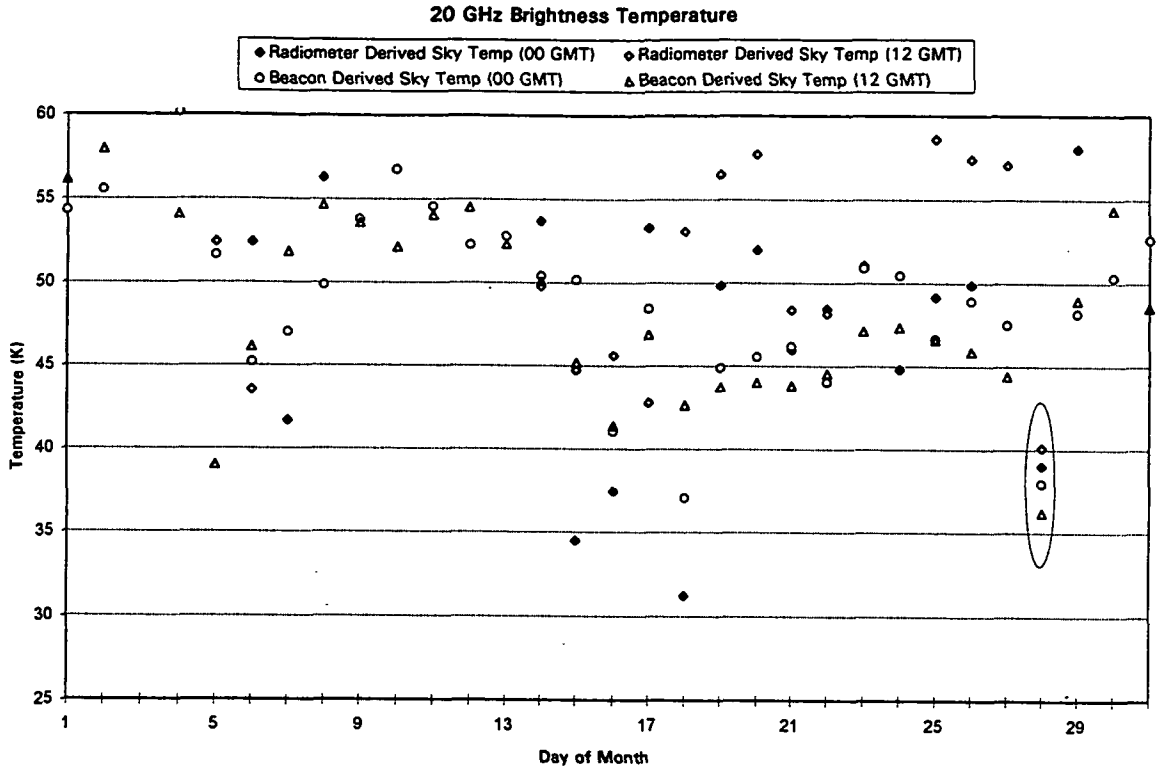

Figure 2. 20 GHz Brightness Temperature - 10/28 used for calibration
Antenna Efficiency: 68%, Antenna Spillover 87°

6/22/95 | 10:02 AM

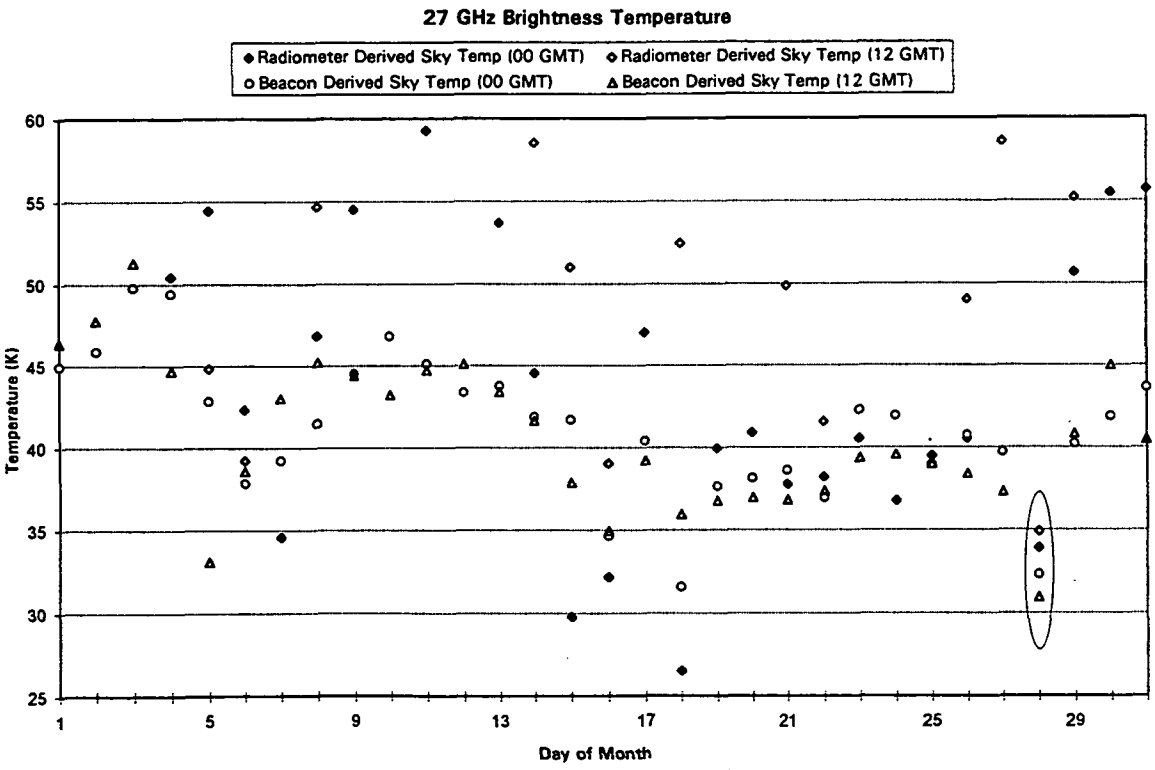

Figure 3. 27 GHz Brightness Temperature - 10/28 used for calibration
Antenna Efficiency: 58%, Antenna Spillover 84°

6/22/95 | 10:02 AM

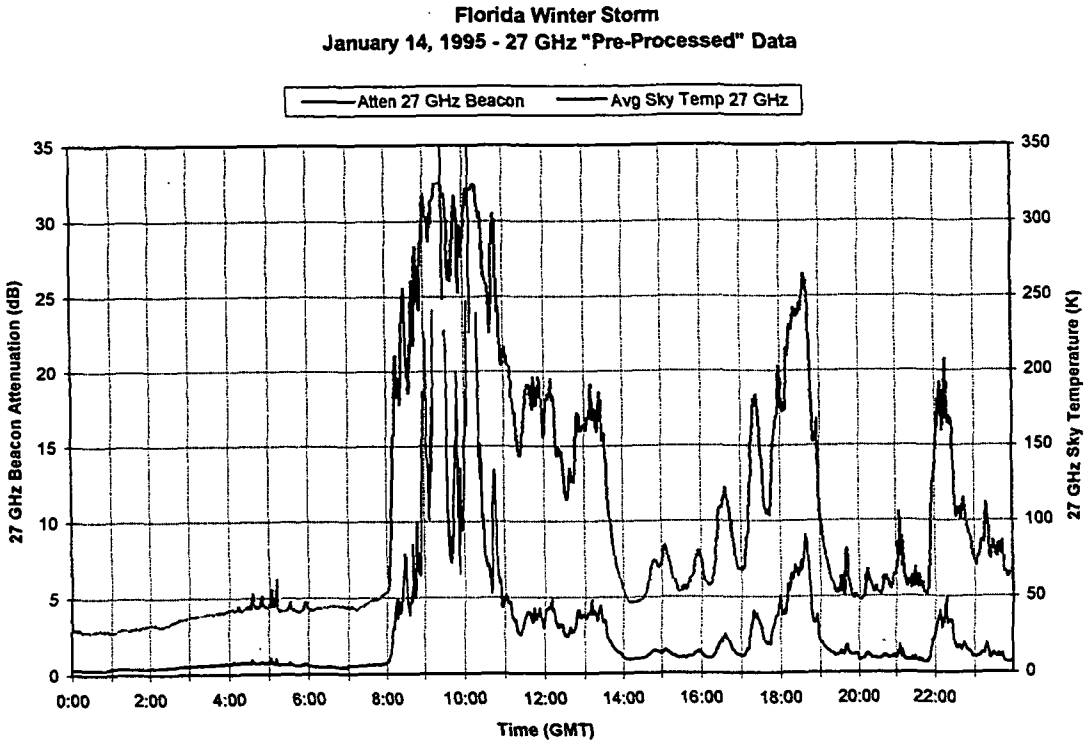

Figure 4. Typical Florida Winter Storm - Pre-processed data - 27GHz

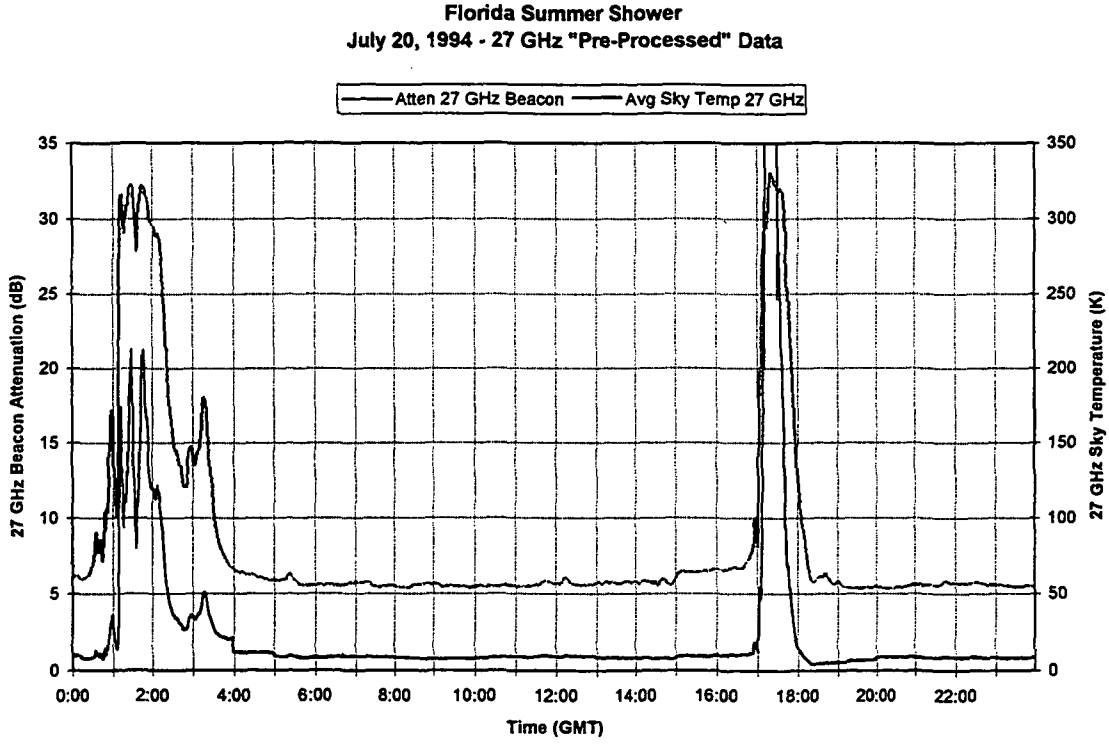

Figure 5. Typical Florida Summer Shower - Pre-processed data - 27GHz

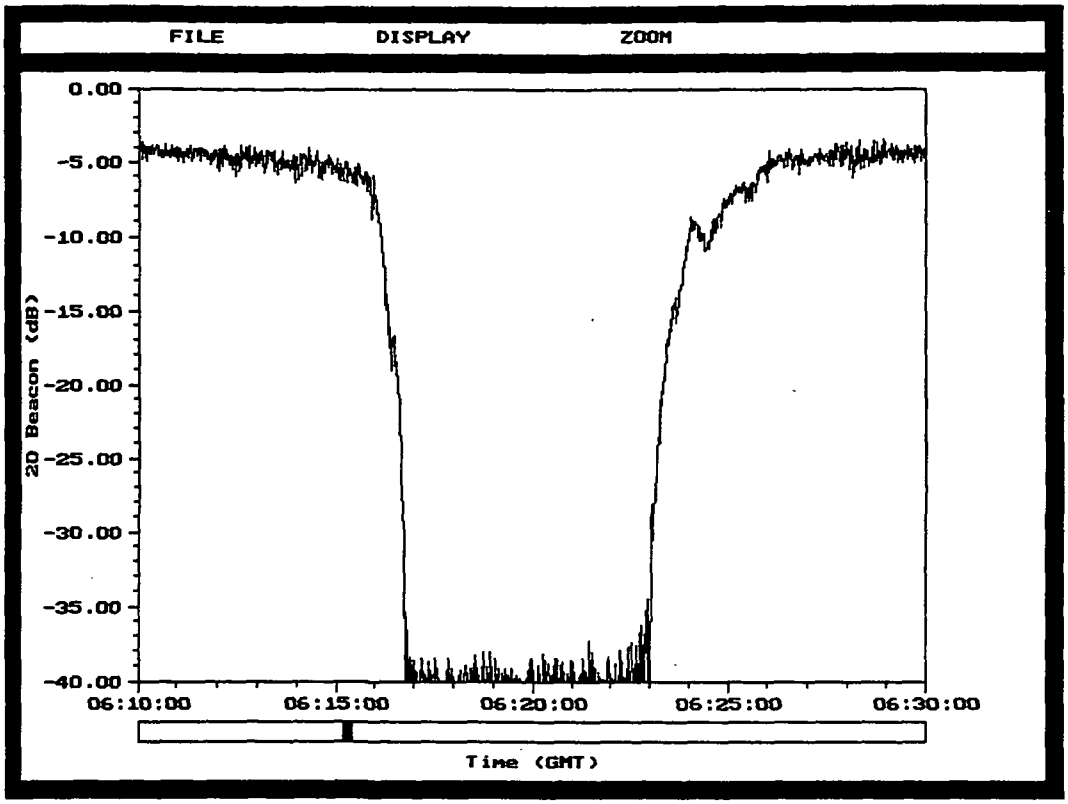

Figure 6. Ran Event - 20 GHz Beacon

May 20, 1995

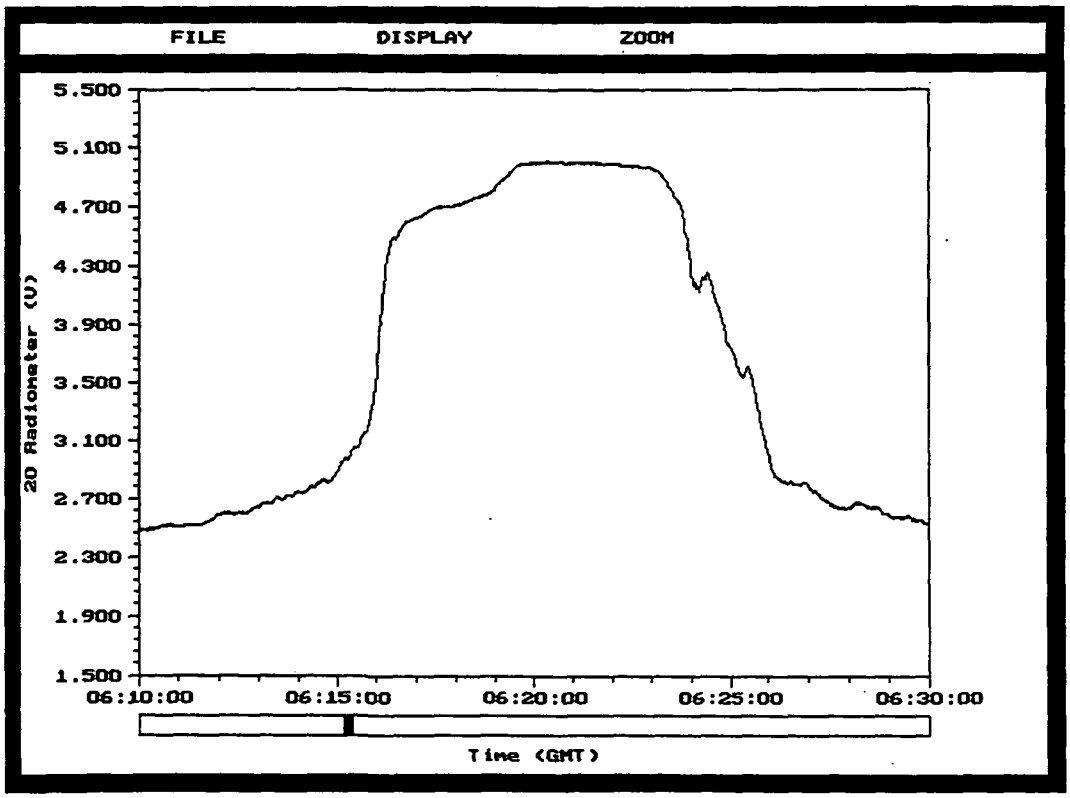

Figure 7. Ran Event - 20 GHz Radiometer - overlaps storm

May 20, 1995

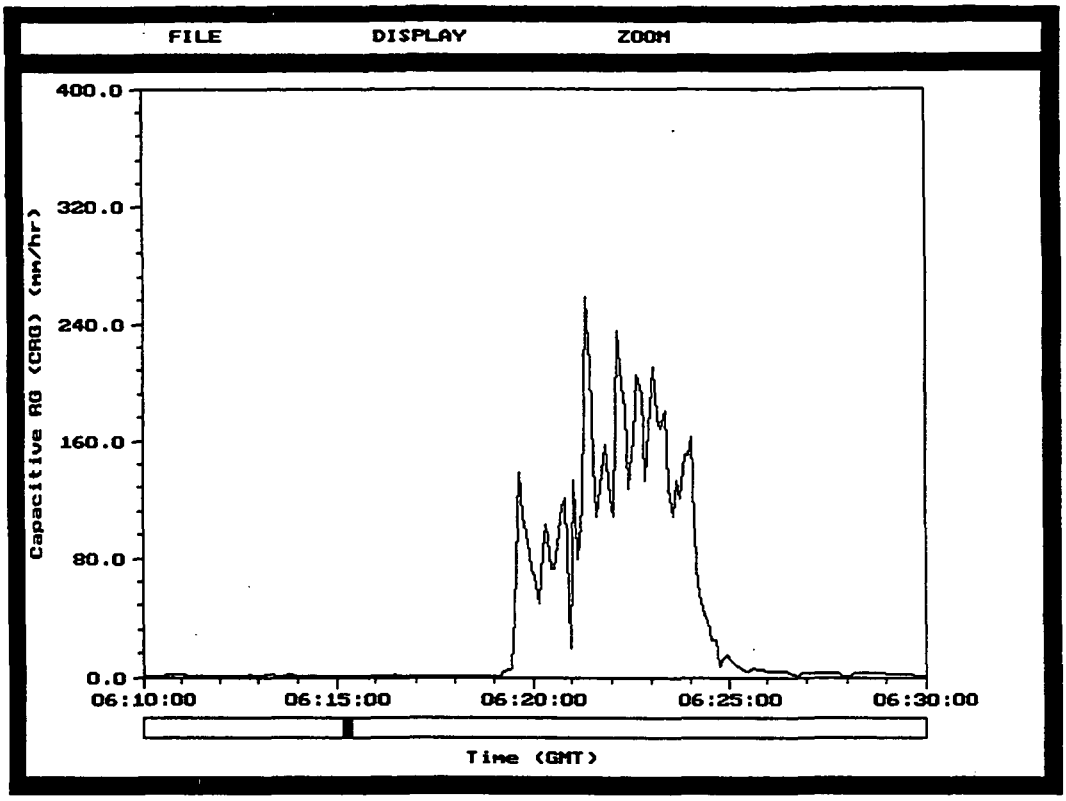

Figure 8. Rain Event - Rain rate - Delayed 2 minutes from fade onset.

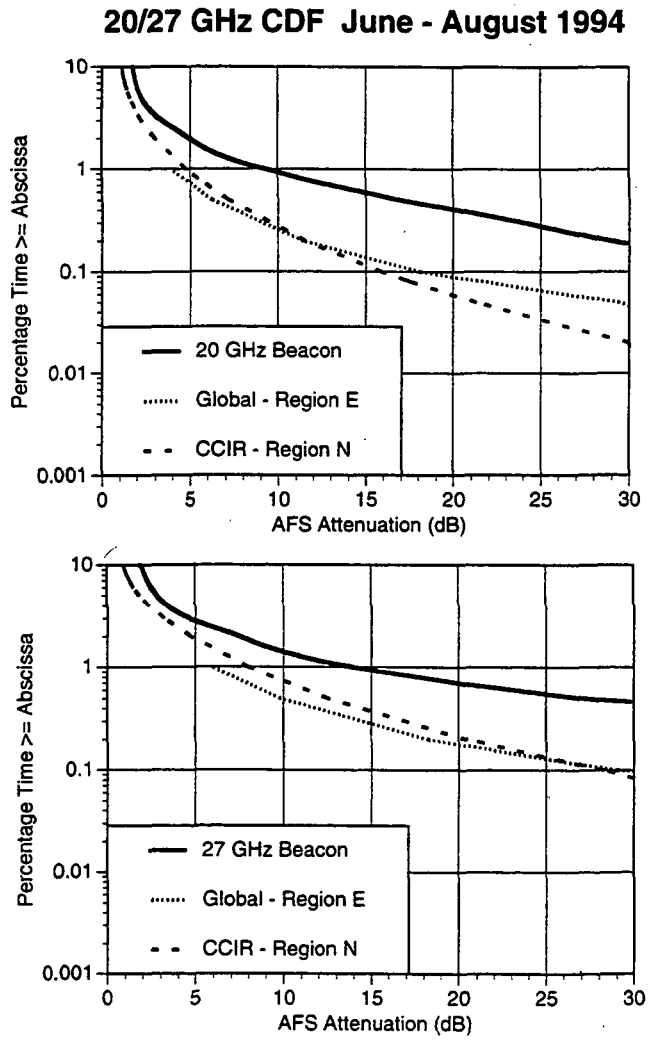

Figure 9. Comparison of pv0 Summer 1994 data with CCIR and Global Rain Models.

FADE ANALYSIS

Step 1 - Generate Binary pv1 file via Version 5.1

Step 2 - Generate Binary pv1a file
Mark Bad Artifact Intervals in Appropriate Channels
Power Outages
Antenna Testing and Other Log Book entries

Step 3 - Data Averaging
Extrapolate Over Calibration Periods
Select Running Average (1 - 30 seconds)
Median Averaging

Step 4 - Fade Analysis
Discard data with values <= 0
Generate CDF with 0.1 dB bins
Fade Duration Matrix
Level: < 1 Db, < 2dB, ... < 30 dB, >30dB.
Durations: < 1 Sec, < 2 Sec .....< 120 Sec.
Slope Matrix
Level: < 1 dB, < 2dB, ... < 30 dB, >30dB.
Slopes: -1.25 dB/sec, -1.20 dB/sec ....1.25 dB/sec.

Figure 10. Proposed Fade Analysis Procedure.

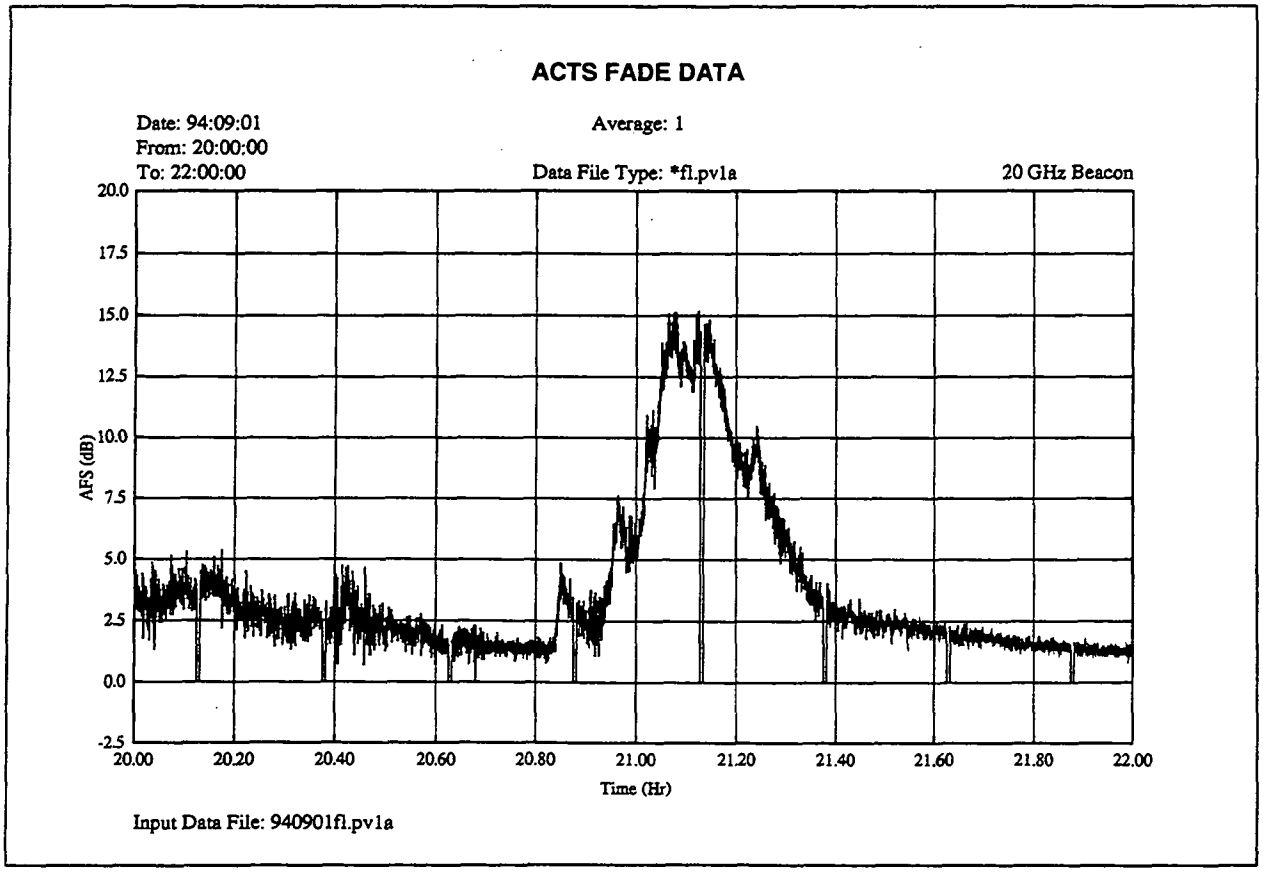

Figure 11. pv1 data: Typical Fade including calibration periods.

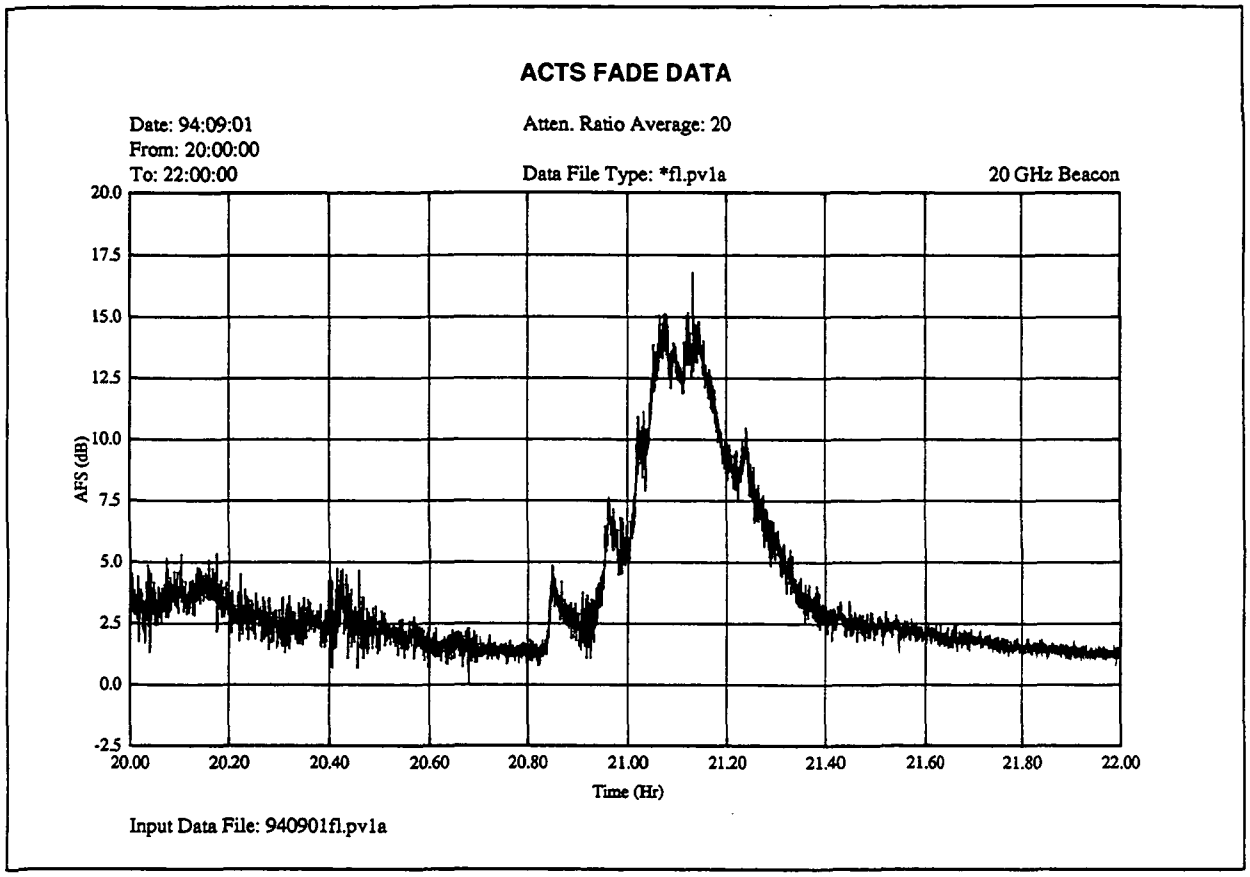

Figure 12. pv1 data: Interpolate calibration data periods with 27 GHZ data and attenuation ratio.

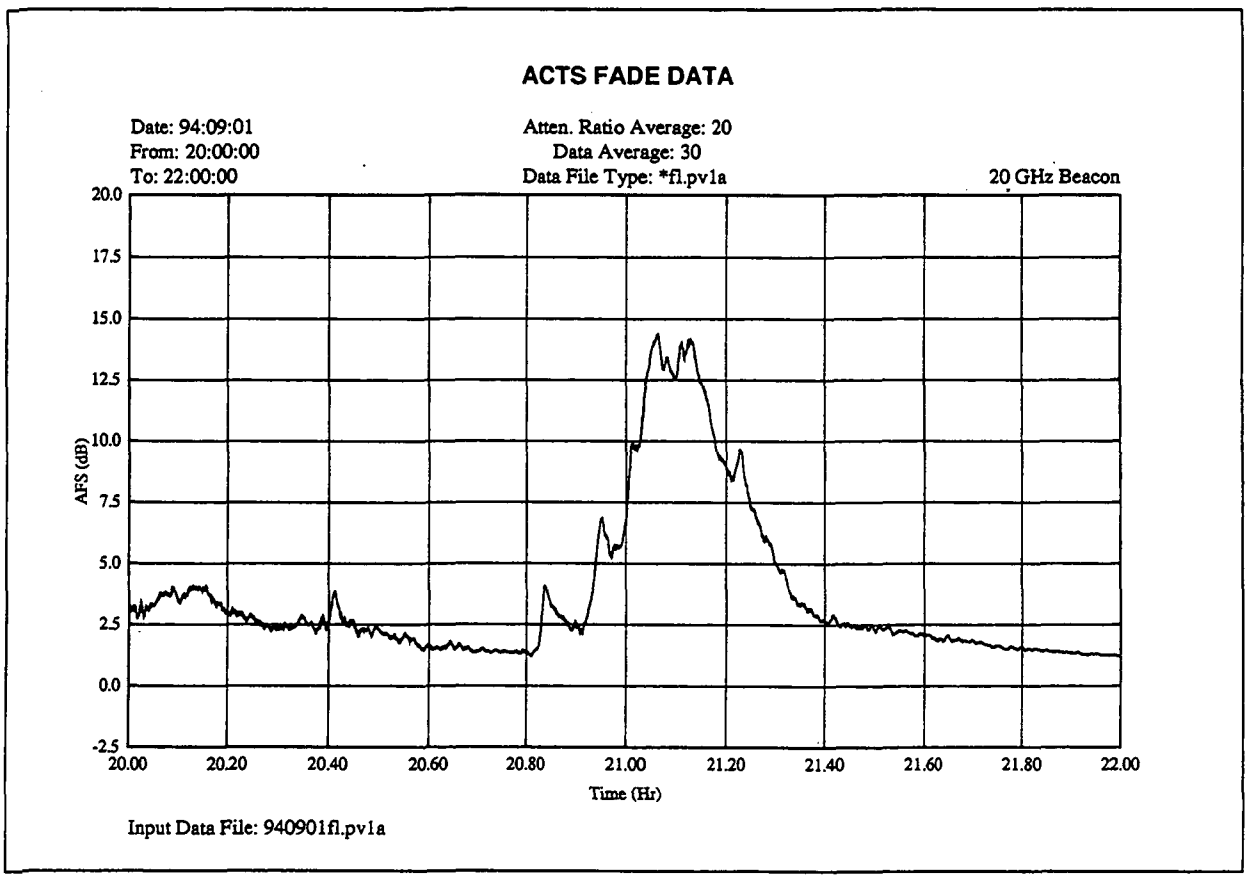

Figure 13. pv1 data: 30 sample running average - episode illustration.

27 GHz Fade Duration - 20 Sample Average

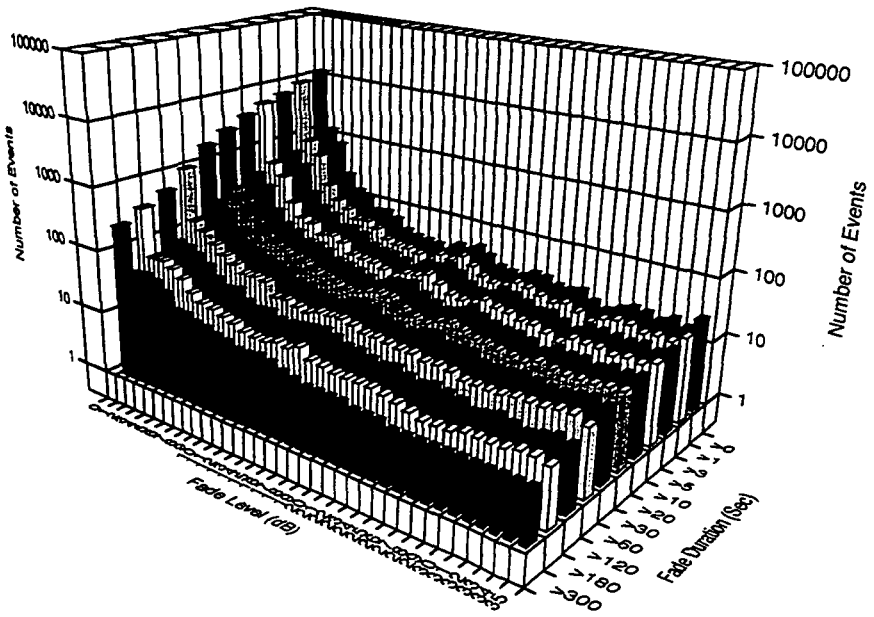

Figure 14. Fade matrix plot number of events vs fade duration and fade level.

SUMMARY

* **ACTS Florida Terminal On-Line Since November, 1993**
  Two Weather Periods: Winter/Dry and Summer/Moist
  Archived Data Available in Texas

* **Pre-processing Software Operational**
  Fine Tuning Post-processing Software

* **Fading Above New CCIR Model Predictions**
  Need Better Sub-Tropical Rain Models

* **Diversity Measurements in Sub-Tropical Areas**
  COMSTAR-GTE Measurements
  New Diversity Measurements to Begin 1995

* **Radiometer Measurements**
  Provides Simpler Fade Measurement Alternative

Figure 15. Summary.

Stanford Telecom / New Mexico State University

ACTS PROPAGATION MEASUREMENTS PROGRAM

Data Analysis Summary

Louis J. Ippolito
Julie H. Feil
Glenn Feldhake
Michael Buehrer

NAPEX XIX and APSW VII
June 14-16, 1995

Fort Collins, Colorado

STANFORD TELECOM® — ACSD

TOPICS

- INTRODUCTION
  - EXPERIMENT OBJECTIVES
  - EXPERIMENT CONFIGURATION
- ACTS K_A BAND MEASUREMENTS SUMMARY
  - SAMPLE MONTHLY ATTENUATION AND WEATHER MEASUREMENTS
  - ANNUAL CY94 STATISTICS
  - FADE DURATION STATISTICS
  - STATUS OF *.PV1 PROCESSING
- APPLICATION OF ACTS MEASUREMENTS TO TDRS SGL'S
  - FREQUENCY SCALING AND ELEVATION ANGLE SCALING
  - PEAK ATTENUATION RATIO MEASUREMENTS
  - CY94 ATTENUATION STATISTICS SUMMARY
  - TDRS SGL PERFORMANCE STATISTICS SUMMARY
- FUTURE ACTIVITIES

STANFORD TELECOM® — ACSD

STel ACTS PROPAGATION EXPERIMENT OBJECTIVES

- MEASURE AND EVALUATE Ka-BAND PROPAGATION EFFECTS AND LINK PERFORMANCE AT LAS CRUCES, NM UTILIZING AN ACTS PROPAGATION TERMINAL (APT)
- DEVELOP LONG-TERM STATISTICS AND PREDICTION MODELING TECHNIQUES FOR LAS CRUCES CLIMATE REGION FOR APPLICATION TO ADVANCED SYSTEM PLANNING AND DESIGN
- APPLY ACTS MEASUREMENTS (20.185 GHz AND 27.5 GHz) TO THE EVALUATION OF CURRENT AND PLANNED TDRS SPACE-TO-GROUND LINK (SGL) PERFORMANCE

STel ACTS PROPAGATION EXPERIMENT MEASUREMENTS

- ACTS PROPAGATION TERMINAL (APT), COLOCATED AT STGT
  - ELEVATION ANGLE TO ACTS: 51^0
  - MEASURED PARAMETERS
    - 20.185 GHGz BEACON
    - 27.5 GHz BEACON
    - 20 GHx RADIOMETER
    - 27 GHz RADIOMETER
    - RAIN RATE (CRG, TBG)
    - TEMPERATURE, RELATIVE HUMIDITY, WATER VAPOR DENSITY, WIND VECTOR
- ANCILLARY MEASUREMENTS FROM TDRS
  - 13.5 GHz SGL DELOGGED SIGNAL ATTENUATION PLOTS FOR IDENTIFIED WEATHER EVENTS ('RAINDANCE')
  - COINCIDENT STEERING DATA: DATE/TIME/ ANTENNA AZ/EL (SINCE APRIL 94)

SITE CONFIGURATION

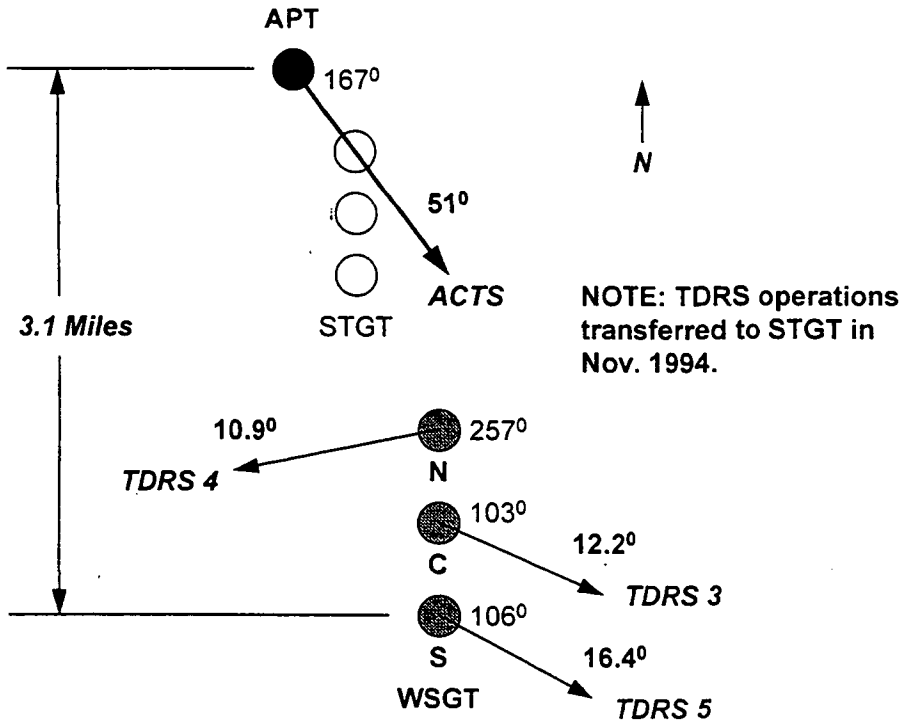

ACTS K_A BAND MEASUREMENTS SUMMARY

MONTHLY CUMULATIVE DISTRIBUTIONS FOR FREE SPACE ATTENUATION (AFS)

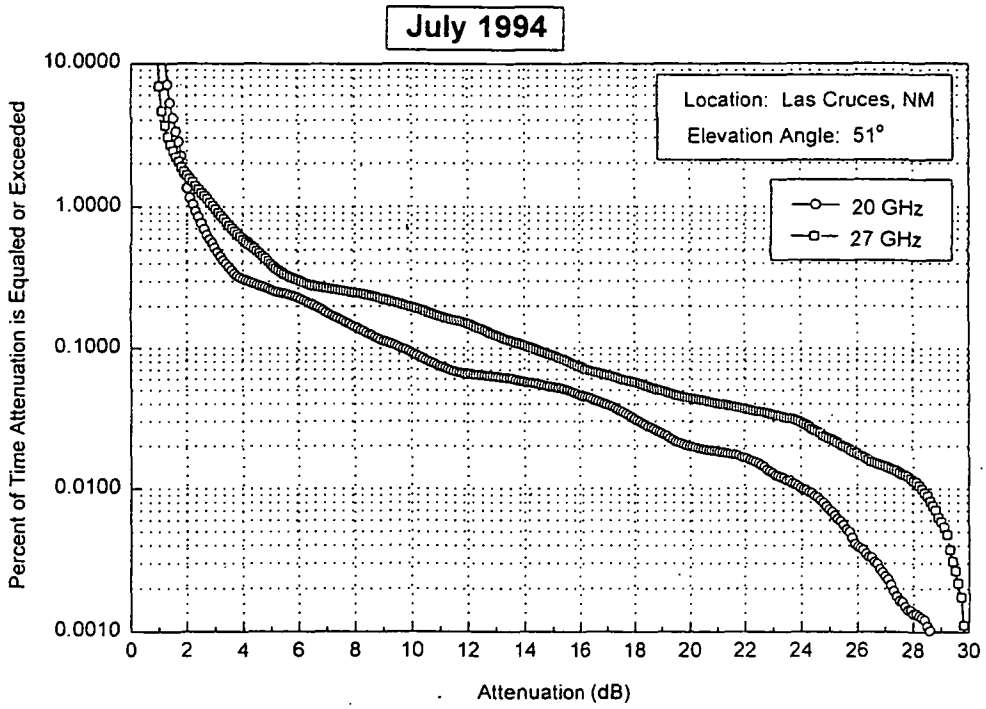

STANFORD TELECOM® — ACSD

MONTHLY CUMULATIVE DISTRIBUTIONS FOR CLEAR AIR ATTENUATION (ACA)

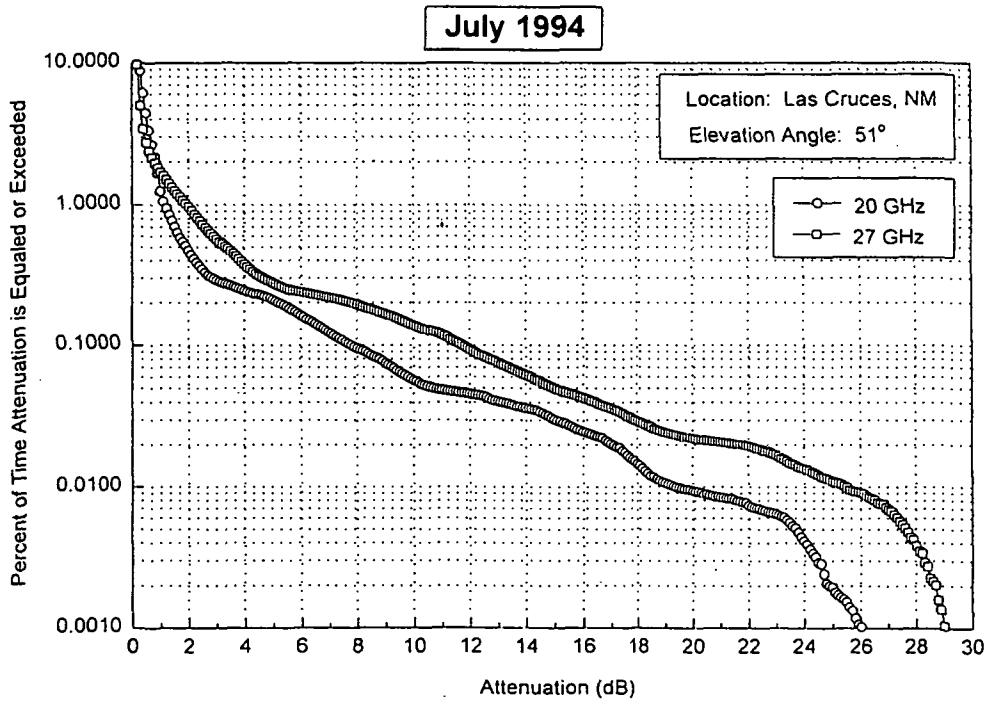

STANFORD TELECOM® — ACSD

MONTHLY SURFACE TEMPERATURE

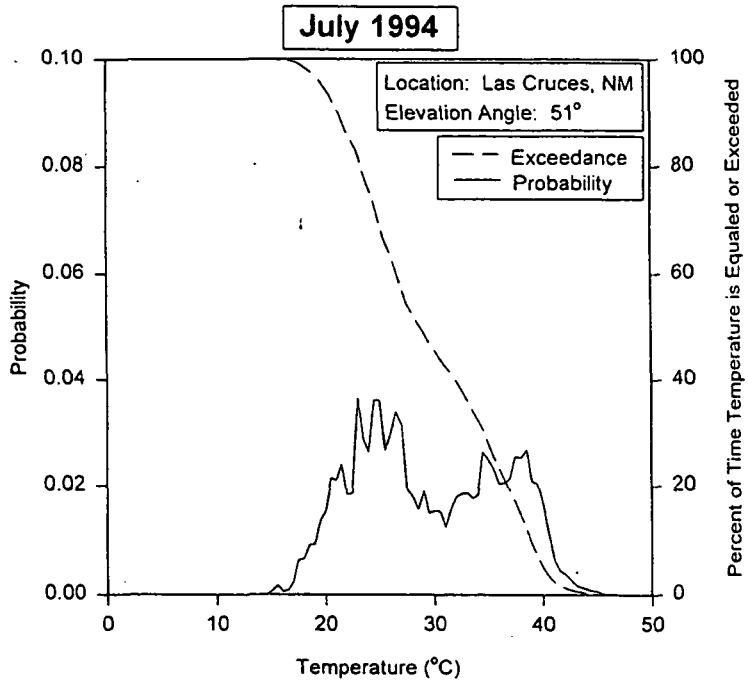

STANFORD TELECOM® — ACSD

No data for July 17-20, 1994

MONTHLY SURFACE RELATIVE HUMIDITY

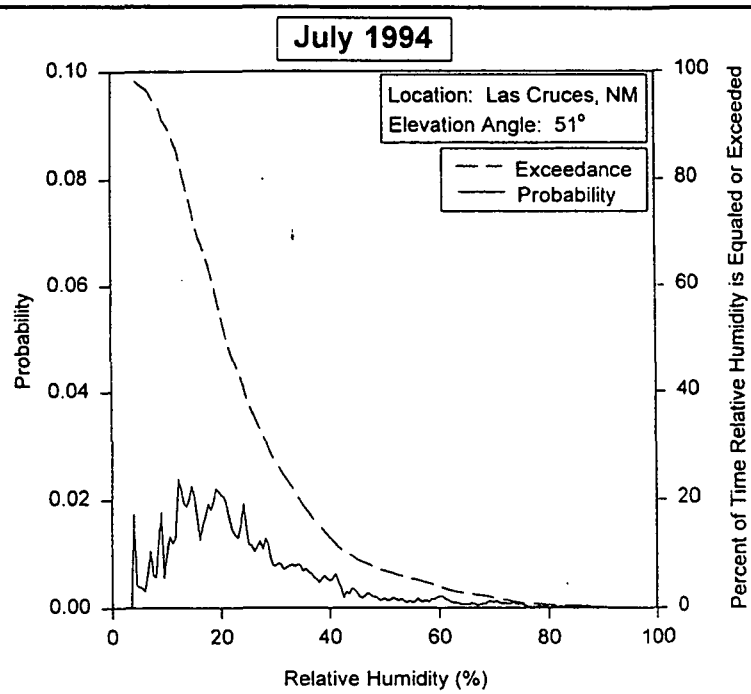

STANFORD TELECOM® — ACSD

No data for July 17-20, 1994

MONTHLY SURFACE WATER VAPOR DENSITY

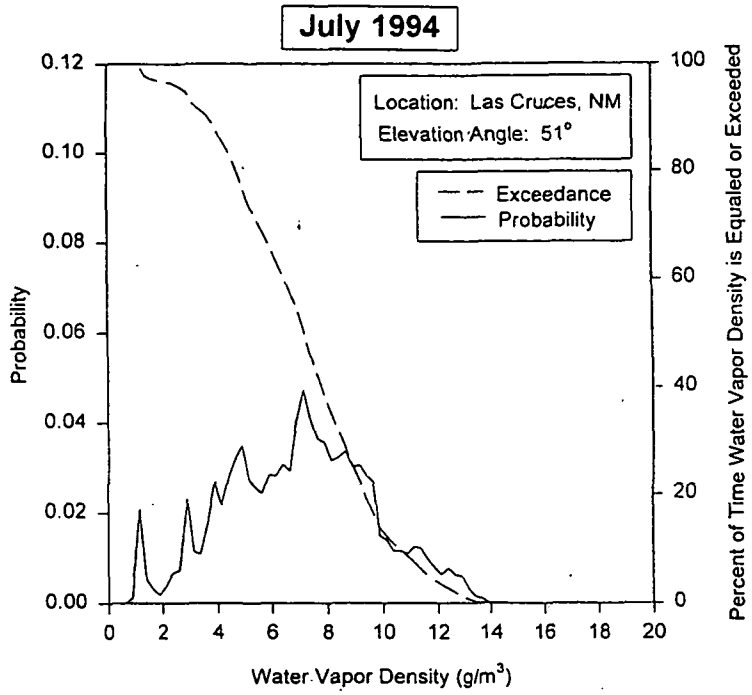

No data for July 17-20, 1994

STANFORD TELECOM® — ACSD

ANNUAL CUMULATIVE DISTRIBUTIONS FOR FREE SPACE ATTENUATION (AFS)

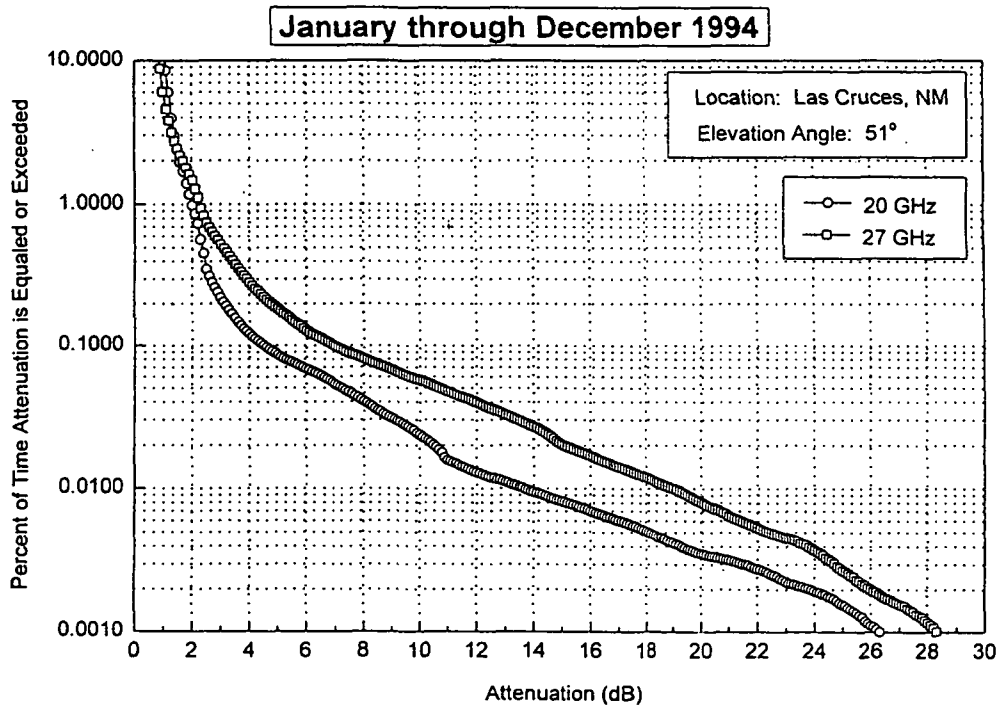

STANFORD TELECOM® — ACSD

ANNUAL CUMULATIVE DISTRIBUTIONS FOR CLEAR AIR ATTENUATION (ACA)

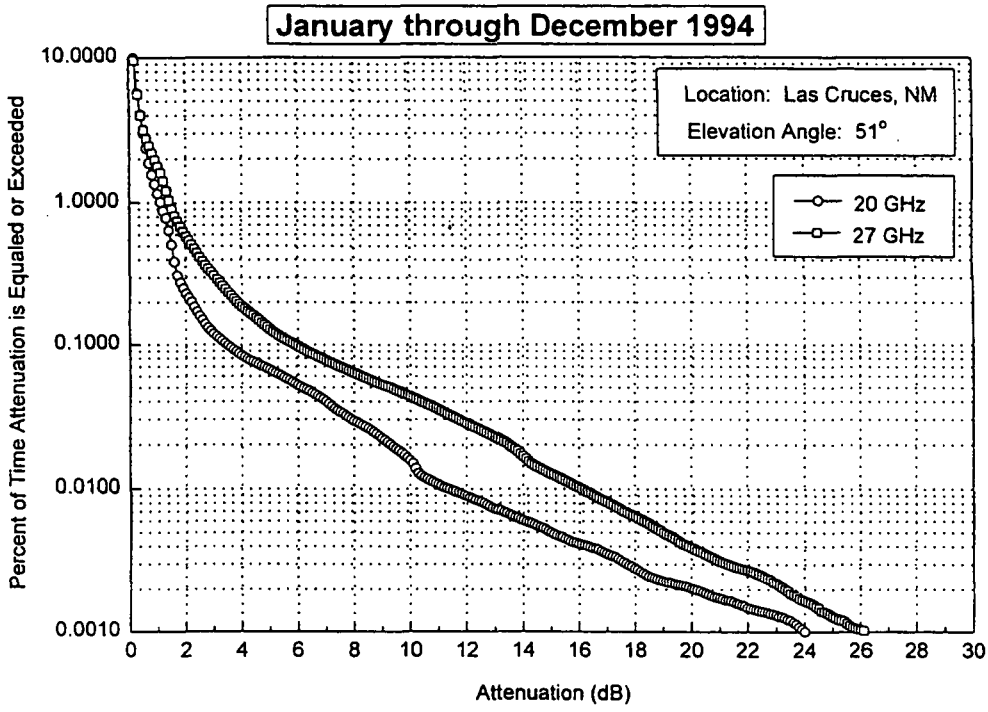

STATISTICAL ATTENUATION RATIO (ARS) FOR CLEAR AIR ATTENUATION (ACA)

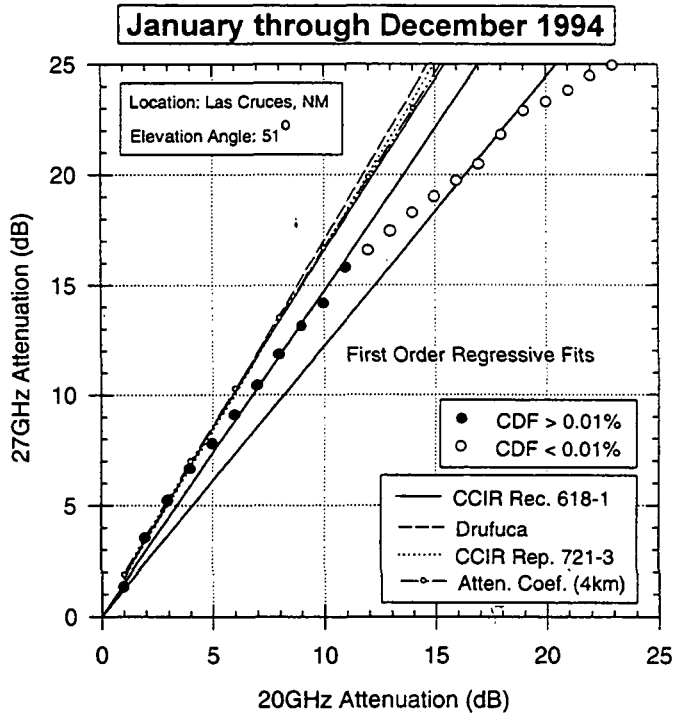

All ARS points
Δ27/Δ20 = 1.2208
Best Fit: CCIR Rec. 618-1
Error: 1.8385

ARS points for CDF > 0.01%
Δ27/Δ20 = 1.4726
Best Fit: CCIR Rec. 618-1
Error: 0.1138

STATISTICAL ATTENUATION RATIO (ARS) FOR RADIOMETER DERIVED ATTENUATION (ARD)

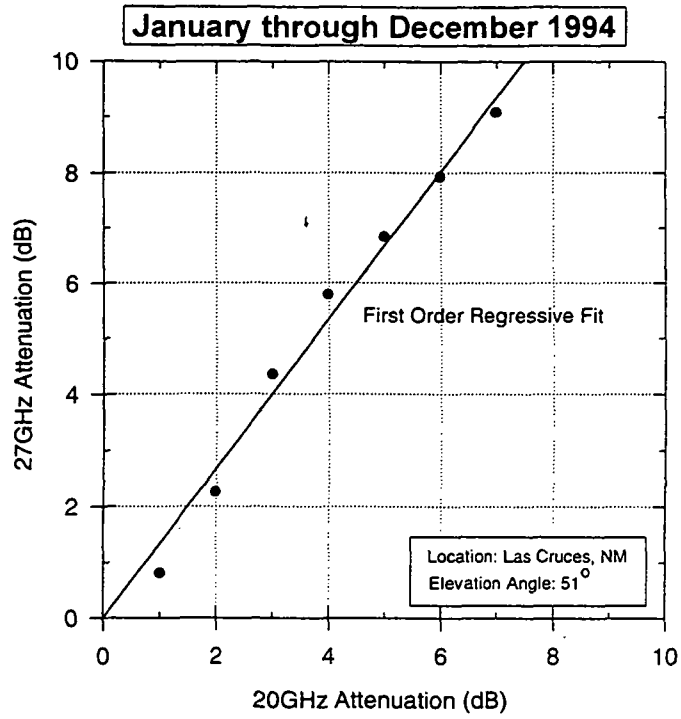

All ARS points Δ27/Δ20 = 1.3356
All points have cdf % > 0.01%.

STANFORD TELECOM® — ACSD

ANNUAL CUMULATIVE DISTRIBUTIONS FOR SURFACE TEMPERATURE

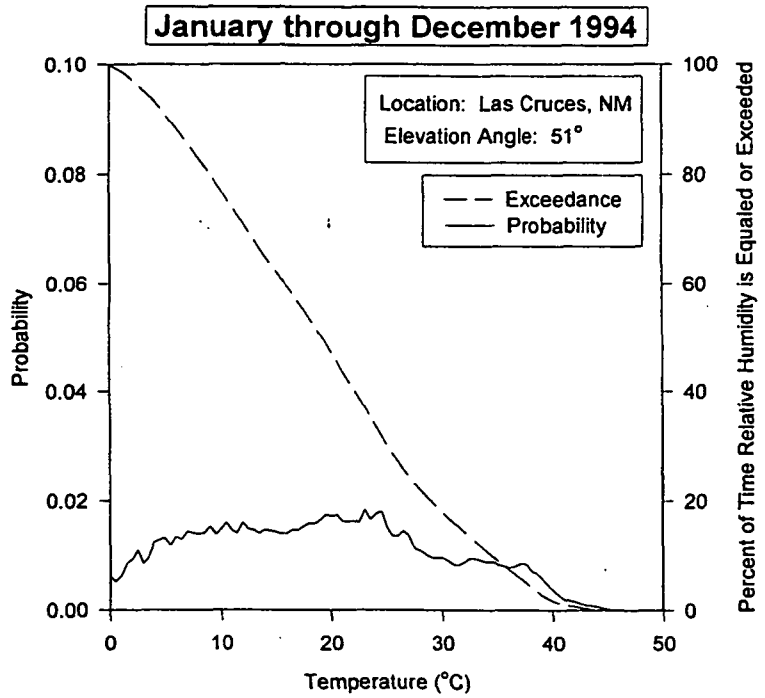

STANFORD TELECOM® — ACSD

ANNUAL CUMULATIVE DISTRIBUTIONS FOR SURFACE RELATIVE HUMIDITY

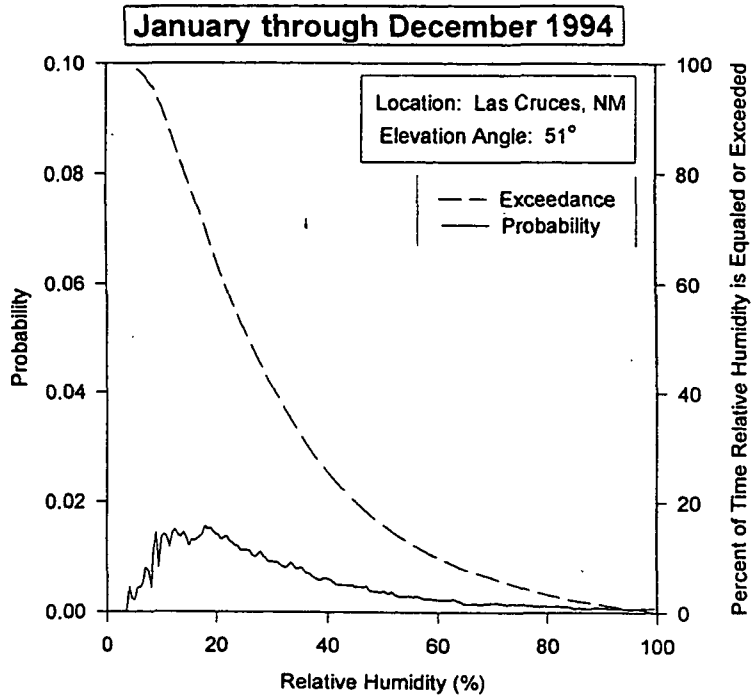

ANNUAL CUMULATIVE DISTRIBUTIONS FOR SURFACE WATER VAPOR DENSITY

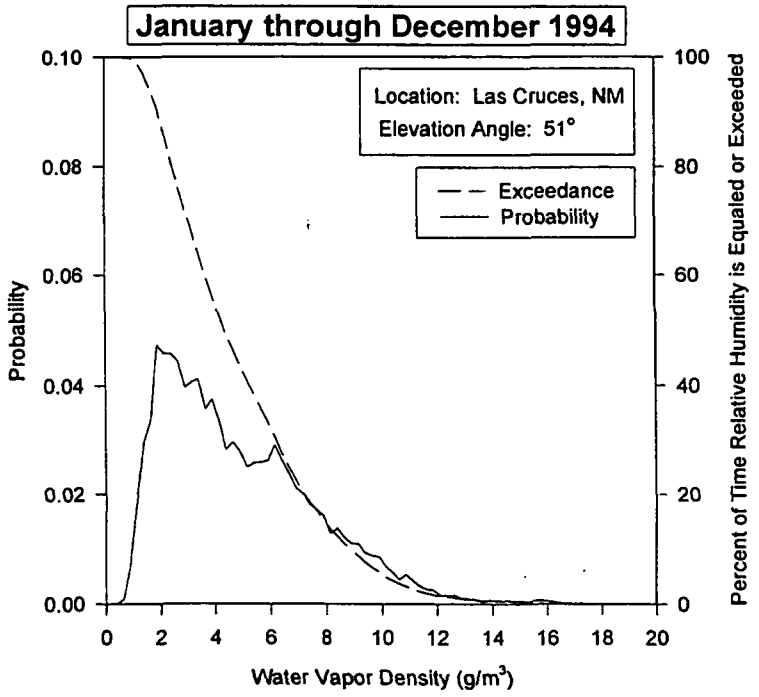

20 GHz FADE DURATION DISTRIBUTIONS

January through December 1994

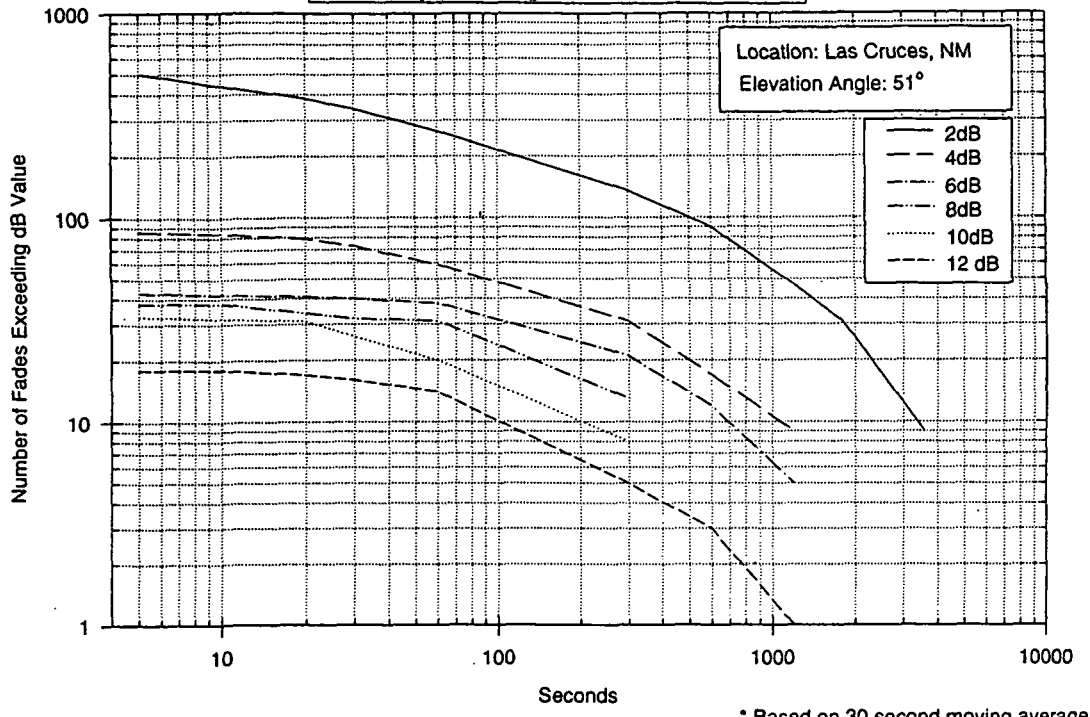

* Based on 30 second moving average

STANFORD TELECOM® — ACSD

27 GHz FADE DURATION DISTRIBUTIONS

January through December 1994

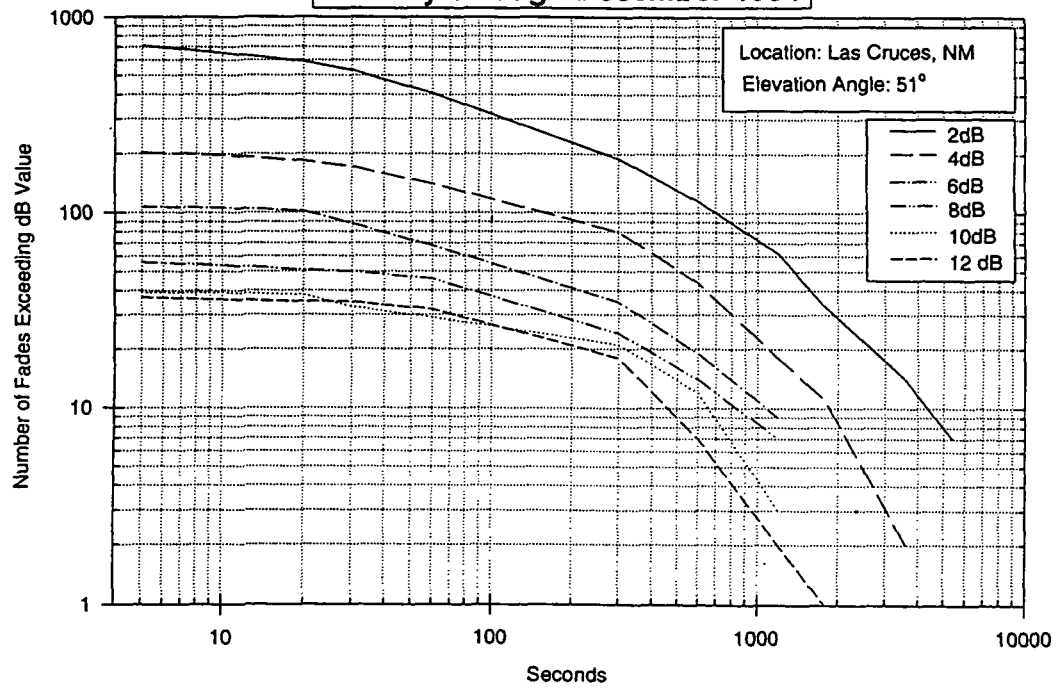

* Based on 30 second moving average

STANFORD TELECOM® — ACSD

FADE EVENT ON NOVEMBER 3, 1994

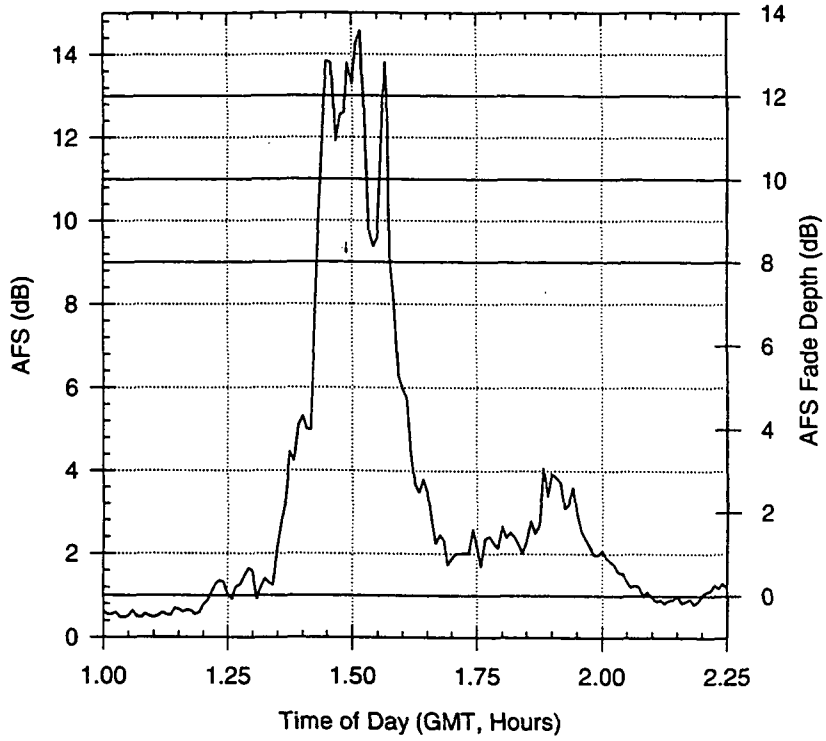

STANFORD TELECOM® — ACSD

COMPARISON OF 20 GHz AFS DISTRIBUTIONS FOR CY 1994

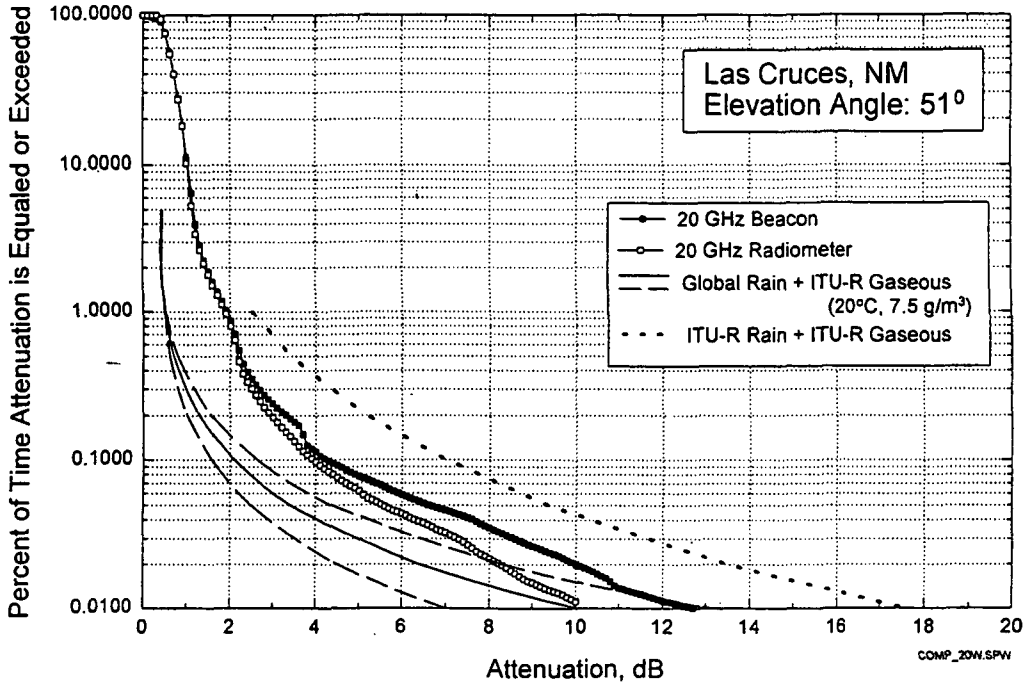

STANFORD TELECOM® — ACSD

COMPARISON OF 27 GHz AFS DISTRIBUTIONS FOR CY 1994

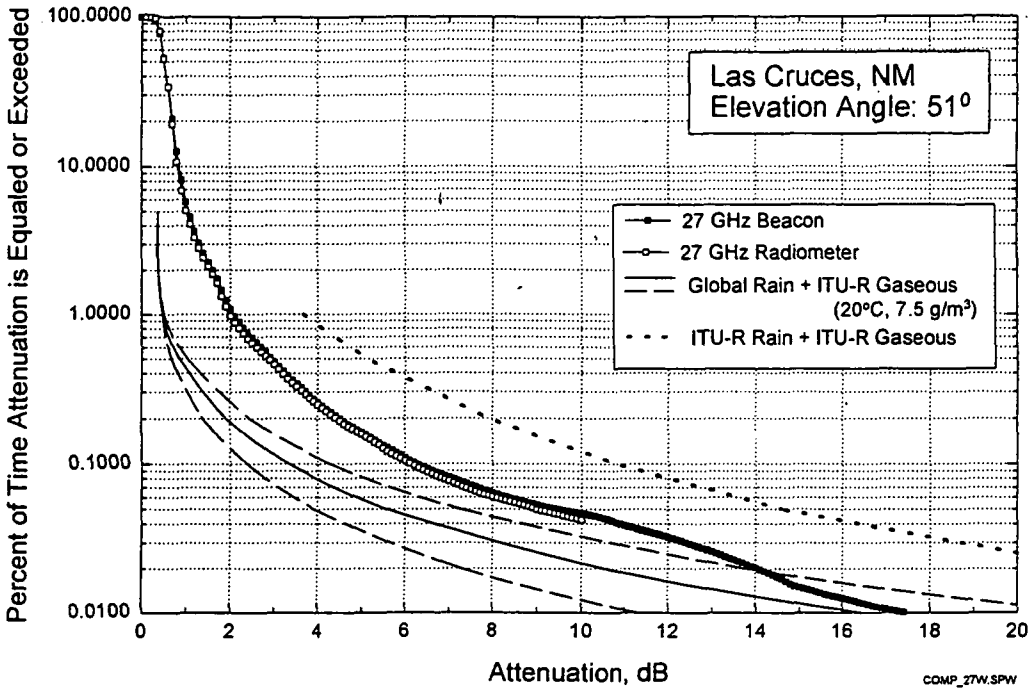

STATUS OF *.PV1 PROCESSING

- FIVE MONTHS PROCESSED
  - 1994: JULY, DECEMBER
  - 1995: JANUARY, FEBRUARY, MARCH
- INCONSISTENCIES BETWEEN CDF's GENERATED FROM *.pv0 AND FROM *.pv1
  - WITHIN EACH MONTH AND BETWEEN MONTHS
- CAUSE(S) OF INCONSISTENCIES UNDER INVESTIGATION
  - ACTSPP51
  - STeL POST PROCESSING

APPLICATION OF ACTS MEASUREMENTS TO EVALUATION OF TDRS SPACE-TO-GROUND LINKS

PREDICTED RAIN ATTENUATION DISTRIBUTIONS FOR TDRS 13.5 GHz SPACE-GROUND-LINKS FROM CRANE GLOBAL MODEL

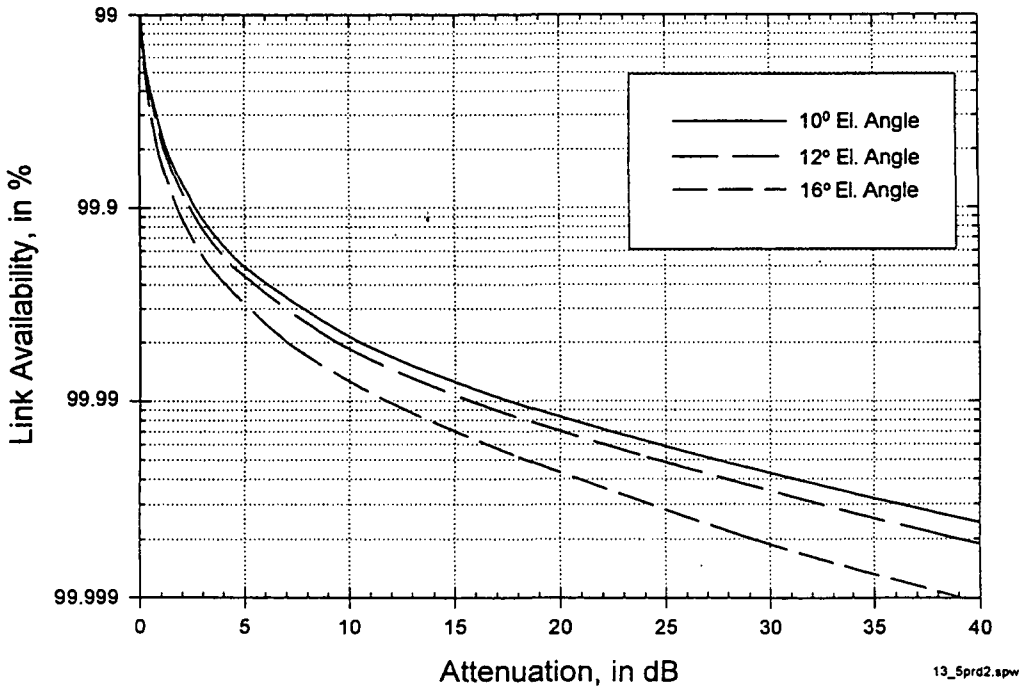

TDRS 13.5 GHz ANNUAL ATTENUATION DISTRIBUTIONS PREDICTED FROM MEASURED 20 & 27 GHz AFS DISTRIBUTIONS

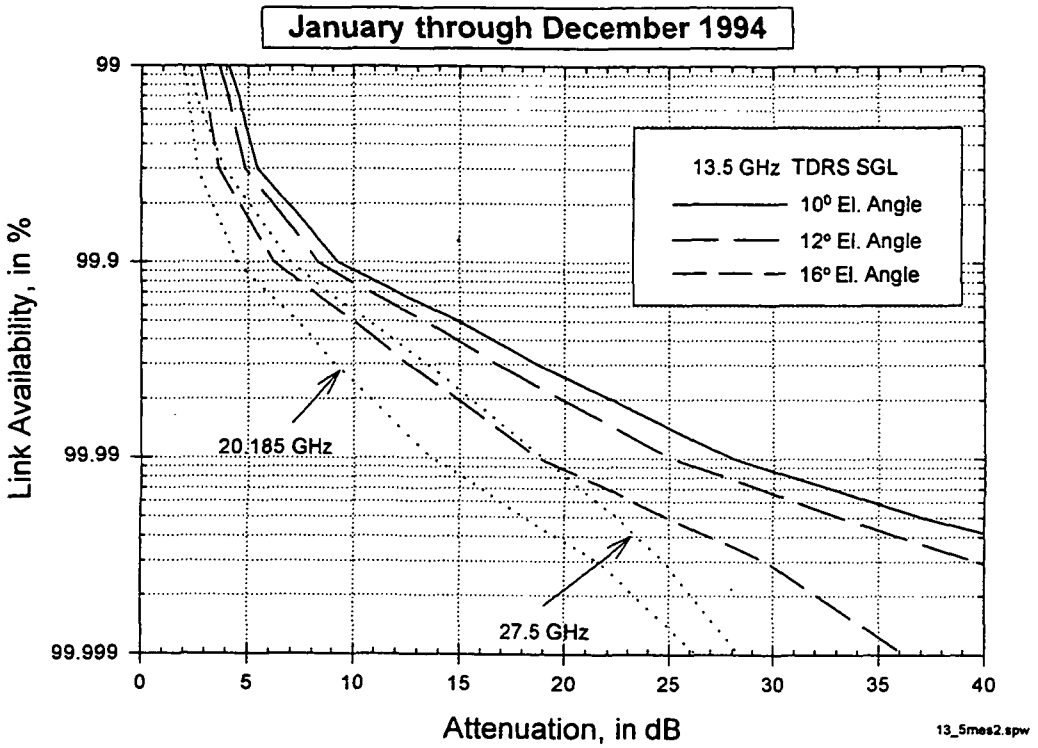

STANFORD TELECOM® — ACSD

TDRS 13.5 GHz ANNUAL ATTENUATION DISTRIBUTIONS PREDICTED FROM MEASURED 20 & 27 GHz ACA DISTRIBUTIONS

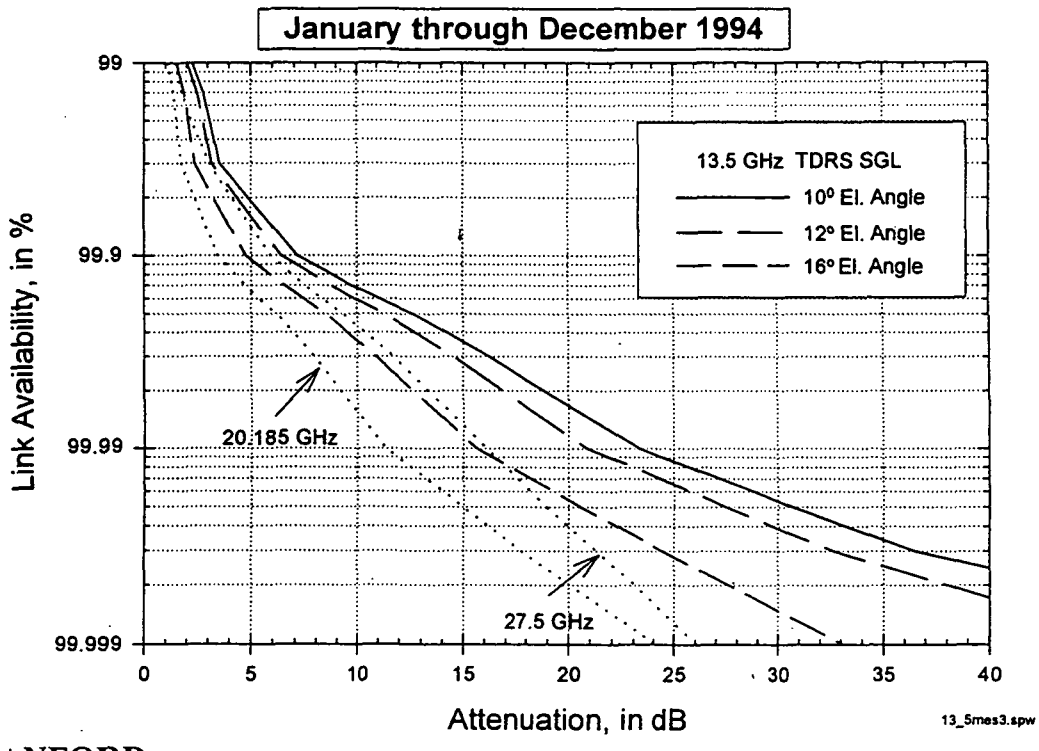

STANFORD TELECOM® — ACSD

ATTENUATION RATIO FOR PEAK 13.5, 20.185, AND 27.5 GHz MEASUREMENTS

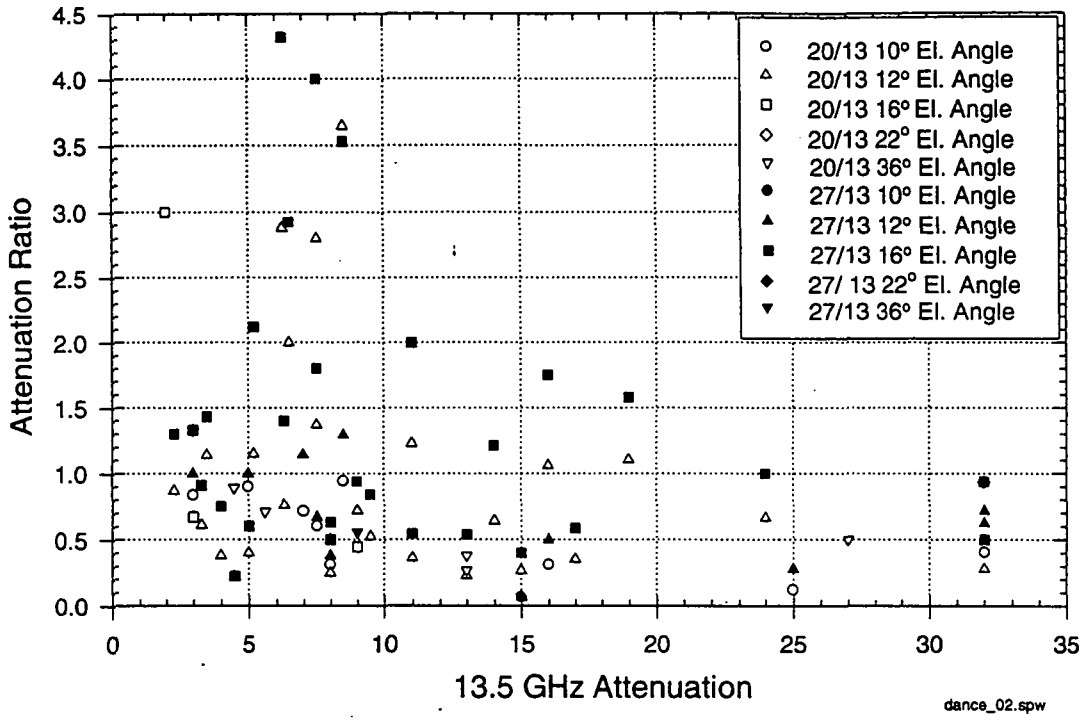

STANFORD TELECOM® —ACSD

ATTENUATION RATIO MEASUREMENTS: ACTS & TDRS-E
Az = 257°, El = 10°

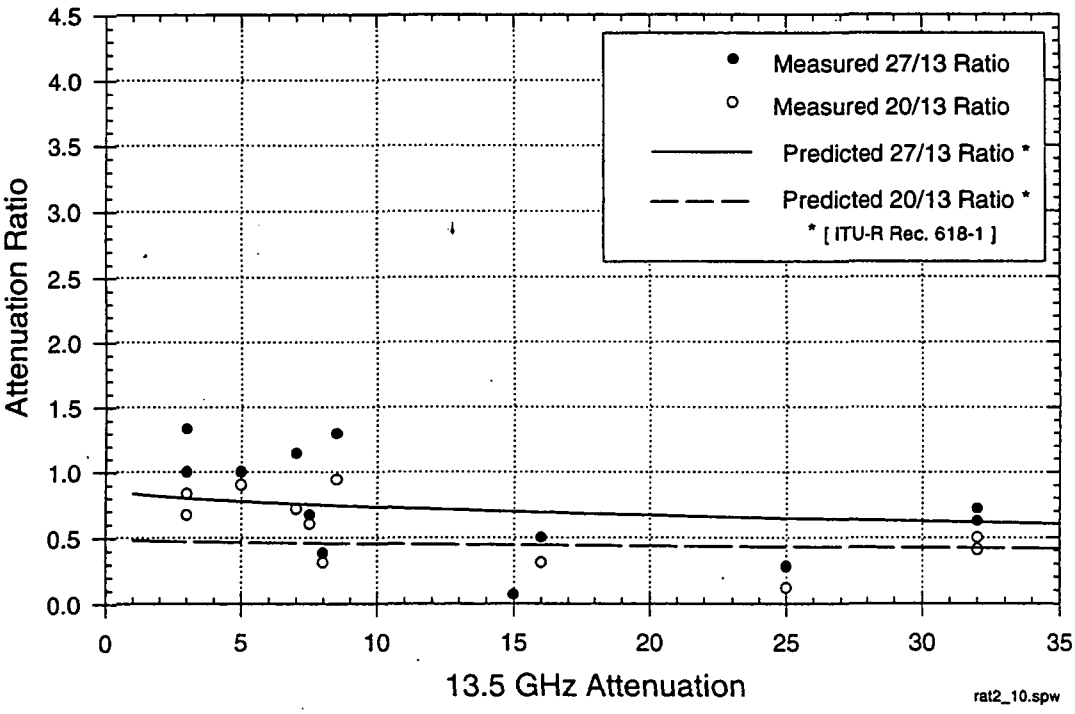

STANFORD TELECOM® —ACSD

ATTENUATION RATIO MEASUREMENTS: ACTS & TDRS-D
Az = 103°, El = 12°

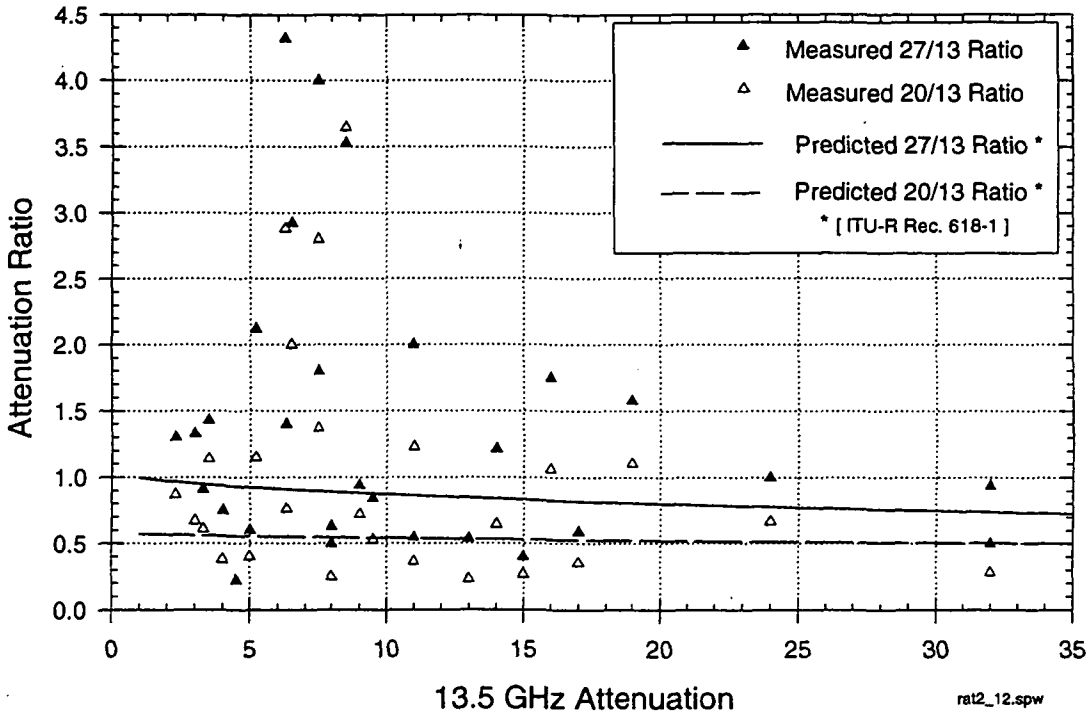

STANFORD TELECOM® — ACSD

ATTENUATION RATIO MEASUREMENTS: ACTS & TDRS-5
Az = 106°, El = 16°

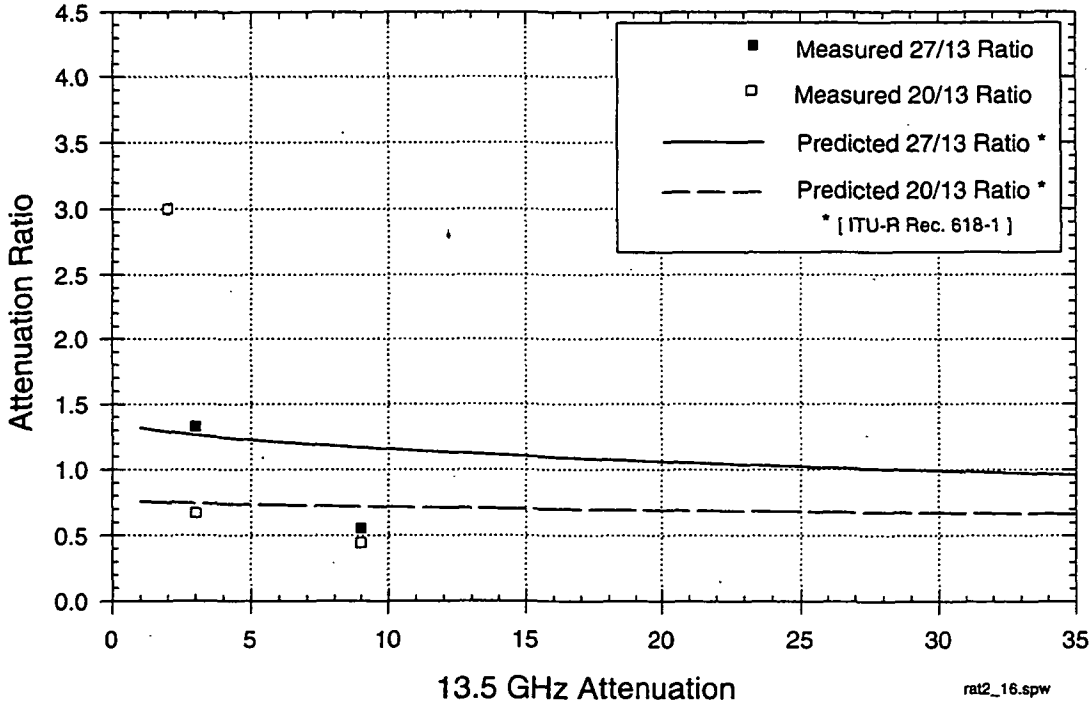

STANFORD TELECOM® — ACSD

ATTENUATION RATIO MEASUREMENTS: ACTS & TDRS-C
Az = 250°, El = 22°

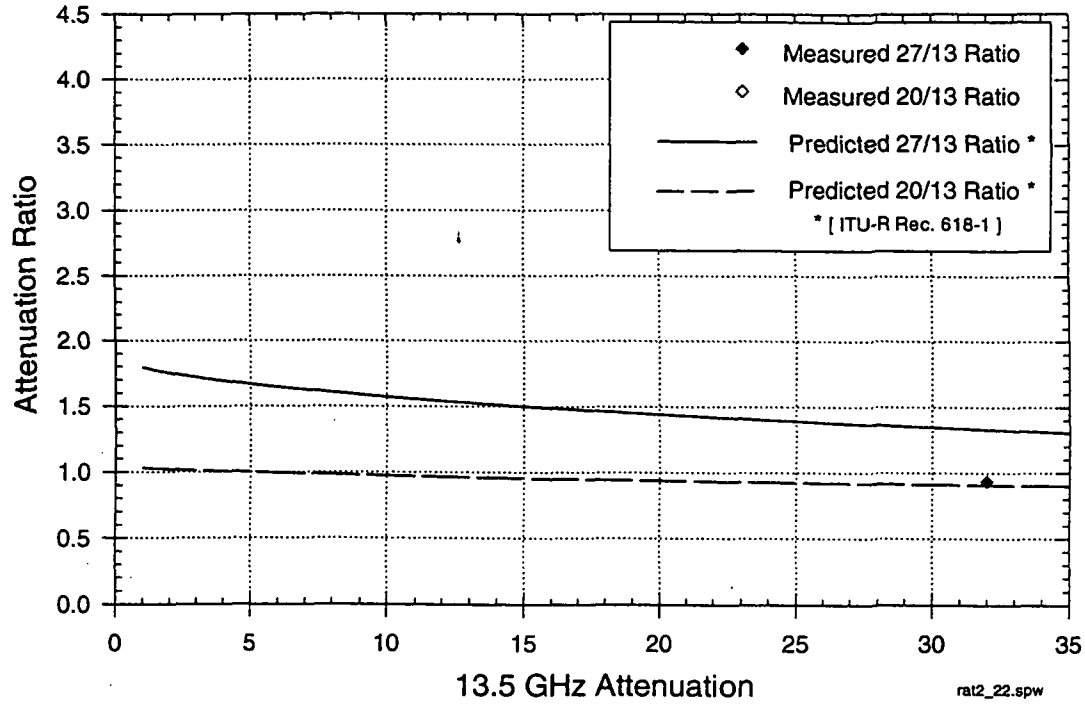

ATTENUATION RATIO MEASUREMENTS: ACTS & TDRS-C
Az = 131°, El = 36°

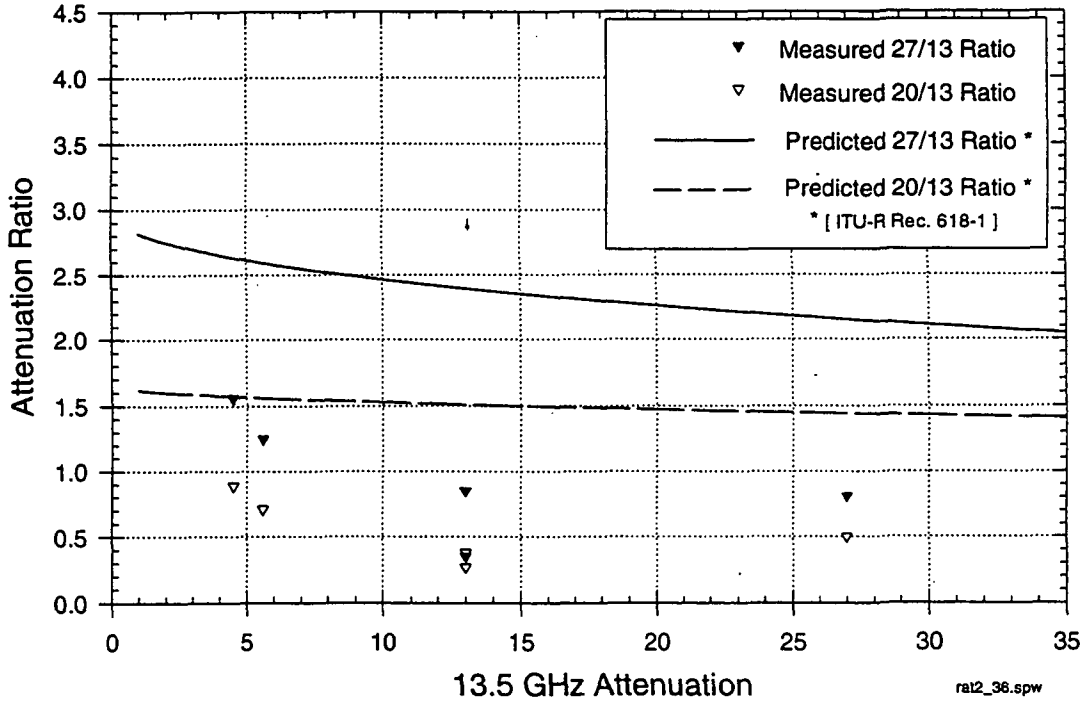

SUMMARY FOR PEAK MEASURED ATTENUATION FOR TDRS 13.5 GHz SGL

January through November 1994

		TDRS SGL Elevation Angle					
		10°	12°	15° - 16°	22°	32°	36°
Measured Peak Attenuation		>32 dB	>32 dB	31 dB	>32 dB	14 dB	27 dB
Date		8/2-3	9/4	9/4	7/17	7/9	5/25
Duration (min)	> 1 dB	115	81	62	49.5	26	51
	>10 dB	33.5	42	27	21	6	6

SUMMARY TDRS 13.5 GHz SGL PERFORMANCE

January through December 1994

Link Availability	*CY94 Attenuation (AFS) Exceedance (dB)**		
SGL El. Angle ►	10°	12°	16°
95%	2.56	2.29	1.72
99%	4.09	3.66	2.74
99.5%	4.85	4.34	3.25
99.7%	5.43	4.86	3.64
99.9%	9.27	8.30	6.21
99.95%	14.92	13.35	9.99
99.99%	28.05	25.10	18.79

* scaled from ACTS 27.5 and 20.185 GHz beacon measurements

SEVERE RAIN EVENT - STel, RESTON, VA

May 18, 1995

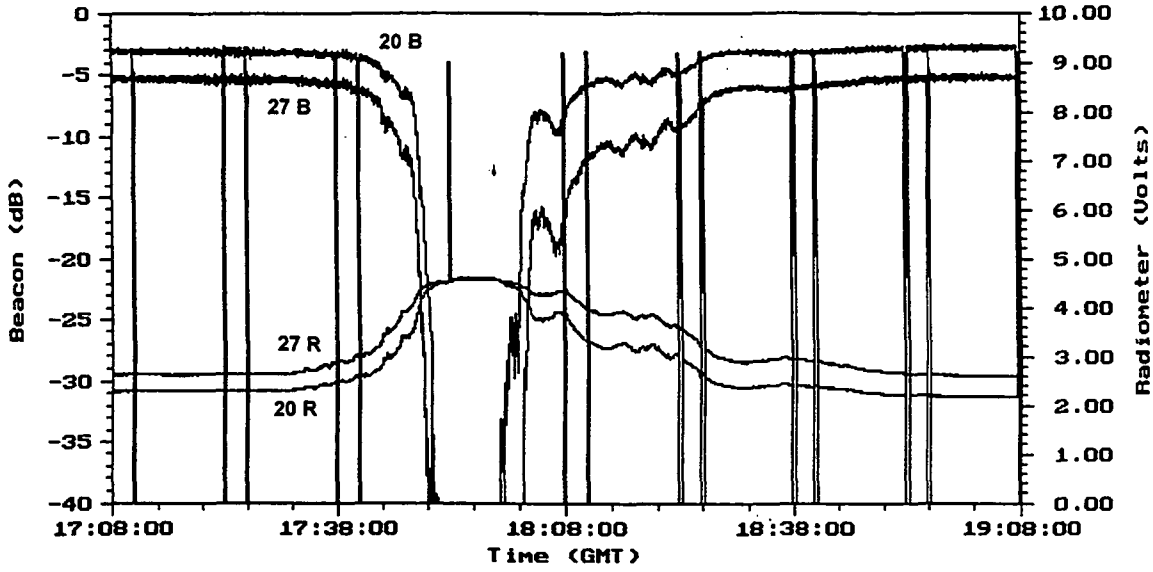

FUTURE ACTIVITIES

- GENERAL
  - COMPLETE DEVELOPMENT/DEBUG OF *.PV1 PRE-PROCESSING SOFTWARE
  - INCLUSION OF WHITE SANDS RADIOSONDE DATA FROM THE ARMY ATMOSPHERIC SCIENCES LAB
  - EXTEND ACTS LINK ANALYSIS WITH INITIATION OF STel RESTON FACILITY APT MEASUREMENTS (APRIL 95)

- APPLICATION OF ACTS MEASUREMENTS TO TDRS SGL'S
  - EXTEND ANALYSIS TO K_A-BAND SGL OPTIONS
  - DEVELOP ANNUAL FADE DEPTH/DURATION STATISTICS FOR SGL LINKS
  - EVALUATE LONG TERM FREQUENCY/ELEVATION ANGLE SCALING ALGORITHMS
  - INTEGRATE ELECTRONIC 'RAINDANCE' DATA INTO ACTS APT ANALYSIS

NEW MEXICO APT STATUS REPORT

Stephen Horan
New Mexico State University

Presented at
ACTS Propagation Studies Workshop VII
June 15, 1995

I.1 STATISTICS: HOURS OF UP TIME

Operational Statistics						
		Total Time				
Month	**Status**	**Days**	**Hours**	**Minutes**	**Seconds**	**% of Total**
December	Up	31	0	0	0	100%
	Down	0	0	0	0	0%
January	Up	30	23	18	0	99.91%
	Down	0	0	42	0	0.09%
February	Up	28	0	0	0	100.00%
	Down	0	0	0	0	0.00%
March	Up	31	0	0	0	100.00%
	Down	0	0	0	0	0.00%
April	Up	29	23	34	50	99.95%
	Down	0	0	25	10	0.05%
May	Up	30	22	18	45	99.77%
	Down	0	1	41	15	0.23%
Total	Up	181	21	11	35	99.94%
	Down	0	2	48	25	0.06%

I.2 CALIBRATION: DATES OF ALL CALIBRATIONS, EXTERNAL AIR TEMP AT CALIBRATION

Calibration Record		
Month	**Day**	**Air Temperature (°C)**
December	none performed	
January	20	12.40
	20	11.30
February	6	17.50
	18	11.50
March	2	16.40
	17	23.70
April	3	23.80
	17	15.40
May	1	27.60
	8	23.20
	26	30.00

I.3 CALIBRATION: DATES OF CRG CALIBRATIONS

CRG Calibration Record	
Month	**Date**
December	7
	16
	19
	27
January	20
February	6
	18
March	2
April	3
	17
May	1
	26

I.4 SUN INTRUSION DATES

March SUN INTRUSION DATES	
DATE	**SATURATING?**
4	no
5	no
6	20 GHz only
7	Both channels
8	Both channels
9	no
10	no

I.5 OPERATIONS CHANGES/PROBLEMS

1. FEED HORN CRACKED IN JANUARY - REPLACED WITH SPARE

2. APRIL 23 LOSS OF TIME DUE TO SITE-WIDE POWER GLITCH?

3. APRIL 28 HAD KEYBOARD HANG AND SYSTEM DID NOT RE-BOOT PROPERLY - LOST DATA
   - TIME ON REAL-TIME DISPLAY AND RUNNING GRAPH IS 3 TO 5 MINUTES DIFFERENT
   - WWV TIME IS USUALLY ONLY RECEIVED A FEW TIMES PER WEEK ACCORDING TO CTS-10 SOFTWARE

4. INSTALLED RF TEMPERATURE CONTROLLER AND UPPER SHROUD

5. UNSUCCESSFUL IN MAKING THE NEW PREPROCESSING SOFTWARE CONVERGE CORRECTLY TO REALISTIC VALUES

2.1 OTHER ACTIVITIES

1. RAIN GAUGE CALIBRATION REPORT FINISHED
   - RECOMMEND THAT A SMOOTHING ALGORITHM BE USED RATHER THAN TWO-POINT SLOPES AS COMPUTED WITH ACTSVIEW

2. SUN INTRUSION PREDICTION PROGRAM GENERATED
   - MARYLAND REPORTS SEVERAL HOURS DIFFERENCE BETWEEN PREDICTED AND ACTUAL INTRUSION
   - NEW MEXICO PREDICTIONS ARE CORRECT
   - IF ANYONE WISHES TO SEND ME THEIR ACTUAL INTRUSION TIMES, I WILL TRY TO FIND THE PROBLEM!

3. GLENN FELDHAKE HAS GRADUATED AND MOVED ONTO WORKING FOR LOU IPPOLITO AT STEL.

Standard Ranging Tone Times Files
OK Radiometer and Beacon Calibrations
11/03/93 - 5/31/95 OK CDFs
Excel Macro - ACTS01.xls

X. Wang, R. K. Crane and P. C. Robinson

June, 1995

School of Meteorology
University of Oklahoma
Norman, Oklahoma

1. Standard Ranging Tone Times Files.

1) A ranging tone is typically switched on around the half hour with 0.36 dB increase in 20G beacon power level, switched off either with or without about 10 seconds 1.4 dB increase in the power level about 5 - 6 minutes later.
2) ACTSPP can find most ranging tones successfully, but fail occasionally, especially during deep fading and system maintenance.
3) ACTSVIEW is used to find the mis-detected ranging tones. But during deep fading and system operation this method is almost useless.
4) By checking with the .rv0 files of the same period from other sites, the missing tones in 3) can be found.
5) Problem arises when the timestamps of these cross-checking sites are not synchronized together. How to handle this problem needs suggestion.
6) Need access to most recent .rv0 files of other sites (at least two sites), so that the standard ranging tone times file can be posted at the end of the month.

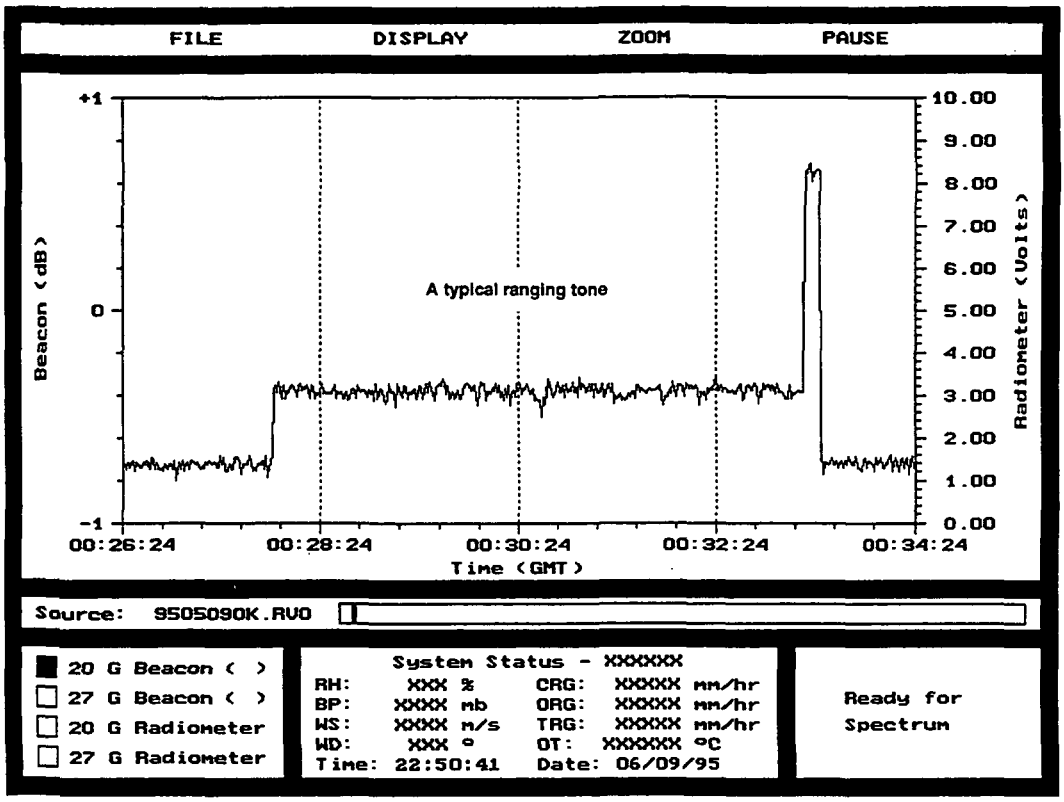
FILE
DISPLAY
ZOOM
PAUSE
+1
0
-1
Beacon (dB)
A typical ranging tone
10.00
9.00
8.00
7.00
6.00
5.00
4.00
3.00
2.00
1.00
0.00
Radiometer (Volts)
00:26:24
00:28:24
00:30:24
00:32:24
00:34:24
Time (GMT)
Source: 9505090K.RVO
20 G Beacon ( )
27 G Beacon ( )
20 G Radiometer
27 G Radiometer
System Status - XXXXXX
RH: XXX %
BP: XXXX mb
WS: XXXX m/s
WD: XXX °
CRG: XXXXX mm/hr
ORG: XXXXX mm/hr
TRG: XXXXX mm/hr
OT: XXXXXX °C
Time: 22:50:41
Date: 06/09/95
Ready for
Spectrum

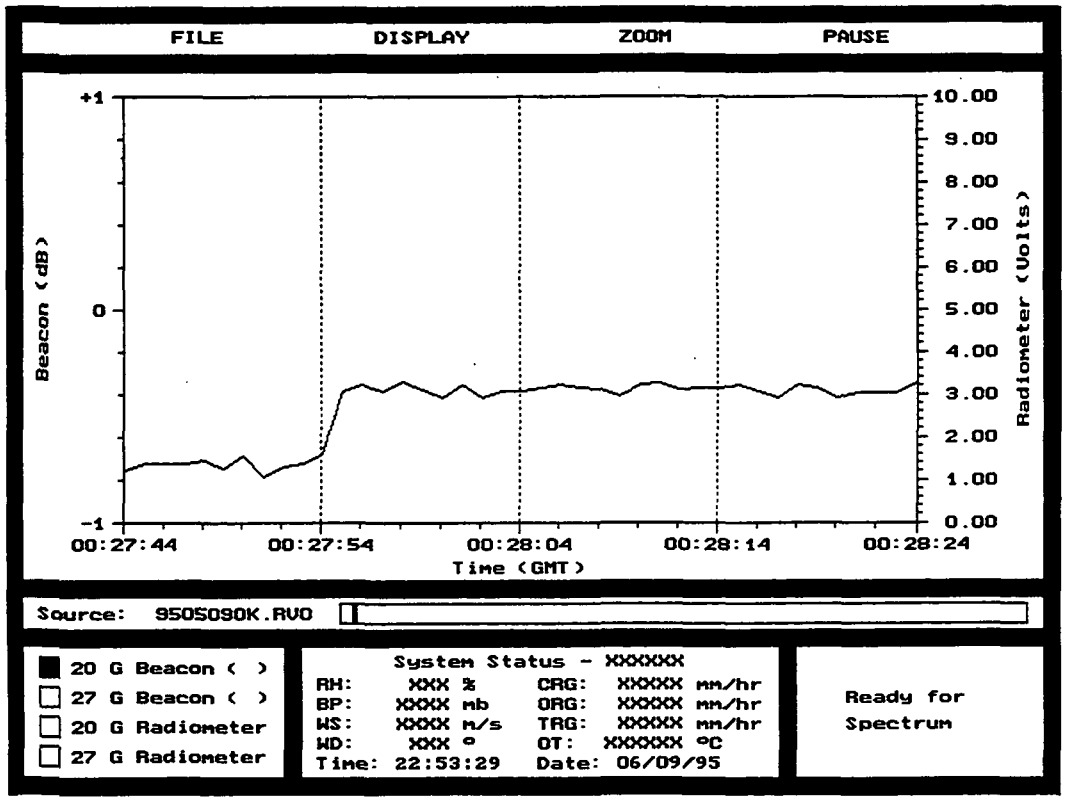
FILE
DISPLAY
ZOOM
PAUSE
+1
0
-1
Beacon (dB)
10.00
9.00
8.00
7.00
6.00
5.00
4.00
3.00
2.00
1.00
0.00
Radiometer (Volts)
00:27:44
00:27:54
00:28:04
00:28:14
00:28:24
Time (GMT)
Source: 9505090K.RVO
20 G Beacon ( )
27 G Beacon ( )
20 G Radiometer
27 G Radiometer
System Status - XXXXXX
RH: XXX %
BP: XXXX mb
WS: XXXX m/s
WD: XXX °
CRG: XXXXX mm/hr
ORG: XXXXX mm/hr
TRG: XXXXX mm/hr
OT: XXXXXX °C
Time: 22:53:29
Date: 06/09/95
Ready for
Spectrum

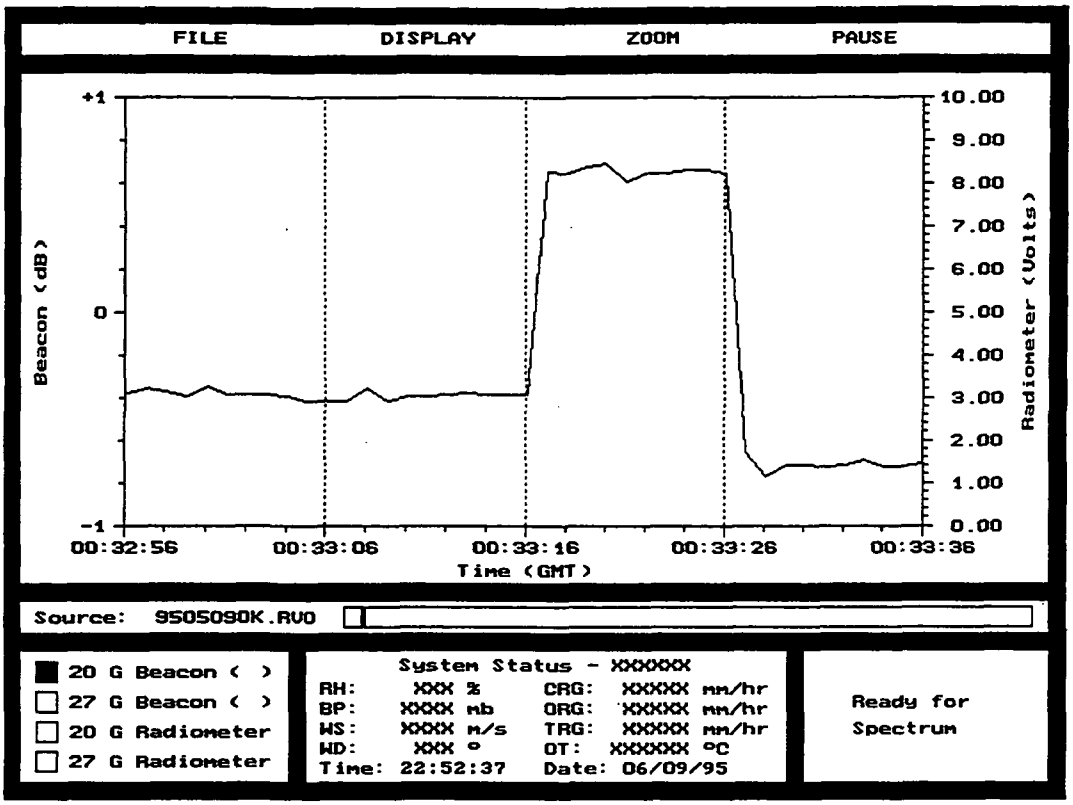
FILE
DISPLAY
ZOOM
PAUSE
+1
0
-1
Beacon (dB)
10.00
9.00
8.00
7.00
6.00
5.00
4.00
3.00
2.00
1.00
0.00
Radiometer (Volts)
00:32:56
00:33:06
00:33:16
00:33:26
00:33:36
Time (GMT)
Source: 9505090K.RV0
20 G Beacon ( )
27 G Beacon ( )
20 G Radiometer
27 G Radiometer
System Status - XXXXXX
RH: XXX %
BP: XXXX mb
WS: XXXX m/s
WD: XXX °
CRG: XXXXX mm/hr
ORG: XXXXX mm/hr
TRG: XXXXX mm/hr
OT: XXXXXX °C
Time: 22:52:37
Date: 06/09/95
Ready for
Spectrum

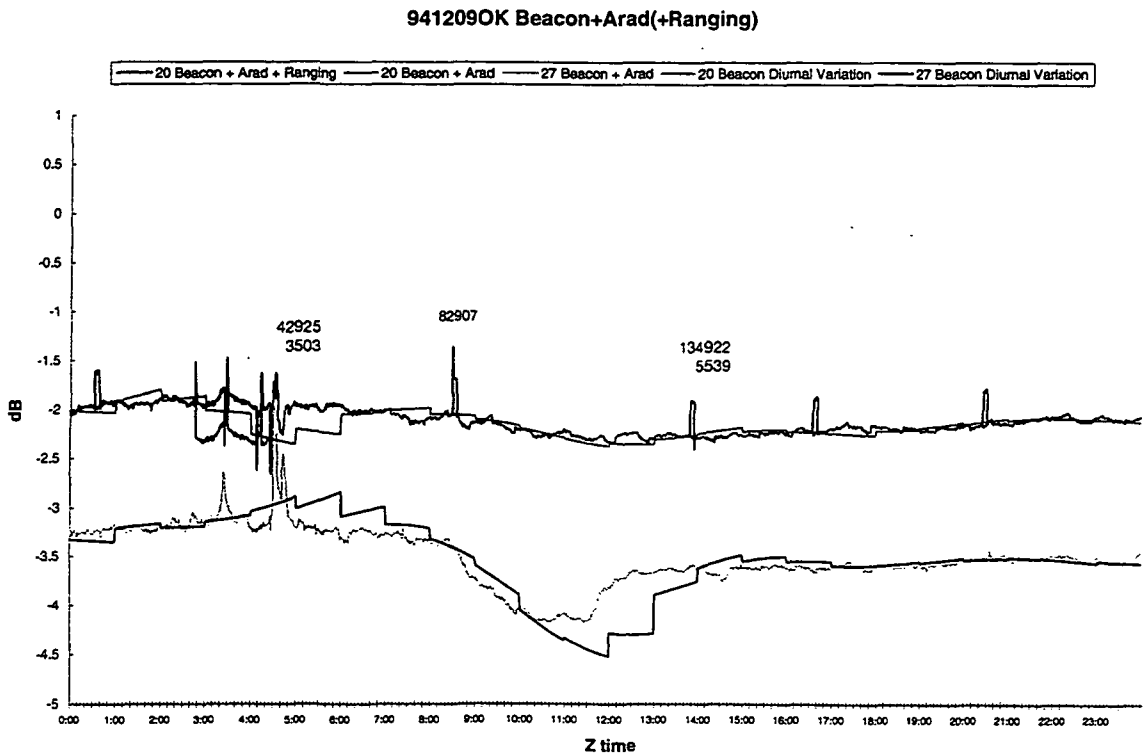
941209OK Beacon+Arad(+Ranging)
20 Beacon + Arad + Ranging
20 Beacon + Arad
27 Beacon + Arad
20 Beacon Diurnal Variation
27 Beacon Diurnal Variation
dB
42925
3503
82907
134922
5539
Z time

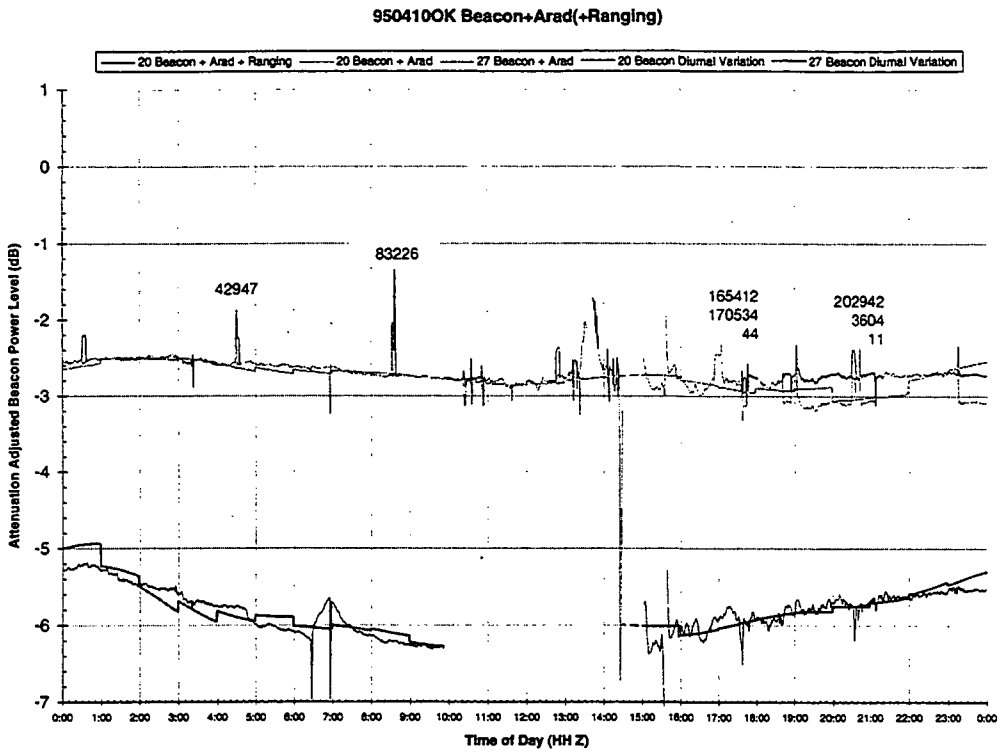
950410OK Beacon+Arad(+Ranging)
20 Beacon + Arad + Ranging
20 Beacon + Arad
27 Beacon + Arad
20 Beacon Diurnal Variation
27 Beacon Diurnal Variation
Attenuation Adjusted Beacon Power Level (dB)
42947
83226
165412
170534
44
202942
3604
11
Time of Day (HH Z)

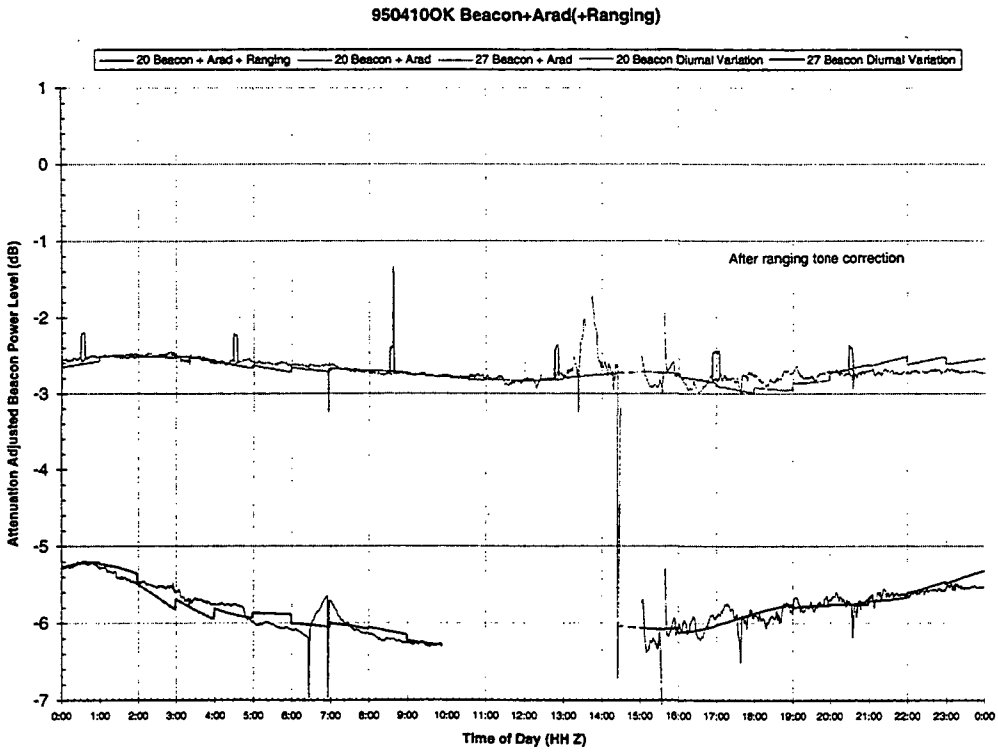
950410OK Beacon+Arad(+Ranging)
20 Beacon + Arad + Ranging
20 Beacon + Arad
27 Beacon + Arad
20 Beacon Diurnal Variation
27 Beacon Diurnal Variation
After ranging tone correction
Attenuation Adjusted Beacon Power Level (dB)
Time of Day (HH Z)

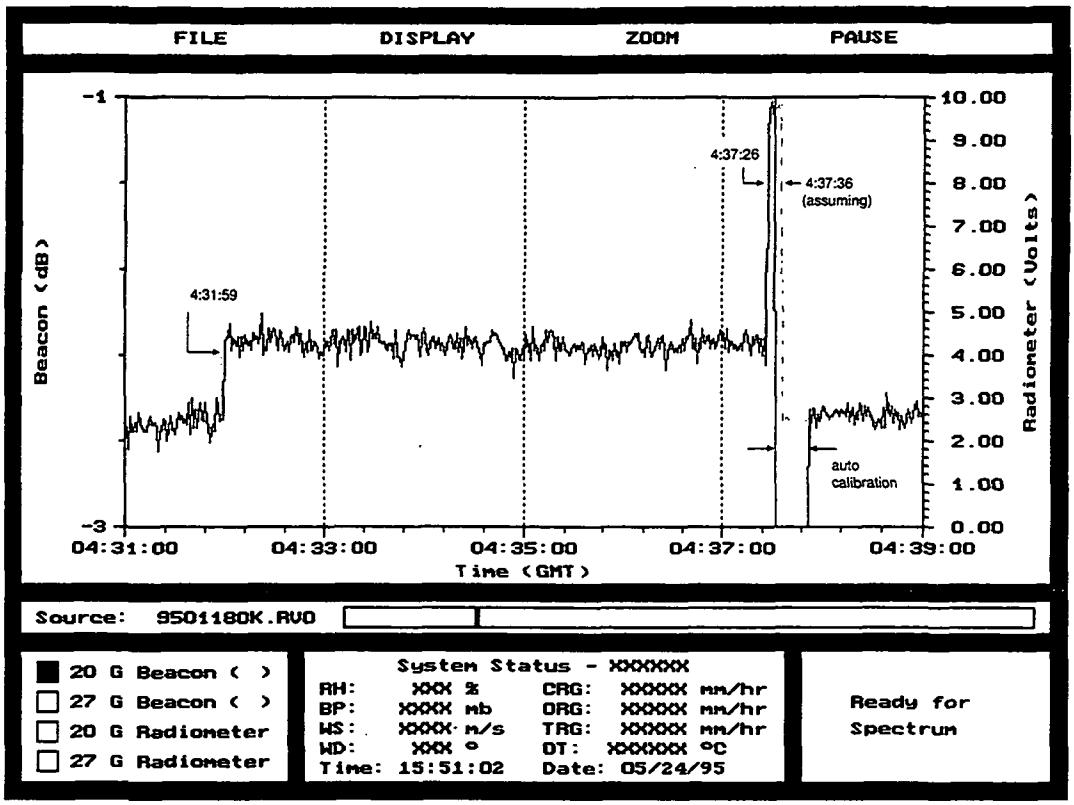
FILE
DISPLAY
ZOOM
PAUSE
Beacon (dB)
Radiometer (Volts)
-1
-3
10.00
9.00
8.00
7.00
6.00
5.00
4.00
3.00
2.00
1.00
0.00
4:31:59
4:37:26
4:37:36
(assuming)
auto
calibration
04:31:00
04:33:00
04:35:00
04:37:00
04:39:00
Time (GMT)
Source: 9501180K.RVD
20 G Beacon ( )
27 G Beacon ( )
20 G Radiometer
27 G Radiometer
System Status - XXXXXX
RH: XXX %
BP: XXXX mb
WS: XXXX m/s
WD: XXX °
Time: 15:51:02
CRG: XXXXX mm/hr
ORG: XXXXX mm/hr
TRG: XXXXX mm/hr
DT: XXXXXX °C
Date: 05/24/95
Ready for
Spectrum

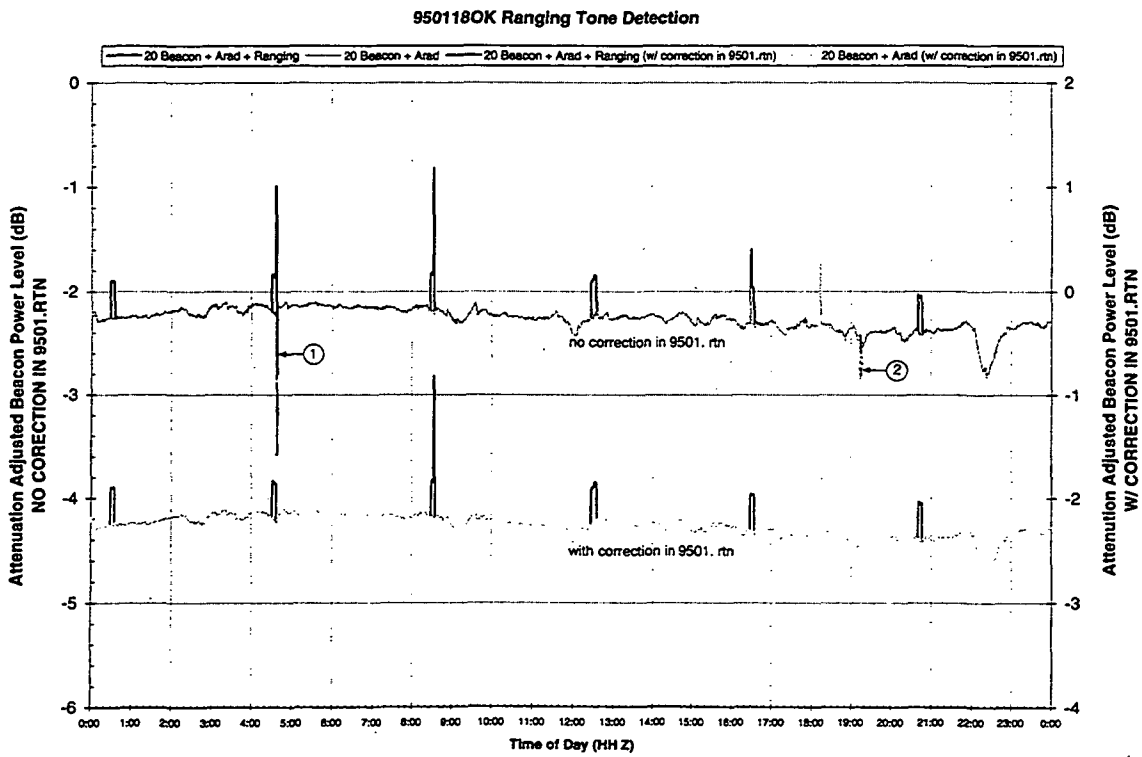
950118OK Ranging Tone Detection
20 Beacon + Arad + Ranging
20 Beacon + Arad
20 Beacon + Arad + Ranging (w/ correction in 9501.rtn)
20 Beacon + Arad (w/ correction in 9501.rtn)
Attenuation Adjusted Beacon Power Level (dB)
NO CORECTION IN 9501.RTN
Attenuation Adjusted Beacon Power Level (dB)
W/ CORRECTION IN 9501.RTN
0
-1
-2
-3
-4
-5
-6
2
1
0
-1
-2
-3
-4
no correction in 9501. rtn
with correction in 9501. rtn
1
2
0:00
1:00
2:00
3:00
4:00
5:00
6:00
7:00
8:00
9:00
10:00
11:00
12:00
13:00
14:00
15:00
16:00
17:00
18:00
19:00
20:00
21:00
22:00
23:00
0:00
Time of Day (HH Z)

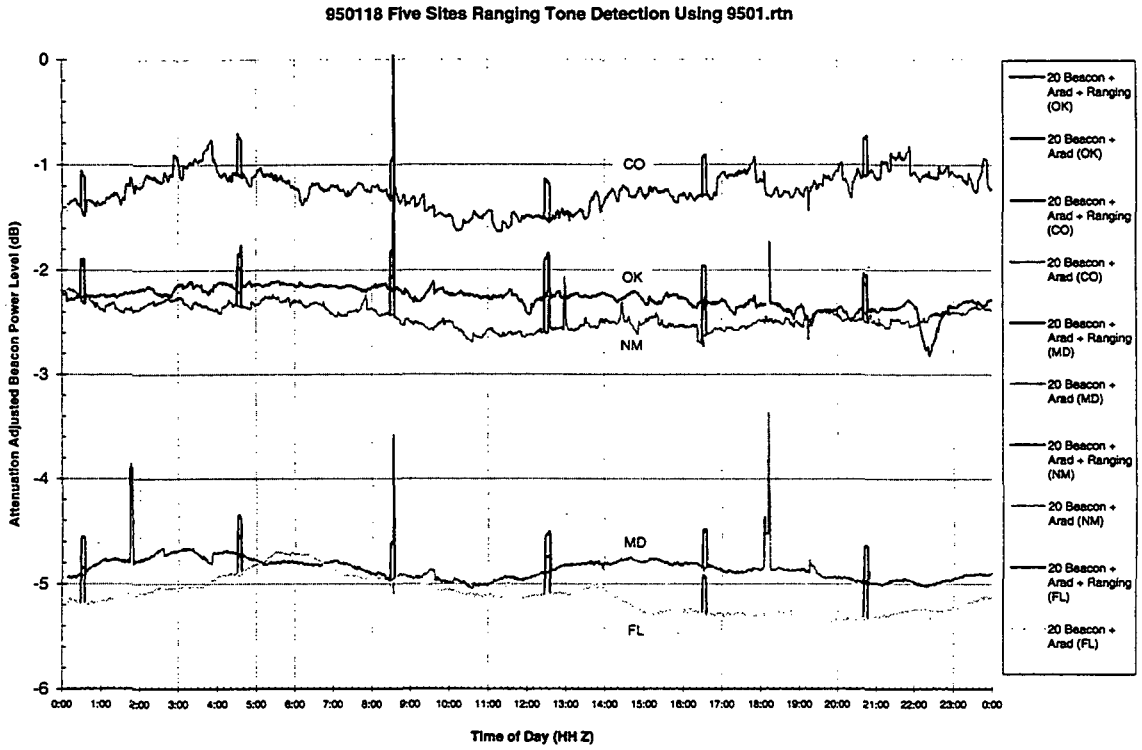
950118 Five Sites Ranging Tone Detection Using 9501.rtn
Attenuation Adjusted Beacon Power Level (dB)
Time of Day (HH Z)
CO
OK
NM
MD
FL
20 Beacon + Arad + Ranging (OK)
20 Beacon + Arad (OK)
20 Beacon + Arad + Ranging (CO)
20 Beacon + Arad (CO)
20 Beacon + Arad + Ranging (MD)
20 Beacon + Arad (MD)
20 Beacon + Arad + Ranging (NM)
20 Beacon + Arad (NM)
20 Beacon + Arad + Ranging (FL)
20 Beacon + Arad (FL)

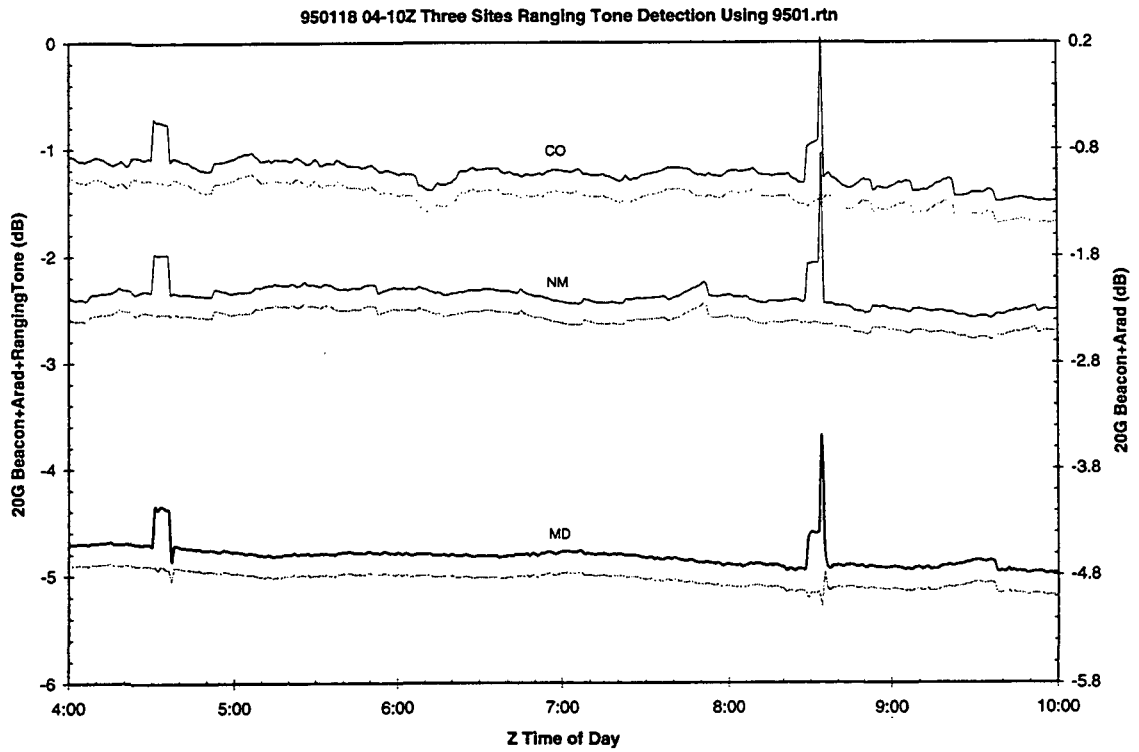
950118 04-10Z Three Sites Ranging Tone Detection Using 9501.rtn
20G Beacon+Arad+RangingTone (dB)
20G Beacon+Arad (dB)
Z Time of Day
CO
NM
MD

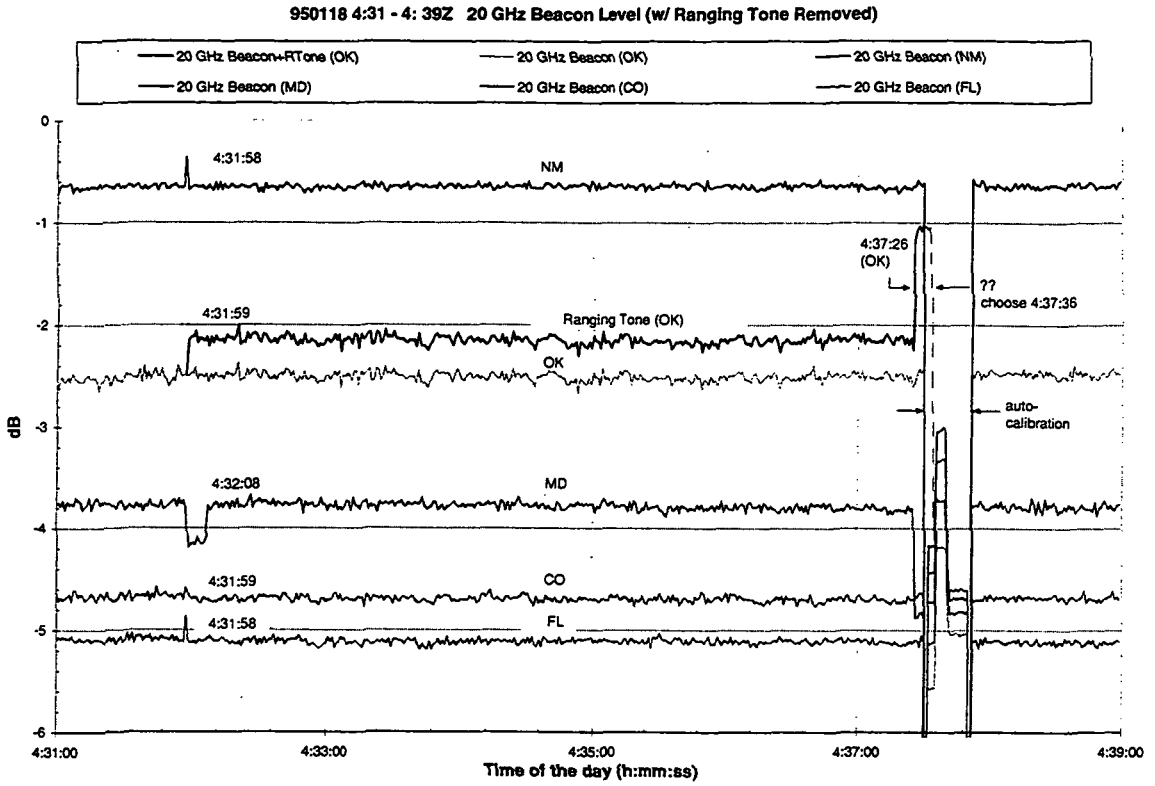

2. Beacon and Radiometer Calibrations at OK

1) On Feb. 14 and May 10, 1995, Dave helped us replaced our 20G LNA and adjusted RF enclosure polarization angle respectively. So calibration constants need to be adjusted for these operations.
2) To correctly calibrate beacon and radiometer, several .rv0 files of 'good' rain days and clear days need to be carefully chosen.
3) The .sum files of the rain days are first generated from ACTSPP. Then beacon to radiometer attenuation ratios are checked graphically for both frequencies. If the ratios are not close to one, re-run the ACTSPP with option 'NC' and change the antenna efficiencies, finally the ratios are adjusted to one.
4) Next with this new calfile, both radiometer attenuations must be close to the estimated gaseous absorptions at the two frequencies for the clear days. If not, spillover temperatures are changed from ACTSPP 'NC' option.
5) Step 3) and 4) are repeated until both criteria are satisfied.
6) Excel macro for above graphical checking purpose is available.
7) Finally whole month the sky brightness temperatures as measured by APT are compared with the sky brightness temperatures calculated from radiosode data.
8) Due to the drifting in noise diodes, we need adjust the noise diode adjustment factors almost every month. (from ACTSPP choosing "NA" option)

Session IV: Plenary

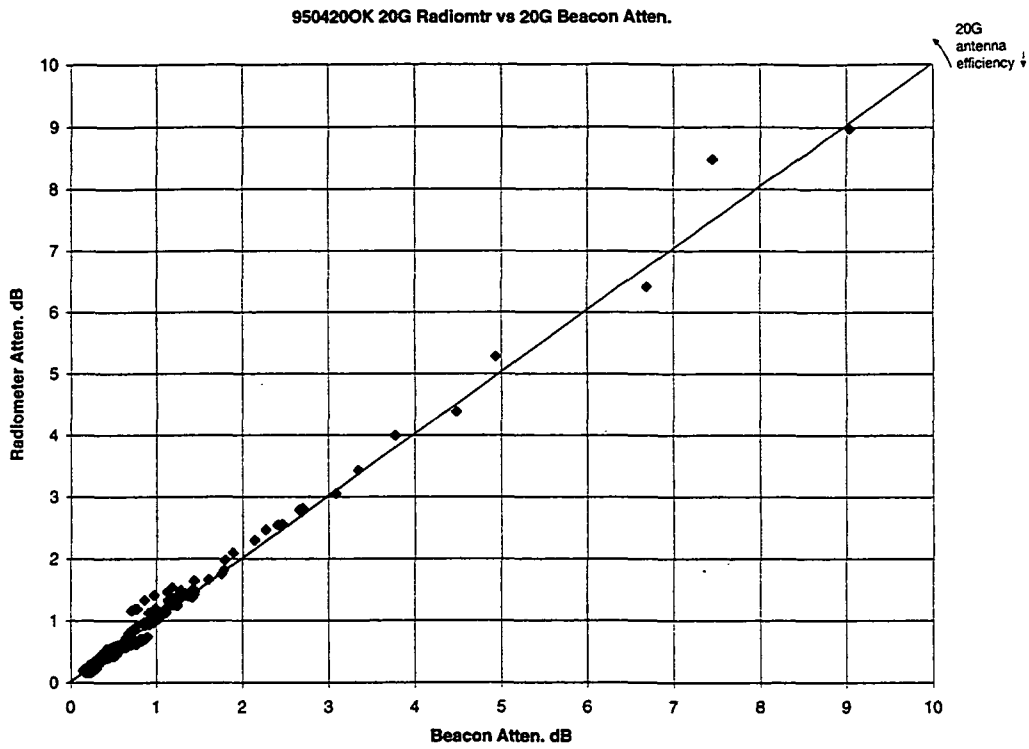
950420OK 20G Radiomtr vs 20G Beacon Atten.
20G antenna efficiency
Radiometer Atten. dB
Beacon Atten. dB
0
1
2
3
4
5
6
7
8
9
10

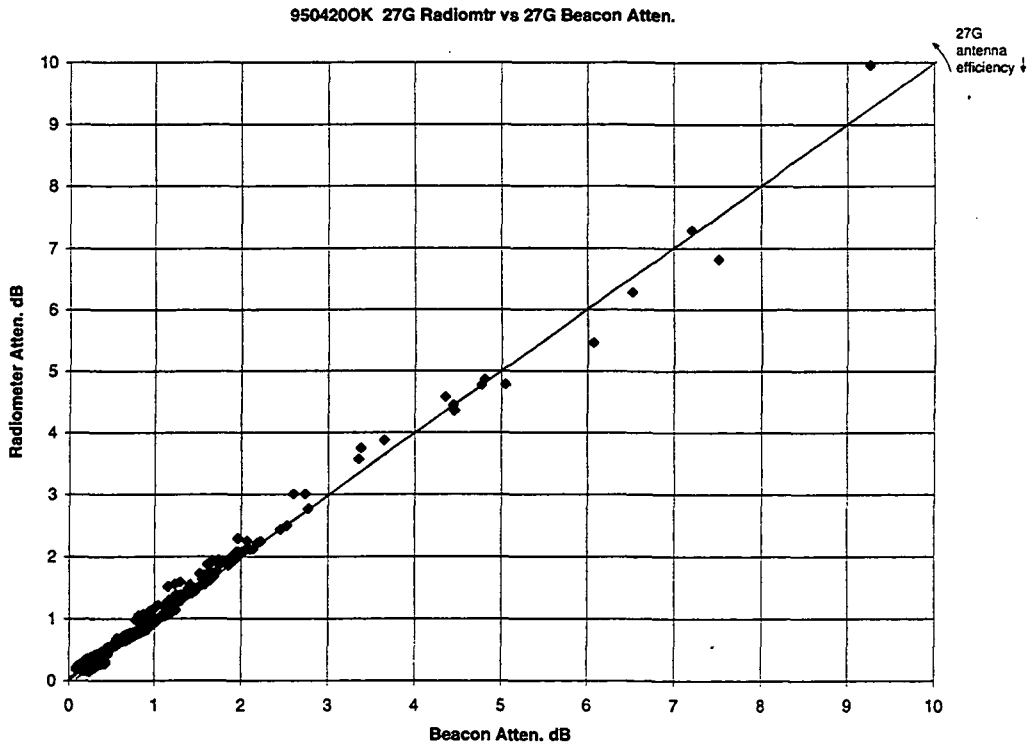
950420OK 27G Radiomtr vs 27G Beacon Atten.
27G antenna efficiency
Radiometer Atten. dB
Beacon Atten. dB
0
1
2
3
4
5
6
7
8
9
10

950420OK Radiometer Atten vs Estimated Gas Absorption in dB

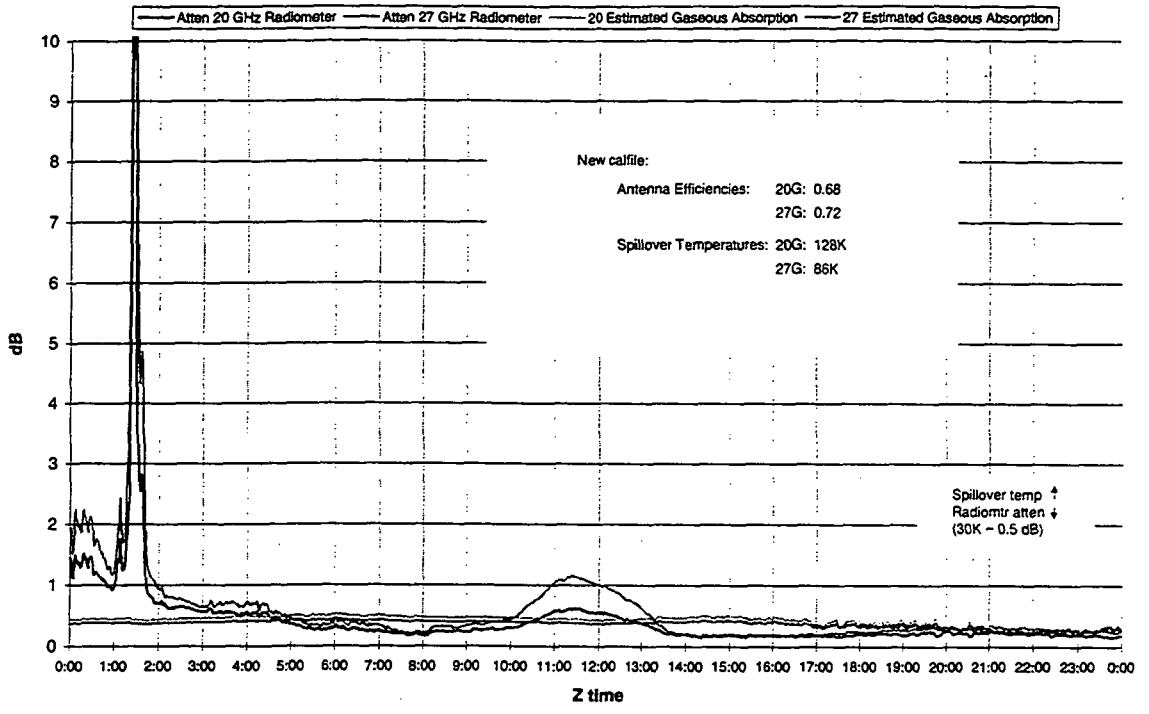

Sky Brightness Temperature, etc Calculated from Radiosode Data (Norman, OK)

By P. C. Robinson

Date	Precip (in)	20GHz Tb (K)	Tau (dB)	Tm (K)	27GHz Tb (K)	Tau (dB)	Tm (K)	Remarks
95011500	.2856	14.75	.2014	267.51	14.31	.1951	265.89	
95011512	.3595	17.29	.2420	271.12	16.10	.2231	269.35	Cs-sct.
95011712	.3075	15.27	.2100	267.92	14.62	.2004	265.88	Cs-sct.
95012000	.2027	12.50	.1645	265.21	12.90	.1726	263.19	
95012012	.2394	13.37	.1790	265.90	13.53	.1831	263.76	
95012312	.2155	12.96	.1742	262.42	13.68	.1884	260.21	
95012400	.1010	9.52	.1151	261.88	10.81	.1381	260.18	
95013100	.1982	12.32	.1609	265.83	12.89	.1724	263.35	
95013112	.1273	10.47	.1289	266.68	11.42	.1464	264.19	
95020112	.1963	12.16	.1548	271.54	12.19	.1560	270.28	Ci-sct.
95020200	.4885	21.39	.3056	277.13	19.16	.2700	275.02	
95020212	.2692	14.25	.1888	273.18	13.82	.1833	270.56	Ci--sct.
95020412	.1880	12.03	.1558	266.02	12.76	.1698	263.73	
95020512	.2735	14.38	.1956	266.84	14.42	.1981	264.35	
95020600	.2173	12.84	.1701	265.35	13.19	.1778	262.90	Cs sct.
95020800	.1764	11.61	.1504	263.16	12.37	.1646	261.30	
95020812	.0926	9.29	.1118	260.16	10.64	.1359	258.86	Cs-sct.
95020912	.3602	17.01	.2391	269.04	16.14	.2259	266.84	
95021000	.2187	12.79	.1668	269.32	12.92	.1703	267.25	Ci-sct.
95021100	.2666	14.23	.1927	267.26	13.94	.1894	265.11	Ci-sct.
95021712	.1803	12.04	.1565	265.19	12.65	.1685	262.86	
95021912	.3471	16.92	.2361	270.65	16.28	.2273	268.20	
95022000	.1521	11.19	.1398	269.21	11.96	.1544	266.38	Ci-sct.
95022012	.3622	17.27	.2388	274.07	16.07	.2207	271.58	Cs-sct.
95022112	.4772	20.59	.2972	272.40	18.50	.2633	270.41	Ci-sct.
95030800	.1831	11.66	.1528	260.65	12.43	.1674	258.93	Cs-sct.
95030812	.1432	10.01	.1251	258.54	11.01	.1437	256.59	
95030900	.2097	12.73	.1684	265.12	13.08	.1758	263.18	Cs-sct.
95030912	.2093	12.81	.1694	265.70	13.09	.1755	263.68	Cs-sct.
95031000	.2041	12.54	.1623	269.80	12.73	.1668	267.48	
95031012	.1892	12.37	.1595	269.60	12.72	.1669	267.17	
95031712	.5128	22.36	.3222	277.00	20.51	.2932	274.74	Cs-ovc.
95032112	.4969	21.47	.3072	276.88	18.83	.2643	275.00	Cs-sct.
95032700	.3785	18.11	.2518	275.40	17.17	.2380	273.08	
95032712	.2475	14.01	.1881	268.42	14.09	.1912	266.12	
95040212	.3247	15.94	.2170	273.41	15.09	.2045	271.05	
95040700	.6585	26.63	.3904	280.60	23.44	.3382	279.02	
95040812	.5789	24.55	.3528	282.11	21.74	.3079	280.14	
95041112	.2428	13.56	.1838	263.56	13.62	.1862	261.86	
95041200	.3083	15.12	.2073	268.27	14.32	.1940	267.63	
95041812	.3000	15.86	.2149	274.31	15.14	.2046	271.97	
95041900	.4135	19.12	.2675	276.71	17.62	.2442	274.69	
95041912	.3635	17.57	.2441	273.87	16.51	.2279	271.79	
95042512	.4187	19.12	.2715	272.82	18.13	.2570	270.44	
95050912	.6208	25.51	.3753	277.63	22.09	.3186	276.11	
95051112	.6608	26.31	.3912	276.23	23.30	.3407	275.14	Cs-sct.
95051312	.8214	32.30	.4779	286.32	28.17	.4092	285.39	

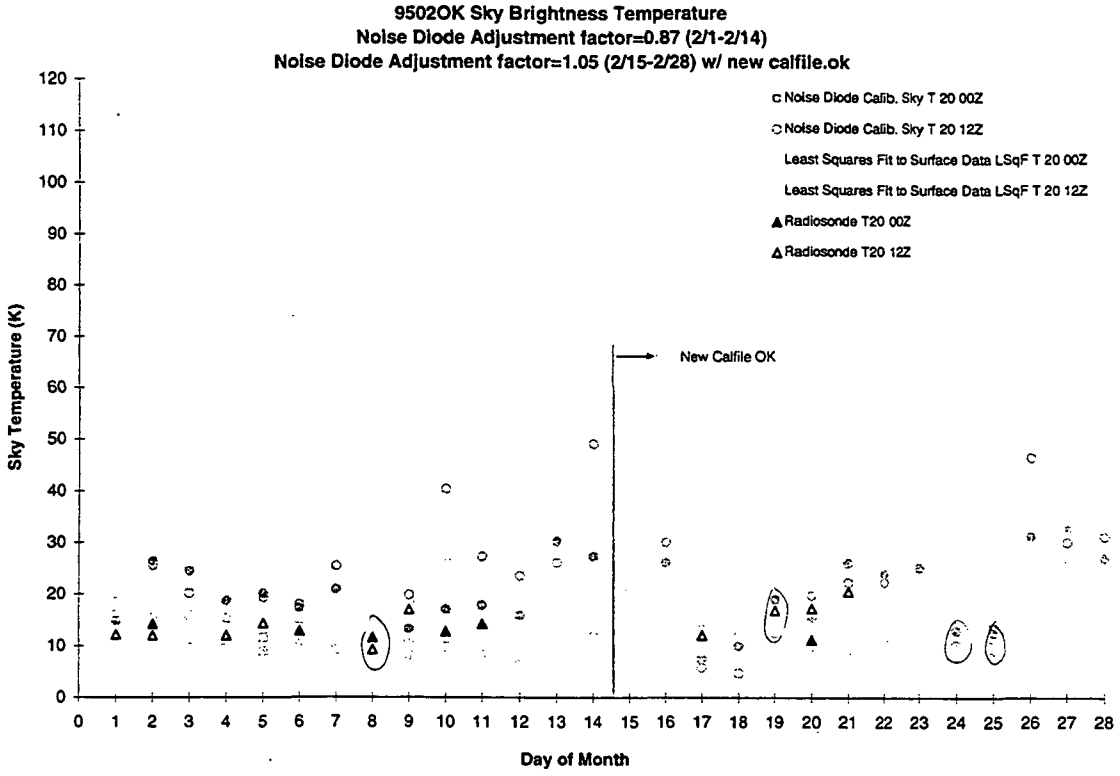
9502OK Sky Brightness Temperature
Noise Diode Adjustment factor=0.87 (2/1-2/14)
Noise Diode Adjustment factor=1.05 (2/15-2/28) w/ new calfile.ok
Noise Diode Calib. Sky T 20 00Z
Noise Diode Calib. Sky T 20 12Z
Least Squares Fit to Surface Data LSqF T 20 00Z
Least Squares Fit to Surface Data LSqF T 20 12Z
Radiosonde T20 00Z
Radiosonde T20 12Z
New Calfile OK
Sky Temperature (K)
Day of Month

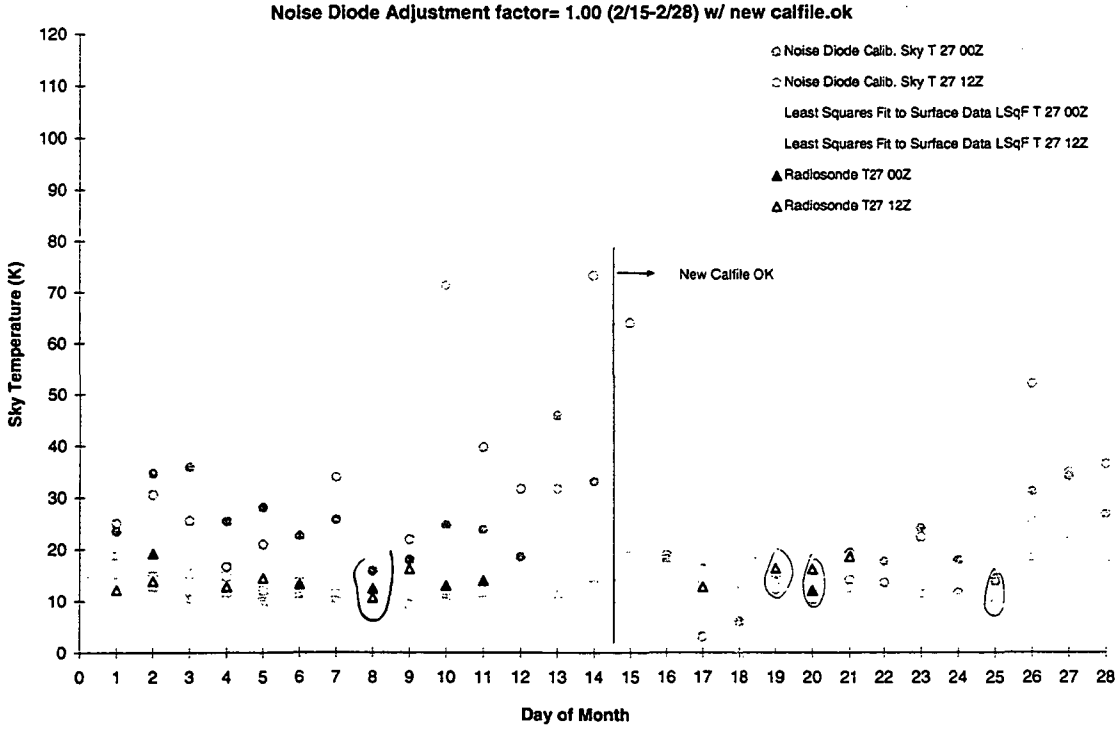
9502OK Sky Brightness Temperature
Noise Diode Adjustment factor=1.04 (2/1-2/14)
Noise Diode Adjustment factor= 1.00 (2/15-2/28) w/ new calfile.ok
Noise Diode Calib. Sky T 27 00Z
Noise Diode Calib. Sky T 27 12Z
Least Squares Fit to Surface Data LSqF T 27 00Z
Least Squares Fit to Surface Data LSqF T 27 12Z
Radiosonde T27 00Z
Radiosonde T27 12Z
New Calfile OK
Sky Temperature (K)
Day of Month

3. 11/03/93 - 5/31/95 OK Experiment CDFs

1) By using the .edf files from ACTSPP, now generating cdfs is a rather easy job.
2) Non-thermal attenuation from system faults/operation, beacon drop-outs, sun/moon intrusions, etc. should be removed from attenuation cdfs.
3) By examining the standard deviation, attenuation charts of each day (which we using the Excel macros as mentioned below to generate), rain, fog, cloud, and condensation events can be roughly distinguished.
4) The 'pure' rain attenuation cdf for 1994 is compared with Crane Tow Component Model. It looks like that the model underestimates the rain attenuation.
5) Rain rate cdf as measured by OK CRG is comparable with Crane's Global Model.

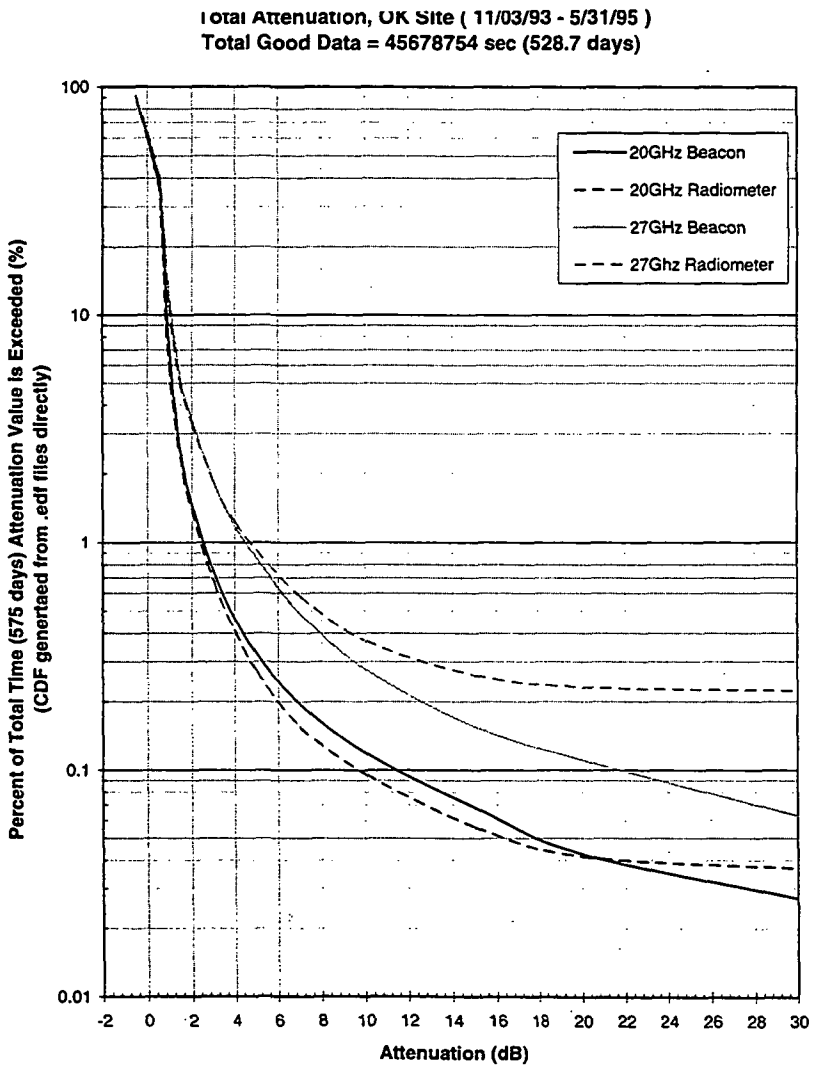

Thermal Attenuation, OK Site (11/03/93 - 5/31/95)
Total Good Data = 45678754 sec (528.7 days)

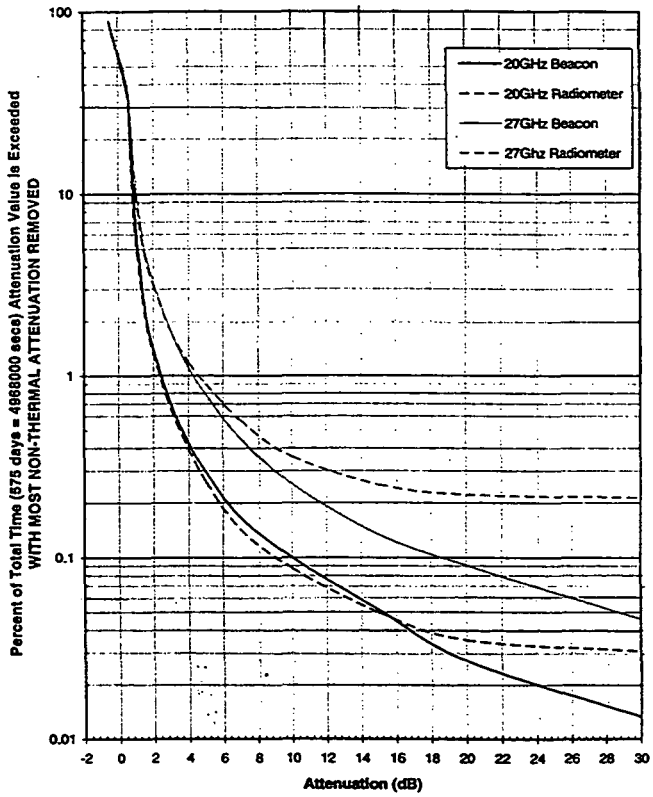

Model Comparison
OK 1994

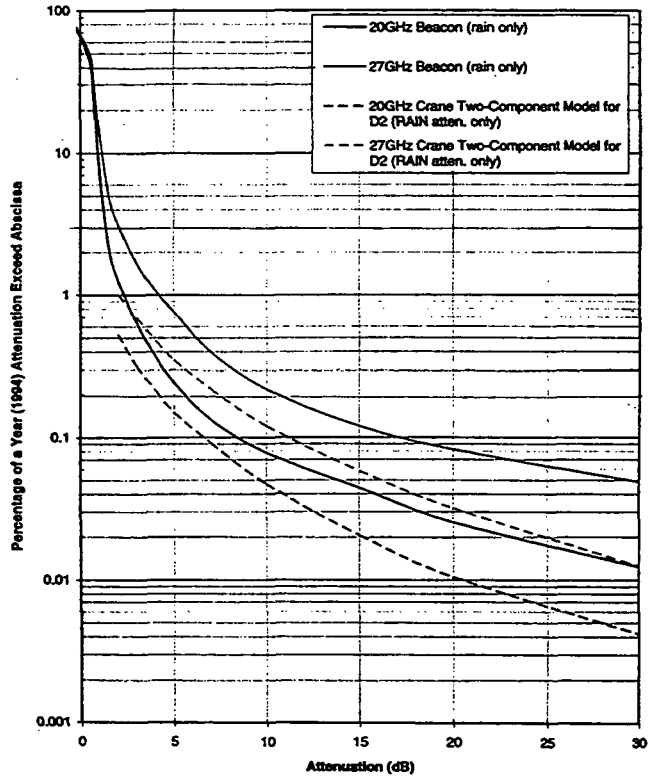

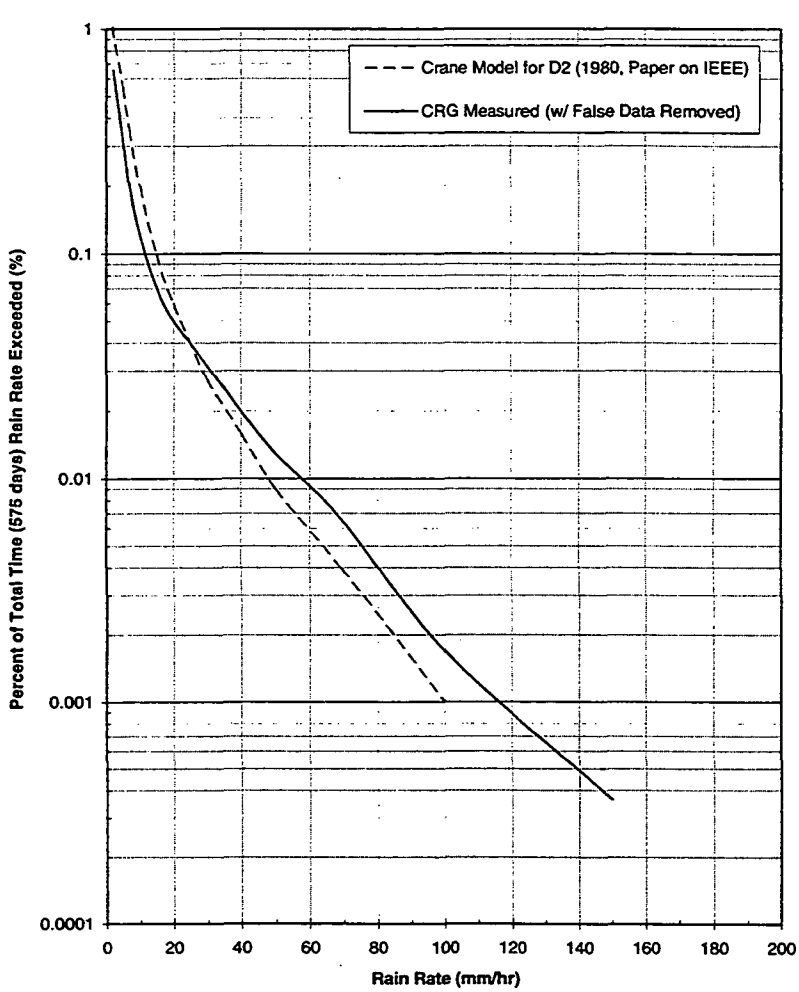

4. Excel Macros - ACTS01.xls

1) Pervious version is a macro used to generate the plots of attenuation adjusted 20G beacon power level for NASA Lewis Center to check ranging tone times.
2) ACTS00.xls is written in response to the request of Bruce Dow (UBC). The macros can automatically generate up to a whole month daily summary plots for each day, beacon power level plots for each day, etc.
3) New ACTS01.xls has save option added in (also in response to Bruce's request).
4) There are still lots of useful columns in .sum file. So any suggestions on new functions, new charts, ..., which the macro should be added in are welcome.
5) Above macros can only run in Microsoft Excel Version 5.0 or up.

950420OK Daily Summuary Plots

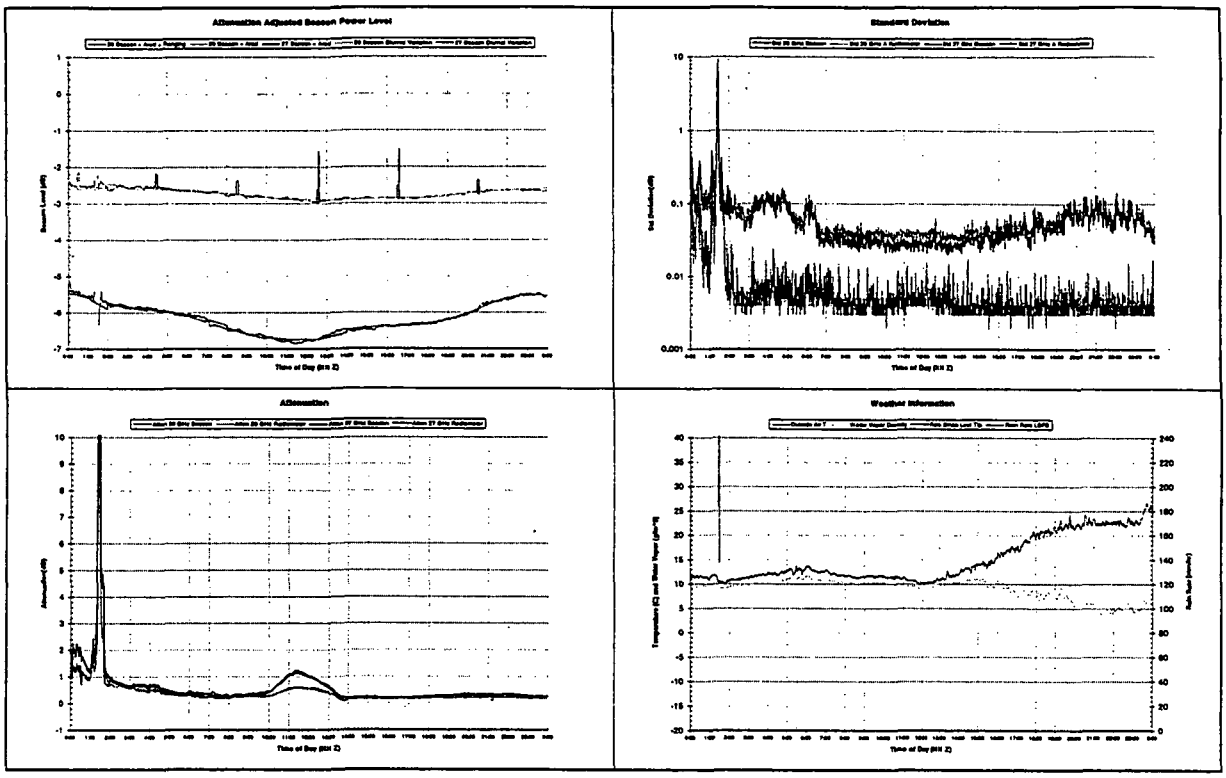

950530OK Daily Summuary Plots

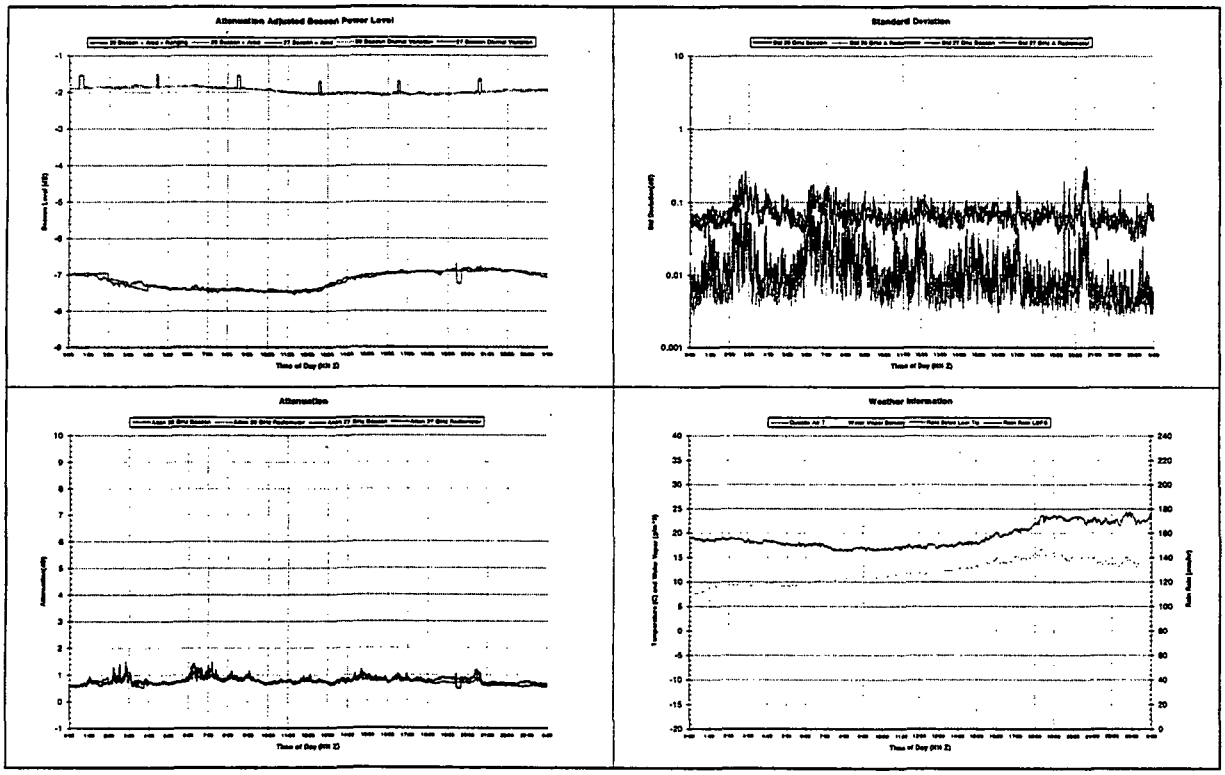

REPORT OF APSW VII PLENARY MEETING

D.V. Rogers and L.J. Ippolito

Results of the APSW VII Plenary meeting, held to discuss issues and action items related to the experiments conducted with the NASA ACTS Propagation Terminals (APTs), are summarized here. As operation of the APTs has become more routine, attention is increasingly focused on issues related to the processing, analysis and dissemination of data.

I. *Issues Related to Contracts and Measurement Period*

R. Bauer noted that the APT measurement contracts for the various sites expire during September-October 1995, which does not cover a full 2-year data-collection period through 30 November 1995. The ACTS budget is undetermined, and continuation of the propagation program beyond the previously-planned 2-year period is not assured. A delayed decision, even if positive, may pose difficulties for some experimenters. No-cost extensions can be arranged for completion of the contract reports, but this action will not relieve problems related to student salaries and costs associated with continued data collection.

A wide-ranging discussion ensued and several experimenters offered helpful suggestions. Based on these deliberations, the group reached a consensus on a preferred approach for current operations as follows.

ACTIONS

In the near term, each experimenter should:

a) focus on analyzing the first year of collected data, which will be advantageous whether contracts are renewed or not;

b) request via the Contract Officer a no-fee contract extension to 31 December 1995 (with copy to the Technical Monitor) to increase the available time to complete a final contract report should additional contract funds not be forthcoming; and

c) if funding renewal is delayed beyond the contract expiration date, continue data collection if possible to avoid gaps in data collection.

Regarding contract administration, R. Bauer stated that about 6 weeks are required to process the no-cost contract extensions.

II. *Data Preprocessing and Analysis*

Experimenters reported on experience to date with the software that performs various data preprocessing tasks, plus beacon and radiometer calibrations, and which outputs files in the .PV1 format. Several noted that, due to editing constraints, the .PV1 files can contain data known to be flawed (*e.g.*, due to maintenance), which is unsatisfactory from the standpoint of quality control of the ACTS data that are to be archived.

H. Helmken asked how to designate "bad" data and what action if any is appropriate for missing data blocks. W. Vogel remarked that archived data are to represent raw data that have been verified as valid, and should not contain derived data. J. Beaver observed that the experimenters require the capability to mark data that they know are invalid.

J. Feil and C. Mayer stated that some problems persist with data preprocessing. The process is slow, and the .PV0 and .PV1 files do not always agree. Comparison of beacon and radiometer distributions also has uncovered some discrepancies.

C. Mayer noted it would be beneficial for experimenters to be aware of the preprocessing constants (antenna efficiencies, etc.) derived by each site. X. Wang stated that he needs .RV0 data from two more sites in order to prepare the ranging-tone files.

D. Westenhaver indicated that he has a copy of software developed by R. Crane to process spectrum data. The software was requested by J. Feil and C. Mayer.

ACTIONS

D. Westenhaver will develop software to permit experimenters to designate start/stop times for bad or questionable data. The general procedure will be to generate and display .PV1 files so that experimenters may insert start and stop times for bad data segments in each channel. The resulting ".PV2" files will be the files archived by the Data Center. It is planned to complete this enhancement by 15 July 1995.

Each APT site is to FTP a table of preprocessing constants to D. Westenhaver, for access by experimenters as desired. Colorado, Maryland and New Mexico .RV0 data will be FTP'd to U. Oklahoma for use in developing the ranging-tone files.

III. *Data Formats and Presentation*

Presentation formats for the ACTS data were discussed, especially in light of the potential need to prepare final contract reports should the measurement program not be continued. It was noted that a format for plotting cumulative statistics had already been agreed. There was brief discussion of the most appropriate venues and methods to disseminate results of the ACTS measurements to the user community and propagation community at large, to demonstrate the progress that has been made and supply results to the user community.

W. Vogel proposed that a general-purpose template be prepared for use by all experimenters when preparing final contract reports so that this chore would need be done only once. J. Goldhirsh recommended that a standard set of data presentation results be established for use by each experiment site (in addition to any data analyses or results particular to that site). H. Helmken noted that standards should also be established for data processing (*e.g.*, time constant for running average used to separate rain attenuation from scintillation) so that results from the various sites could be directly compared in further analyses. It was noted that the NASA Handbooks, VPI&SU reports for Olympus measurements, and the OPEX reports provide useful reference material for such an endeavor.

ACTIONS

L. Ippolito, R. Crane and D. Rogers will draft a report template, and propose standards for a contractually-valid minimum set of data results and data-processing parameters for consideration by the experimenters. The template is to be considered only as a guide. It is planned to complete this draft material by 1 August 1995.

H. Helmken also volunteered to evaluate, using data from Florida and other sites, the provisional data-processing parameters proposed by the aforementioned group to establish optimum data-processing standards.

IV. *Data Dissemination*

R. Bauer reported that he had received several requests for specific segments of ACTS propagation data, and asked as to the proper disposition of such requests (*e.g.*, refer to the Data Center; forward to the relevant experiment site?) Several experimenters also asked how the individual sites should treat any such direct requests.

R. Henning stated that he was considering collaboration with NEXRAD radar experts to evaluate the weather profile in Florida, to assist other government and industrial organizations, and asked who owns the ACTS data and if their use in such joint activity is appropriate. F. Davarian stated that the ACTS data are in the public domain, and there is no restriction on their use; such applications, especially to assist users with implementation issues, are encouraged. However, it was noted that first publication rights for the data reside with the respective experimenters, and interim users should respect this right.

ACTIONS

The group agreed to entrust the development and implementation of the data dissemination procedures to R. Bauer (NASA LeRC) and W. Vogel (ACTS Data Center). Individual experimenters may deal with requests for specific data or analysis results, but in all cases R. Bauer and W. Vogel should be kept apprised of the situation. The group concluded that .PV1 files or software could be provided in response to outside requests if an individual experimenter thought it was really necessary, but such actions should be coordinated with R. Bauer and W. Vogel.

V. *Equipment Issues*

The group discussed the use of hydrophobic paint for the antenna, stimulated by a presentation of J. Goldhirsh on tests involving wetting the antenna dish and feed. Concerns were expressed regarding applying the paint midway through the experiment. It was agreed that the hydrophobic coating has beneficial effects, but that its use and maintenance is the responsibility of each site.

The need for periodic reapplication of the hydrophobic paint was acknowledged. However, the group decided that it be left to each experiment site to determine the appropriate time for reapplication, due to

the variability of local weather conditions from site to site (*i.e.*, from desert to subtropical).

R. Crane, who was unable to attend, forwarded a reminder that the iterative beacon/radiometer calibration technique may be compensating for unknown receiver characteristics, and a complete recalibration is recommended whenever any work is performed on the front end. X. Wang stated that the Oklahoma site uses radiosonde data (from the monthly summary log) to verify the system calibration, and modifies the noise diode factor to compensate for variations.

It was noted that the meteorological sensors are important to the ACTS experiments, and it is important to monitor their performance and address problems promptly. This activity is also the responsibility of each site.

VI. *Other Issues*

While not directly an ACTS issue, the NASA Handbooks were briefly discussed at the end of the meeting. The handbooks still appear to enjoy widespread appeal and use. However, it was noted with some regret that the 4-year revision cycle had slipped due to reduced funding for the Propagation Program. It is therefore inevitable that the value of the handbooks will deteriorate as the contents gradually become obsolete.

End Date
October 11, 1995